

March, Jack (2005) Determining The Location of an Impact Site from Bloodstain Spatter Patterns: Computer-Based Analysis of Estimate Uncertainty. PhD thesis, University of Nottingham.

**Access from the University of Nottingham repository:**

<http://eprints.nottingham.ac.uk/10166/1/JackMarch-Thesis-2005%28HighQuality%29.pdf>

**Copyright and reuse:**

The Nottingham ePrints service makes this work by researchers of the University of Nottingham available open access under the following conditions.

- Copyright and all moral rights to the version of the paper presented here belong to the individual author(s) and/or other copyright owners.
- To the extent reasonable and practicable the material made available in Nottingham ePrints has been checked for eligibility before being made available.
- Copies of full items can be used for personal research or study, educational, or not-for-profit purposes without prior permission or charge provided that the authors, title and full bibliographic details are credited, a hyperlink and/or URL is given for the original metadata page and the content is not changed in any way.
- Quotations or similar reproductions must be sufficiently acknowledged.

Please see our full end user licence at:

[http://eprints.nottingham.ac.uk/end\\_user\\_agreement.pdf](http://eprints.nottingham.ac.uk/end_user_agreement.pdf)

**A note on versions:**

The version presented here may differ from the published version or from the version of record. If you wish to cite this item you are advised to consult the publisher's version. Please see the repository url above for details on accessing the published version and note that access may require a subscription.

For more information, please contact [eprints@nottingham.ac.uk](mailto:eprints@nottingham.ac.uk)

**DETERMINING THE LOCATION OF AN IMPACT SITE FROM BLOODSTAIN  
SPATTER PATTERNS: COMPUTER-BASED ANALYSIS OF ESTIMATE  
UNCERTAINTY.**

**Jack March, BA.**

**Thesis submitted to the University of Nottingham  
for the degree of Doctor of Philosophy**

**September 2005**

## **Abstract**

The estimation of the location in which an impact event took place from its resultant impact spatter bloodstain pattern can be a significant investigative issue in the reconstruction of a crime scene. The bloodstain pattern analysis methods through which an estimate is constructed utilise the established bloodstain pattern analysis principles of spatter bloodstain directionality, impact angle calculation, and straight-line trajectory approximation.

Uncertainty, however, can be shown to be present in the theoretical definition and practical approximation of an impact site; the theoretical justification for impact angle calculation; spatter bloodstain sample selection; the dimensional measurement of spatter bloodstain morphologies; the inability to fully incorporate droplet flight dynamics; and the limited numerical methods used to describe mathematical estimates.

An experimental computer-based research design was developed to investigate this uncertainty. A series of experimental impact spatter patterns were created, and an exhaustive spatter bloodstain recording methodology developed and implemented. A computer application was developed providing a range of analytical approaches to the investigation of estimate uncertainty, including a three-dimensional computer graphic virtual investigative environment.

The analytical computer application was used to generate a series of estimates using a broad spatter bloodstain sampling strategy, with six potentially probative estimates analysed in detail. Two additional pilot projects investigating the utility of a sampled photographic recording methodology and an automated image analysis approach to spatter bloodstain measurement were also conducted.

The results of these analyses indicate that, with further development, the application of similar analytical approaches to the construction and investigation of an estimate could prove effective in minimising the effect that estimate uncertainty might have on informing the conclusions of this forensic reconstructive process, and thereby reaffirm the scientific expert evidential status of estimate techniques within legal contexts.

## Thesis Contributions

The research presented in this thesis contributes to the theory and practice of bloodstain pattern analysis and the construction of an estimate of the location of an impact site from its resultant impact spatter pattern in a number of ways:

- A wide-ranging examination of the potential sources of uncertainty involved in reconstructing the location of an impact site (Chapters 2, 3, and 4).
- The development and implementation of an exhaustive manual impact spatter pattern recording methodology (*Chapter 5*).
- The development of qualitative spatter bloodstain classification methodologies such as the subjective criteria developed during the manual recording process (*Chapter 5*), and quantitative classification through automated image analysis techniques (*Chapter 7*).
- The development of a rapid photographic recording methodology for large-scale sampling of impact spatter patterns (*Chapter 6*).
- The application of an automated image analysis system to demonstrate the potential of reproducible quantitative analyses of spatter bloodstain morphologies (*Chapter 7*).
- The development and implementation of an analytical computer application providing detailed analyses of spatter bloodstain data and precise sample selection, characterisation, and population comparison (*Chapters 8 and 11*); alternative statistical descriptive and analytical methods for a considered approach to the investigation and evaluation of estimate data (*Chapters 8, 9 and 11*); the application of spatial statistical concepts of process and pattern in the interpretation of site of impact estimate data (*Chapters 9 and 11*); an integrated three-dimensional computer graphic interactive environment for the analysis and evaluation of estimate data (*Chapters 10 and 11*).
- The demonstration of the role of such structured quantitative approaches to the analysis of impact spatter patterns, sample selection strategies, and spatter bloodstain morphologies, in increasing reconstructive confidence in site of impact estimates and their construction methodologies (*Chapters 7, 11 and 12*).

## **Acknowledgements**

I would like to acknowledge the following individuals, whose support and assistance during the course of my PhD research has been greatly appreciated.

- Dr Martin Evison, of The University of Sheffield, for setting me on the PhD path.
- Dr Damian Schofield, of The University of Nottingham, for keeping me on that path, and providing directions.
- Dr Ed Lester and Dr Tao Wu, of The University of Nottingham, for their advice and guidance in the ways of image analysis.
- Kev Pritchard, of The University of Central Lancashire, for initial discussions on bloodstain pattern analysis and cabbage bashing experiments.
- Jennie Lewis and Pam Hamer, of Forensic Alliance Limited, for their continued support of this research and generosity with blood.
- Martina Boatfield, of Forensic Alliance Limited, for providing an extra pair of hands during experimentation.
- John March, for his 'novel' but much appreciated proof reading skills.
- Jenny March, for her constant encouragement and entirely misplaced faith.
- Christiane and Peter McAlindon, for mashed potato and Roche Mazet.
- Monica 'Get on with it' McAlindon, for knowing the right thing to say. Oh and paying the mortgage.
- One-Eye and Lucky, for the constant reminder that a life consisting solely of food and sleep can be thoroughly enjoyable.

Thank you all,

Jack

## Table of Contents

1	Bloodstain Pattern Analysis and Crime Scene Reconstruction .....	1
1.1	Introduction .....	1
1.2	A Background to Bloodstain Pattern Analysis .....	1
1.3	Crime Scene Reconstruction .....	4
1.4	BPA: Science or Interpretation?.....	6
1.5	Conclusions.....	12
2	Spatter Bloodstain Patterns and Site of Impact Estimation .....	13
2.1	Introduction .....	13
2.2	BPA In Practice .....	13
2.3	Spatter Patterns .....	15
2.4	Impact Spatter Bloodstains.....	18
2.5	Site of Impact Estimation .....	22
2.5.1	Directionality .....	24
2.5.2	Impact Angle .....	25
2.5.3	Spatter Trajectory .....	28
2.6	Conclusions.....	34
3	Practical Site of Impact Estimation .....	36
3.1	Introduction .....	36
3.2	Site of Impact Estimation .....	36
3.3	2D Convergence Techniques .....	37
3.3.1	Point or Area of Convergence .....	38
3.3.1.1	Point or Area of Origin .....	40
3.4	3D Origin Techniques.....	43
3.4.1	Traditional Stringing.....	44
3.4.2	Computer-Based Methods .....	49
3.5	Conclusions.....	60
4	Site of Impact Estimation: A Critique.....	61
4.1	Introduction .....	61
4.2	Estimate Uncertainty .....	61
4.3	The Impact Event.....	62
4.4	Droplet Dynamics.....	66
4.4.1	Droplet Shape .....	66
4.4.2	Spatter Bloodstain Formation .....	68
4.5	Impact Angle Calculation.....	72
4.6	Spatter Measurement .....	76

4.7	Spatter Bloodstain Sample Selection .....	81
4.8	Conclusions.....	88
4.9	Proposed Investigation.....	95
4.10	Project Outline .....	97
5	Impact Spatter Experimentation .....	100
5.1	Introduction .....	100
5.2	Experimental Impact Spatter Patterns.....	100
5.2.1	Experimentation .....	101
5.2.2	Impact Method.....	102
5.2.3	Target Surface .....	103
5.2.4	Pattern Generation .....	104
5.3	Exhaustive Spatter Bloodstain Recording .....	106
5.3.1	Pre-recording.....	107
5.3.2	Recording Procedure .....	108
5.3.3	Target Surface Grid.....	109
5.3.4	Photographic Recording and Spatter Numbering.....	112
5.3.5	Spatter Measurement.....	114
5.3.6	Specific Pattern Recording and Preliminary Results .....	119
5.3.6.1	Pattern ES-C .....	120
5.3.6.2	Pattern ES-A .....	121
5.3.6.3	Pattern ES-B .....	123
5.3.7	Spatter Location Conversion.....	124
5.4	Discussion.....	127
5.5	Conclusions.....	132
6	Sampled Photographic Recording .....	134
6.1	Introduction .....	134
6.2	Pilot Project Aims and Objectives.....	134
6.3	Recording Design .....	136
6.4	Pattern selection .....	138
6.5	The Recording Process .....	141
6.5.1	Pattern MC-A .....	142
6.5.2	Pattern MC-B .....	144
6.6	Discussion.....	147
6.7	Conclusions.....	151
7	Spatter Bloodstain Image Analysis .....	152
7.1	Introduction .....	152
7.2	Pilot Project Aims and Objectives.....	152
7.3	Methodology .....	154

7.3.1	Idealised Spatter Bloodstains .....	154
7.3.2	Image Analysis Procedure .....	155
7.4	Results .....	158
7.4.1	Centre of Gravity .....	158
7.4.2	Feret Length .....	165
7.4.3	Feret Angles .....	171
7.4.3.1	Directionality .....	171
7.4.3.2	Ellipse Measurement.....	173
7.4.4	Area, Perimeter and the Ideal Ellipse Comparison.....	178
7.5	Discussion.....	187
7.6	Conclusions.....	190
8	Data Pre-processing and Pattern Characterisation .....	192
8.1	Introduction .....	192
8.2	Computer-Based Analysis of Site of Impact Estimation .....	192
8.3	Spatter Bloodstain Data Pre-processing .....	196
8.3.1	Data Acquisition .....	197
8.3.2	Spatter Bloodstain Analysis .....	202
8.3.2.1	Straight-Line Trajectory Determination.....	203
8.3.2.1.1	Vector Decomposition .....	205
8.3.2.1.2	Vector Proof .....	207
8.3.2.1.3	Target Surface Variation.....	208
8.3.2.1.4	An Alternative Directionality .....	210
8.3.2.2	Calculating Additional Trajectory Angles .....	211
8.3.2.3	Independent Trajectory Quality Parameter.....	214
8.3.2.4	Distance from Impact Site .....	216
8.3.2.5	Spatter Bloodstain Size .....	216
8.3.2.6	Subjective Spatter Bloodstain Type.....	217
8.4	Spatter Bloodstain Data and Collection Composition .....	217
8.4.1	Target Surface Distribution .....	220
8.4.2	Spatter Bloodstain Morphology Composition .....	221
8.4.3	Straight-Line Trajectory Composition.....	222
8.4.4	Impact Site Relative Composition.....	224
8.5	Conclusions.....	226
9	Site of Impact Estimate Construction and Analysis.....	228
9.1	Introduction .....	228
9.2	Spatter Bloodstain Selection .....	228
9.3	Site of Impact Estimate Construction .....	231
9.4	Establishing Trajectory Intersections.....	233



9.5	Analysing Trajectory Intersection Data Sets .....	237
9.5.1	Conventional Statistical Analysis .....	238
9.5.1.1	Univariate Analysis .....	239
9.5.1.2	Multivariate Analysis .....	247
9.5.2	Spatial Data Analysis .....	255
9.5.3	Spatial Point Patterns .....	256
9.5.3.1	Distance-Based Methods .....	258
9.5.3.2	Area-Based Methods .....	270
9.6	Single and Multiple Sample Specific Analyses and Data Recording .....	273
9.6.1	Single Sample Site of Impact Estimation Data .....	273
9.6.2	Multiple Sample Site of Impact Estimation Data .....	276
9.7	Conclusions .....	279
10	Three-Dimensional Estimate Visualisation .....	283
10.1	Introduction .....	283
10.2	Forensic Data Visualisation .....	283
10.3	Visualisation Development .....	287
10.4	Constructing a Visualisation .....	290
10.4.1	General Visualisation Features .....	290
10.4.1.1	Environment and Camera Creation .....	290
10.4.1.2	Geometry Selection and Numerical Data Presentation .....	292
10.4.1.3	Known Site of Impact Visualisation .....	294
10.4.1.4	Spatter Bloodstain Visualisation .....	295
10.4.2	Single Sample Estimate Visualisation .....	296
10.4.2.1	Straight-Line Trajectory and Intersection Visualisation .....	297
10.4.2.2	Visualisation of Intersection Data Set Analyses .....	299
10.4.3	Multiple Sample Visualisation .....	304
10.4.4	Mean Data Visualisation .....	305
10.4.5	Sampling Distribution Confidence Interval Visualisation .....	306
10.5	Conclusions .....	307
11	Experimental Data Analysis .....	309
11.1	Introduction .....	309
11.2	Impact Spatter Pattern Screening .....	309
11.3	Site of Impact Estimate Sampling Strategy .....	311
11.4	Total Spatter Bloodstain Population Analysis .....	314
11.4.1	Single Sample Estimation .....	315
11.4.2	Multiple Sample Estimation .....	324
11.5	3D Data Quality Sub-Population Analysis .....	333
11.5.1	Sub-population Composition .....	333

11.5.1.1	Vertical Angle .....	335
11.5.1.2	Width-to-Length Ratio .....	337
11.5.1.3	Minimum Droplet Flight Distance .....	339
11.5.2	Single Sample Estimation .....	341
11.5.3	Multiple Sample Estimation .....	348
11.6	Conclusions .....	352
12	Research Conclusions .....	360
12.1	Introduction .....	360
12.2	The Limitation of Current Site of Impact Estimation .....	360
12.3	Results of the Research .....	363
12.4	Future Work .....	368
	References .....	372
	Appendix A – Forensic Alliance Limited Examination of Biological Contaminated Material Information Sheet .....	387
	Appendix B – Forensic Alliance Limited Bloodstain Experimentation Information Sheet .....	389
	Appendix C – Forensic Alliance Limited Experimentation Risk Assessment .....	391
	Appendix D – Forensic Alliance Limited Laboratory Working Procedure .....	395
	Appendix E – Spatter Bloodstain Recording Process Assessment .....	396
	Appendix F – Spatter Bloodstain Recording Risk Assessment .....	397
	Appendix G – Plasti-Kote Material Safety Data Sheet .....	398
	Appendix H – Sodium Hypochlorite Material Safety Data Sheet .....	400
	Appendix I – Experimental Impact Spatter Pattern Photographic Recording ...	403
	Scaled Grid .....	403
	Numbered .....	405
	Appendix J – Sampled Photographic Recording .....	409
	Pattern MS-A .....	409
	Pattern MS-B .....	411
	Appendix K – The Automated Image Analysis Macro .....	414
	Appendix L – Automated Image Analysis Results .....	416
	Shape IS-A .....	416
	Shape IS-B .....	417
	Shape IS-C .....	418
	Shape IS-D .....	419
	Shape IS-E .....	421
	Shape IS-F .....	422
	Appendix M – Experimental Impact Spatter Pattern ES-A .....	424
	Appendix N – Converted BackTrack®/Win Experimental Data .....	445

Front Wall .....	445
Back Wall .....	445
Right Wall .....	446
Left Wall .....	446

# **1 Bloodstain Pattern Analysis and Crime Scene Reconstruction**

## **1.1 Introduction**

This chapter will introduce the forensic reconstructive disciplines of bloodstain pattern analysis, and crime scene reconstruction. A brief review of the aims, development, and current methodological approach to reconstructing a scene from patterned bloodstain evidence will be presented. The relationship of bloodstain pattern analysis to the broader discipline of crime scene reconstruction will be discussed, and some of the fundamental concepts and limitations of this general approach to reconstructing crime scenes will be addressed. The position of bloodstain pattern analysis within the field of forensic science will also be highlighted, and a number of the potential difficulties with the general application of the findings of bloodstain pattern analysis in legal contexts, where the criteria for the admissibility of such expert forensic evidence is becoming increasingly stringent, will be addressed.

## **1.2 A Background to Bloodstain Pattern Analysis**

Blood is one of the most common forms of evidence found at the scene of violent crimes, and its utility as evidence in criminal investigation has been exploited since the times of some of the earliest historical medico-legal systems, and probably even before (Bevel and Gardner, 2002). By the 1950's, the development of serological analysis had made possible the determination of blood as human, the determination of blood groups, and biological sex identification from small blood droplets and dried bloodstains (Marriner, 1991). Since the mid 1980's, and the discovery of genetic fingerprinting, an almost definite individualisation of blood has been possible through the development of increasingly sensitive DNA analysis techniques (Jackson and Jackson, 2004; Watson, 2004). Currently, it is possible, through the scientific investigation of blood at a crime scene, to provide significant information regarding the identification and possible individualisation of a person who has shed even the smallest amount of blood. This forensic determination of 'who', however, is not the only investigative potential provided by blood deposited at a crime scene. A level of 'what', more associated with the realms of forensic pathology than forensic science, can also be inferred from the analysis of bloodstain patterns at a crime scene (Bevel and Gardner, 2002). The investigation and analysis of

bloodstain patterns can provide an insight into the physical crime scene dynamic, and in certain circumstances, such as when the individuals involved are not in question, or no eye-witnesses are available, or those that were present provide conflicting statements, it has been argued that this 'what' function can actually be of equal or greater investigative significance than the 'who' (Ristenbatt and Shaler, 1995; Lee et al., 2001; Pizzola et al., 1986a; Raymond et al., 1996a).

The means by which the physical, spatial, and temporal components of a crime can be inferred from bloodstains is often referred to as Bloodstain Pattern Analysis (BPA). The objectives of this type of analysis are to apply concepts of biology, biochemistry, physics and mathematics to reconstruct events associated with the 'static aftermath' of a violent crime that bloodstains can often represent (MacDonell, 1982 cited in Bevel and Gardner, 2002). Despite the common misconception that BPA is a relatively new forensic discipline, bloodstain evidence has a long history of use in legal contexts, stretching back to at least the records of 13<sup>th</sup> Century Germanic law (Bevel and Gardner, 2002). It was not until the late 19<sup>th</sup> and early 20<sup>th</sup> centuries, however, that the medium of blood, and bloodstain patterns began to be investigated in a scientific manner (e.g. Gross, 1894, Poitrowski, 1895, Haberda, 1914 and Ziemke, 1914, cited in Pizzola et al., 1986, MacDonell, 1996 and Bevel and Gardner, 2002), and the presence of bloodstain evidence at crime scenes began to be utilised in a more rigorous fashion than previous medico-legal attempts (Marriner, 1991). The 1960's have been suggested as a period of modern renaissance for the discipline of BPA, with the work of renowned figures such as Dr. Paul Kirk, and Herbert MacDonell paving the way for the increased interest, acceptance, use, and significance of BPA in criminal investigation involving scenes of bloodshed through to the 1990's and beyond (Bevel and Gardner, 2002; James, 1998a; Chisum, 2000; MacDonell, 1996; Kou et al, 1991, cited in Kou et al, 1992).

Through its continued development and application, BPA is now recognised as a valuable tool in Crime Scene Reconstruction (CSR) techniques, with a number of organisations appearing to support, advance, and regulate its practice. The International Association of Bloodstain Pattern Analysts (IABPA) was set up in 1983 with the aims of promoting education and research into BPA, as well as standardising BPA training and terminology. This organisation currently has over 600 members worldwide, convenes an annual BPA training conference in the United States of America, as well as producing a BPA newsletter, which contains amongst others research articles (IABPA, 2004a). The International Association

of Identification (IAI) recognised BPA as a discipline distinct from general crime scene analysis in 1990 and now operates BPA accreditation based on fulfilling course requirements, with at least 40 hours basic training, a level equivalent to that required for Provisional membership of the IABPA (Bevel and Gardner, 2002; IAI, 2004; IABPA, 2004a). More recently, the Federal Bureau of Investigation (FBI) laboratory has set up the Scientific Work Group on Bloodstain Pattern Analysis (SWGSTAIN). Since its inception in March 2002, SWGSTAIN has aimed to:

'...serve as a professional forum in which BPA practitioners, and practitioners from related fields, can share, discuss, and evaluate methods, techniques, protocols, quality assurance, education, and research relating to BPA'

The group is also committed to working toward 'best practice' guidelines for the enhancement of BPA and its practice (SWGSTAIN, 2002). Despite having multinational representation, SWGSTAIN is geared towards the use of BPA within an adversarial judicial system, and more specifically the federal system of the US. This situation has led to the call by some European bloodstain pattern analysts for the creation of an affiliated European workgroup, to address the specific concerns of BPA within an inquisitorial judicial system (Eikelenboom, 2003).

Modern BPA is a broad and complex mix of formal training, experimentation, research and casework, relying upon the application and appreciation of a wide range of other scientific and technical disciplines in both its theory and practice (James, 1998a). The actual practical process of BPA as part of the investigation of a crime scene involves a range of procedures that includes (Wonder, 2001):

- The recording and collection of evidence.
- Pattern categorisation and identification.
- Individual pattern and total crime scene pattern interpretation and reconstruction.
- Experimental design and experimentation.
- The presentation of the culmination of these processes in the form of expert testimony in court.

### 1.3 Crime Scene Reconstruction

The Association of Crime Scene Reconstruction defines CSR as (ACSR, 2005):

'The use of scientific methods, physical evidence, deductive and inductive reasoning and their relationship to gain explicit knowledge of the series of events that surround the commission of a crime'.

Although some form of CSR has always been an implicit part of criminal investigations, it was not until the 1980's, and the high profile development of criminal profiling, that CSR began to be explicitly recognised, and studied and developed as a discipline in its own right (Bevel and Gardner, 2002). The general aim of modern CSR is to provide an insight into an overall incident involving the commission of a crime, through the analysis of a broad spectrum of evidence, which includes the locations, position and distribution of the physical evidence in conjunction with its laboratory examination (Lee et al. 2001). CSR attempts to construct a crime scenario narrative in which the presence, movements and actions of individuals and objects are described in terms of their spatial and temporal position, given the available evidence. To facilitate this reliance on the physical evidence and crime scene patterning, the overall crime scene scenario can be broken down into components parts of 'events' and 'event segments'. CSR events represent specific stages during an incident, such as the forced entry to a property, while event segments represent specific actions connected with the events, to which evidence, such as the presence of fingerprints a shattered pane of glass, or specific glass fragments found on a suspect's clothes, can be directly linked (Lee et al., 2001; Bevel and Gardner, 2002). Through relative, and less frequently, absolute time referencing, it may be possible to link event segments into chronological event scenarios. It may then be possible to time reference the events themselves to provide a degree of understanding of the incident as a whole.

Despite its potential utility, and frequent use in Crime Scene Investigations (CSI), the use of CSR and its reliance on pattern evidence has often been criticised as unscientific, and subjective by the more fact driven forensic science community (Bevel and Gardner, 2002; Lee et al., 2001; Cooley, 2001). To counter such suggestions, proponents of modern CSI and associated CSR approaches often stress their reliance on a 'scientific' method, which is often referred to as '*the scientific*' method, explicitly linking it to that used by more mainstream sciences.

The scientific method utilised within CSR, like its pure science counterpart, has its basis in both inductive and deductive reasoning, and to a certain degree has a revisable hypothesis testing procedure, which is often implemented (Bevel and Gardner, 2002; Cooley, 2001). Problems arise in the scientific standing of CSR, however, as no real standards exist against which to test its ultimate conclusions (Figure 1-1).

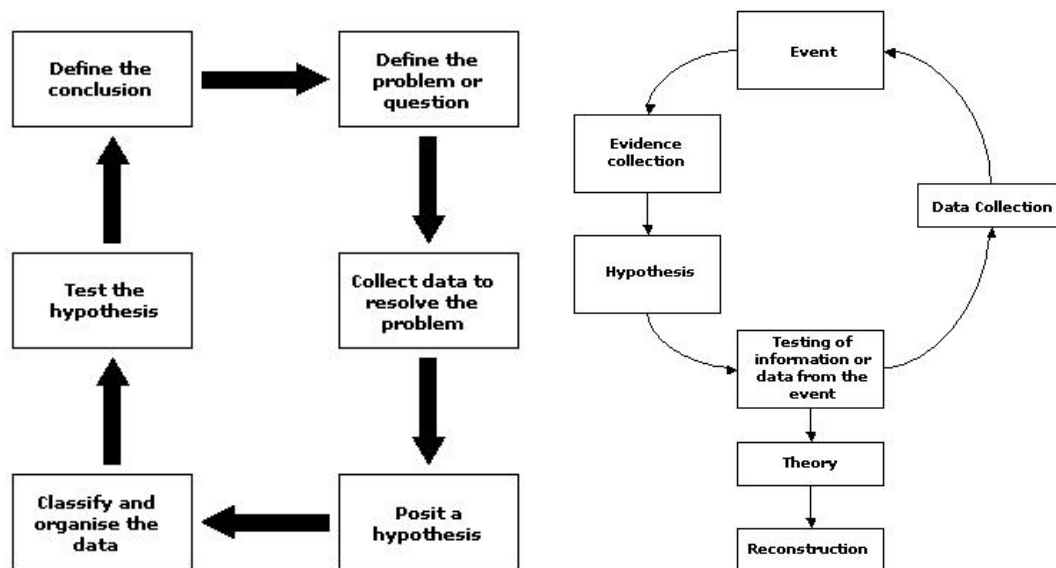


Figure 1-1 - Diagram of 'the' scientific method (left, after Bevel and Gardner, 2002), and the 'scientific' CSR process (right, after Lee et al., 2001).

While the circular methodology of 'the scientific' method means hypothesis generation, testing and conclusion is a potentially continuous and refinable process, the CSR 'scientific' method is forced to break this circle at some point. This break from 'the scientific' circle usually occurs when no more meaningful evidence can be gathered, and the CSR process is forced to posit some type of conclusions, which fit the available evidence, but cannot necessarily be effectively retested. Although new data can be incorporated within CSR hypotheses and conclusions, and experimentation can be conducted in an attempt to replicate evidence found at the scene, it is impossible to exactly replicate the crime scenario with the kind of tight control over independent and dependent variables that is central to pure scientific investigation. The double checks that are present in empirical scientific investigation are, therefore, not necessarily present in the testing methods employed in CSR (Cooley, 2001). In this sense, if two, or possibly more competing CSR hypotheses can explain the crime scene evidence, it may be impossible to differentiate between them. CSR, it can be argued, is



based on more fluid and uncontrollable dynamics than the tightly defined scientific laws of pure science (Bevel and Gardner, 2002). As such, the objectives, techniques and results obtainable through CSR as a whole, and with BPA in particular, can, and should, achieve a more reliable utility in eliminating possible crime scene scenarios, rather than in attempting to prove a definitive incident narrative (Lee et al, 2001; Bevel and Gardner, 2002).

While the methodology of CSR is arguably 'scientific', describing the process as employing 'the scientific' method is perhaps a step too far, to a certain extent overlooking the limitations that the nature of the data places on CSI and CSR practitioners. A middle ground has been suggested by Bevel (2001, cited in Cooley, 2001), who describes CSR not as a 'science' but as the 'application of science' to solve problems regarding the events in a crime. But no matter how the process is packaged, its limitations in term of scientific fact remain, and these limitations are somewhat re-emphasized by the advocacy of conservative CSR interpretations by several authors, and the restriction of reconstructions to 'events', or even 'event segments', if a complete case narrative, or competing narratives are not exclusively supported by the evidence (James, 1998a; Murray, 2000a, 2000b; Lee et al. 2001; Saccoccio, 1998).

#### **1.4 BPA: Science or Interpretation?**

A BPA scene reconstruction, conducted in isolation, provides only a partial CSR in the sense that only one form of evidence is considered. At scenes of violent crime, however, it may often be the case that BPA evidence proves to be the most probative aspect of a full CSR (Lee et al., 2001). Holding this position within CSR, BPA has also been hindered by questions over its scientific basis. One area where this is perhaps the most obvious is in the various names given to the techniques of CSR using bloodstain patterns by practitioners and authors alike. Although for the sake of convention and consistency the term BPA is used throughout this thesis, others have offered titles varying from 'bloodstain pattern interpretation' through to 'blood dynamics' (Bevel and Gardner, 2002; James, 1998a; Eckert, 1997 cited in van Zyl, 2001; Kish, 1998; McDonnell, 1996; Wonder, 2001). These descriptive titles place different emphases on the position of BPA within forensic investigative sciences (Bevel and Gardner, 2002; Wonder, 2001). The explicit inclusion of 'interpretation' suggests a more subjective approach to the examination of bloodstain patterns, whereas a stress on

'analysis' or 'dynamics', attempts to place the discipline firmly within the realms of scientific endeavour, countering the still common view that BPA lacks scientific credibility in legal contexts (Murray, 2000a).

The state of BPA within legal contexts is a fairly complex one, which differs in different judicial systems. The majority of examples discussed here originate from the US, as legal examples are more widely available, and the bulk of published BPA literature stems from the US. All of the points raised are, however, of importance to the practice and application of BPA in the context of any legal system, and as a discipline. The interpretations of patterned bloodstain evidence have been admitted into court in the US and the UK for over a century (Cooley 2001; Saccoccio, 1998; Henderson, 1998; Bevel and Gardner, 2002), with modern scientific BPA being offered as expert testimony in America from the 1940's and 1950's (Murray, 2000a; Cheatham and Flach, 2003). While some courts have historically had little problem with the expert status of BPA evidence, others have both rejected and allowed the admission of BPA testimony on the basis that it is within the realms of common experience (Veilleux, 1993; Saccoccio, 1998). The discipline as a whole, as well as the conclusions inferred from its practice, has often been viewed as the simple application of 'common sense' or just 'interesting guesswork' (van Zyl, 2001).

Although the present-day admissibility of BPA is based more on the position it holds as a scientific or applied scientific forensic discipline, problems with the perception of BPA still exist (Saccoccio, 1998). Despite a more than likely universal agreement that the interpretation of bloodstains is not within the realms of general experience, nearly everybody has and does experience the actions of fluids on a daily basis, and probably less frequently have some experience of the physical nature and flow of blood (Saccoccio, 1998). Unlike BPA, however, this experience does not systematically study, characterise and interpret the bloodstains resulting from violent crimes, but in conjunction with the often inadequate presentation of BPA as a complex scientific discipline it can result in the perception of BPA as either relatively simple, unscientific, or both. The presentation of BPA in court presents somewhat of a paradox for BPA expert witnesses. An appreciation of the underlying scientific theory and applied science involved in the documentation, interpretation and reconstruction of the bloodstain pattern evidence is necessary for a court in an adversarial system to establish what weight to attribute to such reconstructions, as with all expert evidence (Murray, 2000b). While attempting to present the processes of BPA to a non-

scientific audience the theories and practice of BPA are, however, often presented in a simplified manner. The analysis of bloodstain pattern evidence can, as a result, appear inherently unsophisticated, an impression reinforced by the emphasis that is regularly placed on the more immediately understandable visual aspects of the BPA process (Murray, 2000a; Wonder, 2001). The possible consequences of such perceptions are both the undervaluing of potentially probative and significant BPA reconstruction evidence within the legal process, and the potentially dangerous overextension of 'common sense' bloodstain evidence to provide answers to legal arguments where no expert opinion has been offered (Murray, 2000a).

At a broader level, it can even be argued that the respective objectives of 'truth' and 'justice' of scientific investigation and the legal process, and their methodologies, techniques and epistemological stances, are not entirely compatible. The bifurcated dichotomy of 'yes' or 'no' usually required by legal counsel from their expert witnesses is generally at odds with the multifarious shades of grey surrounding scientific knowledge. Cooley (2001) argues that where science and legal process do overlap, however, is in the concepts of reliability and validity, and it is these attributes that in a legal context are typically held synonymous with science. By adopting a scientific tag, it is these attributes that the reconstruction methodologies of CSR and BPA are trying to associate themselves with, but as has already been mentioned, any scientific realisation of pattern evidence reconstruction is generally unobtainable through the inability to perform direct empirical study with regards to the actual reconstruction (Cooley 2001). There is, however, no reason why increased reliability and validity of reconstruction methodologies cannot be aimed towards, and even achieved. Whether this development is through the application of scientific procedures in the documentation, characterisation, interpretation and reconstruction of bloodstain pattern evidence at crime scenes, or by advancing the potential of these processes through direct scientific experimentation with closely defined research aims, procedures and conclusions. This broad level of experimentation within BPA, however, is generally lacking. Although reconstructive experimental design and experimentation are often an essential part of the interpretation of evidence in specific cases, the funding for more general research into BPA techniques, methodologies and their theoretical basis tends not to be forthcoming. As a result experimentation and research is predominantly casework-based, and as such is often limited by time constraints, and the relative narrowness of the investigative questions being addressed

(Wonder, 2001). This situation is probably partly responsible for the general lack of published BPA research material. Such a restricted research base, combined with a conceptual association of science with experimentation in legal contexts, and the common misconception that case-specific experimentation is necessary in the identification and interpretation analysis of all bloodstains, can only further any critique of the scientific nature of BPA (Cooley, 2001; Wonder, 2001).

The differing abilities and conceptual approaches to BPA of different practitioners is an additional concern for the discipline, despite attempts to standardise the quality of BPA evidence and expert testimony through professional accreditation. Anyone who has completed a short basic training course run by numerous institutions and different professional bodies can, theoretically, give expert evidence in court (Eikelenboom, 2003). Although the more qualified an 'expert' is in terms of knowledge gained through study and experience, and the higher standing they have amongst their peers, the more influential, and less open to question their evidence is likely to be, this situation still represents a potentially damaging position for BPA (Murray, 2000a). Not only could the presentation of inaccurate testimony in a specific case have considerable consequences for the individuals involved in that case, but could combine to seriously affect the perceived standing of the BPA in general. It is also difficult to perceive BPA as a unified forensic discipline given that different schools of thought about the training and nomenclature of BPA exist, and are usually stressed by the different groupings of practitioners (Wonder, 2001; Eikelenboom, 2003). Expert testimony on BPA and bloodstain pattern evidence has been accepted in courts from a wide variety of trained professionals, including forensic scientists with backgrounds in chemistry, biology, physics, serology and pathology and from members of the law enforcement community, including crime scene investigators, evidence technicians and detectives (Veilleux, 1993; Henderson, 1998; James, 1999, cited in van Zyl, 2001). Within this broad range of backgrounds, the experience of Wonder (2001), a renowned BPA specialist, suggests that detectives tend to concentrate their efforts on spatter identification, whereas technicians tend to be more concerned with transfer patterns, and pathologists are most interested in patterns which are indicative of arterial damage.

This lack of standardisation within BPA is mirrored in the use of terminology. Although the IABPA (2004b) published a suggested terminology for the characterisation and interpretation of bloodstain evidence, the document also includes the caveat that:

'It is strongly recommended...that Bloodstain Analysts be able to individually define terms as it pertains to their own use. If this is readily available to the reader or reviewer, then there should be no question as to the particular or unique use of a term'.

The flexible use of terminology to address specific BPA methodologies and individual practitioners preferences is certainly an admirable and utilitarian stance, but even where terminology is made explicit, the use of a different lexicon by different practitioners arguably can only complicate the review of BPA work by other practitioners, as well as present a general feeling of confusion within the discipline (Eikelenboom, 2003). It can also be argued that a general lack of standardisation within the discipline, both in terms of terminology and protocol, whether this is actually practical or not, is partially responsible for the perceived lack of the scientific credibility of BPA by those viewing the discipline from the outside (e.g. Cooley, 2001).

It is hardly surprising then, that BPA can be accused of being subjective and unduly reliant on the interpretational elements of its reconstruction methodologies (Cooley, 2001). Proponents of BPA assert, however, that the reluctance of legal systems, and other forensic sciences to accept the more subjective elements of BPA is not necessarily due to the fact that they are actually prejudicially subjective, but more a result of the inadequate understanding of the processes through which BPA inferences are made. It is argued by Murray (2000b), for example, that it is the very judgement that can be interpreted as subjective that is necessary to combine all of the numerous strands of bloodstain pattern evidence and the analysis of this evidence in determining investigational significance. Murray (2000b) also suggested that it is just this contextual consideration of evidence, which rather than inhibiting the discipline, enables an accurate and appropriate analysis of specific case evidence to be made. Perhaps more interesting is the stance taken by Bevel (Bevel, 2001 cited in Cooley, 2001; Bevel and Gardner, 2002), who argues for a retention of the scientific tag for CSR and BPA as applied sciences (Bevel, 2001 cited in Colley 2001), while questioning the foundations of the modernist stance from which science gains much of the weight attributed to it as the elucidator of truth. Bevel and Gardner (2002) challenge scientific knowledge, suggesting that it is logic and rationalism, both forms of interpretation, that combine with empirical observations to make sense out of abstract and complex scientific issues,

arguing, therefore, that it is the interpretation of data that leads to knowledge, not just the collection of it. While science can be questioned in terms of its ability to be completely objective, suggesting that the more subjective components of CSR are not that dissimilar to the processes of the knowledge generation of pure science, a scientific tag in terms of an applied scientific technique is arguably a necessary goal for the credibility of the discipline.

It can be shown from even a brief review of the techniques and research involved in BPA that the situation is more complex than any interpretation-science dichotomy, with a significantly blurred transition from the more scientific and theoretical to the more interpretative and practical aspects of the methodologies and reconstructive techniques employed throughout the discipline. Even within BPA the techniques utilised do not really differ between the interpretative and analytical epistemological schools of thought, and it can be argued that there is actually a greater division between the science and the practice of BPA than there is between the science and the interpretation, the interpretation itself often being based on scientific study, observation, experimentation and research. Wonder (2001) asserts that BPA is a scientific endeavour beyond the application of simple physics and biology because of the presence of technical and scientific literature on the subject. But it can also be argued that the presence of scientific rigour in the literature does not necessarily translate into practical application. It will be shown later in this thesis (see Chapter 4) that this is specifically the case for the estimation of the location of an impact event from its resultant bloodstain pattern, where, despite advancing technical applications, the methodologies currently used fail to represent some of the more recent scientific research into, and critiques of, the fundamental assumptions on which this analysis is based. BPA in general, and specifically the approaches to the estimating of the location of an impact event from its resultant bloodstain pattern, have also largely failed to address the relatively recent trend in forensic science of the statistical analysis and probabilistic evaluation of evidence, even though such inferential approaches are likely to become, out of necessity, central to BPA and its role in CSI in the near future (Emes and Price, 2004).

One of the main missions of SWGSTAIN has recently been identified as preparing BPA as a discipline for Daubert admissibility hearings in US courtrooms (Van Stratton, 2003; Van Stratton, 2004). Whether BPA is offered as an expert scientific testimony or as expert technical testimony in the form of an applied science, the gatekeeper role of the judiciary in terms of the quality of expert

evidence allowed into court requires a number of issues to be addressed. These include, amongst others (Henderson, 1998):

- Is the proposition testable?
- Has it been tested?
- Has it been subject to peer review?
- Does the methodology or technique have known error rates?
- Are there standards for using the methodology employed?
- Are the methods generally accepted?

Given the current state of BPA SWGSTAIN acknowledges that:

'It is quite evident that an enormous amount of time and work is needed in preparing for Daubert hearings and that we should start now as a group and use our combined efforts to address potential issues which may face us in the future' (Van Stratton, 2003).

## **1.5 Conclusions**

Despite being established and functional features of criminal investigation, CSR and BPA both face some relatively complex issues in terms of how best to provide themselves with a theoretical, methodological and interpretational base, that can satisfy the questions that are increasing being asked of scientific and technical expert forensic evidence in legal contexts. The processes of evidential collection, identification, interpretation and experimentation employed throughout modern BPA are underpinned arguably by sound scientific principles, and can provide a degree of objective confidence in their findings (Emes and Price, 2004; Bevel and Gardner, 2002; Wonder, 2001). A large amount of work, however, is still required within BPA to prepare for the future challenges which may present themselves in terms of the potential utility and admissibility of, as well as weight given to its reconstructive conclusions (Van Stratton, 2003). While some of this work will probably have to be undertaken at the disciplinary level, research into some of the more specific techniques of BPA, and the analysis of its results could begin to provide BPA with an inferential toolkit that is complicit with a more rigid evidential framework. The remainder of this thesis will attempt to address a number of these issues as they pertain to the process of estimating the location of a bloodstain-producing impact event from its resultant bloodstain pattern.

## **2 Spatter Bloodstain Patterns and Site of Impact Estimation**

### **2.1 Introduction**

This chapter will introduce some of the practical aspects of BPA including commonly recognised pattern types and the kinds of inferences possible from employing BPA at a scene where bloodstains are present. The main focus of this chapter will address spatter bloodstains, with specific attention given to impact spatter patterns, before the theoretical and practical foundations of estimating the location of a spatter-producing impact event from its resultant impact spatter pattern are discussed.

### **2.2 BPA In Practice**

When blood is exposed to the physical environment by some trauma it will behave in a predictable manner according to the principles of physics (James, 1998a; van Zyl, 2001). BPA uses an understanding of these principles in relation to the physical properties of bloodstains to infer facts, actions and behaviours which have combined to produce the bloodstain patterns observable at a crime scene (James, 1998a; Murray, 2000a). The location, size, shape and distribution of bloodstain patterns deposited at a crime scene during some blood-shedding event can consequently be used to produce a reconstruction of those events (James, 1998a; Lee et al., 2001; Bevel and Gardner, 2002; Wonder, 2001).

For a bloodstain pattern to be created at a crime scene there needs to be some open blood source available, a target surface upon which the bloodstain can be deposited, and some incident dynamic involving the deposition of a volume of the blood source, from its origin, onto the recording target surface. This by no means a necessarily simple process, and it is the complex nature of blood as a liquid, and the nature of the deposition dynamic that combine to form frequently distinctive bloodstain patterns. The creation of multiple bloodstains, and the presence of intervening events recorded in already deposited bloodstains can combine to indicate some form of temporal sequence, and, consequently, a crime scene narrative. The interpretation of bloodstains, however, does not usually occur at such an early stage in the time-line of the existence of a crime scene. The passage of time, which can occasionally be significant, allows the potential intervention of additional events, which can complicate, mask or even completely



obliterate the original interpretative potential of bloodstain patterns, or the bloodstains themselves. Even where bloodstains remain in a state comparable to that of their deposition, they have to be found, recognised and correctly interpreted by the analyst before they have any real investigative value. It is important that the location, size, shape and distribution of bloodstain evidence, from the macro-scale, down to the micro-scale be treated as evidence, as the reconstructive narratives of BPA are developed from inferences, which are ultimately based on these facets of bloodstains and their relationship to their methods of creation (Lee et al., 2001; Murray, 2000a).

Modern BPA recognises a number of different categories of bloodstain that can be used in the reconstruction of crime scene event segments, crime scene events, and total crime scene incidents. The inferential potential of the analysis of these bloodstain types is often credited with a capacity to determine a number of significant investigative issues that frequently include (James, 1998a; Emes and Price, 2004; Bevel and Gardner, 2002; Wonder, 2001):

- The origins of bloodstains.
- The type, direction and location of an impact that produced a bloodstain pattern.
- The nature of force involved in creating a bloodstain.
- The identification of objects that produce specific patterns.
- The positions and movements of victim(s), assailant(s) and objects during various stages of the commission of a crime.
- The probable sequence of events during the commission of a crime.
- The number of blows and/or gunshot injuries inflicted during an assault.
- The providing of corroborative or refuting evidence for witness statement evaluation.
- The provision of information on the progression of the blood-shedding incident or incidents.
- The provision of additional criteria for post-mortem interval estimation.
- Combining with other forensic evidence in crime scene as well as general criminal investigations.

Although, as previously discussed, there does tend to be a general lack of consistency in the terminology of BPA, the recognition of the various types of bloodstain patterns, whatever name or grouping they are assigned, and an understanding of the dynamics involved in their creation, is central to the

inferential potential of BPA (Emes and Price, 2004). Common characterisation of bloodstain patterns types in BPA includes:

- Transfer or contact patterns.
- Void and shadow patterns.
- Pooled or volume bloodstains.
- Flow patterns.
- Arterial breach or projected patterns.
- Physically altered bloodstains.
- Composite bloodstains.
- Spatter patterns, which can include the sometimes-separate categories of single, free-fall or passive drop patterns, cast-off bloodstain patterns, and impact spatter patterns.



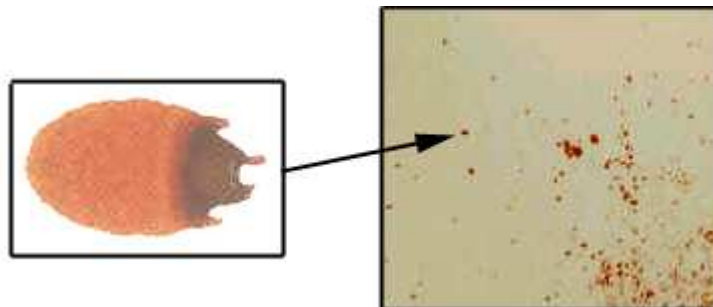
Figure 2-1 – Examples of a contact transfer pattern (left [James and Eckert, 1998]), a void pattern (centre [Lee et al., 2001]), and a flow pattern (right [James and Eckert, 1998]).

### 2.3 Spatter Patterns

An individual spatter bloodstain is created by the contact of a small droplet of blood with a target surface, and the larger spatter pattern is some conceptual linked grouping of these individual spatters, as illustrated in Figure 2-2. Semantically, the term spatter can be either a verb or a noun (Tulloch, 1995; Bevel and Gardner, 2002), referring to both the action of the dispersal of a liquid, and the result of that dispersal. As BPA is primarily a discipline concerned with interpreting the aftermath of bloodshed events the term spatter is usually used in reference to the actual bloodstain evidence. The term, however, can still refer to the action of the blood sources' dispersal. The IABPA (2004b), for example, defines spatter in terms of its creation mechanism rather than solely on the resulting bloodstain evidence:

'[Spatter is] That blood which has been dispersed as a result of force applied to a source of blood.'

What the IABPA definition lacks, perhaps, is the detail of the causative class characteristics that all spatter patterns share. Firstly, a force has to be applied to the blood source. Second, some of the blood source is separated into droplets. Third, these droplets are distributed over a flight path, and finally they are intercepted by a target surface, upon which they form a spatter bloodstain (Wonder, 2001). As blood is a liquid, mechanically it can be considered to be an incompressible fluid, and as such the application of some force to a volume of blood requires that some of this volume be displaced (Nakayama and Boucher, 1999; Douglas et al., 1995; Bevel and Gardner, 2002). Where the magnitude of this force overcomes the viscosity and surface tension of the blood source, the dispersed volume usually takes the form of a droplet or droplets. Each droplet is then subject to a specific flight dynamic and the system of external and internal mechanical forces that this entails before it creates a spatter bloodstain on some target surface.



*Figure 2-2 - An individual spatter and its parent spatter pattern (After James and Eckert, 1998 and Slemko, 2005).*

Given this force-droplet-flight definition of spatter, which is by no means universally applied within BPA, it is apparent that a number of scenarios can produce spatter patterns. Individually, however, it is often impossible to determine the cause of spatter bloodstains. Specific spatter morphologies are not exclusive to one particular creation dynamic, and it is typically only through an examination of the entire distribution of a spatter pattern that the cause of the pattern can be determined through the specific individualising characteristics of some of these distributions (Wonder, 2001; James and Sutton, 1998b; Bevel and Gardner, 2002). It is generally the specific nature, source, and application of the force involved in producing spatter that generates these diverse and identifiable

spatter pattern configurations. Spatter pattern types that are formed by the direct application of force to a blood source include (James and Sutton, 1998a; Wonder, 2001; Bevel and Gardner, 2002; Lee et al., 2001; Emes and Price, 2004):

- Free-fall or passive drop patterns, caused by the action of gravity on the mass of the volume of a blood source.
- Cast-off patterns, caused by the interaction of centrifugal, centripetal, and gravitational forces as well as the effects of momentum acting on the mass of a blood source.
- Blood-into-blood patterns, where a droplet contacting an already present volume of blood generates and projects a number of small droplets from the volume.
- Certain cases of arterial projected blood, where the unstable stream of projected blood forms distinct droplets during flight.
- And impact spatter patterns, which are the focus of this thesis, and are examined in more detail below.

An additional category of spatter bloodstain commonly known as satellite spatter is also identifiable within spatter taxonomy. These bloodstains, however, are represented by a special case where a small separate droplet is generated during the collapse of a parent blood droplet as it makes contact with a target surface, and as such are not considered as a distinct pattern type. The consideration and identification of this type of spatter bloodstain can be significant in the accurate interpretation of the spatter bloodstain pattern types. It is as a central part of the analysis and interpretation of a number of aspects of these spatter bloodstains and their patterning that the full combination of a knowledge of physics, ballistics, trigonometry and the biochemistry of blood, often quoted as being the foundations of BPA, really begin to provide detailed information about the nature of the crime scene dynamic and the creation of spatter patterns (Moore, 2002). This is especially true for impact spatter bloodstain patterns, where all of these disciplines combine in the theory and practice of estimating the physical location of a site of impact from the resultant spatter pattern of an impact event.

## 2.4 Impact Spatter Bloodstains

Impact spatter is generated by the application of some force to a blood source in the form of an impact event, which causes the random dispersal of multiple small blood droplets (IABPA, 2004b). The separation of blood droplets from their source is a result of the pressure gradients, and the nature of the flow set up within the blood source as a result of the impacting force. The impulse applied to the blood volume by this force causes the blood to flow from high-pressure regions, around the location of the application of this force, towards other lower-pressure regions. Where this flow becomes turbulent, which can vary with the nature of the flow and the physical characteristics of the liquid, the dispersal of the blood volume becomes chaotic and blood droplets are formed (Fischer, 2001).

Impact spatter patterns are among the most common type of bloodstain patterns experienced in casework in the UK, and are usually associated with incidents of blunt force trauma and gunshot injury (Emes and Price, 2004). Two distinct methodologies are typically used to categorise impact spatter patterns within BPA. These can be defined as:

- Velocity classification methods.
- Descriptive classification methods.

The velocity-based classification of impact spatter bloodstains relies upon the division of impact spatter patterns into three basic types:

- Low Velocity Impact Spatter (LVIS).
- Medium Velocity Impact Spatter (MVIS).
- High Velocity Impact Spatter (HVIS).

The division is dependent on the size of the individual spatter bloodstains within the overall impact spatter patterns, with the size ranges being explicitly linked to a velocity range of the impacting object, which is often interpreted in the terms of the causative mechanisms of the impact. LVIS includes bloodstains produced by the application of force up to the level of that applied by gravity or an impact velocity of up to 5 feet per second or  $1.5 \text{ ms}^{-1}$ . The typical size of bloodstain created in this spatter group is generally 3mm and greater in diameter (James, 1998a; James and Sutton, 1998a; IABPA, 2004b; Benecke and Barksdale, 2003). MVIS is associated with impact velocities of 5 to 25 feet per second or 1.5 to 7.6

$\text{ms}^{-1}$ , and is typically consistent with the majority of blunt force trauma incidents, although higher impacting velocities of between 25 and 100 feet per second (7.6 to  $30 \text{ ms}^{-1}$ ) are possible with golf clubs, whips and various specialist martial art weapons (James, 1998a; James and Sutton, 1998b). Typical sizes of individual spatters encountered within the MVIS range measure between 1mm and 3mm in diameter (James, 1998a; James and Sutton, 1998b; Bevel and Gardner, 2002; IABPA, 2004b). HVIS classification is associated with an impact event velocity greater than 100 feet per second or  $30 \text{ ms}^{-1}$ , and is most commonly associated with gunshot injuries, and high-speed machinery. The typical spatter bloodstain size in this range is less than 1mm in diameter (IABPA, 2004b; James, 1998a; James and Sutton, 1998b; Bevel and Gardner, 2002).

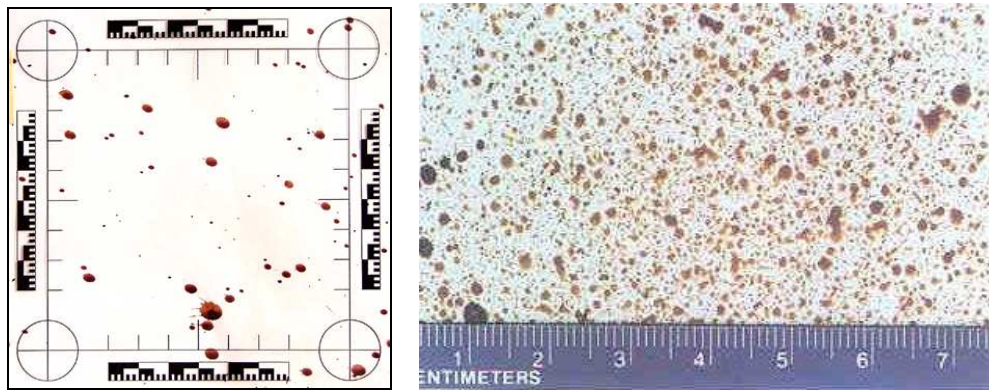


Figure 2-3 -Examples of a MVIS (left), and a HVIS (right [James and Eckert, 1998]) bloodstain pattern with scales.

Despite its widespread and continued use, velocity-based impact spatter classification presents a related mechanical incongruity and BPA anachronism. Firstly, the size and distribution of blood droplets from an impact is not solely dependent on velocity, but requires an appreciation of the degree of mechanical force applied to a blood source through the conservation of energy and momentum, and the pressure gradient that this induces within the blood. Far more mechanical data is needed to assess the effect of an impact including knowledge of (Fischer, 2001; Emes and Price; 2004):

- The mass of the object.
- The size and shape of the contacting surface area.
- The elasticity of both the impacting and receiving surfaces.
- The force exerted by the impact-receiving surface.
- Some concept of the time component of the impact.
- The paths of least resistance available to a blood source.

- The physical flow characteristics of the particular blood source.

Secondly, the velocity-based division of impact spatter was originally derived from concepts based on a normal blood droplet volume, and the subsequent possible division of impact spatter patterns based on the inferred velocities of droplets on contact with a target surface (Pizzola et al., 1986a; Wonder, 2001; Bevel and Gardner, 2002). Standard droplet sizes, however, are now largely rejected, but the terminology of velocity-based impact spatter division has endured, with the velocity referring to that of the impacting object (Wonder, 2001). Even practitioners and authors who routinely use and incidentally propagate this velocity division are often critical of its basis, stressing the rather arbitrary nature of the overlapping velocity and spatter-size divisions, the variations in spatter size observable within impact spatter patterns, and the often restrictive and possibly misleading nature of its divisions (Pizzola et al., 1986a; James, 1998a; Bevel and Gardner, 2002; Emes and Price, 2004). Despite these heavy criticisms, the velocity-based division of impact spatter bloodstains is still perpetuated within BPA. The continued use of this approach is arguably a product of its inclusion in many basic BPA courses and BPA literature (Fischer, 2001). The tendency of spatter size to vary inversely with the level of force applied to a blood source, which has become synonymous with object velocity in this system, also provides a relatively simple explanatory and inferential tool to describe and quantify impact spatter patterns, as well as to suggest possible causes of the impact event (Bevel and Gardner, 2002; James, 1998a; Lee et al, 2001).

Although the descriptive classification of impact spatter patterns is not a single coherent system, the general process is based on approaches that allow the generation of hypotheses concerning the cause of a spatter pattern to be developed independently from the recording and documentation of the patterns themselves (Bevel and Gardner, 2002, Wonder, 2001; Emes and Price, 2004). One type of descriptive method which has gained in popularity is also based on the size of individual spatter bloodstains, but, in contrast, the system can be used in the classification of all spatter pattern types, and the specific size groupings are not inherently linked to any assumed causation. The spatter size-cause link is still applied in impact spatter pattern interpretation using these methods, but this association has to be made explicitly, and can be considered in relation to other relevant information about the crime, the crime scene, as well as other evidence (Laber cited in Emes and Price, 2004; Wonder, 2001, Emes and Price,

2004). The divisions of one such size-based descriptive method advocated by Wonder (2001) are:

- Large, with predominant spatter diameter greater than 6mm.
- Medium, with predominant spatter bloodstain diameter greater than 3mm but less than 6mm.
- Small, with predominant spatter bloodstain diameter greater than 1mm but less than 3mm.
- Fine, with predominant spatter bloodstain diameter greater than 0.1mm but less than 1mm.
- Mist, with predominant spatter bloodstain diameter under 0.1mm.

Whatever classification system is used, impact spatter bloodstain patterns are arguably one of the most complex single bloodstain pattern types in BPA, in terms of both their creation and their analysis and interpretation. Where this is linked to causative mechanisms one can only really state that it is consistent with and not conclusive of one creation mechanism or another (MacDonell, 2004). The careful and detailed analysis of this complexity, however, can often provide information on a number of significant investigative issues including (Bevel and Gardner, 2002; Wonder 2001; Emes and Price, 2004; James and Sutton, 1998a; James and Sutton, 1998b):

- The nature of the force applied during the impact event.
- The identification of potential impacting objects and mechanisms.
- The minimum number of potential impact events at a scene.
- The relative positions of people and objects within a scene.
- An indication as to the likelihood of bloodstains being present on an assailant or other people present at the scene.
- The opportunity to estimate what can be a pertinent issue in CSR and criminal investigations, the physical location of an impact within a crime scene.

The location within a scene where a blood source encounters an impacting force is commonly referred to as an impact site (IABPA, 2004b). The location of this site of impact can be estimated from its resultant impact spatter pattern by employing a number of theoretical models and practical techniques in the analysis of the patterns constituent spatter bloodstains. While the various processes by which this locative estimation is undertaken have been given a number of



descriptive titles within BPA, for reasons which it is hoped will become clear during the course of the discussion of these techniques, the term 'site of impact estimation' is used here to describe this general approach to impact spatter pattern interpretation.

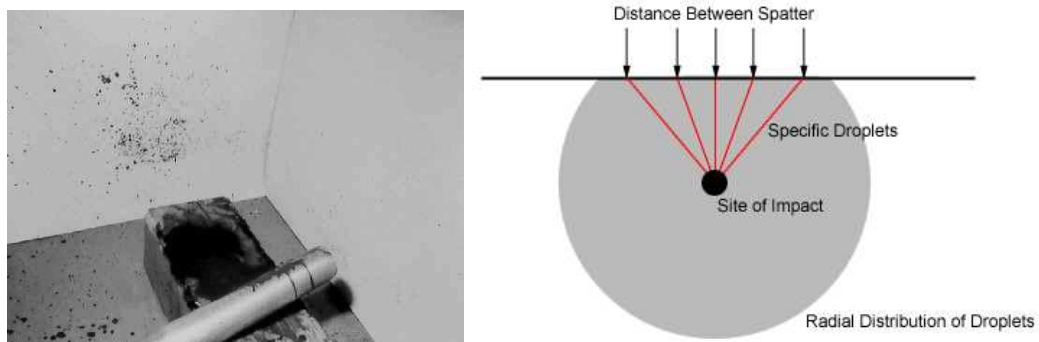
## **2.5 Site of Impact Estimation**

Impact spatter bloodstain patterns can be considered appropriate for site of impact estimation, and therefore distinct from the other spatter bloodstain groups for two principal reasons. Firstly, all of the individual spatters that make up a single isolated impact spatter pattern are generated by a single impact event at the same restricted location in time and space. Unlike other spatter pattern creation mechanisms, where droplet generation is more dependent on time and space, and tends to be sequential in nature, the separation of multiple droplets from a blood source through a single impact event is generally considered to be instantaneous, and all of the droplets generated through this single impact are projected from the same spatial location, the site of the impact. Secondly, impact spatter droplets are typically dispersed from the blood source in a radial pattern. The precise character of this distribution is, however, generally hard to predict and impossible to replicate as the distance, direction and quantity of spatter depend on a number of variables including (Emes and Price, 2004; Bevel and Gardner, 2002; James and Sutton, 1998b; Wonder, 2001):

- The volume of the blood source.
- The size and shape of the weapon.
- The nature and surface properties of the weapon and the object that it impacts.
- The relative positions of the assailant and the impact site.
- The magnitude and direction of the force applied by the weapon at the moment of impact.

These variations in the nature of an impact and subsequent droplet generation tend to produce radial droplet distributions and spatter patterns that often are restricted to a particular direction or area of a target surface. These potential sources of pattern variation, however, do not usually affect the salient features of this radiation:

- That each droplet in the distribution tends to have a distinct flight path, making inter-droplet collision unlikely (Sirignano, 1999; Bevel and Gardner, 2002, Moore, 2002).
- That each droplet maintains a trajectory that originates from its separation from the blood source, and is not prone to break-up in flight or deviation from this flight path, unless acted upon by a force other than aerodynamic and gravitational forces (James, 1998a; Moore, 2002).
- That impact spatter patterns exhibit a degree of spatial separation between many of their component spatter bloodstains, with the density of spatter within an overall impact pattern decreasing the further the target surface is from the site of impact (Wonder, 2001; Bevel and Gardner, 2002; Figure 2-4).



*Figure 2-4 – Experimental impact spatter pattern exhibiting directional radial patterning (left, Slemko, 2002), and a diagram illustrating the changes in spatter density with distance from the site of impact (right).*

An isolated impact spatter pattern, where identifiable, therefore, presents a situation where a significant number of individual spatters are known to have been produced at the same location in time and space by the same single impact event. These multiple individual spatters constitute a spatter pattern that has both spatial range and diversity, created by multiple blood droplets with separate and diverging trajectories. Given these features of impact spatter patterns, two observable properties of spatter bloodstains can be used to estimate the trajectories of spatter causing blood droplets, and subsequently the intersections of these trajectories, to estimate the spatial origin of a spatter causing impact event. These two properties are commonly defined as the directionality, and impact angle of spatter bloodstains.

### **2.5.1 Directionality**

Blood droplets that have undergone a flight dynamic are generally thought of as being spherical in shape. Although a large degree of oscillation in droplet shape can be observed at and shortly after droplet separation from its blood source, it has frequently been argued that the viscous properties of blood and the surface tension of the droplet combine to produce a rapid reduction in this oscillation (James and Sutton, 1998a; Wonder, 2001; Bevel and Gardner, 2002; Raymond et al., 1996b, Lee et al, 2001). Where a spherical droplet contacts a recording target surface it can leave a distinctive directional indicator of its flight path, with spatter bloodstains exhibiting a degree of elongation depending on the angle with which they strike a target surface. Droplets that make perpendicular contact with a target surface tend to produce circular bloodstains, but as the impact angle of the spatter, which can be defined as the internal angle between the trajectory of the droplet and the plane of the recording target surface, becomes more acute the elongation of the spatter bloodstain becomes more pronounced (IAPBA, 2004b). This elongation tends to produce elliptical, or near-elliptical spatter bloodstains, whose major axis indicates the orientation of the droplet's trajectory in the plane of the particular target surface that it strikes. The directional component of the stain, the direction along this orientation that the droplet was travelling, can then be inferred from the edge of the bloodstain that exhibits the most tapering or distortion, which is a function of the collapse of the liquid droplet through its contact with the target surface (James and Sutton, 1998a; Bevel and Gardner, 2001; Wonder, 2001; Moore, 2002; Lee et al., 2001; Van Zyl, 2001). Figure 2-5 illustrates the concept and interpretation of the directionality of a spatter bloodstain. This directional feature of spatter bloodstains was recognised and documented as early as 1895, and as a general rule the more well formed and pronounced the ellipticity of the spatter bloodstain, the more accurate one is likely to be in assigning directionality (Bevel and Gardner, 2002). The only spatter type, which does not, as a general rule, adhere to this directionality, is satellite spatter. The specific aetiology of this type of spatter produces a reversal of this directional indicator, and as such their identification, and exclusion from a site of impact estimate is necessary to provide a consistent and appropriate consideration of spatter directionality (Bevel and Gardner, 2002; Jackson and Jackson, 2004).

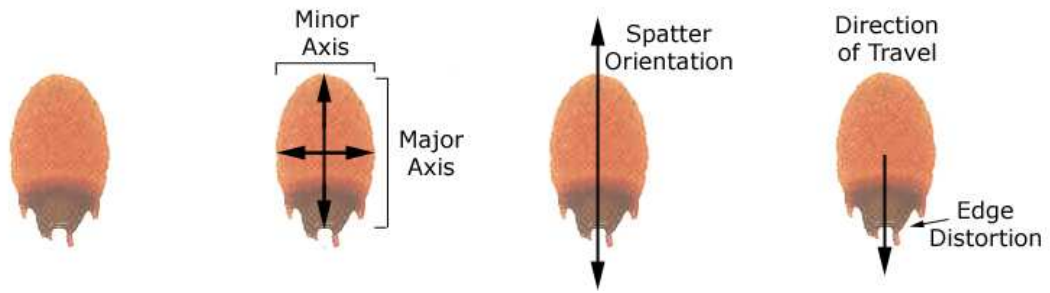


Figure 2-5 – Spatter bloodstain directionality.

### 2.5.2 Impact Angle

Through the same droplet-target contact dynamic that results in an observable spatter directionality, the ellipticity of a spatter bloodstain can also be used to estimate the impact angle at which a blood droplet struck a target surface. Balthazard et al. first published a relationship between the relative axial dimensions of elliptical spatter bloodstains and their impact angles in 1939 (James, 1998a; Bevel and Gardner, 2002; Pizzola et al., 1986a; Ristenbatt and Shaler, 1995). This morphological relationship is demonstrated in Figure 2-6, where the spatter bloodstains produced by blood droplets of the same size have been recorded on target surfaces of different known inclinations.

Impact Angle (degrees)	90	80	70	60	50	40	30	20	10
Typical Spatter Image									

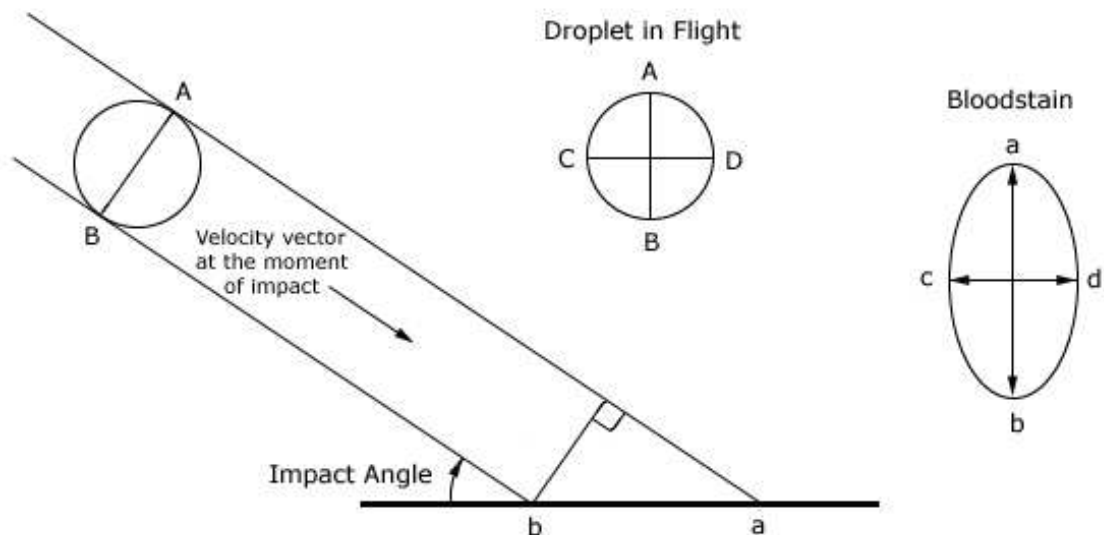
Figure 2-6 – Spatter bloodstain impact angles (after Lee et al., 2001).

Initially, this relationship between spatter morphology and the impact angle of the causative droplet was only reported in terms of a correlation. It was not until 1971 that MacDonell and Bialouze (Fischer, 1998; Bevel and Gardner, 2002; James, 1998a) published a more refined trigonometric relationship between the width (minor axis) and the length (major axis) of a spatter bloodstain and its impact angle. Although both Balthazard et al., and MacDonell and Bialouze have been credited with laying the foundations for the techniques of estimating a site of impact through the development of impact angle assessment, it is arguably only through the development of the practical and relatively transparent trigonometric relationship that these techniques have become widely accepted and employed throughout BPA and CSR (Willis et al., 2001; Bevel and Gardner, 2002; Pizzola et al., 1986b; Risenbatt and Shaler, 1995; Chafe, 2003). This relationship states that:

$$\theta = \sin^{-1}\left(\frac{w}{l}\right)$$

*Formula 2-1 – The impact angle calculation for spatter bloodstains.*

where  $\theta$  is the angle of impact,  $w$  is the width of the spatter bloodstain and  $l$  is the length of the bloodstain.



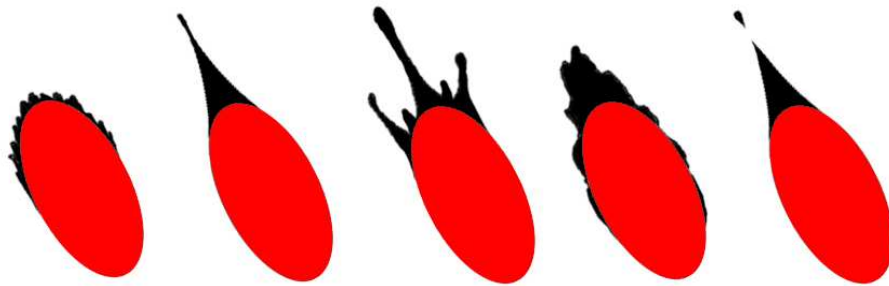
*Figure 2-7 - The trigonometric relationship between the size of a blood droplet, its angle of impact, and the elliptical stain it produces (after Bevel and Gardner, 2002).*

Figure 2-7 illustrates a common theoretical justification for this impact angle formula. As a blood droplet is generally considered to be spherical by the time it contacts a target surface, the diameter of the droplet is the same from any point on its surface. **A** and **B** are two diametrically opposite points on the surface of the spherical droplet so that the line **AB** is perpendicular to the direction of travel. The distance **CD** is equal to **AB**, and the points **C** and **D** are also diametrically opposite one another, with the line **CD** at right angles to the line **AB**. The line **CD** in the diagram of the droplet in flight is perpendicular to the plane of the illustration, and the upper case labels marked on the droplet diagram correspond to the same lower case labels on the bloodstain diagram. Theoretically then, the distance **cd** on the bloodstain is equal to **CD**, and represents the width of the droplet. The points **a** and **b** are where the extreme edges of the droplet make contact with the target surface, and represent the length of the spatter bloodstain, as well as indicating the orientation of its travel in the plane of the target surface. The impact angle of the spatter bloodstain at **a**, which is the same angle as at **b**, can be defined in terms of a right-angled triangle where the hypotenuse is the line **ab**, and the opposite side is the width of the droplet, which is also the width of the bloodstain (**AB**, **CD**, or **cd**). Basic trigonometry states that the sine of an angle in a right-angled triangle is the length of opposite side divided by the length of the hypotenuse, which in this case is equal to the width of the elliptical spatter bloodstain divided by its length.

The majority of spatter bloodstains experienced in practice, however, do not form perfect ellipses, and a technique known as 'ellipse fitting' is typically used to take width and length measurements from spatter bloodstains (Carter, 2001; Bevel and Gardner, 2002; Chafe, 2003; Moore 2002). This 'ellipse fitting' technique involves the superimposition of a perfect ellipse over a spatter bloodstain so that any excess crenulations or extended spines are rounded off, providing a measurable ellipse that corresponds to the morphology of the main body of the bloodstain (Figure 2-8). The superimposition of an ellipse can include elements of:

- The comparative, utilising ellipse templates (Bevel and Gardner, 2002; Carter, 2001).
- The conceptual, through visual assessment and experience (Bevel and Gardner, 2002).
- The mathematical (Chafe, 2003; Carter, 2001).

To minimise any inaccuracy in ellipse fitting, and consequently, improve the accuracy of spatter bloodstain measurement, spatters that exhibit a relatively well-formed elliptical shape are usually chosen for use in site of impact origin estimations (Chafe, 2003; Bevel and Gardner, 2002; James and Sutton, 1998a). A well-formed spatter bloodstain can be considered to be approximately symmetrical about the two axes represented by the width and length of the bloodstain (Bevel and Gardner, 2002).



*Figure 2-8 - Five idealised spatter bloodstains with the same fitted ellipse (red), but different extraneous morphological features (black).*

### **2.5.3 Spatter Trajectory**

When combined, the directionality and impact angles provide information on the trajectory of a spatter-causing blood droplet. The directionality of the spatter bloodstain provides the orientation and direction of this trajectory in the plane of the target surface, while the impact angle provides the final elevation of this trajectory relative to both the plane and the normal of the target surface. If measured as an angle relative to some datum assigned to the target surface, the directionality of a spatter bloodstain combined with its impact angle can be used to produce a relative 3D unit vector that can be thought of as representing the trajectory of the droplet immediately prior to its contact with the target surface (Carter, 1998 and 2001). This trajectory takes the form of a unit vector, as the relative sizes of the components of the 3D trajectory, and therefore, the direction of travel of the droplet are known, but the magnitude of this vector, the absolute speed of the droplet, is not, as demonstrated in Figure 2-9. The trajectory vector is also relative, as it relies upon the position, orientation and surface normal of the plane of a target surface to have any consistent meaning within a 3D environment, especially where this is composed of multiple target surfaces, as in Figure 2-10. The vector equivalence of the directionality and impact angle of spatter bloodstains and the proportional velocities of a droplet's trajectory

relative to a recording target surface have been demonstrated through the comparable dimensions of spatter bloodstains observed under several different trajectory-target contact conditions. These conditions include free-falling droplets contacting angled target surfaces, and free-falling droplets contacting a moving horizontal target surface, as well as angled droplet trajectories contacting horizontal and vertical target surfaces (Moore, 2001; Willis et al., 2001; Pizzola et al., 1986a and 1986b).

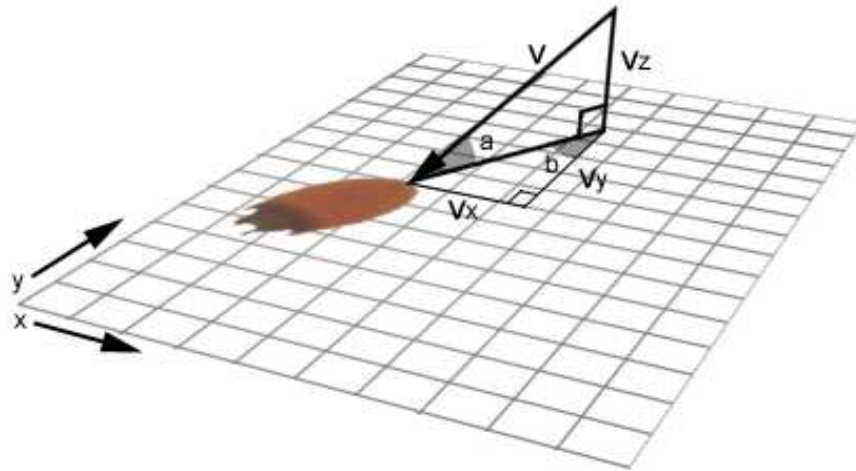
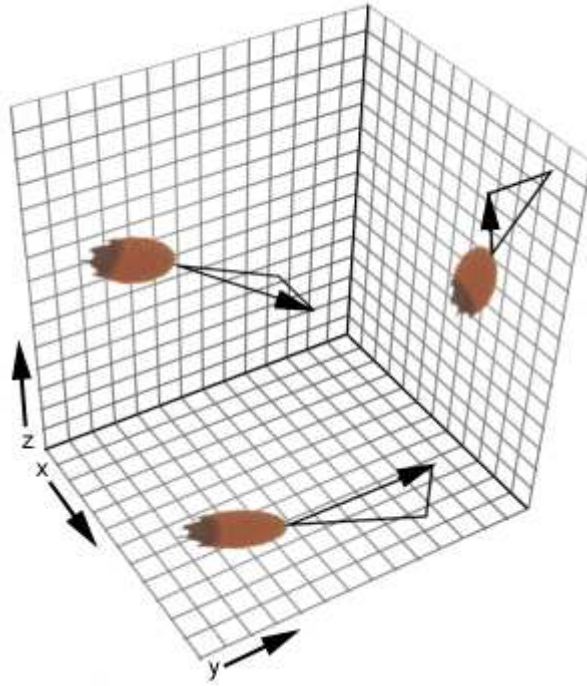


Figure 2-9 – The 3D trajectory unit vector formed from the impact angle (a), and directionality angle (b) of a spatter bloodstain.

Considering the trajectory information provided through the analysis of the directionality and impact angle of spatter bloodstains as a 3D unit vector highlights a number of key issues that are arguably central to the estimation of droplet trajectories from the analysis of spatter bloodstains. These issues include:

- That some knowledge of the position, orientation and normal of the target surface is inherent in the accurate interpretation and estimation of blood droplet trajectories.
- That the morphology of a spatter bloodstain is not solely a function of the velocity of its trajectory on contact with a target surface, but is dependent on its velocity relative to the target surface on which it is recorded.
- That it is only the directional components, or the relative velocity of a droplet's trajectory that can be established through the analysis of the two recognized and observable characteristics of spatter bloodstains, directionality and impact angle.





*Figure 2-10 - Multiple spatter trajectory vectors from the same spatter bloodstain on differently orientated target surfaces.*

The entire flight path of a spatter causing blood droplet can be approximated by projecting the directional trajectory of the droplet as it contacts a target surface, as inferred from the directionality and impact angle of the spatter bloodstain, back through the crime scene towards the droplet's origin. This reconstructed flight path takes the form of a straight-line trajectory, which can be considered to be an accurate representation of the droplet's actual flight path in the horizontal plane, the plane in which flight path curvature is not typically evident. In the vertical plane, however, this straight-line trajectory approximation is limited by an inability to represent any curvature in the droplet's flight path caused by the effects of aerodynamic and gravitational forces (Moore, 2001; Bevel and Gardner, 2002; Carter and Podworny, 1991; Carter, 1998 and 2001). The curvature of the flight paths of blood droplets is omitted from the flight path reconstruction because of two significant limitations. Firstly, the nature of the directional unit vector, inferred from spatter bloodstains, is such that it is time independent, having no absolute velocity, and theoretically the time dependent acceleratory effects of aerodynamic force, and gravity cannot be evaluated in respect to this directional vector alone. Secondly, the practical calculation of the degree of curvature that aerodynamic force and gravity would have had on the flight path of a specific blood droplet is essentially precluded by a general lack of knowledge concerning the specific dynamics of the droplet's flight. The application of

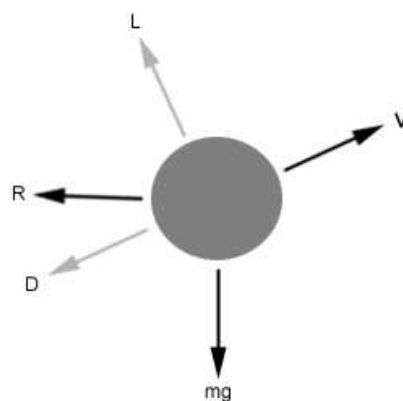
relatively simplistic physical models of droplet flight, however, has proved effective in BPA through the computer simulation of droplet trajectories and resultant spatter bloodstains. But even under such modelling conditions, where droplets tend to be modelled as solid spheres of a fixed size and mass moving through a homogeneous still atmosphere, an approximation of the curved trajectory of a blood droplet still cannot be constructed exclusively from the information gleaned from its spatter bloodstain (Carter, 1998 and 2001; Bevel and Gardner, 2002;).

As a droplet moves through the air it is constantly subject to changing forces and acceleration. The effect that these forces and the resulting acceleration have on the velocity of the droplet defines the curvature of its flight path. To resolve the forces acting on a droplet at each and any stage in its flight two principal attributes are necessary:

- Droplet velocity.
- Droplet size.

The absolute velocity of a droplet affects both the direction and magnitude of aerodynamic force, but also determines the relative effect that the acceleration induced by this force and the downward acceleration of gravity will have on the droplet's current velocity and, therefore, on the curvature of its flight path. The size of a droplet is important, as it is also an influencing factor in the magnitude of aerodynamic force (Figure 2-11). More fundamentally though, it is also central to establishing the volume, and by extension, mass of a blood droplet, on which the resolution of forces acting on a droplet, and the resultant acceleration of the droplet during its flight rely. Both of these essential features to curved flight path reconstruction, however, are absent from the knowledge of the droplet inferred from its spatter bloodstain directionality and impact angle. As already discussed the absolute velocity of the droplet on contact with a target surface is not known, but additionally, despite the theoretical justification for spatter bloodstain impact angles outlined above, the actual diameter of the spatter causing blood droplet also cannot be accurately estimated from its resultant spatter bloodstain (Moore, 2002; Carter, 1998 and 2001). Depending on the level of accuracy required, modelling the flight characteristics of a fluid droplet in less abstracted physical terms may also require additional information. This information can include details of the oscillation of droplet shape, and the variable mass and viscosity of blood, which are dependent to a large extent on blood haematocrit, as well as

information on the conditions of any air currents present during the droplets flight, and any spin or rotational velocity applied to the droplet during separation from its source (Hart and Croft, 1988; Nakayama and Boucher, 1999; Douglas et al., 1995; Sirignano, 1999; Frohn and Roth, 2000). Each of these factors can affect the degree of influence that gravitational and aerodynamic forces have on the flight path of a droplet, but as with the case of absolute velocity and droplet size, they cannot be established solely from a droplet's spatter bloodstain, or necessarily reconstructed to any accurate degree from other sources. The general lack of knowledge concerning the specific dynamics of the flight of an individual blood droplet means that the straight-line trajectory model, despite its limitations, can be considered to be the best approximation of a blood droplet's flight path that is available using current trajectory reconstruction techniques, and ultimately to the estimation of a site of impact from impact spatter patterns (Carter, 1998 and 2001).



*Figure 2-11 - A blood droplet modelled as a particle in flight.  $V$  is the velocity of the droplet,  $mg$  the force of gravity, and  $R$  the aerodynamic force resolved from aerodynamic drag ( $D$ ) and lift ( $L$ ) that act on a body in flight.*

The application of the straight-line trajectory model in reconstructing droplet flight paths from spatter bloodstains has three main consequences for both the practice and interpretation of these estimates. Firstly, the utility of straight-line trajectory estimation is often restricted to providing relatively accurate horizontal trajectory estimates, with the vertical component of the straight-line trajectory only excluding possible flight paths that would have occurred above this upper straight-line limit, as shown in Figure 2-12 (Bevel and Gardner, 2002; Carter, 1998 and 2001; James and Sutton, 1998a). Secondly, a straight-line trajectory model will tend to produce estimates for the height of a droplet's trajectory that are higher than the actual height of the droplet's true flight path at most points

along its path. Where the spatial origin of this flight path can be established, the height estimate provided by the straight-line trajectory at this point will, as a result, tend to be higher than the actual height of the droplet's origin (James and Sutton, 1998a; MacDonell, 1997 cited in Brady et al., 2002; Balthazard et al., 1939 cited in Bevel and Gardner, 2002; Carter, 1998 and 2001).

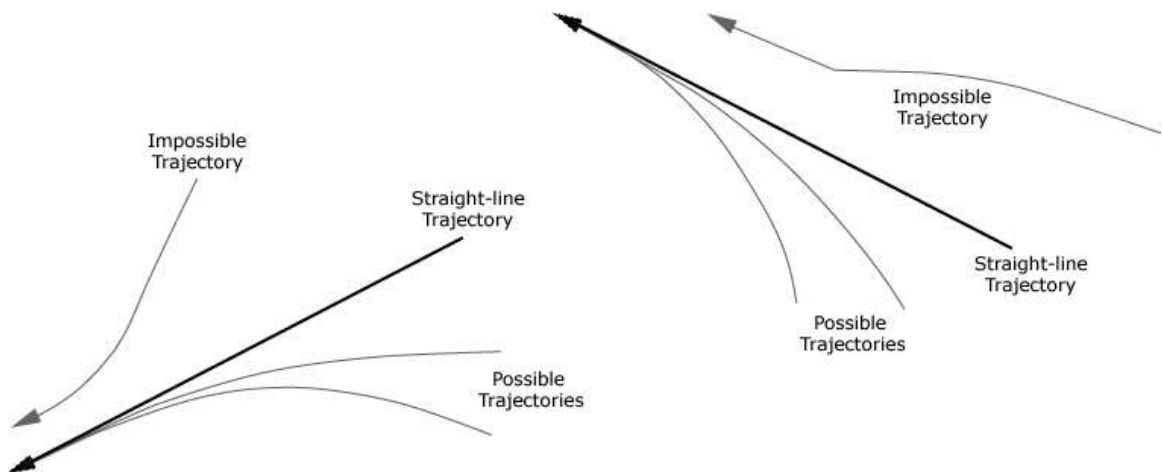


Figure 2-12 – Two straight-line trajectory estimates, and examples of the corresponding possible and impossible flight paths (after Bevel and Gardner, 2002).

And thirdly, spatter bloodstains that can be considered to represent fast upward-moving droplets are typically chosen for use in trajectory reconstruction where height estimation is a significant issue. The flight paths of fast moving droplets are the most likely to correspond to a straight-line trajectory model, while it is only spatter bloodstains that represent upward moving droplets that can be considered to have had a single vertical direction of movement, rather than representing a fast downward portion of an initially upward trajectory, as demonstrated in Figure 2-13. The consideration of a consistent vertical direction of travel can be significant, as the straight-line representation of an upward moving droplet can provide a potentially close approximation to the actual flight path of a droplet, while the straight-line approximation of a downward moving droplet can result in a considerable over-estimation of the height of a trajectory (Carter and Podworny, 1991; Carter, 1998 and 2001). As the trajectory approximations of spatter bloodstains are relative to the plane of the target surface upon which they are recorded, the distinction between these two types of spatter bloodstains is only generally possible on walls, or surfaces with some vertical component.

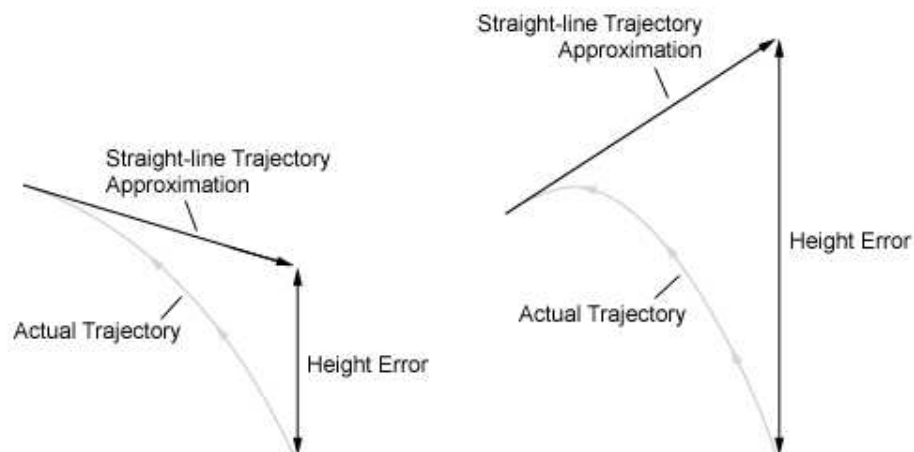


Figure 2-13 - Straight-line trajectory correspondence to solely upward, and downward travelling droplets.

## 2.6 Conclusions

BPA, in its identification and interpretation of bloodstain patterning at crime scenes, can provide significant information to CSR and the wider criminal investigation in terms of what, and how the distinct types and configurations of bloodstains found at a scene could have been formed. Of the categories of bloodstain patterning commonly recognised within BPA, spatter patterns can represent one of the most complex in terms of both their creation and interpretation. While the interpretation of impact spatter patterns can provide a scene investigation with information such as the potential nature of the impact force and impacting mechanisms, and the minimum number impact events within a scene, the inferential process defined here as 'site of impact estimation' can also provide information on the likely spatial location within a scene at which a particular spatter-producing impact event took place. At its core, site of impact estimation has a number of fundamental theoretical and practical principles based on aspects of the disciplines of physics, ballistics, biochemistry, fluid dynamics and mathematics that make such a locative inference possible. This chapter has outlined how the construction of straight-line trajectory approximations is made possible through the related practical techniques of ellipse fitting, directionality determination, and the measurement of the elliptical dimensions of spatter bloodstains. The theoretical principles behind these practical inferential methods such as the fluid properties of blood promoting a spherical droplet shape, and the

elliptical morphological relationship of spatter bloodstain with impact angles have also been addressed.

### **3 Practical Site of Impact Estimation**

#### **3.1 Introduction**

While the previous chapter outlined the theoretical and practical foundations of the process of site of impact estimation, this chapter will introduce some of the common methodologies through which an estimate can be constructed. The specific procedures involved in the various techniques of estimation will be described, and the advantages and limitations of each of these methods discussed. While each of the techniques discussed is not without its practical limitations, all have proved a degree of effectiveness in establishing a site of impact estimate. This chapter will present the computer-based techniques that are currently gaining favour in the BPA community as providing perhaps the most appropriate approach to constructing a site of impact estimate. The increased interpretative validity that can be attributable to these techniques may not, however, necessarily provide site of impact estimation with the sound scientific basis that could be required of it for its future application as expert scientific or technical forensic evidence.

#### **3.2 Site of Impact Estimation**

Although straight-line droplet trajectories can be used in the analysis of most spatter patterns with varying inferential results, it is only in the particular case of impact spatter pattern interpretation that a number of droplet trajectory estimates can be combined to provide an estimate of the location of the origin of the spatter-producing event. The distinctive features of impact spatter generation, and their resultant impact spatter patterns, mean that a number of droplet trajectories from a single impact spatter pattern can be estimated and traced back across the crime scene. The location in which a number of these trajectories intersect can then be interpreted as the spatial location of the site of impact that produced the impact spatter pattern under analysis. In less complex scenes, or CSR conditions that require less detailed analyses, an experienced BPA practitioner can often judge the location of a site of impact by eye, but where a more detailed and accurate assessment is required more structured reconstruction methodologies are usually applied (Emes and Price, 2004). A number of different techniques for site of impact estimation have been proposed and used within BPA. The variations in these techniques, however, can be

broadly divided into two main estimation methodologies. These methodologies can be defined as:

- Those based on 2D convergence techniques.
- Those based on 3D origin techniques.

Each methodology has specific interpretational advantages and limitations, as do the specific techniques that utilise these methods, although all of the techniques rely on the key systemic assumptions of site of origin estimation already outlined. The choice of which particular technique to use at a crime scene usually depends on which procedures a practitioner is most familiar with, and what the specific objectives of the site of impact estimation are within the general CSR and overall criminal investigation (Bevel and Gardner, 2002). The division of these techniques into 2D convergence, and 3D origin techniques does not correspond with the traditional classification of techniques in BPA. Instead of referring to the spatial nature of the estimate, the 2D or 3D classification here corresponds to the treatment of droplet trajectory approximations within a particular site of impact estimation technique. Specifically, this refers to whether a trajectory is considered in its 3D form from the outset of the estimation process, or whether the trajectory is initially treated as a 2D planar estimate, regardless of the circumstances of its use.

### **3.3 2D Convergence Techniques**

While BPA literature commonly defines convergence techniques as methods that conduct a locative estimate in the 2D plane on which an impact spatter pattern was observed, they are defined here as both 2D and 3D site of impact estimation techniques which involve at least an initial 2D planar estimate in the plane on which the spatter pattern was observed. While the latter 3D techniques are commonly grouped under an 'origin' estimate category they are grouped with 2D convergence techniques here, as the initial 2D planar estimate stage means that both of these approaches result in the inconsistent, and potentially erroneous treatment of trajectory estimates and intersection locations, depending upon the target surface the impact spatter pattern was observed in.



### 3.3.1 Point or Area of Convergence

Point or Area of Convergence (PAC) analysis is a site of impact estimation technique that relies solely on the application of spatter directionality. PAC estimates have been defined as the first stage in the estimation of a 3D site of impact (James and Sutton, 1998a; Bradley et al., 2002; Lee et al., 2001; Bevel and Gardner, 2002), but the technique can also be applied to impact spatter patterns in its own right (Wonder, 2001). The construction of PAC estimates takes place in the same plane that an impact spatter pattern is observed. If the bloodstain is on a wall, for example, then strings, tape, or drawn lines are applied to the wall, retracing the straight-line trajectory of a selection of spatter bloodstains that are, or are likely to have been produced by the same impact event. Where a number of these 2D straight-line trajectory estimates converge can subsequently be interpreted as the location of the site of impact within that particular plane of analysis (Lee et al., 2001; Wonder, 2001; Brady et al., 2002; Figure 3-1). This PAC estimation technique is illustrated in Figure 3-1. As PAC estimates are based in a single plane, it is possible to construct multiple PAC estimates from a single spatter causing impact event, if a number of different planar surfaces within the crime scene record a sufficient amount of spatter (Wonder, 2001).

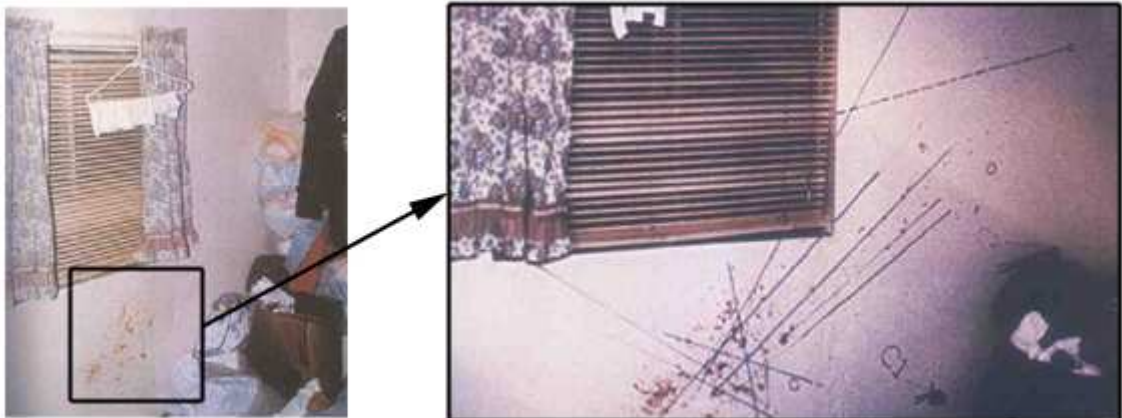


Figure 3-1 - An impact spatter bloodstain pattern (left), and the subsequent in situ PAC estimate (right [after Wonder, 2001]).

Wonder (2001), who is an advocate of this technique, describes its two main advantages as:

- The relative speed of the procedure as opposed to those techniques that utilise spatter bloodstain measurement and impact angle calculation.
- That the PAC technique is less prone to the inaccuracies that can be introduced to both measurement and calculation through human error.

There are, however, considerable interpretational difficulties with this technique that arguably overshadow its practical simplicity. Despite the previous claims, PAC estimates are not free from human error. Wonder (2001) herself reports observing a phenomenon in experimental PAC construction where, once the intersection of the first two lines has been established, subsequently constructed trajectories tend to gravitate towards this location to a greater degree than the directionality of the spatter suggests. Although this phenomenon could have an effect on the accuracy of the technique it is likely that it applies equally to all site of impact estimation methods that involve the physical construction and placement of estimated trajectories either within a scene, or some representation of it. The main specific limitation of convergence estimation is that it is only consistently valid for impact spatter patterns that are observed and analysed in a horizontal plane, as it is only in this plane that droplet trajectory estimates can be accurately represented as straight-lines. The application of the PAC method to impact spatter patterns on vertical surfaces, like all straight-line trajectory approximations, cannot adequately account for the potential curvature of droplet flight paths in this plane. Where PAC estimation is potentially compromised, however, is that its analysis in a vertical plane does not restrict the inaccuracies of the straight-line trajectory model to height estimation but includes this error in establishing a horizontal estimate for the location of a site of impact.

Figure 3-2 illustrates this effect by comparing the intersections of the same three 3D straight-line trajectories in both the horizontal plane, and the vertical plane of PAC analysis. The images were created using the droplet flight path and spatter bloodstain simulation computer package Tracks<sup>®</sup> 2.2, using a provided droplet simulation example (Forensic Computing of Ottawa Inc., 2001a). The straight-line trajectories (thin red lines) generated from the virtual spatter bloodstains show an exact correspondence between the intersections of the droplet trajectories and the hypothetical site of impact when the 3D straight-line trajectories are resolved in the horizontal plane. In the vertical plane, however, the 2D resolution of these 3D straight-line trajectories intersect at a point above the simulated site of impact, as would be expected, but also to its right. The accuracy of the intersection of the simulated curved trajectories (thin black lines)

in the vertical plane is evident, but the intersection of the 2D straight-line trajectory approximations, with the green line being an extension of one of these trajectories, produces an erroneous location estimate in both the vertical and horizontal axes of the vertical plane of analysis. Consequently, any site of impact estimation that uses convergence methodologies in a vertical plane is prone to error, as the intersection of straight-line trajectories in the vertical plane of PAC analysis do not necessarily represent a 2D projection of the 3D origin of the site of impact, or even the horizontal position of this origin in that specific plane (Carter and Podworny, 1991; Carter, 1998, 2001 and 2004a).

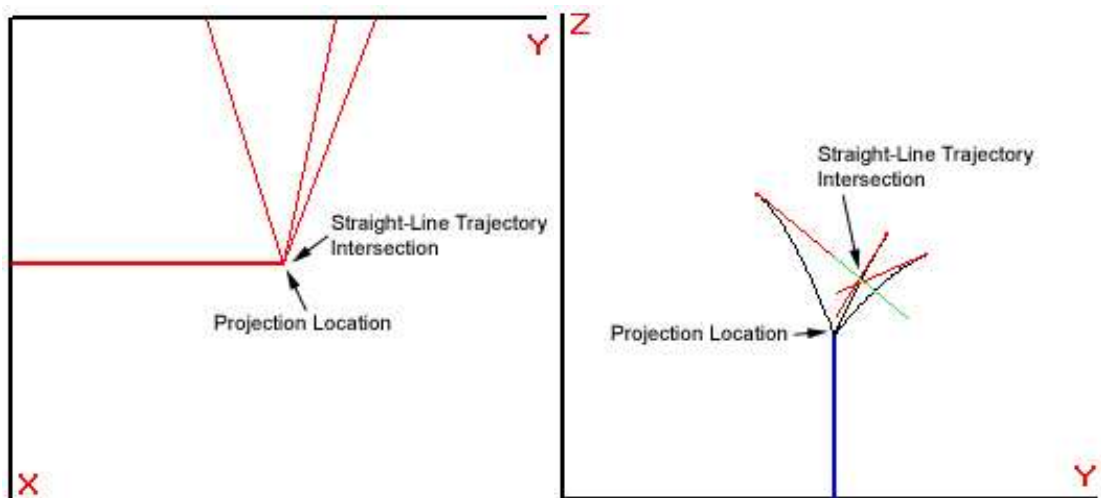


Figure 3-2 - The comparison of viewing straight-line trajectory intersections in the horizontal (left) as opposed to the vertical plane in which the spatter bloodstains are recorded (right) as generated by simulated droplet trajectories (after *Forensic Computing of Ottawa Inc.*, 2001a).

### 3.3.1.1 Point or Area of Origin

Traditionally, convergence techniques are defined as those procedures that produce an estimate of the site of impact in a single plane. The term, however, is also used here to also describe 3D location techniques that are based around the initial construction of 2D PAC estimates, with a third dimension estimate added afterwards. Such techniques would typically be described as Point or Area of Origin (PAO) techniques within BPA, but as will become clear with the discussion of 3D origin techniques, the methodology, assumptions and possible inferences associated with the two essentially separate estimation techniques do differ.

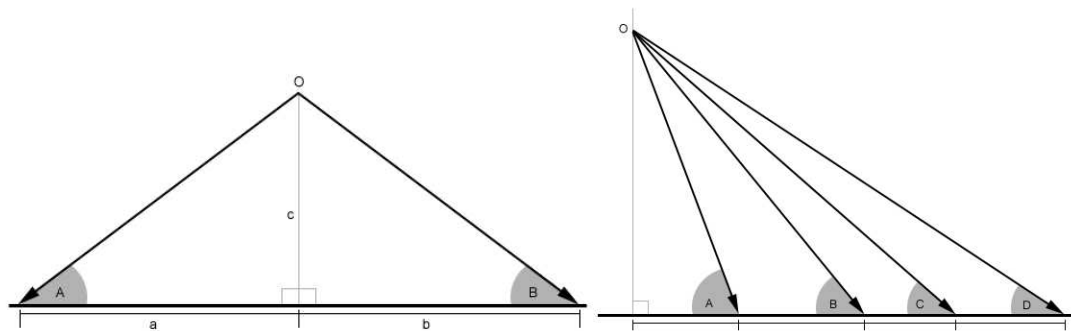


Figure 3-3 - The right-angled triangles involved in the mathematical 'tangent' method (left), and the graphical method (right).

Both graphical and mathematical 'tangent' methods can be used in conjunction with a completed 2D convergence estimate to provide an approximate 3D location for a site of impact (Emes and Price, 2004; Bevel and Gardner, 2002; James and Sutton, 1998a; Jackson and Jackson, 2004; Fischer, 1998; Brady et al., 2002). Both of these methods rely on reconstructing the perpendicular distance of a straight-line trajectory estimate from the plane of PAC analysis, at the location of 2D convergence, by using the distance of a spatter bloodstain from this location in conjunction with the impact angle (Figure 3-3). In graphical methods this distance, angle, and perpendicular distance are represented in a scale plan, whereas in the 'tangent' method, this is done using relatively simple trigonometry.

The graphical method is potentially limited by scale effects, the number of trajectories that can be considered and accurately drawn on a single plan, and the over-convergence of physically constructed trajectories. The mathematical method is limited in that each trajectory is essentially analysed in isolation, and that the physical calculation of these perpendicular distances can be both error prone, and time-consuming if a significant number of spatter bloodstains are considered. More fundamentally, however, any assessment of the 3D site of impact based on an initial 2D convergence in a vertical plane is likely to be flawed in all three axes (Carter and Podworny, 1991; Carter, 1998, 2001 and 2004a). The reliance on an erroneous 2D convergence to calculate or graphically construct a 3D estimate of a site of impact also includes a degree of error into the second horizontal axis, although this may well be reduced if the intersections are averaged (Carter, 2004a). The intersection of a straight-line trajectory, and the projection of an erroneous 2D convergence in the horizontal plane will not necessarily be in the same location as the intersections of 3D straight-line trajectories fully resolved in the horizontal plane (Figure 3-4). As a result, the

potential error associated with the inability of straight-line trajectories to account for flight path curvature in the vertical plane is not limited to the vertical axis in 3D estimates based on 2D convergence techniques in a vertical plane, but is also propagated through to the estimate to both axes of the horizontal plane (Carter, 2001).

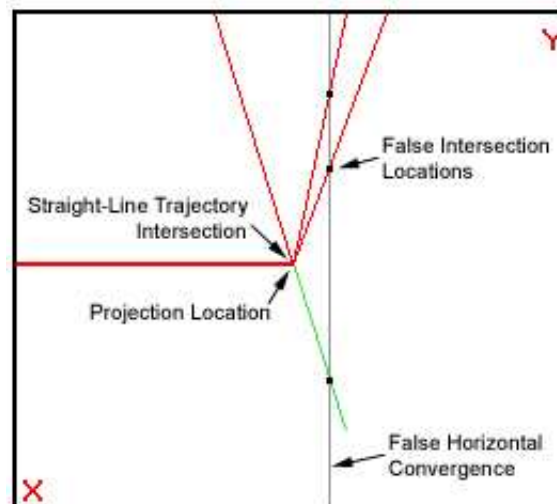


Figure 3-4 - The accurate intersection of 3D straight-line trajectories resolved in the horizontal plane, and the erroneous intersection of these straight-line trajectories with a horizontal projection of a vertical 2D convergence (after Forensic Computing of Ottawa Inc., 2001a).

The majority of descriptions of convergence techniques in BPA literature, however, are conducted in a horizontal plane, where a 2D convergence estimate can construct reliable straight-line trajectory intersections and provide a potentially accurate horizontal site of impact estimate (Bevel and Gardner, 2002; Fischer, 1998; Emes and Price, 2004; James and Sutton, 1998a; Jackson and Jackson, 2004). The inferential limitations placed on height estimation as a function of the straight-line trajectory model are often addressed in these descriptions, but there tends to be little explicit discussion of its potential effect on convergence in vertical surfaces, with the notable exceptions of Carter and Podworny (1991), Carter (1998, 2001 and 2004a), and Bevel and Gardner (2002). This reliance on the horizontal plane for estimate accuracy arguably further limits convergence estimates. The estimation of vertical height is often the most problematic in a horizontal plane, especially where it is upward facing, such as in the case of a floor. This is primarily a function of the fact that the selection of spatter bloodstains that more closely represent straight-line trajectories is more difficult under these circumstances. Spatter bloodstains that represent blood droplets with significantly curved trajectories cannot easily be

distinguished from those with relative straight flight paths, which can significantly increase the potential scale of any error in the estimation of site of impact height. It may also be the case that an accurate site of impact estimate in the horizontal plane is impossible using 2D convergence techniques, if an impact spatter pattern, or the most appropriate section of it for site of impact estimation is only evident in a vertical plane.

In contrast to the theoretically error-prone methodology already described, the practical application of these convergence methods is not necessarily as clear-cut. Although the technique is often referred to as 'point' of convergence (Lee et al., 2001; Brady et al., 2002; IABPA 2004b; Bevel and Gardner, 2002), it is generally accepted that the assumptions, and potential inaccuracies involved in the straight-line trajectory model, as well as the general site of impact estimation procedure, result in straight-line trajectory intersections that do not converge on a single point, but produce an area of intersection, when constructed in either the horizontal or PAC vertical plane of analysis (Wonder, 2001; Bevel and Gardner, 2002; Carter, 2001; James and Sutton, 1998a). As site of impact estimates have spatial size as well as location, the absolute error of convergence estimates may, as a result, be reduced. This reduction in absolute error, in terms of whether a real horizontal site of impact is within the estimate area suggested by PAC analysis, however, is likely to be achieved, and to some degree offset, by an increased relative error. The relative estimate area is itself likely to be larger as a result of the combined individual errors in establishing trajectory intersections. Any error associated with the application of convergence techniques in a vertical plane, arguably, can be reduced where spatter bloodstains are selected that better correspond to the straight-line trajectory model in a vertical plane and the ability to apply PAC methods successfully has been demonstrated, under both experimental and case work conditions (Carter, 2001 and 2004a; Wonder, 2001). The fact remains, however, that there is an additional source of error that places limitations on site of impact convergence estimates that are not inherent to 3D origin techniques.

### **3.4 3D Origin Techniques**

3D origin techniques are defined here as methods which involve the full 3D reconstruction of straight-line trajectories from the outset, or which use knowledge of this 3D trajectory to resolve it into its more accurate horizontal and

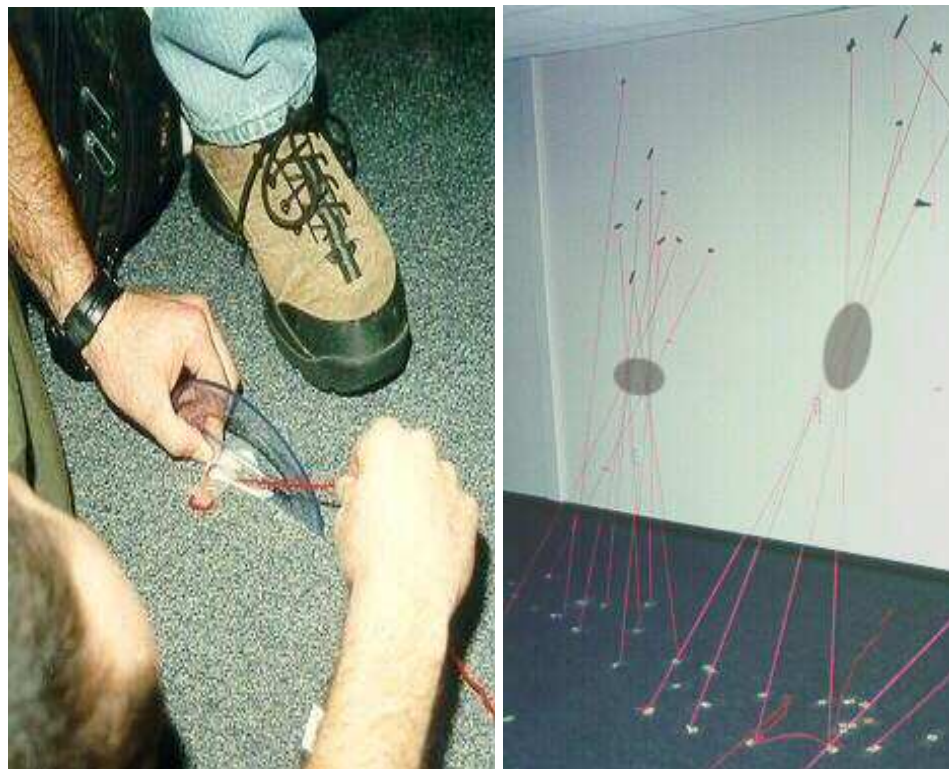
less reliable vertical components regardless of the plane in which the impact spatter pattern is observed. Typically, these methods would be grouped with 3D convergence estimates in BPA, under the PAO heading. These methods are presented in a different grouping here, however, to make explicit the differences involved in what could be considered 'true' 3D site of impact estimation, and the arguably more limited convergence estimation. The two main methods in which 3D origin estimations have been made are through traditional stringing and more recently through computer-based simulated string methods.

### **3.4.1 Traditional Stringing**

The traditional process of crime scene 'stringing' uses the 3D directional vector of spatter bloodstains, as inferred from directional and impact angles, to produce string matrices in the estimation of a site of impact. As with 2D convergence techniques the determination of the numerical value of the angle of directionality is not necessary, as it is only important that the string is aligned using this direction. The string used to represent a straight-line trajectory estimate is then angled according to the calculated impact angle from the manual measurement of spatter bloodstains. The location where a number of these strings cross can be subsequently interpreted as the position of the site of impact for that particular impact event in 3D, as shown in Figure 3-5.

The stringing technique, arguably, has been in existence in one form or another since the introduction of the correlation between spatter bloodstain dimensions and impact angle by Balthazard et al. in 1939, and has been taught as an integral part of basic BPA courses for a number of years (Bevel and Gardner, 2002; Risenbatt and Shaler, 1995; Pizzola et al., 1986a). Stringing has been described as the physical manifestation of mathematical convergence methods and is frequently considered to be an additional step in the inference of site of impact estimations after the construction of a 2D convergence (Bevel and Gardner, 2002; Lee et al., 2001; James and Sutton, 1998a). Such comparisons are understandable given the fact that the alignment of strings using spatter directionality and angling to correspond to impact angle can be viewed as analogous to the two-stage process of 3D estimation based on 2D convergence. The process of crime scene stringing, however, even if preceded by a 2D convergence estimate, does not treat directionality and impact angle singularly, but considers straight-line trajectories in their 3D form. The string matrices

constructed at a scene represent a full 3D realisation of the straight-line trajectory estimates and any intersections that may occur between them. 3D stringing techniques effectively allow the visualisation of a site of impact estimation away from the plane in which an impact spatter pattern may be observed, and as a result avoid a number of the limitations of the 2D treatments of site of impact estimation (MacDonell, 1997, cited in Brady et al., 2002).



*Figure 3-5 – The traditional stringing technique. Directionality and impact angle alignment (left), and two multiple string matrices with the likely zones of intersections marked (after Nelson, 1999).*

The reliance on a full 3D realisation of straight-line trajectories in the form of traditional crime scene stringing has a number of benefits for site of impact estimation. Firstly, the technique is based on the physical geometry of the target surface. As with PAC techniques, the physical placement of strings at a crime scene means that the actual physical geometry of the target surface upon which the impact spatter pattern is observed is inherent in the construction of straight-line trajectories. Although the physical fixing or drawing of lines at a scene requires a significant amount of interaction with the evidence, potentially resulting in destructive techniques, the inclusion of the estimate within the physical scene can provide the potential for a fully integrated scene-based analysis of the site of impact estimate. This contrasts with the other more abstracted estimation techniques, as well as providing a potentially accurate

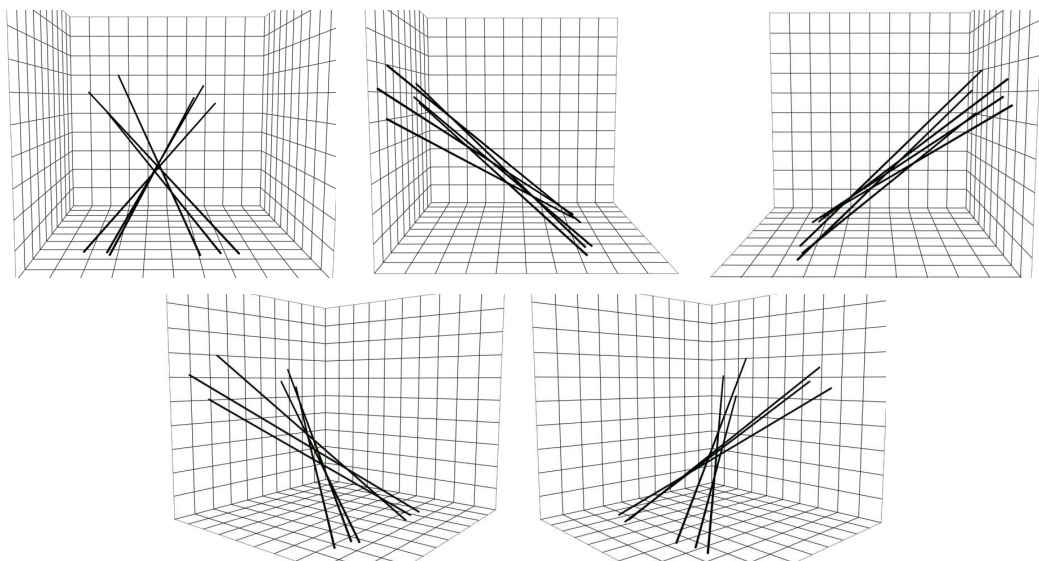


trajectory approximation based on the actual physical geometry of a target surface upon which the relative vector indicated by spatter bloodstain morphology depends. Secondly, the stringing technique is theoretically applicable to any target surface, or target surfaces, regardless of their orientation or geometry. Convergence methods are limited in the application of straight-lines estimates directly onto a target surface, with multiple target surfaces having to be treated independently before combining into a single estimate. The stringing method, conversely, only relies on the geometry of the target surface at the point at which an individual spatter is observed and the physical string is fixed. Rather than the generation of straight-line trajectories being conditional on the orientation and geometry of an entire target surface, as in 2D convergence estimations, the 3D trajectory estimates of stringing mean that a single estimate can be constructed from impact spatter observed on multiple target surfaces, regardless of their orientation and geometry, with a consistent theoretical treatment and representation of each reconstructed trajectory. Finally, these factors combine in providing the potential of a full 3D appreciation of the geometry of the straight-line trajectories, their intersections, and the resultant site of impact estimate.

As with the intersection of straight-line trajectories resolved in a single plane, the intersections of straight-line trajectories in 3D, despite the frequent use of 'point' of origin terminology, do not intersect at a single point. The likelihood of just two straight-line trajectories intersecting perfectly in 3D space, in the sense that they occupy the same space in 3D somewhere along their lengths, is low, and as the numbers of strings used increases the likelihood of highlighting an exact point for a site of impact estimate decreases further (Bevel and Gardner, 2002; Fischer, 1998). The chances of an exact point intersection are such that any estimate that produces this result should be regarded with serious suspicion (Wonder, 2001; Bevel and Gardner, 2002; Lewis, 2003; Laber and Epstein, 2004). The 3D nature of the strings, and their intersections can have significant implications for the interpretation of any site of impact estimate constructed.

Figure 3-6 demonstrates how different perspectives of a 3D realisation of straight-line trajectories can affect their interpretation. As the intersection of two strings is rarely an exact location in 3D, the perspective from which a string matrix is viewed can significantly change the perceived location of the string intersections, and by extension, the size and shape of the site of impact estimate. The complete 3D realisation of the straight-line trajectories in traditional stringing should mean that any view of the scene, including the horizontal plane in which

straight-line trajectories and their intersections can be considered to be unbiased, could be achieved regardless of the surface upon which the impact spatter pattern is observed. In theory, this would mean that the stringing of a impact spatter pattern in a vertical plane site could provide both an accurate horizontal estimate for a site of impact, and a height estimation with a significantly reduced scale of error through the selection of appropriate fast-upward moving spatter bloodstains. The limitations of the physical scene, however, frequently mean that achieving this idealised horizontal view is difficult if not impossible (Carter, 1998). The majority of visual perspectives of string matrices that are generally obtainable at crime scenes are those that incorporate some vertical component, and as a result will include a degree of error in estimates of horizontal location, in a similar way to PAC estimates conducted in a vertical plane. The danger in relying on these perspectives of the 3D string matrices to infer a site of impact estimate is that an additional unknown degree of error is unavoidably included within the estimate. These subjective views of the physical estimate, either chosen by the analyst, or imposed by the physical circumstances of the estimate, could affect both the results of the estimate and the inferential base of any conclusions made from them.



*Figure 3-6 – Five separate 3D views of the same site of impact estimate, similar to those one might experience of traditional stringing at a crime scene. The five views shown are a front view, two side views, and two isometric views, respectively.*

Traditional stringing has also come under criticism in regard to the implementation and appropriateness of string-based approximations of straight-line trajectories, and the effect that this could have on establishing an accurate

site of impact estimate. These criticisms have included (Carter, 1991, 1998, and 2001; Wonder, 2001; Bevel and Gardner, 2002; Emes and Price, 2004; Rinehart, 2000):

- A lack of precision in string placement.
- The potential sag in strings that lack sufficient tension.
- Human error in spatter bloodstain measurement and impact angle calculation.
- The over-convergence phenomenon in physically constructed straight-line trajectories.
- The lack of potential re-analysis by others.
- The time-consuming and cumbersome methodology of stringing in complicated or physically restricted scenes.
- That its procedures are more suited to conditions with relatively small numbers of spatters, such as those found in relatively simple crime scenes.



*Figure 3-7 - A laser pointer developed for aiding the placement of strings as part of a 'stringing' site of impact estimation procedure (Mavin, 2002).*

Recent advances in stringing methodology have introduced laser protractors to more precisely define straight-line trajectory estimates, and significantly aid the accuracy of string placement (Figure 3-7). The application of this laser technology has been generally considered to be an improvement on the traditional stringing, and has been shown to perform well in experimental comparisons with computer-based site of impact estimation (Wonder, 2001; Bevel and Gardner, 2002; Mavin, 2002). Despite this advance in both straight-

line estimate definition and placement, the majority of theoretical and practical limitations of stringing methodologies at crime scenes arguably remain.

Whatever the limitations of stringing techniques, the basic method can, and has been routinely and successfully applied in both experimental and casework scenarios for at least 30 years. Physical stringing techniques are still used in the investigation of impact spatter patterns at crime scenes, but their main function is increasingly being restricted to educational and visual aids used to promote understanding of site of impact estimation assumptions, techniques and limitations in both basic BPA courses, and courtrooms (Bevel and Gardner, 2002). In the UK, as in the rest of the world, physical crime scene stringing is gradually being replaced by more sophisticated computer-based 'virtual stringing' techniques (Emes and Price, 2004; Bevel and Gardner, 2002; Carter 1998, 2001 and 2004a).

### **3.4.2 Computer-Based Methods**

The use of computers in the analysis of site of impact estimates from impact spatter patterns has been pioneered by Dr. Alfred Carter, formerly of the University of Carleton, Canada, through his BackTrack™ software range. Involved with the teaching of the physics and mathematics for spatter bloodstain interpretation with the Royal Canadian Mounted Police from 1982, Carter introduced the use of computer processing power to site of impact estimation as early as 1987 (Bevel and Gardner, 2002; Carter, 2004b). A fully functioning site of impact estimation tool, based on the creation of 'virtual strings' was developed by 1989, with a Windows version and an additional digital image spatter measurement program released in 1992 (Carter, 2004b), with the experimental validity of 'virtual string' methodology demonstrated to the IABPA at its annual conference in 1993 (Carter, 1998). In the meantime Carter and Podworny (1991) had published a method for determining the intersection of straight-line trajectories in the horizontal plane using 3D geometry and a scientific calculator for impact spatter patterns that were observed in the previously problematic vertical plane. Through his continued efforts in improving site of estimation techniques, as well as promoting the understanding of the physics and mathematics behind accurate site of impact estimation, Dr. Carter was awarded the title of Distinguished Member of the IABPA at its annual conference in 1999 (Carter, 2004b). BackTrack®/Win and its spatter bloodstain measurement

counterpart, BackTrack®/Images, are probably the most well-known, and widely used computer applications for site of impact estimations within BPA.

The core program of the suite of impact spatter analysis programs, BackTrack®/Win, is now on its third major release, and is distributed by Dr. Carter's company, Forensic Computing of Ottawa Inc. (Carter, 2004a). The BackTrack®/Win program uses a number of measurements of impact spatter bloodstains and the 3D environment in which they are situated to generate 'virtual strings' of straight-line trajectory estimates, and produce a site of impact estimate based on the intersections of these trajectories via a method Carter (1998, 2001 and 2004a) has termed 'Directional Analysis'. The measurements required for this analysis involve setting up a 3D grid for the environment containing the impact spatter pattern to ascertain the spatial location and plane upon which each individual spatter is recorded, the measurement of the width and length dimensions, and the angle of directionality of each spatter bloodstain to be analysed. An example of this data is illustrated in Figure 3-8, which shows sample data supplied with BackTrack®/Win in tabular form. The 'Status' column of this table indicates which target surface that the spatter is observed on. The 'Alpha' and 'Gamma' columns represent the impact and directionality angles, respectively, and the 'Xpos', 'Ypos' and 'Zpos' represent the location of the spatter in 3D space.

Drop#	Status	Width	Length	Alpha	Gamma	Xpos	Ypos	Zpos	Visible
1	0	16.7	35.7	28.	316.1	0	76.2	173.7	Y
2	0	21.	38.5	33.	327.	0	89.	164.	Y
3	0	21.9	41.2	32.	327.3	0	90.5	158.	Y
4	0	19.7	39.5	30.	319.	0	81.6	147.9	Y
5	0	15.	25.6	36.	338.	0	103.2	149.8	Y
6	0	21.3	34.	38.7	303.1	0	90.7	133.	Y
7	0	22.	42.7	31.	22.	0	143.3	149.6	Y
8	0	16.3	30.	33.	38.1	0	151.2	143.2	Y
9	0	24.8	51.5	28.8	46.	0	169.1	152.	Y
10	0	21.9	49.8	26.	47.	0	177.5	151.	Y
11	0	18.3	44.9	24.	55.2	0	179.4	146.9	Y
12	0	23.3	44.9	31.3	60.	0	173.	133.2	Y

Figure 3-8 - Example data table from BackTrack®/Win showing the data inputted for 12 spatter bloodstains from an experimental impact spatter pattern (Carter, 2004a).

The 'Directional Analysis' of impact spatter bloodstains uses 3D geometry to decompose the straight-line trajectory inferred from spatter directionality and

impact angle, and the orientation of the target surface into its three Cartesian X, Y and Z components (Carter, 1998). Once fully resolved into these three components a relatively accurate horizontal location for the site of impact can be estimated by considering the horizontal components of the straight-line trajectory estimates and their intersections in isolation, regardless of the plane in which the actual impact spatter pattern is observed. The result of the estimate is subsequently reported both numerically, if the form of an average of the locations of the straight-line intersections, and via three orthographic plan views of the 3D site of impact analysis. The horizontal plane of analysis, and the horizontal location of the site of impact estimate can be viewed in 'top' view provided by BackTrack<sup>®</sup>/Win, while a 'side' view of the straight-line trajectories can also be analysed to provide tentative site of impact height estimates or more firm estimates of the upper limit of this height (Carter, 1998). An additional 'end' view corresponds to the PAC vertical plane of analysis, and routinely illustrates the differences between site of impact horizontal intersection locations with those created by convergence analysis in this vertical plane (Carter, 1998, 2001 and 2004a). These three orthographic projections of the 'virtual string' estimation provided by BackTrack<sup>®</sup>/Win are shown in Figure 3-9.

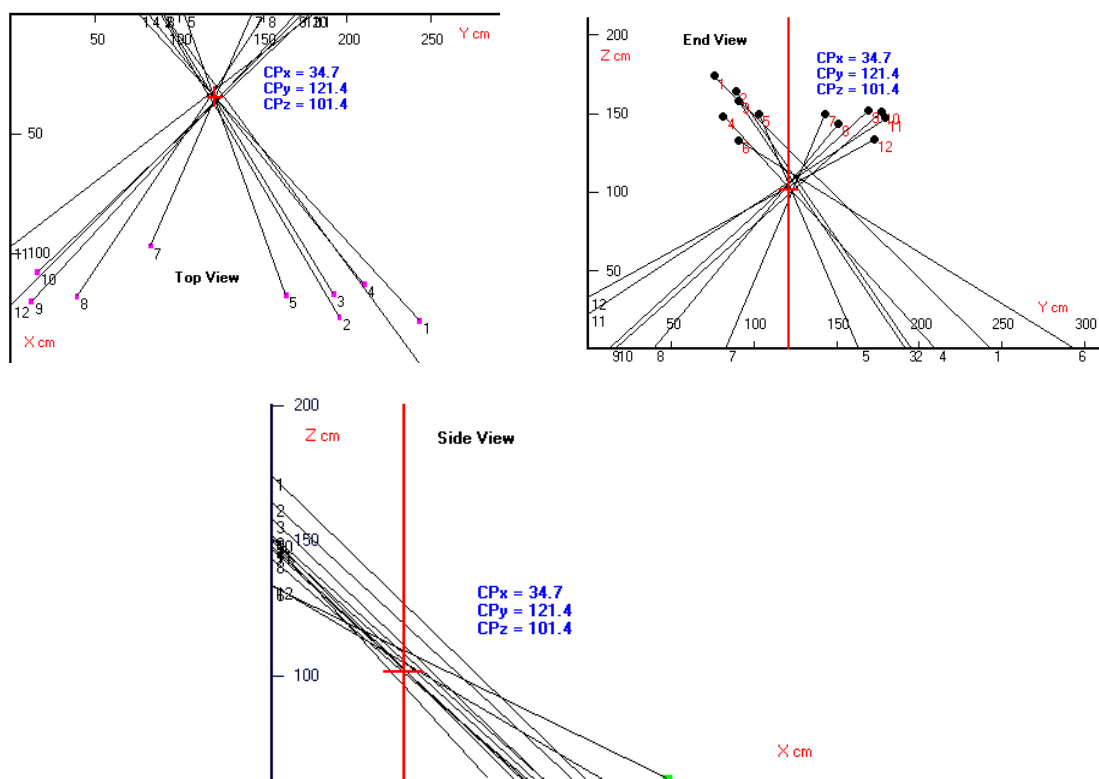


Figure 3-9 – Orthographic projections of the 'top', 'end' and 'side' views produced by BackTrack<sup>®</sup>/Win (Carter, 2004a).

The 'virtual stringing' technique of BackTrack<sup>®</sup>/Win has been described as the computer application of the traditional stringing technique' or at least its fundamental principles (Carter, 1998; Emes and Price, 2004). The computer application of straight-line trajectory analysis, however, does improve upon traditional stringing in a number of key areas. These improvements include:

- Mathematically defined and precise representations of straight-line trajectories (Bevel and Gardner, 2002; Carter, 1998).
- Error-free placement of strings (Carter, 1998).
- A numerical as well as graphical representation of an estimate of the location of a site of impact (Carter, 1998; Bevel and Gardner, 2002).
- Straight-line trajectory intersections, and the site of impact estimate being considered in the horizontal plane, providing a potentially unbiased horizontal site of impact estimation in terms of flight path curvature (Carter, 1998 and 2001).
- The provision of horizontal intersection analysis whether an impact spatter pattern is observed on a vertical or horizontal plane.
- The ability to apply accurate horizontal estimation to impact spatter patterns observed in a vertical plane, providing an increased opportunity to select fast-upward moving spatter bloodstains for potentially more accurate site of impact height estimation (Carter 1998; Carter, 2001).
- The separation of horizontal and vertical analysis so that potentially all types of impact spatters can be used to establish horizontal intersections, with height estimation based on the spatters that represent fast-upward moving blood droplets, where present (Carter and Podworny, 1991; Carter 1998).
- Orthographic projections presenting planar straight-line trajectories with no perspective effects, including the unbiased horizontal plane (Carter, 1998 and 2001).
- A potentially quicker and less cumbersome reconstruction methodology (Bevel and Gardner, 2002; Carter, 1998; Wonder, 2001).
- An intersection analysis that can be conducted independently of the physical scene.
- Computer processing power, providing the potential for a greatly increased number of spatter bloodstains to be used in a single site of impact analysis.
- The provision of a valuable presentational tool.

The other program in the BackTrack™ suite, BackTrack®/Images, can be used to provide the raw spatter bloodstain dimension and angle data necessary for 'virtual stringing' through digital image processing, albeit with significant user involvement. Close-up scaled photographs of each spatter bloodstain to be used in the site of impact estimation are analysed separately. The angle of directionality is calculated by the software from lines, manually positioned in the software interface, that correspond to the major axis of the spatter, and the directionality datum line, which has to be included in the photograph itself. The width, and the length of the spatter are then manually marked in the interface, before the software generates an ellipse of this data upon which the impact angle is based. Once generated this ellipse can be manipulated to provide the best fit for each particulate spatter bloodstain. This image analysis process is illustrated in Figure 3-10. The raw spatter bloodstain data, which includes manually inputted 3D location and plane data for each spatter, can then be saved and imported directly into BackTrack®/Win for site of impact estimation. The combined use of BackTrack®/Images and BackTrack®/Win can significantly speed up the generation of site of impact estimates when a practitioner has become competent in the process of measurement, photography, and image and data manipulation, even where larger samples of spatter bloodstains are used than would normally be practical with manual estimation techniques (Bevel and Gardner, 2002).

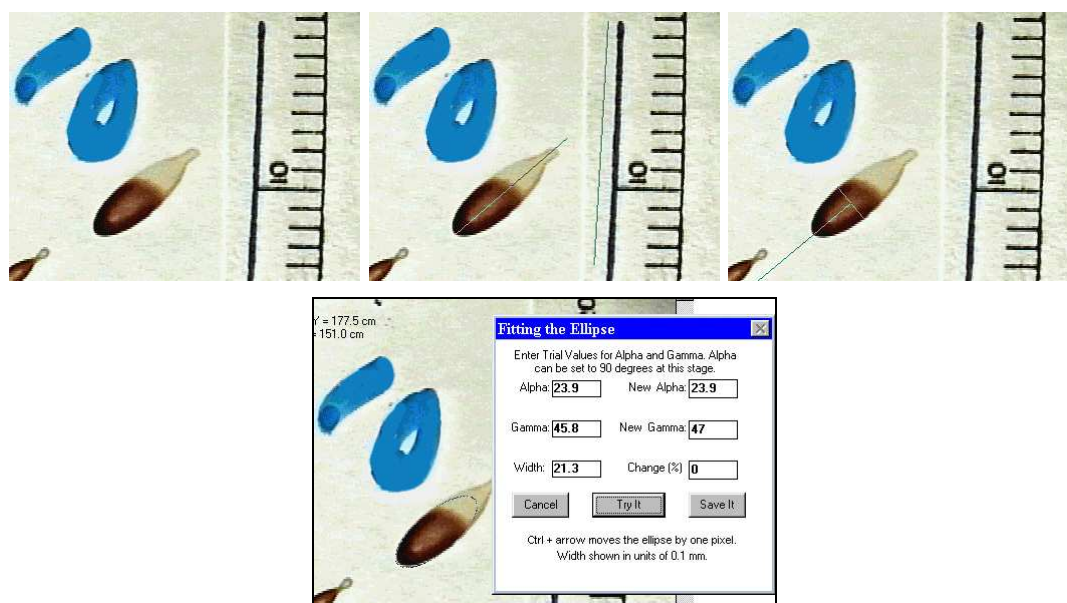


Figure 3-10 - BackTrack®/Images ellipse fitting procedure. Close-up photograph of spatter (top left), directionality and datum line marked (top middle), spatter width marked (top right), and software generated ellipse (bottom, after Carter, 2004a).



Once the spatter bloodstain data has been entered into BackTrack<sup>®</sup>/Win, whether this is done manually or through BackTrack<sup>®</sup>/Images, the horizontal location of the site of impact estimate can be established by taking an automatic average of the horizontal locations of the trajectory intersections, the average of horizontal trajectory intersections in a manually selected area, or the average of a number of manually selected individual horizontal trajectory intersections. Once the horizontal aspect of the estimate has been established a mean average vertical estimate can subsequently be constructed from the heights of a selection of trajectories as they pass over this horizontal location, as represented in the 'side' view of BackTrack<sup>®</sup>/Win (see Figure 3-9).

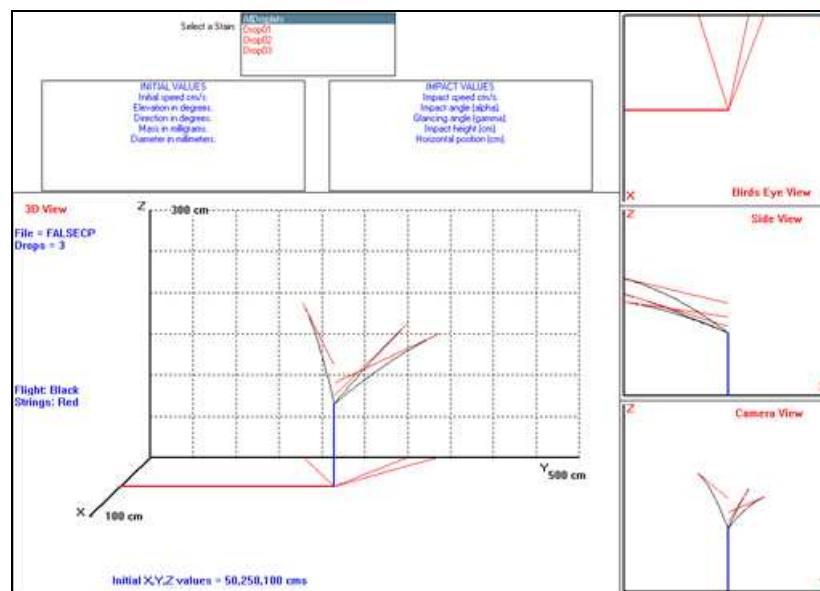


Figure 3-11 - Tracks<sup>®</sup> blood droplet and bloodstain simulation visual interface (after Forensic Computing of Ottawa Inc., 2001a).

The droplet simulation program Tracks<sup>®</sup> is an additional spatter bloodstain interpretational tool developed by Dr. Carter, and is now released with the BackTrack<sup>™</sup> suite (Forensic Computing of Ottawa Inc., 2001a). Tracks<sup>®</sup> allows a BPA analyst to project hypothetical blood droplets from a source at any direction and speed to examine both the curvature of the trajectory of the droplet in the vertical plane, and the resulting spatter bloodstain impact angle and directional angle that the droplet would create on a target surface (Figure 3-11). While not directly involved in site of impact estimates, Tracks<sup>®</sup> has proved useful as both an educational tool for demonstrating the dynamics of droplet flight path curvature, and resultant spatter bloodstain morphology, and as an investigative

tool for postulating 'consistent' droplet sizes and initial trajectory velocities with documented spatter bloodstain morphologies. Site of impact estimation that combines trajectory intersection technique and droplet flight dynamics in a single analysis have been attempted, but the undeterminable variables of droplet size, mass and velocity have largely precluded such programs from having any improved interpretational utility beyond that possible with straight-line trajectory analysis. The original version of BackTrack<sup>®</sup> released by Forensic Computing of Ottawa attempted to estimate actual parabolic flight paths of droplets in the construction of a site of impact estimate, although this was quickly followed up by a straight-line trajectory approach, BackTrack<sup>®</sup>/Strings, upon which current BackTrack<sup>®</sup>/Win versions are based (Bevel and Gardner, 2002).

Despite the history of use and acceptance by the BPA community of the BackTrack<sup>™</sup> suite of programs, other computer-based site of impact estimate applications are also used in the interpretation of impact spatter patterns. CAD-based techniques, which utilise 3D CG design and modelling technology to reconstruct and present information on site of impact estimations are currently used in constructing site of impact estimates, and are taught in IABPA advanced BPA courses (Figure 3-12). The methods employed in such analyses, however, are essentially an extension of BackTrack<sup>™</sup> 'virtual stringing' techniques into existing 3D design and modelling computer packages, and as such share many of the BackTrack<sup>™</sup> system's advantages but also a number of its limitations (Pace, 2004a).

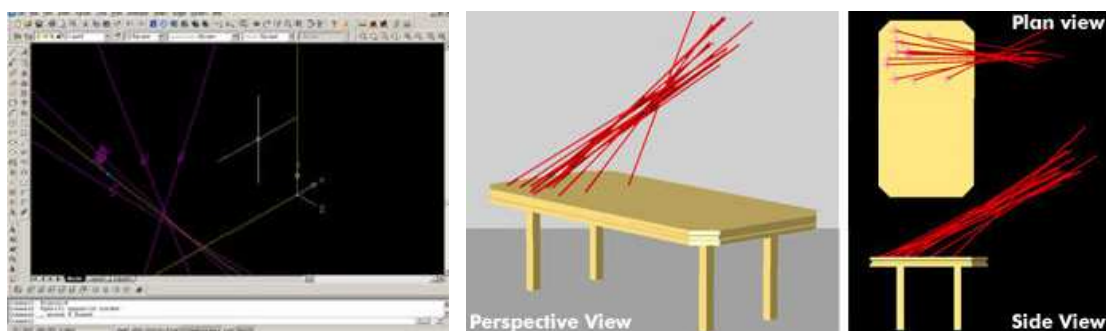
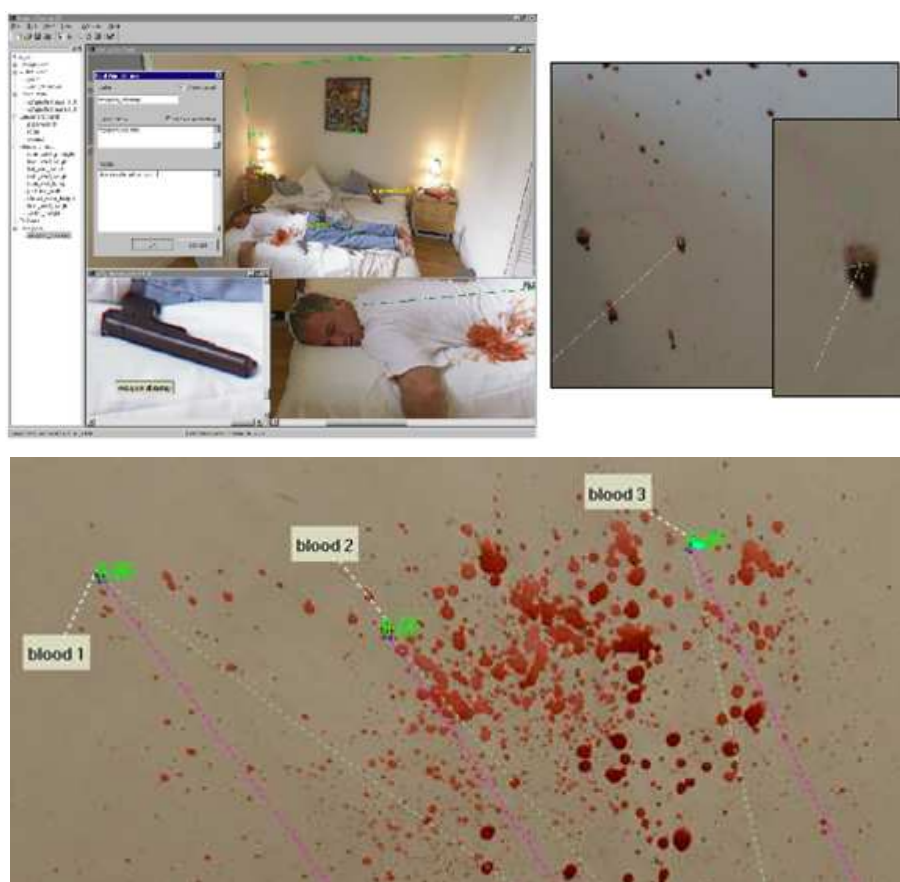


Figure 3-12 - 3D CAD environment used for site of impact estimation (left, Pace [2004a]), and still rendered images of various views of a virtual CAD site of impact estimation (right, Pace [2004b]).

The use of such 3D CG technology arguably has an advantage over the present BackTrack<sup>™</sup> suite in that the fully interactive 3D environment permits an investigative experience similar to that of physical stringing at a crime scene, in which many BPA practitioners are already trained. 3D modelling software can

also produce various renders of the site of impact estimate, not just the interpretatively-valid orthographic projections of BackTrack®/Win, but also perspective-based 3D views of the scene that include relevant environmental features, and other significant investigational information. The use of the animation features of a number of 3D modelling packages also provide the opportunity to produce virtual walkthroughs of BPA reconstructions that include both the final site of impact estimations and the data upon which they are based. Where this type of technology is combined with virtual reality software, the potential also exists for interactive 3D crime scene investigation and reconstruction.



*Figure 3-13- SceneVision-3D crime scene scanning, visualisation and measurement tool, with preliminary 3D straight-line trajectory estimation (after 3rdTech, 2004b and 2005).*

As computer-based site of impact estimation is gradually replacing physical estimation methods, so 3D computer-based environmental modelling and analysis are beginning to complement 'virtual stringing', especially where 3D CG crime scene reconstruction and presentation are becoming more commonplace. The potential of this type of 3D analysis has been recognised by both Forensic Computing of Ottawa Inc., and 3rdTech of North Carolina, USA. From the end of

2004, 3rdTech who develop and sell the DeltaSphere-3000 3D Scene Scanner and SceneVision-3D crime scene capture, analysis and reconstruction software, have entered into a collaboration with Forensic Computing of Ottawa Inc. to incorporate BackTrack™ analysis into their software, which has already proved useful in taking 3D crime scene measurements and representing rudimentary impact spatter trajectory information (3rdTech, 2004a and 2004b). Examples of this crime scene software are illustrated in Figure 3-13.

Despite the many advantages of computer-based methods of site of impact estimation, there are a number of potential limitations that need to be highlighted. Firstly, the potential for increased precision, and reduced subjectivity and propensity for error in the handling of mathematical data in computer-based analysis compared to manual estimation techniques is not in doubt. What has been questioned, however, is whether the actual level of this precision provides a more accurate estimate, in terms of representing a 'true' site of impact, given that site of impact estimation has a number of inherent modelling assumptions and uncertainties associated with its basic methodology (Bevel and Gardner, 2002). A second, but associated criticism is that despite the 3D analytical nature of computer-based site of impact estimation, the numerical results of the analysis are predominantly reported in terms of a mean point average. This single point description of the estimate data is arguably inadequate in terms of representing both the areal nature and any spatial variation present in the straight-line trajectory intersection data set, as well as providing a limited statistical analysis of the potentially large and detailed intersection data sets given the processing power of modern PCs. Thirdly, it has been suggested that any overemphasis on the average point precision of computer-based analysis could lead to misinterpretations of the results of a site of impact estimate. While any such misinterpretation is unlikely by trained analysts, it could be a significant factor if such data is either generated by, or presented to individuals who lack an understanding of the processes and assumptions involved in both the general site of impact estimate methodology, and the specific computer-based estimate technique (Bevel and Gardner, 2002). In any criticisms of mean point average estimates it should be remembered, however, that the horizontal area of intersection can always be viewed from a 'top' view, in which the location of the mean point is also included in BackTrack®/Win. As Figure 3-14 demonstrates though, even this visualisation-based approach can become fairly complicated when a larger number of trajectories are considered.

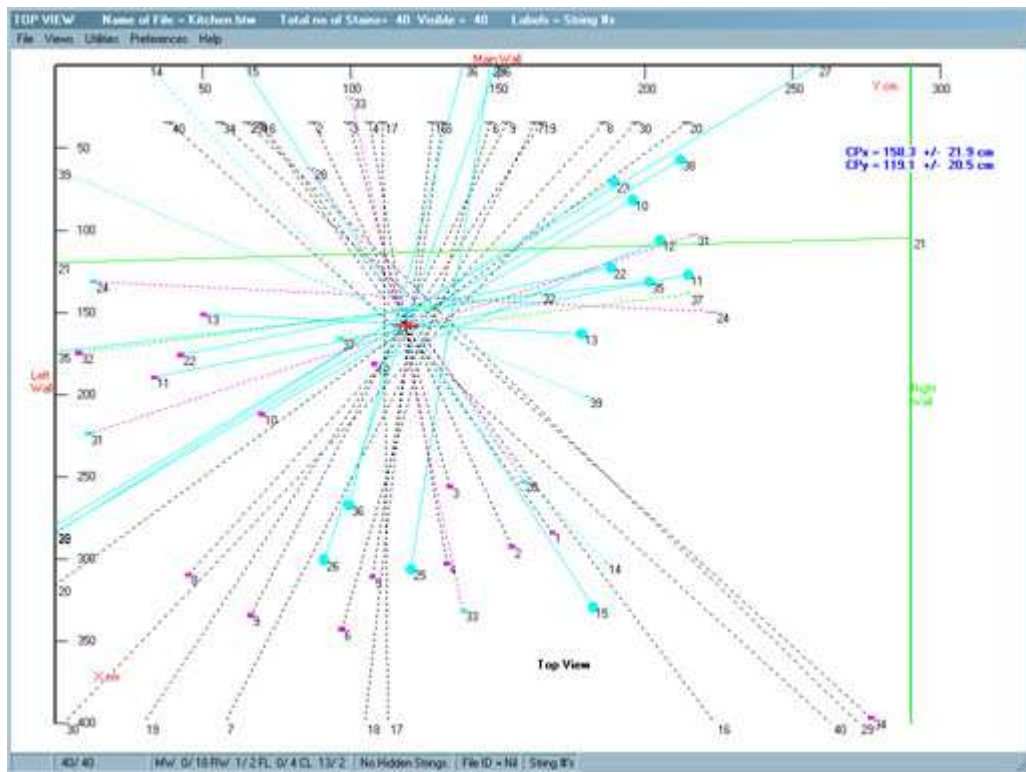


Figure 3-14 - The 'top' view of a BackTrack®/Win site of impact estimate using 40 experimental spatter bloodstains (Forensic Computing of Ottawa, 2001b).

Carter and Podworny (1991) and Carter (2001) have suggested that the accuracy of the horizontal site of impact estimate from spatter bloodstains observed in a vertical plane depends solely on the precision of the measurement of the two angles that define the straight-line trajectory estimate. For an impact spatter pattern observed in a horizontal plane any estimate, by extension, could be considered to depend solely on the measurement of the directionality angle of the spatter bloodstain. There are, however, a number of other factors that could also affect the accuracy of the computer-based estimates. These factors include:

- Any errors in the increased numbers of measurements required to locate each spatter bloodstain in 3D space.
- The accurate definition of, and adherence to, a suitable 3D coordinate system within the crime scene environment.
- The selection of appropriate spatter bloodstains for measurement and inclusion within the average intersection estimate.
- The architectural complexity of the scene, and variations in the geometry of the target surfaces.

Despite comparisons to traditional physical stringing techniques, computer-based analysis presents a number of unique considerations as a result of its abstraction from the physical crime scene. The benefits of this abstraction include one of the defining features of computer-based analysis, the provision of an accurate view of the horizontal plane of analysis, but also include other advantages such as a string-free working environment, a potentially less destructive estimate methodology, and the potential for a more lengthy and considered analysis, as well as the chance to reanalyse the data and replicate an estimate even after the physical crime scene no longer exists. Conversely, however, the abstraction of the estimate methodology from the physical location of the evidence means that both the practice and interpretation of an estimate are decontextualised to a certain extent. While the generation of straight-line trajectory estimates in traditional stringing techniques inherently uses the physical geometry of a target surface to constructing relative directional unit vectors from spatter bloodstains, computer-based methods, as a result of their abstraction, require some approximation of this geometry to accurately conduct any analysis. In the current version of BackTrack<sup>®</sup>/Win this approximation of the 3D geometry of a crime scene is limited to 12 planar surfaces that represent the six surfaces of a cube with the potential for an additional parallel offset for each surface. Every surface within the analysis is assumed to be planar and parallel to one of the three 3D Cartesian planes, presenting a situation which can be limiting in real world environments with complex surface geometry, and can have an effect on both the accurate measurement and positioning of spatter bloodstains upon a particular 'virtual' target surface, and the accuracy of the construction of the 3D direction of a 'virtual string' relative to the orientation and geometry of the target surface. The potential for this limitation has been recognised, however, and is beginning to be addressed. Future versions of BackTrack<sup>®</sup>/Win are to include the analysis of spatter on planar sloped target surfaces, and the inclusion of BackTrack<sup>™</sup> technology in 3D scene scanning, reconstruction and visualisation packages presents the opportunity to generate accurate 3D coordinate registration of spatter bloodstains, and to more precisely define the general and localised geometry of target surfaces (Carter et al, 2004; 3rdTech, 2004a and 2004b). The fact may still remain, however, that the estimate of straight-line trajectories from spatter bloodstains in computer-based methods is not inherently based on the geometry of the crime scene, but on some approximation of it.

### **3.5 Conclusions**

As with the other practical methods of site of impact estimation, despite its theoretical limitations, the application of computer-based methods have been shown to provide reasonably accurate approximations of sites of impact for CSR purposes in both experimental and casework conditions (Carter, 1998 and 2001; Pace. 2004a). The methods employed in the 'Directional Analysis' of spatter bloodstains, however, can be attributed a greater degree of interpretational confidence than the other estimation techniques, and it has even been suggested that the BackTrack™ treatment of site of estimation satisfies the criteria of a sound scientific methodology, which is becoming increasingly required of scientific and technical expert forensic evidence for its utility in the wider legal process (Carter, 2001; Henderson, 1998; Van Stratton, 2003; Emes and Price, 2004). While it is arguably the case that the BackTrack™ methodology is the closest manifestation of site of impact estimation to this ideal through its consistent 3D treatment of straight-line trajectory estimates, its mathematically defined 'virtual strings', and its provision of a potentially unbiased horizontal plane of analysis, it could also be argued that a critique of the fundamental assumptions and inaccuracies in the general site of impact estimate procedure, as well as the ability of current investigative techniques to represent these uncertainties, might cast some doubt on this assertion.

## **4 Site of Impact Estimation: A Critique**

### **4.1 Introduction**

While the previous chapter discussed the specific methodological approaches to constructing a site of impact estimation, and some of the limitations specific to these approaches, this chapter will discuss the more fundamental theoretical and practical limitations of site of impact estimation. The estimation process will be highlighted as being inherently prone to uncertainty, and will be specifically addressed in terms of how this might affect the comparatively more sound inferential methodology employed by computer-based techniques. The conclusions section of this chapter will provide a brief synopsis of the discussion of BPA, and site of impact estimation so far, before outlining a number of research questions derived from the discussion of estimate uncertainty, and what effect these could have on the position of the technique within the forensic scientific and technical investigation and the reconstruction of crime scenes. The final project intention section of this chapter will outline the experimental computer-based analytical research design that will be used in an attempt to address a number of the issues raised during this discussion of site of impact estimation uncertainty.

### **4.2 Estimate Uncertainty**

No matter what technique is used to establish the location of a site of impact, Bevel and Gardner (2002) emphasise that the results of the analysis:

*'...are an estimate.'* [their emphasis]

As an estimate, there will always be a degree of uncertainty surrounding the determination of this location. While the different approaches to site of impact estimation each impose their own specific limitations on the production of any particular estimate, the general approach of site of impact estimation is itself surrounded by a number of methodological and theoretical uncertainties. The principal source of this uncertainty can be considered to be a consequence of the fact that any particular estimate represents a single static depiction of an event, constructed from the results of what is an inherently dynamic process. This dynamism is evident at every stage in the generation of an impact spatter



pattern, from the impact event, to droplet generation, projection and flight, and droplet-target contact and spatter bloodstain creation. Even the estimation procedure can be viewed as a dynamic process participated in by an analyst, whose responsibility it is to identify, interpret, and measure spatter bloodstains upon which to base the analysis, as well as evaluate and comment upon the investigational significance of the results of this analysis. The potential practical and inferential implications of the inability of site of impact estimation to account for such dynamism have already been highlighted to a certain degree in the case of straight-line trajectory approximations (see Sections 2.5.3). The following discussion will explore the extent to which the inability to incorporate this pervasive dynamism in other areas of site of impact estimation theory and practice could influence both the methodological application, and inferential utility of this approach to impact spatter pattern interpretation. The main topics that will be addressed are:

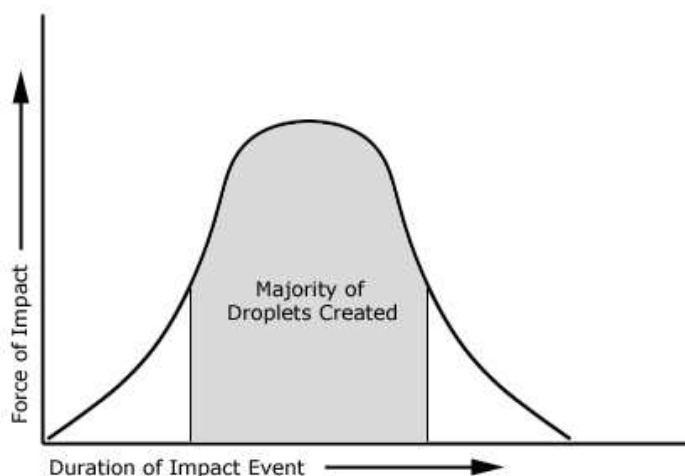
- The dynamic impact event.
- Droplet dynamics.
- Impact angle calculation.
- Spatter bloodstain measurement.
- Spatter bloodstain sample selection.

### **4.3 The Impact Event**

For the purposes of site of impact estimation, an impact event is generally modelled as instantaneous. In reality, however, the dynamic nature of any impact event means the generation and projection of blood droplets from some blood source will involve at least some spatio-temporal component (Fischer, 1998; Wonder, 2001; Fischer, 2001; Bevel and Gardner, 2002). The spatial aspect of an impact event can involve a number of factors including:

- The spatial size of the blood source.
- The size of the portion of the surface of the object that impacts with the blood source.
- Any movement of both of these components during the complex and violent dynamics that occur around, and during an impact event.

While the temporal component of an impact event, which is implied in the suggestion of possible movement of an event's constituent parts during the event, is arguably very small, it remains an integral part of any impact process that can affect both the size and distribution of impact spatter patterns. The physical process of the development of an impact, the build up of a pressure gradient, and movement within the blood source volume, and the distribution of droplets from it, are essentially temporal in nature, and although the timeframe involved is usually considered to be so small that it is suppressed in the theoretical basis of site of impact estimation, it can still have implications for the creation of, and inference from impact spatter patterns. Bevel and Gardner (2002), for example, have suggested that the temporal application of force to a blood source during an impact event is partly responsible for the variable spatter bloodstain sizes that can be observed from a single event. As the general mechanics of droplet separation typically adhere to an inversely proportional relationship between the magnitude of force and droplet size, any single impact event can produce a range of spatter droplet sizes as the level of force exerted varies over the duration of the impact event (Figure 4-1). The variable and largely unpredictable nature of a dynamic impact event, the generation and projection of spatter blood droplets, and the manifestation of impact spatter patterns, however, effectively precludes the extension of any experimental quantification of such temporal components to specific estimation circumstances.



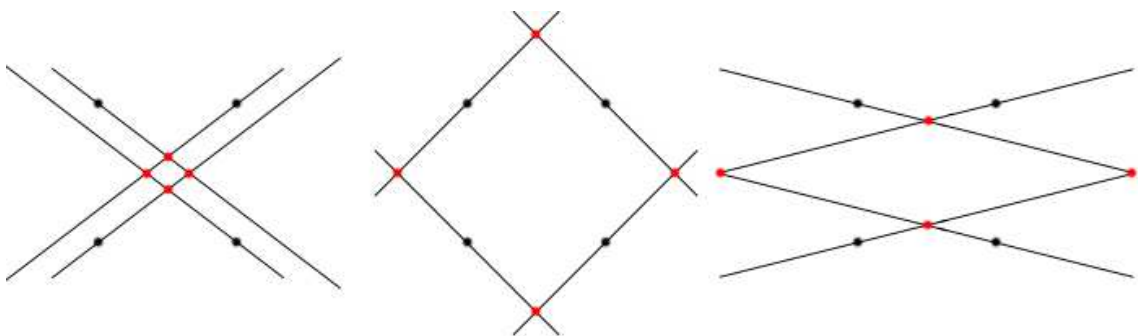
*Figure 4-1 – The variation in force with time during impact event. In general the larger the force of an impact, the smaller the resulting blood droplets are likely to be (after Bevel and Gardner, 2002).*

In terms of site of impact estimation, the implications of a dynamic impact event, which can involve aspects of both spatial and temporal size, and movement, is that any event rarely occurs in a precise XYZ coordinate point (Bevel and

Gardner, 2002; Wonder, 2001). The definition of an exact point location in any site of impact estimation can, as a result, be generally considered to be impossible, and inconsistent with the nature of the impact event itself. While the consideration, discussion, and use of 'point' of convergence, or 'point' of origin terminology is still prevalent in BPA, many analysts consider an 'area'-based representation of any estimate to be more appropriate, both in terms of representing the available trajectory intersection data, and at least some aspect of the spatial nature of impact events (James and Sutton, 1998a, Bevel and Gardner, 2002; Wonder, 2001). Both the 'point' and 'area' depictions of a site of impact estimate, however, represent a reduction in dimensionality. While the data and conclusions of an estimate are typically present in terms of a more accurate horizontal location, and a less accurate vertical approximation of a site of impact, or some vertical upper limit, the nature of the estimate remains inherently 3D. As such, just as 'point' estimate may be considered a dimensional reduction from an estimate's spatial size, to a spatial location, the use of 'area'-based terminology signifies a reduction of dimensionality from the 3D volumetric nature of any estimate to a 2D areal representation. If 'area' is more appropriate than 'point', then could 'volume' be still more appropriate in considering the 3D spatial nature of an estimate? Even in cases where a horizontal estimate is presented in isolation, the third, vertical dimension of the estimate should not be considered to be absent. As no restriction is actually placed on the height of the 3D spatial estimate, a horizontal areal estimate simply represents the cross section of a 3D volumetric shape that extends from the lowest to highest possible vertical positions within an environment. Where an upper limit on vertical height is provided, the 3D estimate volume could be considered to cut off above this level, and where a firmer vertical approximation is possible, the variation in the available data could suggest a volumetric estimate region suspended within the investigational environment.

The implications of a dynamic impact event take on two further implications, whether an estimate is conceptualised, as 'point', 'area' or 'volume'. Firstly, any site of impact estimate, in effect, reduces the dimensionality of the impact event under investigation. A degree of uncertainty in the estimate can stem from the fact that a dynamic event is reconstructed, or an estimate of it is constructed, as a static representation of the entire dynamic impact event. While this reduced dimensionality is largely imposed on the estimate process by the nature of its evidential base (the final spatter bloodstain pattern), it arguably impinges on the way in which any single estimate can be interpreted. Any representation of the

site of impact constructed through a site of impact estimation can be considered as a long exposure image where the various phases of an impact event, or at least those aspects that produce spatter, are recorded. Even in an ideal situation where all other sources of error in estimate accuracy are avoidable, an areal representation of an impact site does not simply represent the physical size of the impact, but could conceivably include elements of any spatio-temporal size and movement that are also recorded in any particular impact spatter pattern. A 'point'-based representation can conceivably reduce this dimensionality still further by presenting this spatio-temporal area as a single locative but dimensionless point. Secondly, in emphasizing the need for a representation of spatial size in site of impact estimation, the fact that no two droplets originate from the exact same spatial location has been emphasized (Wonder, 2001). While this arguably demonstrates the need for some appreciation of the spatial size of an impact event, it also highlights an additional source of uncertainty in the site of impact estimation process. If no two droplets originate from the same location, even if the straight-line estimates of their trajectories are accurate, they will not intersect at a physically significant point in terms of the site of impact. The two trajectories will not intersect at a common point of dispersal from the blood source, which they do not share, but at some other undefined approximation of this point. The locations of a number of trajectory intersections and their spatial relationships, as a result, can vary not inconsiderably, depending not only on the location of the real origin of the droplets but also on the relationships between the trajectory approximations of their flight paths, as illustrated in Figure 4-2.



*Figure 4-2 - Three idealised intersection scenarios. The location of dispersal of four droplets from a blood source (black dots), the accurately estimated trajectories (black lines), and the actual locations of intersection (red dots) are shown.*

Uncertainty in a site of impact estimate can, as a result, stem from the fact that the analysis of trajectory intersection data does not necessarily correspond with,

but is an approximation of the property under investigation, the spatial origin of the droplets. The dynamic and unpredictable nature of impact events, and the limited potential of the interpretation of a resultant impact spatter pattern to inform of this nature, means that any impact event is not necessarily easy to define in any concrete dimensional terms (both spatial and temporal) through site of impact estimation techniques.

#### **4.4 Droplet Dynamics**

The need to better understand blood droplet dynamics within BPA, despite being identified as early as the mid 1960's, remains a limiting factor in site of impact estimation, with BPA challenged both in and out of court on its lack of research in this area (Kirk, 1967 cited in Risenbatt and Shaler, 1995; Pizzola et al., 1986a; Bevel and Gardner, 2002). The fluid dynamics of blood droplets can affect the interpretation of spatter bloodstains for the purposes of site of impact estimation through two key areas:

- Droplet shape during flight.
- Spatter bloodstain formation through droplet collapse.

##### **4.4.1 Droplet Shape**

The assumption of droplet sphericity is fundamental to the accurate interpretation of directionality and impact angle from spatter bloodstain morphology, with any distortion of droplet shape on contact with a target surface potentially influencing both this morphology and the accuracy of any resultant straight-line trajectory estimate (Bevel and Gardner, 2002; Raymond et al, 1996b). While some oscillation of blood droplet shape is instigated by the distortion of both the blood source and the separating droplet during spatter generation, the specific fluid characteristics of blood with its relatively high viscosity and relatively low surface tension, compared to other fluids such as water, and the relatively small size of impact spatter droplets are frequently claimed to reduce this oscillation rapidly, promoting a spherical droplet shape during flight (Beard cited in Bevel and Gardner, 2002; Wonder, 2001; Raymond et al., 1996a; James and Sutton 1998a; Sirignano, 1999). In impact spatter droplet generation, however, the initial oscillation of droplet shape has been shown to be as much as 40% of the droplets

diameter, with experimental impact spatter observations suggesting a reduction to below 10% within 0.05 seconds of dispersal (Gardner, 1996, cited in Bevel and Gardner, 2002; Bevel and Gardner, 2002). This rapid damping may not be insignificant, however, where the selection of spatter bloodstains is based on those thought to represent fast-moving droplets. Raymond et al., (1996b), for example, have applied experimentally established oscillation damping times to a 1% level from blood droplets generated through a controlled free-fall method to possible flight speeds of impact spatter droplets. The results of this research have been used to suggest that impact spatter droplet oscillation should not be regarded as negligible in droplets of 1 mm in diameter with a flight distance of less than 1 m, and less than 0.25 m for droplets with a diameter of 0.5 mm (Raymond et al, 1996b), both sizes being consistent with experimental ranges of impact spatter droplets observed by Bevel and Gardner (2002). The practical application of such findings is not simple, however, as there is difficulty in interpreting any such inaccuracy solely from impact spatter bloodstains. Oscillatory lifetime and flight distance are not necessarily linked in terms of their actual relationship in site of impact estimation, as it is only the straight-line trajectory that is examined, and not the actual curved flight path distance. An assessment of the absolute velocity of the spatter causing blood droplet, upon which flight time depends, in conjunction with flight distance, as well as an accurate determination of the size of a spatter-causing droplet, are generally not possible solely from their resultant spatter bloodstains. The extension of free-fall dynamics to impact spatter droplets may also be limited due to reduced aerodynamic force in the potentially slower flight of the droplet, the smaller amount of causative force, and the initial oscillation in droplet shape, with Raymond et al. (1996b) only reporting a 13-22% oscillation following free-fall droplet separation, around half that of the maximum of impact spatter droplet oscillation reported by Bevel and Gardner (2002).

Despite the demonstrated potential for droplet oscillation, the bulk of BPA literature maintains that impact spatter droplets are likely to be spherical or near spherical on contact with a target surface, giving a level of confidence to the interpretation of spatter bloodstain morphology that is arguably confirmed in the frequent experimental proof of impact angle calculation and site of impact estimation (Bevel and Gardner, 2002; Wonder, 2001; Pizzola et al, 1986a; Pizzola et al. 1986b; Carter 1998 and 2001; Moore, 2002). The possibility nevertheless remains that larger impact spatter droplet sizes and droplets that contact a target surface after only a short flight time may deviate from the

spherical droplet model. While the general level of accuracy of site of impact estimation does not seem to be significantly affected by this situation, deviations from a spherical droplet shape cannot, as a result, be totally discounted during site of impact estimation (Bevel and Gardner, 2002; Raymond et al., 1996b).

#### **4.4.2 Spatter Bloodstain Formation**

Whether a blood droplet is spherical, or only near spherical on its contact with a target surface, the actual mechanism of this contact, and the collapse of the droplet in creating a spatter bloodstain is not currently well understood, the process having lacked detailed investigation in both general fluid mechanics and droplet studies, as well as in its application to BPA (Sirignano, 1999; Bevel and Gardner, 2002). Rather than simply being a function of the trajectory of the droplet as it makes contact with a target surface, the morphology of spatter bloodstains also depends on the complex dynamic collapse of the droplet as it makes contact with, and spreads across a target surface. This process of droplet collapse involves aspects of the mechanical conservation of momentum, the conservation of energy, and if contact is angled, the conservation of angular momentum of a fluid droplet (Sirignano, 1999). Attempts to define this collision and its effect on the structure of a blood droplet and spatter bloodstain formation within BPA have generally been descriptive, with the spatio-temporal process involving some form of contact, displacement, dispersion, and retraction phases (Bevel and Gardner, 2002). This general process of the collapse of a blood droplet is also accompanied by complex internal wave-like movements within the droplet's fluid volume (Pizzola et al., 1986a). One result of this dynamic collapse process is that the width of a spatter bloodstain is typically larger than that of its causative droplet (Bevel and Gardner, 2002). The dynamic nature of spatter bloodstain creation can be considered to present spatter bloodstain interpretation with a paradox, as the determination of spatter directionality is largely dependent on this dynamic, whereas impact angle calculation for the most part suppresses it. The reduction of the volume of the droplet as it moves along a target surface during its collapse, as well as the wave-like movement of the remaining blood volume are essential in the interpretation of directionality. It is the resultant tapering and edge distortions of spatter bloodstain morphology that are indicative of the direction of travel of a spatter-causing droplet. Spatter impact angle theory, illustrated in Figure 2-7, however, largely denies this dynamic, requiring the preservation of both the spherical shape droplet and its pre-contact trajectory

throughout the formation of the spatter bloodstain to provide the idealised elliptical morphology upon which the impact angle relationship is based.

The inconsistencies and current inadequacies in spatter bloodstain formation theory resulting from the suppression of this dynamic can be demonstrated through the consideration of two influential factors in spatter bloodstain formation:

- Collision energy.
- Target surface properties.

The effect of the energy involved in the collision of a blood droplet with a solid target surface on spatter bloodstain morphology can be demonstrated through the change of size in free-fall droplet spatter bloodstains solely as a function of the height of their fall. Released from rest, free-fall droplets accelerate downwards, due to gravitational force until the opposing aerodynamic force equals that of the gravitational force, and the droplet reaches its terminal velocity. Any increase in the distance of drop of a free-fall blood droplet results in an associated increase in the size of its resultant spatter bloodstain. Once a height is reached where the terminal velocity of the droplet is achieved during its fall, however, the resultant bloodstain size will not increase even with further increases in the fall height. The velocity, and momentum of the droplet, as well as the energy involved in the collision, are restricted by this terminal velocity, which in turn limits the amount that the volume of the droplet is displaced on contact with a particular target surface, as demonstrated in Figure 4-3.






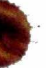



<b>Height of Fall (Inches)</b>	3	6	12	24	36	48	60	72	
<b>Bloodstains</b>									

Figure 4-3 – Increase in spatter bloodstain sizes produced by the free-fall of a defined droplet size from different heights. Above the 36 inch height there is no difference in stain size (after Lee et al., 2001).

This feature of free-fall droplets and their resultant spatter bloodstain size has meant that the estimation of the height of fall of such droplets is problematic (James and Sutton, 1998a; Willis et al., 2001). Recent research has, however, suggested that some utility may be found in an experimentally established



mathematical relationship between the measurement of spatter bloodstain diameter and the number of spines around the bloodstains edge, and the final velocity and diameter of the causative droplet, although this remains to be thoroughly tested under a broad range of conditions (Hulse-Smith et al., 2005).

It can also be shown that the fall distance of a free-fall blood droplet onto an angled target surface has a similar effect on the size of the resultant elliptical spatter bloodstains. Fundamentally for site of impact estimation, with this increase in size the relative proportions of the spatter bloodstains' shape tend to be maintained, preserving the width-length relationship. As blood droplets produced during an impact event are not subject to terminal velocity, however, the increase in the size of the resultant spatter bloodstain is not limited in the same fashion as free-fall droplets. The momentum of the droplet, and the energy involved in the collision depend not only on the volume and mass of the droplet but also on the velocity of the collision (Moore 2002). As a result, inferring droplet size and final velocity, two important factors in reconstructing the curvature of flight paths in a vertical plane, remains largely undeterminable to any accurate degree using established techniques of dimensional spatter bloodstains analysis.

The size, shape and edge characteristics of spatter bloodstains are also heavily influenced by the texture and absorbency of the target surface on which the bloodstain is formed. Figure 4-4, for example, shows a number of spatter bloodstains created by free-fall droplets of the same volume, with the same height of fall, on different target surfaces.

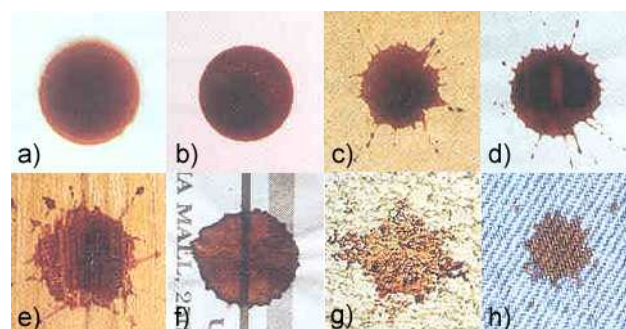


Figure 4-4 – Free-fall bloodstain size and shape variation of droplets of the same volume with the same distance of fall on different target materials. A) glass, b) polished tile, c) cardboard, d) non-corrugated cardboard, e) wood panelling, f) newspaper, g) concrete, h) denim cloth (after James and Sutton, 1998a).

Those surfaces that are smooth, and of low absorbency, tend to produce well defined regular stains. Conversely, rough or irregular surfaces tend to produce stains with irregular crenulated edges (Emes and Price, 2004; James and Sutton, 1998a; McDonell, 1993 cited in Saferstein, 1995; Moore, 2002). Surfaces of lower absorbency also tend to produce larger stains as the total volume of the droplet is dispersed across the exterior of the surface, whereas more absorbent surfaces can produce smaller bloodstains as some of the blood volume is likely to be absorbed within the surface (Lee et al., 2001; Emes and Price, 2004).

These variations in spatter size and morphology distortion can be significant in impact angle estimation in two key areas. Firstly, the level of distortion of a spatter bloodstain can make accurate and appropriate ellipse fitting problematic, which can consequently affect the accuracy of determining both the dimensions and directionality of spatter bloodstains. While only those spatter bloodstains with a well-formed elliptical shape are generally chosen for use in site of impact estimation in an attempt to reduce such errors, the use of site of impact estimation in conditions where spatter bloodstains are distorted to some degree cannot always be avoided. In such situations a generally unknown additional degree of error may be introduced in straight-line trajectory estimation (Chafe, 2003; James and Sutton, 1998a; Bevel and Gardner, 2002). Recent research has, however, begun to address the levels of confidence that an analyst may be able to apply to impact angle estimates produced from spatter bloodstains on a number of common spatter bloodstain-distorting crime scene target surfaces (Reynolds, 2004a). Secondly, the effect of the dynamism of spatter bloodstain formation in terms of the disparity between spatter bloodstain size and that of its causative droplet, and the exclusion of spatter bloodstain edge distortions, and spines in ellipse fitting, is that three fundamental assumptions of the theoretical inverse-sine model are not necessarily met (Reynolds, 2004b; Bevel and Gardner, 2002):

- The width of a spatter bloodstain is not necessarily that of the causative droplet.
- The length of the spatter bloodstain, or even the truncated ellipse does not necessarily represent the distance a spherical droplet travelled across the target surface.
- The total volume of the blood droplet, in terms of the physical extent of its resultant spatter bloodstain, is frequently not represented within the fitted ellipse approximation.

## 4.5 Impact Angle Calculation

Despite the seemingly ambiguous theoretical aetiology, the determination of impact angles and its role in site of impact estimation has been a long established and accepted principle of BPA (Willis et al., 2001; Chafe, 2003). As early as 1939, however, Balthazard et al. (1939, cited in Bevel and Gardner, 2002) cautioned that:

'In practical application, it [impact angle determination] should not be looked after for an illusionary accuracy...[impact angle determination] permits an estimate of the impact angle with an acceptable accuracy, sufficient for practical purposes.'

This statement, although referring to the earlier correlated relationship between spatter bloodstain dimensions and impact angle, is equally applicable to the more refined inverse-sine model of impact angle determination. The theoretical limitations of this model, in terms of its practical application, emphasize that a calculated impact angle is only an approximate determination, albeit both experimentally and practically reasonable (Carter, 1998; Bevel and Gardner, 2002). It is only recently, however, that such error rates have begun to be discussed explicitly within BPA literature with regards to this 'acceptable accuracy', and the consequences that this may have for site of impact estimation (Willis et al, 2001; Raymond et al., 1996a, and 1996b; Bevel and Gardner, 2002; Reynolds, 2004a). One study, conducted by Willis et al. (2001) investigated the variance associated with the estimation of impact angles from spatter bloodstains, using both theoretical mathematical models and practical experimentation. Applying ISO 9000 mathematical error treatment to the inverse-sine impact angle model, Willis et al. (2001) developed and tested the theoretical proposition that any variation in impact angle calculation will grow without limit as the impact angle approaches the perpendicular. Both experimental and calculated levels of variance were established through the determination of impact angles of multiple spatter bloodstains generated by free-fall droplet contact with target surfaces inclined at known angles. The results of this study indicate that a demonstrable level of variance does exist between repeated spatter bloodstain generation and impact angle estimation, and that this variance does increase as the impact angle becomes less acute (Table 4-1).

<b>Impact Angle (°)</b>	<b>Experimental Variance (°)<sup>2</sup></b>	<b>Calculated Variance (°)<sup>2</sup></b>
15	1.74	1.75
30	2.01	2.13
45	2.23	2.29
60	6.46	6.57
75	20.5	13.3

Table 4-1- The experimental and calculated variance of impact angle calculation from free-fall droplets contacting target surfaces at known angles (Willis et al., 2001).

The reporting of this variance, however, is arguably limited in a number of areas including:

- How the actual calculated impact angles and the variance in this calculation corresponds to the known impact angles.
- How appropriate the calculation of variance is in describing the experimental data set.
- The validity of the application of large free-fall droplet data to all spatter pattern creation dynamics.
- The probable sources of the variation in this particular case.

The study does nevertheless highlight the dynamic variability in droplet formation and impact angle estimation even under controlled conditions, as well as drawing attention to the fact that the inverse-sine model of impact angle determination is itself a significant factor in the effect that any initial error may have on establishing an accurate impact angle. The variable propagation of error through the mathematical formula for impact angle determination is a product of its two component non-linear functions:

- The proportional width-length ratio.
- The inverse-sine function.

Figure 4-5 illustrates the relationship between possible impact angles and the corresponding sine, or width-length ratio of each angle, whereby increases in angle result in progressively smaller increases in the sine of that angle.

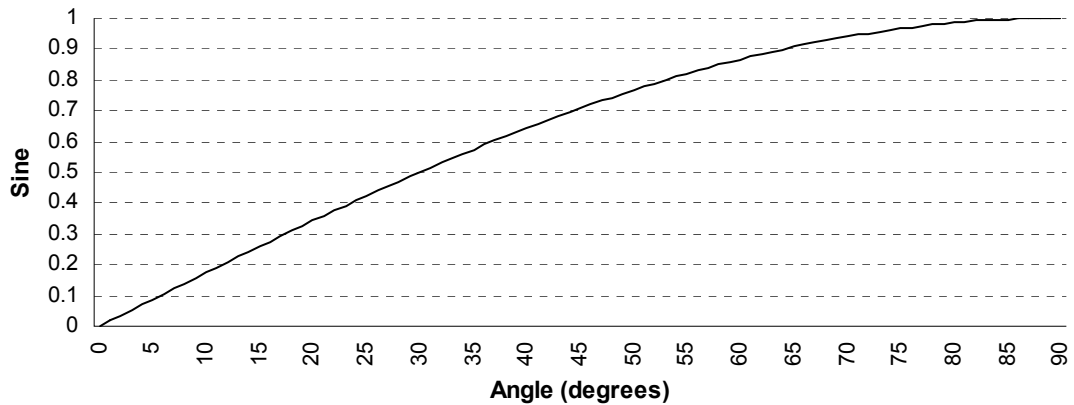


Figure 4-5 - Sine curve for acute angles, corresponding to possible droplet impact angles.

The effect that this non-linear relationship can have on the determination of an angle of impact can be demonstrated by grouping this data into successive 0.1 wide width-length ratio ranges, as shown in Figure 4-6. Viewed in this way it is evident that the consistent rise in width-length ratio corresponds to increasingly larger ranges of impact angles. As a result an equal error in establishing a width-length ratio, if applied to spatter bloodstains with an impact angle closer to 90 degrees, will result in a proportionally larger error in angle estimation than if applied to a spatter bloodstain with a more acute impact angle.

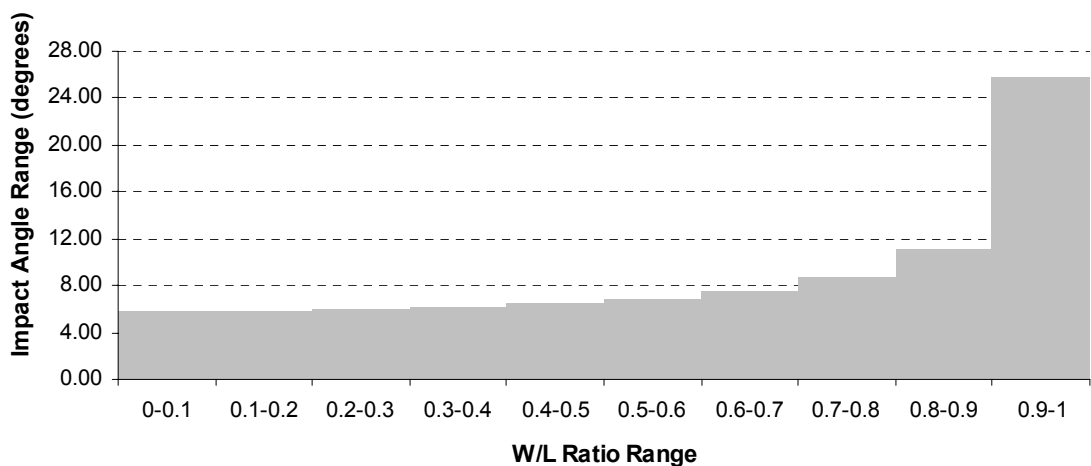


Figure 4-6 - Graph showing the difference between angles returned within 0.1 W/L ratio groups.

Figure 4-7 illustrates the proportional relationship between the width-length ratio and the length-width ratio in elliptical spatter bloodstain measurements. It can be seen from this graph that to achieve progressively smaller width-length ratios an idealised ellipse requires a significantly larger length in relation to its width.

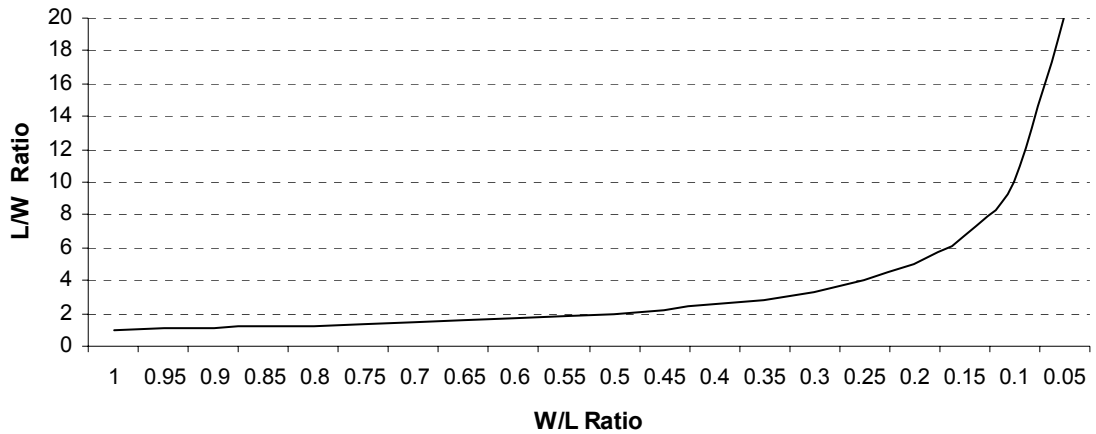


Figure 4-7 – Graph to show the relationship between the width-length ratio, and the length-width ratio.

Grouped in a similar way to Figure 4-6, this data indicates that smaller width-length ratios correspond to increasingly larger increases in ellipse length proportional to width, suggesting that small errors in determining elliptical dimensions at higher ratios can have a larger effect in terms of the resultant width-length ratio, than at lower ratios. This relationship, illustrated in Figure 4-8, is effectively the reverse of that demonstrated in Figure 4-6 between the width-length ratio groupings and impact angles, where the higher ratios cover the larger range of angles.

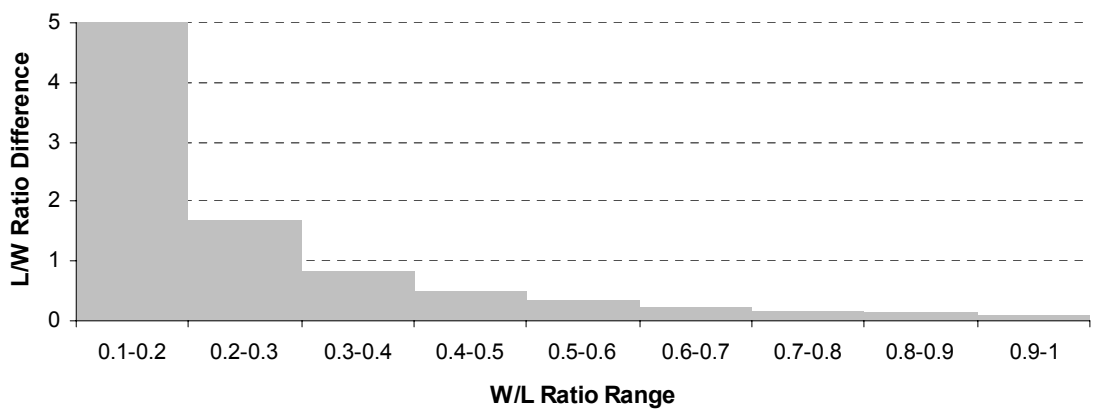


Figure 4-8- Graph to show the length-width ratio differences

The combination of these two non-linear functions in the inverse-sine impact angle calculation results in a situation where the smallest group in terms of the proportional difference between the width and length of an idealised ellipse encompasses the largest range of impact angles, and vice versa. This has the

effect that a smaller error in establishing a width-length ratio for impact angles representing contact closer to the perpendicular can produce a larger degree of error in impact angle determination than a larger width-length ratio error for spatter bloodstains with a more acute angle of contact. Willis et al. (2001) use the results of their study, which stresses this mathematical relationship, to suggest that in site of impact estimation more confidence should be given to spatter bloodstains with acute impact angles, and less reliance attributed to those closer to the perpendicular.

#### **4.6 Spatter Measurement**

Establishing the raw data for site of impact estimation through the interpretation and measurement of spatter bloodstain morphology can be a potentially significant source of uncertainty within site of impact estimation methodologies. As measurement is in essence an experimental procedure, and the true value of any measurable quantity is an abstract concept, there is always an unavoidable uncertainty in scientific measurement (Rabinovich, 1997; Taylor, 1997). The accuracy of any particular measurement is determined by the interplay of the accuracy of the measurement instrument, the method of measurement used, and the skill of the individual taking the measurements (Rabinovich, 1997). In site of impact estimation these factors can be crucial in the assessment and quantification of spatter bloodstain impact angle and directionality, where this is a measured property, which in turn can effect the level of uncertainty attributable to subsequent straight-line trajectory approximations, and any final site of impact estimate (Moore, 2002; Bevel and Gardner, 2002).

For the measurable property of some phenomena, such as the physical dimensions of a spatter bloodstain, to be meaningful the measurement has to be definable in two ways (Rabinovich, 1997):

- Quantitatively, in terms of the actual physical measurement.
- Qualitatively, in terms of describing the specific physical property that the quantitative measurement refers to.

While subjective elements of correct and accurate use of a measurement instrument cannot be discounted as sources of error in producing a quantitative measurement, one of the main concerns in spatter bloodstain interpretation is the

scale and accuracy of the measurement instrument itself (Bevel and Gardner, 2002; Moore, 2002). The scale of the instrument used in measuring spatter bloodstains can be significant, as accurate interpolation between the divisions of an analogue device, such as a micrometer or a photographic loupe, is typically limited to the mid-point between scale divisions. The general accuracy of such measuring devices, as a result, is typically cited as being one-half of the smallest scale graduation of the device either side of the quantitative measurement taken (Bevington and Robinson, 1992). This consideration of scale can be important in site of impact estimation as the smaller a spatter bloodstain is the more effect any consistent error can have on determining its dimensions, as the error will be proportionally greater than for larger spatter bloodstains (James and Sutton, 1998b; Bevel and Gardner, 2002). The percentage errors of the accuracy of two typical measurement device scale divisions for two likely spatter bloodstain widths is shown in Table 4-2.

		<b>Width (mm)</b>	
		2	4
<b>Scale (mm)</b>	0.1	±2.5%	±1.75%
	0.2	±5%	±2.5%

*Table 4-2 - The percentage error of common scale divisions of 0.1 and 0.2 mm of more sensitive measurement devices for spatter bloodstains widths of 2 and 4 mm.*

The predominant source of subjective and methodological error in spatter bloodstain measurement is arguably in the qualitative definition of the measurements. This qualitative aspect of measurement can compound any uncertainty present in the physical quantitative measurement, as the qualitative definitions of the properties necessary for site of impact estimation are based on the construction of fitted ellipse approximations of potentially complex spatter bloodstain morphology. The measurement of both the dimensions and directionality of spatter bloodstains can, as a result, suffer from a 'problem of definition' whereby the actual qualitative properties to be measured are not necessarily clearly defined (Taylor, 1997). Rather than being the result of a lack of definition in terms of the actual concepts of the properties to be measured, in spatter bloodstain analysis additional measurement error can stem from the uncertainty in how these concepts are realised physically. The process of ellipse



fitting in spatter bloodstain interpretation is intrinsically subjective, with no absolute rules applicable to the construction of fitted ellipses for the diverse manifestations of spatter bloodstain morphology (Bevel and Gardner, 2002; James and Sutton, 1998a). Each spatter bloodstain must be judged separately in an attempt to exclude surplus morphological features and construct an ideal elliptical shape whose dimensions correspond to the fundamental physical models of impact angle and directionality interpretation for any particular spatter bloodstain. The accuracy and precision obtainable through this process is largely a product of analyst skill and experience (Bevel and Gardner, 2002; Chafe, 2003). Even in computerised spatter bloodstain measurement, such as in BackTrack<sup>®</sup>/Images, despite the increased potential for the re-evaluation and re-analysis of evidence, the process is still inherently subjective, with all stages, bar the mathematical calculation of the impact and directionality angles, involving significant elements of user interaction.

While accurate ellipse fitting is critical in site of impact estimation, in casework conditions it is unclear how a number of key aspects of this process can be assessed. These aspects include three associated but conceptually different levels of accuracy:

- The appropriateness of any particular fitted ellipse in describing the gross morphology of a specific spatter bloodstain.
- The extent to which the features of a fitted ellipse correspond to the theoretical justification of spatter bloodstain interpretation.
- The extent to which this assessment corresponds to the actual trajectory of a spatter-causing blood droplet on contact with the target surface.

While some of the difficulties in the accurate and consistent generation of fitted ellipses have been highlighted in terms of analyst skill, and distorted spatter bloodstain morphology (see above), the elliptical eccentricity of the spatter bloodstain itself can be significant in accurate spatter bloodstain interpretation. The impact angles of elongated spatter bloodstains, for example, can frequently be overestimated as a result of the fitted ellipse being cut too short, returning a wider angle estimate than that of the actual impact angle (Wonder, 2001). In determining the directionality of spatter bloodstains Bevel and Gardner (2002) have suggested that the low level of ellipticity demonstrated in spatter bloodstains with impact angles between 75 and 90 degrees can reduce the reliability of any inferred directionality, compared to those spatter bloodstains

with more acute impact angles, and a more pronounced and elongated elliptical shape with a more distinctive longitudinal line of symmetry. This situation is exacerbated by the presence of edge crenulations that are frequently distributed around a larger portion of the leading edge of spatter bloodstains with impact angles nearer the perpendicular, as opposed to the often more distinct and directionally-isolated spines or individual tails of spatter bloodstains that contact target surfaces at more acute angles. As establishing directionality, ellipse fitting and the dimensional measurement of spatter bloodstains are related processes, any uncertainty in assigning directionality to spatter bloodstains is also likely to have an associated effect on the accuracy and reliability of the dimensional measurements of the bloodstain.

While uncertainty in the determination of both directionality and impact angle can have significant effects on the accuracy of any straight-line trajectory estimate, the numerical treatment of error in site of impact estimation has predominantly focused on impact angle estimation. This investigational bias may be the product of a number of factors, including:

- Directionality error being considered to be more controllable through appropriate spatter bloodstain selection.
- The aetiology and interpretation of directionality being less rigidly based on fundamental modelling assumptions.
- Directionality being a direct measurement, rather than an indirect measurement based on a theoretical mathematical relationship and formula.
- Quantitative uncertainty being limited to  $\pm 0.5$  degrees even when using relatively inaccurate protractors with 1-degree divisions, representing only a small degree of relative error given the potential 360-degree range.

The numerical treatment of the error in impact angle calculation is, however, not without its difficulties. The recent focus on definable error rates can be criticised in a number of areas. Firstly, studies have tended to focus on a single source, or limited sources of potential impact angle error. While this compartmentalised approach is arguably necessary in the identification and scientific investigation of the potential sources of error and how these may affect site of impact estimation, it is not without limitations. For example:

- It may not be possible to identify or quantify all of the potential sources of uncertainty operating in the specific circumstances of any particular estimate.
- Knowledge of the potential relationships between the individual source of error may be restricted.
- Any definitively quantified levels of error are unlikely to be universally applicable to all situations given the variable generation and manifestation of impact spatter patterns.
- The total level of uncertainty of a specific estimate could, as a result, remain largely unknown.

Secondly, while the majority of recent studies have been based on experimentation and numerical analysis, their conclusions have tended to be limited to making suggestions for the improvement of spatter bloodstain selection for inclusion within a site of impact estimate, rather than explicitly including and recording demonstrable error levels within the estimates themselves (e.g. Willis et al., 2001; Raymond et al., 1996b). The presence of these detailed scientific investigations into site of impact estimation error and uncertainty in the BPA literature do not, therefore, necessarily translate into a scientific application of their findings in practical estimation methodology. Where some form of numerical error range has been suggested, such as the general 5 to 7 degrees suggested by Bevel and Gardner (2002) to account for droplet creation dynamics in standard spatter bloodstains, the application of this range to a total estimate methodology is likely to be unworkable using physical site of impact estimation techniques.

A final consideration for the error of impact angle determination is that for spatter bloodstains observed in a horizontal plane any error in this angle only affects the vertical intersection of straight-line trajectories in site of impact estimation. Although these errors can be significant, the vertical plane, through the limitations in straight-line trajectory approximations, is already well recognized as containing a potentially significant degree of uncertainty, albeit not quantitatively determined. For spatter bloodstains observed in a vertical plane, however, the horizontal intersection of straight-line trajectories is also affected by any error in impact angle determination, as the horizontal component of this trajectory vector is dependent on both the directionality and impact angle of the spatter bloodstain. The propagation of this error into the resolution of straight-line trajectories in the horizontal plane could have considerable consequences for

computer-based site of impact estimation, as the trajectory intersections established in the accessible horizontal plane provided by these methods can arguably be attributed a greater degree of interpretational reliability (Carter, 1998 and 2001).

#### **4.7 Spatter Bloodstain Sample Selection**

Levels of site of impact estimation uncertainty can also be affected by the sampling methods employed in the selection of spatter bloodstains for use in any site of impact analysis. As Carter (1998 and 2001), and Carter and Podworny (1991) have suggested that theoretically only two straight-line trajectories, and the location of their intersection are needed to indicate the position of a site of impact. This theoretical proposition is, however, dependent on three main conditions:

- That both spatter bloodstains originate from the same impact event.
- That the straight-line trajectories accurately represent the flight-path of their causative blood droplets.
- That the trajectories intersect at, or close to the site of impact.

While the first condition is generally precluded in controlled experimental conditions, in casework settings more complex situations of multiple and overlapping spatter patterns are distinct possibilities. The presence of separate spatter patterns within an analysis environment increases the possibility that the intersection of any two spatter bloodstain trajectories may be coincidental, and not representative of the location of a common site of impact that the two spatter bloodstains do not necessarily share (Bevel and Gardner, 2002; Fischer, 1998). The second condition (the accuracy of a straight-line trajectory estimate) has already been demonstrated to contain at least some degree of uncertainty in both its vertical and horizontal resolution (see Sections 2.5.3 and 6.6). The reliance on a limited number of straight-line trajectories in constructing a site of impact estimate effectively increases the influence that any individual uncertainties present in these trajectory approximations can have on the final outcome of the estimate. While the third consideration is a source of estimate uncertainty because two droplets of even the same impact event do not share the same exact location of origin, they do not indicate this location, but some other point that is likely to be close to their respective origins if the spatial size of the impact event

is small. As a result, it is generally considered good practice to include a larger number of spatter bloodstains in a site of impact estimate, in an attempt to increase both the interpretational reliability, and investigation significance of any site of impact analysis (Lee et al., 2001; James and Sutton, 1998b; Bevel and Gardner, 2002; Raymond et al, 1996b; Carter 2001). The larger the sample of spatter bloodstains, and the more straight-line trajectories that intersect around a given location, the more confidence is typically attributed to this location as representing a 'true' site of impact (Bevel and Gardner, 2002).

How well any such sample corresponds to a 'true' site of impact can, however, be largely determined by the nature of the available spatter bloodstain evidence, the sampling strategy employed, and the level of analysis of the available data. In site of impact estimation the explicit selection of spatter bloodstains for inclusions within any analysis is typically based on a purposive sampling strategy. Specific spatter bloodstains that can be considered to provide as accurate as possible an approximation of a site of impact, both in terms of any potential uncertainty in their interpretation, and its correspondence to a vertical straight-line trajectory model where necessary, are selected by an analyst for use in the analysis. Typically selection criteria for a purposive sample can include factors such as:

- Well-formed, undistorted spatter bloodstains.
- Elongated spatter bloodstains, typically representative of an impact angle between 20 and 45 degrees (Reynolds, 2004a; Yen et al., 2003; Willis et al 2001).
- The exclusion of bloodstains that could be satellite spatter, or the result of droplet ricochet (Bevel and Gardner, 2002).
- Spatter bloodstains recorded on stationary target surfaces (Pizzola et al., 1986b; Bevel and Gardner, 2002).
- Spatter bloodstains that represent fast-upward moving droplets to correspond to a vertical straight-line trajectory hypothesis where necessary.
- Spatter bloodstain that bracket a site of impact to reduce the influence of straight-line trajectory estimate errors upon establishing intersection locations from spatter bloodstains in close proximity to one another (Carter and Podworny, 1991; Laber and Epstein, 2004).
- Spatter bloodstains of a size and distance from the site of impact that their causative droplets are unlikely to exhibit any shape oscillation on contact with the target surface (Raymond et al., 1996b).

- Spatter bloodstains that are not so small as to be prone to significant measurement error.

While such purposive sampling strategies are arguably fundamental in limiting the practical level of uncertainty in current estimate methodologies, they can also be an additional source of uncertainty within the wider application of site of impact estimation, and any assessment of its results. The size of a spatter bloodstain sample, for example, is usually limited either by physical or time constraints imposed by the specific estimate technique employed. Even in computer-based analysis, which has the potential to analyse considerable numbers of spatter bloodstains, a large sample in a typical site of impact estimation can be considered to be 20 droplets or more, with traditional stringing methodologies typically using less (Bevel and Gardner, 2002). Where such sample sizes only make up some proportion of the purposive population of interest, some uncertainty in the resulting estimate can stem from the fact that the result of the analysis is an estimate of some wider population parameter. Depending on the distribution of the population, and the sampling strategy employed, the results of several estimates from different samples of a single population are likely to vary to some degree.

A second, but associated issue is that the specific characteristics of, and relationships between the total spatter bloodstain population, the purposive population of interest, and the selected sample of spatter bloodstains are largely undetermined in current site of impact estimation techniques. This is predominantly a product of practical limitations, as the exhaustive manual recording and interpretation of even an entire population of interest, from an impact spatter pattern composed of potentially several hundred individual spatter bloodstains, can be unrealistic in casework conditions. It does, however, present site of impact estimation with a situation where the potential variance in estimate results, the representativeness of any particular sample selected with regard to the larger population of interest, and the appropriateness of any extension of the analysis of sample data to the population from which it was drawn, are largely unknown.

The ability to assess and accurately represent the uncertainty in the data under investigation takes on additional significance in computer-based estimation techniques, whose results are frequently reported in terms of a precise statistical description of the available intersection data. For many statistical descriptions of

a data set to have a consistent, and interpretatively appropriate meaning, some knowledge, or assumption regarding the distribution of the data that is being described is often necessary. Current computer-based techniques, despite numerically evaluating all straight-line intersections selected for analysis, give little explicit consideration to the distribution, or multivariate spatial nature of this intersection data. In attempting to simplify the interpretation of potentially large and complex spatial intersection data sets current techniques arguably provide only a limited and potentially inappropriate set of statistical tools through which data is analysed, and results are often evaluated and reported. This situation can be highlighted by a consideration of the numerical techniques of BackTrack<sup>®</sup>/Win, which provides a mean point average of the intersection data, as well as the standard deviation in each axis. Both of these statistical measures, however, are sensitive to the nature of the distribution of the data they are used to describe, and considered in isolation do not consistently provide a good approximation of either the central tendency, or the distribution of the data around this point. The mean of a data set, for example, is not necessarily an appropriate measure of central tendency in distributions that are skewed, have any extreme outliers, or are clustered around two or more locations within the data set, as exemplified in Figure 4-9.



*Figure 4-9 - Five idealised intersection patterns that produce a mean point average at their centre, but are considerably different in their distribution around this point.*

The standard deviation of a data set, being the result of a mean squared distance function, is also sensitive to outliers in the data, and only provides an a-directional measure of dispersal around a mean point. In a multidimensional data environment, standard deviations reported in isolation are further limited, as they are indicative of the marginal distributions of the data in each axis, but do not provide any information on the joint distribution of the data, or how the data varies between the axes. The practical limitations of this type of statistical description are highlighted by the developers of BackTrack<sup>®</sup>/Win, who stipulate that the inclusion of the standard deviation to indicate the spread of intersections around the mean is only an investigative aid, and is not entirely suitable for the reporting of estimate results (Forensic Computing of Ottawa, 2001b). The

development of computer-based methods has provided the means for a more detailed examination of intersection data compared to other site of impact estimation techniques, both in terms of the increase in size of potential data sets upon which to base estimates, and the numerical processing power available for their investigation. Uncertainty in an estimate, however, can also stem from the fact that the numerical precision possible using computer-based techniques is higher than the accuracy with which a phenomena can be described, or the evidence of it can be acquired and analysed (Zhang and Goodchild, 2002; Bevel and Gardner, 2002). The currently available techniques may, consequently, be limited by the level and nature of the numerical analyses they conduct, and the appropriateness of these typically point-based summaries to the dynamic nature of impact events, and the aims, methodologies, and quality of data available to site of impact estimation. This situation is exemplified by the fact that while the more straight-line trajectories that intersect around a given location are typically associated with an increased level of confidence in a site of impact estimate, little explicit quantitative investigation of the spatial distribution of this data is actually undertaken in the analysis and interpretation of the results of site of impact estimation (Bevel and Gardner, 2002). This may be of increasing significance as sample sizes grow because for any given increase in the number of spatter bloodstains considered during an estimate there is a considerably greater increase in the number of possible trajectory intersections, as illustrated in Figure 4-10. Point-based summaries arguably become even less appropriate in conveying the spatial distribution, variation, and clustering of these larger spatial intersection dataset.

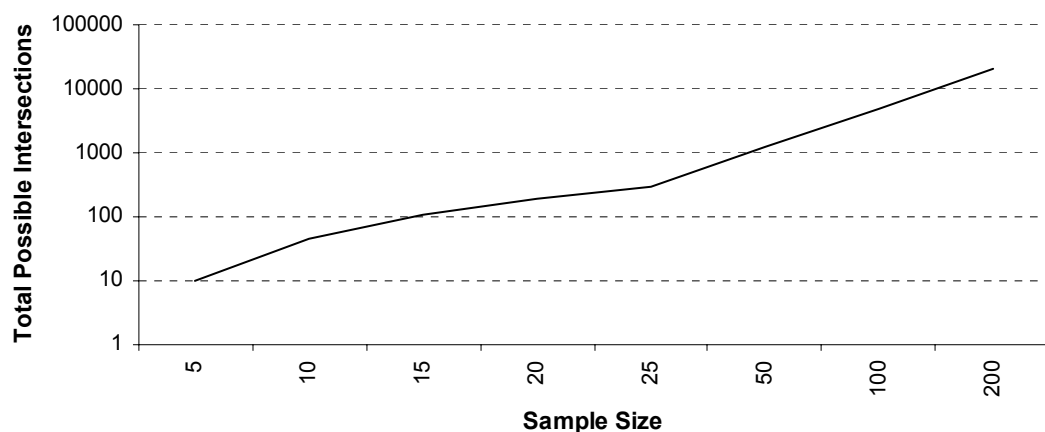


Figure 4-10 – A graph to show the increase in the number of potential trajectory intersections with the increase in spatter bloodstain sample size.



A review of some of the experimental proofs of the BackTrack™ suite can highlight a number of the issues surrounding spatter bloodstain sampling, and the accuracy and appropriate representation of the data upon which site of impact estimate results are based. Carter (1998 and 2001), for example, has shown that the accuracy obtainable in a horizontal site of impact estimate can be within 5cm of a known impact site in both axis in relatively simple cases using 6 and 12 bloodstains on a single vertical target surface. Other experimental data, collected by Dr. Carter and the Royal Mounted Canadian Police, consisting of 40 individual spatters on 11 different surfaces, and supplied with BackTrack®/Win (see Figure 3-14), can be used to show that the accuracy obtainable in more complex situations using the automatic averaging function of the software can be within 7cm of the known impact site in either horizontal axis (Forensic Computing of Ottawa, 2001b). While the difference in accuracy between these two conditions is negligible given the variable and dynamic nature of impact events, the standard deviations of the mean in each axis are considerably different, being approximately 2.5 cm in the first case, and 20 cm in the final case (a standard deviation is not reported in the second case). Although the sampling strategies employed in each case are not known, and the distribution of the intersection data is not known in any detail beyond that provided in the standard deviation of the mean, the results can highlight a number of issue surround numerical site of impact estimation. Firstly, the results go some way to indicating that the more spatter bloodstains used in an analysis, and the more complex a situation is, the larger the potential variation there can be in a site of impact estimate. This is hardly a surprising point, however, given the variable nature of individual straight-line trajectory estimates, and the fact that in selecting six spatter bloodstains a total of only 15 intersections are possible, whereas for 40 spatter bloodstains some 780 trajectory intersections can occur. Even where the bracketing intersection strategy of BackTrack®/Win is used as part of its automatic averaging function the maximum number of possible intersections are still nine, and 400 respectively. The difference in the scale of data between the two conditions is considerable. Secondly, while the results do suggest that an estimate can correspond well to the location of a site of impact with the appropriate selection of just a few spatter bloodstains, the larger degree of variation in the latter experiment can be used to reinforce the potential dangers of such a limited selection. As the intersection data of the larger sample appears to be widely spread about its mean estimate, the construction of an alternative estimate using only six spatter bloodstains from the 40 recorded would utilise a maximum of only nine out of the potential 400 intersections analysed, and could

provide a considerably different mean point estimate. Thirdly, in casework conditions, where no independent standard against which to test an estimate is likely to be available, the differentiation between an accurate and erroneous estimate based on a limited number of spatter bloodstains may not necessarily be possible. The only other consistently available evidence against which to test any results are likely to be the remaining evidence of the impact event, the other spatter bloodstains within the impact spatter pattern. While larger samples may provide a less precise estimate than a smaller sample in terms of the spread of the intersection data, the interpretational base for the evaluation of its results could ultimately be more representative of the evidence of the impact event.

The combination of purposive sampling strategies and the restricted analysis of intersection data can leave an additional issue in site of impact estimation open to question. What sort of confidence should be attributable, or how could any data be effectively used, in situations where no 'appropriate' spatter bloodstains are present? The reliance on the selection of spatter bloodstains in current site of impact estimation methodologies to reduce, rather than explicitly include and analyse uncertainty in intersection data, arguably can restrict both the interpretational value and application of site of impact estimation in situations that may be critical to a particular CSR but where no 'appropriate' spatter bloodstains exist. While the assessment of estimate accuracy remains essentially qualitative, the construction of a site of impact estimate in such circumstances may be consistently considered to have a low confidence level, or may not even be attempted without any detailed consideration being given to the potentially available intersection data. To broaden both the application and interpretative potential of site of impact estimation, alternative investigational methodologies are likely to be necessary. The morphology of the majority of spatter bloodstains in an impact spatter pattern that are not significantly distorted can, after all, be considered to contain some information on the trajectory of the blood droplet that formed them. Current questions asked of these spatter bloodstains amount to how appropriate are they in informing about a site of impact, and to what extent a straight-line trajectory estimate can be accurately inferred from them. An alternative but equally pertinent perspective that might be explored is to what extent can the information available be applied in an estimate regardless of its potential quality. The methodology of traditional stringing, for example, relies heavily on straight-line trajectory estimates that can be considered to be representative of a droplet's trajectory in a vertical plane in order to provide reasonable estimate accuracy. The development of computer-based analysis has

increased the range of spatter bloodstains that can be considered useful, with spatter bloodstains whose straight-line trajectories provide both good, and poor vertical approximations being usable in the resolution of a horizontal site of impact estimate (Carter and Podworny, 1991; Carter, 1998; Carter, 2001). The data available to each method remains the same, but the alternative treatment of the construction of the estimate enables a wider application of the physical process of estimation and its potential results.

Arguably this situation is compounded by the fact that the current application of selection criteria is essentially subjective, relying on the skill of the analyst in identifying, selecting and interpreting spatter bloodstains that are 'appropriate' to the aims of the analysis. As Wonder (2001) points out, while computer-based estimation may be able to more accurately assess the data that it is supplied, the selection, and therefore quality of this data, is still reliant on the analyst. The subjective application of selection criteria is emphasized further by the fact that spatter bloodstain selection criteria do not represent an absolute set of universal rules applicable to all impact spatter patterns, in all circumstance, or applied by all analysts. In their practical application, the specific selection criteria employed by an analyst can be considered to be more akin to a sliding scale where some compromise is reached between the various identifiable and controllable potential sources of estimate error in a particular impact spatter pattern, in an attempt to provide the best possible estimate given the available evidence. As Bevel and Gardner (2002) stress, however, there are no perfect spatter patterns. Just as the dynamic nature of impact spatter pattern creation means that a particular pattern is unlikely to correlate perfectly with either velocity- or descriptive-based categorisation, so an ideal set of spatter bloodstains in terms of the theoretical and interpretational accurate representation of a site of impact are just as improbable.

#### **4.8 Conclusions**

While some doubt has been cast on the position of BPA within forensic science as a scientific discipline, the reconstructive aims and methodology of BPA can be considered to be based on the application of science, of scientific techniques, and of experimental research in the construction, comparison, and discrimination of possible scenarios surrounding an incident from the available bloodstain pattern evidence. Site of impact estimation is arguably at the forefront of this application

of science. The interpretation of the spatial origin of an impact spatter pattern represents an area of investigation within BPA that involves the explicit application of aspects of physics, ballistics, fluid dynamics, blood biochemistry, and mathematics. The information derived from these fields combines to aid the analyst in constructing useful information about an event segment, the specific spatter-producing impact, from its resultant bloodstain evidence. In conjunction with other interpretative aspects of bloodstain evidence, this locative analysis of the evidence can subsequently provide significant investigative information concerning the event itself, and the dynamic scenario in which the impact took place.

Locating the position from which an impact spatter originated can be an important element in reconstructing a crime scene, and the application of site of impact estimation is both a long established, and widely accepted facet of BPA (Emes and Price, 2004; Bevel and Gardner, 2002; Raymond et al., 1996b). The fundamental principles of site of impact estimation, the directionality and impact angle of spatter bloodstains, have been documented features of BPA since the early to mid 20<sup>th</sup> century, and while the origin of practical techniques of site of impact estimation is debatable, the traditional stringing technique has been in existence since at least the 1970s. Site of impact estimation, and the general principles of reconstructing the trajectories of spatter-causing blood droplets are typically considered as standard procedures in BPA, and are often taught as part of modern basic BPA training courses (Raymond et al., 1996b; Bevel and Gardner, 2002; IABPA, 2004c; IAI, 2004). Of the different techniques for establishing a site of impact estimate that can, and have been used effectively in site of impact estimation, computer-based techniques are beginning to predominate as the analytical methods of choice within the BPA community. The benefits to site of impact estimation that computer-based techniques have provided have led to claims that the precise mathematical treatment of trajectory approximation; the separation of these 3D trajectories into potentially unbiased horizontal and more variable vertical aspects of an estimate; the consistent methodological treatment of spatter bloodstains observed in either a horizontal or vertical plane; the numerical representation of the physical evidence and numerical construction of an estimate; and the potential for the re-evaluation of evidence:

'...satisfies the criterion of a sound scientific methodology (Carter, 2001).'

While this assertion can be considered to be true in terms of a methodological and interpretative comparison to the other common site of impact estimation techniques, current computer-based estimation techniques are not without their limitations. Some of the specific limitations of these techniques, such as the decontextualisation of analysis, and the need for increased numbers of measurements in a tightly controlled 3D coordinate system are beginning to be addressed to a certain extent by the inclusion of site of impact estimation techniques within 3D crime scene capture and analysis technologies. Other limitations, however, stem from the theoretical and methodological foundations of site of impact estimation that employ systems of evidence investigation, interpretation and evaluation that are intrinsically prone to uncertainty. The discussion of site of impact estimation in this chapter has arguably demonstrated that aspects of uncertainty are present in the site of estimation process from the theoretical definition and approximation of the impact site, and the theoretical justification for impact angle calculation; through the practical processes of spatter selection, the dimensional interpretation of spatter bloodstain morphology, and the practical limitations imposed by the inability to fully incorporate droplet flight dynamics; and culminating in the potential restrictions placed on the interpretation of the results of an estimate by a general lack of explicit consideration of such uncertainty, and the specific numerical methods employed by current computer-based site of impact estimation techniques in representing the potential available estimate data.

Even though uncertainty has been shown to be largely pervasive throughout site of impact estimation theory and practice, it does not necessarily preclude the process from achieving a level of accuracy that is typically considered sufficient for practical reconstruction purposes. The results of an estimate often allow an analyst to determine with some degree of confidence locations within a crime scene from which an impact spatter pattern could and could not have originated (Emes and Price, 2004; Bevel and Gardner, 2002; MacDonell 1997 cited in Brady et al, 2002). While this practical level of accuracy has proved effective within BPA and the discipline's reconstructive aims, it is debateable as to what extent this 'practicality' can satisfy the more rigid investigative and conclusive criteria that is increasingly demanded from the scientific and technical interpretation of evidence in legal contexts.

The discussion of site of impact estimation uncertainty in this chapter has highlighted a number of potential research questions that may be of significance in terms of the future of the practical and theoretical application of computer-based site of impact estimation, as well as its grounding in scientific implementation, investigation and interpretation. Firstly, could the investigation of site of impact estimation benefit from a more explicit and considered 3D volumetric estimation process? While one of the main advantages of computer-based techniques is the consistent and appropriate 3D treatment of trajectory approximations in establishing horizontal and vertical estimates, the detailed spatial nature of the intersection data generated during this analysis is largely suppressed. The point-based numerical representations of the results of an estimation process has been identified as a potential limiting factor in current computer-based estimation methods, and arguably represents a reduction in dimensionality not only in terms of the representation of the data upon which the results of an estimate are based, but also in terms of the dynamic spatio-temporal nature of impact events themselves and the general level of uncertainty present in the estimation process (Bevel and Gardner, 2002). Additional questions could therefore be asked as to whether a more explicit consideration and visual representation of the 3D spatial nature of the investigative process, and the data upon which it relies, could provide a more appropriate and informative analytical tool in the construction of site of impact estimates. Similarly, whether the identification, evaluation and provision of alternative statistical and spatial analyses of site of impact estimation data can provide a more detailed, representative, and informed assessment of the evidential basis of the estimate, and so provide a firmer basis for the consideration and evaluation of the spatial conclusions required from locative reconstructive aims of the process? The explicit development, evaluation and discussion of 3D volumetric and spatial approaches to conducting and representing site of impact estimations will more than likely become a necessary part of computer-based site of impact estimations. With such a methodological shift prompted by a move towards fully interactive 3D investigative and presentational environments, and as the need for a more appropriate statistical or probabilistic approach to the inference of results, in which other areas of forensic scientific investigation are becoming increasingly entrenched, becomes explicitly required of BPA and CSR conclusions.

Secondly, how can some assessment of the uncertainty that is pervasive within site of impact estimation be explicitly incorporated within an estimate, and inform the conclusions generated from its results? In scientific investigation, the

assertion of a best estimation of some analyses without explicitly stating the error or uncertainty present in establishing the estimate can be potentially misleading. Without some explanation as to how a level of uncertainty was determined, even the provision of some level of confidence in the reporting of an estimate can be ambiguous (Taylor, 1997). This can be of considerable consequence for forensic disciplines as the role of the forensic expert is not only to analyse the evidence, but to testify to the worth of the results of this analysis, and by extension the worth of the evidence itself in the context of some legal process (Aitken, 1995). In site of impact estimation it has been demonstrated that such a measured inferential process is not without its practical difficulties. The sources of error within site of impact estimation are both numerous and varied, and while some quantification of specific error rates has recently been undertaken, the potential problems with identifying, quantifying and applying error rates to specific site of impact estimation circumstances and processes have largely precluded the generation of any model of total estimate error. While the quantitative investigation of error within specific areas of site of impact estimate has provided additional criteria for purposive sampling strategies, the qualitative assessment of error that this allows does not necessarily correspond to a scientific demonstrable, quantifiable, and comparable level of uncertainty, with which differing reconstructive hypotheses could be explicitly and consistently evaluated. Within the numerical and visual representation of site of impact estimation produced by computer-based methods, such considerations of uncertainty can be additionally significant, as an experienced user may know that the quality of their data is not reflected by the quality of the graphical or numerical output, but they cannot necessarily benefit from this knowledge as the level of uncertainty in the data remains largely unknown (Heuvelink, 1998). In current techniques this arguably is compounded by the fact that the common point-based numerical representations of an estimate typically reduce the scale of the available data, which could, if approached differently, at least provide some assessment of the uncertainty of the result of the estimate in terms of how well it represents the data upon which it was based, if not a level of uncertainty associated with how well this result is likely to correspond to an actual impact site. The questions could therefore be asked as to what extent could the provision of alternative statistical and spatial analyses of the intersection data in site of impact estimation provide a more detailed and representative assessment of the uncertainty in the construction of an estimate. Alternatively, it could also be asked as to what extent could computer-based analysis of site of impact estimation evidence be extended to provide a more standardised and quantifiable approach to aspects of

the estimation process, like ellipse fitting, where some computer-assisted analysis is already aiding investigation. Could a less subjective approach to the quantitative description of spatter bloodstain morphology begin to provide the investigation of a site of impact with some degree of reproducible quantitative, and quantifiable qualitative analysis of the evidence upon which the analysis depends?

Finally, could site of impact estimation benefit from a more structured approach to its sampling procedures? While purposive sampling strategies are routinely employed in site of impact estimation techniques the undetermined nature of the sample taken, and the subjective and variable application of the selection criteria pose a number of questions for the practice of the locative estimation techniques. For example, the specific sample selected during the construction of an estimate is largely undetermined in terms of how representative it is of the population of interest it was selected from, or its relation to the wider spatter bloodstain population, the entire impact spatter pattern. The question could as a result be asked, as to whether more could be learned about, and inferred from site of impact estimation where a more comprehensive assessment of an entire spatter pattern is undertaken, and the nature of the chosen sample, and its relationship to the remaining spatter bloodstain evidence is explicitly investigated. Could the complete enumeration of entire spatter bloodstains under experimental conditions also indicate other approaches to sample selection that might be useful in the construction of a site of impact estimate? The effect that the selection of an undetermined sample might have on the uncertainty of the estimate itself may also be a pertinent area of investigation. In the evaluation of forensic evidence an estimate may be considered to be good if it is both accurate and precise, in that its measure is both close to the true value of the parameter of interest, and the variability of repeated estimates is low (Aitken, 1995). While some research into the variability of the fundamental process of site of impact estimation, such as impact angle determination, has been conducted, most experimental proofs of site of impact estimations are typically based on the appropriate selection of spatter bloodstain (see Section 4.7), and although largely proving a reasonable level of precision, have not tended to address issues of reproducibility, or potential variability in their results (Willis et al, 2001; Carter, 1998 and 2001; Pace, 2004a; Brady et al., 2002). The question could therefore be asked as to how any particular estimate may differ if an alternative but equally appropriate sample were selected from the same population of interest, and how appropriate any single estimate methodology may be in assessing the extent of the data that



may be indicative of the location of an impact site. The application of idealised spatter selection criteria in an attempt to minimise estimate uncertainty, and by extension assign some level of qualitative confidence to an estimate is also the source of a number of questions. Given the potential subjective and variable application of selection criteria, that may result from the highly variable generation and manifestation of impact spatter patterns, the question could be asked as to what extent does a qualitative assessment of uncertainty correspond with some quantifiable level of uncertainty. By extension, perhaps a more pertinent question in expanding the interpretative potential of site of impact estimation could be what level of confidence should be attributable, or how could any data be effectively used, in situations where only less appropriate or no appropriate spatter bloodstains are present, but a site of impact estimation may be critical to a CSR, and a wider criminal investigation?

In conclusion, the potential sources of estimate uncertainty identified during the discussion of site of impact estimation techniques have been addressed separately in an attempt to isolate distinct research areas that could be addressed as part of this research project. The combination of these potential sources, when viewed as part of a whole system of evidence interpretation, however, could present site of impact estimation with its most challenging question. This question, or questions like it, could, and may well be asked in defining the future of site of impact estimation and specifically computer-based methodologies as part of a scientific and technical toolkit for the forensic investigation and reconstruction of crime scenes. Given:

- The relatively subjective qualitative assessment of estimate accuracy based on spatter selection.
- The potentially variable application of standard site of impact estimation procedures.
- A generally undetermined total estimate error rate.
- The limited interpretation, representation, and evaluation of the potentially available evidential data.

To what extent can current site of impact estimation techniques provide a sufficient means for the assessment of confidence in their results, and the potential investigative significance of these results, if this is to be conducted under the auspices of, or at least satisfy, some scientific or technical investigative paradigm? Bevel and Gardner (2002) have suggested that computer-aided

analysis is an area that is ripe for development within CSR and BPA, allowing the analyst to test beliefs regarding an event, determine if the data available matches the circumstances, and in general allow for more in-depth analyses. They, go on to state, however, that unfortunately little effort has been put into exploring and defining the future of computers in these fields, and that a number of issues including the scientific validity of the 3D reconstructions and presentations of these techniques require explicit investigation. Computer-based site of impact estimation has been in development for over 20 years, and is becoming increasingly entrenched within BPA. While one imminent future for computer-based site of impact estimation appears to be its integration within wider 3D crime scene capture, reconstruction and investigation technologies. An alternative, or complementary future, which the research project presented in the remainder of this thesis will set out to investigate, is how site of impact estimation could benefit from the explicit investigation and incorporation of the uncertainty inherent in this 'reconstructive' estimation process within the analysis, evaluation, and presentation of its results, and how this might be achieved.

#### **4.9 Proposed Investigation**

The remainder of this thesis will describe, discuss, and evaluate the attempts made to address a number of the issues highlighted in the discussion of site of impact estimation, through an experimental computer-based analytical research design. The proposed investigation into the construction of site of impact estimates and estimate uncertainty will involve three distinct processes. Firstly, a series of experimental impact spatter patterns will be generated to provide raw spatter bloodstain data for the construction and analysis of site of impact estimates. The creation of new experimental impact spatter bloodstain data will be necessary to provide a degree of control over the spatter-producing impact event both in terms of the impacting mechanism and providing a known location of the site of impact against which spatter bloodstain data, and constructed estimates can be compared. The generation of new experimental impact spatter patterns will also provide the potential to record and analyse entire impact spatter patterns. To provide this level of data, a manual spatter bloodstain recording technique will be developed and implemented, which will provide a total enumeration of the observable experimental impact spatter patterns, in terms of the information required on each spatter bloodstain for the construction of a site

of impact estimate. It is envisaged that such an extensive recording process will provide sufficient spatter bloodstain data to enable a detailed analysis of the composition of an impact spatter pattern and any specific spatter bloodstain samples drawn from it for the purposes of estimate construction. The comprehensive nature of the data collected could also form the basis of a database of spatter bloodstain information, which could make available an evidential base for future research into the interpretation of impact spatter patterns, and the construction of site of impact estimates.

Secondly, the design, development and implementation of a computer-based site of impact estimation system will be undertaken to provide a number of innovative features for the analysis of the large-scale spatter bloodstain data sets. This site of impact estimation application will perform a number of analytical functions in an attempt to enhance the amount and type of data generated during the construction of an estimate, and develop the inferential and evidential potential of computer-based estimation procedures. The analytical estimate system will provide methods for the precise and detailed selection of spatter bloodstain samples, and the characterisation of the composition of collections of spatter bloodstains to facilitate the investigation, comparison and evaluation of alternative spatter bloodstain sampling strategies. Alternative methodological approaches to the investigation, description and analysis of the straight-line trajectory intersection data sets, which constitute the basis of a site of impact estimate, will also be examined. These will include a range of statistical techniques to provide a comprehensive descriptive assessment of the distribution of trajectory intersections with any particular estimate, and the application of analytical methods developed specifically for the investigation of spatially referenced data. An integrated interactive virtual 3D CG investigative environment will be produced to aid the investigation and evaluation of the potentially large amount of complex data generated through the approach to the analysis of a site of impact estimate adopted during this project, and facilitate the presentation and dissemination of this technical data to others. Two alternative approaches to the construction and analysis of site of impact estimates will also be utilised in an attempt to provide a two-fold assessment of the uncertainty the estimation process. The first approach will construct and analyse the potential uncertainty in a single site of impact estimate, while the second approach will facilitate the investigation of the variation between estimates constructed using identical sampling strategies.

Thirdly, the analytical site of impact estimation computer application developed for this research project will be utilised in the analysis of the experimentally-produced impact spatter patterns, and a series of site of impact estimates constructed from them. A number of spatter bloodstain sampling strategies will be examined, and their ability to accurately indicate the location of the known impact sites for each experimental impact spatter pattern will be assessed. The degree of estimate uncertainty both within and between specific spatter bloodstain samples will be analysed, and an evaluation will be conducted of the innovative techniques introduced to site of impact estimation during this research project, in terms of their ability to inform, and improve upon the interpretative potential of site of impact estimation techniques, and the application of computer-based analyses and 3D CG reconstructions within this field of forensic crime scene investigation and reconstruction.

#### **4.10 Project Outline**

The methodologies employed and results achieved during the investigation of estimate uncertainty undertaken within by research project are presented in the remaining eight chapters of this thesis. Chapter 5, Impact Spatter Experimentation, will describe the methodology employed during this research project in the generation of a number of experimental impact spatter patterns, including the impact method, target surface configuration, and blood source used. The manual total-pattern recording procedure developed and implemented during this project, to provide the level of spatter bloodstain data necessary for the proposed investigation of site of impact estimation and estimate uncertainty, will also be outlined, and a number of issues will be raised concerning the validity of the extension of the experimental data generated and collected to casework conditions.

Chapter 6, Sampled Photographic Recording, will describe an additional pilot project conducted into the development and implementation of a procedure to rapidly record large amounts of potential spatter bloodstain information. The sampled photographic methodology developed for the purposes of recording two additional impact spatter patterns within a mock crime scene environment will be discussed, and the potential for the future development and implementation of such methodologies in the construction of site of impact estimates and investigation of estimate uncertainty will be examined.

Chapter 7, Spatter Bloodstain Image Analysis, will describe an additional pilot project conducted during the research into site of impact estimate uncertainty. The development of a prototype automated image analysis procedure for the quantification of spatter bloodstain morphologies will be discussed, and the results of this analysis examined in relation to the ability of the procedure to provide accurate and reproducible quantitative spatter bloodstain data for the purposes of the construction of site of impact estimates.

Chapter 8, Data Pre-processing and Pattern Characterisation, will introduce the analytical site of impact estimation computer application developed as part of this research into estimate construction and uncertainty. The choice of programming language, and development and run-time environments made for the design and implementation of the analytical research application will be described initially. The specific procedures through which the raw spatter bloodstain data is processed for the purposes site of impact estimation, and the methods used to characterise any collection of spatter bloodstains analysed for the purposes of comparing the composition of spatter bloodstain patterns and samples will subsequently be discussed.

Chapter 9, Site of Impact Estimate Construction and Analysis, will describe and discuss the methods through which the analytical site of impact estimation application constructs and analyses site of impact estimates. The vector-based establishment of straight-line trajectory intersections, and the construction of three alternative trajectory intersection data sets, which correspond to different approaches to the interpretation of trajectory intersection data, will be outlined. The various univariate and multivariate statistical techniques employed in an attempt to provide detailed descriptions of the distribution of trajectory intersections within an estimate will be described and their inferential potential discussed. The application of a number of theoretical concepts and practical techniques of spatial data analysis, which explicitly incorporate ideas of stochastic processes, data uncertainty and spatial relationships within the investigation of data situated in a spatial context, will also be described, and their possible utility in aiding the interpretation of site of impact estimate evidence examined. The two alternative estimate construction methods developed and implemented through the analytical site of impact estimation application will also be discussed.

Chapter 10, Three-Dimensional Estimate Visualisation, will describe the development and implementation of the 3D CG data visualisation component of the analytical site of impact estimation application developed during this research project. The chapter will introduce a number of issues surrounding the production of investigative and presentational 3D CG visualisations within a legal context before discussing the choice of programming language, and the development and run-time environments of this integrated component of the analytical estimation application. The visualisation methodology employed, and specific 3D CG geometries and shading strategies applied in the visual presentation of the detailed numerical data generated during the investigation of a site of impact estimate will be described. The potential benefits of an interactive 3D CG spatial approach to the analysis, evaluation and presentation of site of impact estimation will also be addressed.

Chapter 11, Experimental Data Analysis, will describe a number of the specific analyses conducted using the spatter bloodstain data collected from the experimental impact spatter patterns and the analytical site of impact estimation application. The results of these analyses will be discussed in relation to the uncertainty inherent within the process of site of impact estimation, as well as the potential implications that the results may have for the practical application of the current state of the theory and practice of site of impact estimation.

The final chapter, Research Conclusions, will discuss the implications of this research for the current application of the reconstructive aims and techniques of site of impact estimation. Possible future directions for the advancement of site of impact estimation will be discussed with regards to securing a firm grounding within sound scientific principles of data collection, investigation and analysis, as well as increasing the potential utility and admissibility of any reconstructive conclusions derived from its application will also be addressed.

## **5 Impact Spatter Experimentation**

### **5.1 Introduction**

This chapter will outline the experimental impact spatter pattern generation, and recording processes conducted as an integral part of the proposed investigation into site of impact estimation, and the potential future use of computer-based analysis in this area of BPA. The chapter is divided into three main sections. The first section will describe the experimental generation of four impact spatter patterns used to provide the raw spatter bloodstains for the subsequent construction and analysis of site of impact estimates. The second section will outline the exhaustive identification and recording procedure conducted in order to convert the raw spatter bloodstain evidence into usable site of impact estimation data for the purposes of this research project. The final section will discuss a number of the issues raised during the experimentation and exhaustive recording processes, and how these may impact on the investigation of site of impact uncertainty within this research project.

### **5.2 Experimental Impact Spatter Patterns**

A series of experimental impact spatter patterns were produced to provide the raw impact event and impact spatter pattern data that would be used to construct site of impact estimations and provide the basis for the analysis of the research aims identified during this project. The generation and recording of new impact spatter pattern data was necessary to provide control over the experimentation in terms of both the locations of the impact sites and the nature of the impact events, as well as to conform to the aim of total spatter enumeration which would enable the investigation and comparison of population and sample spatter bloodstain composition. The creation of new impact spatter patterns, with a total spatter recording methodology, would also provide the potential foundations for the general aim of establishing an impact spatter pattern database from which future research can be conducted.

### 5.2.1 Experimentation

The experimental impact spatter patterns were produced in collaboration with Forensic Alliance Limited<sup>1</sup> (FAL), a commercial forensic science laboratory who provided both practical BPA expertise and the necessary facilities and materials for the experimentation. The forensic scientists at FAL are routinely involved in BPA experimentation for the purposes of the investigation of specific casework bloodstain patterns, conducting general bloodstain pattern research, and in the training and continued evaluation of their bloodstain pattern analysts. The impact spatter experimentation was conducted in a purpose-built bloodstain pattern experimentation facility at FAL's Culham laboratories in Oxfordshire. This experimentation environment was a cuboid structure with one wall open to allow access to the experimentation area and provide a wide viewing angle for the recording of experimental bloodstain-producing events (Figure 5-1).



*Figure 5-1 Bloodstain experimentation area at FAL's Culham laboratories (left), and a vial of the blood used during the impact spatter experiments (right).*

The walls of the experimentation structure were constructed using a rigid pole frame covered by stiff cardboard, which was covered with a layer of white lining paper. For the purposes of this experimentation an additional layer of brown

---

<sup>1</sup> Forensic Alliance Limited. F5 Culham Science Centre, Abingdon, Oxon. OX14 3ED. Special mention is required for Jennie Lewis and Pam Hamer for organising the use of these facilities, and Martina Boatfield who assisted in conducting the experiments.



paper was added for each experimental impact event to provide a detachable target surface. The use of such a removable target surface was considered necessary to both maximise the limited time available at this facility, as well as provide the physical record of the impact spatter patterns, which would have to be examined over a larger time scale than usual, given the innovative total spatter recording methodology proposed.

The blood source used throughout the creation of the experimental impact spatter patterns was human blood taken by the National Blood Service (NBS, 2005) for the purposes of transfusion, but which had passed its date for safe use in medical contexts (see Figure 5-1). The handling of this human blood, and the application of impacting forces to it, was conducted under strict health and safety conditions which were already in place, as FAL conduct a number of studies with this type of human blood and spatter-producing methods (Appendices A to D). The blood used during this experimentation was taken from the same batch of transfusion blood, and was at approximate room temperature when subjected to an impacting force.

### **5.2.2 Impact Method**

Two alternative impact methods were compared to determine the most appropriate for use in the generation of the experimental impact spatter patterns, given the aims of this research. The two methods investigated were:

- The closing of a mouse and rat trap mechanism on a blood source.
- The manual application of an impact force by striking a blood source with a hammer.

While the trap mechanisms provided the opportunity to generate relatively tightly controlled and reproducible impact events, the spatter bloodstain distributions produced using this method tended to be restricted in terms of area of the target surface covered, which were predominantly composed of relatively small size of spatter bloodstain, as illustrated in Figure 5-2. The creation of impact spatters through the manual hammer application method, while being more variable in terms of the size and nature of the impacting force between each impact event, produced a significantly more spatially diverse bloodstain pattern with a generally larger size of individual bloodstains (Figure 5-3). This method of impact was also

considered to be more representative of the type of impact events and resulting spatter bloodstain distributions encountered at crime scenes, and more appropriate for the extension of any of the findings of the research to cases of impact spatter patterns resulting from incidences of blunt force trauma. While the more unpredictable nature of this manual application of an impacting force arguably introduces a greater source of impact spatter pattern variation, this was not considered to be contrary to the aims of the research, the investigation of the general application and the evaluation of the process of site of impact estimation.

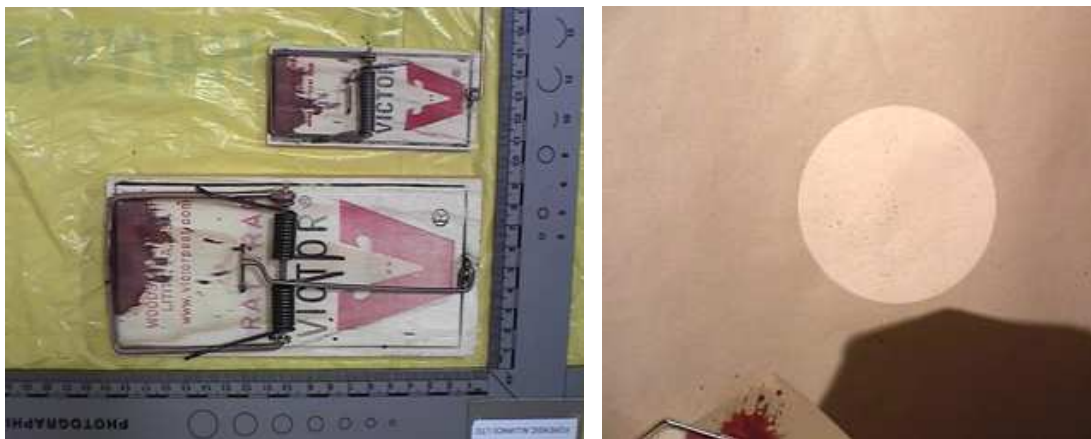


Figure 5-2 Mouse and rat traps used in the initial assessment of impact method (left), and the resultant bloodstain spatters highlighted on the target surface (right).

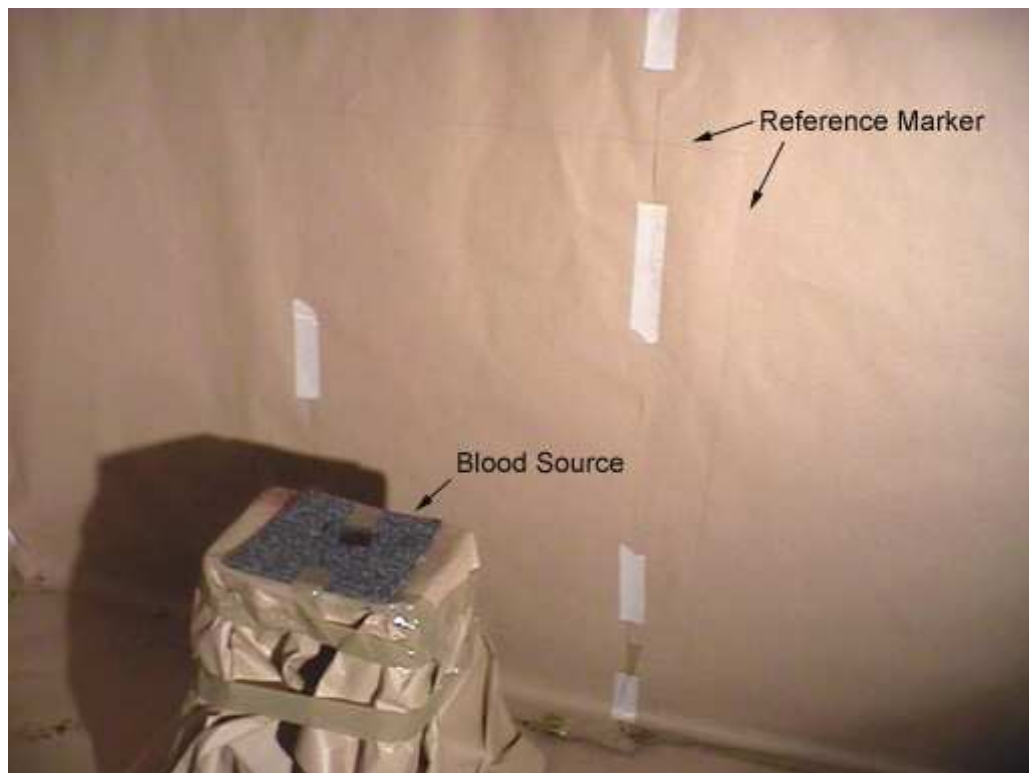


Figure 5-3 Blood source with scale (left) and hammer covered in plastic to avoid excessive contamination (right).

### 5.2.3 Target Surface

A single target surface model was decided upon for the investigation of site of impact estimation in this research project. The use of a single target surface as

the recording medium for impact spatter bloodstains was considered to be a logical starting point for the analysis of site of impact estimation methods from which subsequent and increasingly complex experimental scenarios and site of impact estimation processes could be compared and analysed in future research. To provide a reference from which the spatter patterns could be measured relative to the co-ordinate system of the experimentation environment during the later recording stages, a horizontally and vertically levelled reference marker was drawn onto the removable brown paper target surface, as demonstrated in Figure 5-4. The dimensions of these reference markers was either 1 m by 1m or 0.5 by 1m depending on the extent of the target surface area. Each target surface was labelled to indicate the specific impact event that created them. The axes of the reference marker and positive directions of these axes were also marked to provide a means to re-orientate each target surface during the recording phase.



*Figure 5-4 Experiment set-up for impact event ES-A, showing the raised blood source and vertical target surface with reference metre square.*

#### **5.2.4 Pattern Generation**

Four experimental impact events were produced using the manual impact method with a blood source comprised of a piece of blood soaked carpet, as shown in

Figure 5-3. Each of the four experiments were conducted with the blood source at a different vertical height and perpendicular distance from the target surface, to provide some grounds for the comparison of impact spatter pattern characterisation and site of impact estimation of different impact spatter distributions. Each separate event was assigned a lettered designation, and will be referred to within this project as patterns ES-A, ES-B, ES-C, and ES-D. Of the four experimental impact events three (ES A-C) were recorded on a vertical target surface, and one event (ES-D) was recorded on a horizontal target surface. For events ES-A to C the horizontal position of the blood source relative to the target surface was recorded directly onto the target surface. In addition to this relative position, the height and perpendicular distance of the blood source from the target surface were measured using a 5-metre hand tape to provide a 3D reference location for the impact site, as shown Table 5-1. As event ES-D was administered at ground level, the location of the blood source in this horizontal plane was marked relative to the impact spatter pattern on the target surface. A vertical height was also recorded for this event, although this was only the thickness of the carpet blood source.

	<b>ES-A</b>	<b>ES-B</b>	<b>ES-C</b>	<b>ES-D</b>
<b>Vertical Height</b> (cm)	62.7	35.4	18.9	0.4
<b>Perpendicular Distance</b> (cm)	48	59.5	22	Target Ref.

*Table 5-1 Measured position of blood source for four experimental impact spatter events.*

Each impact event was recorded by digital video as part of the permanent record of the experimentation process. A single frame from each of these digital videos is shown in Figure 5-5. The full-length videos are included on the DVD-ROMs that accompany this thesis. As the images of the experimentation process illustrate full forensic protective suites, latex glove, facemasks and face shields were worn during the experimental creation of each impact spatter patterns.

The bloodstained target surfaces were allowed to dry in position while preparations for the next experimental impact pattern were made. The target surfaces were subsequently carefully removed and stored horizontally until fully dry, so as not to compromise the morphology of the spatter bloodstains with any potential flow characteristics which may have resulted from allowing the patterns to dry at alternative orientations. Each target surface was then rolled up and sealed for transportation from the experimentation facility to the biohazards

laboratory at the University of Nottingham that was to be used in the recording of the impact spatter patterns.



*Figure 5-5 Single frames from the movie sequences of events ES-A to D (top left, top right, bottom left, and bottom right respectively).*

### **5.3 Exhaustive Spatter Bloodstain Recording**

To provide the raw spatter data necessary to conduct the proposed site of impact estimation analysis based on multiple sampled estimates from a single impact spatter patterns, the comparison of the population parameters and sample estimates, the characterisation and comparison of impact spatter populations, and populations of interest and samples taken from them, a total spatter bloodstain recording methodology was developed. This methodology is defined here as 'exhaustive' recording, as each entire impact spatter pattern required explicit examination and each individual spatter bloodstain within each impact spatter pattern required identification and measurement, where possible. Through this exhaustive recording methodology it was envisaged that a significant level of detail concerning each of the four experimental impact spatter patterns could be collect for analysis. Such an extensive impact spatter pattern recording process is not normally conducted in the practical construction of site of impact estimates, whether for experimental or casework purposes.

Three of the four experimental patterns, ES-A to C, were chosen for this exhaustive recording process. These three patterns were selected, as they were the experimental impact spatter patterns recorded on a vertical target surface. It was considered that the examination and analysis of these three patterns within the research into site of impact estimation would provide the potential for a direction comparison between the results generated from each pattern, as well as providing the opportunity to apply more structured sampling procedures, in terms of including spatter, that might adhere to a vertical straight-line flight path hypothesis, as opposed to the more problematic selection of spatter bloodstains observed in horizontal planes. The remaining impact spatter pattern, ES-D, that was recorded in a horizontal plane was considered to provide the potential for a contrasting analysis of site of impact estimation construction in these different manifestations of impact spatter patterns, but ultimately the time scale involved in recording the total spatter patterns meant that it was decided that this pattern would not be considered during this particular research project.

The recording of the impact spatter bloodstains took place in the Biological Hazards Laboratory in the School of Chemical, Environmental and Mining Engineering at the University of Nottingham. This facility provided the means for the safe and controlled examination of the dried blood pattern, as well as disposal facilities for any contaminated recording equipment or materials. Additional health and safety risk assessments were undertaken for this separate recording phase (Appendices E to H). A comparative level of projective clothing was worn during the recording phase of this project as had been used during the experimentation phase. A full protective body suite, latex gloves, and a facemask were worn throughout the exhaustive recording process.

### **5.3.1 Pre-recording**

Prior to the recording of the three impact spatter bloodstain patterns, staff at FAL had advised that the target surfaces be coated with Plasti-Kote Super Spray Paint no. 1138, Clear Acrylic. This would provide an extra layer of protection while recording the spatter bloodstains, as well as preventing any of the dried bloodstains from flaking away from the target surfaces. To this end a number of tests were conducted on sections of the target surface material, which did not include any spatter bloodstains. While some discoloration of the target surface

was evident in areas of denser coverage, this was not considered significant enough to mask the presence of any spatter, and, before the recording of each impact spatter pattern, two coats of this clear acrylic spray were applied to the entire target surface. Where excess portions of the target surfaces exhibited no sign of spatter bloodstaining these were removed, to provide a more practical size for analysis, and to avoid any unnecessary work in terms of extending the recording process to areas of the target surfaces that did not exhibit spatter bloodstains.

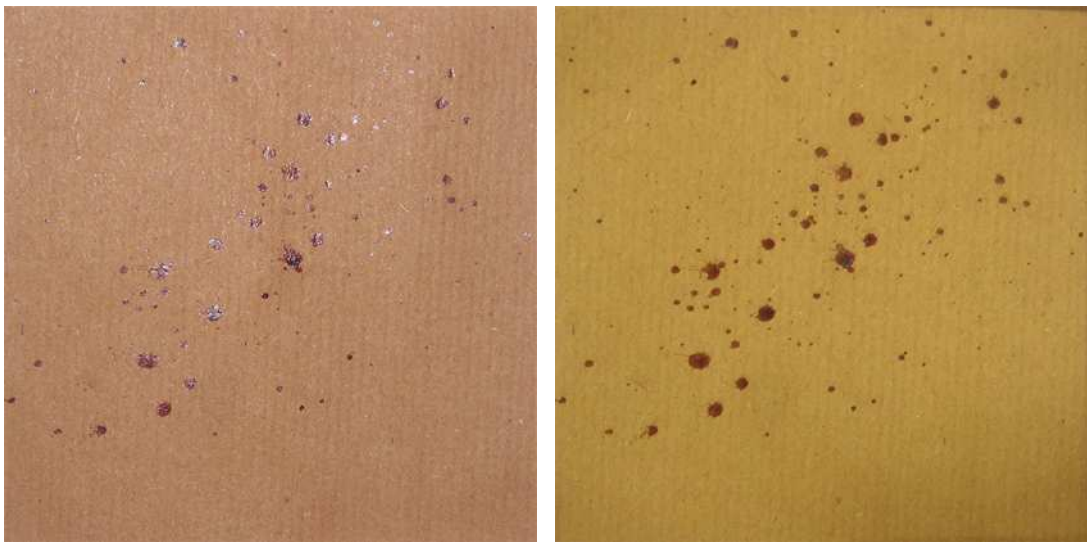
Trial photographs were also taken to determine how best to conduct the photographic phases of the proposed recording procedure (see Section 5.3.2). The camera used throughout the recording process was an Olympus Camedia C350 Zoom, with a 3 megapixel resolution, producing an image size of 2048 by 1536 pixels. The method decided upon to capture the necessary images for the photographic recording of the spatial distribution and size of spatter bloodstains was to mount the camera on a tripod that was set level to the plane of the target surface in order to avoid excessive perspective effects in the images. The camera was used in macro mode to accommodate the close-up nature of the intended photography, and no flash was used during the recording phases, as this tended to result in a 'whiting out' of the bloodstains due to their highly reflective nature (Figure 5-6). To avoid the potential image distortion from the longer exposure time that resulted from this lack of a flash, acute angle lighting was directed at the area of interest for each photograph, with the images captured using the camera inbuilt timer-release function to avoid any camera shake.

### **5.3.2 Recording Procedure**

The exhaustive recording procedure designed to provide the level of impact spatter pattern detail necessary for the proposed research into site of impact estimation incorporated six distinct phases. In order, these phases, conducted for each of the three impact spatter patterns examined, were:

1. The construction of a 10 cm square target surface grid covering the extent of the impact spatter pattern.
2. The scaled photographic recording of all the grid squares within the target surface grid that contained spatter bloodstains to provide a full record of the impact spatter pattern.

3. The examination of each grid square in the target surface grid to identify and number the spatter bloodstains in each grid square.
4. The photographic recording of each grid square within the target surface grid with numbered spatters, to provide a reference for the spatter measurements.
5. The measurement and recording of the spatter bloodstain information necessary for a computer-based site of impact estimation.
6. The conversion of the grid-based location measurements into a total relative location for the impact site and individual spatter bloodstains in the resultant impact spatter pattern.



*Figure 5-6 – A comparison between the recording photography of spatter bloodstains with a flash (left), and without a flash (right). The actual size of these images is approximately 1260x1260 pixels.*

### **5.3.3 Target Surface Grid**

Each target surface was divided into a 10cm square grid to provide a structured method for the identification, recording, and measurement of each individual spatter bloodstain with the separate experimental impact spatter patterns. The division of each target surface into this grid system provides:

- A basis from which the complete photographic record of the impact spatter patterns could be conducted with sufficient resolution..
- A mechanism for recording the identity of the large number of spatter bloodstains using the combination of a grid reference and a number for each spatter identified within a specific grid square.



- A system for assessing the location of spatter bloodstains relative to the orientation of the target surface during experimentation.
- A method for the locative measurement of spatter bloodstains relative to the 10cm grid system rather than a more distant reference point
- A set of datum lines from which directionality angle measurements of spatter bloodstains could be taken.

The grid system for each target surface was set up using the reference markers recorded on each target surface prior to the creation of the experimental impact spatter patterns. The horizontal and vertical axes of the experimentation environment that these markers represent were used to construct the horizontal and vertical components of the grid system, which, once established within this reference area, was extended across the extent of the target surface on which spatter bloodstains were identified. The construction of this target surface grid system is illustrated for pattern ES-C in Figure 5-7, Figure 5-8, and Figure 5-9.



*Figure 5-7 - The reference 0.5m by 1m zone marked on the target surface C during experimental impact spatter pattern production, with the vertical edges extended as the first stage in producing the target surface grid.*

Once the grid system was complete each grid square was labelled with a grid reference, with letters to represent the horizontal axis of the plane of the target surface, and numbers representing the vertical axis of the plane. A preliminary investigation of each grid square was also conducted, with grid squares that contained no spatter bloodstains marked with two diagonal lines through the grid square. Where there was some doubt concerning the presence of spatter bloodstains due to the presence of small inclusions within the paper target

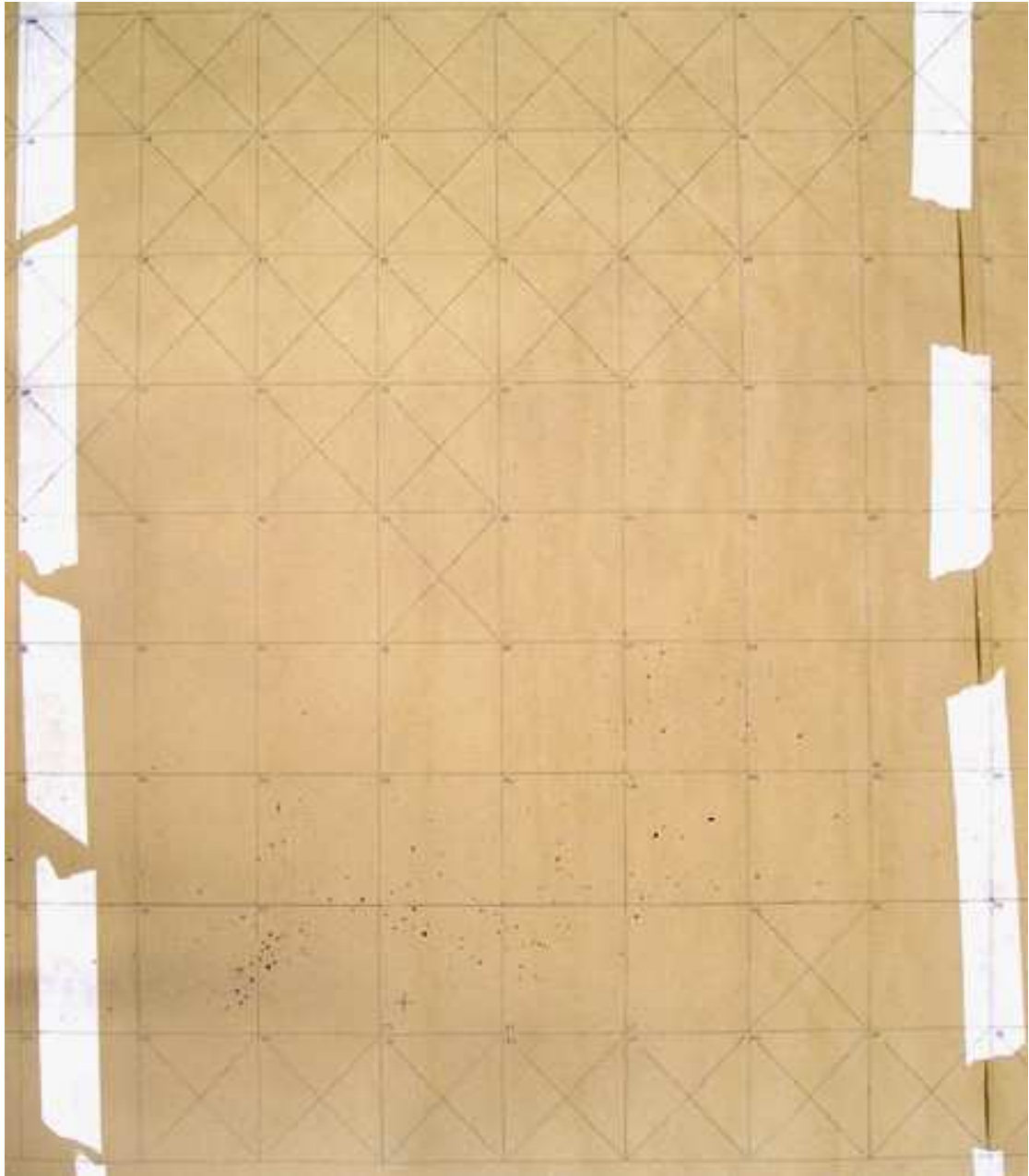
surface, these grid squares were left clear for closer examination during the spatter-numbering phase. A section of the final referenced grid system for pattern ES-C is shown in Figure 5-10.



*Figure 5-8 - Horizontal lines drawn every 10cm within the extended reference zone of pattern ES-C.*



*Figure 5-9 - The full target surface grid of pattern ES-C, expanded from the reference zone to cover the extremes of the impact spatter pattern.*



*Figure 5-10 – The completed grid of a section of target surface ES-C. This image has been manipulated in an attempt to remove perspective effects, and contrast-adjusted to highlight the grid system and spatter bloodstains at such a small scale.*

#### **5.3.4 Photographic Recording and Spatter Numbering**

Following the setting out of the target surface grid, scaled photographs were taken of each grid square that contained spatter bloodstains. These photographs will act as a permanent record of the entire bloodstain pattern and make the raw spatter data available for subsequent re-evaluation, as well as other research into the theory and methodology of site of impact estimation.

Subsequent to this stage of the photographic recording of the impact spatter patterns each grid square that had been previously identified as containing spatter bloodstains was examined in detail. Each confirmed spatter bloodstain was manually circled and given a unique sequential number within the specific grid square, to provide each spatter on the target surface with an identity. The number of spatters within each grid square was recorded to provide a check during the later spatter bloodstain measurement recording phase.

The final photographic recording phase was then carried out. This process was a repeat of the first grid photographic recording procedure, although no scale was included. This photographic record of the specific identities of all of the spatter bloodstains, previously recorded by scaled photography, with a specific reference for each spatter bloodstain, provides a means of tying the numerical representations of the spatter bloodstain morphology back to the original impact spatter pattern and the specific spatter bloodstain they relate to. Figure 5-11 shows an example of the scaled photographic record of a single grid square, and the second photographic record after the spatter bloodstain present within that grid square had been numbered. A sample of the photographs taken for pattern ES-A is included in the appendices of this thesis (Appendix I), while the full series of images used to recorded each of the three target surface grid systems are included on the DVD-ROMs that accompany this thesis.

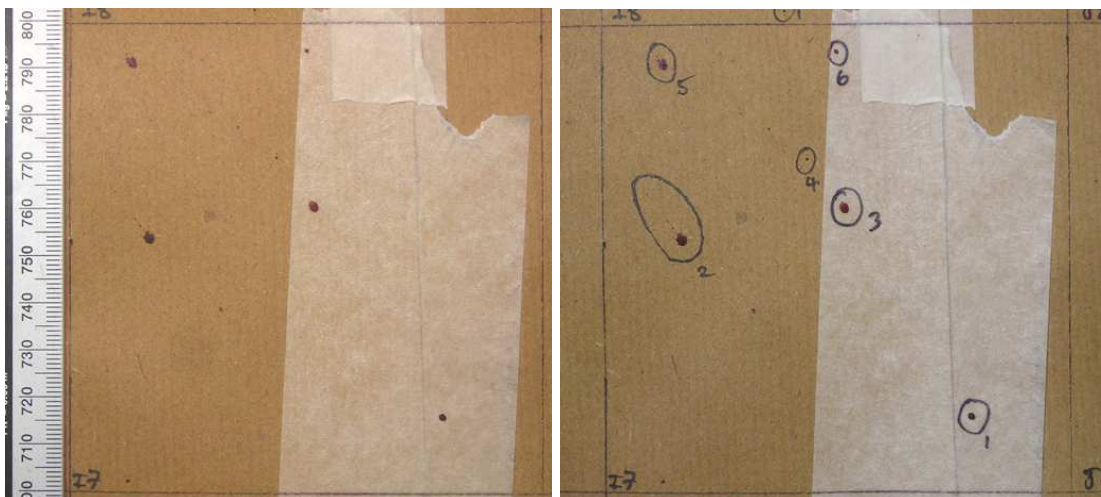
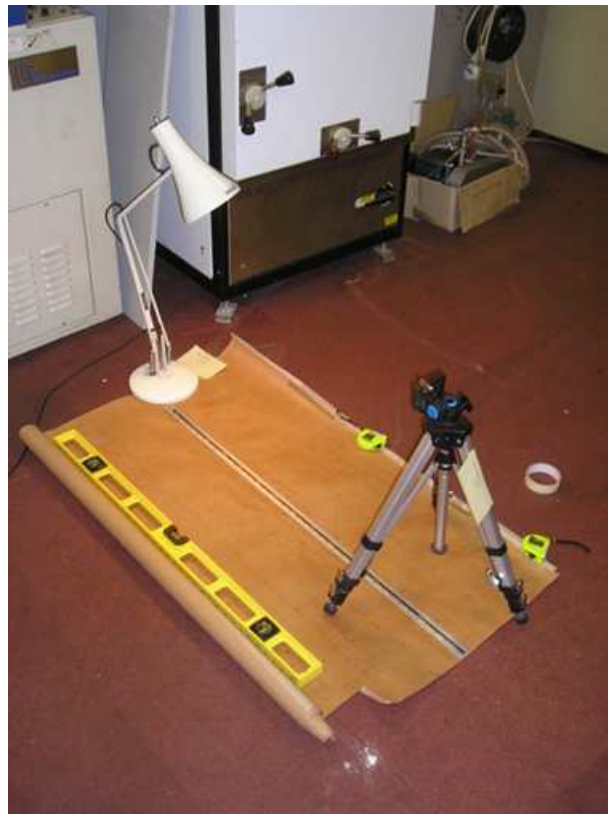


Figure 5-11 - Example of recording of pattern B grid square 17. Scaled photography (left), and numbered spatters (right).

All of the photographs taken during the grid recording process were taken using the method set out during the pre-recording tests (see Section 5.3.1 and Figure 5-12). The photographic plane of the camera was set parallel to the floor of the laboratory, and therefore parallel to the target surface, using a spirit level and the fine adjustment possible with the tripod mounted camera. At least two photographs of each grid square were taken for each of the two recording phases.



*Figure 5-12 - The set-up of the scaled photographic recording process. The camera has been removed from the tripod to take this picture.*

### **5.3.5 Spatter Measurement**

The spatter measurement phase of the exhaustive impact spatter recording procedure involved taking five measurements for each spatter identified in the previous numbering phase. These measurements were:

- The horizontal and vertical locations of the spatter bloodstain.
- The directionality angle of the bloodstain.
- The width and length measurements of the bloodstain.

Both the horizontal and vertical measurements were taken relative to the grid reference of the 10 cm square within which the bloodstain was located, with the (0,0) location being the bottom left hand corner of each square. Where either of the left or bottom edges of the grid square were not available to provide a datum to measure from, a negative measurement was taken from the next available grid line. These positional measurements were taken using a setsquare with an integrated 1mm divided rule to provide measurements at right angles to the axes of the grid system (Figure 5-13, top). The measurements taken using this instrument were interpolated to a 0.5mm level. Where spatter bloodstains exhibited an elliptical morphology the centre of the leading edge of the spatter was measured as its location. Where spatter appeared to be circular the centre of the spatter was measured as its location.

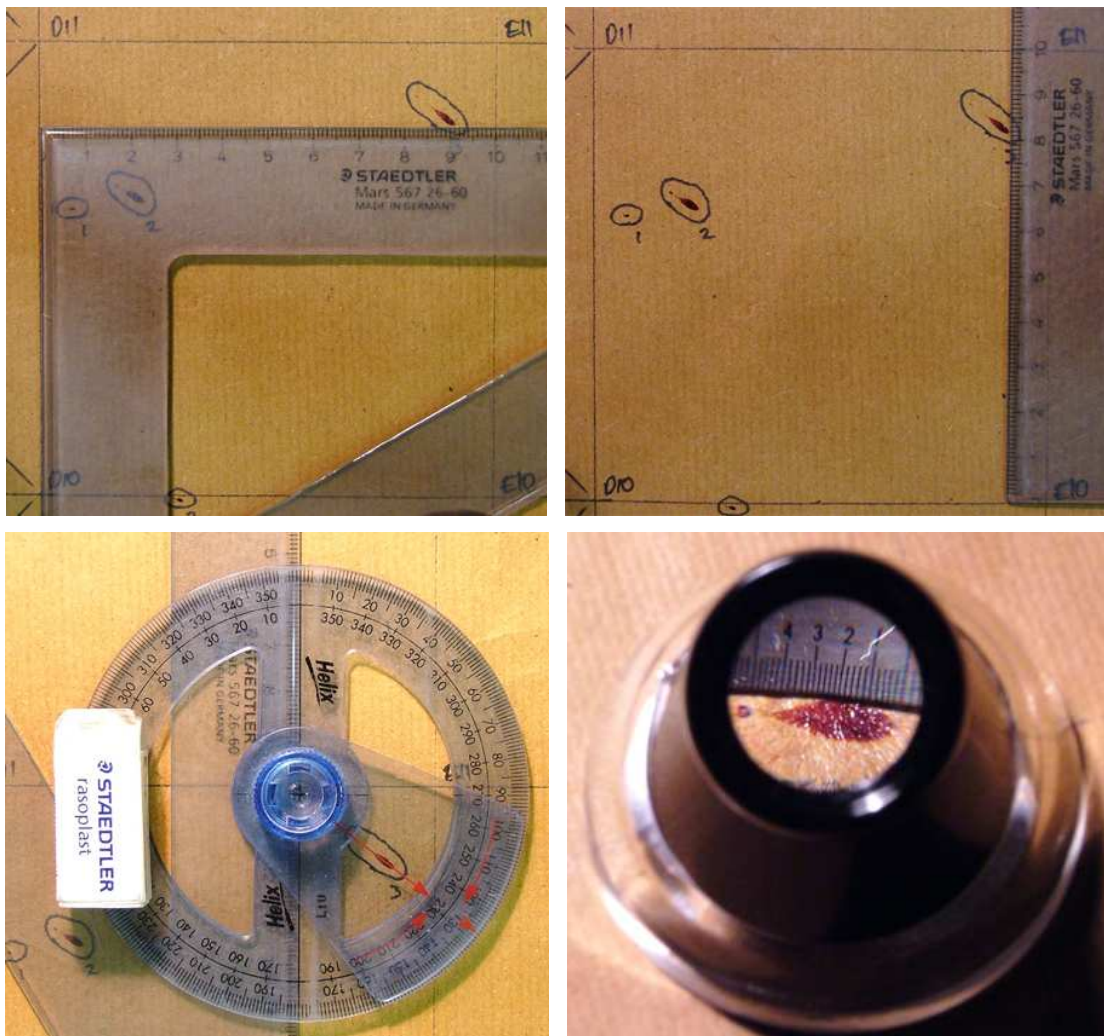


Figure 5-13 - The measurement of the horizontal (top left) and vertical position (top right), the angle of directionality (bottom left), and the width and length of the each spatter bloodstain (bottom right).

The directionality of each individual spatter bloodstain was measured using a conventional 360-degree protractor, with 1-degree divisions, in conjunction with the setsquare to provide a vertical datum away from the vertical grid lines (Figure 5-13, bottom left). The vertical y-axis was used as the zero degree reference and angles were measured in a clockwise direction. For reasons that will be discussed later in this thesis (see Section 8.3.2.1.4) this angle of directionality was measured in the opposite direction to traditional methods, indicating the opposite of the direction in which the droplet was travelling relative to the target surface. The angular measurements taken using this instrument were interpolated to a 0.5-degree level.

The width and length dimensions of the spatter bloodstains were measured using a photographic loupe, with an x5 magnification and divisions of 0.2 mm. Measurements taken using this instrument were interpolated to a 0.1mm level, with the ellipse fitting process used to define the width and length measurements of a spatter bloodstain conducted through visual assessment of the spatter bloodstain morphology (Figure 5-13, bottom right).

In addition to the quantitative measurement necessary for the later construction of a site of impact estimation computer model, a number of qualitative terms were also used to describe spatter bloodstain in order to provide some subjective assessment of the potential nature or quality of the data represented by each spatter bloodstain. A number of subjective criteria were used in the description of the spatter bloodstains analysed, and although some were used throughout the recording process, others had to be added later to account for additional conditions of spatters bloodstains not previously observed during the recording process.

Seven qualitative spatter bloodstain descriptions were used throughout the recording process:

- NDLE = Non-discernable leading edge. These spatter bloodstains exhibit elliptical orientation, but no recognisable traits to indicate directionality. A single directionality angle measurement was taken for these spatter bloodstains but only because the location of the source and therefore the flight direction are known.

- PDLE = Potentially discernable leading edge. These spatter bloodstains are a less extreme case of NDLE, where some directionality indicator is present but is not completely unambiguous.
- CIR = Circular spatter bloodstain. These spatter bloodstains exhibit no discernable ellipticity under x5 magnification. These spatters are recorded with an equal width and length, and the location measured at the centre of the bloodstain. The circular nature of these spatter bloodstains means that they do not exhibit directionality.
- DIST = Distorted spatter bloodstain. These spatter bloodstains exhibit a distorted morphology deemed too complex for measurement for site of impact estimation purposes. The locations of these spatter bloodstains were measured for patterns ES-A and B and were taken to the approximate centre of the bloodstain.
- PDS = Potentially distorted spatter bloodstain. These spatter bloodstains contain some distorting effects, although they are not as severe as in the case of DIST spatter bloodstains. The ellipse fitting and dimensional measurement process could be possible for these spatter bloodstains, although some degree of error is likely to be included.
- OSC = Oscillating spatter droplet. The orientation of the elliptical and the indicators of directionality do not correspond for these spatter bloodstains, presenting the possibility of some non-spherical droplet shape at the point of contact with the target surface.
- Not BS = Not a bloodstain. This is used to distinguish those markings of the target surface paper that were initially thought to be spatter bloodstains but on closer magnified inspection during the dimensional recording of the spatter bloodstains were determined to be inclusions within the paper itself.

The additional qualitative descriptive criteria that were developed during the recording process, and were only applied to patterns ES-A and B were:

- PSAT(no.) = Satellite spatter bloodstain. The spatter bloodstain is a satellite spatter, with the bracketed number referring to the identified parent bloodstain. Where a parent spatter bloodstain cannot be identified this is denoted with a '?' rather than a number.
- ESAT(no.) = Parent spatter bloodstain. The spatter bloodstain is a parent spatter with an associated satellite spatter. The number in brackets refers



to the number of the spatter that has been identified as the satellite bloodstain.

- HSAT = Has satellite spatter included. The spatter bloodstain has a satellite spatter included within its numbered boundary.
- TSAT = Tailed satellite spatter. The spatter bloodstain has some satellite formation, although the body of the satellite is still attached by to the parent spatter bloodstain by an extended tail.
- TAI = A spatter bloodstain with a significant length of tail which could be a source of uncertainty in ellipse fitting.
- CREN = Crenulated edges. The measurement of spatter dimensions may not be as reliable as spatter bloodstain with less crenulated edges.
- FRAG = Fragmentary spatter bloodstain. The morphology of these spatter bloodstain is incomplete with some internal morphological distortion. Some estimation has to be made to construct a complete fitted ellipse in these cases.

Examples of each of these subjective criteria are shown in Figure 5-14, Figure 5-15, Figure 5-16, and Figure 5-17.

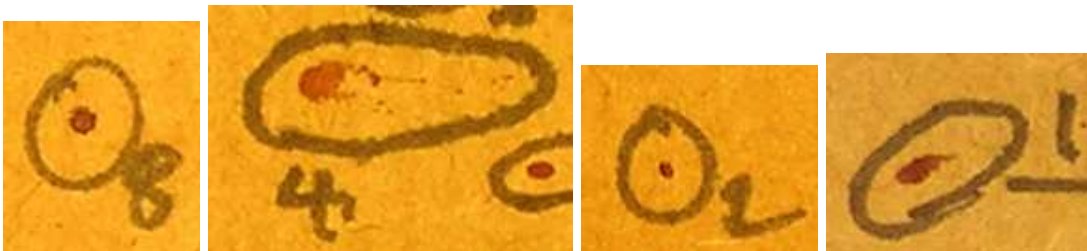


Figure 5-14 - Examples of CIRC (N3-8), FRAG (P4-4), NDLE(M6-2) and PDS (P6-1) spatter bloodstains from pattern ES-A.

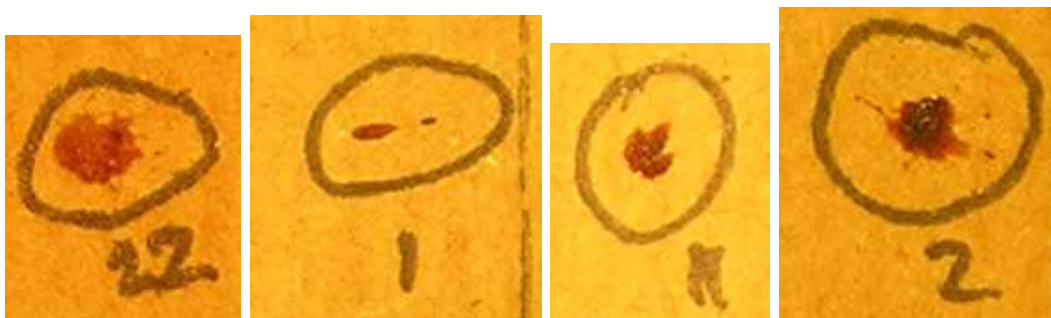


Figure 5-15 - Examples of CREN (O3-22), HSAT (V7-1), OSC (L5-11) and DIST (L3-2) spatter bloodstains from pattern ES-A.

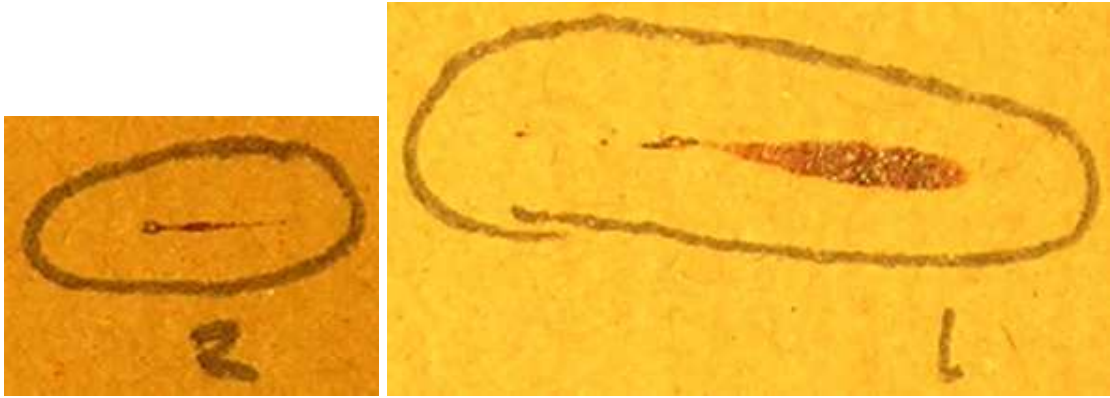


Figure 5-16 - Examples of associated PSAT (A6-2) and ESAT (B6-1) spatter bloodstains from pattern ES-A.

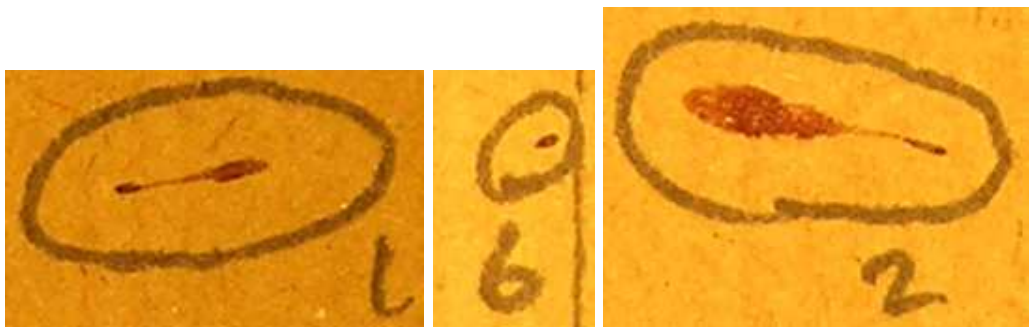


Figure 5-17 - Examples of TSAT (A5-1), PDLE (D5-6) and TAI (U2-2) spatter bloodstains from pattern ES-A.

An example of the tabulated results generated during this recording process for seven spatter bloodstains within pattern ES-C is illustrated in Table 5-2

Grid Square	Spatter Number	x (cm)	y (cm)	Width (mm)	Length (mm)	Directionality Angle (degrees)	Qualitative Description
G3	1	1.1	1.1	0.7	1.4	76.5	NDLE
	2	3.5	1.1	0.9	1.6	79.5	
	3	1.3	6	0.4	0.6	73	
	4	0.45	9.1	0.6	1	95	
	5	1	9.1	0.6	1.1	100.5	PDLE
	6	1.8	8.85	0.4	0.4		CIR
	7	2.25	9.7	0.5	0.7	82	NDLE

Table 5-2 - An example of the results of the data recording process for pattern ES-C.

### 5.3.6 Specific Pattern Recording and Preliminary Results

The specific recording of each of the three impact spatter patterns, as well as some of the preliminary results of this exhaustive recording are described in this

section. The three impact spatter patterns are presented in the order in which they were recorded.

### 5.3.6.1 Pattern ES-C

The first pattern to be recorded was ES-C. This pattern was chosen because on preliminary inspection it appeared to be the smallest of the four patterns in terms of the areal distribution of the impact spatter pattern. Of the three patterns recorded, this pattern was created with the impact site at its lowest height and closest to the plane of the target surface.

The experimentation environment reference marker included on the target surface for pattern ES-C was a rectangle of 0.5 m vertically by 1 m horizontally. Re-examination of this reference marker in the recording position revealed that the upper left corner and the respective left vertical and top horizontal sides of the marker were the most accurate in terms of the length of the side, and the angle of the corner created between the two sides. These two sides were therefore used as the basis for the construction of the grid system for this target surface, with the corner created between these two sides representing the top left corner of grid square F8.

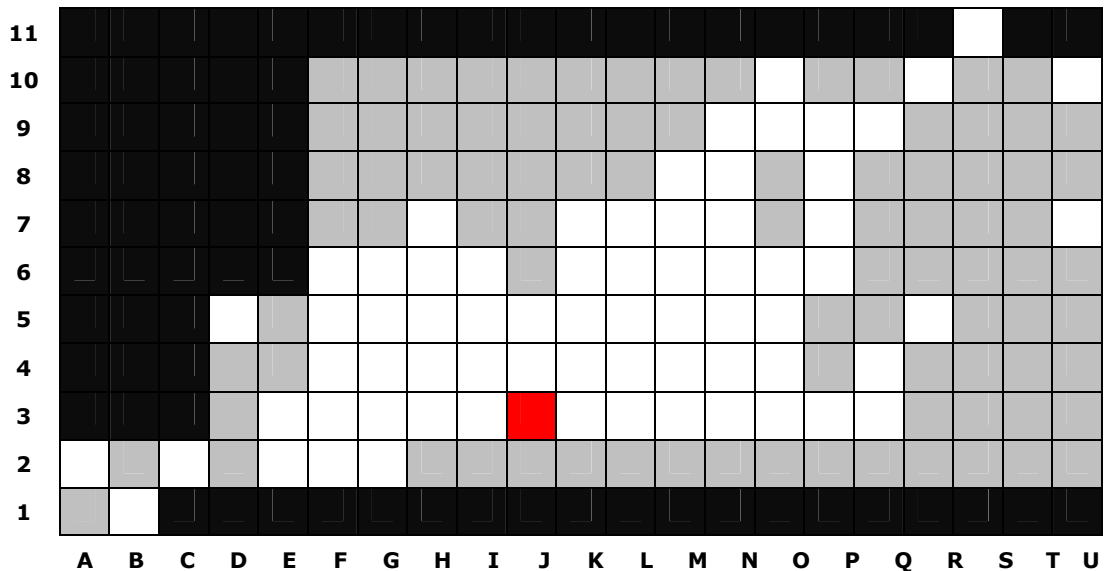


Figure 5-18 - The target surface grid of pattern ES-C. Black = not included in grid system, Grey = contained no spatter bloodstains, Red = contained reference marker representing the location of the impact site.

The grid system layout for pattern ES-C is illustrated in Figure 5-18. The grid system for this pattern contains 158 grid squares, seventy of which exhibit spatter bloodstaining giving an approximate impact spatter coverage of 0.7 square metres. The location of the impact site marker within the grid system for ES-C is square J3 with a relative x measurement of 1.9 cm and a relative y measurement of 2.45 cm. The lowest row in the grid system, row 1, did not form a complete row due to the extent of the target surface. The relative vertical heights for spatters in grid square B1 were, as a result, measured negatively from the lower horizontal line of grid square B2.

A total of 957 spatter bloodstains were identified and recorded for pattern ES-C.

#### **5.3.6.2 Pattern ES-A**

The second impact spatter pattern to be recorded was ES-A. As with the previously recorded pattern the target surface for pattern ES-A was comprised of three horizontally adjacent sheets of brown paper. In this case, however, while the second and third sheets appeared to be well aligned due to the consistency of the metre square experimentation environment reference marker, the first sheet seemed to have slipped by around 5 mm to the left along its lower horizontal line during transportation from the experimental laboratory to the recording laboratory.

Each section of target surface paper was secured to the adjacent section on its front surface by a cream coloured masking tape. In the case of pattern ES-A, the first section of target paper was attached by two separate strips of tape. The lower of these two strips exhibited no sign of spatter bloodstains and was removed to realign the first section of the target surface relative to the reference marker, which extended across all three target surface sections. The upper section of tape had a number of spatters bloodstains adhered to it and, as a result, was reused to align and attach the upper section of this section of target surface by removing it from one surface only, and reattaching it after the reference marker was re-aligned. Following the re-alignment of the reference marker the spatter bloodstains and target surfaces were fixed using the acrylic spray. The entire target surface was subsequently turned over and the three sections of the target surface were secured in position with tape on the reverse

of the target surface. Additional tape was also used to secure the target surface sections.

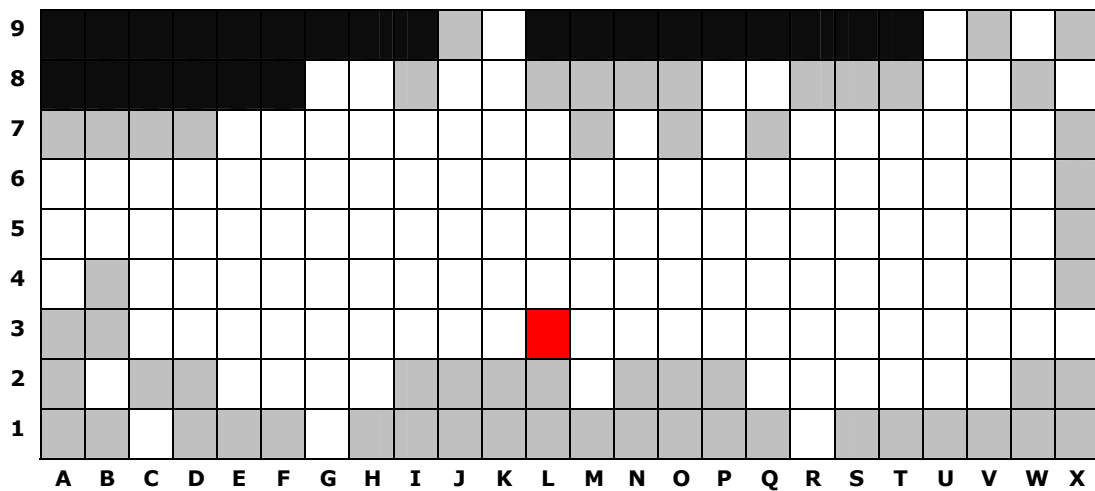


Figure 5-19 - The target surface grid of pattern ES-A. Black = not in grid system, Grey = contained no spatter bloodstains, Red = contained reference marker representing the location of the impact site.

The top left corner of the experimentation environment reference grid was used as a basis for the target surface grid system for pattern ES-A, as the vertical and horizontal sides of the metre square reference that made up this corner appeared to be the most accurate in terms of length and internal angle. The target surface grid system constructed for pattern ES-A is illustrated in Figure 5-19. The grid system contained 192 squares, 133 of which exhibit spatter bloodstaining, giving the impact spatter pattern an approximate area of 1.33 square metres. The relative location marker for the impact site in this case was located in grid square L3, with a x measurement of 2.2 cm and a y measurement of 5.55 cm. Columns A and X were not complete 10 cm wide columns due to the extent of the target surface, and as a result the x-axis measurements for column A were taken negatively from the horizontal line marking the boundary between columns A and B. As column X is not complete on its extreme right edge the measurement of the x-axis was not compromised and was undertaken in the normal positive fashion.

A total of 1022 spatter bloodstains were identified and recorded for pattern ES-A.

### 5.3.6.3 Pattern ES-B

Pattern ES-B was the final pattern to be recorded. It also appeared to have fared the worst in the transportation from the experimentation laboratory to the recording laboratory. As with the other two impact spatter pattern target surfaces, pattern ES-B was comprised of 3 horizontally adjacent sheets of brown paper. Each of these three sections of the target surface seemed to have undergone some slippage during transportation, which was evident from the inconsistency in the experimentation environment reference marker across the sections. Each section was re-attached with additional tape along the joins of their front surfaces in an attempt to re-establish the integrity metre square reference marker. As with pattern ES-A, once the reference marker had been re-established, and the target surface fixed with the acrylic spray, the sections of the target surface were also attached to each other on the reverse side of the target surface to prevent potential future slippage of the target surface sections during the recording process. The top left corner and the vertical and horizontal lines that coincide to create this corner of the metre square reference marker were again used as the basis for setting out the target surface grid system. The final layout of this grid system is illustrated in Figure 5-20.

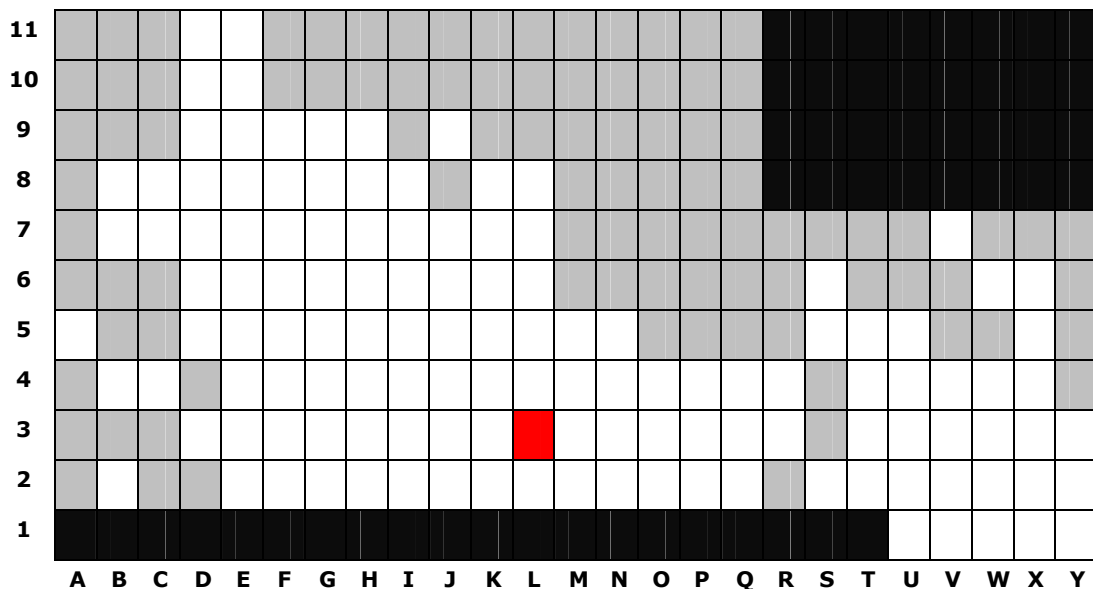


Figure 5-20 - The target surface grid of pattern ES-B. Black = not in grid system, Grey = contained no spatter bloodstains, Red = contained reference marker representing the location of the impact site.

The grid system for this impact spatter pattern contained 223 squares, 128 of which exhibit spatter bloodstaining, giving an approximate impact spatter pattern

areal converge of 1.28 square metres. The positional marker of the impact site was located in grid square L3, with an x measurement of 8.35 cm and a y measurement of 0 cm (although noted as L3 the marker was observed on the line between L2 and L3). The first row of the grid system did not form a complete 10 cm square, with the bottom line being below the extent of the target surface. As a result the spatter bloodstains in grid squares U1, V1, W1, X1, and Y1 had their locations measured negatively in the y-axis from the upper horizontal line of their grid squares.

A total of 430 spatter bloodstains were identified and recorded for pattern ES-B.

### 5.3.7 Spatter Location Conversion

As the spatter bloodstain locations measured during the recording process were relative to the grid square in which they were located within the pattern specific target surface grid systems, some conversion of these measurements was needed to provide absolute locations for the three impact spatter patterns in terms of their location within their overall target surface grid systems.

<b>Grid Square</b>	<b>Spatter Number</b>	<b>x (cm)</b>	<b>y (cm)</b>	<b>Cal x (cm)</b>	<b>Cal y (cm)</b>
A2	1	4.2	0.9	4.2	10.9
B1	1	5.85	-1.2	15.85	8.8
C2	1	10	4.95	30	14.95
D5	1	6.85	0.6	36.85	40.6
E2	1	4.05	8.7	44.05	18.7
E3	1	5.5	1.35	45.5	21.35

*Table 5-3 - An example of the conversion of the grid specific measurements into absolute grid locations for spatter bloodstains positions in pattern ES-C.*

Table 5-3 shows an example of a number of spatter bloodstain locations converted from the relative measurements taken using each grid squares within the grid system of pattern ES-C to an absolute grid location. The conversion of patterns ES-A and C were conducted in a labour intensive process, whereby the locations of each spatter bloodstain (approximately 2000 individual spatters) were converted manually. The horizontal measurements, the recorded x-axis, were converted in relation to the lettered designation of the grid square in which the spatter was observed, and the vertical measurements, the recorded y-axis, were converted in relation to the numbered designation of the grid square as shown in Table 5-4. During the conversion process the recorded xy reference of

the grid system was converted back into the experimentation environment coordinate system where the locations of entities within the plane of the target surface are represented in the vertical yz plane. The measured x-axis was converted to the experimentation environment y-axis, and the measured y-axis converted to the experimentation environment z-axis. To provide the 3D spatial data necessary to construct 3D site of impact estimations from the recorded spatter bloodstain data, an additional x-axis spatter bloodstain location measurement, and a plane and plane normal designation for each experimental target surface were also included for each spatter bloodstain during this conversion process. The target surface for each impact spatter pattern was assigned an yz plane designation, with a positive normal to correspond with the configuration of the three target surfaces within the experimentation environment. An x-axis location of 0 cm was also assigned to each spatter bloodstain to indicate that the spatter bloodstains were observed in this single yz plane, and not on some offset from it.

....	....	....	....	....	....
<b>4</b>	+30,0	+30,10	+30,20	+30,30	....
<b>3</b>	+20,0	+20,10	+20,20	+20,30	....
<b>2</b>	+10,0	+10,10	+10,20	+10,30	....
<b>1</b>	+0,0	+0,10	+0,20	+0,30	....
	<b>A</b>	<b>B</b>	<b>C</b>	<b>D</b>	....

Table 5-4 - The conversion method used for patterns ES-A and C.

For the conversion of pattern ES-B an alternative semi-automated method was attempted in which multiple spatter bloodstains were converted within a Microsoft Excel Spreadsheet. For the calibration of this pattern an alternative height calibration was employed in which the first row of the grid had 10 cm added to the y-axis measurement, 20 cm to the second row, 30 cm to the third row, and so on. The horizontal x-axis measurement conversion remained the same as in the conversion of the two previous patterns. As the locations of the impact spatter pattern and the impact site (see below) are known relative to the target surface grid system within the plane of the target surface, this alteration in conversion methodology has no affect on the consistency or accuracy of the eventual absolute grid locations provided for the impact spatter pattern and impact site for this event. The conversion of this pattern did not, however, account for the negative measurements taken in the lowest grid squares of the last four columns of the grid system, squares U1, V1, W1 and Y1, where no lower grid boundary was present. The result of this omission was an error in



positioning nine spatter bloodstains relative to the target surface grid system. The nine spatter bloodstains (U1-1, V1-1, W1-1, W1-2, W1-3, X1-1, X1-2, X1-3, Y1-1, Y1-2) were assigned an absolute grid position 10 cm lower than their actual position within target surface grid system. Unfortunately this error in calibration only came to light after the impact spatter pattern characterisation and complete site of impact estimation analysis had already been conducted, a procedure which was both computer-processor intensive and time-consuming to such an extent that re-analysing the data was not possible given the time constraints imposed on the research project. While the inclusion of this locative conversion error in the later data analysis stages of this research is likely to introduce some error into the analysis of this specific impact spatter pattern, any effects that these may have on the final results of the analysis are deemed to be slight given:

- The uncertain and relatively spatially imprecise nature of site of impact estimation.
- That the erroneous spatter bloodstains will only be included in certain site of impact estimation depending on the specific sampling methodology used.
- That the nine spatter bloodstains only constitute approximately 2% of the impact spatter population of pattern ES-B.
- That the range of statistical and spatial tools provided for the analysis of site of impact estimation data may reduce the overall affect of any erroneous trajectory intersection data.
- That only the height of these nine spatter bloodstain is affected. The horizontal locations and therefore the horizontal site of impact estimation analyses in which they are included will be unaffected.
- That the relatively large numbers of spatter bloodstains used to construct the site of impact estimates will reduce the influence of these erroneous spatter bloodstains on any single estimate.
- That the conclusions of this research will be based on trends evident in all three impact spatter patterns.

The inclusion of these erroneous spatter bloodstain locations within pattern ES-B, as a result, are not considered to adversely effect the analysis or conclusions of the analysis of the spatter bloodstain data presented in the remainder of this thesis.

<b>Impact Spatter Pattern</b>	<b>x (cm)</b>	<b>y (cm)</b>	<b>z (cm)</b>
ES-A	48	112.2	25.55
ES-B	59.5	118.35	30
ES-C	22	91.9	22.45

*Table 5-5 - The calibrated relative 3D positions of the known impact site of the three experimental impact spatter patterns.*

In addition to the conversion of the spatter bloodstain locations for each of the three impact spatter patterns, the conversion of the location of the spatter-producing impact sites was also necessary to provide a known impact site location against which constructed site of impact estimations could be compared. Table 5-5 shows the relative location of the site of impact in 3D to their specific spatter bloodstains. The same rules used to convert the relative grid measurements of the spatter bloodstain were used to calibrate the location of the site of impact for each of the three impact spatter patterns recorded. While the absolute vertical height of the impact site of each impact spatter pattern is known from the measurements taken at the time of experimentation (see Table 5-1), this height was not used in the conversion process. The vertical and horizontal locations of each impact site relative to their specific spatter bloodstain patterns and target surface grid system were already known and measured from the reference marker included on the target surface during the experimentation phase. The absolute position of the site of impact in the x-axis, the axis perpendicular to the plane of the target surface, was used, however, to provide the location of each of the three sites of impact in this third dimension. While this relative conversion method results in impact spatter patterns and impact site locations that are consistent within each pattern, but not between patterns, the absolute heights of the known impact sites can still be utilised to compare and contrast the pattern characterisations and site of impact estimations possible from the different spatial locations of the three experimental impact events.

#### **5.4 Discussion**

The experimental impact spatter creation and exhaustive spatter bloodstain recording methodologies employed during this research project were developed to provide the level of data necessary for the detailed analysis of impact spatter patterns and the construction of multiple site of impact estimates proposed in the aims of this research. The results of the experimentation and recording

processes have provided three fully enumerated impact spatter patterns, recorded on three separate vertical target surfaces for the purposes of this analysis. The consideration of each impact spatter pattern was restricted to a vertical surface in order to provide the widest range of spatter differentiation and sample selection possible in terms of the discrimination of spatter-producing droplet flight paths. The single vertical target surface was also considered to be a logical starting point for research into impact spatter pattern characterisation and site of impact estimation against which any future investigation of more complex impact spatter pattern distributions might be compared. The spatter bloodstain recording procedure employed to extract the necessary data from each of these impact spatter patterns was designed not only to provide information for the purposes of computer-based site of impact estimation, but also to create a permanent record of the entire impact spatter pattern which could be re-evaluated, or re-used in future research into impact spatter patterns, site of impact estimation techniques, and spatter bloodstain morphological analysis.

While the impact spatter generation and exhaustive data collection processes described here have provided the necessary data to conduct the computer-based analysis of impact spatter patterns and site of impact estimation proposed by this research project, a number of issues concerning this data require explicit consideration. First, there is likely to be a certain degree of decontextualisation present in the recorded spatter bloodstain data. Given the limited time available in the facilities provided by FAL for the experimental impact spatter pattern generation, and the extensive and time-consuming exhaustive spatter bloodstain recording methodology, it was necessary to implement a procedure where the experimentation and recording processes could be conducted at separate locations. While the experimental target surfaces were constructed to be as planar as possible at the time of impact spatter creation, the slight differences that are likely to be present between the actual geometry of the target surface during experimentation, and that of the target surface during the separate recording phase could introduce some small inconsistencies into the recording process. This degree of inconsistency, however, is unlikely to be any greater than that resulting from the spatter-target surface decontextualisation imposed by current computer-based site of impact estimation techniques that employ the manual measurement of spatter bloodstain locations, and the use of a limited axis-aligned, planar surface representation of potentially complex crime scene environments. A more precise validation of site of impact estimation models might be conducted through the construction of an experiment environment in

which the geometry of the environment and its target surfaces is strictly defined. The experimental and recording methodology applied here, as a result, is arguably more appropriate to the detailed investigation of the application of site of impact estimation modelling assumptions to casework scenarios, including this aspect of decontextualisation, rather than an idealised and isolated proof of the reconstructive concept itself. Conversely, it may also be the case that the level of reconstructive decontextualisation introduced by this separation of experimental pattern creation and spatter bloodstain recording is offset to some degree by the fact that the removal of the target surface from its experimentation position provided an opportunity to study the impact spatter patterns in a more accessible position in which the entire impact spatter patterns could be analysed in significant detail.

Second, the manual construction of the target surface grid systems through which the individual spatter bloodstains and site of impact markers were referenced and measured can also introduce some degree of error in the raw spatter bloodstain data. During the scaled photographic recording phase small inaccuracies in the target surface grid system were noticed. The most extreme of these inaccuracies was around 2 mm, or 2% of the individual 10 cm grid square. Although the majority of the grid squares do not exhibit this degree of error, if extended across the entire target surface grid systems the total error in positional measurement could be as indicated in Table 5-6.

While error within the target surface grid system will result in some errors in the locative measurement of the impact spatter pattern features within the grid system, the level of this error, even in the most extreme scenario, where the maximum 2% error is repeated in every grid square in both axes, is not considered to be detrimental to the aims of the research. This level of error is not considered to be any greater than measurements taken from reference points further removed from the spatter bloodstain being measured, or more than in the situational environment-dependent recording carried out at crime scenes where a reference grid system as structured or well-defined as in this recording exercise may not be possible. The total potential level of error that could be present in these grid systems is also not considered to be significant given the spatially uncertain nature of site of impact estimation. The accuracy in the target surface grid system is also likely to provide a more appropriate investigation of the reconstructive system of site of impact estimation, and the evaluation of computer-based analysis proposed by this research project under conditions

similar to those experienced in casework conditions rather than an isolated, scientific proof of the principles of site of impact estimation.

<b>Impact Spatter Pattern</b>	<b>x-axis total potential error (cm)</b>	<b>y-axis total potential error (cm)</b>
ES-A	4.8	1.8
ES-B	5	1.8
ES-C	4.2	2.2

*Table 5-6 - The total potential error in the target surface grid system for the three experimental impact spatter patterns given the extreme 2% error.*

Third, the issue of the potential target surface grid system error could be exacerbated by the fact that in patterns ES-A and B the three sections of target surface that made up these impact spatter patterns were found not to be in their original experimental configuration after transportation to the recording laboratory. The re-alignment and re-fixing of the target surface sections in these two cases, although based around re-establishing the integrity of the experimentation environment reference markers, could introduce some additional small error to the recording process in terms of the actual impact spatter configuration. As the experimentation reference markers were reinstated to their original configuration the level of error that this factor could introduce is likely to be minimal, although it cannot be completely discounted in the future analysis of the recorded impact spatter patterns.

Fourth, the target surface material used needs to be considered in terms of the nature of the spatter bloodstain data. While the use of a large roll of brown paper provided the means for a removable target surface that covered an area sufficient to capture the entire extent of each impact spatter pattern within the single vertical investigative plane, the nature of this target surface material also presented some recording issues in terms of small inclusions within the matrix of the paper itself, and the surface morphology of the paper. The inclusions present within the paper matrix introduced an additional complexity to the recording process, as a number of these inclusions, especially in the recording of the first impact spatter pattern (ES-C), were initially mistaken for small spatter bloodstains. It was only during the more detailed, magnified analysis of these features of the target surface that they were discounted from the spatter bloodstain recording process. On closer examination the paper target surface also exhibited some minute striations within its surface morphology which may be the cause of some of the distortion present in a number of the spatter bloodstains

subjectively identified as PDS, or CREN. Both of these factors, in addition to the reduced contrast between spatter bloodstain and target surface that can be provided through the use of alternative target surface colour (see Chapter 6), however, can be considered to enhance the position of this research in terms of providing a set of conditions that could be more consistent with impact spatter pattern analysis in casework conditions. In these conditions numerous and variable complex target surface can be experienced, as opposed to a more sterile scientific investigation of the individual reconstructive elements of site of impact estimation, where a more uniform and predictable target surface may be employed. In contrast to this, the extension of any findings generated from this experimental data require some consideration given the nature of the out-of-date transfusion blood, and the impact surface employed throughout the experimentation process.

Fifth, the issue of target surface inclusions and the potential distortion of spatter bloodstain morphology as a result of the variable nature of the target surface become important in this research due to the attempted exhaustive recording process. In other sample-based recording methodologies, the size and type of spatters recorded could exclude from consideration spatter bloodstains whose identification or measurement are likely to be significantly affected by these factors. The exhaustive spatter bloodstain recording methodology employed here may have an additional effect on the quality of the data recorded. By attempting to measure all spatter bloodstains it may be that some spatter bloodstains were too small to measure their dimensions and directionality effectively given the manual recording techniques and instruments employed. Such considerations may be of specific importance in the accurate quantification of spatter bloodstains that exhibit only slight ellipticity or are sufficiently small to warrant an increased margin of error in their measurement given the relative size of the error of the measurement instruments used to the size of the spatter bloodstains. While the potential levels of error in the quantification of spatter bloodstain morphology in the recording methodology employed here are not likely to be any greater than those where manual recording methods are employed in casework conditions, the fact that all of these spatter are recorded rather than discounted from analysis, as may occur in sampled methodologies, could be considered to incorporate an additional, albeit necessary, error within the impact spatter recording process.

Finally, while the generation of the four impact spatter patterns produced was completed within a single day, the completion of the exhaustive recording methodology for the three impact spatter patterns captured on the vertical target surfaces, comprising the identification and measurement of approximately 2500 individual spatter bloodstains, and the taking of over 650 grid squares photographs, took approximately three months. The experimental and recording methodologies employed during this project are arguably more representative of the conditions of investigation of impact spatter patterns at crime scenes than the scientific proof of the reconstructive elements of site of impact estimation. As a result, they are likely to be more appropriate in the investigation, analysis and evaluation of uncertainty under the conditions in which forensic investigative site of impact estimation is employed. The exhaustive recording process, from which the analysis of uncertainty proposed by this research will stem, however, is largely untenable in casework scenarios given the time-scales involved. While any findings of this research may well provide site of impact estimation with further areas for investigation, and potentially more rigorous and innovative data analysis techniques, the application of such an approach to actual site of impact estimation using manual spatter bloodstain recording methods is not currently a practical proposition.

## **5.5 Conclusions**

Four experimental impact spatter patterns were created during this research project to provide the raw spatter bloodstain and impact spatter pattern data necessary for the proposed investigation of site of impact estimation. Each impact spatter pattern was generated through the use of a hammer to manually apply an impacting force to the blood source, which was comprised of out-of-date human transfusion blood soaked into a square of carpet material. A removable target surface methodology was developed to maximise the limited time spent at the purpose-built bloodstain experimentation facility. This removable target surface methodology was designed to maintain the spatial configuration of spatter bloodstains upon the recording target surfaces, as well as provide a known 3D location of the impact sites of each experimental impact event against which the spatter bloodstain data collected and site of impact estimation methodologies employed during this research could be evaluated and validated. Four experimental impact spatter patterns were generated during this research project, each of which was recorded on a single planar target surface to provide a

logical starting point for the investigation of site of impact estimation uncertainty. Of the four experimental patterns generated, the three that were recorded on a vertical target surface were recorded using the exhaustive recording process developed for this research project to provide the level of spatter bloodstain data necessary for the proposed investigation of the uncertainty in the construction of site of impact estimates.

While the experimental impact spatter pattern generation and recording methodologies developed and implemented during this research project do not correspond exactly to conditions likely to be experienced, or represent methods that could be practically applied in casework conditions, the validity of the extension of the results of these experimental processes to the investigative forensic construction of site of impact estimates is considered to be as appropriate as possible given the exhaustive spatter bloodstain recording design. Some degree of error in the quantification of the spatter bloodstain data is conceivably introduced through the decontextualisation of the recording process from the experimental pattern generation, the presence of small errors in the definition of the target surface grid systems, and the relatively inexperienced (at least initially) skill level employed in the manual interpretation and measurement of spatter bloodstain morphologies. Although no effort is made within the research to compare this level of error with spatter bloodstain quantification in casework conditions, the recording methodology employed within this project is not considered to be inherently any more error prone in this initial data gathering stage of the process of site of impact estimation than other manual recording approaches.



## **6 Sampled Photographic Recording**

### **6.1 Introduction**

This chapter will describe the additional sampled photographic recording pilot project conducted during the investigation of site of impact estimate uncertainty. This pilot project, which involved the development and implementation of a rapid method for collecting considerable amounts of potential spatter bloodstain data, will be discussed in five main stages. The first section of this chapter will outline the aims and objectives of this pilot project, while the second section will describe the sampled photographic recording design developed for the recording of large numbers of spatter bloodstains from an impact spatter patterns will be described. The third section of this chapter will discuss the impact spatter patterns selected from a series of mock crime scene bloodstain patterns for the purposes of this pilot project. The implementation and results of the sample recording process, as applied to two independently produced impact spatter patterns will be described in the fourth section of this chapter, before the final section discusses a number of the issues that were highlighted during this pilot project. This final section will examine a number of the potential implications that the type of recording methodology developed could have for both the future construction, analysis and evaluation of site of impact estimates, as well as the continued investigation of estimate uncertainty.

### **6.2 Pilot Project Aims and Objectives**

An additional opportunity to record and investigate impact spatter patterns was offered by FAL following the creation of a series of mock crime scenes for the training and evaluation of their employees who routinely conduct bloodstain pattern analysis at crime scenes. These mock crime scenes were constructed in purpose-built scene environments with bloodstain patterning created using human blood that was no longer suitable for the purposes of transfusion. The purpose-built environments were constructed of a timber framework, with the walls of the structure provided by large wooden boards. A white paper target surface covered the internal walls of these structures to provide a contrasting surface against which bloodstain patterns could be identified. Although the experimental bloodstain patterns were not created specifically for the purposes of this research project, and the aims of the generation of these bloodstain patterns

did not correspond exactly with those of the experimental pattern creation described above (see Section 5.2), this opportunity was felt to correspond with the general project objective of beginning to build up a database of information on impact spatter patterns, and would provide additional raw data for future research into site of impact estimation methodologies. As the mock crime scenes were designed and constructed to correspond as closely as possible to realistic forensic investigative scenarios this opportunity was also considered to present a chance to collect impact spatter pattern data within a less structured and more representative framework of impact spatter investigation at crime scenes as opposed to the experimental impact spatter pattern analysis outlined above. This more representative investigative framework was compounded by the fact that the accurately located impact sites of each impact spatter pattern within the mock crime scenes were not available for analysis. While this factor does restrict the analysis of any impact spatter data collected from these impact spatter patterns in terms of the correspondence of any site of impact estimation to known impact sites, it does provide the potential for alternative avenues of research, including:

- Applying any findings generated using the exhaustive experimental data to a more realistic estimate scenario.
- The analysis of variation of site of impact estimates in developing conclusions from an estimate where the impact site is not known *a priori*.
- The initial development and evaluation of image analysis (IA) systems for spatter bloodstain recognition and morphological quantification of large impact spatter samples.
- The comparison of manual, assisted IA, and automated IA techniques in collecting reproducible quantitative data on both individual spatter bloodstains, and larger multiple spatter bloodstain samples.

An alternative recording strategy to that employed in the exhaustive recording process was required for the recording of the impact spatter patterns constructed within these mock crime scenes. While the exhaustive recording of the three impact spatter patterns already described took approximately three months to complete, a single day was allocated to gather as much impact spatter pattern data as possible from the mock crime scenes. This limited time frame would have been sufficient to conduct some practical and comparative site of impact estimations using current computer- and non-computer-based methodologies. However, to adhere to the more structured investigation, characterisation, and

quantification of impact spatter bloodstain patterns and site of impact estimates that is the focus of this research project, it was decided to employ an alternative sampled photographic recording design to capture the raw spatter bloodstain data present within the impact spatter patterns. It was also hoped that such a recording design, with future development, analysis, expansion and evaluation, could provide site of impact estimation with a level of spatter bloodstain data comparable level to that of exhaustive spatter recording techniques, but by a means that is tenable within the context and time constraints of the forensic investigation of a crime scene.

### **6.3 Recording Design**

A photographic recording design was considered to be the most appropriate way of gathering the largest amount of spatter bloodstain evidence possible, given the restricted time-scale available for recording the impact spatter patterns. To this end a 10 square centimetre photographic scale was developed which would be used to capture multiple 10cm<sup>2</sup> areas of each impact spatter pattern recorded using digital photography. The images and associated scales could then be used either to measure the spatter bloodstains manually from printed reproductions, via an interactive computer-based measurement procedure such as BackTrack<sup>®</sup>/Images (Forensic Computing of Ottawa, 2001c), or in the development and testing of automated computer-based spatter bloodstain measurement systems.

The photographic scale, shown in Figure 6-1, was produced using a vector basic graphics package, Adobe<sup>®</sup> Illustrator<sup>®</sup> (Adobe Systems Incorporated, 2001). The scale was a 10 cm square, comparable to the grid square system used in the exhaustive recording process (see Section 5.3), with 1 cm divisions marked along each side of the square by vertical (on horizontal line) and horizontal (on vertical line) 0.5 cm lines. The 5 cm division on each axis of the scale square was marked with a 1cm internal line. Cross-haired circles with a 1 cm radius were also placed in each corner of the scale. The intersection of these circles with the lines of the scale square make up the first and last 1cm division line along each side of the scale. The circles also provide a reference for any subsequent image manipulation which might be required to re-orientate, re-squaring or removing perspective or lens effects from any of the images, if any are introduced during the digital photography recording procedure. A monochrome scale with 1cm,

0.5cm, and 1mm divisions was also included parallel to each of the scales axes to provide a more accurate means of image-size calibration and image correction across both the vertical and horizontal extents of the recorded images. The potential use of this scale for the measurement of the recorded spatter bloodstains is illustrated in Figure 6-2 where the 1 mm scale division provided demonstrated an approximate ratio of 0.1 mm per pixel for the measurement of the spatter bloodstain image, a scale sufficient to capture the dimensional detail of most impact spatter bloodstains.

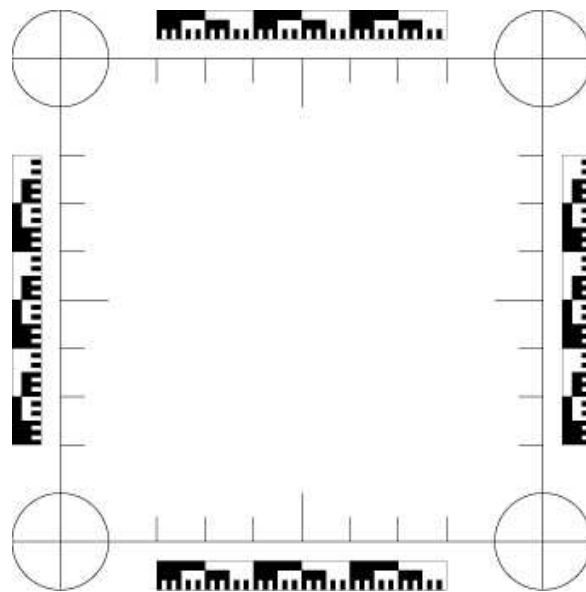


Figure 6-1 - The photographic scale used in the sample recording of impact spatter bloodstains.

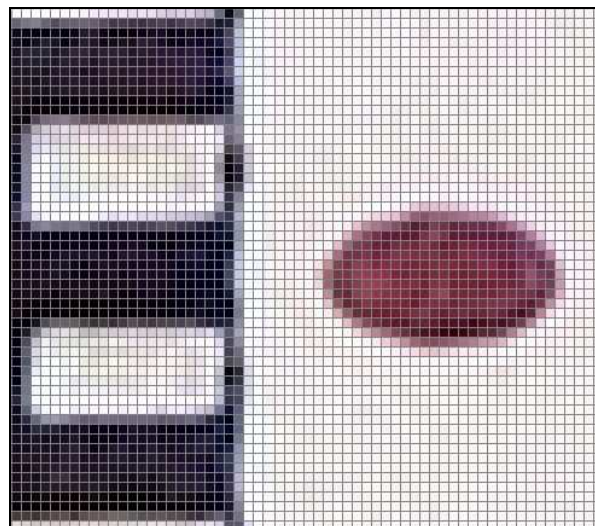


Figure 6-2 - An example of a spatter bloodstain and the millimetre divisions of the photographic scale with a single pixel grid in Photoshop.

As a total recording strategy had already been ruled out due to time constraints imposed on the recording procedure, a sampled methodology was decided upon to record the impact spatter patterns within the mock crime scenes. The placement of multiple scales across the target surface of each impact spatter pattern would be random in nature in the attempt to provide an unbiased representation of the whole of the impact spatter patterns. Some purposive sampling elements would also be employed to provide information on as many of the different types of spatter bloodstains in relation to the aims and practice of site of impact estimation as possible. It was felt that this purposive aspect of the sampling methodology would provide the potential for future comparison with the results obtained in the exhaustive recording process of the previous experimental impact spatter patterns, as well as further investigation of the objectives of this research project.

The photographic scale was designed to be re-used and attached flush to the spatter-bearing target surface using removable masking tape. To preserve the dimensional integrity of the scale the original image was printed onto an entire A4 sheet of clear acetate, and the scale re-measured to eliminate the possibility of any distortion during this reproduction. An electronic version of the image was also saved as an Adobe® Photoshop® (Adobe Systems Incorporated, 1999) file to provide a reference against which the digital images taken during the recording process could be compared to and corrected against using the image manipulation features of this powerful digital imaging package. Both the original scale and the Photoshop version are included on the DVD-ROMs that accompany this thesis.

#### **6.4 Pattern selection**

Numerous scenes had been created at the Culham laboratories of FAL as part of a weeklong bloodstain pattern analysis training and evaluation course<sup>2</sup>. These mock crime scenes contained a variety of bloodstain types used to test the analysts' identification, analysis and interpretation of both isolated bloodstain types, and the possible dynamics of entire bloodstained scenes. Of these mock scenes, a bar scenario was chosen for the sampled photographic recording process. This scene exhibited two distinct impact spatter patterns, one situated in each of the rear corners of the environment. This particular mock crime scene

---

<sup>2</sup>Course facilitated by T. Laber and B. Epstein, February 2004.

provided the potential to record two impact spatter patterns for future analysis in isolation, but also presented the possibility of constructing and investigating a multiple site of impact estimate scene reconstruction. The two impact spatter patterns were also of a type comparable to the experimental impact spatter patterns produced for exhaustive recording in that they were predominantly recorded on vertical target surfaces. Figure 6-3 and Figure 6-4 show the layout of this mock bar crime scene. Both of the impact spatter patterns within this mock crime scene were distributed across the two vertical walls that made up the particular corner in which they were situated. For this recording procedure, however, the collection of spatter data was limited to a single vertical target plane to facilitate the potential future comparison of this spatter data with the exhaustive experimental impact spatter pattern data already collected (see Chapter 5).

The plan view of bar scene, the locations of the two impact spatter patterns, and the planar designation assigned to the three target surfaces upon which the two patterns were visible are illustrated in Figure 6-5. The two impact spatter pattern situated in the left and right corners of the bar scene are identified here as pattern MC-B and MC-A respectively.



*Figure 6-3 - The rear right corner of the bar scene.*



Figure 6-4 - The rear left corner of the bar scene, with reference grid system outlined.

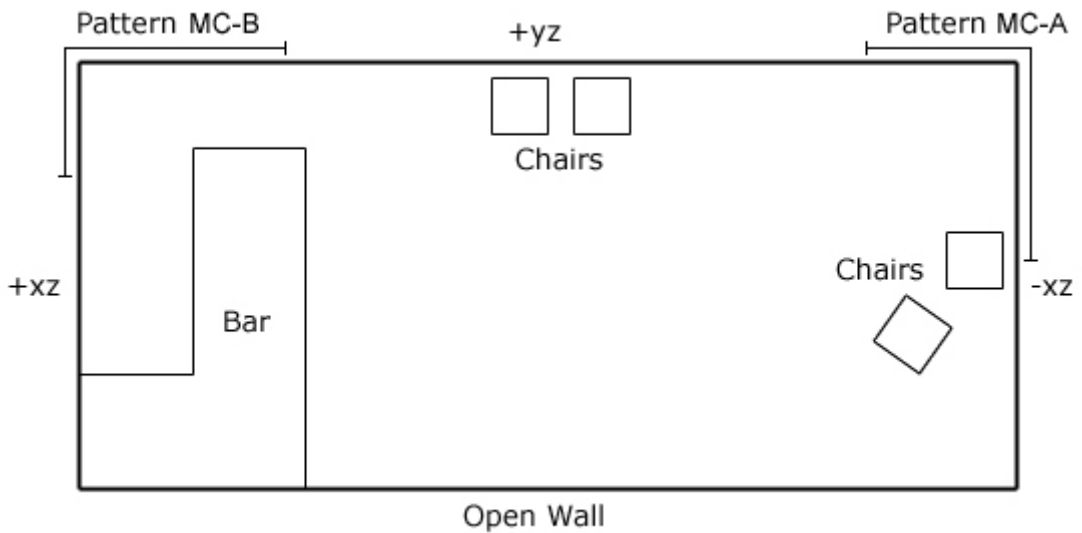


Figure 6-5 - A diagram showing position of the impact spatter patterns identified for sampled photographic recording, and the labelling of vertical target planes (not to scale).

The planar designation of the target surfaces within the mock bar environment was assigned relative to the 3D environment co-ordinate system shown in Figure

6-4, and the dimensions of the axes of this co-ordinate system are given in Table 6-1.

Axis	Measurement (cm)
x	244
y	365
z	241

Table 6-1 - The axial dimensions of the mock bar crime scene at FAL's Culham Laboratories.

## 6.5 The Recording Process

The photographic scale was attached to the target surface upon which the impact spatter pattern was observed according to the sample strategy outlined above (see Section 6.3). For each placement of the photographic scale the horizontal and vertical axis of the scale were aligned using a spirit level to correspond with the environmental co-ordinate system. The location of the lower bottom corner of the photographic scale was subsequently measured using a 5-metre hand tape, to provide a reference location for each sampled spatter area within the specific target surface examined (Figure 6-6).



Figure 6-6- The levelling (left), and surface reference measurement of the horizontal (middle) and vertical (right) locations of the photographic scale in the sampled photographic recording of the two impact spatter patterns.

At least two digital images were then taken for each position of the photographic scale. The camera used throughout the recording process was a Fuji FinePix S5000 set at a resolution of 3 megapixels. Where possible the camera was mounted on a tripod, which was levelled using a spirit level and positioned to provide a photographic plane perpendicular to that of the photographic scale. In situations where the use of the tripod was not possible the images were taken from a hand-held position.



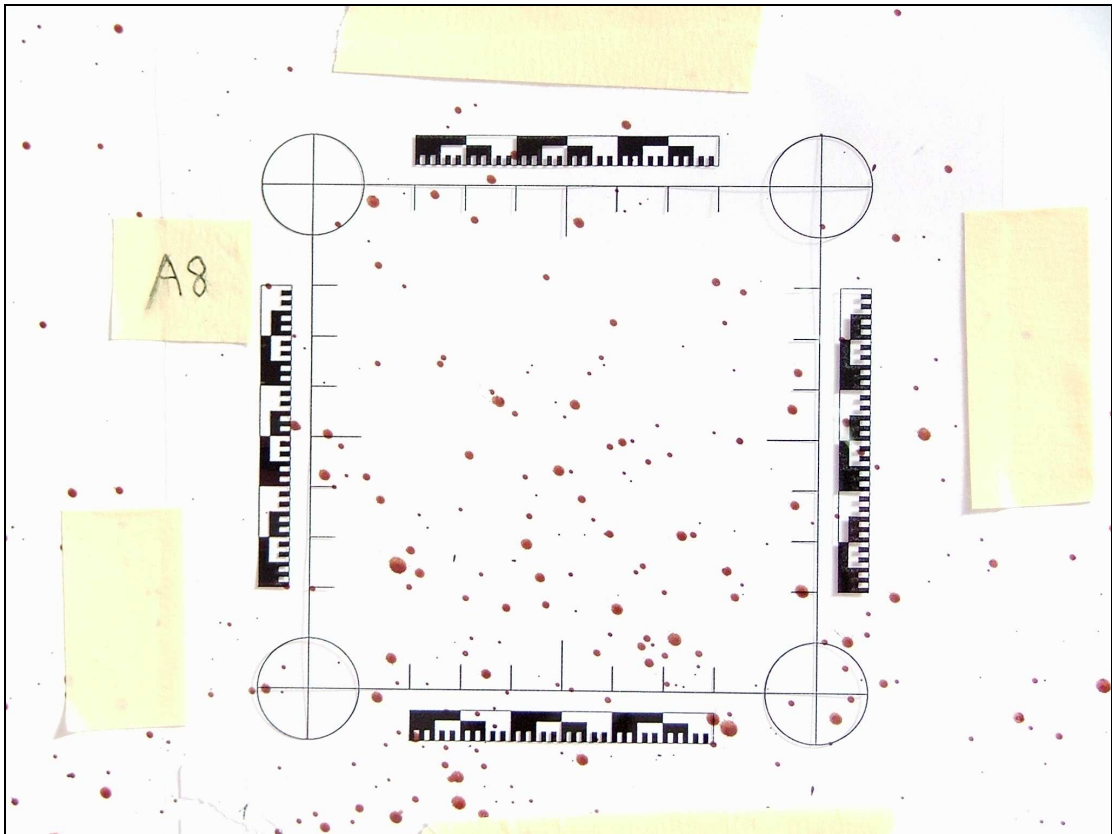


Figure 6-7 – An example of scaled impact spatter bloodstain sample photograph. The real size of this image is 2048 by 1536 pixels.

An example of the scaled photographic images taken during this recording procedure is shown in Figure 6-7. The size of this full frame image is 2048 by 1536 pixels, providing an approximate resolution of 1000 by 1000 pixels for the 10 square centimetre area covered by the photographic scale, although this is expected to vary to some degree between each image.

### 6.5.1 Pattern MC-A

The first impact spatter pattern to be recorded using the sampled photographic recording method was located in the rear right corner of the mock bar crime scene. This pattern was visible on both vertical target surfaces that made up this corner of the environment, although the majority of the spatter bloodstains were observed in the  $-xz$  plane, the wall with the framed picture and the telephone in Figure 6-8. This  $-xz$  plane was chosen for the purposes of the recording exercise.

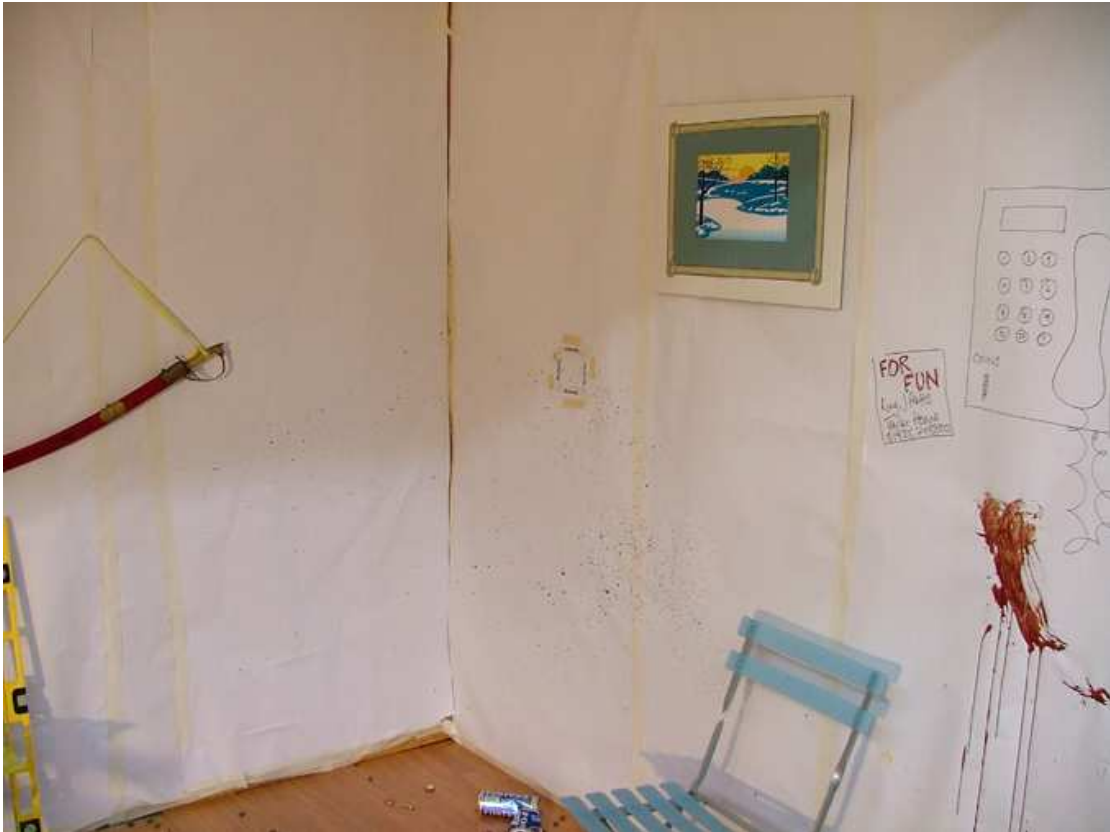


Figure 6-8- The location and extent of impact pattern MC-A within the mock crime scene.

Photograph Reference	x (cm)	z (cm)
A1	6.9	122.6
A2	39.4	117.4
A3	56.9	115.7
A4	50.3	98.9
A5	72.6	111.0
A6	24.8	73.9
A7	68.6	81.9
A8	99.5	87.6
A9	91.4	68.3
A10	112.0	63.7
A11	90.9	51.9
A12	53.1	42.3
A13	75.0	78.3
A14	25.0	119.4
A15	54.8	120.0

Table 6-2 – The measured location of the bottom left corner of each photographic sample area in MC-A.

Fifteen different locations were used to record impact spatter pattern MC-A in the  $-xz$  target surface plane. The locations of each of these sampled areas were measured along the x-axis from the internal corner of the  $-xz$  wall out to the horizontal position of left vertical edge of the photographic scale, and measured

along the z-axis from ground level to the vertical height of the lower horizontal edge of the photographic scale. The locations of bottom left corner of each recorded 10 square centimetre area are shown in Table 6-2 and Figure 6-9. All of the images taken as part of this recording process are included at a small scale in the appendices of this thesis (Appendix J). The full size images of each photographic spatter bloodstain sample are included on the DVD-ROMs that accompany this thesis.

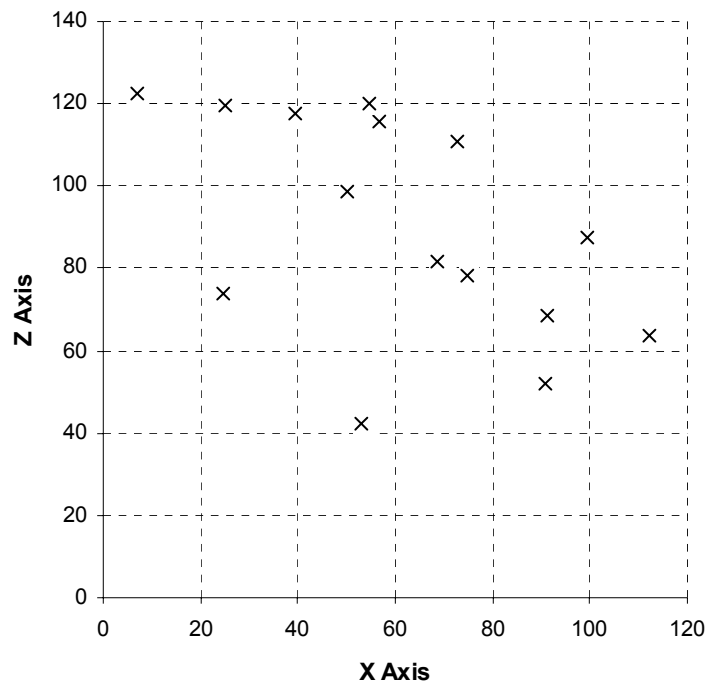


Figure 6-9 - A graph showing the locations of the bottom left corner of each scaled photograph taken of pattern MC-A.

### 6.5.2 Pattern MC-B

The other pattern to be recorded as part of this sampled photographic recording procedure, pattern MC-B, was located in the rear left corner of the mock bar crime scene, close to the bar itself. This pattern was distributed over a larger area than pattern MC-A and provided a more problematic photographic procedure as it was not possible to position the tripod around the bar structure in all cases, nor was it possible to extend the tripod high enough to reach some of the distal spatter bloodstains. The majority of the photographs in the recording of this pattern were, as a result, taken from a hand-held position. This impact spatter pattern was distributed across both +xz, and +yz vertical planes, although the

majority of spatter bloodstains were evident on the latter target surface. The +yz plane, the wall with the cocktail sign and the clock in Figure 6-10, was therefore chosen for the purposes of this recording procedure.

Twenty-two locations were used to provide the sampled photographic record of this impact spatter pattern. The locations of each of these sampled areas was measured out along the y-axis from the internal corner of the environment to the left vertical edge of the photographic scale, and upward along the z-axis from ground level to the lower horizontal edge of the photographic scale. The locations of bottom left corner of each photographically recorded area are shown in Table 6-3 and Figure 6-11. As with pattern MS-A, all of the images taken during the recording of this impact spatter pattern are included at a small scale in the appendices of this thesis (Appendix J). The full size versions of these images are included on the DVD-ROMs that accompany this thesis.

The dimensions of the bar, and its position relative to the walls that make up this corner of the mock scene were also taken during the recording of this impact spatter pattern. This feature was assumed to be immovable, and therefore any estimate results should be considered relative to the location of this environmental feature. In addition to the plan view measurements shown in Figure 6-12, the height of the bar was measured at a consistent 90.5 cm above ground level.



Figure 6-10 - The location and extent of pattern MC-B within the mock bar crime scene.

<b>Photograph Reference</b>	<b>y (cm)</b>	<b>z (cm)</b>
B1	13.0	175.7
B2	12.0	156.8
B3	13.1	120.3
B4	14.4	104.4
B5	13.2	73.4
B6	23.8	33.0
B7	31.1	62.4
B8	34.5	85.4
B9	36.4	155.9
B10	41.8	186.8
B11	61.6	54.8
B12	73.9	77.1
B13	71.7	101.2
B14	61.3	141.9
B15	61.4	163.0
B16	95.0	103.5
B17	85.0	160.9
B18	95.1	137.8
B19	119.0	102.9
B20	150.3	91.4
B21	39.8	210.2
B22	57.9	202.5

Table 6-3 - The measured location of the bottom left corner of each photographic sample area in MC-B.

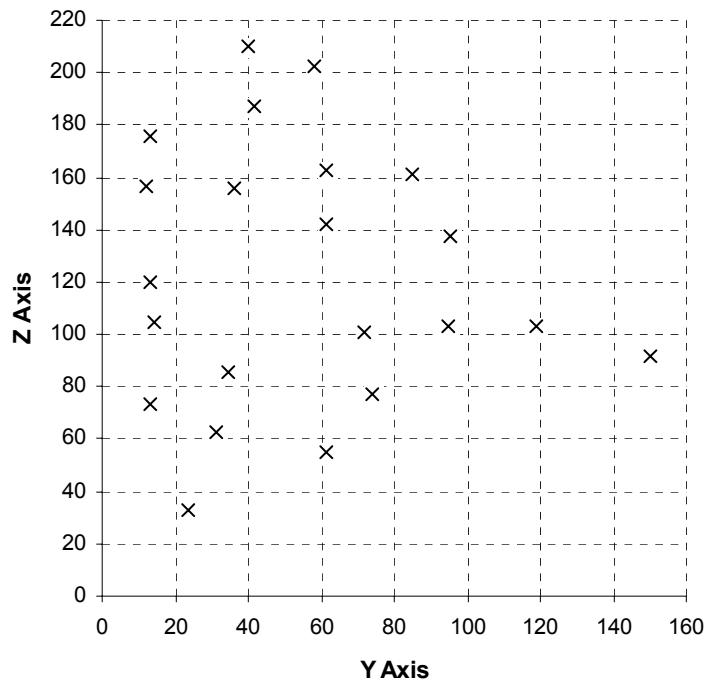


Figure 6-11 - A graph showing the locations of the bottom left corner of each scaled photograph taken of pattern MC-B.

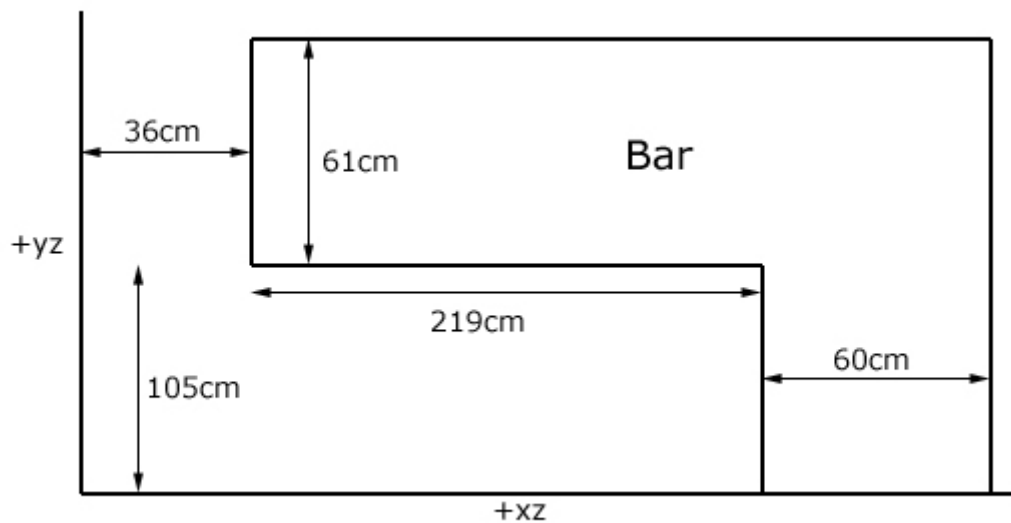
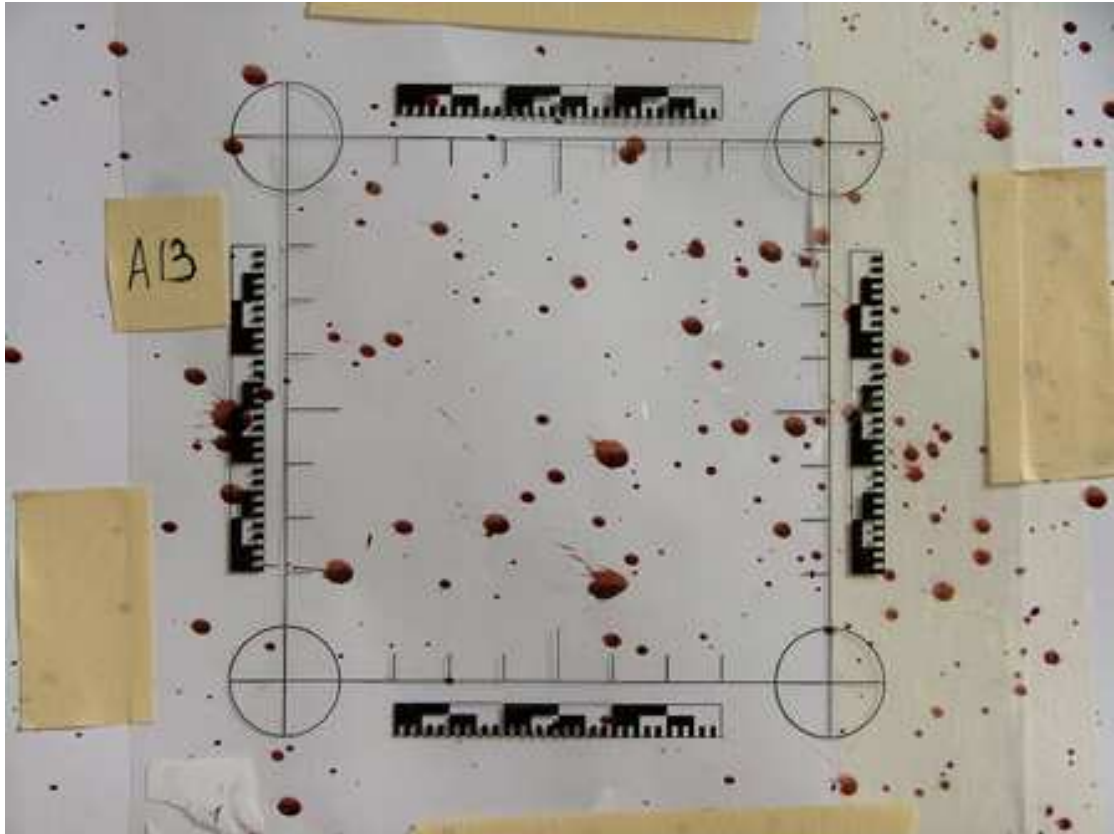


Figure 6-12 - A diagram to show the dimensions and location of the fixed bar structure.

## 6.6 Discussion

For any future use of the sampled photographic impact spatter pattern data collected during this recording exercise a number of issues need to be explicitly considered. Firstly, the locating of the sampled areas within their specific target surfaces, and the combining of the locations of these areas within a single environment reconstruction using the dimensions of the bar environment, require the assumption that the 3D co-ordinate system employed is consistent across the entire environment, and that the walls and target surfaces of the environment are both planar, and axis-aligned. While establishing the precise 3D geometry of the bar environment was beyond the scope of this exercise, any inconsistency with the true geometry of the environment could produce erroneous site of impact estimation results. The level of this inconsistency is, however, not likely to be any greater than in current computer-based site of impact estimation techniques that employ the manual measurement of spatter bloodstain locations, and the use of a limited axis-aligned, planar surface representation of crime scene environments. Such a recording methodology may therefore, given further research, be applicable to collecting larger spatter bloodstain datasets in such estimation techniques, although the appropriateness of the representation of the environmental geometry should be explicitly considered in the discussion of the results. A second, but associated factor, is that a number of the images captured

using the sampled photographic recording methodology show signs of some lifting-off of the photographic scale from the target surface, as demonstrated in Figure 6-13.



*Figure 6-13 - An example of the scaled photographic recording process with some lift-off of the scale from the target surface, and examples of the acetate reflectance.*

In locations where the target surface itself is coplanar with the underlying wooden board walls of the crime scene environment structure this lifting-off of the scale does not appear to be an issue. Where the target surface, the white paper layer, had begun to come away from the walls of the structure the non-planar nature of the target surface results in the entirety of the photographic scale no longer being parallel to the target surface. This lifting-off of the photographic scale from the target surface has implications for any accurate image correction and spatter measurement, as well as for the application of such a methodology in real crime scene scenarios where non-planar target surfaces are likely to be experienced. This situation, however, does also provide the potential to compare the accuracy of spatter bloodstain measurements between images of the sampled areas with planar and non-planar photographic scales, and the comparison of spatter bloodstains measurements taken from a single image

across both planar and non-planar sections of the image. If applied either in the form presented here or in a modified state, in future impact spatter pattern recording exercises a more uniform planar target surface could be constructed to eliminate this issue. The target surface in this particular case, however, was still in a reasonable state, given that the environments had previously been used for training purposes over a weeklong period, and the majority of the sampled areas included a coplanar photographic scale.

Thirdly, some variation in the quality of the photographic images is evident both between individual images and even within single images. These variations in quality are predominantly due to the lighting conditions within the environment, producing images of variable contrast, and the reflectance of the acetate photographic scale, as illustrated in Figure 6-14. While these variations are present in some of the recorded spatter bloodstain images, a preliminary visual assessment indicated that these features do not significantly distort the morphology or identification of spatter bloodstains, at least in the visual examination of the images. Any automated IA computer-based spatter morphology quantification methods developed and evaluated using such variable image data could initially be trained using more consistent images with greater contrast between target surface and spatter bloodstain. The methods developed could subsequently be tested on more realistic image scenarios where variable contrast between the target surface and the spatter bloodstains is evident, as might be expected to be found at crime scenes during casework.

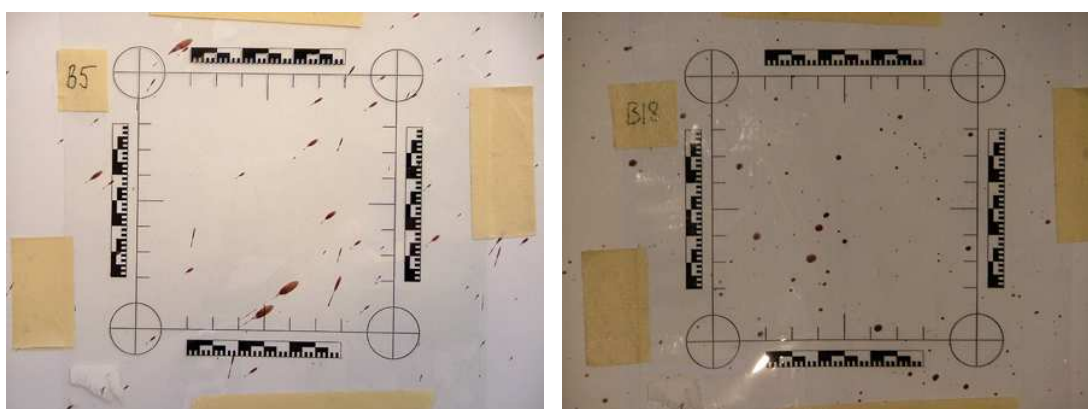


Figure 6-14 - An example of a scaled photograph image with relatively good and consistent contrast between the target surface and spatter bloodstains (left), and an image with poor contrast, and strong reflective highlights (right).



An additional point of comparison may be possible between the image-capture processes of each of the two impact spatter patterns. While the images for pattern MC-A were taken using a tripod mounted camera, the images of pattern MC-B, due to the restricted space around the bar area and the height of the impact spatter patterns, were taken from a hand-held position. Although the former method can provide a controllable and more consistent photographic recording method, the latter can conceivably be conducted significantly quicker. An interesting area for further research into this photographic recording methodology might be to compare the image qualities, necessary image manipulation, and potential spatter bloodstain measurement accuracies given the differences between these approaches. Such research might provide some direction for the future application of rapid spatter bloodstain capture techniques that can be used to collect large amounts of spatter bloodstain data from an impact spatter pattern, or even provide the means to record an entire impact spatter pattern in sufficient detail for the purposes of site of impact estimation.

Finally, given the restricted time-scale involved in the sampled photographic recording process presented here, a quantification or evaluation of how representative the sampled spatter bloodstain data is of the wider impact spatter patterns was not possible. Such an undetermined sampling procedure could well have implications for expressing confidence in a site of impact estimate given the discussion of data representation in the literature review section of this thesis (see Section 4.7). This sampling limitation may be most significant for pattern MC-B since it covered a larger area than pattern MC-A, and therefore may be less well represented in the limited samples recorded here. In contrast, however, the samples taken during this recording process represent significantly more spatter bloodstain information than those usually taken in current site of impact estimation methodologies, and the sampling strategy employed was not purposive in the sense usually applied in spatter bloodstain selection, but was employed to cover as many possible types of spatter bloodstain, but in a random fashion. To provide a means of quantification and comparison for such recording techniques a future potential avenue of research may be to select random grid squares from the exhaustive spatters, or randomly place a window of investigation over all of the enumerated spatter patterns to compare site of impact estimations based on this and other recording methodologies.

## **6.7 Conclusions**

The sampled photographic recording methodology was developed during this research project to record two additional impact spatter patterns generated by FAL for the purposes of training BPA practitioners. This photographic recording design was considered to be the most appropriate way of gathering the largest amount of spatter bloodstain evidence possible given the time constraints, as well as reflecting a potential methodology for the development and application of spatter bloodstain recording techniques similar to those employed in the exhaustive recording phase of this research project under more casework-appropriate conditions. A 10 square centimetre photographic scale was developed for this recording methodology, and the two impact spatter patterns selected for analysis were recorded on a single vertical target surface using multiple samples to correspond to the target surface configuration employed in the creation of the previous experimental impact spatter patterns. The location of each photographic sample on the plane in which each impact spatter patterns was situated was recorded, and the dimensions of the mock crime scene environment and the immovable scene furniture were taken to provide a 3D reference environment within which a site of impact estimation could be constructed at a later date. While no further analysis of this data has been undertaken during this research project, the collection of the spatter bloodstain data was felt to correspond to the general aim of building up an impact spatter bloodstain database for use in additional research into impact spatter pattern interpretation and the construction of site of impact estimates. The development of a rapid large-scale data collection methodology was considered to present a potential future direction for the capture of raw spatter bloodstain morphologies for the purposes of site of impact estimation, whether the quantification of these morphologies would subsequently be conducted through manual measurement or IA techniques. Given further development, and the integration of site of impact estimation techniques within 3D crime scene geometry-capture techniques, rapid large-scale photographic recording methodologies are likely to become increasingly possible within site of impact estimation. Where this data collection can be achieved with a reliable degree of accuracy, the potential amount of information available for the analysis, interpretation and evaluation of impact spatter patterns and their associated site of impact estimates will undoubtedly be greatly increased, and a more structured approach to the construction and evaluation of site of impact estimates facilitated.

## **7 Spatter Bloodstain Image Analysis**

### **7.1 Introduction**

This chapter will describe and discuss the additional automated spatter bloodstain measurement IA pilot project conducted as part of this project's wider investigation of site of impact estimation and estimate uncertainty. The pilot project was undertaken to assess the potential utility of an automated IA system in the measurement of spatter bloodstains for the purposes of trajectory reconstruction, and site of impact estimate construction. This chapter is divided into four main sections. The first section of the chapter will outline the aims and objective of this IA pilot project. The second section will describe the methodology employed during the project, which includes a discussion of the spatter bloodstain images analysed and the specific IA software and procedures utilised. The third section of this chapter will describe and discuss the detailed numerical results generated during the pilot project, while the final section will examine the implications of these results for the further development of automated IA techniques within site of impact estimation, and the potential consequences similar technologies could have on the both the construction of estimates, and the continued investigation and evaluation of estimate uncertainty.

### **7.2 Pilot Project Aims and Objectives**

IA systems, such as BackTrack<sup>®</sup>/Images (Forensic Computing of Ottawa, 2001c), have already been used effectively in site of impact estimation through an increased methodological productivity, a more structured consistent approach to the ellipse fitting process, and the potential to re-analyse the raw spatter bloodstain data collected. However, as previously discussed in the site of impact estimation methods section of this thesis (see Section 3.4.2), the current IA techniques employed tend to rely on significant user input in both the identification, selection, and measurement of the spatter bloodstains, and as a result, continue to use relatively small spatter bloodstain sampling strategies. The analysis, development and evaluation of an automated IA system were considered to present the potential for additional benefits to each of the three areas already experienced within site of impact estimation through the introduction of IA techniques. The development of an automated IA system was

also considered paramount for any future application or detailed analysis of the exhaustive and photographic sampling methodologies employed as part of the wider research project into site of impact estimation uncertainty. The main advantages of an automated IA system for site of impact estimation in general, and specifically the aims of the wider research project present here were considered to include:

- The potential for the development of a time- and cost-effective method for the recording and processing of total, or at least large scale, spatter bloodstain-sampling strategies in the development and analysis of impact spatter pattern databases.
- The potential for reproducible and quantifiable spatter bloodstain measurements through which spatter data could be collected rapidly, and its quality assessed for the purposes of both spatter bloodstain selection and site of impact estimate evaluation.
- The possibility of a practical recording methodology enabling the re-calculation and re-evaluation of large-scale impact spatter pattern data, in contrast to the limited re-analysis of pre-selected data provided in current IA techniques.

The collection of an impact spatter pattern in the form of digital images at a sufficient resolution to provide detailed spatter bloodstain data, and the identification and separation of individual spatter bloodstains from background information are not necessarily straight-forward tasks given the diverse manifestation of impact spatter patterns in casework conditions. The aim of this pilot project was to investigate the more immediate application of available IA procedures in taking the specific measurements of spatter bloodstains necessary for site of impact estimation. The image-based analysis of spatter bloodstain undertaken in this pilot project was conducted in collaboration with Dr Edward Lester and Dr Tao Wu from the School of Chemical, Environmental and Mining Engineering at the University of Nottingham. Both Dr Lester and Dr Wu have extensive experience in the morphological analysis and characterisation of individual small-scale features from large digital image data sets using image analysis technologies in a number of research applications.

### **7.3 Methodology**

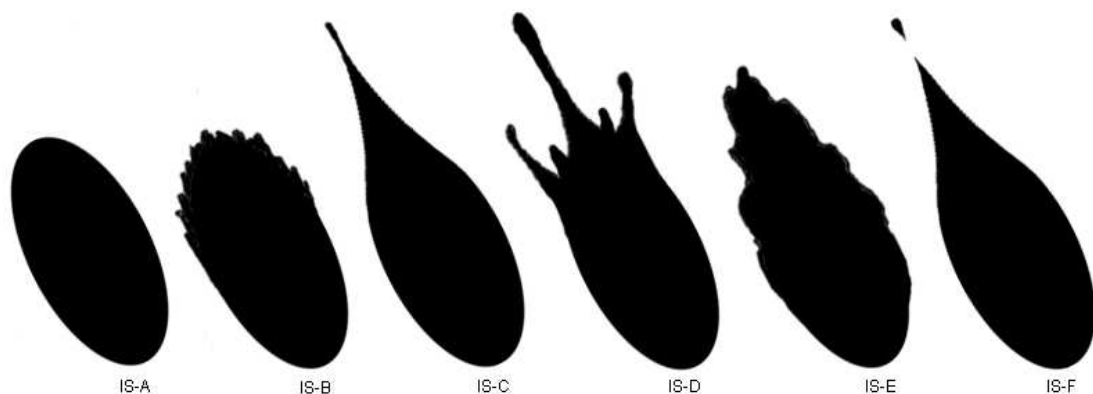
The methodology employed in the pilot IA project is described in this section. The creation of the six idealised spatter bloodstain shapes, the IA software employed, and specific morphological measurements, and image manipulation processes employed during the project are addressed.

#### **7.3.1 Idealised Spatter Bloodstains**

For the purposes of this project the investigation of a number of idealised spatter bloodstain shapes was deemed to be a useful starting point from which to analyse the potential of automated IA technologies in quantifying spatter bloodstain morphology. Six idealised spatter bloodstain greyscale images were generated in Adobe® Photoshop® (Adobe Systems Incorporates, 1999) to act as the test data against which to compare and contrast the results of IA processes given the different possible spatter bloodstain morphologies, and to present the system used with a number of potentially problematic spatter quantification scenarios. These idealised spatter bloodstain images, shown in Figure 7-1, were all based on the same elliptical shape of spatter bloodstain IS-A, with the approximate elliptical measurements of 90 by 180 pixels, providing an impact angle of 30 degrees. Each of the idealised spatter bloodstains was rotated to provide an arbitrarily selected directionality angle (using the definition of directionality applied during this research into site of impact estimation) of 153 degrees from the positive vertical axis in a clockwise direction.

These shapes were given the labels IS-A to F. Shape IS-A forms the basis for all of the other five spatter bloodstain shapes. This shape is included in the analysis to provide both a simple elliptical shape against which to evaluate the ability of the IA techniques employed to accurately quantify the morphology of the shape, and to provide a comparative base against which the analysis of the other spatter bloodstain shapes can be assessed. Shape IS-B largely maintains the base ellipse shape of IS-A, but has the addition of some edge crenulations to both indicate directionality and to provide a relatively slight distortion of the predominant elliptical form. Shape IS-C includes a single long spine extension to the basic ellipse spatter bloodstain shape, and while the main elliptical body of the shape is maintained, the inclusions of a long spine masks the curvature of the ellipse, and could result in the erroneous measurement of the long axis of the spatter

bloodstain long axis. Shape IS-D has a multi-spine morphology, with five separate spines protruding from the main elliptical shape. The elliptical morphology of this shape is distorted to a greater extent than in IS-C, with the inclusion of additional spines either side of the predominant central spine. Shape IS-E provides an alternative but equally complex elliptical morphology with the inclusion of distorting edge effects distributed around the majority of its perimeter. Some extension to the ellipse is included to demonstrate directionality, although this is represented by a continuation of the edge effected rather than by distinct spines. The distribution of the edge effects around this shape are likely to complicate both the measurement of both the long and short axes of the base elliptical shape. Shape IS-F is similar in form to IS-C, although here the spine is truncated and a separate satellite spatter is added to provide an example of the complex and multi-component morphology that can be associated with a spatter bloodstain.



*Figure 7-1 - The six idealised spatter bloodstain shapes used to test the prototype automated image analysis procedure.*

### **7.3.2 Image Analysis Procedure**

The IA software used throughout this project was the Zeiss KS400 version 3.1 (Carl Zeiss Ltd, 2005). This versatile professional IA package provides a wide range of predefined functions, including those needed to analyse and measure geometric features within an image, combined with the ability to produce customised routines in its MacroEditor, through which application specific IA requirements can be addressed. For the analysis of the idealised spatter bloodstain shapes an automated macro was developed to provide detailed geometric and morphological information on each idealised spatter bloodstain

image (Appendix K). A number of predefined IA functions were included within this macro to extract the information necessary to construct a site of impact estimation, the elliptical width and length, the angle of directionality, and the location of the idealised spatter bloodstain shapes. An example of the raw numerical results produced through this analysis for shape IS-A is shown in Table 7-1. Where the data presented is a calculated measurement generated during the IA procedure, the results will be reported correct to 1 decimal place throughout the discussion of the results of this pilot project. This is considered to be a reasonable level of accuracy given that the smallest real unit in each of the images analysed is a single pixel.

<b>Iteration</b>	<b>Area</b> (pixels)	<b>Perimeter</b> (pixels)	<b>Feret</b> <b>Maximum</b> <b>Length</b> (pixels)	<b>Feret</b> <b>Minimum</b> <b>Length</b> (pixels)	<b>Centre</b> <b>Gravity X</b> (pixels)	<b>Centre</b> <b>Gravity Y</b> (pixels)	<b>Feret</b> <b>Maximum</b> <b>Angle</b> (degrees)	<b>Feret</b> <b>Minimum</b> <b>Angle</b> (degrees)
1	12038	450.8	177.7	88.2	87.6	102.4	118.1	28.1
2	11658	445.1	175.9	86.5	87.6	102.4	118.1	28.1
3	11282	438.9	174.2	84.7	87.6	102.4	118.1	28.1
4	10911	433.2	172.4	82.9	87.6	102.4	118.1	28.1
5	10544	427.5	170.7	81.2	87.6	102.4	118.1	28.1

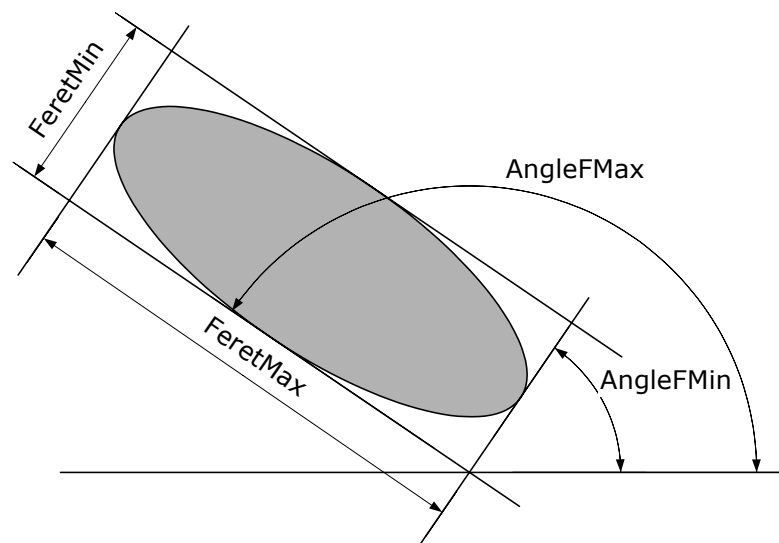
*Table 7-1 - An example of the data retrieved from five of the 47 iterations of the IA process for spatter bloodstain IS-A.*

The functions included within the spatter bloodstain macro performed a number of different operations and analyses on each of the six idealised spatter bloodstain shapes. The first operation performed by the macro was to convert the greyscale image into a binary black and white image. As the shape images were generated with a pure white background and dark subject, the black and white conversion did not produce any significant alterations in the image shapes. The binary image was subsequently inverted to adhere to typical IA convention where the subject to be analysed is presented in white and the 'background' presented in black.

In this binary form, each image was subjected to a series of analyses at each successive stage of an iterative image manipulation process. The iterative procedure applied in the spatter bloodstain analysis macro was a distance transform erosion process, where at each successive stage of the process a single layer of pixels are removed from around the perimeter of the shape being analysed. This process is designed as a structured mechanism through which the extraneous portions of a shape can be removed while the basic morphology of the

shape remains largely intact, at least until the final steps of the process when the shape becomes so small its morphological characteristics cannot be maintained. At each stage of this iterative process a number of measurements were taken to establish the area, perimeter, centre of gravity, feret lengths, and feret angles of the resultant shape.

The area and perimeter of the shapes are recorded to provide a means of shape analysis, and to provide a comparison to which calculated ellipse areas and perimeters can be compared given the dimensional measurements taken during the shape analysis. The centre of gravity of the shape is calculated to provide a mean location around which the pixels that make up the shape under analysis within the image are distributed. In conjunction with the distance transform process the centre of gravity of the shape can also provide a measure of shape uniformity and consistency depending on the degree of movement of this location throughout the image reduction process.



*Figure 7-2 – The definitions of the feret minimum and feret maximum measurements, and the feret maximum and feret minimum angles as they apply to an ideal ellipse.*

The feret maximum and feret minimum of a shape are determined by rotating two parallel lines around the centre of gravity of the shape, with each line touching the edge of the shape. Where the perpendicular distance between these two lines is at a maximum is defined as the feret maximum, and where this distance is at a minimum is defined as the feret minimum. In conjunction with the distance between the two lines in each of these cases, the angle that the lines make with a horizontal line is also established. Where the shape under



investigation is elliptical the feret maximum and feret minimum should indicate the length and width of the ellipse respectively, and the angle of the feret maximum should indicate the orientation of the long axis of the ellipse, as shown in Figure 7-2.

## **7.4 Results**

The tabulated results of the IA process employed during this pilot project for each of the six idealised spatter bloodstain shapes are included in the appendix of this thesis (Appendix L). The following sections of this report will describe and analyse the potential application of these results to the quantification and measurement of spatter bloodstain morphologies. This analysis will highlight a number of the trends observed in both the raw IA data, and the analysis of this data in terms of evaluating the ellipticity of the each of the six shapes.

### **7.4.1 Centre of Gravity**

The locations of the centres of gravity for the six spatter bloodstain shapes at each successive iteration of the distance transform process are shown in Figure 7-3 to Figure 7-8. The centres of gravity for each spatter bloodstain shape are calculated relative to their specific image sizes, and as a result the specific locations recorded are not directly comparable to the control shape IS-A or each other. The location of each centre of gravity is measured from the top left corner of each image, which is assigned the (0,0) reference position.

The centre of gravity of shape IS-A maintains a virtually constant position during the iterative distance transform procedure. The range of the x-axis location of the centre of gravity was recorded as between 87.5 and 87.6 pixels, while the y-axis location ranged between 102.2 and 102.5 pixels. The centre of shape IS-A, as a result, varies by less than a single pixel during the distance transform process, suggesting that shape is both consistent and uniform throughout the process, and that the centre of gravity of the shape provides a reasonable approximation for the centre of the gross morphology of this shape. The slight variation in the location of the centre of gravity in both axes towards the end of the distance transform process is likely to be a result of the distortion of the predominant morphology of the shape caused by the transform process itself, and

is a feature that appears in the analysis of the centre of gravity of all of the ideal spatter bloodstain shapes.

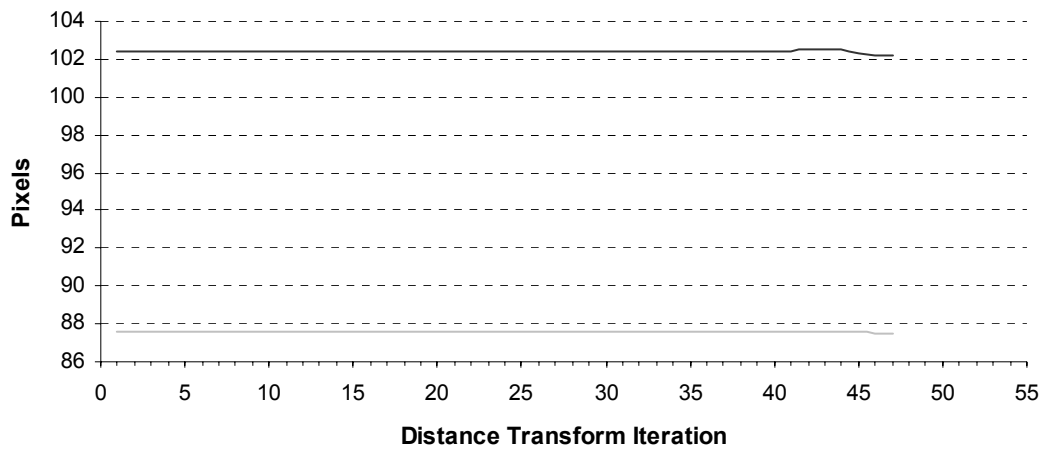


Figure 7-3 - A graph showing the location of the centre of gravity for shape IS-A at each successive stage of the distance transform process. The location of this point within the x-axis is indicated by the light grey line, and in the y-axis by the black line.

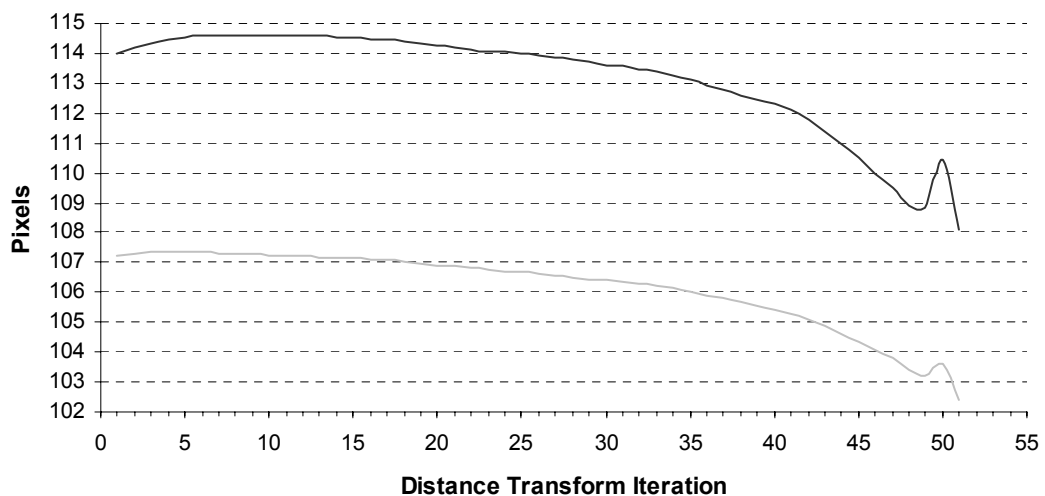


Figure 7-4 - A graph showing the location of the centre of gravity for shape IS-B at each successive stage of the distance transform process. The location of this point within the x-axis is indicated by the light grey line, and in the y-axis by the black line.

The location of the centre of gravity for shape IS-B demonstrates a degree of variation during the distance transform process. The range of locations for the centre of gravity in the x-axis was measured between 103.8 and 107.4 pixels. The location in the y-axis was measured between 109.5 and 114.6 pixels, giving an approximate variation of 5 pixels in each axis. The predominant trend of movement of the centre of gravity for this shape in both axes is towards the lower figures, or top left of the image, during the distance transform process.

This movement only becomes relatively extreme around the 35<sup>th</sup> iteration of the process. Before this the variation in the location of the centre of gravity in both axes is limited to approximately 1.5 pixels.

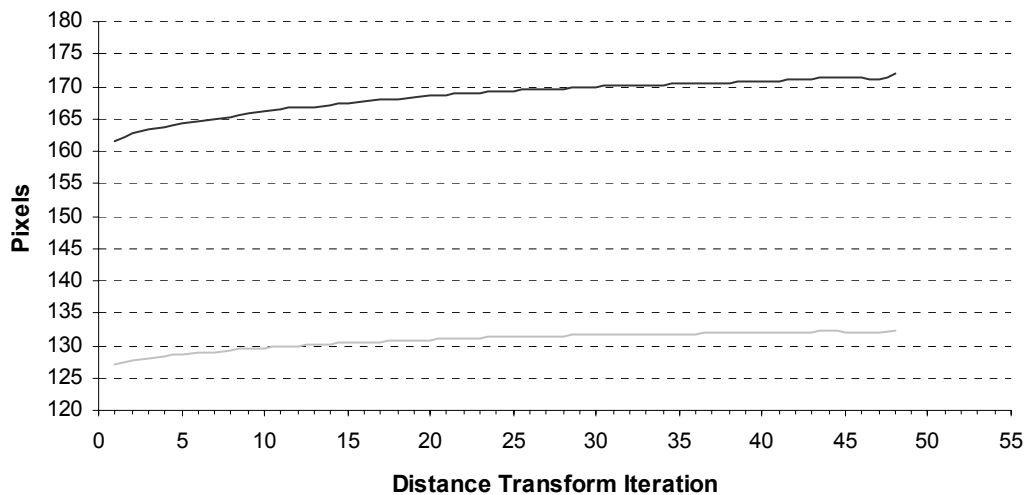


Figure 7-5 - A graph showing the location of the centre of gravity for shape IS-C at each successive stage of the distance transform process. The location of this point within the x-axis is indicated by the light grey line, and in the y-axis by the black line.

The centre of gravity for shape IS-C was measured over a range of 127.2 to 132.4 pixels in the x-axis, and 161.6 to 172 pixels in the y-axis, providing a variation of approximately 5 pixels and 10 pixels in the x and y axes respectively. The movement of the centre of gravity during the distance transform process for this shape exhibits a trend of movement from the top left of the shape (the lower figures) towards the lower right (the higher figures). The locations of the centre of gravity also appear to become more stable as the number of iterations of the processes increases.

The location of the centre of gravity of shape IS-D exhibits some of the most extreme variation of any of the six idealised spatter bloodstain shapes during the distance transform process (Figure 7-6). The x-axis locations were recorded as ranging between 50.6 and 132.2 pixels, and the y-axis between 32.9 and 191.2 pixels. The extreme low readings returned during this analysis are restricted, however, to the 4<sup>th</sup>, 5<sup>th</sup> and 6<sup>th</sup> iterations of the distance transform, suggesting some morphological anomaly during these stages. With these seemingly anomalous measurements removed from consideration the centre of gravity of shape IS-C varies between 124.8 and 132.2 pixels in the x-axis, and 176.4 and 191.2 in the y-axis, providing a variation of approximately 8 pixels in the x-axis,

and 15 pixels in the y-axis. With this section removed the location of the centre of gravity exhibits an upward trend before remaining relatively constant between the 10<sup>th</sup> and the 45<sup>th</sup> iterations of the distance transform process. Between these iterations a variation of approximately 1.5 pixels is evident in both axes.

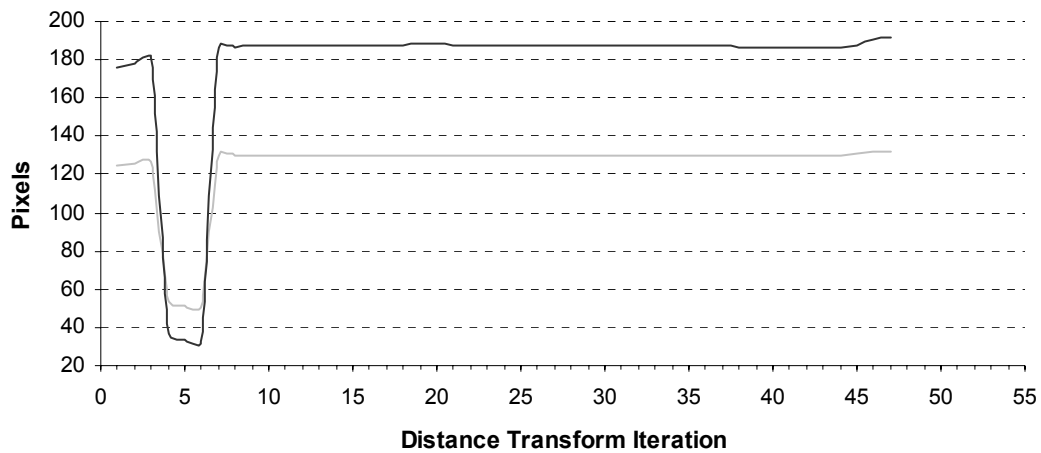


Figure 7-6 - A graph showing the location of the centre of gravity for shape IS-D at each successive stage of the distance transform process. The location of this point within the x-axis is indicated by the light grey line, and in the y-axis by the black line.

The analysis of the centre of gravity of shape IS-E, illustrated in Figure 7-7, recorded a range of results between 122.7 and 137 pixels in the x-axis, and between 170.4 and 205.6 pixels in the y-axis. The overall variation in the location of the centre of gravity exhibited a difference of approximately 15 and 35 pixels in the x and y axes respectively. The extreme minimum and maximum results recorded for both axes in the analysis of this shape are, however, a product of the seemingly anomalous readings taken between the 49<sup>th</sup> and 52<sup>nd</sup> iterations of the distance transform process. While variations in reading towards the end of the iterative image reduction process were both predicted and experienced in the analysis of the other ideal spatter bloodstain shapes, the variation seems to be particularly extreme in this case. With the removal of these potentially anomalous readings the range of location of the centre of gravity of shape IS-E varies between 126.6 and 132.3 pixels in the x-axis and 182.8 and 194 pixels in the y-axis, providing a variation of approximately 6 pixels in the x-axis, and 11 pixels in the y-axis. The movement of the centre of gravity during the distance transform process for this shape also exhibits a trend from the lower to higher figures as the number of iterations of the process increase.

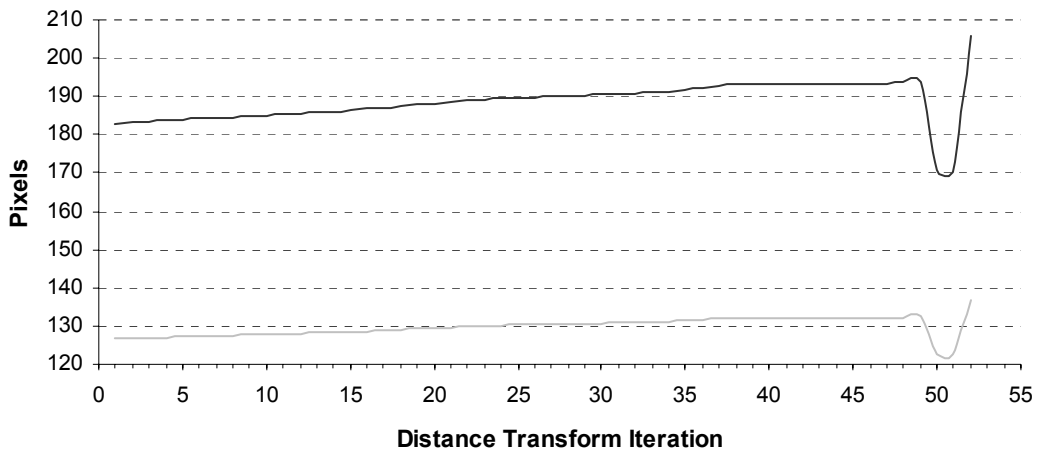


Figure 7-7 - A graph showing the location of the centre of gravity for shape IS-E at each successive stage of the distance transform process. The location of this point within the x-axis is indicated by the light grey line, and in the y-axis by the black line.

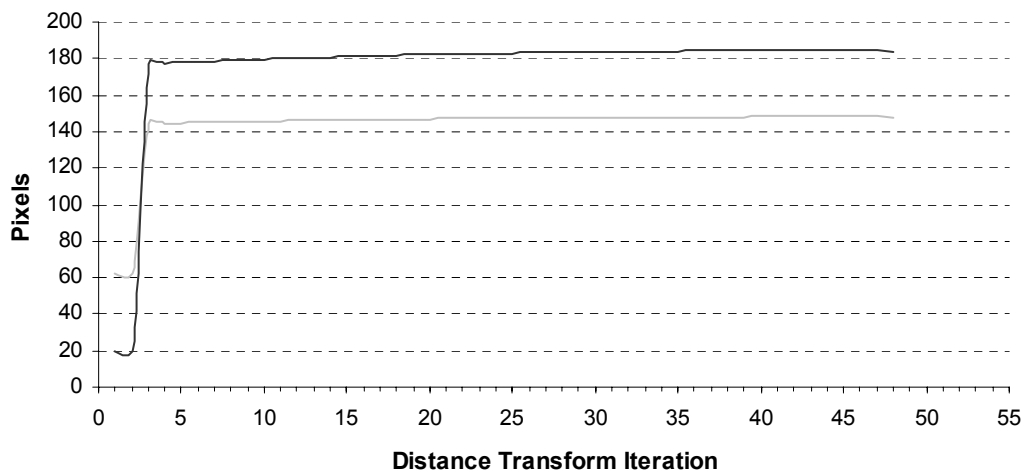


Figure 7-8 - A graph showing the location of the centre of gravity for shape IS-F at each successive stage of the distance transform process. The location of this point within the x-axis is indicated by the light grey line, and in the y-axis by the black line.

Shape IS-F exhibits a large degree of variation in the locations of its centre of gravity during the distance transform process in a similar fashion to that recorded for shape IS-D, as illustrated in Figure 7-8. The range of locations of the centre of gravity of this shape was recorded between 62.4 and 148.3 pixels in the x-axis and between 19.8 and 185.2 pixels in the y-axis. With seemingly anomalous reading taken during the first three stages of the iterative distance transform process removed, however, this variation is reduced to between 144.2 and 148.3 pixels in the x-axis and between 177.1 and 185.2 pixels in the y-axis, providing a range of approximately 4 and 8 pixels in the x and y axes respectively. The

predominant trend exhibited during the analysis of this shape is the movement of the centre of gravity from the lower towards the higher figures, again suggesting a movement from the upper left of the image towards the lower right.

The analysis of the centres of gravity of the six idealised spatter bloodstain shapes reveals a number of features which could be applicable to quantification of spatter bloodstain morphology for the purposes of site of impact estimation. Firstly, the consistency of the centre of gravity of shape IS-A demonstrates that the distance transform, if applied to a uniform and consistent elliptical shape, can return a relatively constant location for the centre of gravity. As a result this process can be considered to provide both a reasonable approximation of the location of a uniform elliptical shape within its image frame, but also to provide a comparative benchmark against which other shapes, whose morphologies are known to be predominantly elliptical, can be evaluated. Such a comparative functionality can be demonstrated in the consideration of the consistency of the centre of gravity of shape IS-D. The relatively high consistency in the majority of the centre of gravities of shape IS-D during the distance transform process, for example, suggest that in this case the image erosion process was successful in removing the extraneous spines from the shape, leaving the predominant elliptical morphology for subsequent analysis. In contrast to this situation, however, the analysis of shapes IS-C, which also exhibits an extended spine morphology, is unlikely to have been as successful in removing these features from subsequent stages of the analysis, as a larger degree of variation in the location of the centre of gravity is experienced throughout the distance transform process in this case. The analysis of shape IS-F does support the interpretation of revealing elliptical shape suggested in the results of shape IS-D, although the anomalous readings present at the very beginning of the analysis of this shape do mask this potential relationship.

Secondly, the variation evident in the centre of gravity, even in shapes where consistency is not achieved, could be a useful indicator as to spatter shape and orientation. The larger variation demonstrated in the y-axis compared to the x-axis of the shapes with extended morphologies such as IS-C, IS-E and IS-F, for example, is in direct contrast to shapes that exhibit, at least at some stage in the distance transform process, a similar variation in the location of the centre of gravity in both axes. This similar variation is evident in shapes IS-A, IS-B and IS-D, and could be both an indicator of establishing a more uniform morphology,

as well as being indicative of the general direction of the long axis of the shape for those that exhibit greater variation in one axis.

Third, the movement of the centre of gravity of shapes IS-C, IS-D, IS-E and IS-F during the distance transform process suggest that this function could be applicable to determining the directionality in spatter bloodstain that exhibit extended spines of significantly tapered morphologies. Each of the four shapes demonstrated a movement of the centre of gravity during the distance transform process from the upper left of the image towards the lower right, corresponding to the movement of this location from the direction of the extended portion of the morphology towards the main elliptical body.

Fourth, and in contrast to the previous point, the trend of movement of the centre of gravity in the analysis of shape IS-B is opposite to that of the extended spine morphologies. It may, therefore, be the case that the more distributed crenulations included in this shape constitute a more significant and integral part of the morphological structure, resulting in the rear portion of the shape maintaining a greater influence over the shape during the distance transform process. Such a situation is also indicated by the fact that the consistency of the centre of gravity of shape IS-B is relatively high, suggesting a greater correspondence to a uniform elliptical morphology in the early stages of the iterative image erosion. The opposing conditions in terms of directionality could present some confusion in terms of establishing this direction if considered in isolation, but if used in conjunction with other shape defining functions, such data may not only be useful in defining directionality but could also provide additional mechanisms for spatter shape categorisation.

Fifth, the similarity in the anomalous reading in shapes IS-D and IS-F suggest that these are a result of the initial separate satellite spatter morphology included in shape IS-F, and the generation of a separate morphological structure from the predominant spine of shape IS-D during the distance transform process. The likely cause of the anomalous readings is also reflected in the results of the measurements of the feret lengths, area and perimeter of these two shapes. To counteract this problem, future attempts to develop this automated IA method will require additional functions to identify the presence of multiple structures within each single spatter bloodstain image, and provide analysis of one or both of these structures.

Finally, the relatively large variation demonstrated towards the end of the distance transform process for shape IS-E in comparison to the other idealised spatter bloodstain shapes may indicate that morphologies with more distributed crenulations could experience considerable variation in the final stages of the distance transform process. This result is likely to be a product of the fact that the distance transform process was not able to effectively remove the more distributed crenulations included in this shape during the early stages of the iterative process. The crenulations in shape IS-E, as a result, may maintain an influence over the morphology of the shape throughout the analysis procedure. While this possibility, if considered in isolation, could have implications on the accurate quantification of the elliptical morphology of the shape, it could also provide automated IA mechanisms with additional means of identifying this type of spatter morphology. This relatively high level of variation towards the end of the distance transform process, however, is not mirrored in the analysis of shape IS-B, which also exhibits distributed crenulations, but not to the extent of shape IS-E.

#### **7.4.2 Feret Length**

Figure 7-9 shows the results of the feret minimum measurements taken for all six spatter bloodstain shapes at each iterative stage of the distance transform process. The results indicate a relatively constant decrease in the size of this measurement for each spatter bloodstain shape, with a relatively close correspondence between the measurements of shapes IS-A, IS-C, IS-D, and IS-F. While shapes IS-B and IS-E demonstrate a similar feret minimum decrease as the other shapes, they represent a separate group where this feret measurement is noticeably higher, with shape IS-E consistently returning the greatest measurement.

Shapes IS-D and IS-F, whose results demonstrate significantly low anomalous readings towards the beginning of the distance transform process, are the two notable exceptions to this linear trend in the decrease of the feret minimum measurement. The feret minimum measurements of shape IS-D also demonstrate additional variation, returning a measurement similar to that of the consistently larger measurements of shape IS-E during the first three iterations of the distance transform process, before closely corresponding to the measurements of the ideal ellipse shape IS-A after the anomalous results of the



4<sup>th</sup>, 5<sup>th</sup> and 6<sup>th</sup> iterations of the distance transform. The first feret minimum measurement taken for the ideal elliptical shape IS-A during the distance transform process was recorded as 88.2 pixels. Given that a single layer of pixels had already been removed, the original feret minimum length of this shape is likely to be close to 90 pixels, a length consistent with the known width of the ellipse constructed for shape IS-A.

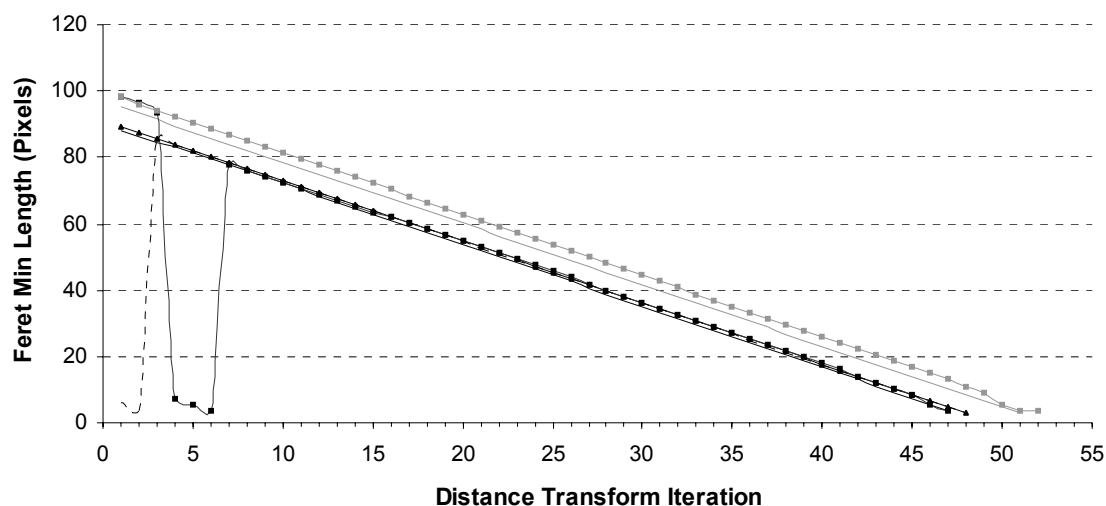


Figure 7-9 – The feret minimum measurements taken for each spatter bloodstain shape at each stage of the iterative IA process. IS-A = solid black line, IS-B = solid grey line, IS-C = solid black line with triangles, IS-D = solid black line with squares, IS-E = solid grey line with squares, IS-F = dashed black line.

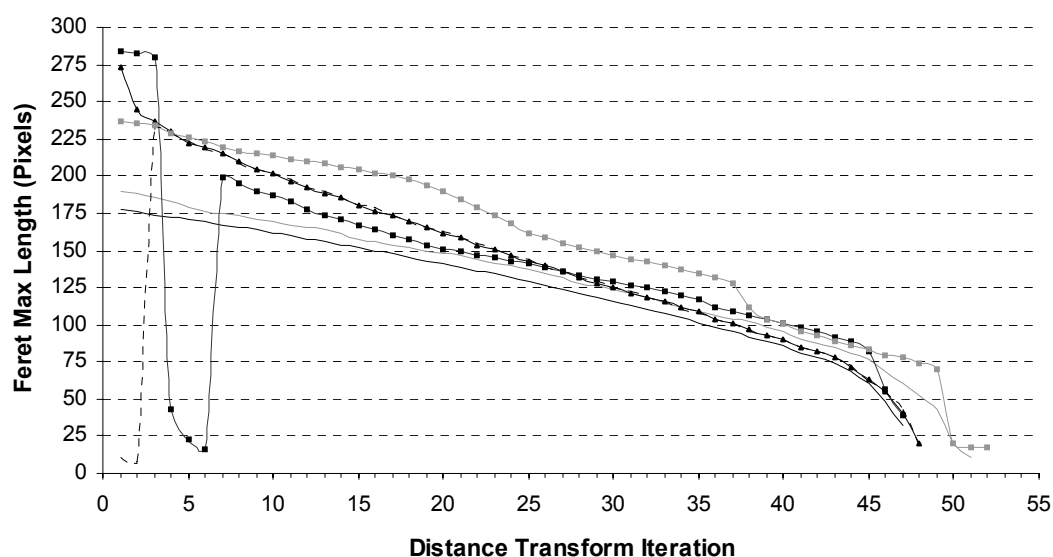


Figure 7-10 – The feret maximum measurements taken for each spatter bloodstain shape at each stage of the iterative IA process. IS-A = solid black line, IS-B = solid grey line, IS-C = solid black line with triangles, IS-D = solid black line with squares, IS-E = solid grey line with squares, IS-F = dashed black line.

The feret maximum measurements taken for each of the six spatter bloodstain shapes at each stage of the distance transform process are shown in Figure 7-10. The predominant trend in the results of the feret maximum for the majority of the six shapes analysed demonstrates a relatively consistent decrease in the feret length during the central section of the distance transform process. In contrast to the feret minimum measurements, however, the results of the feret maximum length exhibit significantly more variation between the six different shapes. The feret maximum results for shape IS-A exhibit a relatively consistent decrease at each stage of the distance transform process until the final stages of the analysis. The initial feret maximum reading for this shape was recorded as 177.7 pixels indicating an approximate original shape measurement of 180 pixels, a length consistent with that of the known length of the elliptical shape constructed for shape IS-A. Shape IS-B demonstrates a comparable pattern in feret maximum decrease to shape IS-A, although the measurements for this shape are consistently higher than that of shape IS-A. Shapes IS-D and IS-F exhibit a series of anomalous low feret maximum readings towards the beginning of the distance transform process comparable to those demonstrated in the analysis of the centre of gravity and feret minimum of these shapes. Following these anomalous readings for shape IS-F the pattern of the feret maximum measurements corresponds closely to that of shape IS-C, and both of these converge on, but never correspond to, the measurements for IS-A during the distance transform process. The feret maximum measurements for shape IS-C also indicate a rapid decrease in this length during the first few iterations of the distance transform process before reaching a consistent decline until the final iterations of the procedure. The initial rapid decrease in the feret maximum measurement also appears to be mirrored by shape IS-D, although for this shape the anomalous readings between the 4<sup>th</sup> and 6<sup>th</sup> iterations of the distance transform mask this detail. After the 6<sup>th</sup> iteration the pattern of feret maximum measurements for shape IS-D exhibits a consistent decline, comparable to that of shape IS-A, but returning consistently larger measurements. Shape IS-E represents the most variable shape in terms of feret maximum measurements, exhibiting a relatively inconsistent decline in this feret length throughout much of the distance transform process. Sections of the analysis of shape IS-E, between the 25<sup>th</sup> and 37<sup>th</sup> iterations, and 40<sup>th</sup> and 49<sup>th</sup> iterations, however, do demonstrate a relationship similar to that of the decrease in shape IS-A, although these measurement are larger than that for shape IS-A, with the former section demonstrating the greatest difference.

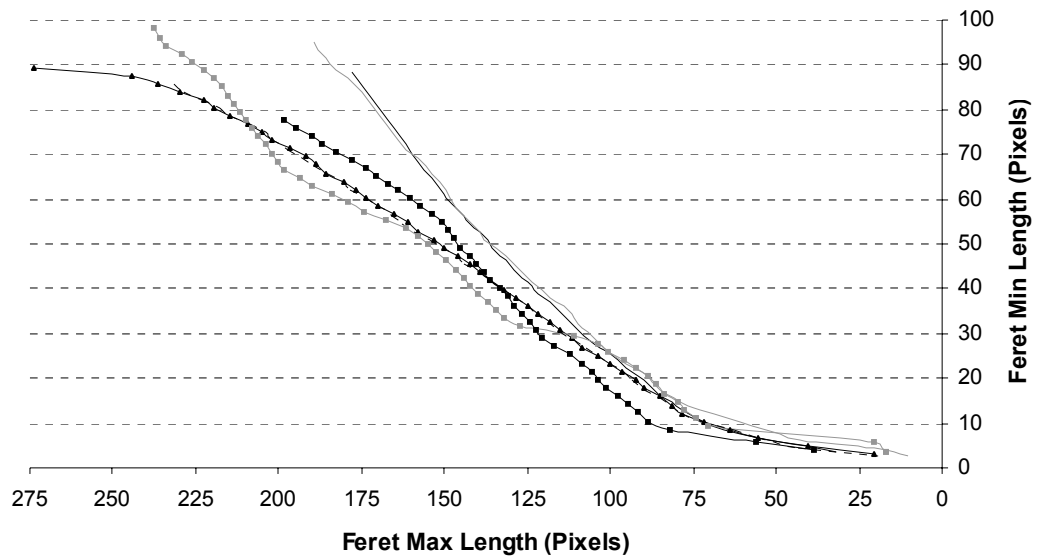


Figure 7-11 - The feret minimum measurement plotted against the feret maximum measurement taken for each spatter bloodstain shape at each stage of the iterative IA process. IS-A = solid black line, IS-B = solid grey line, IS-C = solid black line with triangles, IS-D = solid black line with squares, IS-E = solid grey line with squares, IS-F = dashed black line.

The feret minimum and feret maximum measurements recorded for each of the six idealised spatter bloodstain shapes and the relationship between these two measurements are shown in Figure 7-11. The anomalous measurements recorded for shapes IS-D and IS-F are omitted from this analysis to provide a greater clarity in evaluating the relationships between the feret lengths. Of the six shapes analysed, three main groups appear to be present in this data. Shapes IS-A and IS-B make up the first grouping with both shapes demonstrating a comparable feret length relationship across the range of feret length, although IS-B does depart from this relationship as these measurements become significantly small, demonstrating a larger feret minimum measurement than shape IS-A. The predominant feret relationship exhibited by this group demonstrates a relatively consistent linear relationship up to a feret length of approximately 40 and 125 pixels for the feret minimum and feret maximum respectively. Below this feret size relationship the decrease in the size of the feret minimum becomes progressively less in relation to the decrease in feret maximum length. The second predominant shape grouping in terms of the relationship between the feret minimum and feret maximum measurements is that of shapes IS-C and IS-F. Both of these shapes show a relatively high level of correspondence, as well as demonstrating some convergence on the measurements of shape IS-A as the dimensions of all three shapes become small. The association between the feret minimum and feret maximum in these groups

indicated that at the larger and smaller sizes of both ferets the decrease in the feret maximum measurement is relative great compared to that of the feret minimum measurement, whereas in between these two cases a relatively constant linear relationship is evident. The third grouping suggested in this feret data consists of shapes IS-D and IS-E, in the sense that the feret relationships exhibited by both shapes are relatively distinct in terms of their correspondence to the other shapes, as well as demonstrating a greater degree of variation in their respective feret relationships. While shape IS-E appears to present the most variable feret relationship of this shape grouping, the associated feret maximum and feret minimum lengths of this shape do correspond to some degree with those of shape IS-A between the feret lengths of 25 and 10 pixels for the minimum feret, and 100 and 75 pixels for the maximum feret. The feret measurements and relationships for shape IS-D do not appear to correspond closely to those of shape IS-A until the final stages of the iterations process.

The feret measurement functions applied in the analysis of the six idealised spatter bloodstain shapes during this pilot IA project suggest a number of potential ways in which this type of analysis could be applied in the quantitative assessment of the morphology of spatter bloodstains. Firstly, the measurements of both the feret minimum and feret maximum lengths of shape IS-A for the first iteration of the distance transform process suggest that a high level of correspondence between the actual axial measurements of an elliptical shape, and the IA feret measurements can be achieved. The implication of these results is, therefore, that if the base elliptical morphology that was used to construct each of the six idealised spatter bloodstain shapes can be separated from the total morphology of the shape, then the application of the feret minimum and feret maximum functions should provide a reasonable approximation of the axial dimensions of these ellipses.

Secondly, the fact that the measurements of the feret minimum for each shape demonstrate a consistent decrease at each stage of the distance transform could suggest that this geometrical function is consistently measuring the same morphological feature within each specific shape at each successive iteration of the distance transform procedure. For the group of shapes whose feret minimum measurements correspond closely to that of shape IS-A such a possibility could also indicate that this feret minimum function is measuring the width of the elliptical morphology of the shapes in these cases, as in shape IS-A the smallest edge to edge distance of its known elliptical morphology should consistently be its

width, or minor axis. The consistently larger feret minimum measurements returned for shapes IS-B and IS-E suggest that while a consistent width measurement may be being taken, this width is likely to incorporate the more widely distributed crenulations included in these shapes, and the distortion of the elliptical width presented by these features are influential in shape morphology throughout the distance transform process.

Third, as in the analysis of the centre of gravity of the six idealised spatter bloodstain shapes, the anomalies observed in the feret measurements of shapes IS-D and IS-F are thought to be due to a separate morphological feature from the main body of the shapes during these iterations of the analysis. This hypothesis is reinforced by these feret length results, because not only does a dramatic change in the centre of gravity of the two shapes take place, but a severe reduction in both feret lengths also occurs over the same iterations of the distance transform.

Fourth, the ability of the distance transform process to remove the extraneous morphological features from the analysis of the predominant shape of each image is further suggested in the analysis of the feret functions. The feret minimum results for shape IS-D suggest an early width comparable to that of shape IS-B and IS-E. After the anomalous readings of this shape, however, the feret minimum results are comparable to those of shape IS-A, suggesting that the extraneous spines projecting from the side of the rear of this shape have been removed, to reveal the shape's principle elliptical morphology. The influence of the extended spines over the morphology of shapes IS-C, IS-D and IS-F also appears to be lessened during the distance transform process, with the analysis of the feret maximum of all three of these shapes exhibiting a relatively rapid drop in the results of these measurements early in the iterative shape erosion process. Such a rapid decline in feret maximum length, if restricted to spatter bloodstains with extended morphologies, as suggested by the shapes analysed during this project, could also provide an additional means of spatter bloodstain categorisation.

Finally, the analysis of the feret minimum and feret maximum together suggests that the application of these functions can provide information on the consistency of potential spatter bloodstain shape and size, as the result for similar shapes such as IS-A and IS-B, and IS-C and IS-F correspond relatively well to each other. This type of shape information, as a result, could provide some potential

in the quantitative categorisation and classification of spatter bloodstain morphologies. In addition, the analysis of the two feret function also indicates that the distance transform process, at least for shapes IS-B, IS-C, IS-E and IS-F, can provide a reasonable approximation to the eroded shape of IS-A at some point during the process, as indicated by the correspondence of both of the feret lengths for these shapes. As a result, it is possible that the distance transform process could achieve some degree of success in revealing the underlying elliptical structure of a spatter bloodstain shape. The difficulty with the application of these results to real situations, where no known base elliptical structure is available for comparison, is that the identification when this stage is reached is not possible from this data alone. If this stage can be identified by alternative means, however, the structured decomposition of each shape during the distance transform process suggests that the original elliptical structure of a shape could possibly be reconstructed, through a reversal of this image erosion process.

### **7.4.3 Feret Angles**

In addition to measuring the lengths of the maximum and minimum ferets of each of the six idealised spatter bloodstain shapes at each successive iterations of the distance transform process, the angles at which each of these measurements were taken was also recorded, as shown in Figure 7-2. While an analysis of the angles at which at the minimum and maximum ferets were established can be a useful means of shape analysis in their own right, this angular data was evaluated during this project with reference to data required from spatter bloodstains for the purposes of site of impact estimation. To this end the angular information collected on the orientation of the two feret measurements for each shape at each stage of the distance transform process was analysed in terms of its potential in providing information on the directionality of each shape, and in the evaluation of the adherence of the feret measurements to an ideal elliptical shape.

#### **7.4.3.1 Directionality**

As each of the six idealised spatter bloodstain shapes created for this IA project were based around a relatively pronounced elliptical morphology, it was

considered to be a reasonable assumption that the feret maximum established for each shape was likely to corresponded to the long axis of the elliptical body of the shapes, or in terms of droplet trajectory reconstruction, the orientation of the directionality of the spatter bloodstain shape. To investigate this premise the angle recorded for each feret maximum measurement was converted into an angle of orientation consistent with the definition of directionality employed during the exhaustive spatter bloodstain recording process described above (see Section 5.3.2). The conversion of the obtuse feret maximum angle recorded for each shape, measured from the horizontal in an anti-clockwise direction (as illustrated in Figure 7-2) to a directionality angle, measured in a clock-wise direction from a vertical datum, was made using Formula 7-1, where  $\theta_d$  and  $\theta_{fmax}$  are the angles of directionality and the feret maximum respectively.

$$\theta_d = 90 + |\theta_{fmax} - 180|$$

Formula 7-1 - Conversion of the feret maximum angle into a directionality angle.

The resulting directionality angles calculated for each of the six idealised spatter bloodstain shapes at each successive iteration of the distance transform process are illustrated in Figure 7-12.

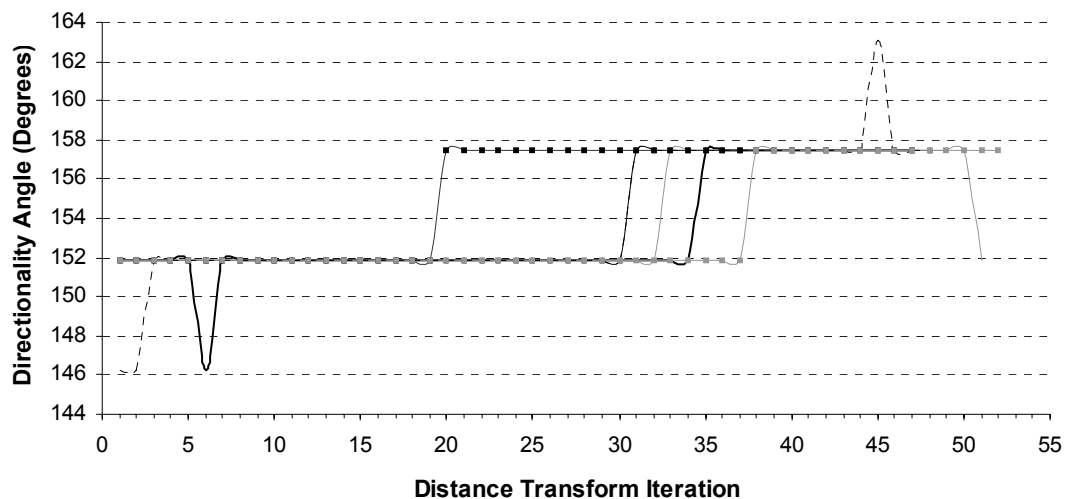


Figure 7-12 - The calculated directionality angle for each of the spatter bloodstain shapes at each stage of the iterative IA process. IS-A = solid black line, IS-B = solid grey line, IS-C = solid black line with triangles, IS-D = solid black line with squares, IS-E = solid grey line with squares, IS-F = dashed black line.

The majority of directionality angles calculated for the six idealised spatter bloodstain shapes indicate an approximate directionality of 152 degrees,

corresponding approximately to the known directionality of 153 degrees for each of the shapes analysed. All six shapes, apart from IS-D, demonstrate a consistent directionality angle up to the 30<sup>th</sup> iteration of the distance transform process, where the predominant directionality angle becomes 158 degrees. Both shapes IS-D and IS-F exhibit anomalous directionalities of approximately 146 degrees during the early iterations of the distance transform process, although these measurements do coincide with the anomalous readings observed in the results of the other IA functions during the image erosion procedure. Shape IS-D also demonstrates some difference to the other five shapes, returning a consistent directionality angle of approximately 158 degrees from the 20<sup>th</sup> iteration of the distance transform process. As well as providing one of the lowest directionality angles shape IS-F also demonstrates the highest directionality angle of approximately 163 degrees at the 45<sup>th</sup> iteration. Table 7-2 demonstrates that the majority of feret maximum angles established for each shape during the distance transform process, with the exception of shape IS-D, return an angle close to that of the known directionality of the idealised spatter bloodstain shapes. The analysis of shapes IS-A and IS-B provides an approximate directionality angle in around 70% of iterations of the distance transform, while shapes IS-B, IS-C and IS-F are consistent with this measurement in approximately 60% of iterations.

<b>Shape</b>	IS-A	IS-B	IS-C	IS-D	IS-E	IS-F
<b>Number of iterations</b>	47	51	48	47	52	48
<b>Number of approx. angles</b>	33	33	30	19	37	28
<b>Ratio</b>	0.70	0.65	0.63	0.40	0.71	0.58

*Table 7-2 - The numbers and ratios of directionality angles calculated as approximately 152 degrees during the distance transform process.*

#### **7.4.3.2 Ellipse Measurement**

To calculate the impact angle of a spatter bloodstain the lengths of both the major and minor axes, or the width and the length, of the fitted ellipse generated for that particular spatter bloodstain must be taken. The IA process, as already discussed above, employed two dimensional measurements, the feret minimum and feret maximum lengths, at each iteration of the distance transform process.



In the case of a perfect ellipse the feret minimum and feret maximum of the shape should correspond to the minor and major axes of the ellipse respectively. To assess the ability of the two feret measurements taken for each spatter bloodstain shape at each stage of the distance transform process to adhere to this elliptical axes measurement the angle between the two established ferets was analysed. The angle between each minimum and maximum feret was calculated by subtracting the acute feret minimum angle from the obtuse feret maximum angle, as they were measured relative to the consistent orientations of the six shapes analysed (see Figure 7-2). To correspond to the elliptical measurements required for the calculation of the impact angle of a spatter bloodstain shape, at least in terms of the orientation of the measurements, the two ferets would have to be established at right angles to one another. The angles between the orientations of the two ferets for each of the six spatter bloodstain shapes during the distance transform process are shown in Figure 7-13.

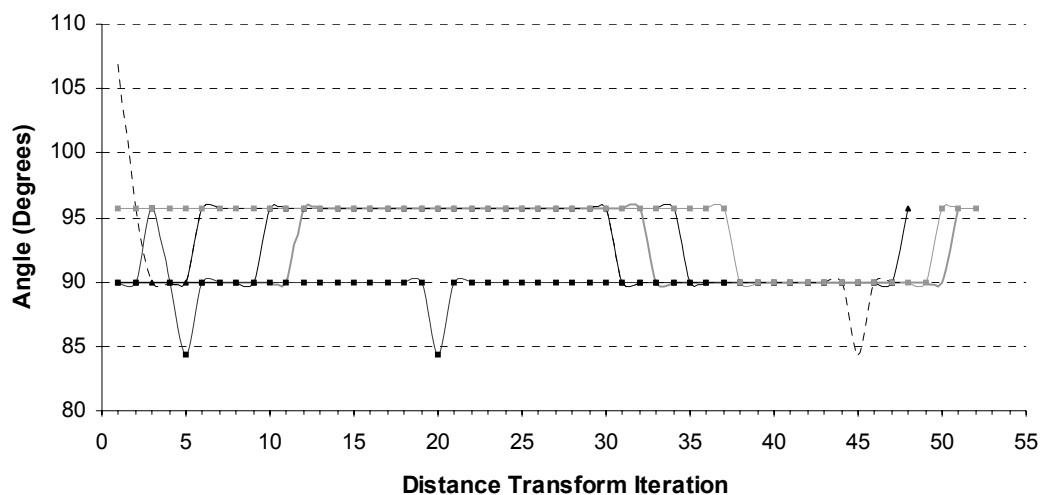


Figure 7-13 – The angle between the feret minimum angle and the feret maximum angle at each iteration of the distance transform process for each of the six shapes analysed. IS-A = solid black line, IS-B = solid grey line, IS-C = solid black line with triangles, IS-D = solid black line with squares, IS-E = solid grey line with squares, IS-F = dashed black line.

The predominant angular relationship between the orientations of the two ferets established for each of the six shapes appears to vary between 90 and approximately 96 degrees during the distance transform process. The majority of shapes return relative angles of 90 degrees towards the beginning and end of the distance transform process, with a predominant trend towards an approximately 96 degree angle between 10<sup>th</sup> and 33<sup>rd</sup> iterations of the procedure. The ferets established for shape IS-A demonstrate a 90-degree separation for the first five

iterations of analysis, and return from a consistent angle of approximately 96 degrees to 90 degrees around the 35<sup>th</sup> iterations. The results for shape IS-B demonstrate a similar relationship to shape IS-A, although for this shape an approximate 96 degree angle of separation between the two ferets is exhibited between the 12<sup>th</sup> and 32<sup>nd</sup> iterations of the distance transform procedure. The angle between the ferets for shape IS-B also returns to an approximate 96 degrees for the final iteration of the analysis of this shape. Shape IS-C exhibits a similar feret angle relationship to shape IS-B, although for this shape the results indicate an approximate 96-degree separation of the ferets between the 10<sup>th</sup> and 30<sup>th</sup> iterations. The final iteration of analysis for this shape also returns an approximate angle of 95 degrees, although this final iteration is the 48<sup>th</sup> for shape IS-C in contrast to the 51<sup>st</sup> for shape IS-B. The angle between the established ferets for shape IS-D provides the most consistent 90-degree separation of all of the six idealised spatter bloodstain shapes. Of the 47 iterations of the distance transform process conducted for shape IS-D only three return results other than 90 degrees. The third iteration of the distance transform process of shape IS-D returns an approximate angle of 96 degrees, whereas the fifth and 20<sup>th</sup> iterations return two of the three lowest angles of separation of approximately 84 degrees. The angle between the two ferets for shape IS-E during the distance transform process demonstrates the consistent result of approximately 96 degrees up to the 37<sup>th</sup> iteration. An angle of 90 degrees is then evident for 12 iterations before the angle of separation of the orientation of the established ferets returns to an approximate angle of 96 degrees for the final three iterations of the distance transform process. The angle between the ferets for shape IS-F demonstrates a similar relationship to shapes IS-A, IS-B and IS-C in that a section of results between the 6<sup>th</sup> and 30<sup>th</sup> iterations return an approximate separation angle of 96 degrees. In addition shape IS-F also exhibits the largest degree of angular separation between the orientation of the two ferets at its first iteration of analysis, returning a result of approximately 107 degrees, as well as returning one of the three lowest results of approximately 84 degrees at the 45<sup>th</sup> iteration of the distance transform process.

Table 7-3 shows the number of iterations for each shape in which the feret measurements are taken at right angles as a ratio of the total number of iterations of the distance transform applied to each of the six shapes analysed. The feret measurements for shapes IS-B and IS-C were taken at right angles to each other in just over half of the distance transform iterations conducted from these shapes, while for shape IS-E approximately 90% of the analyses provided

right-angled feret measurements. For the other three shapes this rate was significantly less, with shapes IS-A and IS-F providing right angled feret measurements in approximately 40% of the distance transform iterations, and shape IS-E adhering to an ideal elliptical measurement in terms of the orientation of feret measurements in only 23% of iterations.

<b>Shape</b>	IS-A	IS-B	IS-C	IS-D	IS-E	IS-F
<b>Number of iterations</b>	47	51	48	47	52	48
<b>Number of right angled ferets</b>	18	29	26	44	12	20
<b>Ratio</b>	0.38	0.57	0.54	0.94	0.23	0.42

*Table 7-3 – The numbers and ratios of feret measurements taken at right angles during the distance transform process for each of the six idealised spatter bloodstain shapes.*

The analysis of the angle of orientation of the two feret functions employed during this pilot IA project suggests a number of relevant features for the analysis of spatter bloodstain morphology for the purposes of site of impact estimation. Firstly, the use of the orientation of the feret maximum angle to provide a reasonable approximation of the known angle of directionality in the majority of analyses for each of the six idealised spatter bloodstain shapes indicates that the use of such a feret function could be used effectively in the analysis of the orientation of spatter bloodstains which exhibit an elliptical morphology. The fact that the directionality indicated by this feret angle remained relatively consistent during the first 30 iterations of the distance transform process suggests that the orientation of five of the six idealised shapes was maintained to a large degree during the image erosion process. In addition, this analysis of directionality was relatively successful for the shapes that exhibit both predominantly elliptical morphologies, such as shapes IS-A and IS-B, and pronounced spine or tail morphologies, such as shapes IS-C, IS-E and IS-F. The comparable results across these spatter shapes could signify a relatively comprehensive technique, at least for the shapes analysed in this project, although any such conclusion is complicated by the exception presented by shape IS-D.

Second, the predominant correspondence of the feret maximum orientation with the angle of directionality during this analysis indicates that the associated feret length measurement, in the majority of cases, was approximately orientated

along the long axis of the elliptical morphology of shapes during the distance transform process. The orientation of this feret maximum function, as a result, provides the potential for the measured length of the feret maximum function to correspond closely to this elliptical dimension. It does not necessarily indicate, however, that this measurement corresponds to the axial dimensions.

Third, while the angle calculated for the directionality of each shape during this analysis corresponds relatively well with the known directionality angle of the idealised spatter bloodstain shapes, the actual analysis of the angle of orientation of the feret maximum only provides information on the orientation of the shapes analysed and not the actual directionality of the shape. For the analysis undertaken during this pilot project, as the directionality was known *a priori*, the feret maximum angle was converted to a directionality angle using this prior knowledge. For a truly automated system where no user input is necessary, additional means independent to the feret maximum function, will be necessary to interpret this essential feature of spatter bloodstain shape in the construction of site of impact estimations.

Fourth, the angle of orientation indicated by the feret maximum angle does not correspond exactly with the known angle of directionality of the six idealised spatter bloodstain shapes produced for the purposes of this IA pilot project. While the angle of directionality in the majority of analyses does correspond well with the known directionality angle of 153 degrees, the actual result returned in these cases was 151.9 degrees. The most accurate determination of the angle of directionality in this project, as a result, demonstrates an error of 1.1 degrees, or approximately 0.3%. While such an amount of error would not necessarily invalidate these results in terms of the already uncertain nature of manual spatter bloodstain interpretation and site of impact estimation techniques, further analysis is needed to investigate the source of this error and improve this figure. One of the potentially redeeming features of this inaccuracy is, however, that it is consistent across all of the shapes analysed.

Finally, the comparatively low correspondence of the angle between the orientation of the feret minimum and feret maximum with the ideal right-angled separation between the two measurements could have considerable consequences for the interpretation and potential accuracy of the feret length functions in terms of measuring elliptical axial dimensions. While the level of disparity of the actual angle between the orientations of the two ferets and the 90

degree ideal in most cases is restricted to plus or minus five degrees, this level of inconsistency, which is even evident in the analysis of the ideal ellipse shape, suggests that the distance transform process, as well as removing extraneous morphological features from the analysis, may also eventually distort the elliptical morphology of each shape.

#### 7.4.4 Area, Perimeter and the Ideal Ellipse Comparison

The area and perimeter of each of the six idealised spatter bloodstain shapes at each iteration of the distance transform process were also recorded during the IA procedure. As the aim of this pilot project was to investigate the potential of this type of automated IA in establishing and measuring, amongst other morphological characteristics, the ellipticity of the spatter bloodstain shapes, the results of these two functions were analysed in respect to their correspondence to the areas and perimeters of ideal elliptical shapes. Both the area and an approximation of the perimeter of an ideal elliptical shape with the same axial dimensions as those measured by the two feret functions were calculated for each of the six shapes analysed at each stage of the distance transform iteration using the mathematical formula shown in Formula 7-2 and Formula 7-3, where  $a$  and  $b$  are the semi-major and semi-minor axes of an ellipse.

$$e_a = \pi ab$$

$$= \pi \left( \frac{F_{\max}}{2} \right) \left( \frac{F_{\min}}{2} \right)$$

*Formula 7-2 - The area of an ideal elliptical shape calculated using the lengths of the semi-major and semi-minor axes.*

$$e_p = 2\pi \sqrt{\frac{a^2 + b^2}{2}}$$

$$= 2\pi \sqrt{\frac{\left( \frac{F_{\max}}{2} \right)^2 + \left( \frac{F_{\min}}{2} \right)^2}{2}}$$

*Formula 7-3 - The approximate perimeter of an ellipse calculated from the semi-major and semi-minor axes (after eFunda, 2005).*

To compare the shapes analysed and the measurements taken for each of the six images during the distance transform process the ratios of the calculated ideal elliptical area and measured area of the shapes, the calculated ideal elliptical perimeter and the measured perimeter of the shapes, and the angles between the orientation of the two feret measurements and the 90 degree ideal necessary for the measurement of the axial dimension of an ellipse were analysed as part of this pilot project. The three ratios of the area, perimeter, and feret orientation measurements taken and the corresponding elliptical ideals for each of the six idealised spatter bloodstain shape at each successive stage of the iterative IA procedure are illustrated in Figure 7-14 to Figure 7-19.

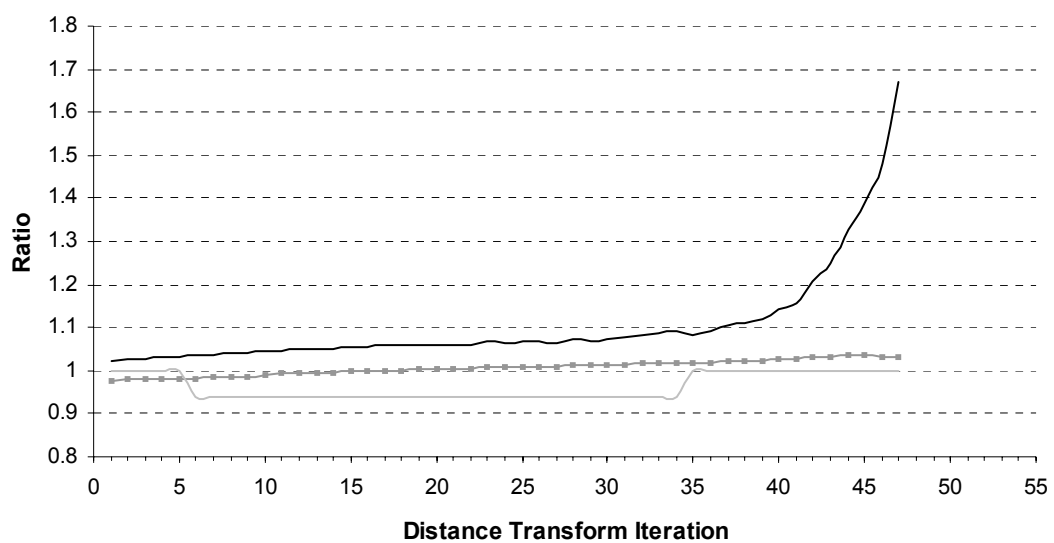


Figure 7-14 – The ideal ellipse ratios for shape IS-A. Area ratio = solid black line, perimeter ratio = solid grey line with squares, angle ratio = light grey solid line.

The ratio for the areas of shape IS-A demonstrates a relatively consistent increase between the first iteration where a ratio of 1.02 was calculated, and the 37<sup>th</sup> iterations where a ratio of approximately 1.10 was returned. After the 37<sup>th</sup> iteration of the distance transform process the increase in the ratio of the ideal to the measured area becomes increasingly rapid. The ratio of the perimeters of shape IS-A also exhibits a relatively constant linear relationship between the ideal and measured perimeters, although in this case the relationship is evident throughout the distance transform process. The initial perimeter ratio for shape IS-A was calculated at approximately 0.98, rising to 1.03 by the final iterations of the shape erosion procedure. The feret angle ratio for shape IS-A demonstrates an ideal ratio of one between the first and fifth iterations, and the 35<sup>th</sup> and 47<sup>th</sup> iterations of the distance transform process. The section of the analysis of shape

IS-A that appears to correspond most closely to the elliptical ideal, when all three ratios are considered is between the first and fifth iterations of the procedure.

The ratio of the calculated and measured areas for shape IS-B demonstrates a relationship similar to that of shape IS-A, exhibiting a predominantly linear association early in the distance transform process, before increasing rapidly towards the end of the procedure. The area ratio results for this shape, however, are consistently higher than for shape IS-A, with the predominantly linear relationship between iterations 5 and 34 exhibiting an increase from approximately 1.06 to 1.12. The area ratio of shape IS-B also demonstrates considerably more variation within this relationship. The perimeter ratio for shape IS-B demonstrates a relatively constant linear relationship after an initially rapid increase in the first three iterations of the process. The perimeter ratio provides its closest correspondence to the ideal between the 43<sup>rd</sup> and 50<sup>th</sup> iterations of the shape erosion procedure, returning a ratio of between approximately 0.99 and 1. The feret angle ratio for shape IS-B corresponds with the ideal between the first and 11<sup>th</sup> iterations, and the 33<sup>rd</sup> and 50<sup>th</sup> iterations of the distance transform process. The section of the analysis of this shape that appears to correspond most closely to the elliptical ideal with respect to all three ratios is between the 5<sup>th</sup> and 11<sup>th</sup> ratios of the shape erosion process.

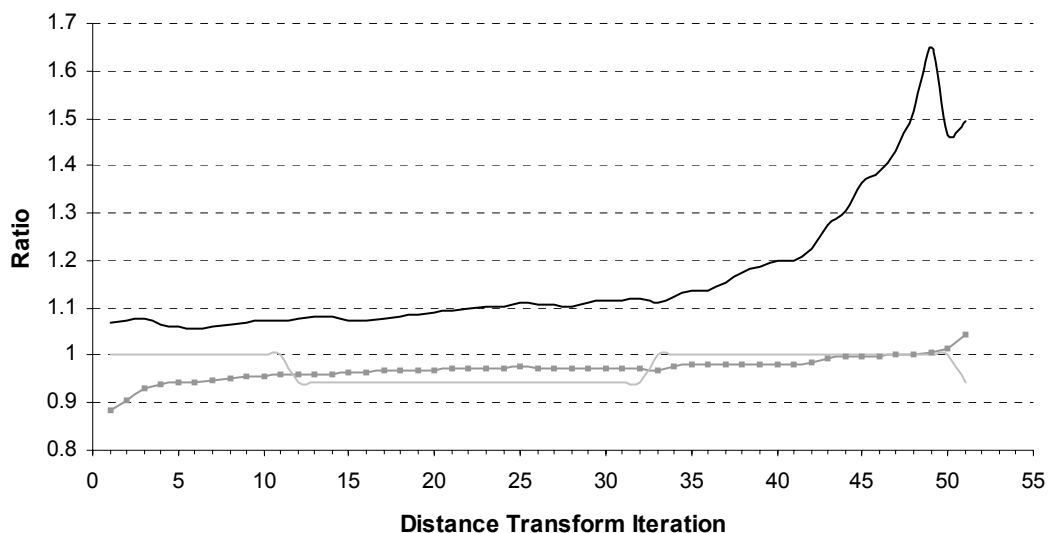


Figure 7-15 - The ideal ellipse ratios for shape IS-B. Area ratio = solid black line, perimeter ratio = solid grey line with squares, angle ratio = light grey solid line.

The relationship between the calculated and measured areas for shape IS-C demonstrates a departure for the general relationship observed with shapes IS-A and IS-B. The area ratio for this shape demonstrates a relatively rapid decrease

in the first two iterations of the process before gradually declining to a level of approximately 1.13 by iteration 28 of the distance transform procedure. The area ratio for shape IS-C subsequently remains relatively constant between approximately 1.13 and 1.14 up to the 39<sup>th</sup> iteration of the shape erosion, after which a rapid increase in ratio, similar to that exhibited by shape IS-A, prevails until the final iteration of the analysis. The perimeter ratio calculated for shape IS-C for each stage of the distance transform process demonstrates a relatively consistent linear relationship, increasing steadily from approximately 1.00 at the first iterations to approximately 1.04 by the final iteration. The feret angle ratio for this shape exhibits two sections of correspondence to the elliptical right-angled measurement ideal between iterations 1 and 9, and iterations 31 and 47. The section of the analysis of shape IS-C that corresponds most closely with the elliptical ideal with respect to each ratio is between the 31<sup>st</sup> and 39<sup>th</sup> iterations of the distance transform procedure.

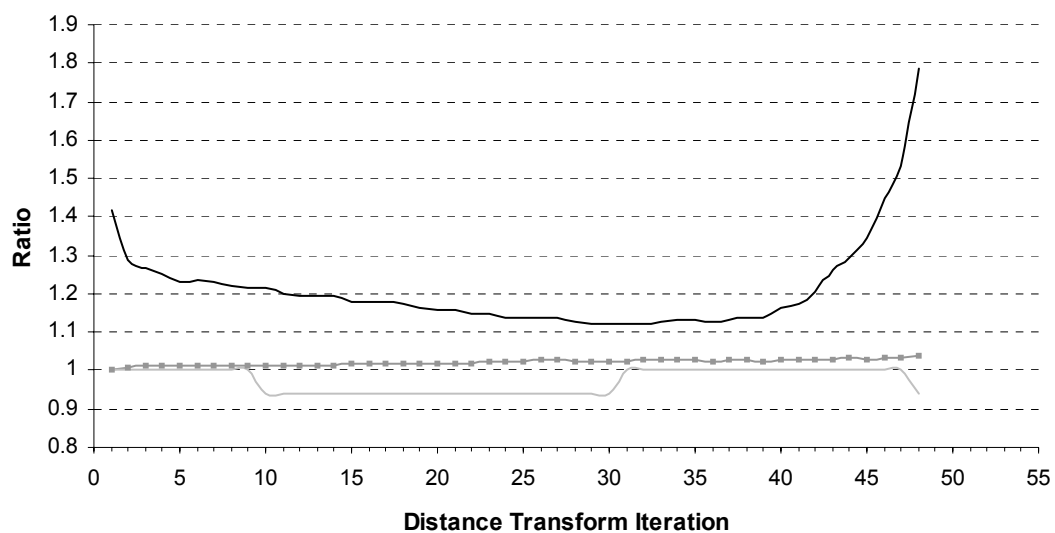


Figure 7-16 - The ideal ellipse ratios for shape IS-C. Area ratio = solid black line, perimeter ratio = solid grey line with squares, angle ratio = light grey solid line.

The ratio of the calculated and measured areas for shape IS-D throughout the distance transform process demonstrates a relationship similar to that observed for shape IS-C. While the early part of this relationship appears to be masked by a series of relatively inconsistent and erratic results between the 4<sup>th</sup> and 6<sup>th</sup> iterations of the process, the predominant trend for the area ratio of shape IS-D demonstrates a decrease in ratio to the 20<sup>th</sup> iteration, where the lowest result of approximately 1.04 is recorded for this shape. Following this result the ratio for shape IS-D increases relatively steadily until the 35<sup>th</sup> iteration of the procedure, where a result of approximately 1.13 was recorded, and with the exception of a



minor decrease around the 36<sup>th</sup> and 37<sup>th</sup> iterations the ratio proceeds to increase rapidly up to the 45<sup>th</sup> iteration of the analysis. Two further seemingly inconsistent ratios are returned for the final two iterations. The perimeter ratio for shape IS-D demonstrates, as with the previous shapes analysed, a relatively consistent linear increase during the distance transform process. With the exception of the irregular ratios recorded at the beginning of the distance transform process the perimeter ratio for this shape appears to process steadily from approximately 0.92 at iteration 7, to 1.03 at iteration 47. The apparent anomalous ratio readings providing during the early stages of the distance transform process are also mirrored in the feret angle ratio for shape IS-D. Two predominant sections, however, correspond to the right-angled ideal feret separation, returning a ratio of 1 between the 5<sup>th</sup> and 19<sup>th</sup> iterations, and the 21<sup>st</sup> and final iteration of the image erosion process. The section of the analysis of shape IS-D that corresponds most closely to the elliptical ideal with respect to all three ratios appears to be between the 21<sup>st</sup> and 33<sup>rd</sup> iterations of the distance transform process.

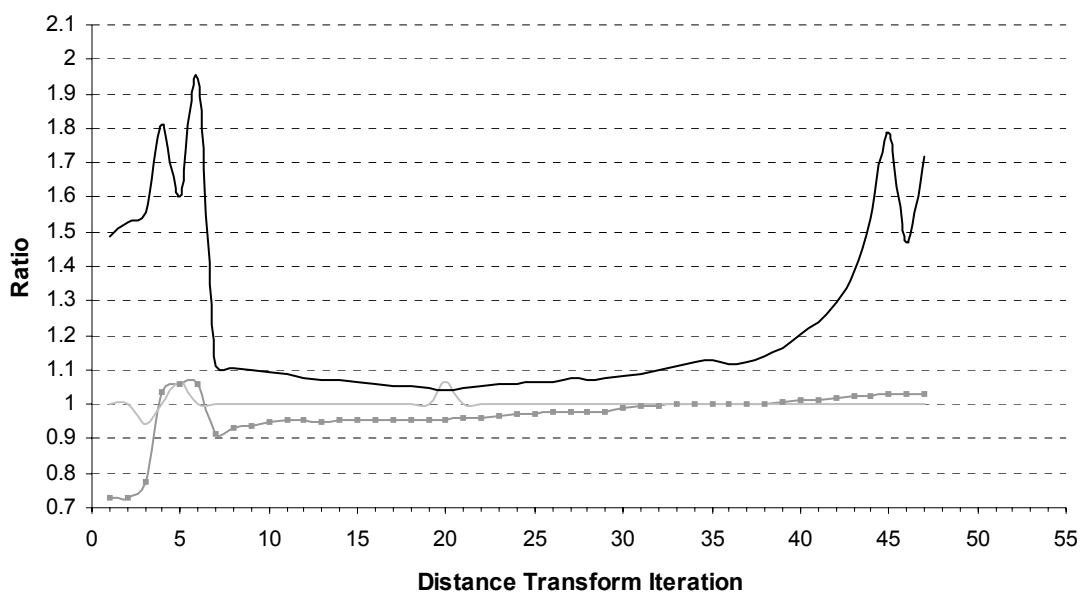


Figure 7-17 - The ideal ellipse ratios for shape IS-D. Area ratio = solid black line, perimeter ratio = solid grey line with squares, angle ratio = light grey solid line.

The area ratio for shape IS-E represents possibly the most inconsistent relationship demonstrated by any of the six idealised spatter bloodstain shapes analysed during the project. The only significant similarity demonstrated in the analysis of shape IS-E is the relatively rapid increase in the area ratio towards the final stages of the distance transform process, although this is interrupted with an

apparently inconsistent reading at the 50<sup>th</sup> iteration. The variable area ratio of shape IS-E provides its lowest results of approximately 1.12 to 1.15 between the 39<sup>th</sup> and 44<sup>th</sup> iterations of the shape erosion procedure. The perimeter ratio for this shape, however, demonstrates a relatively consistent ratio of between approximately 0.99 and 1.01 between the 16<sup>th</sup> and 49<sup>th</sup> iterations of the shape erosion process. Prior to the relatively consistent level the perimeter ratio demonstrates a steady increase from approximately 0.96 at the first iteration, and returns three relatively inconsistent results for the last three iterations of the distance transform procedure. The feret angle ratio for shape IS-E only returns a result of 1, corresponding to the right-angled measurement ideal, for 12 iterations of the distance transform process, between iterations 38 and 49. The region of analysis that appears to correspond most closely with an elliptical ideal in relation to all three ratios is between the 39<sup>th</sup> and 44<sup>th</sup> iterations of the distance transform process.

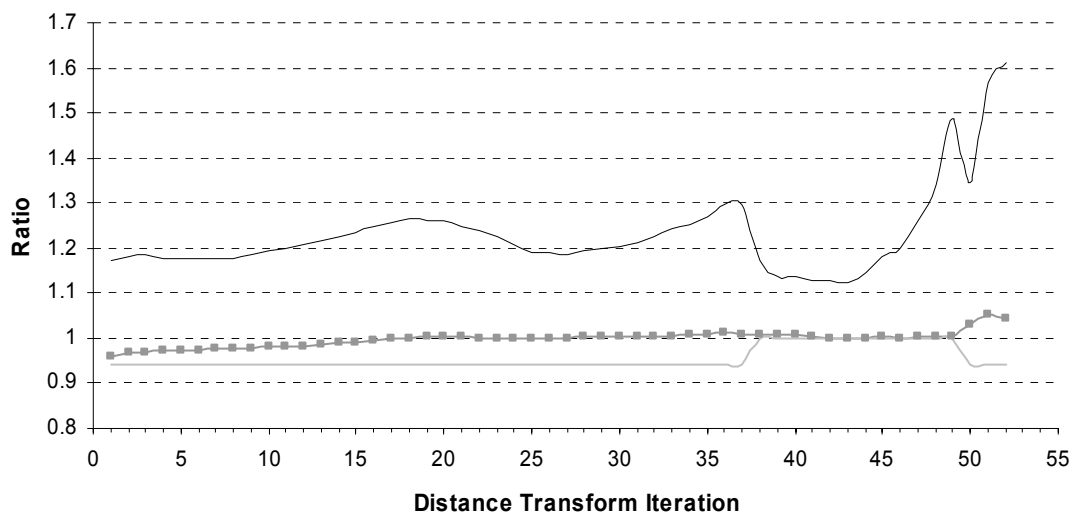


Figure 7-18 - The ideal ellipse ratios for shape IS-E. Area ratio = solid black line, perimeter ratio = solid grey line with squares, angle ratio = light grey solid line.

The relationship demonstrated between the calculated and measured areas by shape IS-F throughout the distance transform process is similar to that of shape IS-C. The area ratio for shape IS-F exhibits a gradual decrease from the 3<sup>rd</sup> iterations of the distance transform process following an apparent extreme value returned for the second iteration. This decrease continues until the 27<sup>th</sup> iteration, where a relatively consistent ratio of between approximately 1.12 and 1.13 is returned until the 38<sup>th</sup> iterations of the shape erosion. The ratio results subsequently demonstrate a rapid increase in ratio, which appears to prevail, with

the exception of the ratio calculated for the 45<sup>th</sup> iterations, until the conclusion of the analysis of this shape.

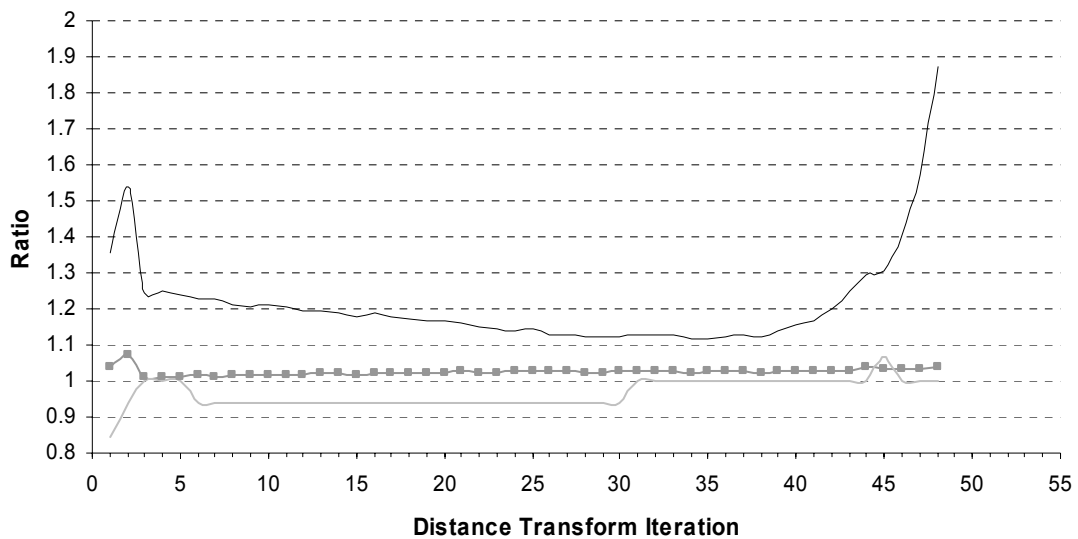


Figure 7-19 - The ideal ellipse ratios for shape IS-F. Area ratio = solid black line, perimeter ratio = solid grey line with squares, angle ratio = light grey solid line.

The perimeter ratio for shape IS-F, as with the other shapes, demonstrates a predominantly linear increase during the distance transform process. Following two ratio results for the first and second iterations of the analysis, which do not correspond to this predominant relationship, the perimeter ratio for this shape tends to increase gradually from 1.01 at the third iteration to approximately 1.04 by the final iteration. The feret ratio, in comparison to the area and perimeter ratios, also returns an apparently anomalous reading early in the distance transform process, with the lowest ratio recorded for any of the shapes analysed of 0.84. The feret angle ratio for shape IS-F exhibits three sections where the angle of separation between the two ferets measured is consistent with the ideal right-angled separation. These sections are evident between the third and the fifth iterations, the 31<sup>st</sup> and 44<sup>th</sup> iterations, and the 46<sup>th</sup> and 48<sup>th</sup> iterations of the shape erosion process. The section of the analysis of this shape that most closely corresponds to the elliptical ideal, in respect to all three ratios, appears to be evident between the 31<sup>st</sup> and 38<sup>th</sup> iterations of the IA procedure.

The analysis of the correspondence of the data obtained during this IA project to an ideal elliptical shape presents a number of implications for this type of image-based investigation of the quantification of spatter bloodstain morphologies. First, the analysis of the area ratio for each shape at each successive stage of the

distance transform process may prove useful in the quantitative categorisation and classification of spatter bloodstain shapes. The elliptical shapes of IS-A and IS-B, for example, appear to demonstrate a similar relationship between the area ratio and the progression of the distance transform process, whereby the ratio steadily increases through the iterative procedure. The area ratio of shapes IS-C, IS-D and IS-F, which were constructed with extended spine morphologies, in contrast, exhibit a relationship whereby the ratio first decreases, and reaching a minimum before subsequently increasing again. This relationship may be indicative of the gradual removal of these extended spines during the distance transform process. The only shape to exhibit a distinct morphology, shape IS-E, also demonstrates a distinct area ratio. This ratio exhibits the least consistent trend of all of the shapes, and possibly signifies the more variable morphology of this shape, with the predominant crenulations influencing the morphology of shape throughout much of the distance transform process.

Second, the area ratio results do suggest that the distance transform process encourages the more complex ideal spatter bloodstain morphologies, such as shapes IS-C to IS-F, to reveal at least some elliptical morphological tendencies. Of these shapes, the results for IS-C, IS-E and IS-F suggest the closest approximation to the elliptical ideal as being 13 to 15% above the expected, possibly suggesting that the more incorporated spine or tail morphologies of these shapes are maintained throughout the shape erosion process. The results for shape IS-D, however, demonstrate a closest elliptical area approximation of only 4% above the ideal, suggesting that the analysis of this shape may have been successful in identifying the elliptical features of this shape to a greater extent than the other shapes with spine morphologies. It may, therefore, be the case that while the distance transform process does appear to reveal some of the ellipticity of the shapes analysed, the procedure performs better on shapes with more distinct spine morphologies where these morphological features are not significantly incorporated within the elliptical morphology of the spatter bloodstain shape. The results provided from the analysis of the more pronounced elliptical shapes, such as IS-A and IS-B, also suggest that the distance transform process could have a detrimental affect on the elliptical nature of these shapes throughout the iterative shape erosion procedure, as the trend of analysis for these morphologies appears to be a steady movement away from the elliptical ideal.

Third, the perimeter ratio does not appear to be as discriminatory, in terms of shape morphology, to the same degree as that exhibited by the area ratio. In the majority of analyses the perimeter ratio, regardless of shape morphology, demonstrates a predominantly linear relationship during the distance transform process, with the ratio tending to increase gradually throughout the procedure. The analysis of the perimeter ratio, however, should be approached with some degree of caution, as the calculation of an ellipse perimeter solely from its axial dimensions is only an approximation of this geometric feature, with the potential maximum error of ten percent (eFunda, 2005). The effect of this of potential error in the approximation of elliptical perimeter could be suggested in the results of the analysis of shape IS-A. While the area ratio for the first iteration of the distance transform process is slightly above one, the trend of this data suggests that if analysed before a layer of pixels has been removed from the shape, the area ratio could be even closer to one. In the case of the perimeter ratio, however, at the first iteration of analysis the ratio is already below one, and the trend exhibited by the following analyses suggests a previous perimeter ratio of even lower than one. The inability of this perimeter analysis to accurately identify the initial elliptical morphology of shape IS-A, in direct contrast to the results of analysis of the area ratio, feret angles, and feret measurements of this shape, could, as a consequence, have implications for the appropriate use of this calculated metric in the analysis of ellipticity conducted during this pilot IA project.

Fourth, the anomalous readings observed at the beginning of the distance transform process for shapes IS-D and IS-F in the other analyses conducted as part of this IA project are also present within the analysis of the area and perimeter ratios of these shapes. While some analysis of the original area and perimeter data recorded for each of the six idealised spatter bloodstain patterns may have provided a more detailed analysis of this phenomenon, the fact that these anomalous readings are present in the same distance transform iterations as the feret and centre of gravity analyses does go some way to reinforcing the hypothesis that these readings are due to the already present separate morphological structure in shape IS-F, and the creation of a separate morphological structure in the case of shape IS-D through the distance transform process.

Finally, in the previous analyses of the IA functions employed during this pilot project, the data generated for the idealised spatter bloodstain shapes IS-B to IS-

F have been repeatedly compared to the data generated for shape IS-A in the evaluation of the ability of the IA procedure to reveal the underlying elliptical morphology of each of these shapes. In the real quantification of spatter bloodstains, however, this type of comparative elliptical shape, with known widths, lengths and orientations is unlikely to be available for the assessment of shape during each stage of the distance transform process. Given the measurements taken during this pilot IA project, the data presented in the analysis of the ratios of the area, perimeter and feret angles of each shape represent the type of data that could be appropriate in establishing the ellipticity of actual spatter bloodstain shapes. While the analysis of this ratio data in this project has been largely based on the visual assessment of the trends exhibited in the data, an automated approach based around the minimisation of similar comparative morphological concepts, could be developed. Although not attempted as part of this pilot project, the minimisation of some function, if achieved, could potentially provide the basis for a reconstruction of the elliptical shape of the original spatter bloodstain morphology.

## **7.5 Discussion**

The research into the use of automated IA procedures in measuring spatter bloodstain shape conducted during this pilot project represents a preliminary investigation of both the potential volume of data generated through the use of such technologies, and the variety of IA techniques that could provide information on spatter bloodstain shapes for the purposes of trajectory reconstruction and site of impact estimation. The relatively limited scope of this pilot project, however, has not precluded the results of this analysis from indicating at least some of the potential that the application of such technologies could bring to the analysis, evaluation and interpretation of spatter bloodstains. The quantitative IA functions applied during this project have been shown to provide the potential for a variety of analytical features applicable to the interpretation of spatter bloodstain morphologies. These features include:

- The classification and identification of specific spatter bloodstain morphologies.
- The determination of approximate angles of shape orientation and directionality indicators.
- The accurate measurement of the axial dimensions of elliptical shapes.

- The comparison of shape data to elliptical ideals.
- The reduction of the influence of extraneous morphological features in the geometric analysis of spatter bloodstain shapes.
- The identification of aspects of the elliptical morphologies of spatter bloodstain shapes.

The preliminary nature of this research does limit the extension and application of the tentative conclusions based on the results of this project, with the practical application of any such automated IA methodologies requiring further investigation and development before providing the quality of data envisaged in the aims of this project. The analysis of the results of this pilot study, however, has highlighted a number of areas in which the specific IA techniques employed, and the nature of the idealised spatter bloodstain shapes analysed could be improved in any future attempts to further this development. These improvements include:

- The provision of an additional stage in the iterative process to investigate the morphology of shapes before any image erosion takes place.
- The inclusion of an additional feret function where the orientations of the minimum and maximum ferets are set at right angles to provide comparative feret data for the evaluation of potential elliptical morphology.
- The comparative analysis of the centre of gravity function for each of the six idealised spatter bloodstain shapes by providing the same absolute location for the elliptical base morphology of each of these shapes within their image frames.
- The analysis of additional spatter bloodstain shapes, sizes and morphological configurations, as well as larger spatter bloodstain data sets to provide a firmer evidential basis for the tentative conclusions of this pilot study.
- The analysis of shapes not commonly associated with spatter bloodstains to investigate the possibility of spatter bloodstain discrimination from background features.
- The inclusion of some mechanism to overcome the anomalous shape data recorded through the inclusion, or generation of separate morphological structures in the analysis, as experienced for shapes IS-D, and IS-F.

The results generated during this pilot project have indicated the capacity of automated IA technologies to accurately measure the axial dimensions of elliptical shapes, and identify stages in the analysis where an elliptical, or close to elliptical spatter bloodstain shape can be inferred. However, it was felt to be beyond the scope of this preliminary analysis to use this elliptical data to reconstruct and analyse the potential elliptical nature of the original idealised spatter bloodstain shape. Further studies are planned, however, in which the minimisation of some elliptical determination function, such as the area, perimeter and angle ratios investigated during this project, could be used to identify those sections of the analysis where a shape corresponds most closely to an elliptical ideal. The possible elliptical section of the original morphology of the shape could subsequently be reconstructed using additional data concerning the centre of gravity of the shape, and the stage of the shape erosion process at which the minimisation of the ellipse function occurred. This reconstructed elliptical shape, generated through the addition of the same number of pixels removed from perimeter of the shape during the distance transform process, could then be quantitatively compared to the original shape morphology and evaluated in terms of any potential correspondence to the morphology of the original spatter bloodstain shape. Where a number of elliptical options are presented, each of these could be analysed, compared and evaluated in relation to each other to establish the most appropriate elliptical shape, or range of shapes for the interpretation of the particular spatter bloodstain morphology in respect to trajectory reconstruction and site of impact estimation.

The possible automated IA project described above, however, represents the analysis, evaluation and development of a relatively small number of IA techniques in relation to the aims of the quantitative analysis of spatter bloodstain morphologies outlined for this project. While the specific analytical IA procedures employed during this project have demonstrated some potential in the analysis of spatter bloodstain, it would likely be restrictive to limit future analyses to the investigation of this data to the exclusion of all others. Alternative approaches, such as the inclusion of ellipse fitting and edge detection algorithms, line-profiling functions, and bivariate and multivariate statistical analyses could provide additional significant information for the evaluation and quantification of spatter bloodstain morphologies. Other approaches, such as analyses based on image colour and intensity, could also provide additional avenues of investigation, and provide both complementary and comparative information to that provided through the analysis of binary image data.



The circumstances under which the idealised spatter bloodstain shapes were analysed during this pilot project may also have implications for the extension of the analytical IA procedures employed to a fully automated spatter bloodstain quantification system. The six shapes analysed during this project were, as frequently referred to, idealised. The six spatter bloodstain shapes were produced and analysed in separate image frames, and were generated in a greyscale format, with a distinct separation between the subject shape to be analysed and the background to be ignored. Providing this level of data in casework conditions could present some difficulties to a totally automated spatter bloodstain quantification system. The accurate thresholding, identification, and separation of each individual spatter bloodstain from its target surface background, as well as the other spatter bloodstain within the impact spatter pattern given, is by no means necessarily straightforward given the variable conditions experienced at crime scenes and the variable manifestation of impact spatter patterns.

The difficulties that total automation presents, however, do not preclude the development of IA systems through a more modular approach. Even the development of a limited automated IA system similar to the methodology of BackTrack<sup>®</sup>/Images (Forensic Computing of Ottawa, 2001c), where a spatter bloodstain image would be selected and thresholded manually, for example, could provide site of impact estimation methodologies with a powerful tool for the quantification of spatter bloodstain morphologies.

## **7.6 Conclusions**

The results of the automated IA pilot project described in this chapter have demonstrated that the detailed analysis of raster images of typical spatter bloodstain shapes, even given a relatively restricted IA approach, can provide site of impact estimation with a large amount of potentially useful quantitative information on spatter bloodstain morphology. The innovative application and development of existing IA techniques to provide the necessary data from spatter bloodstain morphologies for the purpose of site of impact estimation do present a number of specific analytical requirements that could benefit from further explicit investigation. The potential advantages of the development and use of an automated IA system, even where applied to single spatter bloodstain images,

could ultimately provide BPA with a more structured and consistent scientific approach to the interpretation of spatter bloodstain morphology and enable the collection and analysis of considerably larger spatter bloodstain data sets than is currently practical. As a result, the development of a practical and effective automated IA approach to spatter bloodstain morphology quantification may ultimately provide a firmer basis for the construction of site of impact estimates and the further investigation of estimate uncertainty.

## **8 Data Pre-processing and Pattern Characterisation**

### **8.1 Introduction**

This chapter will outline the preliminary analyses conducted for the research project using the data collected from the three experimental impact spatter through the exhaustive spatter bloodstain recording process. The chapter is divided into three main sections. The first section will introduce the Visual Basic programming language and the embedded programming environment of Visual Basic for Applications that were chosen for the development of the analytical system and user interface for the project's computer-based investigation of site of impact estimation. The second section will describe the data pre-processing procedures employed to prepare the raw spatter bloodstain data for the construction of site of impact estimates and aid the detailed characterisation of any collection of spatter bloodstains analysed. The discussion of these methods will include the analysis of a vector trajectory reconstruction approach, the use of the alternative opposite directionality measurement throughout the research project, and the construction of an independent data quality assessment for each spatter bloodstain analysed. The final section of this chapter will describe the specific methods employed in the analysis and characterisation of the composition of a collection of spatter bloodstains, which provide data through which the composition of spatter bloodstain samples and their parent spatter bloodstain populations can be compared and evaluated.

### **8.2 Computer-Based Analysis of Site of Impact Estimation**

The computer application developed for the purposes of constructing, visualising and investigating site of impact estimates during this research project is based on two distinct components:

- The numerical construction and analysis of 3D site of impact estimates.
- The 3D interactive visualisation of the results of these analyses.

The functionality of both of these components is integrated into a single program interface within the final site of impact estimation application, as shown in Figure 8-1. Each of the components was, however, developed using separate programming languages and application development environments that provided

specific advantages for the particular role of each of these components. The development and implementation of the numerical construction and analysis component of the application is addressed within this and the following chapter of this thesis. The development and implementation of the 3D visualisation component of the application is also addressed later in this thesis (see Chapter 10).

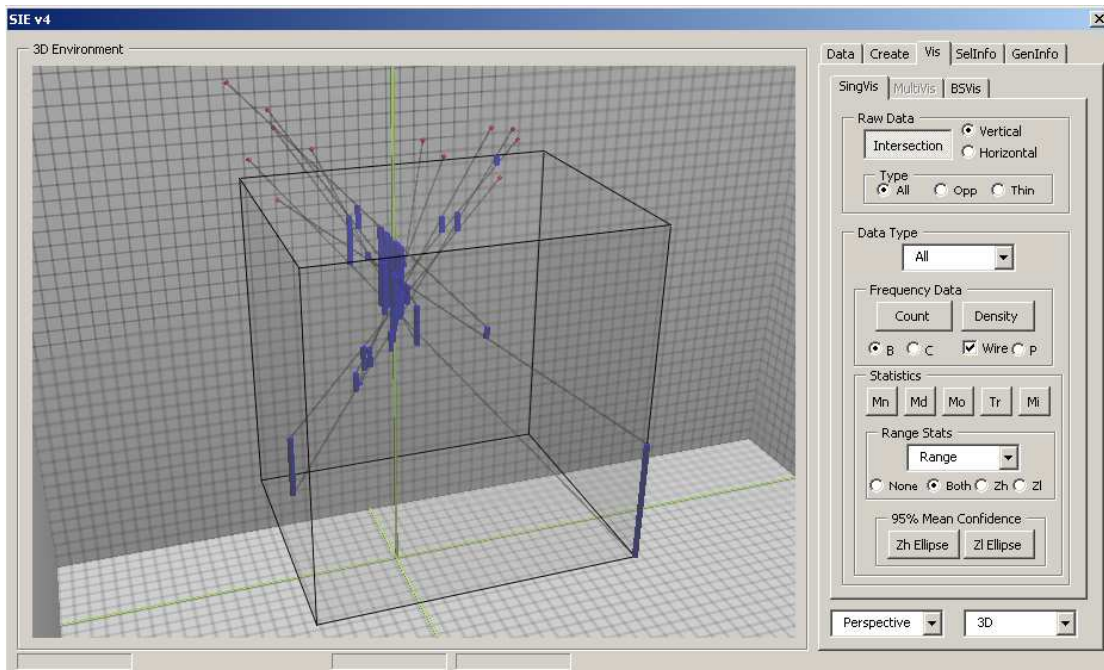


Figure 8-1 - The integrated site of impact estimation analysis and visualisation application.

The construction and analysis component of the analytical site of impact estimation computer application, as well as the general application interface, was designed and developed using the Visual Basic<sup>®3</sup> 6.0 programming language within the Visual Basic<sup>®</sup> for Applications programming environment embedded within the Microsoft<sup>®</sup> Office suite of programs (Microsoft Corporation, 1999). The programming language and development environment were chosen for the development of the site of impact estimation application for a number of reasons. Firstly, Visual Basic<sup>®</sup> (VB) and Visual Basic<sup>®</sup> for Applications (VBA) Application Programming Interface (API) provide the means for the Rapid Application Development (RAD) of programs that run within the common Windows<sup>®</sup> operating system. Secondly, the versatile VB programming language is designed to be human-readable, and is a widely accessible language implemented through

<sup>3</sup> Microsoft, Visual Basic, Windows, ActiveX and Excel are either registered trademarks or trademarks of Microsoft Corporation in the United States and/or other countries.

an integrated development environment (Microsoft Corporation, 2005). Thirdly, the VB API and Windows®-based execution of the program code facilitated the integration of the Macromedia®<sup>4</sup> Shockwave® ActiveX® plug-in within the application to provide the 3D interactive visualisation of the numerical results. Finally, the embedded nature of Visual Basic® for Applications provides the means to extend, automate, and customise the already powerful functionality of the Microsoft® Office (Microsoft Corporation, 2005) suite of programs to meet the specific needs of a varied user base. For the purposes of this project the provision of the Integrated Development Environment (IDE) of VBA within the Excel® (Microsoft Corporation, 2005) spreadsheet application was considered to be advantageous in a number of respects (Figure 8-2). These advantages include:

- Excel® is a commonly used data collation, analysis and presentation tool that can be used to present information in a format both familiar and accessible to a wide range of users.
- The functionality of Excel® includes a number of numeric, trigonometric, and statistical operations applicable to the pre-processing and analysis of site of impact estimation data.
- The conventional graphical representations of data possible within Excel® provide an additional means for the analysis and presentation of any site of impact estimation data generated.
- The large spatter bloodstain datasets collected from the three experimental impact spatter patterns were already recorded in a tabulated Excel® format.
- The proprietary '.xls' file format of Excel® provides an immediate means of providing a structured and accessible record of the large amounts of tabulated data generated through the proposed analysis of site of impact estimates.

The analytical site of impact estimation application was, as a result, developed as an embedded VB macro within an Excel® workbook, and is run from within the Excel® spreadsheet application. The development of a stand-alone analytical site of impact estimation program, as opposed to the embedded version developed during this research project, was not considered necessary due to the experimental research-based nature of the application design. The inclusion of the site of impact estimation analysis program within an Excel® spreadsheet

---

<sup>4</sup> Macromedia and Shockwave are trademarks or registered trademarks of Macromedia, Inc. in the United States and/or other countries.

format also provided a widely distributable format from which few complications in terms of the compatibility of the program with specific computer systems were considered to be likely to occur. The Excel<sup>®</sup> workbook containing the VB macro and the full VB code for this macro are available on the DVD-ROMs which accompany this thesis.

The analytical design of the site of impact estimation application required six main processes to be conducted by the VB macro. These six processes were:

- The acquisition and pre-processing of the spatter bloodstain data.
- The selection of a sample to examine in terms of constructing a site of impact estimation.
- The construction of a particular site of impact estimation.
- The analysis of the data generated through the construction of a site of impact estimation.
- The recording of the results of this analysis.
- Passing these results to the visualisation component of the program for their presentation in a 3D interactive environment.

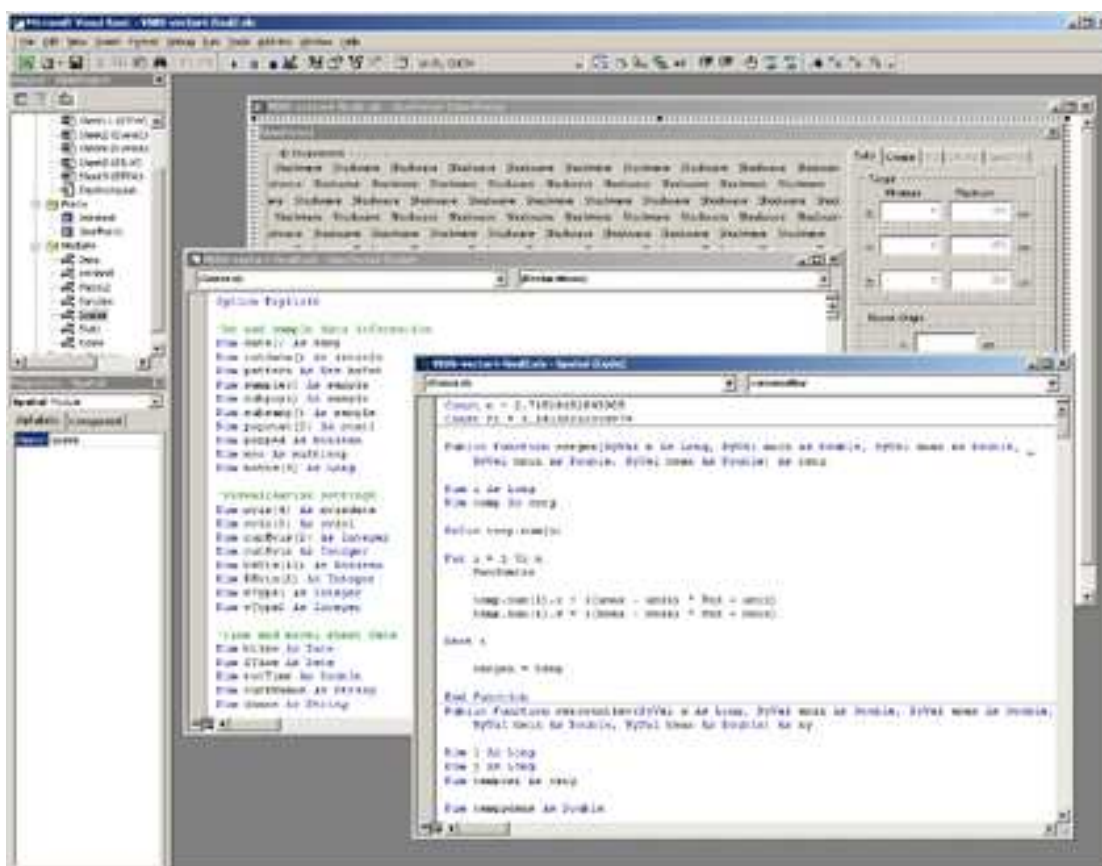


Figure 8-2 – The VBA IDE included embedded within the Excel<sup>®</sup> spreadsheet package.

The first of these six processes, the acquisition and pre-processing of the spatter bloodstain data, while constituting only a small part of the site of impact estimation application in terms of program code and processing time is an essential part of the analytical application design. This initial analysis of the raw spatter bloodstain data was developed to provide a sufficiently detailed level of data to conduct the following sample selection and estimation construction phases of the program. It was also designed to provide additional relevant data for a more detailed analysis of the structure of impact spatter patterns, the spatter bloodstain samples selected from these patterns, and the ability of these samples to construct accurate site of impact estimations. The acquisition and pre-processing of the raw spatter bloodstain data conducted within the analytical site of impact estimation macro is discussed in the remainder of this chapter.

### **8.3 Spatter Bloodstain Data Pre-processing**

An example of a small sample of the raw spatter bloodstain data collected during the exhaustive spatter bloodstain recording process in a form necessary for the construction of 3D site of impact estimates using the Excel® VB macro is provided in Table 8-1. The information provided by this raw spatter bloodstain data includes:

- The plane and normal of the target surface upon which each spatter bloodstain was observed.
- The 3D location of each spatter bloodstain.
- The elliptical width and length dimensional measurements recorded for each spatter bloodstain.
- The directionality angle recorded for each spatter bloodstain.
- The subjective comments on data quality employed during the exhaustive recording process for each spatter bloodstain.

As the raw spatter bloodstain data for each of the three impact spatter patterns was already recorded with Excel® worksheets, this data was imported into the Excel® workbook containing the VB macro and stored in separate worksheets. An additional four experimental spatter bloodstain samples, provided with the demonstration version of BackTrack®/Win (Forensic Computing of Ottawa, 2001b), were also entered into separate worksheets within the Excel® workbook. These spatter bloodstain samples were included to provide an additional method

of testing and evaluating the analytical site of impact estimation program during development, as well as evaluating the implementation of the additional data analysis techniques included within this application. Unlike the three experimental impact spatter patterns created and recorded during this project, the BackTrack<sup>®</sup>/Win data did not include subjective data comments, and, as will be discussed in Section 8.3.2.1.4, the directionality measurements provided with this data had to be converted to correspond to the definition of directionality employed throughout this research project. The absence of this subjective data quality assessment for each spatter bloodstain was not, however, considered to be detrimental to the analysis of these spatter bloodstain samples. Each spatter bloodstain would simply be treated with equal weight, with the lack of any subject comment corresponding to an uncompromised spatter bloodstain classification in terms of the subjective criteria employed during the exhaustive recording process.

Plane	Normal	x (cm)	y (cm)	z (cm)	Width (mm)	Length (mm)	Orientation (degrees)	Comments
YZ	+	0	7.2	37.65	1.4	5.6	86.5	TAI
YZ	+	0	6.45	46.4	0.7	2	80	TSAT
YZ	+	0	5.5	57.3	2	8.2	93	TSAT
YZ	+	0	8.9	56.4				PSAT(B6-1)
YZ	+	0	14.75	10.3	0.4	1.6	26	
YZ	+	0	15.5	11.35	0.6	1.2	47	

Table 8-1 - A small sample of raw spatter bloodstain data for pattern ES-A (blank cells indicate data which was not necessary for the analysis of a particular spatter bloodstain).

### 8.3.1 Data Acquisition

Before the impact spatter pattern data can be processed the VB macro first has to access the data for each individual spatter bloodstain within the impact spatter patterns. The spatter bloodstain data contained within the seven Excel<sup>®</sup> worksheets is selected for pre-processing by the site of impact estimation macro through the 'Data' tab of the application interface. Figure 8-3 illustrates this data selection process. The spatter bloodstain data within one of the three experimental impact spatter patterns, or four spatter bloodstain samples to be analysed, is selected from a drop-down box which is populated with the names of all of the worksheets included within the Excel<sup>®</sup> workbook when the VB macro is run. Additional impact spatter patterns, or spatter bloodstain samples can, as a



result, be processed by the macro if the data is imported into a separate worksheet within this Excel® workbook, and the format, definition and scales of the data correspond to that shown in Table 8-1, and described in the recording process section of this thesis (see Section 5.3). Of the seven possible data sources shown in the data selection drop-down box in Figure 8-3, the 'EventA', 'EventB' and 'EventC' worksheets correspond to the experimental impact spatter patterns ES-A to ES-C, while the 'BTFW', 'BTBW', 'BTRW', 'BTLW' worksheets correspond to the BackTrack®/Win front, back, right and left wall spatter bloodstain data as defined by the grid co-ordinate system used by the VB macro. These four spatter bloodstain sample patterns correspond to the East wall, West wall, South wall and North wall datasets respectively, as defined in the BackTrack®/Win software, due to the differences in the investigative grid co-ordinate systems employed. The raw spatter bloodstain data of experimental impact spatter pattern ES-A and the four BackTrack®/Win spatter bloodstains samples are included in the appendices of this thesis (Appendices M and N), while the entire spatter bloodstain data for each of seven experimental spatter bloodstain collections is including on the DVD-ROMs that accompany this thesis.

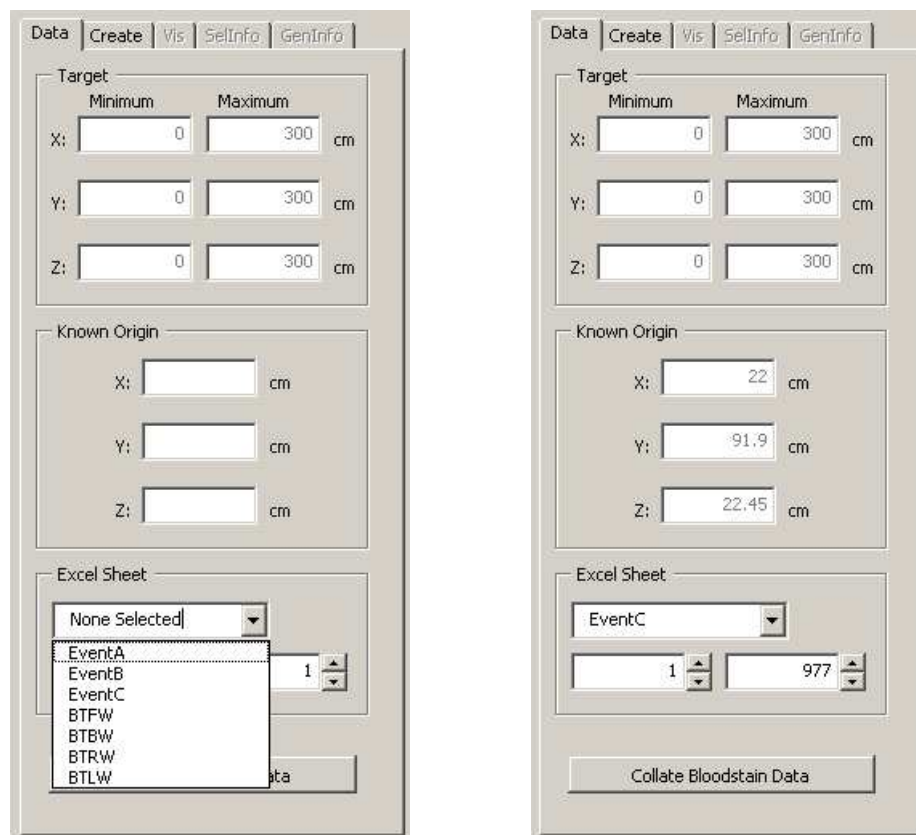


Figure 8-3 - The data selection menu of the analytical site of impact estimation macro.

Once the source data for the analysis is selected the location of the known impact site for each impact spatter pattern is displayed in the 'Known Origin' section of the data selection interface. These known locations are hard coded into the VB macro to avoid any estimate errors resulting from the repeated manual inputting of the figures, a situation which could be significant given the repeated spatter sample site of impact estimation analysis proposed as part of this research project. The dimensions of the investigational environment used by the VB site of impact estimation macro is also set to a 3 by 3 by 3 meter cube, as shown in the 'Target' dimensions of the data selection interface (see Figure 8-3). This constant environment size was included to provide a comparable environment for the examination of multiple constructed site of impact estimates, that was large enough to incorporate the extent of the distribution of each of the three experimental impact spatter patterns, and their known sites of impact, and to avoid any potential errors in repeated manual data input.

The known location of the impact site for the spatter bloodstain sample datasets provided with BackTrack<sup>®</sup>/Win were derived from the analysis of the experimental spatter bloodstain sample data as outlined in a published proof of the BackTrack<sup>®</sup>/Win site of impact estimation system (Carter, 2001). This original experimental spatter bloodstain data is represented by the data included in the BTLW worksheet within this project. The other three sample datasets provided with BackTrack<sup>®</sup>/Win are transpositions of this original experimental spatter bloodstain data onto the three remaining vertical walls of the investigative environment. To correspond to the predefined investigational environment of the VB macro, each of these three additional spatter bloodstain samples were converted from the 2 meter square floor plan a 3 meter square floor plan using the origin of each environment as a constant reference. The known location for the impact site for the BTLW data was also transposed to correspond with each of these additional constructed spatter bloodstain samples.

On the selection of an Excel<sup>®</sup> worksheet containing the spatter bloodstain data to be analysed, a pre-defined VBA function for Excel<sup>®</sup> worksheets establishes the number of rows of cells that are in use within that worksheet. The maximum number of rows of data, and therefore the provisional number of spatter bloodstains to be analysed is displayed in the 'Excel Sheet' section of the data selection interface. Some errors can appear in the application of this function in determining the number of currently active rows within a worksheet, as cells which have contained data at one time, but were subsequently deleted still

register as active. An example of this is provided in the selection of the data for pattern ES-A, where 1032 consecutive rows of the worksheet contain data, but 1046 used rows are returned by this function. Any error in the determination of the number of rows used within a worksheet is not significant to the analysis since any erroneous value returned is always greater than the actual number of rows of spatter bloodstain data. This number is used to establish the row at which the data acquisition process should finish, and the data screening built into this process means that rows of data that do not conform to the pattern outlined in Table 8-1 are discarded from the analysis. The range of spatter bloodstain data to be considered can also be manipulated using the spinner buttons next to start and finish rows for the pre-processing of the spatter bloodstain data, as indicated by the left and right textboxes within the 'Excel Sheet' section of the data selection interface, respectively. This functionality allows the analysis of selected sections of an impact spatter pattern dataset in isolation, although this function is not utilised in the analyses conducted during this research project.

With a spatter bloodstain dataset selected from the worksheets within the Excel® workbook the 'Collate Bloodstain Data' button begins the acquisition and preliminary analysis of this specific dataset. The iterative data acquisition process is conducted through the 'populate' function within the VB macro. This cycles through each row of spatter bloodstain data within the range specified by the start and finish position within the 'Excel Sheet' section of the data selection interface. If these positions are not altered from those established by the selection of a dataset then the iterative function will cycle through from the first to the last row of spatter bloodstain data contained within that particular Excel® worksheet. Each time the iterative data acquisition function accesses a new row of potential spatter bloodstain data, the first nine cells of the row that contain the recorded spatter bloodstain data, as shown in Table 8-1, are stored in the temporary memory of the application. This data is subsequently checked to establish the correspondence of this data to the necessary format for further analysis. If data is present in the plane column then the row examined is assumed to contain a real spatter bloodstain record. The numerical status of the directionality columns and the values of the width and length columns are then examined. If the data within the directionality column is not numerical, then the spatter bloodstain is of the OSC type, with two recorded directionality angles. If the width and length data within the row analysed is not greater than zero, then the row represents either a distorted, or satellite spatter bloodstain, or a record of a potential spatter bloodstain that, on closer magnified inspection, was decided

not to be a bloodstain, as no data was recorded for the width and length on these occasions, and an empty Excel® cell returns a value of zero. If any of these three data screening methods are not satisfied then the data with that particular row is omitted from further analysis, as the data in these cases is not useable in the construction of site of impact estimates.

If the above data screening criteria are met then the spatter bloodstain data is deemed to be useable for the purposes of site of impact estimation, and the data contained in this row of the Excel® worksheet is passed to a separate sub-routine, the 'Addbs' sub-routine, in the VB macro in which some pre-processing of spatter bloodstain data takes place. The width and length data passed to this sub-routine are examined. Where the width and length dimensions are not equal to each other an additional variable defined in the applications temporary memory is set to the impact angle defined by these two dimensions using the following formula:

$$\sin^{-1}(x) = \tan^{-1}\left(\frac{x}{\sqrt{1-x^2}}\right)$$

$$\sin^{-1}(w/l) = \tan^{-1}\left(\frac{w/l}{\sqrt{1-(w/l)^2}}\right)$$

*Formula 8-1 - The inverse tangent formula used to calculate impact angles from the width and length dimensions of spatter bloodstain within the VB macro (Weisstein, 1999).*

Formula 8-1 uses the known relationship between the inverse tangent of an angle and the inverse sine of an angle to calculate the impact angle of a spatter bloodstain from its width and length dimensions, as the mathematical inverse sine function normally associated with the calculation of the impact angle of a spatter bloodstain is not a native function of VBA. The resulting impact angle is returned in radians, the unit of angular measurement that both VBA and Excel® use in the calculation of trigonometric functions. Where the width and length dimensions for a spatter bloodstain are equal the morphology of the spatter bloodstain is known to be circular, with an impact angle perpendicular to the target surface upon which the bloodstain was observed. The temporary variable used to store the impact angle for each spatter bloodstain at this stage of pre-processing is consequently assigned an angle of 90 degrees, which is converted into radians using a programmed function within the VB macro.

Following this initial data processing, the type of data analysis to be conducted by the VB macro is then assessed. If a known location of an impact site was inputted in the data selection interface then the spatter bloodstain data, and the location of the known impact site is passed to a Class Module within the VB macro to define and set the spatter bloodstain data as an object in the application's memory. A number of pre-processing functions are conducted during the establishment of this spatter bloodstain object, including quality analysis based on the known location of the impact site (see Section 8.3.2.3). Where no location for the site of impact of a collection of spatter bloodstains is inputted in the data selection interface, only the spatter bloodstain data is passed to the spatter bloodstain object-defining Class Module, and the analysis of the spatter bloodstain data proceeds without the additional features included for the analysis of experimentally produced impact spatter patterns. The analytical site of impact estimation macro can, as a result, be used to analyse experimental impact spatter patterns and site of impact estimates in terms of their correspondence to a known impact site, but also construct conventional site of impact estimates where the only information available on the location of an impact site comes from the impact spatter pattern itself.

### **8.3.2 Spatter Bloodstain Analysis**

Each spatter bloodstain object is defined in the 'Add' function of the 'bsStains' Class Module within the VB macro and is stored in a collection that defines the impact spatter pattern, or sample of spatter bloodstains entered, as the source data for analysis. This collection of spatter bloodstain objects is defined as the 'pattern' variable within the variable declaration section of the VB macro. The collection of spatter bloodstain objects created during the raw spatter bloodstain data pre-processing phase of the program can be examined to query the total number of spatter bloodstain objects stored in the application memory, as well as those reset once the collection of spatter bloodstain data stored in the application memory is no longer required, or a new impact spatter pattern is chosen for analysis. The elements, or variables contained within each spatter bloodstain object are defined with a separate Class Module 'bsDat', and each of these variables is set for each new spatter bloodstain object within the 'Add' function of the 'bsStains' Class Module.

While the variables of the spatter bloodstain object include those already defined in the recording of the raw spatter bloodstain data and the pre-processing conducted during the 'Addbs' sub-routine, additional analyses are conducted during the spatter bloodstain object definition stage to provide the necessary information to construct a site of impact estimation, and provide additional pattern characterisation and sample selection criteria. These analyses include:

- The determination of the straight-line trajectory approximation.
- The determination of trajectory angles for spatter bloodstain characterisation and visualisation.
- The determination of an independent data quality metric where a known impact site location is provided.
- The categorisation of spatter bloodstain size.
- The calculation of the distance of the spatter bloodstain from the known impact site location, where provided.
- The categorisation of the spatter bloodstain in terms of a subjective data quality comment, where provided.

#### **8.3.2.1 Straight-Line Trajectory Determination**

While the directionality and impact angle of a spatter bloodstain describe the direction of the straight-line trajectory approximation of the flight path of a spatter-causing blood droplet, some processing of these two angles is required to provide a consistent mathematical method through which the location of intersection of any two such trajectory approximations can be calculated. The main focus of this processing is on the determination of the separate horizontal and vertical aspects of a trajectory to provide distinct and interpretatively isolated horizontal and vertical components to a site of impact estimation. Establishing the horizontal and vertical components of a straight-line trajectory from spatter bloodstains observed on a horizontal plane is conceptually quite straightforward, with the directionality of the bloodstain indicating the direction of the horizontal trajectory, and the impact angle describing the vertical elevation. In situations where spatter bloodstains are observed on vertical target surfaces, however, the determination of the horizontal and vertical components of a trajectory indicated by the directionality and impact angles requires the application of a number of principles of 3D geometry and trigonometry.

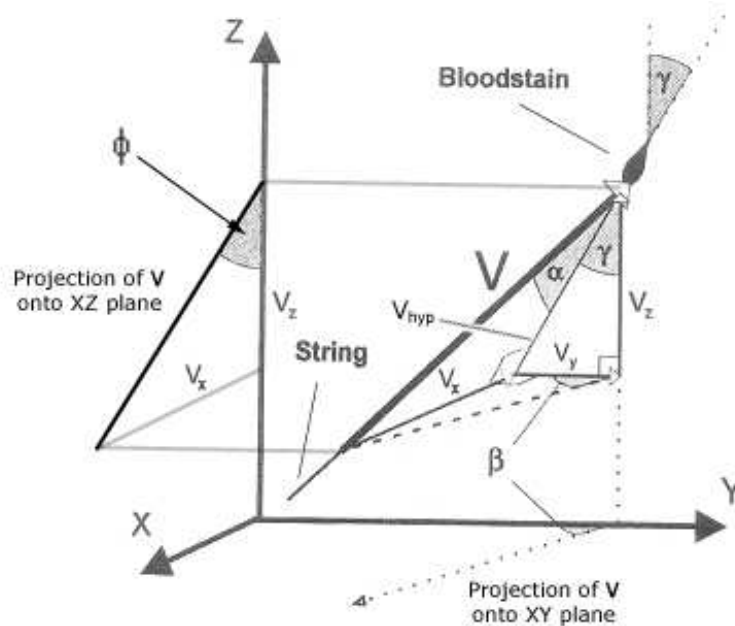


Figure 8-4 – The straight-line trajectory vector defined by the directionality and impact angle of a spatter bloodstain and its relationship to a horizontal and vertical angle, and its three vector components [after Carter (2001)].

Carter and Podworny (1991) and Carter (1998 and 2001), for example, have published a mathematical method for the angular decomposition of straight-line trajectory approximations from spatter bloodstain observed on a vertical target surface that form the basis of both a manual calculation method, and the justification of the BackTrack<sup>®</sup>/Win site of impact estimation technique. The set of two formulae enable a horizontal and a vertical angle that define a straight-line trajectory to be calculated from the known directionality and impact angles of a spatter bloodstain. As Figure 8-4 shows, the horizontal angle,  $\beta$ , and the vertical angle,  $\phi$ , are formed by the projection of the straight-line trajectory onto the horizontal and vertical planes that comprise the Top and Side views within BackTrack<sup>®</sup>/Win. The directionality and impact angles are represented in the figure by  $\gamma$  and  $\alpha$  respectively.

The two formulae developed by Carter and Podworny (1991) and Carter (1998 and 2001) to establish these horizontal and vertical angles are show in Formula 8-2 and Formula 8-3.

$$\beta = \tan^{-1}[\tan(\alpha)/\sin(\gamma)]$$

Formula 8-2 - The horizontal angle formed by the straight-line trajectory vector (Carter and Podworny, 1991; Carter, 1998 and 2001)

$$\phi = \tan^{-1}[\tan(\alpha)/\cos(\gamma)]$$

*Formula 8-3 - The vertical angle formed by the straight-line trajectory vector (Carter, 2001).*

### **8.3.2.1.1 Vector Decomposition**

An alternative method in establishing the horizontal and vertical components of a straight-line trajectory approximation, however, is employed within the investigative site of impact estimation program developed as part of this research project. In contrast to the angular decomposition published by Carter and Podworny (1991) and Carter (1998 and 2001), the spatter bloodstain object-definition section of the VB macro relies solely on a vector-based approach, through which the straight-line trajectory approximation is expressed in terms of its three constituent x, y, and z components. These components are labelled  $\mathbf{v}_x$ ,  $\mathbf{v}_y$ , and  $\mathbf{v}_z$  in Figure 8-4.

While Carter and Podworny (1991) and Carter (1998 and 2001) use the vector properties of a 3D straight-line trajectory in the derivation of their angular formulae, the x, y, and z components of each trajectory vector form the basis of the analyses conducted within the VB macro developed for this research. This vector-based approach was adopted for three main reasons. Firstly, a vector representation of each spatter bloodstain trajectory approximation was considered to provide a consistent single estimation model for the analysis of straight-line trajectory approximations and site of impact estimates. Rather than defining each trajectory approximation with a consistent horizontal but variable vertical angle depending on which plane a spatter bloodstain is observed, the vector-based definition of each straight-line trajectory provides a consistent inter- and intra-trajectory description of each trajectory analysed. The vector definition of each straight-line trajectory can still be used to calculate horizontal and vertical angles, or a wide range of other angular relationships that may be of interest in the detailed analysis of site of impact estimation. A consistency in analysis is also achieved in the construction and evaluation of each straight-line trajectory approximation, whether the spatter bloodstain is observed in the relatively straightforward angular representation achievable in a horizontal plane, or the more complex vertical plane (see below). Each spatter bloodstain trajectory, as indicated by the directionality and impact angles, receives a comparable degree of processing to generate the vector-based representation of



the straight-line trajectory that these two spatter bloodstain angles define. Secondly, the vector-based decomposition of the 3D straight-line trajectory specified by the directionality and impact angles of a spatter bloodstain enables the application of established vector-based mathematical equations in the calculation of both 2D and 3D trajectory intersections (see Section 9.4), and the assessment of independent trajectory data quality (see Section 8.3.2.3). Finally, the vector approach to describing straight-line trajectory approximations was considered to provide an extendable estimation methodology that in future applications could include increasingly complex target surface geometries, and consistent representations of straight-line trajectory approximations of spatter bloodstain observed on and measured from these complex surfaces. Although not addressed as part of this research, an explicitly vector-based system, while removing the need for multiple and complex angular trajectory definitions, makes little conceptual or analytical distinction between horizontal, vertical, and non-horizontal and non-vertical target surfaces as long as the orientation of the targets plane within the 3D Cartesian environment of the crime scene can be accurately and appropriately quantified and recorded.

As a straight-line trajectory vector,  $\mathbf{v}$ , inferable from the morphology of a spatter bloodstain is a unit vector with a dimensionless length of one, the three components of this vector, assuming a target surface configuration corresponding to that shown in Figure 8-4, can be constructed using the following three formulae:

$$\begin{aligned}\mathbf{v}_x &= \mathbf{v} \sin(\alpha) \\ &= \sin(\alpha)\end{aligned}$$

*Formula 8-4 - The x-axis component of the straight-line trajectory vector.*

$$\begin{aligned}\mathbf{v}_{hyp} &= \mathbf{v} \cos(\alpha) \\ &= \cos(\alpha)\end{aligned}$$

$$\begin{aligned}\mathbf{v}_y &= \mathbf{v}_{hyp} \sin(\gamma) \\ &= \cos(\alpha) \sin(\gamma)\end{aligned}$$

*Formula 8-5 - The y-axis component of the straight-line trajectory vector.*

$$\begin{aligned}\mathbf{v}_z &= \mathbf{v}_{hyp} \cos(\gamma) \\ &= \cos(\alpha) \cos(\gamma)\end{aligned}$$

Formula 8-6 - The z-axis component of the straight-line trajectory vector.

### 8.3.2.1.2 Vector Proof

The correspondence of this vector-based approach to the established angular decomposition techniques documented by Carter and Podworny (1991) and Carter (1998 and 2001) can be shown through a comparison of the two sets of formulae. In terms of the horizontal angle as defined in Figure 8-4:

$$\tan(\beta) = \frac{\mathbf{v}_x}{\mathbf{v}_y}$$

Substituting in Formula 8-4 and Formula 8-5 to represent the  $\mathbf{v}_x$  and  $\mathbf{v}_y$  components of the trajectory vector this formula becomes:

$$\begin{aligned}\tan(\beta) &= \frac{\sin(\alpha)}{\cos(\alpha) \sin(\gamma)} \\ &= \left( \frac{\sin(\alpha)}{\cos(\alpha)} \right) \left( \frac{1}{\sin(\gamma)} \right) \\ &= \frac{\tan(\alpha)}{\sin(\gamma)}\end{aligned}$$

Therefore the horizontal angle,  $\beta$ , formed by the projection of the straight-line trajectory onto the horizontal 'Top View' plane is equal to  $\tan^{-1}[\tan(\alpha)/\sin(\gamma)]$ , the same as Formula 8-2 as described by Carter and Podworny (1991) and Carter (1998 and 2001).

In terms of the vertical angle as defined in Figure 8-4:

$$\tan(\phi) = \frac{\mathbf{v}_x}{\mathbf{v}_z}$$

Substituting in Formula 8-4 and Formula 8-6 to represent the  $\mathbf{v}_x$  and  $\mathbf{v}_z$  components of the trajectory vector:

$$\begin{aligned}\tan(\phi) &= \frac{\sin(\alpha)}{\cos(\alpha)\cos(\gamma)} \\ &= \left(\frac{\sin(\alpha)}{\cos(\alpha)}\right)\left(\frac{1}{\cos(\gamma)}\right) \\ &= \frac{\tan(\alpha)}{\cos(\gamma)}\end{aligned}$$

Therefore the vertical angle,  $\phi$ , formed by the projection of the straight-line trajectory onto a vertical 'Side View' plane is equal to  $\tan^{-1}[\tan(\alpha)/\cos(\gamma)]$ , the same as Formula 8-3 as described by Carter (2001).

### 8.3.2.1.3 Target Surface Variation

The formula used to derive the three vector components of the straight-line trajectory approximation described above, however, are specific to the analysis of spatter bloodstain on an yz+ target surface, as illustrated in Figure 8-4. The three formula are appropriate for the vector decomposition of the trajectory indicated by the directionality and impact angle of spatter bloodstain observed on other horizontal or vertical planes, but require some alterations to provide consistent  $\mathbf{v}_x$ ,  $\mathbf{v}_y$ , and  $\mathbf{v}_z$  vector components. The variations on Formula 8-4, Formula 8-5 and Formula 8-6 for each of the six potential orientations of horizontal or vertical target surfaces within the idealised 3D investigative environment illustrated in Figure 8-5 are shown in Table 8-2.

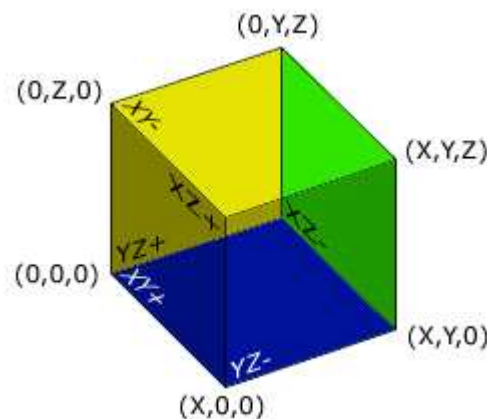


Figure 8-5 - An idealised investigative environment depicting the six specific target surface.

<b>Surface</b>	<b>Description</b>	<b>v<sub>x</sub></b>	<b>v<sub>y</sub></b>	<b>v<sub>z</sub></b>
XY+	Floor	$\cos(\alpha)\sin(\gamma)$	$\cos(\alpha)\cos(\gamma)$	$\sin(\alpha)$
XY-	Ceiling	$\cos(\alpha)[- \sin(\gamma)]$	$\cos(\alpha)\cos(\gamma)$	$- \sin(\alpha)$
YZ+	Left Wall	$\sin(\alpha)$	$\cos(\alpha)\sin(\gamma)$	$\cos(\alpha)\cos(\gamma)$
YZ-	Right Wall	$- \sin(\alpha)$	$\cos(\alpha)[- \sin(\gamma)]$	$\cos(\alpha)\cos(\gamma)$
XZ+	Back Wall	$\cos(\alpha)[- \sin(\gamma)]$	$\sin(\alpha)$	$\cos(\alpha)\cos(\gamma)$
XZ-	Front Wall	$\cos(\alpha)\sin(\gamma)$	$- \sin(\alpha)$	$\cos(\alpha)\cos(\gamma)$

*Table 8-2 - The variation in formula for the vector decomposition of a straight-line trajectory approximation depending on target surface alignment.*

Each spatter bloodstain passed to the object-definition section of the VB macro is analysed using these formulae relative to the planar designation assigned to the target surface upon which the spatter bloodstain was observed, with the three vector components of the trajectory recorded as variables within the spatter bloodstain object. The directionality angle recorded for each spatter bloodstain is also converted into radians using the programmed VB function at this stage to adhere to the requirements of the trigonometric functions of VBA. Where a circular spatter bloodstain is encountered by the VB macro, however, these vector decomposition formulae are negated and the known trajectory vector components shown in Table 8-3 are assigned to the spatter bloodstain relative to the planar configuration of the target surface.

<b>Surface</b>	<b>Description</b>	<b>v<sub>x</sub></b>	<b>v<sub>y</sub></b>	<b>v<sub>z</sub></b>
XY+	Floor	0	0	1
XY-	Ceiling	0	0	-1
YZ+	Left Wall	1	0	0
YZ-	Right Wall	-1	0	0
XZ+	Back Wall	0	1	0
XZ-	Front Wall	0	-1	0

*Table 8-3 - The vector assigned to circular spatter bloodstains depending on the target surface upon which they were observed.*

While the investigational environment is limited to six planar target surface configurations in an attempt to replicate current computer-based site of impact estimation methods, an alternative approach in future applications could be to treat each spatter bloodstain as if recorded on a horizontal surface, for example. The resultant 3D trajectory unit vector could subsequently be rotated so that the initial horizontal surface plane corresponds with the orientation and plane normal

of the actual geometry of the target surface, providing an accurate trajectory vector relative to the specific target surface geometry. Such an approach could have been applied during this project, but was not deemed necessary given the restricted number of target surface configurations employed. In the development of future applications, however, where more complex target surface geometries are considered, and more sensitive surface geometry capture technologies potentially employed, such an approach could provide a more appropriate investigation methodology than currently presented by applications that only consider idealised target surface geometry (see Section 3.4.1).

#### 8.3.2.1.4 An Alternative Directionality

The alternative definition of spatter bloodstain directionality employed during the practical aspects of this research project, in the sense that it is measured in the opposite direction commonly associated with directionality, is a product of the vector-based decomposition of the straight-line trajectory approximations employed in the VB macro. The difference between the common definition of directionality, indicating the direction in which the spatter-forming droplet was travelling, and the definition applied within this research, indicating the direction in which the spatter-forming blood droplets originate from, is illustrated in Figure 8-6. Where a traditional directionality measurement is less than 180 degrees, then the alternative directionality angle is equal to this measurement plus 180 degrees, and where a traditional directionality measurement is equal to or greater than 180 degrees, then the alternative directionality angle is equal to this measurement minus 180 degrees.

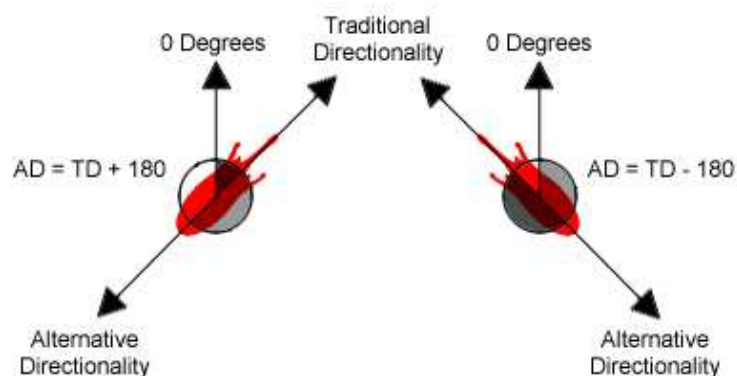


Figure 8-6 - Established directional angle measurement, and the more appropriate vector approach measurement used during this research project.

While both of these effectively measure the same orientation of spatter bloodstains, and the conversion between these two approaches to directionality is not complicated, the alternative definition of spatter bloodstain directionality is used during this research project as it can be considered to be more consistent with the vector-based estimation methodology employed within the analytical site of impact estimation macro. The construction of a straight-line trajectory approximation in terms of the aims of site of impact estimation is based around retracing the straight-line trajectory of a spatter-causing blood droplet back through the scene towards the location of its origin (see Section 2.5). As the unit vector representation of a trajectory inherently includes information on trajectory direction as well as trajectory angle, it is this retracing direction that the vector representation of each trajectory is required to describe within the vector-based trajectory intersection and independent data quality assessment formulae applied later in the VB macro (see Sections 8.3.2.3 and 9.4). The alternative directionality is, as a result, employed within this research project as it explicitly measures directionality in terms of retracing this vector trajectory. Due to the differences in these definitions, however, the alternative directionality used during this project will be referred to as 'angle of orientation' in the remainder of this thesis, and 'directionality angle' will be used to refer to the traditional concept.

### **8.3.2.2 Calculating Additional Trajectory Angles**

While the straight-line trajectory determination is constructed in terms of the vector components of the trajectory, two angular components that define each trajectory are also established during the pre-processing of the spatter bloodstain data. Neither of these trajectory angles are utilised in the construction of the site of impact estimates within the VB macro, but are used in the characterisation and investigation of the impact spatter patterns and spatter bloodstain samples used to construct these estimates. The two angles are also used in the alignment of the 3D structures used to represent the straight-line trajectory approximations within the 3D visualisation component of the program (see Chapter 10).

The two angles calculated from the vector representation of each straight-line trajectory are defined here as the horizontal and vertical angle of a trajectory. In contrast to the definitions used by Carter and Podworny (1991) and Carter (1998 and 2001), however, the vertical angle calculated within the VB macro

corresponds to the degree of elevation of the trajectory above or below a horizontal level, and the horizontal angle corresponds to a bearing, with a zero angle indicating the positive y-axis direction and angular direction measured in a clockwise direction. These two trajectory-defining angles are illustrated in Figure 8-7.

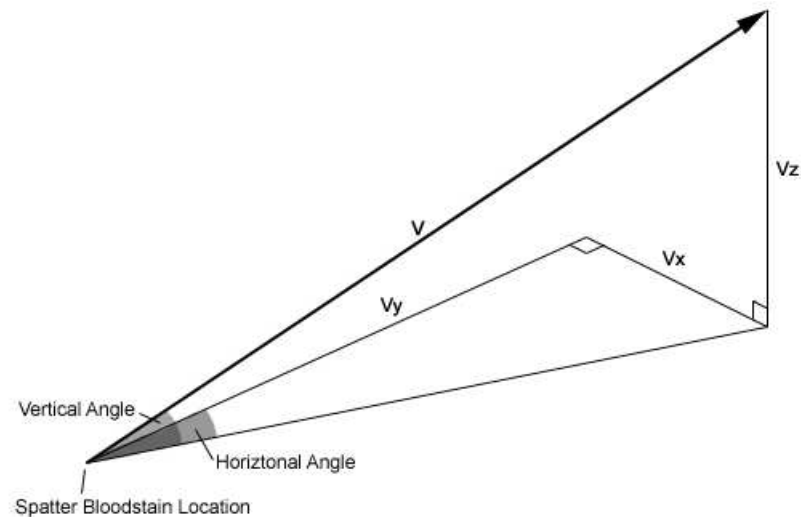


Figure 8-7 - The horizontal and vertical trajectory angles calculated within the VB macro from the trajectory vector components.

The horizontal angle of each straight-line trajectory approximation is calculated using the formulae shown in Table 8-4. The angle is calculated using the  $v_x$  and  $v_y$  components of the straight-line trajectory vector, with an additional angle added to correspond to a 360-degree bearing depending in which of four horizontal sectors the trajectory lies. Where either the  $v_x$  or  $v_y$  component of the trajectory vector equals zero, then the known bearing corresponding to this direction is automatically set for each spatter bloodstain. In addition to assigning a horizontal trajectory angle, the analysis of the horizontal sector in which a trajectory vector lies is also used to assign each spatter bloodstain with a type number between 0 and 4. The eight possible sectors, four horizontal sectors at two vertical levels, are shown in Figure 8-8.

The categorisation of the horizontal components of each spatter bloodstain trajectory is utilised later in the analytical site of impact estimation macro, where the horizontal direction of the trajectory is used to approximate a bracketing intersection hypothesis. This bracketing hypothesis is often assumed to be less error-prone than the consideration of all trajectory intersections and is applied in the automatic averaging function of BackTrack<sup>®</sup>/Win (Cater and Podworny, 1991;

Laber and Epstein, 2004; Forensic Computing of Ottawa, 2001b). The use of this horizontal sector characterisation in the analysis of site of impact estimates will be described in more detail in Section 9.4 of this thesis.

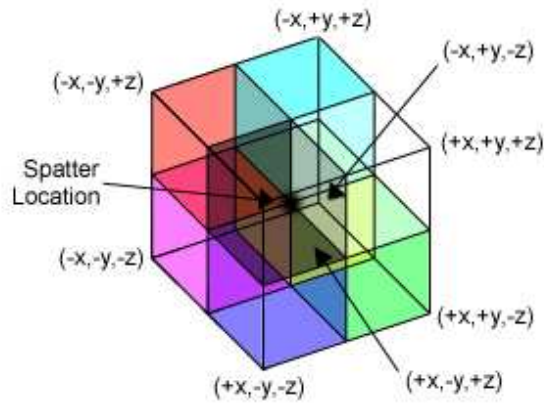


Figure 8-8 - The 8 sectors of the 3D investigation space, relative to any location within the space.

Horizontal Sector	Horizontal Angle (radians)	Bloodstain Type
$\mathbf{v}_x > 0$ And $\mathbf{v}_y > 0$	$\beta = \tan^{-1}(\mathbf{v}_x / \mathbf{v}_y)$	1
$\mathbf{v}_x > 0$ And $\mathbf{v}_y < 0$	$\beta = \pi + \tan^{-1}(\mathbf{v}_x / \mathbf{v}_y)$	4
$\mathbf{v}_x < 0$ And $\mathbf{v}_y < 0$	$\beta = \pi + \tan^{-1}(\mathbf{v}_x / \mathbf{v}_y)$	3
$\mathbf{v}_x < 0$ And $\mathbf{v}_y > 0$	$\beta = 2\pi + \tan^{-1}(\mathbf{v}_x / \mathbf{v}_y)$	2
$\mathbf{v}_x = 0$ And $\mathbf{v}_y > 0$	$\beta = 0$	0
$\mathbf{v}_x = 0$ And $\mathbf{v}_y < 0$	$\beta = \pi$	0
$\mathbf{v}_x > 0$ And $\mathbf{v}_y = 0$	$\beta = \pi / 2$	0
$\mathbf{v}_x < 0$ And $\mathbf{v}_y = 0$	$\beta = 3 / 2\pi$	0

Table 8-4 - The method used to establish the horizontal angle of a trajectory within the analytical site of impact estimation macro.

The vertical angle calculated for each straight-line trajectory approximation corresponds to a degree of elevation of the trajectory from the horizontal. This angle is formed between the unit vector,  $\mathbf{v}$ , and the horizontal components of the vector, the line  $\mathbf{v}_x\mathbf{v}_y$ . Unlike the definition of a vertical trajectory angle employed by Carter and Podworny (1991) and Carter (1998 and 2001), the vertical angle defined within this project is not dependent on its relationship with the four vertical planes of the 3D investigation environment. As the angle is dependent on the trajectory vector in isolation, and not on the projection of the trajectory onto a vertical surface, the angle is entirely consistent and comparable in all of the 3D sectors illustrated in Figure 8-8. This form of the vertical elevation angle



also provides an appropriate basis for spatter bloodstain assessment in terms of the upward or downward direction of the spatter-causing blood droplet on contact with the target surface. The vertical angle of each straight-line trajectory is calculated using a unit vector approach as shown in Formula 8-7. The vertical elevation angle,  $\theta$ , is positive if  $\mathbf{v}_z$  is positive, and negative if  $\mathbf{v}_z$  is negative. Where the straight-line trajectory approximation for a spatter bloodstain has no vertical component, the vertical elevation angle is zero.

$$\mathbf{v}_z = v \sin(\theta)$$

$$\theta = \sin^{-1}(\mathbf{v}_z)$$

*Formula 8-7 - The formula used to calculate the vertical elevation of each straight-line trajectory approximation.*

### 8.3.2.3 Independent Trajectory Quality Parameter

The vector components of each straight-line trajectory approximation are further utilised within the spatter bloodstain object-definition phase of the VB macro in the construction of an assessment of the independent quality of the each straight-lien trajectory, in terms of its correspondence to the known location of an impact site, where such information is provided. The two functions used to generate this data, 'hDistToSegment' and 'vDistToSegment', use the vector components of each trajectory through a parameterised mathematical process shown in Formula 8-8, Formula 8-9 and Formula 8-10. The three components of each trajectory vector are used in conjunction with information recorded on the location of the spatter bloodstain, or origin of the trajectory being retraced,  $\mathbf{o}$ , and the known location of the spatter-causing impact event, to calculate a scaling factor,  $t$ , of the vector,  $\mathbf{v}$ , needed to reach the nearest point along the trajectory to the known point location of the impact site,  $\mathbf{n}$ .

$$t = \frac{\mathbf{v}_x(\mathbf{n}_x - \mathbf{o}_x) + \mathbf{v}_y(\mathbf{n}_y - \mathbf{o}_y) + \mathbf{v}_z(\mathbf{n}_z - \mathbf{o}_z)}{\mathbf{v}_x^2 + \mathbf{v}_y^2 + \mathbf{v}_z^2}$$

*Formula 8-8 - The vector scaling factor necessary to reach the nearest point along a trajectory to a known point in 3D (after Geometric Tools, 2005).*

If the scaling factor  $t$  is less than zero, then the point along the trajectory is located behind the trajectory's origin. In this case the nearest point on the

trajectory to the known point is its origin, **o**. Where the scaling factor is greater than zero then the nearest point along the retraced trajectory to the known location of the impact site is calculated by adding the scaled vector to the location of its origin, the recorded position of the spatter bloodstain. This process is shown in Formula 8-9 where **a** is the nearest point along the straight-line trajectory to the known impact site.

$$\mathbf{a} = \mathbf{o} + tv$$

*Formula 8-9 - The 3D location of the nearest point along a line (after Geometric Tools, 2005).*

The distance of this closest point along the straight-line trajectory, or to give its computer geometry term, this ray, from the known location of the impact site is calculated by subtraction. Formula 8-10 illustrates this process, with **d** being the vector that describes distance between the nearest point along the straight-line trajectory and the known impact site location in terms of the three axes of analysis.

$$\mathbf{d} = \mathbf{n} - \mathbf{a}$$

*Formula 8-10 - The distance between the nearest point along a straight-line trajectory and the known impact site location in the three spatial axes.*

This same independent data quality assessment process is also conducted solely in the horizontal plane to give an indication of horizontal trajectory data quality. In this case the z-axis component of the unit trajectory vector is omitted from the above formulae. The 2D and 3D straight-line distances between the nearest point along each trajectory approximation and the known location of the impact site are subsequently calculated from the axial distances derived from Formula 8-10 using Pythagoras' Theorem, and the scaling factor, the locations and distances in terms of each axis, and the total straight-line distance for both the 2D horizontal and 3D nearest point along each trajectory to the known location of the impact site are recorded for each separate spatter bloodstain object.

The 2D and 3D data quality assessments calculated during the pre-processing of the spatter bloodstain data are defined as 'independent' assessments because, although the data generated provides information on how well each specific straight-line trajectory corresponds with a known location of an impact site, this data does not indicate how each trajectory will interact and intersect with other

trajectories analysed during the construction of a site of impact estimation. It is this intersection, or 'dependent' data quality, that is used in site of impact estimates to indicate the location of an impact site, and as such the independent data quality assessments made at this stage in VB macro can only be used as indicators of the potential, or independent ability of a trajectory to intersect with another trajectory close to the location of the impact site. The independent data quality assessments established are utilised, however, during the analysis of site of impact estimation undertaken in this research project in spatter bloodstain sample selection, and as a means of characterising collections of spatter bloodstain in the form of impact spatter patterns, and smaller spatter bloodstain samples selected from them.

#### **8.3.2.4 Distance from Impact Site**

In addition to providing an independent data quality assessment, the known location of an impact site, where provided, is also used to determine the distance of each spatter bloodstain from this location. The straight-line distance of each bloodstain from the known impact site is calculated in 2D and 3D using Pythagoras' Theorem, and is used as an indicator of the minimum possible flight distance of each spatter-causing blood droplet.

#### **8.3.2.5 Spatter Bloodstain Size**

The size of each spatter bloodstain according to the classification system described by Wonder (2001) is also determined by a separate programmed function during the pre-processing of the spatter bloodstain data. Table 8-5 shows the size classification criteria employed.

<b>Size Category</b>	<b>Spatter Bloodstain Width (mm)</b>
Mist	$0 < \text{Width} \leq 0.1$
Fine	$0.1 < \text{Width} \leq 1$
Small	$1 < \text{Width} \leq 3$
Medium	$3 < \text{Width} \leq 6$
Large	$6 < \text{Width}$

*Table 8-5 - The criteria used to assign size designations to each spatter bloodstain during the pre-processing phase of the VB macro.*

<b>Velocity Category</b>	<b>Spatter Bloodstain Width (mm)</b>
High	$0 < \text{Width} \leq 1$
Medium	$1 < \text{Width} \leq 3$
Low	$3 < \text{Width}$

*Table 8-6 - The velocity-based size division classification system employed within the VB macro.*

The VB macro also categorises the spatter bloodstain size in terms of the velocity based classification system as described by James and Eckert (1998). This classification system is shown in Table 8-6, although while the VB macro does assign each spatter bloodstain a velocity category based on the recorded spatter bloodstain width, this information is omitted from further analysis in favour of the more consistent and less presumptive sized-based classification system outlined above (see Section 2.4).

### **8.3.2.6 Subjective Spatter Bloodstain Type.**

The subjective spatter bloodstain quality assessments, if recorded for a spatter bloodstain, are also processed during the spatter bloodstain object definition stage of the pre-processing performed within the VB macro. As the comments are in text form, this data is processed using the inbuilt string manipulation and parsing functions within VBA. Twelve of the subjective spatter bloodstain assessment criteria, as outlined in Section 5.3.5 of this thesis, are searched for within the comment data string. The subjective 'CIRC' criterion corresponding to a spatter bloodstain with a circular morphology is not included within this analysis, as the circularity of a spatter bloodstain is inferable from its width and length measurements, and its lack of orientation. Where one of the other twelve subjective comments is found, the specific Boolean variable declared within the spatter bloodstain object to record each subjective criterion is set to 'True'. If any of the twelve subjective assessment criteria are not present within the comment string data, then the associated Boolean variable is set to 'False'. This data is utilised in the spatter bloodstain screening process employed during the analysis of the three experiment impact spatter patterns (see Section 11.2).

## **8.4 Spatter Bloodstain Data and Collection Composition**

In addition to providing the necessary means to construct a site of impact estimate from the raw spatter bloodstain data (outlined in the following chapter

of this thesis), the pre-processing phase of the analytical site of impact estimation macro provides a considerable amount of information on each spatter bloodstain that can be used in the analysis and characterisation of the composition of a collection of spatter bloodstains. A sample of this detailed pre-processed spatter bloodstain data generated for a single bloodstain by the VB macro is shown in Table 8-7, which includes information on:

- The orthogonal plane of the 3D investigative environment in which the spatter bloodstain was observed under the 'Plane' column.
- The x-, y-, and z-axis location of the spatter bloodstain within the 3D investigative environment in the 'X', 'Y' and 'Z' columns respectively.
- The measured width and length of the spatter bloodstain in the 'W' and 'L' columns respectively.
- The orientation and impact angle of the spatter bloodstain in the 'ORA' and 'IMPA' columns.
- The size of the spatter bloodstain as defined by Wonder (2001) under the 'Size' column.
- The horizontal and vertical angles of the straight-line trajectory approximation constructed for each spatter bloodstain under the 'Hdeg' and 'Vdeg' columns respectively.
- The locations of the nearest point along the straight-line trajectory to the known impact site in the horizontal plane in the 'HqX' and 'HqY' columns.
- The axial directional distances of the nearest point along the straight-line trajectory from the known impact site in the horizontal under the 'HXerr' and 'HYerr' columns.
- The distance of the nearest point along the straight-line trajectory from the known impact site in the horizontal plane in the 'HQual' column.
- The locations of the nearest point along the straight-line trajectory to the known impact site in 3D in the 'VqX', 'VqY' and 'YqZ' columns.
- The axial directional distances of the nearest point along the straight-line trajectory from the known impact site in 3D under the 'VXerr', 'VYerr', and 'Vzerr' columns.
- The distance of the nearest point along the straight-line trajectory from the known impact site in 3D in the 'VQual' column.
- The status of the spatter bloodstain in terms of each the 12 subjective assessment criteria under the 'TAI', 'TSAT', 'PSAT', 'ESAT', 'PDS', 'NDLE', 'PDLE', 'CREN', 'FRAG', 'HSAT', 'OSC', and 'DIST' columns.

- The distance of each spatter bloodstain from the known impact site in columns 'bsHD', 'bsVD' and 'bsTD' representing the horizontal distance, vertical distance and total 3D straight-line distance respectively.

Plane	X (cm)	Y (cm)	Z (cm)	W (mm)	L (mm)	ORA (degrees)	IMPA (degrees)	SIZE
YZ+	0	7.2	37.65	1.4	5.6	86.5	14.48	small

Hdeg (degrees)	Vdeg (degrees)	HqX (cm)	HqY (cm)	Hqual (cm)	VqX (cm)	VqY (cm)	VqZ (cm)	Vqual (cm)
14.5	3.39	28.47	117.25	20.17	28.19	116.19	44.32	27.57

BsHD (cm)	BsVD (cm)	BsTD (cm)	TAI	TSAT	PSAT	ESAT	PDS	NDLE
115.45	12.10	116.08	TRUE	FALSE	FALSE	FALSE	FALSE	FALSE

PDLE	CREN	FRAG	HSAT	OSC	DIST	Hxerr (cm)	HYerr (cm)	Vxerr (cm)
FALSE	FALSE	FALSE	FALSE	FALSE	FALSE	-19.53	5.05	-19.81

Vyerr (cm)	Vzerr (cm)
3.98	18.77

Table 8-7 – An example of the data available for the analysis of a single spatter bloodstain after the pre-processing stage of the analytical site of impact estimation macro for pattern ES-A (results reported to two decimal places where necessary).

The characterisation of the composition of a group of pre-processed spatter bloodstains is conducted by the VB macro through the 'Bstat2', and 'Bstat3' subroutines of the 'Userform' code module. This characterisation process provides an assessment of the distribution of a number of the spatter bloodstain variables within a collection of spatter bloodstains, which are either central to the construction of a site of impact estimation or can be considered to be important in the selection of potentially accurate spatter bloodstain samples. The VB macro constructs frequency distributions, which can be converted into relative and cumulative relative frequency distributions for the purposes of inter-collection comparison, for the following spatter bloodstain variables:

- Target surface location.
- Width-to-length ratio.
- Orientation Angle.
- The horizontal angle of the straight-line trajectory approximation.
- The vertical angle of the straight-line trajectory approximation.
- Size.

- Subjective data quality assessment.

Three additional distance-based variables for each spatter bloodstain are also characterised for any collection of spatter bloodstains where the known location of an impact site is provided for analysis. These variables are:

- The 3D straight-line distance from the location of the known impact site.
- The horizontal independent data quality assessment.
- The 3D independent data quality assessment.

#### 8.4.1 Target Surface Distribution

The distribution of spatter bloodstains within the target surface upon which they are observed is analysed by the VB macro through the construction of a joint distribution count of the number of spatter bloodstains within 5 by 5 centimetre square regions across the extent of the target surface.

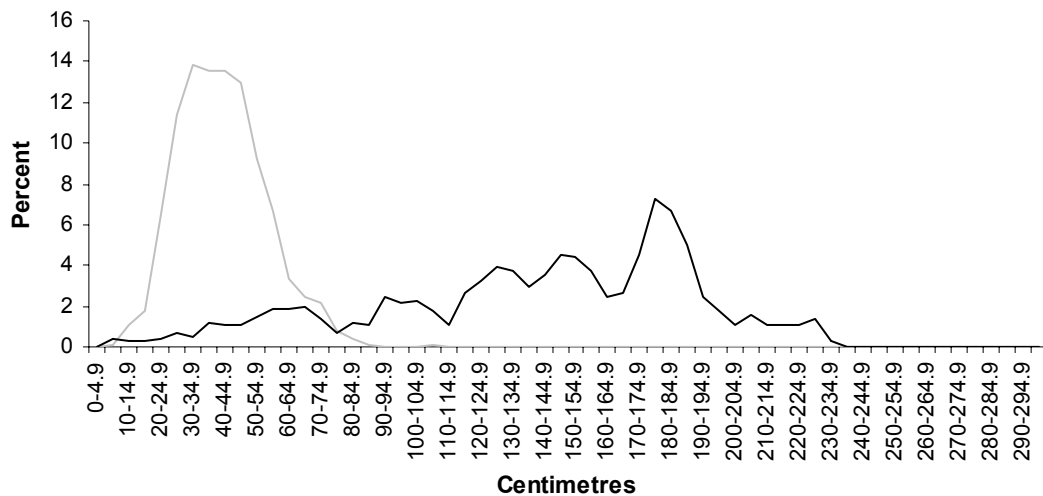


Figure 8-9 - An example of the marginal relative distributions of a collection of spatter bloodstains in the y- (black line) and z-axis (grey line) of the vertical target surface.

As the three experimental impact spatter patterns generated for the purposes of this research are all observed on a +yz vertical target surface plane, the distribution or density of spatter bloodstains within this target surface is assessed in terms of 3600 class intervals which cover the 300 by 300 centimetre extent of this target surface defined by the size of the investigative environment employed throughout this research. The marginal distributions of the frequency of spatter

bloodstains within 60 class intervals on each of the y- and z-axes can also be calculated and analysed from this joint distribution frequency data, as illustrated in Figure 8-9.

#### 8.4.2 Spatter Bloodstain Morphology Composition

The distribution of spatter bloodstain morphologies within a collection of spatter bloodstains is assessed by the analytical site of impact estimation macro through the construction of frequency distributions for the width to length ratios, the orientation angles, the sizes, and subjective morphological assessment of the collection's constituent spatter bloodstains. The frequency distribution for the width-to-length ratios, which provides an approximation of the relative elliptical size and impact angles associated with each spatter bloodstain, is constructed in 0.02 wide class intervals between the theoretical minimum of 0 and real maximum of 1, providing 50 individual classes into which the spatter bloodstain data can be grouped. The distribution of the orientation angles within a collection of spatter bloodstains is divided into 72 five-degree wide class intervals by the VB macro, covering the range of 0 to 360 degrees possible in the measurement of spatter bloodstain orientation. As the experimental impact spatter patterns analysed during this research project are all situated on single vertical target surfaces, the distribution of the orientation angles of a collection of spatter bloodstains can be compared and interpreted in a directional sense that would not be possible if multiple target surfaces were considered.

Size	Count	Percent	Cumulative
Mist	1	0.13	0.13
Fine	575	77.08	77.21
Small	164	21.98	99.20
Medium	6	0.80	100
Large	0	0	100

*Table 8-8 - An example of the size-based characterisation generated for a collection of spatter bloodstains analysed by the analytical site of impact estimation macro.*

The sizes of spatter bloodstain within a collection of spatter bloodstains is assessed by the analytical site of impact estimation macro according to the five ordinal size-based categories described in Section 8.3.2.5, which provides a numerical comparative means of determining the predominant spatter bloodstain size within any given spatter bloodstain collection. An example of the



constructed frequency distribution of the sizes of a collection of spatter bloodstain is shown in Table 8-8.

The final morphological data distribution analysed by the VB macro for any collection of spatter bloodstains is that of the subjective morphological criteria assigned to certain spatter bloodstains during the exhaustive spatter bloodstain recording process employed during this research project. The analytical site of impact estimation macro determines the number of spatter bloodstains within any particular collection that are assigned any of the 12 nominal subjective criteria described in Section 8.3.2.6. The proportion of spatter bloodstains within any collection that corresponds to a morphology that could be considered to be potentially unreliable or problematic to interpret for the purposes of site of impact estimation can, as a result, be determined, as illustrated in Figure 8-10.

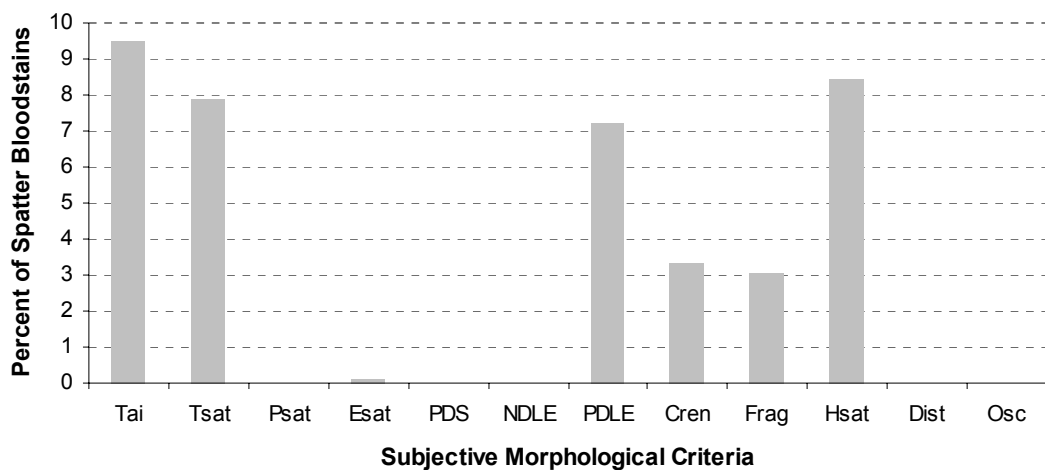


Figure 8-10 - An example of the relative frequency distribution of spatter bloodstains assigned one of the 12 subjective morphological criteria within a collection of spatter bloodstains.

### 8.4.3 Straight-Line Trajectory Composition

The distribution of the straight-line trajectory approximations constructed for a collection of spatter bloodstains is assessed by the analytical site of impact estimation macro to provide a consistent method of evaluating the reconstructive information provided by the spatter bloodstain morphological variables whose definition can be dependent on the target surface configuration. The frequency distributions of both the horizontal and vertical angles calculated for each vector-based straight-line trajectory approximation are analysed by the VB macro to

provide an isolated evaluation of the horizontal and vertical components of the constructed trajectories within any particular collection. The analytical site of impact estimation macro evaluates the distribution of the horizontal angle of the each straight-line trajectory approximation in terms of a series of five-degree wide class intervals that encompass the possible horizontal angle range of 0 to 360 degrees. As the three experimental impact spatter patterns analysed during this research project are all situated on a +yz vertical target surface plane, however, the range presented in this project is restricted to the 36 class intervals which cover the range of angles between the theoretical minimum and maximum of 0 and 180 degrees respectively.

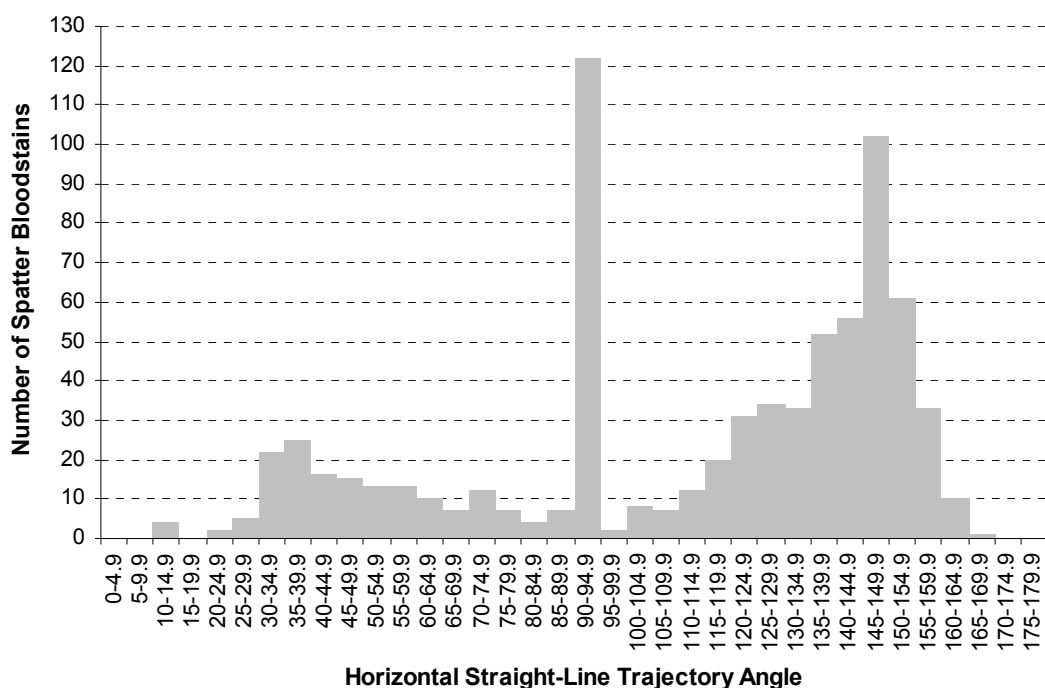


Figure 8-11 - An example of the raw count data generated during the characterisation of a collection of spatter bloodstains based on the horizontal angle of the constructed straight-line trajectory approximations.

The distribution of the vertical angle of the straight-line trajectory approximation constructed for each spatter bloodstain within a collection is also analysed by the VB macro in relation to 36 five-degree wide class intervals. For this trajectory elevation angle, however, a range covered by the analysis is between the theoretical minimum of -90 to the theoretical maximum of 90 degrees. An example of the distributions of the straight-line trajectory approximation of a collection of spatter bloodstains constructed by the analytical site of impact estimation macro is provided in Figure 8-11 and Figure 8-12.

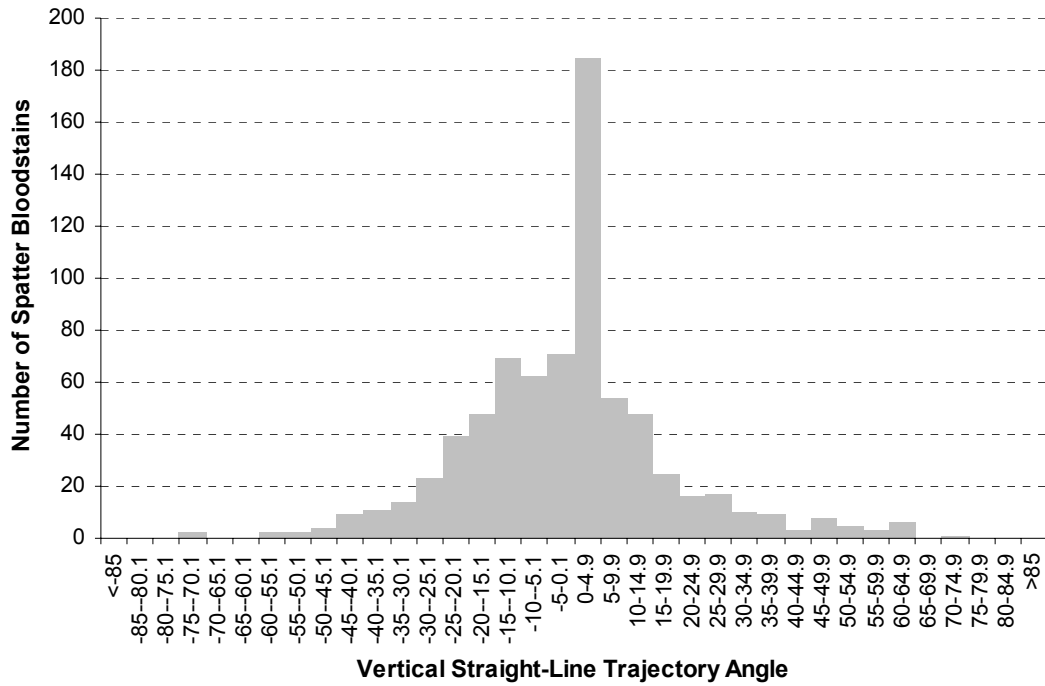


Figure 8-12 - An example of the raw count data generated during the characterisation of a collection of spatter bloodstains based on the vertical angle of the constructed straight-line trajectory approximations.

#### 8.4.4 Impact Site Relative Composition

Where the location of the known spatter-producing impact site is available for analysis, the analytical site of impact estimation macro provides an assessment of the composition of a collection of spatter bloodstains based not solely on observable or calculated spatter bloodstain data, as described above, but on the relationship of this data to its causative impact site. The distribution of the 3D straight-line spatter-impact site distances is evaluated by the VB macro through 29 five-centimetre wide class intervals, which cover the range of 0 to 145 centimetres. Although this range encompasses the maximum distances observed for each of the three experimental impact spatter patterns analysed during this research project, an additional class interval which incorporates distance of 145 centimetres and greater is included in the analysis to enable at least some characterisation of other impact spatter patterns that might include greater 3D straight-line distances.

Quality (cm)	3D			Horizontal		
	Count	Percent	Cumulative	Count	Percent	Cumulative
0-1.9	14	1.9	1.9	105	14.1	14.1
2-3.9	28	3.8	5.6	108	14.5	28.6
4-5.9	41	5.5	11.1	88	11.8	40.3
6-7.9	52	7.0	18.1	97	13.0	53.4
8-9.9	61	8.2	26.3	76	10.2	63.5
10-11.9	73	9.8	36.1	66	8.8	72.4
12-13.9	62	8.3	44.4	52	7.0	79.4
14-15.9	44	5.9	50.3	39	5.2	84.6
16-17.9	38	5.1	55.4	26	3.5	88.1
18-19.9	38	5.1	60.5	24	3.2	91.3
20-21.9	46	6.2	66.6	12	1.6	92.9
22-23.9	24	3.2	69.8	9	1.2	94.1
24-25.9	29	3.9	73.7	3	0.4	94.5
26-27.9	20	2.7	76.4	8	1.1	95.6
28-29.9	17	2.3	78.7	4	0.5	96.1
30-31.9	20	2.7	81.4	5	0.7	96.8
32-33.9	10	1.3	82.7	5	0.7	97.5
34-35.9	8	1.1	83.8	3	0.4	97.9
36-37.9	16	2.1	85.9	2	0.3	98.1
38-39.9	6	0.8	86.7	3	0.4	98.5
40-41.9	14	1.9	88.6	4	0.5	99.1
42-43.9	9	1.2	89.8	2	0.3	99.3
44-45.9	12	1.6	91.4	0	0.0	99.3
46-47.9	7	0.9	92.4	0	0.0	99.3
48+	57	7.6	100.0	5	0.7	100.0

Table 8-9 - An example of the frequency, relative frequency, and cumulative relative frequency distributions of the horizontal and 3D data quality assessments for a collection of spatter bloodstains.

The distributions of both the independent horizontal and independent 3D data quality assessments of a collection of spatter bloodstains are evaluated by the analytical site of impact estimation macro using 24 two-centimetre wide class intervals over a range of 0 to 48 centimetres, as illustrates in Table 8-9. A final 25<sup>th</sup> class interval includes all quality assessment at distances of greater than 48 centimetres from the known location of the impact site. This analysis of the distribution of independent data quality provides information on the proportions of a spatter bloodstain collection that can be considered to provide very good, through to very poor accuracy in terms of providing an approximation of the location of their causative impact site. Any particular collection of spatter bloodstain selected, as a result, can be evaluated in terms of the likely accuracy of its constituent spatter bloodstains, and the selection criteria employed assessed accordingly.

## 8.5 Conclusions

The spatter bloodstain data pre-processing, conducted through the analytical site of impact estimation macro, performs a number of important functions within the analysis of any specific site of impact estimate constructed for the purposes of the research into estimation uncertainty proposed during this project. Firstly, the pre-processing of the spatter bloodstain data provides the necessary mathematical and geometrical information on the straight-line trajectory approximation, defined by the orientation and impact angles of a spatter bloodstain, to construct a 3D site of impact estimate. The vector-based approach to the definition of straight-line trajectory approximations employed within the analytical VB macro provides a consistent and accurate methodology for mathematically defining the 3D direction of a trajectory, regardless of the target surface upon which a spatter bloodstain is observed, or the direction that the straight-line trajectory describes relative to that target surface.

Secondly, the pre-processing of the raw spatter bloodstain data provides the analytical site of impact estimation macro with detailed information on each spatter bloodstain presented for examination, which, in turn, provides the potential to apply precise sampling strategies to the selection of specific collections of spatter bloodstain for further analysis. Detailed information is stored within the application on the location of each spatter bloodstain within the investigative environment, the dimension of the width and length of the bloodstain, the size category of the bloodstain, the measured angle of orientation, the horizontal and vertical angles of the bloodstain's straight-line trajectory approximation, and the potential data quality of the straight-line trajectory where a known impact site is provided. Each variable stored on the pre-processed spatter bloodstain data can theoretically be applied in the selection of a spatter bloodstain sample. The procedure through which the VB macro provides such a sample selection functionality is detailed in the following chapter of this thesis.

Finally, the pre-processing of the spatter bloodstain data provides the means to conduct a detailed examination of the composition of any specific collection of spatter bloodstains analysed, in relation to the stored spatter bloodstain data relevant to the construction of a site of impact estimate. The generation of this composition data provides a method for comparing the data available within and between spatter bloodstain populations, and any specific spatter bloodstain samples drawn from them, as proposed in the aims of this research project.

Especially relevant to the experimental investigative process proposed by this research project is the fact that, where the location of a known spatter-producing impact site is provided, significant amounts of information on the potential quality of the collected spatter bloodstain data can be generated, and subsequently analysed and evaluated in relation to any specific sampling strategy employed. The interpretative functionality of such an investigative approach is demonstrated in Chapter 11 of this thesis, where the results of a series of analyses of the three experimentally produced impact spatter patterns, conducted using the analytical site of impact estimation application, are examined.

## **9 Site of Impact Estimate Construction and Analysis**

### **9.1 Introduction**

This chapter will discuss the numerical construction and analysis of a site of impact estimate conducted by the analytical site of impact estimation macro developed for this research project. The first section of this chapter will outline the selection of populations of interest from an impact spatter pattern and describe the two alternative approaches available within the VB macro to construction and analysis of a site of impact estimate. The second and third sections will discuss the processes through which a spatter bloodstain sample is selected by the VB macro, and the subsequent straight-line trajectory intersection data set of this sample is established, forming the basis of each site of impact estimate. The fourth section of this chapter will describe and discuss the numerous univariate, multivariate and spatial statistical analyses that are employed by the VB macro in the investigation of each trajectory intersection data set, in an attempt to provide detailed and appropriate summaries of this estimate data. The final section of this chapter will outline the specific analyses and data-recording conventions that are used in the construction and reporting of the two alternative approaches to constructing and analysing site of impact estimates available within the analytical site of impact estimation macro.

### **9.2 Spatter Bloodstain Selection**

Following the data acquisition and spatter bloodstain data pre-processing phases of the VB macro (as described in the previous chapter of this thesis), each spatter bloodstain object stored in the application memory can be evaluated in terms of satisfying some spatter bloodstain selection criteria. This evaluation is conducted within the 'subsamppop' subroutine, where an iterative procedure checks the data contained within each spatter bloodstain object against hard coded logic statements which can be programmed prior to any site of impact estimation analysis. The logic statements contained within this subroutine are used to define subpopulations of interest within the total spatter bloodstain object population, which are used to construct specific site of impact estimates based on different spatter bloodstain sampling criteria. Where the data included within each spatter bloodstain object satisfies the specific pre-programmed logic statements, the location of the spatter bloodstain object within the spatter

pattern object collection is stored, and the subpopulation of interest is established from the impact spatter pattern presented for analysis. A maximum of two separate subpopulations can be generated for any single site of impact estimate analysis, but the number of spatter bloodstain selection criteria imposed through the pre-programmed logic statements is limited only by the amount of spatter bloodstain data recorded within each bloodstain object.

Once established the spatter bloodstain subpopulation(s) of interest can be used to construct and analyse site of impact estimates through the 'Create' tab of the VB macro interface shown in Figure 9-1. This interface provides a number of options for both the construction and visualisation of a site of impact estimate. The current impact spatter patterns stored as spatter bloodstain objects within the pattern object collection in the applications memory is indicated in the 'Active Data' panel of the interface tab. Using the subpopulation(s) of interest selected from this impact spatter pattern the VB macro can construct a single sample site of impact estimation, or a multiple sample estimate. A single sample site is constructed by choosing the 'Single Sample' and the 'New' option buttons. On activating the 'New' option button the total number of spatter bloodstains within the chosen subpopulation(s) are indicated in the 'No. of Sample' textbox. This number can be altered to change the size of the spatter bloodstain sample to be used in constructing the site of impact estimate. The single sample option constructs a single site of impact estimate based on the selected sample size and pre-defined subpopulation sampling. A multiple sample estimate can be constructed by selecting the 'Multisample' option button. This multiple sample site of impact estimate analysis technique constructs a series of single sample estimates based on the pre-defined subpopulation to provide a means of analysing the potential variation in an estimate caused by variable spatter bloodstain selection. Up to 400 individual site of impact estimates are constructed, with 100 samples taken for spatter bloodstain sample sizes of 10, 20, 50 and 100, where the total number of spatter bloodstains within the subpopulation(s) of interest allows. The maximum sample size to be analysed using the multiple sample technique is controlled in the 'Sample Sizes' textbox with the numbers 1 to 4 corresponding to the increasing sample sizes. The number of spatter bloodstains within each subpopulation is indicated by the 'Subpop' label, which shows the total number of spatter bloodstains available for analysis, and the number of spatter bloodstain within each of the two possible subpopulations.



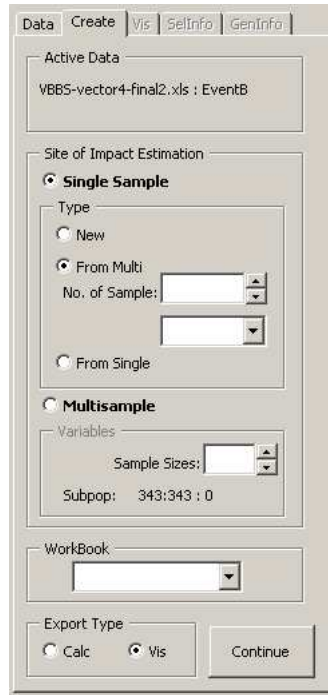


Figure 9-1- The 'Create' interface of the analytical site of impact estimation macro.

Once the method of analysis has been chosen the VB macro begins the process of constructing and analysing the site of impact estimation on the pressing of the 'Continue' button. Two additional choices are available, however, at this stage, with the 'Export Type' option buttons allowing the estimate to either be visualised using the 3D interactive virtual environment or recorded numerically in a separate Excel<sup>®</sup> workbook. While the same process of construction and analysis of a site of impact estimate is employed, regardless of the selected output media, the results of these analyses will be illustrated in this chapter in relation to the numerical recording approach, with the visualisation of site of impact estimation data addressed in the following chapter of this thesis.

Before outlining the procedures through which the analytical site of impact estimation macro constructs and analyses a site of impact estimate, the additional functionality made available through the 'Create' tab of the VB macro interface is worth describing. In addition to analysing new site of impact estimates using the data selected and processed via the 'Data' tab of the VB macro interface, the 'Create' tab also provides a number of alternative choices where site of impact estimation data previously recorded in an Excel<sup>®</sup> workbook can be re-examined. This functionality of the VB macro enables the construction, recording and visualisation of any single sample site of impact estimate that has been pre-recorded in a multiple sample format, as well as enabling a pre-

recorded single or multiple sample estimate to be visualised within the integrated 3D interactive environment. To perform a re-analysis of any pre-recorded site of impact estimation data the specific Excel® workbook in which the data is stored has to be open, and the name of this workbook selected in the dropdown box within the 'Workbook' frame of the 'Create' tab. In the re-analysis of single samples, whether this is from a pre-recorded single or multiple sample, the impact spatter pattern collection of spatter bloodstain objects stored in the application memory is re-populated with the specific pattern data the original analysis was based upon. The raw spatter bloodstain data of each recorded analysis is stored as a separate Excel® worksheet in the workbook used to record the estimate data. The subpopulation of interest specified for the original analysis is also redefined by the VB macro using the subpopulation data of each analysis also stored in the Excel® workbook. Once re-analysed, whether numerical recorded or visualised, the impact spatter pattern collection and subpopulation selection criteria are retained within the application memory for any further analyses which may be required of the data. The source of the active spatter bloodstain data, as with the acquisition of raw impact spatter pattern data through the 'Data' tab of the VB macro interface, is indicated in the 'Active Data' frame of the 'Create' tab, where the name of both the Excel® workbook, and the raw spatter bloodstain worksheet are displayed.

### **9.3 Site of Impact Estimate Construction**

A single site of impact estimate is constructed by the same process within the VB macro, whether the estimate is of a single or multiple sample type, or the data generated is to be visualised by the integral 3D interactive environment or numerically recorded in a separate Excel® workbook. Firstly, a sample of spatter bloodstain from within the subpopulation(s) of interest is selected relative to the size of the spatter bloodstain sample, as chosen through the 'Create' tab. The VB macro utilises the 'randSelect' function within the 'Sample' code module to select the specified number of spatter bloodstains from within the subpopulation. This process uses the pseudo-random function integral to VBA to provide a randomly selected sample in which each spatter bloodstain within the subpopulation(s) of interest can only be included once. Where two subpopulations are defined within the VB macro, then the number of spatter bloodstains drawn from each subpopulation is taken as half the total specified sample size. For the construction of site of impact estimates for the multiple sample approach this

selection process is relatively straightforward, as the sample sizes of 10, 20, 50 and 100 are all divisible into two equal size sample, and the maximum sample size to be constructed is selected relative to the subpopulation containing the fewest spatter bloodstains. In the single sample approach, however, where an odd number sample size is selected, the additional spatter bloodstain is selected from either subpopulation at random. Where a subpopulation of interest contains too few spatter bloodstains to adhere to either of these random selection strategies, then all of the spatter bloodstains from that subpopulation are selected, and the remainder of the sample size is comprised of randomly selected spatter bloodstain from within the other subpopulation. Once selected the spatter bloodstain sample is passed to the 'popSamp' subroutine, where the variable used to stored the current site of impact estimation data and analysis results by the VB macro is re-dimensioned, and the sample specific spatter bloodstain object data stored within it. This spatter bloodstain sample selection process is illustrated in

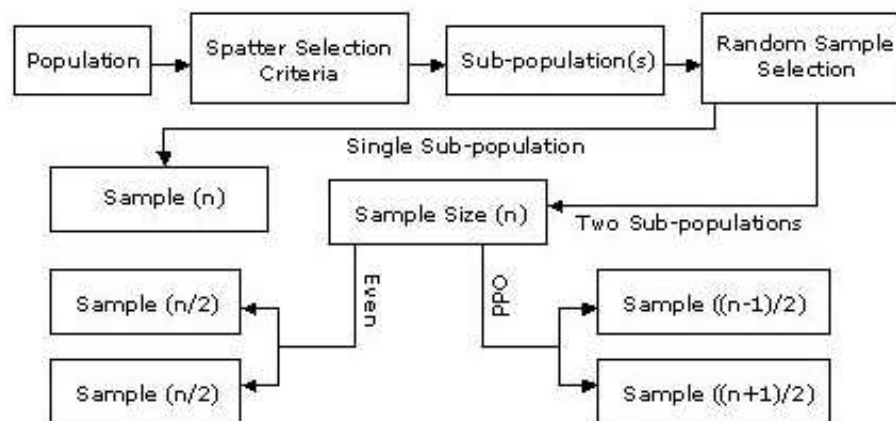


Figure 9-2 - A flow chart showing the sample selection process employed by the VB macro.

The spatter bloodstain data stored within the current estimation variable is subsequently analysed by the VB macro through two distinct sequential procedures in the construction of a site of impact estimate. The first process establishes the location of all of the intersections of the straight-line trajectories inferred from the directionality and impact angle of the spatter bloodstain within the select sample, while the second process analyses and summarises the complete trajectory intersection data set in an attempt to provide an accurate, meaningful, and appropriate site of impact estimation.

## 9.4 Establishing Trajectory Intersections

The construction of a site of impact estimate for any specific sample approach is instigated by the 'Calculate' subroutine within the VB userform code module. This subroutine performs three basic functions. Firstly, the current estimate variable used to store the selected spatter bloodstain sample data is re-dimensioned to include additional sub-variables to store all the possible trajectory intersections that may occur for each specific spatter bloodstain. Secondly, an iterative process scrolls through every combination of two spatter bloodstains to extract and pass the relevant trajectory data to the 'checkInt' subroutine, where the presence and location of the straight-line trajectory intersections is assessed. Finally, before passing this data to the trajectory intersection subroutine for analysis, the 'Calculate' subroutine evaluates the potential trajectory bracketing status of each set of two trajectories, based on the criteria assigned to each spatter bloodstain during the pre-processing stage of the VB macro (see Section 8.3.2.2). Where the bracketing variables of either spatter bloodstain within the sample are the same, or either is equal to zero, the Boolean variable used to store the bracketing status of the two trajectories is set to 'False', and in all other cases set to 'True'. The designation of these bracketing values, and the analysis of the relationship between them was devised to approximate the bracketing sample strategy, and intersection analysis that is often applied in practical site of impact estimation. Where a true bracketing approach would only tend to consider spatter bloodstain trajectories and trajectory intersections from opposite sides of a likely impact site, the use of *a priori* knowledge in the construction of the site of impact estimates was explicitly avoided, and reserved for the analysis of the estimates. This method of approximating a bracketing approach to site of impact estimation was, as a result, deemed to be the most appropriate way of replicating and investigating this approach to estimate construction within this research project.

The presence and location of an intersection of two straight-line trajectories is established using the  $\mathbf{v}_x$ ,  $\mathbf{v}_y$ , and  $\mathbf{v}_z$  vector components of the each straight-line trajectory approximation determined in the pre-processing stage of the VB macro (see Section 8.3.2.1). A similar parameterised vector scaling approach, such as that employed in calculating the independent data quality of each straight-line trajectory, is applied through a series of formulae to assess the presence and position of any intersection between the two trajectory vectors in the horizontal plane (the only unbiased straight-line trajectory plane). The first two calculations

performed in this process are illustrated in Formula 9-1 and Formula 9-2, where the horizontal components of two unit trajectory vectors,  $\mathbf{v}_1$  and  $\mathbf{v}_2$ , and the origins of these trajectories, the horizontal locations of the two spatter bloodstains,  $\mathbf{o}_1$  and  $\mathbf{o}_2$ , are analysed.

$$a = (\mathbf{v}_{1x}\mathbf{v}_{2y}) - (\mathbf{v}_{1y}\mathbf{v}_{2x})$$

*Formula 9-1 - The first preliminary trajectory vector intersection tests (after Geometric Tools, 2005).*

$$b = [\mathbf{v}_{2x}(\mathbf{o}_{1y} - \mathbf{o}_{2y})] - [\mathbf{v}_{2y}(\mathbf{o}_{1x} - \mathbf{o}_{2x})]$$

*Formula 9-2 - The second preliminary trajectory vector intersection test (after Geometric Tools, 2005).*

If both Formula 9-1 and Formula 9-2 return a value of zero then the two trajectory vectors analysed are collinear in the horizontal plane, and as a result will have no single definable point of intersection. If Formula 9-1 returns a value of zero and Formula 9-2 returns a value other than zero then the two trajectory vectors are parallel in the horizontal plane, and the trajectories will never intersect. The intersections variables declared for these spatter bloodstains are recorded as 'Collinear' or 'Parallel'. If both Formula 9-1 and Formula 9-2 return values other than zero, however, then the two unit trajectories cross at some point along an extension of their lengths, and two more formulae can be applied to establish the location of this horizontal trajectory intersection. These two formulae are shown in Formula 9-3 and Formula 9-4, where  $f_1$  and  $f_2$  are the scaling factors that are needed to be applied to the first and second unit trajectory vectors, respectively, to reach the location of their intersection.

$$f_1 = \frac{[\mathbf{v}_{2x}(\mathbf{o}_{1y} - \mathbf{o}_{2y})] - [\mathbf{v}_{2y}(\mathbf{o}_{1x} - \mathbf{o}_{2x})]}{\mathbf{v}_{1x}\mathbf{v}_{2y} - \mathbf{v}_{1y}\mathbf{v}_{2x}}$$

*Formula 9-3 - Determining the scaling factor of the first trajectory to the location of its intersection with the second trajectory (after Geometric Tools, 2005).*

$$f_2 = \frac{[\mathbf{v}_{1x}(\mathbf{o}_{1y} - \mathbf{o}_{2y})] - [\mathbf{v}_{1y}(\mathbf{o}_{1x} - \mathbf{o}_{2x})]}{\mathbf{v}_{1x}\mathbf{v}_{2y} - \mathbf{v}_{1y}\mathbf{v}_{2x}}$$

*Formula 9-4 - Determining the scaling factor of the second trajectory to the location of its intersection with the first trajectory (after Geometric Tools, 2005).*

If either or both Formula 9-3 and Formula 9-4 return a negative scaling factor, then the two trajectories analysed would only intersect in the horizontal plane if one or both of the unit trajectory vectors were extended behind their origin. As the location of the origin of each trajectory vector, the spatter bloodstain, is fixed and represents the termination of the blood droplet flight path that the VB macro is attempting to retrace, then the two trajectories analysed cannot be considered to intersect in the horizontal plane of analysis, and are likely to be divergent. If both Formula 9-3 and Formula 9-4 return positive results then the horizontal trajectory intersection can be considered to be real, and the location of this intersection in the horizontal plane and the vertical heights of each of the trajectories at this horizontal location can be established using Formulae 9-5, as illustrated in Figure 9-3.

$$\begin{aligned} \mathbf{p}_x &= \mathbf{o}_{ix} + (f_i \mathbf{v}_{ix}) \\ \mathbf{p}_y &= \mathbf{o}_{iy} + (f_i \mathbf{v}_{iy}) \\ \mathbf{p}_{iz} &= \mathbf{o}_{iz} + (f_i \mathbf{v}_{iz}) \end{aligned}$$

Formulae 9-5 - Establishing the location of the intersection point for two trajectory vectors.

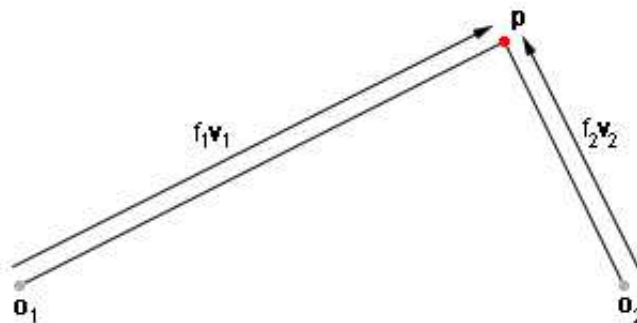


Figure 9-3 - An illustration of the vector-scaling of two straight-line unit trajectory vectors to establish the location of their intersection.

Formulae 9-5 is applied to both trajectory vectors analysed for intersection, with  $i$  taking the values of 1 and 2, and  $\mathbf{p}$  representing the intersection point. As the two trajectories will intersect at the same horizontal location, the  $\mathbf{p}_x$  and  $\mathbf{p}_y$  for both trajectories are calculated and compared to check for consistency. If the intersection locations for each trajectory are the same then the intersection is recorded as the intersection vector,  $[\mathbf{p}_x, \mathbf{p}_y, \mathbf{p}_z, \mathbf{p}_{zh}]$ , representing the horizontal

location of the trajectory intersection, and the heights of each trajectory above this location where  $p_{zi}$  is the lower and  $p_{zh}$  is the higher of the heights.

Once calculated, each intersection vector is subsequently examined in relation to the physical extent of the 3D investigative environment as inputted during the data acquisition phase of the VB macro (see Section 8.3.1). Where the intersection location resides outside of the predefined investigative environment, then the intersection location is recorded as void with a result of either 'OutR' in terms of the horizontal extent of the environment, or 'UnrealZ' where either of the intersection heights lie outside the vertical extent of the environment. If the trajectory intersection analysis procedure fails to establish a intersection point, in terms of the trajectories being collinear, parallel, or intersection occurring outside of the investigative environment, then the 'nullInt' variable of the current estimate data set is re-dimensioned to contain an extra variable, and the number of the two spatter bloodstains analysed and the string variable describing the reason for the failure to intersect are recorded. Where a true trajectory intersection is established the horizontal distance from each of the two spatter bloodstains to the location of the intersection of their trajectories is calculated using Pythagoras' Theorem, and the 3D straight-line distance between the points is recorded in the form of the vector scaling factor.

Once the analytical site of impact estimation macro has established a single trajectory intersection, a variable declared to store the number of intersections within a constructed site of impact estimation is advanced by one to keep track of the total number of intersections established within an estimate. The intersection data variable of the current estimate data set is re-dimensioned to contain an extra variable, and the specific intersection data generated is recorded. The distance of each trajectory intersection point from the known impact site, where provided, is also calculated by the VB macro. The distance and direction of each axial component of the intersection location and the known impact site is determined, and the straight-line distance between the two points calculated. This trajectory intersection procedure is repeated until all the combinations of two spatter bloodstains within the currently selected spatter bloodstain sample have been analysed, and their trajectory intersection data recorded.

The basic intersection data generated by this trajectory intersection procedure is shown in Table 9-1, where data from five of the 2043 trajectory intersections established during the analysis of a spatter bloodstains sample from pattern ES-A

is displayed. This data includes the number assigned to the intersection point, **p**, in the order in which they were established (IntNum), the horizontal location and two vertical heights of the intersection point (X,Y,Zl, and Zh), the identification numbers assigned to the spatter bloodstains within the selected sample (BS1 and BS2), the status of the trajectory bracketing approximation (Opp), the horizontal axial and straight-line distance between the intersection point and the known impact site (XDKP, YDKP, HDKP), and the two vertical height distances and the 3D straight-line distance between the 3D intersection point and the known impact site for both of these heights (ZLDKP, ZHDKP, TZLDKP and TZHDKP).

IntNum	X (cm)	Y (cm)	Zl (cm)	Zh (cm)	Zdif (cm)	BS1	BS2	Opp
1	48.35	115.53	20.28	24.09	3.81	2	1	FALSE
2	46.68	113.36	24.74	25.22	0.48	3	1	FALSE
3	40.46	105.25	26.60	29.44	2.83	4	1	FALSE
4	46.71	113.41	23.24	25.19	1.95	5	1	FALSE
5	45.36	111.64	26.11	29.93	3.81	1	6	FALSE

IntNum	XDKP (cm)	YDKP (cm)	HDKP (cm)	ZLDKP (cm)	ZHDKP (cm)	TZLDKP (cm)	TZHDKP (cm)
1	0.35	3.33	3.35	-5.27	-1.46	6.25	3.66
2	-1.32	1.16	1.76	-0.81	-0.33	1.94	1.79
3	-7.54	-6.95	10.25	1.05	3.89	10.30	10.96
4	-1.29	1.21	1.76	-2.31	-0.36	2.90	1.80
5	-2.64	-0.56	2.70	0.56	4.38	2.76	5.14

Table 9-1 - A sample of the basic trajectory intersection data from five of 2043 intersections established during the analysis of the 0-5 cm 3D data quality sample of pattern ES-A (results reported to 2 decimal places where necessary).

## 9.5 Analysing Trajectory Intersection Data Sets

Even at relatively low numbers of spatter bloodstains, compared to the number made available through the exhaustive recording methodology, the mathematical computer-based estimation of the location of a site of impact estimation can produce large trajectory intersection data sets. As discussed earlier in this thesis, the number of potential trajectory intersections within an estimate raises rapidly as the number of spatter bloodstains considered increases (see Section 4.7). The manipulation of a standard combinations calculation shown in Formula 9-6 further illustrates this quadratic relationship, where  $i$  is the number of potential trajectory intersections,  $n$  is the size of the spatter bloodstain sample, and  $r$  is two, the number of trajectories analysed for intersection at any one time.



$$i=^nC_r = \frac{n!}{r!(n-r)!}$$

$$= \frac{n^2}{2} - \frac{n}{2}$$

*Formula 9-6- The modification of a standard combination formula for the purposes of establishing the number of potential trajectory intersections given spatter bloodstain sample sizes.*

While a site of impact estimate is essentially constructed through the locating of these straight-line trajectory intersections, some processing of this raw estimate data is necessary to provide a meaningful and appropriate description of the distribution of this data and, as a result, an appropriate interpretation of the site of impact estimate generated. The analysis of the trajectory intersection data set produced for a particular estimate is conducted within the 'minmax' subroutine of the analytical site of impact estimation macro. The intersection data is subjected to a series of analyses within this subroutine using two differing but complementary approaches to the investigation, description and evaluation of a trajectory intersection data set. These two approaches involve the application of conventional descriptive and inferential statistical data analysis methods, and the application of spatial data analysis techniques developed specifically for the investigation of data collected in a spatial context.

### **9.5.1 Conventional Statistical Analysis**

The conventional statistical analyses of the trajectory intersection data conducted through the VB macro include the application of numerical and graphical techniques of Exploratory Data Analysis (EDA), and the application of inferential techniques to estimate population parameters from sample statistics. The descriptive statistical methods of EDA are employed to describe and summarise the structure of the potentially large trajectory intersection data sets in an attempt to reveal not only the central tendency of these distributions but also the nature of their shape and dispersal. While the mean and standard deviation of these data sets are typically generated in other computer-based site of impact estimation, multiple approaches to describing the structure the raw estimate data are applied through this project, using the VB macro. A limited number of inferential statistical techniques are also applied to the trajectory intersection data to provide a method of estimating the likely location of a spatter bloodstain population mean, where the intersection data set is constructed from a spatter

bloodstain sample, providing an indication of at least one aspect of uncertainty in the construction of a site of impact estimate. The conventional statistical analysis conducted through the VB macro is divided into two distinct sections. These sections provide a univariate analysis of the marginal distributions and multivariate analysis of the joint distributions of any particular trajectory intersection data set.

### 9.5.1.1 Univariate Analysis

The distribution of each of four intersection data variables,  $p_x$ ,  $p_y$ ,  $p_{zl}$ , and  $p_{zh}$ , are analysed separately, as marginal distributions, by the VB macro to provide a means of evaluating each specific aspect of the estimate data in isolation. The arithmetic mean,  $\bar{x}$ , and sample variance,  $s^2$ , of each marginal distribution are calculated by the VB macro to provide both a measure of the central tendency of the data, and the dispersion of the data around this location. The standard deviation of each distribution, the square root of the variance,  $s$ , can also be derived from the variance of the distribution to provide a measure of the average distance of the entire data set from the location of the mean.

<b>Number of Standard Deviations about the Mean</b>	<b>Empirical Intervals</b>	<b>Bienayme-Chebychev Intervals</b>	<b>Normal Distribution Intervals</b>
1	67%	N/A	68.22%
2	90-95%	At least 75%	95.44%
3	99-100%	At least 88.89%	99.73%
4	N/A	At least 93.75%	99.9%

Table 9-2 - The percentage of a distribution within a number of standard deviations either side of the distribution mean under three differing modelling assumptions (after NSIT/SEMATECH, 2005).

Having established the mean and standard deviation of a data set the entire distribution can be approximated through the application of appropriate distribution models, as demonstrated in Table 9-2. Where a univariate distribution is known to be normally distributed the 'Normal' model can be applied and an accurate percentage of the data within a number of standard deviations of the distribution mean inferred. Where the distribution is approximately bell-shaped, with no evidence of a significant departure from a normal distribution the 'Empirical' model can be reasonably applied. The most conservative of the three models, the Bienayme-Chebychev model, however, can be applied to any data

with reasonable confidence regardless of the nature of its distribution (NSIT/SEMATECH, 2005; Wiess, 1999; Ott and Longnecker, 2001).

While the mean and mean deviation descriptions of a distribution can provide useful measures of the central tendency and variation of data within a particular data set, the interpretation of both of these descriptive methods in isolation requires some caution. Both of the measures are sensitive to, and potentially biased by, the presence of extreme values within a distribution. The variance and standard deviation of a data set, being the result of a squared distance function, also provide no assessment of any directionality in the variation of the data, where this is present.

To provide a more detailed description of each form of each distribution the skewness and kurtosis of the data set is calculated by the VB macro using Formula 9-7, where  $d = 3$  and  $4$  to establish the measures,  $m$ , of skewness and kurtosis respectively, and  $n$  is the size of the distribution.

$$m = \frac{\sum_{i=1}^n (x_i - \bar{x})^d}{(n-1)s^d}$$

*Formula 9-7 - The formula for calculating the skewness and kurtosis of a distribution (after NIST/SEMATECH, 2005).*

The measure of skewness of a data set provides an assessment of the symmetry of the distribution of this data around the location of its mean. A result of zero indicates a distribution that is symmetrical around the location of the mean. A positive result, however, is indicative of a right-skewed distribution, with an extended distribution to the right of the mean of the distribution, while a negative result indicates a left-skewed distribution, with an extended distribution to the left of the mean of the data set. The kurtosis of a distribution provides a measure of how peaked or flat a distribution is, and is often used to compare a distribution to the known response from a normal distribution. As the kurtosis of a normal distribution is known to be 3, the kurtosis of a distribution can be evaluated as  $m-3$ . Where the result of this calculation is negative the distribution is flatter than a normal distribution, and where the result is positive the distribution is more peaked than a normal distribution.

An example of the summary descriptive data provided for a trajectory intersection data set by the analysis of the mean and mean deviation of the distribution of the four positional variables made available for each intersection point is shown in Table 9-3.

<b>Measure</b>	<b>X</b>	<b>Y</b>	<b>Zh</b>	<b>Zl</b>
Mean (cm)	46.42	112.01	28.65	24.92
Variance (cm <sup>2</sup> )	115.39	108.62	21.52	24.58
Skewness	0.89	-0.22	1.13	-0.54
Kurtosis	8.60	12.77	7.37	6.06
Standard Deviation (cm)	10.74	10.42	4.64	4.96
SD*2 (cm)	21.48	20.84	9.28	9.91
SD*3 (cm)	32.23	31.27	13.92	14.87

*Table 9-3 - The mean, variance, skewness and kurtosis information recorded for each of the four variables of the trajectory intersection data and the derived standard deviation information generated during the analysis of the 0-5 cm 3D data quality sample of pattern ES-A (reported to 2 decimal places).*

Standardised scores, or z-scores for each observation within the marginal distributions of the trajectory intersection data are also calculated by the analytical site of impact estimation macro using Formula 9-8, where  $i = 1$  to  $n$ .

$$Z_i = \frac{(x_i - \bar{x})}{s}$$

*Formula 9-8 - The formula used to calculate the standardised score of each variable for each trajectory intersection location.*

The calculation of these standardised scores provides information on the distance of each observation from the mean of the distribution in terms of the size of the standard deviation of the distribution. This data can subsequently be used to compare the relative standings of observations from different distributions, assess the location of each observations in terms of the rest of the distribution, and through the standard deviation intervals outlined in Table 9-2 indicate how 'typical' each individual observation within the distribution might be (Siegel and Morgan, 1996; Weiss, 1999; Ott and Longnecker, 2001).

In addition to the statistical descriptions based on the arithmetic mean of a distribution and the deviation of the observations from this mean, the VB macro also generates a number of statistical descriptions of the trajectory intersection

data set based on the order of the data within each marginal distribution. To produce these descriptions the data within a particular distribution is first arranged in ascending numerical order using the 'Sortb' function of the 'Stats' class module.

The minimum and maximum values within the distribution are also identified and recorded by the analytical site of impact estimation macro to provide an assessment of the total range of values that the distribution covers. The first and third quartiles of the distribution are identified to construct the Inter-Quartile Range (IQR) of the distribution, the values between which the central 50% of the data is situated, and the second quartile of the distribution, the middle, or median of the data set, is also identified to provide an additional measure of the central tendency of the distribution. An example of the summary of a distribution that these order-based measures provide is shown in Table 9-4.

<b>Measure</b>	<b>X (cm)</b>	<b>Y (cm)</b>	<b>Zh (cm)</b>	<b>Zl (cm)</b>
Minimum	0.81	34.66	2.07	0.37
First Inter-Quartile	43.17	109.54	26.34	23.05
Median	46.28	111.53	28.30	25.06
Third Inter-Quartile	49.63	114.39	29.98	27.03
Maximum	126.87	182.31	55.03	49.16

Table 9-4 - The ordered intersection data measures as generated during the analysis of the 0-5 cm 3D data quality sample of pattern ES-A (reported to 2 decimal places).

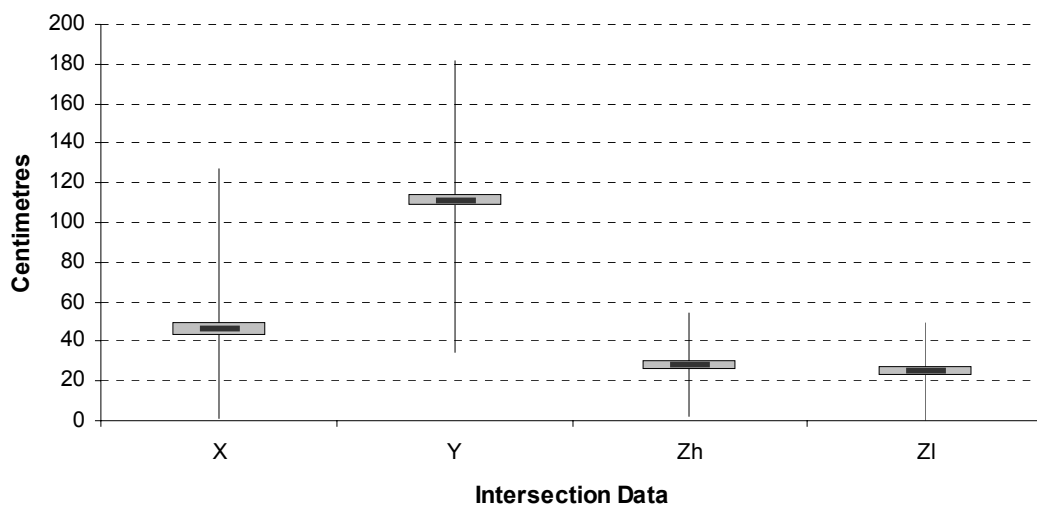


Figure 9-4 - Five-number summary plots of each of the four variables of the trajectory intersection data as generated during the analysis of the 0-5 cm 3D data quality sample of pattern ES-A.

The descriptive measures based on the percentiles of a distribution can provide a more robust alternative to the approximation of the central tendency and variation of a data set than that provided by the mean, and mean deviation-based descriptions of a distribution (Weiss, 1999). The graphical description of the ordered statistics gathered by the VB macro in the form of a five-number summary (also known as a box-whisker plot) can also provide an effective method for describing, assessing and comparing the composition of distributions. An example of the five-point summary graph produced from the data in Table 9-4 is illustrated in Figure 9-4.

The upper and lower limits for each marginal distribution are also calculated by the VB macro, to provide an approximate method for identifying potential outlier values within a data set, the observations that could be considered to fall outside of the overall pattern of the data. These upper and lower limits for each distribution are calculated using Formula 9-9, where  $L_l$  is the lower limit,  $L_u$  is the upper limit, and  $Q_1$  and  $Q_3$  are the first and third quartiles respectively.

$$L_l = Q_1 - \frac{3}{2}(IQR)$$

$$L_u = Q_3 + \frac{3}{2}(IQR)$$

*Formula 9-9 - The method of calculating the upper and lower limits of a distribution (Weiss, 1999).*

While the upper and lower limits of a distribution should not be used in isolation to classify any particular observations as outliers, as extreme values may be a natural feature of some distributions, the range indicated by these limits can also be used to suggest where the predominant portion of a distribution is likely to be situated, as exemplified in Table 9-5.

<b>Measure</b>	<b>X</b>	<b>Y</b>	<b>Zh</b>	<b>ZI</b>
Lower Limit	33.48	102.26	20.89	17.08
Upper Limit	59.32	121.66	35.44	33.00

*Table 9-5 - The lower and upper limit as calculated for the trajectory intersection data generated during the analysis of the 0-5 cm 3D data quality sample of pattern ES-A (reported to 2 decimal places).*

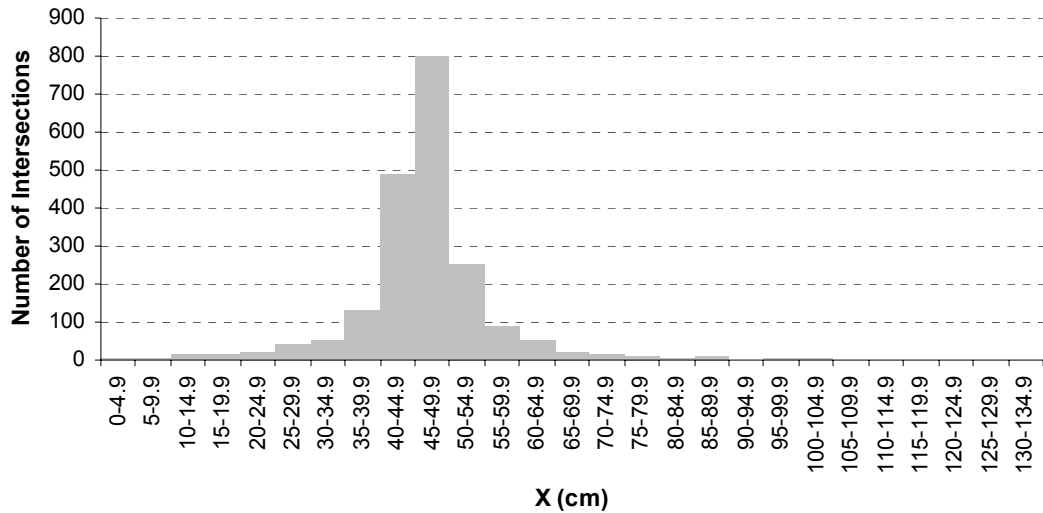


Figure 9-5- The marginal distribution count data of the number of trajectory intersections within five centimetre wide bins in the x-axis of the investigative environment generated during the analysis of the 0-5 cm 3D data quality sample of pattern ES-A.

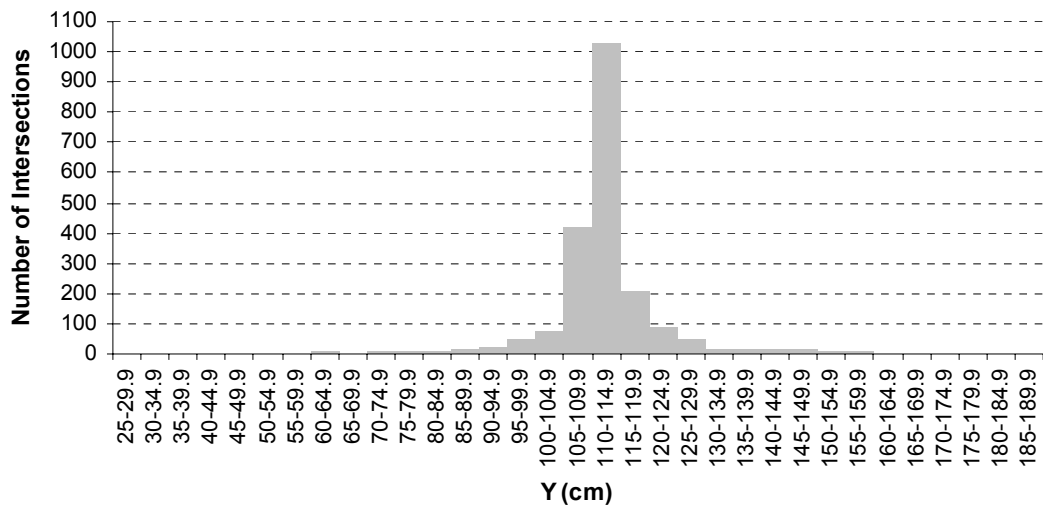


Figure 9-6 - The marginal distribution count data of the number of trajectory intersections within five centimetre wide bins in the y-axis of the investigative environment generated during the analysis of the 0-5 cm 3D data quality sample of pattern ES-A.

The marginal frequency distributions of the trajectory intersection data in each of the two axes of the horizontal plane of analysis are also provided by the VB macro, through the construction of a joint distribution count, which is described later in this chapter (see Section 9.5.1.2). The marginal frequency distributions of the trajectory intersection data in the x- and y-axis of the 3D investigative environment provide a form of marginal distribution summary which can be used to analyse the entire distribution of the data, aiding the appropriate interpretation of the point-based statistical description generated, as well as to identify the

potential modality of the distribution, and provide an approximation of the density of the trajectory intersections with the axes of the horizontal plane. The analysis of the distributions of the trajectory intersection data and their comparison to the distributions of other estimate intersection data sets can also be facilitated by the production of relative frequency distributions, where the count-based class interval data is expressed as a percentage of the total intersection data sets. Examples of the count-based marginal frequency distributions as generated by the VB macro using five centimetre wide classes across the extent of the investigational environment are illustrated in Figure 9-5 and Figure 9-6.

While the majority of the conventional statistical analyses conducted on the marginal distributions of the trajectory intersection data by the VB macro are based on the principles of EDA and statistical description, two inferential statistical processes are also conducted on this data. These two processes involve the construction of confidence intervals for the mean of each distribution using a parametric *t*-distribution, and a non-parametric bootstrap approach. These two methods are included in the VB macro to provide a means of estimating the range within which the mean of a population could be situated where the particular trajectory intersection data analysed can be considered to constitute a sample. The uncertainty of a sample-based description of the mean of a trajectory intersection data, as a result, might be demonstrated.

The *t*-distribution confidence interval for a sample mean when the standard deviation of the population from which the sample was drawn is unknown is calculated by using Formula 9-10, where  $\alpha$  is the confidence level given by  $100(1-\alpha)\%$ ,  $n$  is the number of trajectory intersections within the current sample, and  $\bar{x}$  and  $s$  are the sample mean and sample standard deviation respectively.

$$t_{\text{int}} = \bar{x} \pm t_{\alpha/2} \left( \frac{s}{\sqrt{n}} \right)$$

*Formula 9-10 - The construction of a t-distribution confidence interval when the population standard deviation is not known.*

A confidence level of 95% is calculated by the VB macro for each marginal distribution mean, with the value of the *t*-distribution with  $n-1$  degrees of freedom provided by a predefined statistical function within Excel®. The



application of this confidence interval, however, can be limited as the  $t$ -interval procedure is predominantly based on the assumptions of the sample data having been randomly selected from a normal population distribution. The  $t$ -interval can still be effectively applied in situations where moderate violations of population normality occur, although the analysis of heavy-tailed distributions tends to provide a weaker level of confidence than that calculated, and the analysis of significantly skewed distributions can produce an inappropriate confidence interval given the directionality of the distribution, and the limitations of the arithmetic mean in terms of indicating the central tendency of the distribution (Weiss, 1999; Ott and Longnecker, 2001)

Given the parametric requirements in the appropriate application of the  $t$ -distribution confidence interval, an alternative non-parametric estimator of the sample mean confidence interval for each marginal distribution is also provided within the VB macro. This non-parametric confidence interval is established using a bootstrap technique, whereby the parametric assumptions necessary for the application of the  $t$ -distribution are avoided by replacing the information on the unknown population distribution with that of the known empirical distribution (Chernick, 1999). The confidence interval is calculated through a percentile-based method, which involves repeatedly re-sampling, with replacement, from the empirical sample distribution and calculating the mean of each new data set. The range of values between the 2.5<sup>th</sup> and 97.5<sup>th</sup> percentiles of the series of re-sampled distribution means can subsequently be interpreted as an estimate of the 95% confidence interval for the original sample mean. The bootstrap confidence interval produced by the VB macro, while removing potentially problematic modelling assumptions, still requires some caution in its interpretation. The percentile method does not, for example, perform particularly well with small sample sizes, especially where these are from asymmetric distributions, and generally requires at least 1000 re-samples to provide a sound estimate of a confidence interval (Chernick, 1999). As the bootstrap is a computer-intensive method, and the size of trajectory intersection data sets to be analysed during this research project are potentially very large, only 500 re-samples of each marginal distribution are taken by the VB macro to reduce processing time. As a result, it may be more appropriate to view the attempts at mean confidence interval estimation undertaken within the VB macro as approximations of these inferential statistics, which if identified as potentially beneficial to the analysis of estimate uncertainty can be fully implemented in future developments of the analytical site of impact estimation application.

An example of the mean bootstrap confidence interval information generated by the analytical site of impact estimation macro for a random sample of ten spatter bloodstains taken from a population of interest where the 3D independent data quality assessment of a spatter bloodstain is 5 centimetres or less is provided in Table 9-6.

<b>Measure</b>	<b>X (cm)</b>	<b>Y (cm)</b>	<b>Zh (cm)</b>	<b>Zl (cm)</b>
Bootstrap 2.5%	45.71	109.75	26.43	23.12
Bootstrap 97.5%	50.81	112.41	29.44	26.24
Bootstrap Interval	5.10	2.66	3.02	3.12
Lower Bootstrap	-2.38	-1.44	-1.32	-1.61
Upper Bootstrap	2.72	1.22	1.70	1.50

*Table 9-6 - The confidence interval data for the mean statistic estimation recorded by the VB macro and the derived bootstrap interval information produced from the analysis of the 0-5 cm 3D data quality sample of pattern ES-A (reported to 2 decimal places).*

### **9.5.1.2 Multivariate Analysis**

While the univariate analysis of the marginal distributions of the trajectory intersection data set can provide a considerable amount of information on the structure of the distribution of the data set, each of the four trajectory intersection variables are essentially analysed in isolation. No consideration is given by this analysis to how these four variables, which describe different aspects of the same item (a trajectory intersection location), may be associated. To provide some insight into the relationships that exist between the four locative variables of the trajectory intersection data a series of multivariate statistical techniques are either made available by, or conducted through the analytical site of impact estimation macro.

One of the more straightforward ways of investigating the association of any two variables within a multivariate distribution is graphically, in the form of a scatter plot (Krzanowski, 2000). The relationships between higher dimensional data, such as the four locative variables of the trajectory intersection data, can also be investigated through the presentation of multiple scatter plots (Johnson and Wichern, 2002; NIST/SEMATECH, 2005). As the VB macro records and reports the location of each trajectory intersection established, this detailed site of impact estimate data can be visualised, analysed and compared using such conventional

graphical techniques, as illustrated in Figure 9-7, Figure 9-8, Figure 9-9, and Figure 9-10.

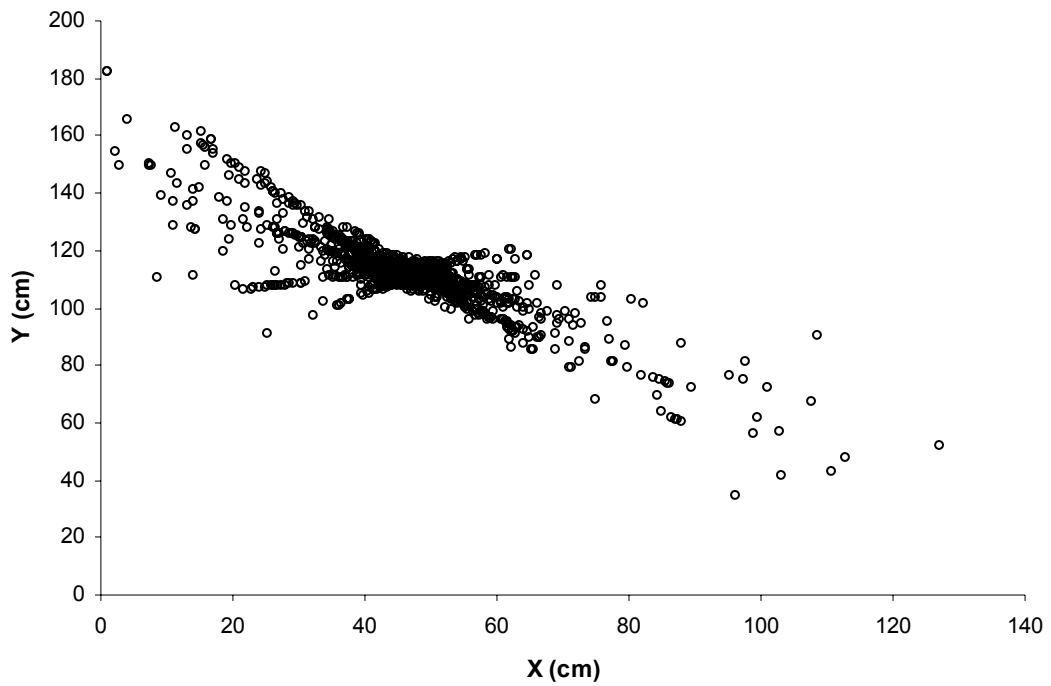


Figure 9-7 - A scatter plot of the  $p_x$  and  $p_y$  trajectory intersection data generated during the analysis of the 0-5 cm 3D data quality sample of pattern ES-A in the horizontal xy plane.

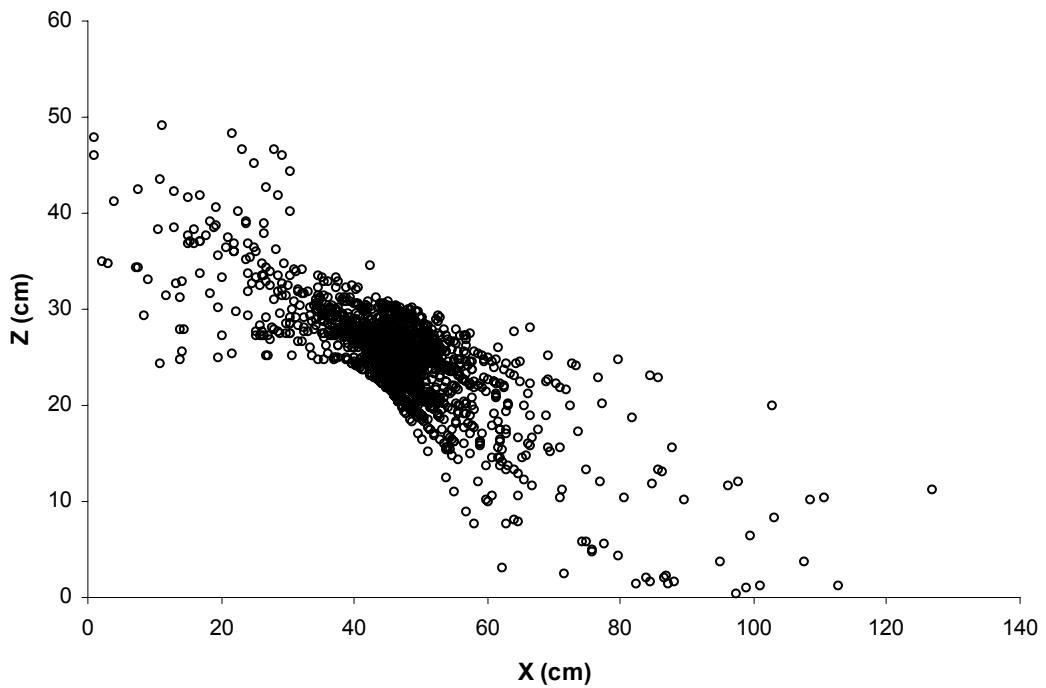


Figure 9-8 - A scatter plot of the  $p_x$  and  $p_z$  trajectory intersection data generated during the analysis of the 0-5 cm 3D data quality sample of pattern ES-A in the horizontal xz plane.

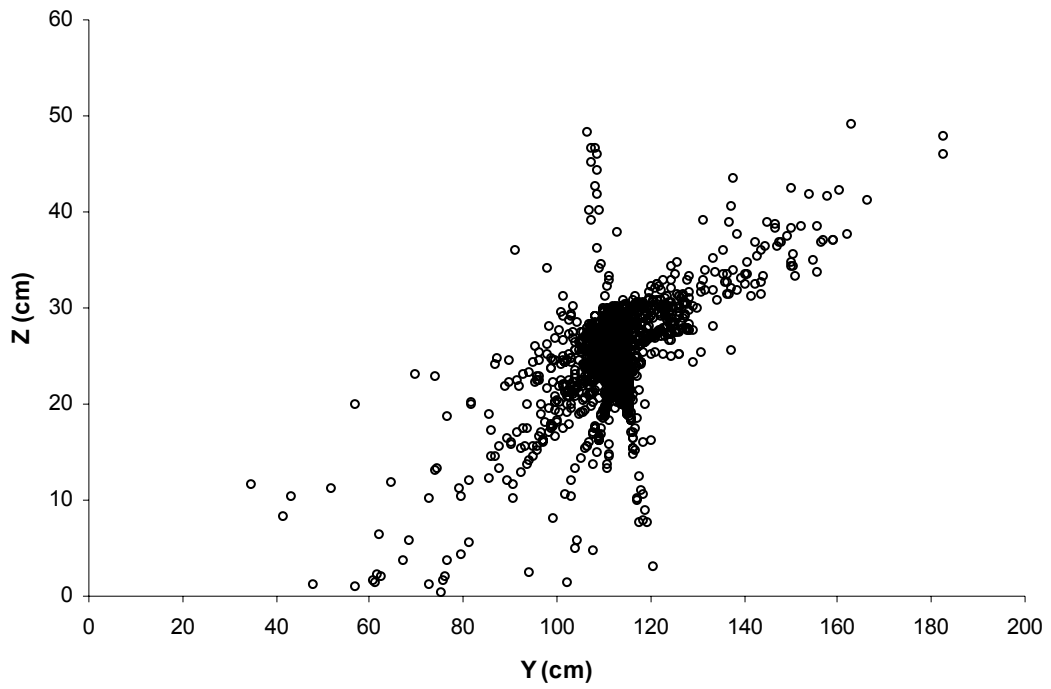


Figure 9-9 - A scatter plot of the  $p_y$  and  $p_{z1}$  trajectory intersection data generated during the analysis of the 0-5 cm 3D data quality sample of pattern ES-A in the horizontal yz plane.

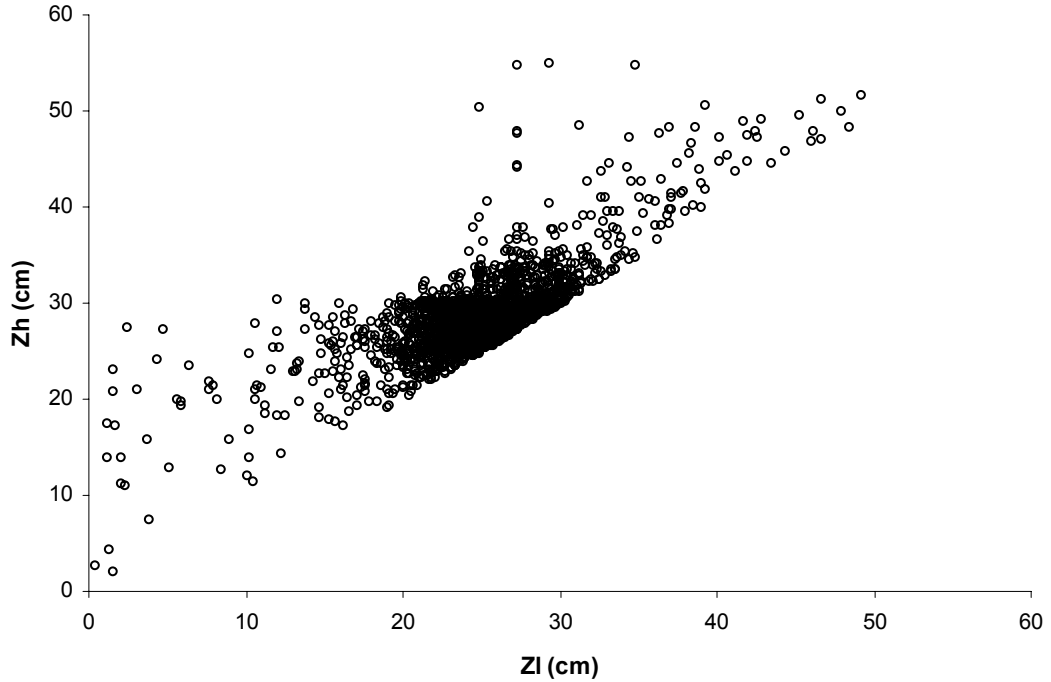


Figure 9-10 - A scatter plot of the  $p_{z1}$  and  $p_{zh}$  trajectory intersection data generated during the analysis of the 0-5 cm 3D data quality sample of pattern ES-A.

		X (cm)					Marginal Y
		35-39.9	40-44.9	45-49.9	50-54.9	55-59.9	
Y (cm)	95-99.9	0	0	0	1	25	26
	100-104.9	7	0	1	21	23	52
	105-109.9	2	77	166	125	25	395
	110-114.9	28	334	562	85	8	1017
	115-119.9	43	57	69	21	6	196
	120-124.9	39	21	0	0	0	60
	125-129.9	11	0	0	0	0	11
Marginal X		130	489	798	253	87	

Table 9-7 - An example of a small section of the horizontal 2D joint distribution count of the trajectory intersection data generated during the analysis of the 0-5 cm 3D data quality sample of pattern ES-A.

To provide an assessment of the aggregation of the individual trajectory intersections within the horizontal plane of analysis, the plane that can be considered to exhibit the least amount of straight-line trajectory bias in the construction of a site of impact estimate, a joint distribution count is also constructed by the VB macro through the 'joint2' function within the 'Dens' code module. The 'joint2' function utilises the  $p_x$  and  $p_y$  trajectory intersection variables to construct a joint distribution count of the number of trajectory intersections within adjacent 5 by 5 cm square class intervals across the extent of the predefined investigational environment, as exemplified in Table 9-7.

In addition to the basic joint distribution count data, the 'joint2' function also identifies the modal class interval(s) within the distribution, the range that the non-zero class intervals cover within the investigative environment, and calculates three mean counts to provide measures of the mean class count across the entire investigative environment, the mean class count within the range of the non-zero class intervals, and the mean class count of the non-zero class intervals only. The marginal distribution counts of the horizontal intersection data variables (see Section 9.5.1.1) can also be calculated by summing the counts of the rows and columns of this joint distribution count data. As with the interpretation of the marginal distributions the horizontal distribution of the trajectory intersection data can be used to analyse the entire distribution of the data set, aid the appropriate interpretation of other statistical descriptions, and provide an approximation of the density of the trajectory intersections with the

horizontal plane of the investigative environment, as demonstrated in see Figure 9-11.

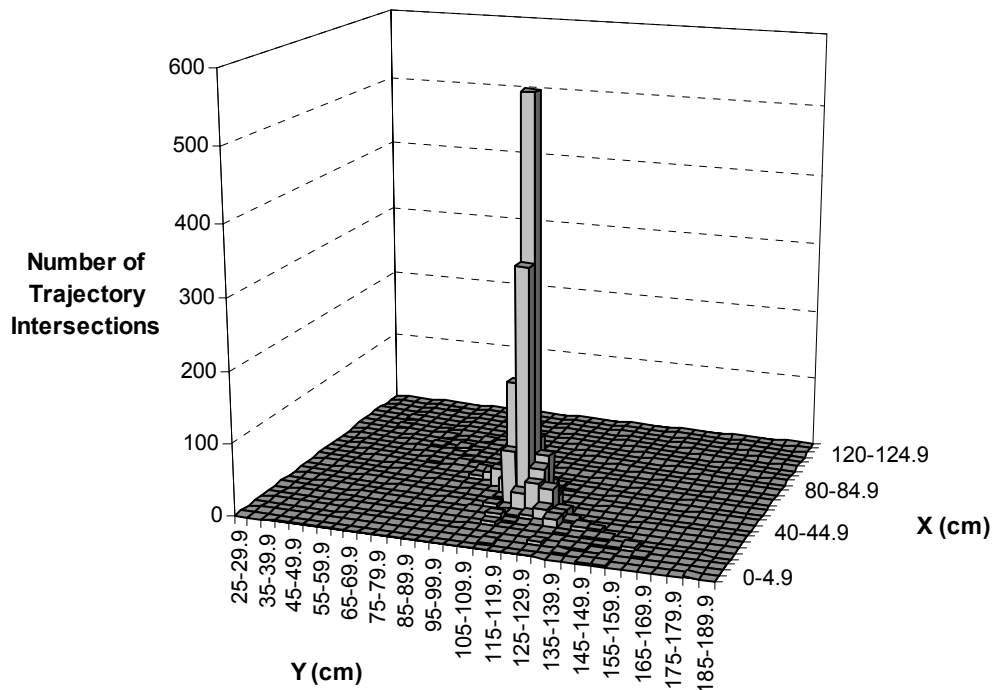


Figure 9-11 - The joint distribution count data of the number of trajectory intersections within five by five cm squares across the extent of the horizontal plane of the investigative environment generated during the analysis of the 0-5 cm 3D data quality sample of pattern ES-A.

Some caution in the interpretation of the horizontal joint distribution count, must be taken, however, because, despite providing considerable information for the evaluation of the results of a site of impact estimate, the representation of the distribution offered through this analysis is essentially a product of the analysis itself. The construction of a frequency distribution with a different size or alternative positioning of class intervals, for example, can indicate alternative interpretations of the same data set (Wand and Jones, 1995; Silverman, 1986). And while the 5 by 5 centimetre class intervals applied during the analysis of the horizontal trajectory intersection data by the VB macro provide a reasonable level of accuracy given the uncertainty present in site of impact estimation, and the class intervals are located to entirely cover the predefined investigative environment, any information on distribution modality, or the identification of regions of high intersection density can only accurately be interpreted as approximations. A range of 5 centimetres or one class interval around such features, while less accurate, is likely to be a more appropriate measure of the actual distribution. The same conservative interpretations are also necessary for

the marginal frequency distributions already discussed (see Section 9.5.1.1) and the 3D joint distribution counts described below.

The VB macro also performs a 3D joint distribution count to identify the 3D modality of the trajectory intersection data set. This 3D distribution count is conducted twice, once using the upper,  $\mathbf{p}_{zh}$  intersection data, and once using the lower  $\mathbf{p}_{zl}$  data. The modality and location of the 3D modes of the intersection data is calculated and reported by the 'tdcount' function within the 'Dens' code module of the VB macro as shown in Table 9-8.

Height Data	Modality	X	Y	Z	Count
Zh	1	10	23	6	413
Zl	1	10	23	5	346

Table 9-8 - The 3D modal data collected during the analysis of the 0-5 cm 3D data quality sample of pattern ES-A.

The number of modes identified, the number of the 5 cm interval within each axis in which each mode is identified in, and the number of individual trajectory intersections within this 25 cubic centimetre class interval are recorded by the VB macro. The data provided in Table 9-8, as a result, indicates that a single  $\mathbf{p}_{zh}$  mode was identified with a total of 413 intersections in the 3D region defined by  $45 \geq x < 50$  cm,  $110 \geq y < 115$  cm, and  $25 \geq z < 30$  cm. A single  $\mathbf{p}_{zl}$  mode was also identified at the same horizontal location containing 346 intersections, but with a height range of  $20 \geq z < 25$  cm.

As the mean of the four marginal distributions of the trajectory intersection data are established during the univariate analysis phase of the VB macro, the multivariate mean vector for the distribution is also definable, as shown in Formula 9-11.

$$\bar{\mathbf{x}} = \begin{bmatrix} \mathbf{p}_{\bar{x}} \\ \mathbf{p}_{\bar{y}} \\ \mathbf{p}_{\bar{z}l} \\ \mathbf{p}_{\bar{z}h} \end{bmatrix} = \begin{bmatrix} 46.72 \\ 112.01 \\ 24.92 \\ 28.65 \end{bmatrix}$$

Formula 9-11 - The definition of a multivariate mean vector, and the mean vector established during the analysis of the 0-5 cm 3D data quality sample of pattern ES-A.

The sample covariance, which provides a measure of the linear association between sets of two variables, is also calculated by the VB macro for the trajectory intersection data using Formula 9-12, where  $n$  is the size of the data set, and  $i$  and  $k$  are 1 to 4, representing the  $\mathbf{p}_x$ ,  $\mathbf{p}_y$ ,  $\mathbf{p}_{zl}$ , and  $\mathbf{p}_{zh}$  variables respectively. The covariance of the combinations of  $\mathbf{p}_x$  and  $\mathbf{p}_y$ ,  $\mathbf{p}_x$  and  $\mathbf{p}_{zl}$ ,  $\mathbf{p}_x$  and  $\mathbf{p}_{zh}$ ,  $\mathbf{p}_y$  and  $\mathbf{p}_{zl}$ , and  $\mathbf{p}_y$  and  $\mathbf{p}_{zh}$  are calculated by the programmed 'covar' function of the 'Matrix2' code module the of VB macro.

$$S_{ik} = \frac{1}{(n-1)} \sum_{j=1}^n (x_{ji} - \bar{x}_i)(x_{jk} - \bar{x}_k)$$

Formula 9-12 - The formula used to calculate the covariance of two associated variables.

The calculation of these covariances enables the generation of two variance-covariance matrices to describe the variation within, and linear association between the variables of the 3D intersection data sets, which represent the point-estimates of the trajectory intersection data set at both the  $\mathbf{p}_{zl}$  and  $\mathbf{p}_{zh}$  heights, as illustrated in Formula 9-13.

$$\mathbf{S}_{zl} = \begin{bmatrix} 115.39 & -94.39 & -41.16 \\ -94.39 & 108.62 & 33.11 \\ -41.16 & 33.11 & 24.58 \end{bmatrix} \quad \mathbf{S}_{zh} = \begin{bmatrix} 115.39 & -94.39 & -36.39 \\ -94.39 & 108.62 & 28.98 \\ -36.39 & 28.92 & 21.52 \end{bmatrix}$$

Formula 9-13 - The construction of a variance-covariance matrix, and the two matrices generated during the analysis of the 0-5 cm 3D data quality sample of pattern ES-A.

The three eigenvectors and three eigenvalues of the two variance-covariance matrices are subsequently resolved by the VB macro through the 'EigenVal' and 'EigenVec' functions of the 'Matrix2' code module of the VB macro using the standard matrix equations shown in Formula 9-14, Formula 9-15, and Formula 9-16, where  $i$  represents the zl and zh variance-covariance matrices in turn, and  $j = 1$  to 3.

$$|\mathbf{S}_i - \lambda \mathbf{I}| = 0$$

Formula 9-14 - The matrix formula defining the eigenvalues of a matrix.



$$\mathbf{S}_i \mathbf{x}_j = \lambda_j \mathbf{x}_j$$

Formula 9-15 - The matrix formula defining the eigenvectors of a matrix.

$$\mathbf{e}_j = \frac{\mathbf{x}_j}{\sqrt{\mathbf{x}_j' \mathbf{x}_j}}$$

Formula 9-16 - The matrix formula to convert an arbitrary eigenvector to its unit length.

Once established the three eigenvectors and corresponding eigenvalues of the two variance-covariance matrices respectively indicate the direction of the three orthogonal axes which maximise the variation, and the size of this variation within the two separated  $\mathbf{p}_{z1}$  and  $\mathbf{p}_{z2}$  estimate data sets. This data is used within the VB macro to construct an  $F$ -distribution multivariate mean confidence ellipsoid for the two 3D mean vectors, where the lengths,  $l$ , from the mean vector along the axes indicated by the three eigenvectors for each estimation are defined by Formula 9-17, where  $n$  is the number of intersections, and  $\alpha$  the level of confidence. This method provides a means of estimating the region of 3D space within which the mean of a population could be situated where the particular trajectory intersection data analysed can be considered to constitute a sample.

$$l_j = \pm \sqrt{\lambda_j} \sqrt{\frac{3(n-1)}{n(n-3)} F_{3,n-3}(\alpha)}$$

Formula 9-17 - The calculation of the lengths of axes of a multivariate confidence ellipsoid (after Johnson and Wichern, 2002).

A confidence level of 95% is calculated by the VB macro for the two height separated 3D estimate data sets, with the value of the  $F$ -distribution provided by a predefined statistical function within Excel®. As with the marginal  $t$ -interval mean confidences calculated for each trajectory intersection variable during the univariate analysis, the appropriate application of an  $F$ -distribution confidence ellipsoid is based on the assumption that the sample data is randomly selected from a normally distributed population, albeit in this case a more complex multivariate normal distribution (Krzanowski, 2000). As no attempt is made to verify this assumption during the data analysis process beyond the analysis of skewness and kurtosis of the marginal distributions, the construction of these confidence regions for the 3D trajectory intersection data, like their univariate counterparts require cautious interpretation.

<b>Eigenvector</b>	<b>X</b>	<b>Y</b>	<b>Z</b>	<b>95% Length (cm)</b>
1	-0.89	0.52	0.03	4.51
2	0.18	0.24	-0.9	0.82
3	0.43	0.82	0.11	2.16

<b>Volume (cm<sup>3</sup>)</b>	33.69
--------------------------------	-------

Table 9-9 - The eigenvector directions, 95% confidence lengths, and volume of the confidence ellipsoid generated for the  $p_{zi}$  trajectory intersection data generated during the analysis of a 10 spatter bloodstain sample selected from the 0-5 cm 3D data quality subpopulation of pattern ES-A.

### 9.5.2 Spatial Data Analysis

The multivariate analysis of the trajectory intersection data generated during the construction of a site of impact estimate is continued within the VB macro through the application of principles of Spatial Data Analysis (SDA) to the investigation of the estimate data sets. While conventional multivariate analysis can be used to investigate the relationships between any set of variables gathered from a collection of items, the application of SDA is concerned with the analysis of data that is spatially referenced in some way, with explicit consideration given to the possible importance of the spatial arrangement of the data, and the problems and potentials that are present when analysing data that is situated in a spatial context (Bailey and Gatrell, 1995; O’Sullivan and Unwin, 2003). The analysis of the spatial properties of these data sets can yield more meaningful results in terms of describing possible spatial relationships between the data and other spatial phenomena than the application of a-spatial analytical techniques, which typically ignore the possible spatial interaction of the data (Fotheringham et al, 2000; Bailey and Gatrell, 1995)

A key concept in the analysis of spatially referenced data through SDA is in the distinction of ‘pattern’ and ‘process’. The pattern, which can be defined as the observed spatial structure of the data set, is a result of some spatial process that operates across the space in which the data set is situated. The process, as a result, can be defined as a description of how a spatial pattern might be generated, with any particular observed pattern being a single ‘realisation’ of this underlying process (O’Sullivan and Unwin, 2003; Unwin, 1981; Bailey and Gatrell, 1996). The primary objective of SDA is in the description and/or explanation of

the underlying spatial process from the analysis of the observed spatial pattern (Bailey and Gatrell, 1995). One of critical features of this analysis, however, is that the underlying spatial process is typically considered to be stochastic, or random in nature, in the sense that the generation of the spatial pattern is subject to some degree of uncertainty (Diggle, 2003; Bailey and Gatrell, 1995; Fotheringham et al, 2000; O'Sullivan and Unwin, 2003). Even where the generation of a spatial pattern can be considered to be theoretically deterministic, approaching the observed pattern as a realisation of some stochastic process can provide a means of incorporating random processes, such as measurement error, introduced into the investigation of this spatial data within its subsequent analysis (Unwin, 1981).

Given the discussion of site of impact estimation uncertainty within this thesis (see Chapters 3 and 4), the trajectory intersection data generated in the construction of a single estimate can, under an SDA approach, be considered to be a realisation of a stochastic spatial process. Instead of approaching site of impact estimation as a deterministic reconstructive enterprise, the generation of a trajectory intersection data set, can be conceptualised as a stochastic estimation process, whereby the underlying deterministic relationship between the straight-line trajectory approximations of spatter bloodstains, the locations of their horizontal intersection, and the location of impact site of the spatter-producing event is blurred to an unknown extent by a number of intervening random processes. While the sources of uncertainty in the construction of a site of impact estimation, as previously discussed, can be considered to be numerous, and not necessarily easily quantifiable in terms of any specific single case, the application of SDA stochastic theory could provide a means of incorporating at least some of this uncertainty, or random error, into the analysis of an entire trajectory intersection data set and, as a result, the interpretation of a site of impact estimate.

### **9.5.3 Spatial Point Patterns**

The SDA of the trajectory intersection data is undertaken within the VB macro as a 2D spatial point pattern, with each point or observation within the pattern representing the location of the straight-line trajectory intersections in the horizontal plane of analysis, the plane that is typically attributed a greater degree of interpretative confidence in site of impact estimation. A spatial point pattern

(SPP) consists of a series of observations within a spatial study region, where each observation represents the existence of one event of the type that the particular investigation is interested in, and the important or often only variable available for analysis is the location of these observations (O'Sullivan and Unwin, 2003; Cressie, 1993). The observed SPP is a realisation of the underlying stochastic spatial process, and while a SPP can be considered to represent the simplest form of spatial data, this does not necessarily mean that these patterns are particularly simple to analyse (Gatrell, 1996; Bailey and Gatrell, 1995; O'Sullivan and Unwin, 2003).

The main objective of the analysis of a SPP is to describe and quantify the spatial distribution of the observations in terms of the degree of aggregation, regularity, or randomness that is displayed within the pattern (Allen and Unwin, 1981; Cressie, 1993; Bailey and Gatrell, 1995; Stoyan et al, 1987). Inferential assessments of the 'typical' or 'unexpected' nature of the spatial patterning in relation to specific statistical models of spatial processes can also be conducted, and can prove useful in determining the possible underlying process that produced the specific SPP (O'Sullivan and Unwin, 2003; Bailey and Gatrell, 1995; Fotheringham et al, 2000; Allen and Unwin, 1981).

In most practical investigations of SPP data the starting point for any analysis is the rejection of a null hypothesis of pattern randomness in favour of an alternative that asserts that some systematic patterning of the spatial data exists (Diggle, 2003; Gatrell et al, 1996; Unwin, 1981; Upton and Fingleton, 1985). The comparison of an empirical SPP realisation to an Independent Random Process (IRP), where any observation has an equal probability of being located in any position within the study area, and the positioning of any observation is independent of all other points, provides a convenient first approximation for three main reasons (Unwin, 1981; Diggle, 2003; O'Sullivan and Unwin, 2003; Stoyan et al, 1987):

- If a hypothesis of IRP is not rejected there is little value in analysing a SPP further.
- The rejection of IRP can provide a valid means of data exploration where the hypothesis is of intrinsic interest to the investigation of the SPP.
- The hypothesis of IRP can act as a dividing hypothesis to distinguish between patterns that are broadly classifiable as demonstrating regularity or aggregation within the SPP.

The typical SDA methods employed in the investigation of a SPP can be divided into two broad types (Gatrell et al, 1996):

- Distance-based methods, where information on the spacing between observations are used to analyse their spatial association and patterning.
- Area-based methods, which rely on the aggregated frequency distribution of observations within a study region to investigate the observed spatial patterning.

Both of these approaches to the investigation of the 2D spatial point patterns, which the horizontal trajectory intersection data set of an estimate can be considered to represent, are conducted through the analytical site of impact estimation macro. The concept of an IRP is used within this analysis to suggest which trajectory intersection points within the pattern could be considered to have been generated by a random process, and to indicate specific areas within the patterning of the horizontal trajectory intersection data where the aggregation of the observed data can be considered to be above that that might be expected of a theoretical random process.

#### **9.5.3.1 Distance-Based Methods**

The first procedure conducted by the analytical site of impact estimation macro is the analysis of the horizontal trajectory intersection SPP in an attempt to identify those intersection locations which could be considered to fall within or below a model of IRP, and as a result, not correspond to a model of spatial aggregation. Each trajectory intersection is analysed individually, and the number of other intersections within 15 concentric circular areas, with radii of 1 to 15 centimetres at one centimetre intervals, are counted. While larger search areas could also have been used effectively in the analysis of the trajectory intersection SPP, the one centimetre divisions, with a maximum of a 15 centimetre radius was considered to provide a reasonable level of analysis given the spatial accuracy, and reconstructive aims of site of impact estimation. The count data for each trajectory intersection location, which is weighted to counter any significant edge effects that might be present in the analysis, is subsequently compared to the number of intersections that would be expected to be found if the pattern was generated by under IRP conditions. The expected count within a circular region

of a study region is calculated using Formula 9-18, where  $n_e$  is the expected number of intersection points,  $d$  is the length of the radius of the circle,  $i$  is 1 to 15 and represents the 15 different radii lengths, and  $\lambda$  is the empirical mean intensity of the SPP.

$$n_{ei} = \pi d^2 \lambda$$

*Formula 9-18 – The number of expected intersection points within a circular area given the empirical intensity of the SPP.*

The mean intensity of an SPP is a basic property of the analysis of SPPs, which can be defined as the number of observations divided by the area of the study region, or the probability that a small area within the study region will receive an observation (O’Sullivan and Unwin, 2003). For the purposes of this analysis the study region is taken as the minimum horizontal rectangular area that encompasses the entire trajectory intersection data set. The definition of a study region with SDA can have considerable consequences for the analysis of an SPP, affecting the concepts of pattern randomness, dispersal and aggregation (Fotheringham et al, 2000; Diggle, 2003; Bailey and Gatrell, 1995; Lawson, 2001). Although any region within the predefined investigative environment used throughout this research project can conceivably be applied as a study region, the minimum area covered by the SPP is considered to provide the most intuitive, and probably most meaningful assessment of aggregation of the horizontal trajectory intersection data, despite the fact that the size of the study region, and as a result, any analysis based on this area, are likely to vary between trajectory intersection data sets.

As the theoretical IRP model implies that the intensity of an SPP does not vary throughout the study region, an excess in the number of observed intersections around any single trajectory intersection compared to the expected number of observations within the same area (which is rounded to the nearest whole number by the VB macro) can be considered to be indicative of a tendency towards spatial aggregation. Where this expected level is not met, the particular trajectory intersection can be considered not to exhibit spatial aggregation, beyond that possible under IRP conditions, within the study region. The VB macro compares the count data collect for each trajectory intersection, across each of the 15 areal resolutions, to the expected IRP counts. The trajectory intersections that exceed the expected level at the majority of resolutions are, as

a result, classified as exhibiting spatial aggregation and a Boolean variable used to store this information for each trajectory intersections is set to 'True'. Where the expected level is not exceeded the Boolean variable is set to 'False', and that particular trajectory intersection is not considered to exhibit a tendency towards spatial aggregation, and could potentially be considered to be more a product of the stochastic, as opposed to the deterministic elements of the underlying spatial site of impact estimation process.

While the discussion of the analysis of the trajectory intersection data set by the VB macro has thus far been presented as analysing a single total trajectory intersection data, the analytical site of impact estimation macro analyses three separate trajectory intersection data sets, where these exist, for each single estimate produced. The univariate and multivariate analyses already described, and the following spatial analyses, are conducted by the VB macro three times (except where explicitly mentioned) using:

- The total trajectory intersection data set (also referred to as the 'All' data set in the subsequent SDA discussion).
- The trajectory intersections that correspond to the approximation of a bracketing trajectory approach used by the VB macro (referred to as the opposite of 'Opp' data set in the subsequent SDA discussion).
- The trajectory intersections that correspond to the model of spatial aggregation applied within the VB macro (referred to as the thinned or 'Thin' data set).

The analysis of the three trajectory intersection data sets enables the construction of three separate estimates from a single spatter bloodstain sample according to the alternative approaches to the interpretation of straight-line trajectory intersections that these groupings represent. Firstly, the analysis of the total trajectory intersection data set provides an assessment of the full distribution of the constructed site of impact estimate data in which no *a priori* interpretation or reduction of the data is involved. The analysis of this data set provides an assessment of an entire estimate data set, which may be valid in terms of estimating the location of an impact site in its own right, but also provides a comparative base for the analysis of the two alternative reduced data sets. Secondly, the analysis of the opposite data set provides an approximation of the estimate results achievable through a bracketing trajectory approach, which is often applied in traditional stringing methodologies and in the

BackTrack<sup>®</sup>/Win automatic averaging function (see Section 4.7). This approach is typically applied in an attempt to reduce random errors, in the form of extreme values within a trajectory intersection estimate data set that can occur where trajectories with similar orientations are located in close proximity to one another (Carter and Podworny, 1991; Cater, 2001; Laber and Epstein, 2004). Thirdly, the thinned data set, developed as part of this research, is included in the analysis of the trajectory intersection data as an alternative to the bracketing approach in an attempt to consistently apply the concept of reducing random error within a trajectory intersection data set. While a bracketing approach may reduce the presence of extreme values within a trajectory intersection data set where trajectories that bracket an impact site can be established, such an approach cannot be used to evaluate impact spatter patterns, for example, that are observed to one side of the impact site only. The analysis of a thinned trajectory intersection data set, and its removal of trajectory intersections that do not correspond to the spatial aggregation model, however, can be applied consistently to any total trajectory intersection data set, regardless of the circumstances of its creation.

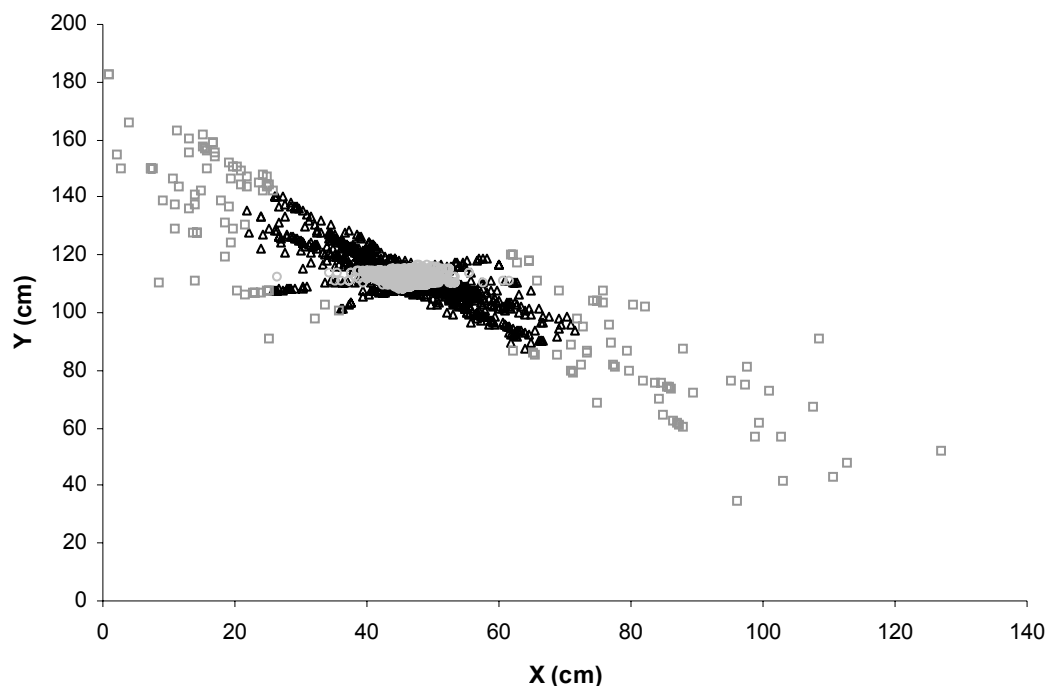


Figure 9-12 - The three separate sets of data analysed during the analysis of the 0-5 cm 3D data quality sample of pattern ES-A.

An example of the horizontal distribution of the three separate trajectory intersection data sets, the total data, the opposite data, and the thinned data,



from an analysis of pattern ES-A is shown in Figure 9-12. The dark grey squares represent the trajectory intersections that are included only in the total data set. The black triangles represent trajectory intersections that are included in both the total and thinned data sets, and the light grey circles represent trajectory intersections that are present in all three of the data sets.

Distance (cm)	NN G(w)	ONN G(w)	TNN G(w)	Distance (cm)	NN G(w)	ONN G(w)	TNN G(w)
0.0	0.0000	0.0000	0.0000	8.0	0.9961	1.0000	
0.5	0.8488	0.9783	0.8899	8.5	0.9971		
1.0	0.9305	0.9910	0.9676	9.0	0.9976		
1.5	0.9506	0.9974	0.9843	9.5	0.9985		
2.0	0.9657	0.9974	0.9922	10.0	0.9990		
2.5	0.9741	0.9974	0.9969	10.5	0.9990		
3.0	0.9804	0.9974	0.9990	11.0	0.9990		
3.5	0.9848	0.9987	0.9995	11.5	0.9990		
4.0	0.9878	0.9987	0.9995	12.0	0.9990		
4.5	0.9902	0.9987	0.9995	12.5	0.9990		
5.0	0.9922	0.9987	1.0000	13.0	0.9990		
5.5	0.9956	0.9987		13.5	0.9990		
6.0	0.9956	0.9987		14.0	0.9990		
6.5	0.9956	0.9987		14.5	0.9995		
7.0	0.9956	0.9987		15.0	1.0000		
7.5	0.9956	0.9987					

Table 9-10 - The ratio of nearest-neighbour distances for each of the three trajectory intersection data sets as during the analysis of the 0-5 cm 3D data quality sample of pattern ES-A.

Once established and analysed using the univariate and multivariate approaches employed within the VB macro, the three alternative trajectory intersection data sets for each site of impact estimate are analysed using additional SDA techniques. One method of investigating the degree of spatial dependence in a SPP is to examine the observed distribution of the smallest inter-event distances, or nearest neighbour distances, of the events within the SPP (Bailey and Gatrell, 1995). The empirical distribution function of the nearest neighbour distances for the total intersection pattern is calculated automatically by the VB macro using Formula 9-19, but as the nearest neighbour distances of each trajectory intersection for each of the three spatial distributions is recorded, the empirical distribution function of the opposite and thinned SPPs can also be constructed, as shown in Table 9-10.

$$\hat{G}(w) = n^{-1} \#(w_i \leq w)$$

*Formula 9-19 – The empirical distribution function of the nearest neighbour distances of a SPP (Diggle, 2003).*

Where the empirical distribution function of the nearest neighbour distances exhibits a steep climb in the early part of its range before levelling out, then the indication is a high degree of short-distance nearest neighbours suggesting a degree of event clustering. Where the opposite is true, and the distribution climbs steeply at the later part of its distance range, then some suggestion of event regularity can be inferred (Bailey and Gatrell, 1995; O’Sullivan and Unwin, 2003). The empirical distribution function can also be compared to the values of the  $G(w)$  function, under the conditions of an IRP, to provide some assessment of the empirical distribution in relation to that expected if the SPP were the result of an IRP. The expected values of the  $G(w)$  function for the total intersection data are calculated by the VB macro using Formula 9-20.

$$G_e(w_i) = 1 - e^{(-\lambda\pi w_i^2)}$$

*Formula 9-20 - The expected distribution function of the nearest neighbour distances of an IRP (O’Sullivan and Unwin, 2003; Diggle, 2003; Bailey and Gatrell, 1995).*

In addition to the empirical distribution function of the nearest neighbour distances the mean and variance of the nearest neighbour distance for each of the three spatial point patterns are calculated, to provide a means of comparison to a completely random spatial pattern. The ratio between the observed and expected mean nearest neighbour values,  $R$ , for any particular SPP can be used to both describe, and infer the type of patterning which might be evident. The nearest neighbour statistic,  $R$ , can vary between 0, where all the points are in a single location, and a theoretical maximum of 2.14, where a pattern is perfectly uniform, with a value of  $R = 1$  indicating that the observed SPP is likely to be random as the observed mean is exactly that expected. In effect, a value of  $0 \geq R < 1$  suggests a tendency towards clustering within the SPP, and a value of  $1 > R \leq 2.14$  is indicative of a SPP with a tendency towards uniformity (Unwin, 1981; Rogerson, 2001). The expected mean of the nearest neighbour distance of an IRP SPP within the same study region of each of the three horizontal trajectory intersection data sets is calculated using Formula 9-21 and Formula 9-22 respectively, where  $A$  and  $P$  are the area and perimeter of the study region.

$$\bar{x}_e = \frac{1}{2} \sqrt{\frac{A}{n}} + 0.051 \frac{P}{n} + 0.041 \frac{P}{n^{3/2}}$$

Formula 9-21 - The expected mean nearest neighbour distance under a hypothesis of IRP for a completely enumerated SPP within a predefined study region (Bailey and Gatrell, 1995; Diggle, 2003; Upton and Fingleton, 1985).

$$s_e^2 = 0.07 \frac{A}{n^2} + 0.037P \sqrt{\frac{A}{n^5}}$$

Formula 9-22 - The expected variance of nearest neighbour distances under a hypothesis of IRP for a completely enumerated SPP within a predefined study region (Bailey and Gatrell, 1995; Diggle, 2003; Upton and Fingleton, 1985).

The statistical significance of the deviation of each SPP from a null hypothesis of an IRP can subsequently be tested through a z-test, where:

$$z = \left( \frac{\bar{x}_o - \bar{x}_e}{\sqrt{s_e^2}} \right)$$

A value of z greater than 1.96 indicates that the SPP under investigation presents a significant degree of spatial uniformity, and where z is less than -1.96 the SPP presents a significant tendency towards clustering, and the null hypotheses of a random pattern can feasibly be rejected (Rogerson, 2001). An example of the results of a nearest neighbour analysis conducted through the analytical site of impact estimation macro is shown in Table 9-11.

<b>Intersection Data Set</b>	<b>NN Mean (cm)</b>	<b>Expected Mean (cm)</b>	<b>Expected Variance (cm<sup>2</sup>)</b>	<b>Mean-Expected Mean Ratio (cm)</b>	<b>Z</b>
All	0.34938	1.52307	0.00033	0.22939	-64.92545
Opp	0.09592	0.31735	0.00004	0.30224	-35.90134
Thin	0.20720	0.59254	0.00005	0.34968	-53.03972

Table 9-11 - Nearest Neighbour statistics calculated for the three trajectory intersection data generated during the analysis of the 0-5 cm 3D data quality sample of pattern ES-A (results reported to 5 decimal places).

One of the problems with the nearest neighbour distance analysis of a SPP is that only the distance to the nearest event in the pattern is analysed. Information on the larger scale of the SPP is, as a result, ignored during these analyses (Bailey

and Gatrell, 1995; Rogerson, 2001). To provide a larger scale exploratory analysis of inter-event dependency within the total intersection SPP, a  $K$  function approach is also applied to the investigation of this SPP through the analytical site of impact estimation macro. The application of this additional process is limited to the total intersection SPP as the areal count data necessary to conduct this analysis is already available following the trajectory intersection thinning process previously described, and, as a result, does not require any considerable additional processing. The formula used to calculate the empirical  $K$  function of the total SPP and the expected function under IRP conditions are shown in Formula 9-23, where  $i = 1$  to 15,  $n$  is the number of intersections, and  $w_j$  is the distance between intersection points  $j$  and  $k$  when  $j \neq k$ .

$$\hat{K}(d_i) = \frac{A}{n^2} \sum_{j=1}^n \sum_{k=1}^n \#(w_{jk} \leq d_i)$$

$$K_e(d_i) = \pi d_i^2$$

*Formula 9-23 - The construction of an empirical  $K$  function and the expected  $K$  function under IRP conditions (after Bailey and Gatrell, 1995).*

$$\hat{L}(d) = \sqrt{\frac{\hat{K}(d)}{\pi}} - d$$

*Formula 9-24 - The  $L$  function of a SPP (Fotherngton et al, 2000; O'Sullivan and Unwin, 2003; Bailey and Gatrell, 1995).*

Where the empirical  $K$  function falls below the expected level given a hypothesis of an IRP, some regularity in the SPP is suggested, and where the empirical  $K$  function exceeds the expected some degree of clustering within the SPP is indicated (Bailey and Gatrell, 1995; Fotheringham et al, 2000). A more practical comparison of an observed  $K$  function to that expected under IRP conditions, given the potentially large values of a  $K$  function, can be made by plotting alternative functions, such as the two shown in Formula 9-24 and Formula 9-25 (O'Sullivan and Unwin, 2003; Fotheringham et al, 2000). Both of these expression return a zero value if the empirical and expected functions are equal, with a positive value indicating a larger than expected aggregation of events, and a negative value suggesting fewer or a greater dispersal of events than expected at each distance analysed (Bailey and Gatrell, 1995; Fotheringham et al, 2000;

O'Sullivan and Unwin, 2003). These two additional distance-based analyses are calculated and recorded for the total intersection SPP through the VB macro.

$$\hat{l}(d) = \frac{1}{2} \log\left(\frac{\hat{K}(d)}{\pi}\right) - \log(d)$$

*Formula 9-25 - The I function of a SPP (Fotherngton et al, 2000; O'Sullivan and Unwin, 2003; Bailey and Gatrell, 1995).*

While the distance-based analyses conducted by the VB macro that have been described so far provide an indication of the degree of spatial aggregation of the SPPs analysed, they do not provide any indication of how the trajectory intersection data is distributed around a known impact site, where this location is available. To provide some means of assessing the spatial aggregation of trajectory intersections around a known impact site, the VB macro conducts an analysis similar to that outlined in the thinning process (see above). In this instance, however, the number of trajectory intersections within the 15 circular areas, with radii from between 1 and 15 centimetres at one centimetre intervals, are counted around the known location of the site of impact. The ratio of the total number of trajectory intersections within each of the three SPP data sets is subsequently calculated for each circular region, and compared to three theoretical distributions as shown in Table 9-12 and Figure 9-13.

<b>d (cm)</b>	<b>All</b>	<b>Opp</b>	<b>Thin</b>	<b>Constant Intensity</b>	<b>Equal Counts</b>	<b>Normal Distribution</b>
1	0.037	0.075	0.040	0.004	0.067	0.159
2	0.150	0.257	0.160	0.018	0.133	0.311
3	0.279	0.481	0.297	0.040	0.200	0.451
4	0.426	0.702	0.454	0.071	0.267	0.576
5	0.549	0.853	0.586	0.111	0.333	0.683
6	0.619	0.917	0.660	0.160	0.400	0.770
7	0.673	0.951	0.718	0.218	0.467	0.838
8	0.710	0.971	0.757	0.284	0.533	0.890
9	0.735	0.980	0.783	0.360	0.600	0.928
10	0.757	0.986	0.807	0.444	0.667	0.954
11	0.774	0.991	0.825	0.538	0.733	0.972
12	0.793	0.992	0.846	0.640	0.800	0.984
13	0.808	0.996	0.862	0.751	0.867	0.991
14	0.824	0.999	0.878	0.871	0.933	0.995
15	0.837	0.999	0.892	1.000	1.000	0.997

*Table 9-12 - The three empirical and three theoretical count ratios generated during the analysis of the 0-5 cm 3D data quality sample of pattern ES-A.*

The three theoretical distribution ratios are based on three separate models of spatial aggregation around the known location of a site of impact, where trajectory intersection data sets are either totally or predominantly distributed within the 15 centimetre maximum radii. The three theoretical models considered are:

- A constant intensity model, where the distribution ratio is dependent on the area of each circular region.
- A model of equal counts, where the distribution ratio set is divided equally between each of the 15 circular regions.
- A normal distribution model, where the distribution ratio corresponds to a normal distribution with a standard deviation radii of 5 centimetres.

The comparison of the empirical count ratios of the three SPP data sets to these theoretical models can be facilitated by plotting the difference in their ratios as shown in Figure 9-13, with positive results indicating where the count ratios of the empirical distributions exceed those expected by the theoretical distributions. Any interpretation of the results of these comparisons must be made cautiously, however, as only the distance of the trajectory intersection locations from the known impact site, and not their absolute locations, are considered. As a result, even though the three theoretical models are conceptually centred on the known impact site, a corresponding or excess ratio observed in any of the empirical distributions can only be interpreted as having an equal or greater ratio of trajectory intersections within a particular circular region that expected, but not necessarily centred on the known impact site.

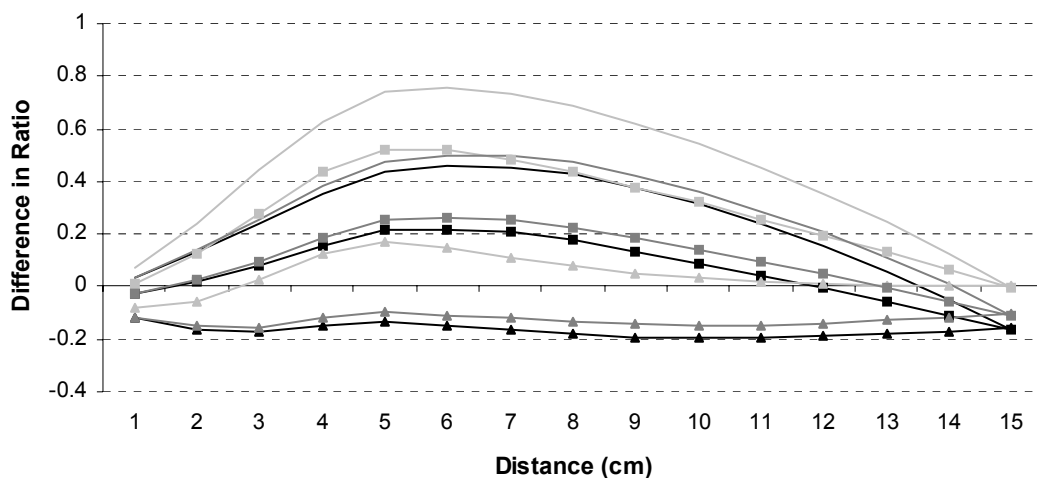


Figure 9-13 - The comparison of the distribution of trajectory intersection events around the location of the known impact site to the empirical distribution of the events.

A measure of the aggregation of each SPP in relation to absolute locations within the investigative environment is also constructed via the VB macro in the form of an empirical probability density function (EPDF). The EPDF of each SPP provides a continuous estimate of the density of trajectory intersection locations across the horizontal plane of analysis, and as a result in relation to the location of a known site of impact. The construction of an EPDF can be considered to be preferable to the joint distribution counts already discussed (see Section 9.5.1.2), as in multivariate cases, a histogram, and, as a result, its presentation of the data and any analysis derived from it, is defined by both the size and location of the class intervals, as well as their spatial orientation (Silverman, 1986; Lawson, 2001; Fotheringham et al, 2000; Wand and Jones, 1995).

The EPDF for each SPP is calculated by the VB macro using a bivariate normal distribution function, as shown in Formula 9-26, where  $x$  and  $y$  are the sampling locations,  $x_i$  and  $y_i$  are the location of each event within the SPP, and  $h_x$  and  $h_y$  are the smoothing parameters of the density estimate function in the  $x$ - and  $y$ -axes respectively.

$$\hat{F}(x, y) = \frac{1}{n} h_x h_y \sum \frac{1}{2} \pi e^{-\frac{1}{2} \left[ \left( \frac{x - x_i}{h_x} \right)^2 + \left( \frac{y - y_i}{h_y} \right)^2 \right]}$$

*Formula 9-26 - The EPDF used in the analysis of the SPP constructed by the VB macro (after Everitt et al, 2001).*

The horizontal plane of the investigative environment is sampled by the VB macro in a grid system at five centimetre sample intervals across the minimum area that encompasses the entire total data set SPP. The EPDF for each of the three trajectory intersection data sets is constructed across this range to provide a means of comparison between the relative densities of each alternative data set, and to correspond to the class interval sizes used in the construction of the joint distribution counts of the horizontal trajectory intersection data. A smoothing parameter of five centimetres for both axes is used by the VB macro in an attempt to provide an assessment of the scale of patterning that could prove useful in establishing an appropriate site of impact estimate. The selection of the smoothing parameters for the construction of an EPDF can be paramount to the successful analysis of a particular SPP, with larger smoothing parameters tending to highlight regional patterns, and smaller smoothing parameters emphasising

local patterning (Fotheringham et al., 2000). While the analysis of multiple resolutions of patterning, through the construction of different EPDF using different smoothing parameters could provide considerable information about the spatial patterning of a trajectory intersection data, the single smoothing parameter was chosen for this research to provide a preliminary investigation of the potential application of the generation and evaluation of an EPDF in the construction and interpretation of a site of impact estimate.

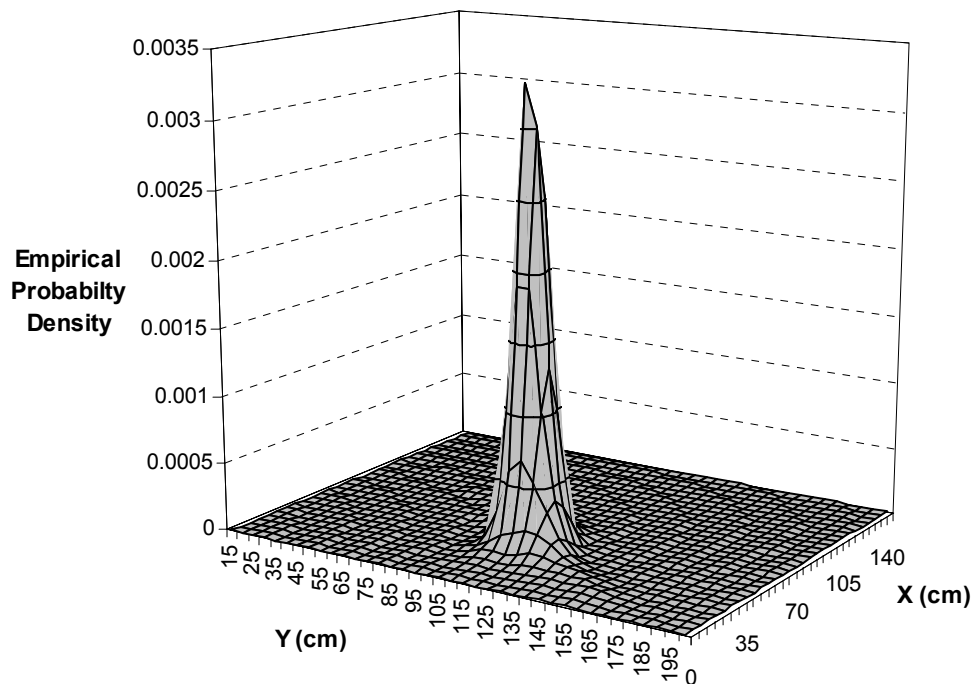


Figure 9-14 - An empirical probability density of the horizontal trajectory intersection data generated during the analysis of the 0-5 cm 3D data quality sample of pattern ES-A.

As an EPDF is a probability function, the volume under the entire surface can be reasonably expected to be equal or very close to 1 where no significant raising of the density surface at the edge of sampled area is evident. To provide a measure of the region of the EDPF that could represent an excess density in terms of a theoretical IRP, and as a result, could be considered to represent a region of spatial aggregation of the horizontal trajectory intersection data sets, an expected uniform density for the study region can be constructed using Formula 9-27, where  $x_h$  and  $x_l$  are the locations of the maximum and minimum sample points on the x-axis, and  $y_h$  and  $y_l$  are the locations of the maximum and minimum sample points on the y-axis that are necessary to cover the extent of the each of the three specific trajectory intersection SPP data sets.



$$d_{IRP} = \frac{1}{(x_h - x_l)(y_h - y_l)}$$

*Formula 9-27 - The theoretical uniform density of an IRP.*

While the theoretical IRP density level constructed for each specific SPP data set analysed may provide a reasonable approximation of the constant density expected, the interpretation of the results of this analysis should be approached conservatively in some cases. Where an SPP exhibits considerable aggregation within a small area, and contains no outlining or more widely distributed observations, for example, the value returned by Formula 9-27 can overestimate the theoretical density level of an IRP. This is primarily a result of the fact that the area used to calculate the IRP density level does not correspond with an area where the volume under the EPDF surface that is approximately equal to one. This problem could be addressed by continually extending the area under consideration until the volume under the EPDF surface of the particular SPP is approximately equal to 1, although this process is not attempted within the analytical site of impact estimate macro. Instead the arguably more intuitive basis for establishing the range of analysis, as described above, is used, with the minimum and maximum values of the trajectory intersection data sets in each horizontal axes enabling some degree of assessment of the extent of the volume under the EPDF surface that is encompassed within this area.

### **9.5.3.2 Area-Based Methods**

An alternative to a distance-based approach to the analysis of a SPP is to compare the distribution of the number of events situated within a number of sub-regions of equal area and size within the study region in which the SPP is situated. Given this aggregated version of the SPP data, a number of SDA methods often referred to as 'quadrat' methods can be applied to the investigation of this areal data (Diggle, 2003; Bailey and Gatrell, 1995). As the three horizontal trajectory intersection SPPs have already been effectively aggregated through the construction of the horizontal joint distribution counts (see Section 9.5.1.2), this data is re-used by the VB macro to provide the basis for the areal investigation of the spatial patterning of the trajectory intersection data sets.

The Index of Cluster Size (ICS) of the aggregated count data is calculated through the VB macro using Formula 9-28, where  $\bar{x}$  is the mean count, and  $s^2$  is the variance of the count data. Where the ICS is greater than zero, the suggestion is that the SPP exhibits a tendency to cluster. Where the ICS is less than zero some regularity in the SPP can be interpreted, and, where the ICS is close to zero, the suggestion is that the SPP corresponds approximately to a randomly generated pattern (Rogerson, 2001; O’Sullivan and Unwin, 2003).

$$ICS = \frac{s^2}{\bar{x}} - 1$$

*Formula 9-28 - Calculating the Index of Spatial Clustering of quadrat count data.*

The significance of the departure of quadrat count data, indicated by the ICS, from that expected under a null hypothesis of generation through an IRP can be assessed by comparing the chi-squared distribution with a  $X^2$  statistic calculated for the quadrat count data using Formula 9-29.

$$X^2 = \frac{(m-1)s^2}{\bar{x}}$$

*Formula 9-29 - The chi-square statistic for the evaluation of a SPP through the mean and variance of a quadrat analysis (after Diggle, 2003; O’Sullivan and Unwin, 2003; Rogerson, 2001).*

If the value returned by Formula 9-29 is greater than the chi-squared distribution at the appropriate degrees of freedom ( $n-1$ ), the null hypothesis of an IRP can be rejected in favour of the spatial relationship indicated by the ICS (O’Sullivan and Unwin, 2003; Diggle, 2003; Rogerson, 2001). An example of this quadrat-based analysis of the spatial patterning of the horizontal trajectory intersection data is illustrated in Table 9-13. The analysis of the aggregated quadrat data is conducted twice for each of the three spatial data sets. The first analysis is conducted over the range of quadrats that encompass each specific SPP, and the second analysis is conducted only on the quadrats whose count is greater than zero. These two different approaches to the analysis are implemented to provide an assessment of the clustering evident over the spatial area covered by each specific SPP, and the potential presence of any significant clustering within the quadrats in which the trajectory intersections are situated.

Measure	All Quadrat	Opp Quadrat	Thin Quadrat	All Non-Zero	Opp Non-Zero	Thin Non-Zero
ChiCalc	195681.07	4868.50	32583.95	27394.83	2278.69	12458.98
ChiLev0.01	901.27	41.64	171.57	157.80	26.22	81.07
ICS	242.08	210.67	247.73	229.21	188.89	229.72

Table 9-13 - An example of the chi-squared analysis of the mean and variance of the quadrat count data generated during the analysis of the 0-5 cm 3D data quality sample of pattern ES-A (results reported to 2 decimal places).

The final analysis of the trajectory intersection data sets conducted by the VB macro, in terms of the construction and evaluation of the site of impact estimate provides a measure of the probability of achieving a specific quadrat count given IRP conditions. While the procedure employed within the VB macro could be used to assess which quadrats within a total range can be considered to exceed a level expected given IRP conditions, the procedure is used here in an attempt to identify any non-zero quadrat counts which could be considered to exhibit spatial aggregation in relation to the other non-zero quadrats only. To this end an iterative process is used to identify the non-zero quadrat counts within each SPP data set that corresponds to an approximate probability level of 0.1, 0.05, 0.01 and 0.001 using Formula 9-30, where  $\bar{c}$  is the non-zero count mean, and  $c$  is the count level being analysed. An example of the quadrat count levels identified for each of the four probability levels and each of the three SPP data sets is illustrated in Table 9-14.

$$P(c) = \frac{\bar{c}^c e^{-\bar{c}}}{c!}$$

Formula 9-30 - The probability of attaining a specific quadrat count under the Poisson distribution (after O'Sullivan and Unwin, 2003).

Data	P=0.1	P=0.05	P=0.01	P=0.001
ALL	17	22	27	31
OPP	60	62	75	83
THIN	34	40	47	53

Table 9-14 - An example of the quadrat count probability levels for each of the three trajectory intersection data sets as generated during the analysis of the 0-5 cm 3D data quality sample of pattern ES-A.

As with the evaluation of the raw joint distribution count data, the interpretation of the spatial analysis of this data requires some caution, as the distribution of the count data analysed is likely to be dependent to a certain extent on the

structure of the quadrats used to define the counts (Bailey and Gatrell, 1995; Fotheringham et al., 2000; O'Sullivan and Unwin, 2003). The result of this dependence is that the aggregated data can be considered to contain a higher degree of uncertainty than the original SPP data, and any significant patterning that may be observed during its analysis could be an artefact of the aggregation process rather than a reflection of the structure of the SPP (Fotheringham et al., 2000; Unwin, 1981). The generation, visualisation and analysis of quadrat count data, however, can provide a reasonable global approximation of the sub-region variation of SPP intensity across a study region, and the comparison of analytical results with complementary distance-based methods can guard against the incorrect interpretation of patterning (Bailey and Gatrell, 1995; Fotheringham et al., 2000). An alternative approach, similar to that proposed for the construction and interpretation of the EPDF, is to provide a multi-resolution quadrat analysis of the SPP data to investigate alternative scales of patterning within the data. While such an approach could reveal additional information on the structure of the an trajectory intersection SPP that could prove useful in the interpretation of specific site of impact estimates, the single resolution analysis of a 5 by 5 centimetre quadrat size conducted by the VB macro is considered to provide a reasonable scale of analysis given the aims of this research, and the potential uncertainty in the construction of a site of impact estimate.

## **9.6 Single and Multiple Sample Specific Analyses and Data Recording**

While the construction and analysis of a single estimate is conducted by the VB macro using essentially the same analytical procedure, regardless of whether a single or multiple sample estimate is being generated, a number of specific analyses are conducted for each of these two alternative approaches to the investigation of a site of impact estimation. This section will outline the specific analyses conducted on the single and multiple sample site of impact estimate data, and outline the format in which the analytical site of impact estimation macro records the specific data of each estimate type.

### **9.6.1 Single Sample Site of Impact Estimation Data**

Following the statistical and spatial analysis of the site of impact estimate trajectory intersection data conducted by the VB macro, an assessment of the

dependent data quality of the straight-line trajectory approximation of each spatter bloodstain is made. This assessment of dependent data quality is constructed in direct contrast to the independent data quality assessment conducted for each spatter bloodstain during the bloodstain data pre-processing phase. While the independent quality assessment is based solely on how close a straight-line trajectory approximation corresponds to the location of a known impact site, the dependent quality assessment is based on the interaction of the trajectories within the construction of an estimate. To provide this dependent quality assessment each spatter bloodstain used in the construction of the site of impact estimate is analysed through the 'BSDist' subroutine within the 'Userform' code module of the VB macro, with an assessment made of how well each trajectory intersection established along their particular associated straight-line trajectory approximations corresponds to the known location of the impact site, where this is available. The distance of each trajectory intersection from the location of the known impact site is calculated in the x-, y- and z-axes, and the total straight-line horizontal and 3D distance between all of the intersection locations associated with a particular spatter bloodstain established. The five univariate quality distributions established for each spatter bloodstain are subsequently processed to provide a description of the dependent data quality of each bloodstain using the mean, variance, quartiles, and minimum and maximum of the distributions.

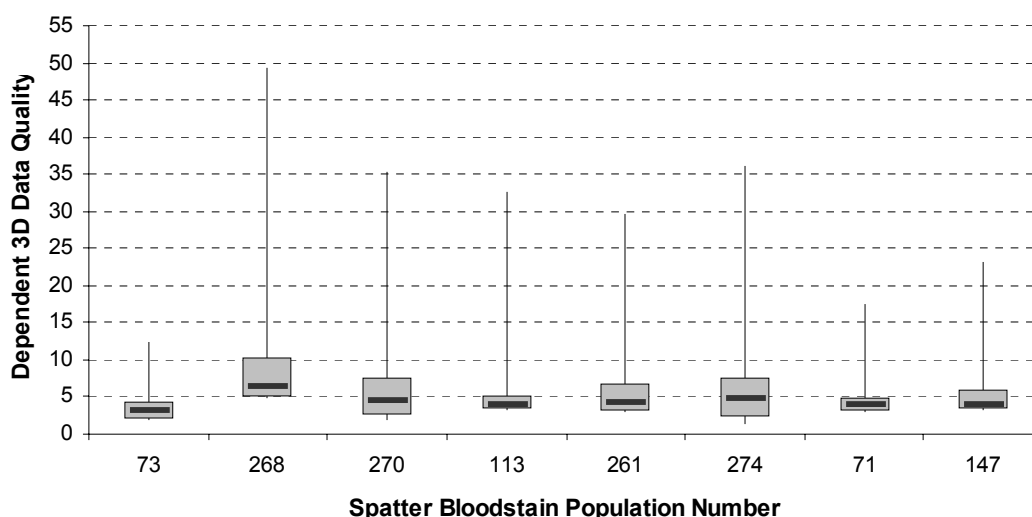


Figure 9-15 - An example of the five figure summary data for the dependent 3D data quality assessment of a sample of eight spatter bloodstains from the 66 spatter bloodstain analysed during the analysis of the 0-5 cm 3D data quality sample of pattern ES-A.

This process is repeated for each of the three alternative approaches to the interpretation of the trajectory intersection data set, providing a total, opposite and thinned assessment of dependent data quality for each spatter bloodstain analysed within a single site of impact estimation. An example of the dependent as opposed to independent data quality of a spatter bloodstain is illustrated in Figure 9-15, where each spatter bloodstain analysed was selected to have a 3D independent data quality of 5 centimetres or less.

Once conducted, the detailed numerical construction and analysis of a single sample site of impact estimate is recorded by the VB macro, where this option is selected, within a separate Excel<sup>®</sup> workbook in which the following worksheets are included:

- Event – The raw spatter bloodstain data from the particular impact spatter pattern analysed are recorded in this worksheet. The worksheet name is also given a designation of 'A', 'B', or 'C', to correspond to the three experimental impact spatter patterns generated and analysed within this research project.
- Popdata – This worksheets contains the pre-processed information on each spatter bloodstain that has the appropriate information recorded about it for the purposes of site of impact estimation within the specific impact spatter pattern analysed.
- Subpopdata - The pre-processed data of each spatter bloodstain within population of intersect which is selected from the total population using the sample criteria specified within the VB macro is recorded in this worksheet.
- Sampdata – This worksheet contains the pre-processed data of each of spatter bloodstain within the random sample selected from the population of intersection. The dependent quality assessment data generated for each spatter bloodstain used within the estimate is also included in this worksheet.
- Sd1 – The spatter bloodstain sample characterisation data, as discussed in Section 8.4, along with the results of the majority of the spatial analyses conducted on the trajectory intersection data sets are contained within this worksheet.
- Intndata – These worksheets contain the information recorded on each trajectory intersection established during the construction of a site of impact estimate. Where more than one worksheet is required to record

the total trajectory intersection data set additional sequentially numbered 'Intdata' worksheets are added to the workbook.

- Stat – This worksheet contains the results of the majority of the univariate and multivariate statistical analyses conducted by the VB macro on the trajectory intersection data of a site of impact estimate.
- Count – This worksheet records the joint distribution count data collected during the analysis of the horizontal trajectory intersection data.
- Density – This worksheet records the results of the EPDFs constructed for the trajectory intersection data.
- NullInt – The numbers of the spatter bloodstains whose straight-line trajectory intersection fail to produce an intersection, and the reason for this failure are recorded within this worksheet.

### **9.6.2 Multiple Sample Site of Impact Estimation Data**

The construction of a multiple sample site of impact estimate for a selected population of interest takes place within the 'Multisamp' subroutine of the 'Userform' code module of the VB macro. A total of four separate estimates based on 100 individual estimates using spatter bloodstain sample sizes of 10, 20, 50, and 100 can be constructed by the VB, depending on the number of spatter bloodstain available within the population(s) of interest. Once constructed, the information on the mean, variance, quartiles, minimum, maximum, skewness, kurtosis, and bootstrap confidence intervals of the  $p_x$ ,  $p_y$ ,  $p_{zh}$ , and  $p_{zl}$  variables, and the number of trajectory intersections established for each of the 100 individual estimates at each sample size is recorded by the VB macro, as illustrated in Figure 9-16.

The error of the mean and median of each variable in terms of its distance from the known impact site, where this is available, is also recorded for each individual estimate, along with the corresponding horizontal and 3D straight-line distances. This data is recorded for each of the three trajectory intersection distributions, the total, opposite, and thinned data sets, analysed by the VB macro during the construction of a single estimate. The distribution of each of these descriptive summaries of the 100 individual single estimates that constitute the multiple sample estimate for each sample size are subsequently analysed by the VB macro through a number of the univariate statistical methods previously described (see Section 9.5.1.1). This analysis provides a descriptive summary of the sampling

distribution of each of the univariate measures used to describe an individual site of impact estimate, enabling an assessment of the variation, or uncertainty, in the construction of a single sample estimate under specific sampling conditions, as illustrated for the mean data of a multiple sample estimate in Table 9-15.

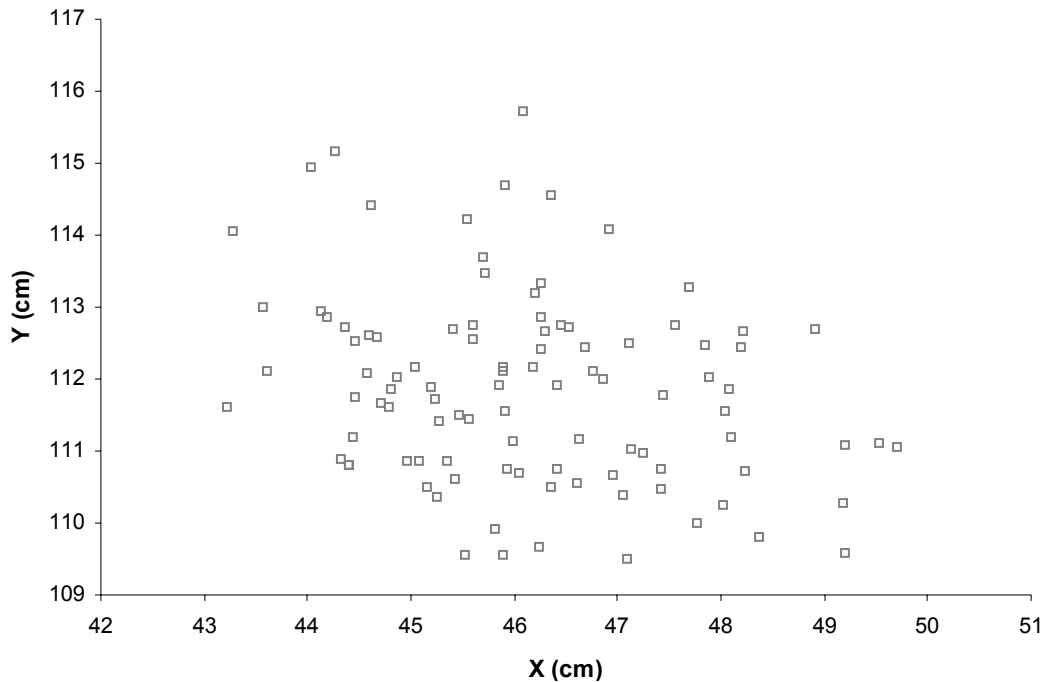


Figure 9-16 - The 100 mean horizontal estimates for a sample size of 10 spatter bloodstains generated during the analysis of the 0-5 cm 3D data quality sample of pattern ES-A.

<b>Measure</b>	<b>X Mean</b>	<b>Y Mean</b>	<b>Zh Mean</b>	<b>ZI Mean</b>
Mean (cm)	46.13	111.86	28.51	24.78
Variance (cm <sup>2</sup> )	2.17	1.77	1.17	1.21
Minimum (cm)	43.22	109.50	25.87	21.19
FIQ (cm)	45.05	110.83	27.77	24.03
Median (cm)	45.96	111.86	28.32	24.74
TIQ (cm)	47.11	112.69	29.18	25.59
Maximum (cm)	49.71	115.71	31.66	27.41
Lower Limit (cm)	41.94	108.03	25.67	21.68
Upper Limit (cm)	50.21	115.49	31.28	27.93
Lower Boot (cm)	45.86	111.62	28.31	24.57
Upper Boot (cm)	46.43	112.11	28.73	25.00
Skewness	0.35	0.51	0.43	-0.07
Kurtosis	-0.43	0.04	0.02	0.39
+/-T0.05 (cm)	0.34	0.30	0.25	0.25

Table 9-15 - The summary statistical data generated for the variables generated in each of the 100 individual estimates of a multiple sample estimate.



In addition to the univariate variables of each of the 100 single sample estimates, the VB macro also records the data on the 3D mode(s), covariances, and the two 3D confidence region constructed for each single estimate. The principles of multivariate central limit theory of the sampling distribution of the mean are also applied through the VB macro to produce 3D confidence regions for each multiple sample estimates constructed. The same process used to generate the single estimate 3D confidence regions is applied to the multivariate estimate data, although in this case the variables analysed are the 100 individual mean estimates constructed for the  $\mathbf{p}_x$ ,  $\mathbf{p}_y$ ,  $\mathbf{p}_{zh}$ , and  $\mathbf{p}_{zl}$  variables of each single site of impact estimate. A total of six confidence regions for each of sample size analysed are constructed by the VB macro based on the separate  $[\mathbf{p}_x \ \mathbf{p}_y \ \mathbf{p}_{zh}]$  and  $[\mathbf{p}_x \ \mathbf{p}_y \ \mathbf{p}_{zl}]$  point estimates constructed for each of the total, opposite and thinned trajectory intersection data sets. In contrast to the construction of the single 3D confidence region, which provides an assessment of the confidence in the sample mean estimate, the multiple sample versions uses Formula 9-31 to estimate the 3D region that encompasses 95 percent of the multivariate distribution of the mean estimates. The volumetric zone constructed can, as a result, be reasonably expected to encompass approximately 95 percent of single sample mean estimates given a particular sample size and sampling strategy.

$$l_j = \pm \sqrt{\lambda_j} \sqrt{\frac{3(n^2 - 1)}{n(n - 3)} F_{3, n-3}(\alpha)}$$

*Formula 9-31 - The calculation of the eigenvector lengths of a multivariate population confidence region (after Krzanowski, 2000).*

Once constructed and analysed, a multiple sample site of impact estimate is recorded by the VB macro, where this option is chosen, within a separate Excel® workbook. A multiple sample estimate workbook contains the same 'Event', 'Popdata', and 'Subpopdata' worksheets that are included within each single sample estimate workbook, as well as the following specific worksheets:

- Subpopstats – This worksheet records the pattern characterisation data of the population of interest, as described in Section 8.4.
- BSdens – This worksheet records three EPDFs constructed for the distribution of the spatter bloodstains within their specific target plane constructed during the multiple sample analysis of a site of impact estimate.

- M – The results of the 100 individual single estimates that make up a multiple estimate analysis and the statistical analysis of this multiple estimate data are recorded in these worksheets. A total of four 'M' worksheets may be present and are labelled to correspond to the four sample sizes of 10, 20, 50 and 100, employed during the construction of a multiple sample estimate.
- S – These worksheets record the population and subpopulation identity reference numbers of the spatter bloodstain selected for each of the 100 individual single sample estimates. As with the 'M' worksheets, a total of four 'S' worksheets can be present in a multiple sample workbook corresponding to which of the four sample sizes are used in the analysis.
- Sd – These worksheets contain the same sample characterisation and SDA data as the 'Sd1' worksheet in the single sample workbooks. In the multiple sample workbooks, however, a total of four 'Sd' workbooks can be present, depending on the sample sizes employed during the analysis, and each individual page contains the characterisation and SDA data on each of the 100 individual estimates constructed for each multiple estimate sample size.
- Z – The standardised scores of the each of the univariate variables of a multiple sample estimate are recorded by the VB macro in these worksheets. As with the previous three worksheets up to four 'Z' worksheets can be present, depending on the sample sizes examined during the analysis.

## **9.7 Conclusions**

Following on from the pre-processing of the raw spatter bloodstain data, described in the previous chapter of this thesis, the analytical site of impact estimate macro provides a range of innovative functionality for the construction and analysis of site of impact estimates. Firstly, the VB macro allows for specific sub-populations of interest to be selected from within the pre-processed spatter bloodstain data for further analysis. The selection of collections of spatter bloodstains, according to the data generated on them during pre-processing, provides a structured method for the comparison of the composition of alternative spatter bloodstain groupings, as well as the construction and analysis of site of impact estimates using samples selected randomly from within these structurally defined collections.

Also the analytical VB macro establishes the horizontal intersections of straight-line trajectory from any collection of spatter bloodstains using a mathematical vector-based procedure. This approach to the analysis of straight-line trajectory intersections provides a consistent methodology for assessing the intersection of straight-line trajectory intersections, regardless of the target surface upon which a spatter bloodstain is observed or the 3D direction described by the trajectory. Not only is the horizontal location of the trajectory intersection established by this method, but the vertical heights of the two intersecting trajectories are also calculated using the same vector methodology for each trajectory intersection established.

Thirdly, the VB macro, as a result of the vector-based approach to trajectory intersection, provides data on the entire distribution of trajectory intersection locations in both the horizontal and vertical planes of analysis for further investigation; an approach not typically associated with other computer-based site of impact estimation techniques. The VB macro also applies three approaches to the interpretation of trajectory intersection data sets within a single estimate. The total established trajectory intersection data set, the opposite trajectory intersection data set, or the intersections which correspond to the macro's approximation of a bracketing hypothesis, and the thinned trajectory intersection data set, the intersections within the total data set that correspond to a model of spatial aggregation, are all analysed, where available. The results generated using each of these alternative approaches can, as a result, be compared and evaluated with respect to each other and the location of a known impact site. The analytical VB macro also provides two separate analyses for each of the three possible trajectory intersection data sets, using the two alternative intersection heights established for each trajectory intersection.

Fourthly, the analytical VB macro conducts a series of detailed statistical analyses on each trajectory intersection data set to provide a comprehensive description of the distribution of straight-line trajectory intersections within the investigative environment for any estimate constructed. While the mathematical construction of a site of impact estimate using computer-based techniques tends to involve the application of statistical procedures to provide a description of the trajectory intersection data, these can be limited in terms of both application and interpretative value (see Sections 3.4.2 and 4.7). The statistical techniques employed within the VB macro provide a variety of complementary techniques for

the investigation of the central tendency of a distribution of trajectory intersections, and also the level and predominant shape of the dispersion of this distribution. Both univariate and multivariate techniques are utilised in the analysis of the trajectory intersection data sets of an estimate in an attempt to provide detailed information on the variation, or degree of uncertainty, present within the trajectory intersect data sets that form the basis of a site of impact estimate.

Fifthly, the VB macro applies concepts and analytical techniques of SDA to the investigation and evaluation of a site of impact estimate. The modelling of the horizontal distribution of the trajectory intersection data sets of an estimate as SPPs allows the explicit application of SDA concepts of spatial randomness and stochastic spatial processes to the investigation of an estimate, with explicit consideration given to estimate uncertainty. The application of SDA to the analysis of site of impact estimation data during this project, however, is only relatively preliminary in nature. If such concepts and analytical techniques do prove useful in the analysis of site of impact estimates, further development of a SDA toolbox could provide significant investigative detail to the analysis of a particular realisation of a site of impact estimation process. Alternative SDA approaches, such as the stochastic analysis of straight-line data, the application of specific aggregated spatial process models, the application of additional computer-intensive Monte Carlo simulation and confidence estimation techniques, the application of cluster analysis techniques, and the expansion of the 2D horizontal model to a multi-dimensional marked SPP model, for example, given further research, could ultimately provide alternative investigative methods for the analysis of site of impact estimation data and the appropriate interpretation of uncertainty within trajectory intersection data sets (O'Sullivan and Unwin, 2003; Diggle, 2003; Rogerson, 2001).

Finally, the analytical VB macro developed as part of the investigation into the construction of site of impact estimates and estimate uncertainty undertaken during this research project provides two alternative modes of analysis. A single sample estimate, which corresponds to the traditional construction of a site of impact estimate, albeit with additional investigative functionality, can be constructed and analysed to provide an evaluation of the likely location of a spatter-producing impact site, given a specific collection of spatter bloodstain analyses. An additional multiple sample estimate, which constructs and analyses a large number of single sample site of impact estimates, given a particular

sampling strategy, can also be easily generated. The development of the analytical VB macro, as a result, provides the innovative possibility to investigate the uncertainty or variation both within a single sample estimate, and between single sample estimates selected using an identical spatter bloodstain sampling criteria.

## **10 Three-Dimensional Estimate Visualisation**

### **10.1 Introduction**

This chapter will outline the development and implementation of the 3D interactive visualisation component of the analytical site of impact estimation application developed during this research project. The visualisation of the site of impact estimate data generated through the analytical VB macro will be discussed in three main sections. Firstly, the investigative and presentational aims and objectives of this visualisation will be discussed in relation to other 3D reconstructions and visualisations of forensic information and the admissibility of such evidence in legal contexts. Secondly, the development environment used to create the visualisation component of the analytical site of impact estimation application will be examined, and the general visualisation methodology employed described. Finally, the methods used to visualise the specific features of an estimate will be presented. The data visualisation options provided within the application, and the interactive functionality made available to facilitate the investigation, evaluation, and presentation of the detailed site of impact estimate data generated by the VB macro will also be addressed.

### **10.2 Forensic Data Visualisation**

In addition to the detailed numerical construction and analysis of a site of impact estimate, the analytical site of impact estimation application developed as part of this research into estimate uncertainty also provides an interactive 3D CG visualisation of the estimate data generated. This interactive 3D CG environment provides a method for displaying, investigating, evaluating and presenting the often large and complex numerical results of an estimate in a computer-generated approximation of the native 3D spatial context of the reconstructive data. As previously highlighted in the discussion of computer-based site of impact estimation techniques (see Section 3.4.2), the provision of such an interactive 3D CG approach to the investigation of site of impact estimate information may provide a more sophisticated, detailed and appropriate method for the generation, investigation, and presentation of site of impact estimates within 3D crime scene capture technologies, and also for CG reconstructions and presentations, which are becoming increasingly common within modern CSR and evidence presentation. Significant examples of this increasing use of 3D CG

environments in the investigation and presentation of forensic and CSR information within the UK include:

- The dynamic animation of road traffic accidents based on police scene survey and crash reconstruction data (Schofield et al., 2002).
- The reconstruction of changed environments from architectural plans and survey data (The Bloody Sunday Inquiry, 2005).
- The reconstruction and presentation of large-scale crime scenes that contain considerable amounts of physical evidence, or complex event timelines, as illustrated in Figure 10-1 (Schofield, 2005).

As modern forensic science and technology is often reliant upon computer-based data and data analysis to provide evidential information, there is a need to rigorously authenticate any CG forensic reconstructions produced and the methods through which these visualisations of the data are generated. This authentication is necessary to ensure that evidential standards are maintained and that the admissibility of the information generated by, and presented through these computer applications is viable (Noond et al., 2002).



Figure 10-1 – The dynamic reconstruction of a road traffic accident (left, courtesy of Damian Schofield), the virtual environment used in the Bloody Sunday Inquiry (centre, The Bloody Sunday Inquiry, 2005), and a crime scene reconstruction involving a complex timeline (right, courtesy of Damian Schofield, copyright West Midlands Police 2003).

When scientific evidence is submitted to a court or inquiry, part of the procedural requirements involves the checking of any methodology employed in the collection, analysis and presentation of this evidence, including any programs and reconstructive processes used. The type of software used and the method through which a reconstruction is generated can have significant implications for admissibility of this type of evidence (Goodwin, 2005). Within the field of accident reconstruction, where 3D CG reconstructions and animations have found varying degrees of utility in the investigation and presentation of complex

dynamic events, computer-based reconstruction technology has been functionally divided into a number of categories that include (Bohan and Yergin, 1999; Grimes, 1994):

- The illustration of a proposed event or sequence of events whose basis is supportable independently of the CG images, environment or animation.
- The creation of simple reconstructions or simulations, where the data and equations built into the application are readily accessible for examination and testing by others, in the same way that expert witnesses are allowed to examine the assumptions and methods of opposing experts.
- The generation of more complex reconstructions or simulations, where analyses cannot be practically conducted without a computer, and the software application is of a level of complexity that even persons knowledgeable in both programming and engineering cannot penetrate the simulation process without considerable investigation.

The main distinction between these three alternative forms of computer-generated evidence is whether the evidence can be considered to be demonstrative or substantive. Where the visualisation of evidence is used to support or demonstrate any evidence or expert opinion already available, the CG visualisation of this evidence is likely to be classifiable as demonstrative, and as such does not tend to be subject to such rigorous admissibility procedures as substantive evidence (Bevel and Gardner, 2002; Goodwin, 2005).

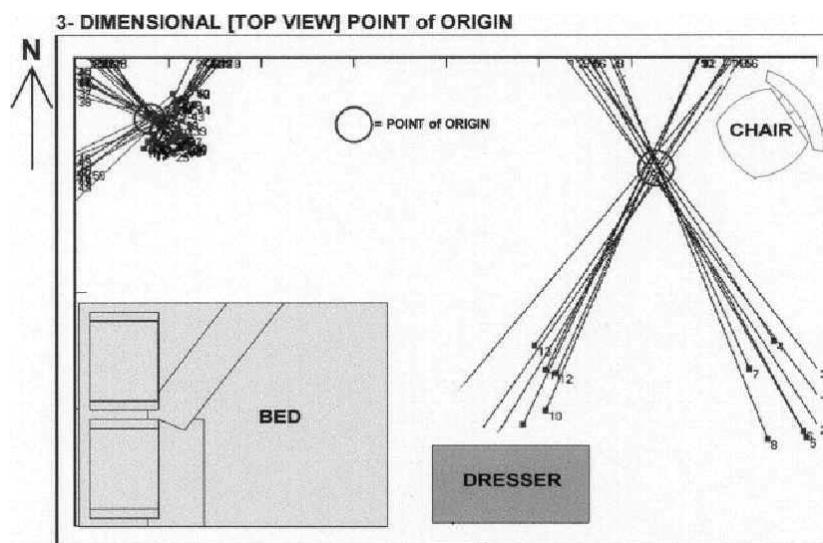


Figure 10-2 - An example of a CG visualisation of data derived through a site of impact analysis using BackTrack<sup>®</sup>/Win (Slemko, 2005).



Where the computer-generated evidence is probative, in the sense that it is evidence in its own right that can be used to prove an occurrence or fact, the CG evidence is typically considered to be substantive, and as such is subject to the same admissibility issues as other forms of expert evidence (Goodwin, 2005). A specific example of a substantive visualisation is provided by Colandero (1997 cited in Goodwin, 2005) where standard mechanical and physical principles are used to accurately depict the motions of physical entities within the scene being visualised. This scenario is conceptually reminiscent of processes involved in site of impact estimation (see Figure 10-2).

Bevel and Gardner (2002), however, take a somewhat more polarised view of the use of computer-generated evidence in terms of site of impact estimation and the presentation of its results. They postulate that while the use of applications such as BackTrack<sup>®</sup>/Win are undoubtedly substantive in nature, the inclusion of the results of an analysis conducted using this software within a CG visualisation of a scene is arguably demonstrative, because the visualisation does not tell the analyst anything new, but helps to express the analyst's expert opinion based on the information derived from the substantive application. With the movement of computer-based site of impact analysis into 3D CG investigational environments and 3D crime scene capture technologies, however, the convenient and significant distinction made between this analysis and visualisation could become somewhat blurred. Where the analysis and interpretation of any substantive reconstructive data becomes increasingly dependent on the visualisation of detailed and complex numerical information, such as in the contextual analysis of estimate uncertainty data, the presentation of CSR, BPA and site of impact estimate evidence is likely to have increasingly complex questions asked of it. This situation is further compounded by the need for BPA and its techniques of evidential interpretation, evaluation, and presentation to become firmly grounded within the realms of scientific expert evidence in legal contexts, as argued at the beginning of this thesis (see Chapter 1). While the analytical estimate construction and data visualisation methodology developed as part of this project are not intended to provide a definitive solution to solve such problems, they may provide one avenue of further investigation for the integration of the scientific investigation, interpretation and presentation of site of impact estimate data within BPA, CSR and the wider forensic and criminal investigation.

### 10.3 Visualisation Development

The 3D interactive data visualisation component of the analytical site of impact estimation application was developed using the multimedia development environment Macromedia® Director® (Macromedia, Inc., 2001). Macromedia® Director® is a commercial software package that enables the development of high-performance content-rich interactive applications for distribution as stand-alone executables or as web-based content over an Internet connection (Macromedia, Inc., 2005). This particular development package was selected for this project for a number of reasons. Firstly, Macromedia® Director® has an inbuilt 3D graphics functionality which supports the development and implementation of textured real-time interactive 3D environments. The 3D graphics media provided by Macromedia® Director® utilises optimised Intel 3D graphics software, which exploits the 3D graphics acceleration capabilities of modern video-card hardware through the industry standard graphics programming interfaces of both OpenGL®<sup>5</sup> and DirectX®<sup>6</sup> (Macromedia, Inc., 2005). Secondly, access to this versatile 3D graphics functionality is provided through Lingo, the proprietary programming language of Director®, and the software's extensible visual IDE, which is illustrated in Figure 10-3. The IDE of Macromedia® Director® provides a convenient method for the design and implementation of program structure and flow, as well as developing and implementing coded behaviours that control how the application responds to both user-interaction, and pre-defined program control elements. The access to powerful 3D graphics feature through the Lingo programming language also allows the dynamic creation and manipulation of 3D CG components and functions such as primitive geometries, viewpoint cameras, scene lighting, individual geometry vertices, geometry shader support and texture mapping, scene navigation, and geometry selection, which are arguably central to the development of an effective investigative interactive 3D CG environment. Thirdly, the ability to deliver Director® content through the Shockwave® ActiveX® Control developed by Macromedia® provides a high level of integration between the VB interface, which acts as an ActiveX® container, and the 3D graphics capabilities of Director® and its web content playback engine Shockwave® Player. Finally, the ability to publish the same 3D visualisation content generated within the analytical site of impact estimation application over the Internet using the free, easily accessible and widely used Shockwave® Player provides the potential,

---

<sup>5</sup> OpenGL is a trademark of Silicon Graphics, Inc., in the United States and/or other countries worldwide.

<sup>6</sup> DirectX is either a registered trademark or trademark of Microsoft Corporation in the United States and/or other countries.

with further development, to distribute site of impact estimate data and their associated 3D CG reconstructions rapidly and with minimal technological requirements or expertise. Such distributional functionality could eventually prove beneficial to the practice of site of impact estimation, with both an increase in the dissemination of, and collaboration on the analysis and interpretation of case specific site of impact estimate data. The Director® file, Shockwave® movie, and full program code are included on the DVD-ROMs which accompany this thesis.

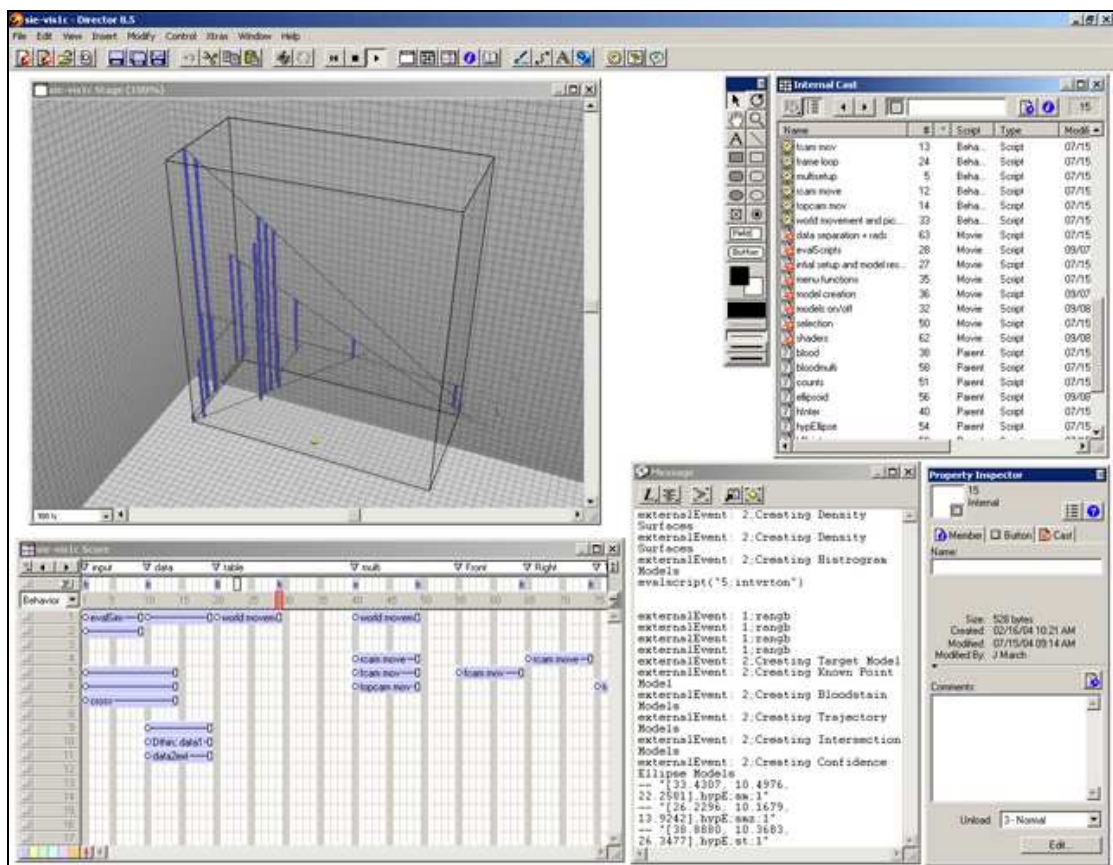


Figure 10-3 - The Macromedia® Director® 8.5 IDE.

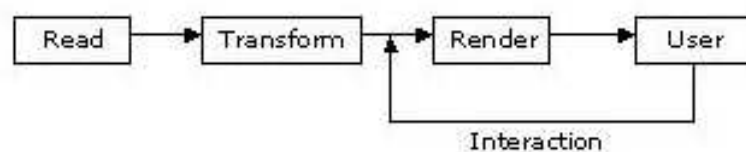


Figure 10-4 - The interactive visualisation methodology of the 3D component of the analytical site of impact estimation application.

The interactive visualisation methodology employed in the development and implementation of the 3D CG environment component of the analytical site of impact estimation application is illustrated in Figure 10-4. This process employs a modular approach common to many data visualisation applications, which involves four distinct stages (Walton, 2003; Ware, 2000):

- The data is *read* into the visualisation software from a source.
- The numerical data is processed or *transformed* into geometrical objects to be displayed within the 3D visualisation.
- The geometry generated is outputted or *rendered* to a display device.
- The user views this output, and *interacts* with the information presented to manipulate the visualisation for some specific investigative purpose.

The visualisation component of the analytical site of impact estimation application, which performs all four of these functions, was developed using the Macromedia® Director® IDE. The visualisation application created was published in the Shockwave® movie file format, which is played back within the VB macro interface using the Shockwave® ActiveX® Control to produce an integrated analysis and visualisation application for the construction and evaluation of site of impact estimation. The site of impact estimation data generated by the analytical site of impact estimation VB macro, whether this is newly created or read in from a pre-recorded estimate, is passed to, or read into the Shockwave® Movie via the Shockwave® ActiveX® Control in the form of a delimited string. This string is subsequently parsed using text manipulation functions intrinsic to Macromedia® Director® to separate and analyse the individual components of data required to produce a 3D visualisation of the estimate data. Once separated the data read into the visualisation Shockwave® movie is screened to assess the type of data being passed to the visualisation. Where this data is part of the interactive control of the visualisation, the information is passed to the relevant geometries within the 3D CG environment and various options made available through the VB macro for the visualisation of the estimate data are implemented and rendered. Where the data passed to the Shockwave® movie represents a new estimate to be visualised the relevant data groups are directed to specific 3D model creation procedures, where the raw estimate data is dynamically transformed into the 3D geometrical data necessary to produce an interactive 3D visualisation of a site of impact estimate constructed by the analytical site of impact estimation VB macro.

## **10.4 Constructing a Visualisation**

The discussion of the dynamic construction of a 3D site of impact estimate visualisation by the Shockwave® movie developed during as part of this research project is divided into three sections within the rest of this chapter. The first of these three sections will outline the general visualisation geometry and interactive features that all of the 3D interactive environments constructed share. The second and third sections will discuss the specific data transformations and rendering options made available for the visual inspection, evaluation and presentation of the distinct single sample estimate and multiple sample estimates generated using the VB macro.

### **10.4.1 General Visualisation Features**

The features of the site of impact estimation visualisation methodology employed within the Shockwave® movie developed for the analytical site of impact estimation macro that are shared between both the single sample and multiple sample estimate visualisations are described in this section. The four areas discussed include the generation of the investigative environment model and the selection and interaction with the 3D environments virtual cameras, the construction of known impact site geometry, and the visualisation of spatter bloodstain information.

#### **10.4.1.1 Environment and Camera Creation**

The 3D investigational environment, within which all other visualisation geometries are positioned, is dynamically created within the visualisation Shockwave® movie. While the size of the environment used through this research project has been pre-defined, the procedure used to create the 3D geometry of the environment was initially designed to generate site of impact estimate visualisations regardless of the size of the environment in which the construction of an estimate took place. To this end a single unit sized cube primitive is scaled to the correct size indicated by the environment data passed to the Shockwave® movie from the VB macro (in the case of this research a 300 x 300 x 300 centimetre cube). Only the back-faces of this geometry are rendered within the visualisation to provide the internal walls of the virtual bloodstained

scene, and each if the six surfaces of this environment are textured to provide a five square centimetre grid system with additional one centimetre divisions, as illustrated in Figure 10-5.

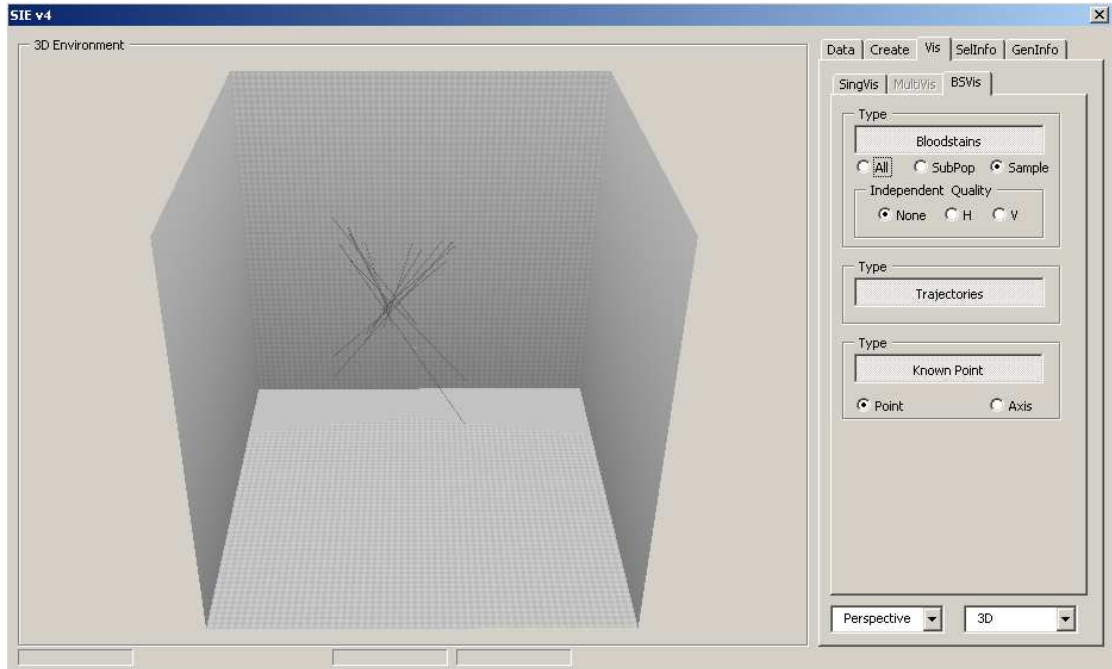


Figure 10-5 - The 3D environment within which an estimate is visualised and analysed, situated within the VB macro interface.

Four virtual cameras are created within the 3D environment to provide alternative viewpoints for the analysis of the site of impact estimate geometry. The virtual camera, and its set-up within a 3D CG environment are crucial to the visualisation process as it is the camera that provides the means by which the 3D numerical model of the environment stored within the application is translated into a 2D image on the computer monitor to be viewed by the application user. One of the four cameras generated for the purposes of the visualisation of the site of impact estimation data provides a perspective projection of the 3D geometry. It is through this camera that the true 3D visualisation and exploration of the site of impact estimate data takes place. The three additional cameras provide orthographic projections of the 3D geometry within the visualisation environment, which replicate the top, side, and front views more commonly associated with computer-based site of impact estimation applications. Each of these orthographic cameras provides a viewpoint for the accurate analysis of the 3D visualisation geometry relative to the grid-textured axis-aligned planes of the 3D investigative environment, as demonstrated in Figure 10-6. A degree of interaction with the 3D virtual site of impact estimation environment is achieved

through the user-controlled movement of each of these four cameras within the investigative environment. The cameras can be panned, rotated, and zoomed using the movements of a mouse and three function keys, as shown in Table 10-1, to provide a flexible user-led investigative experience through which the 3D geometrical representations of the site of impact estimation data can be analysed and evaluated.

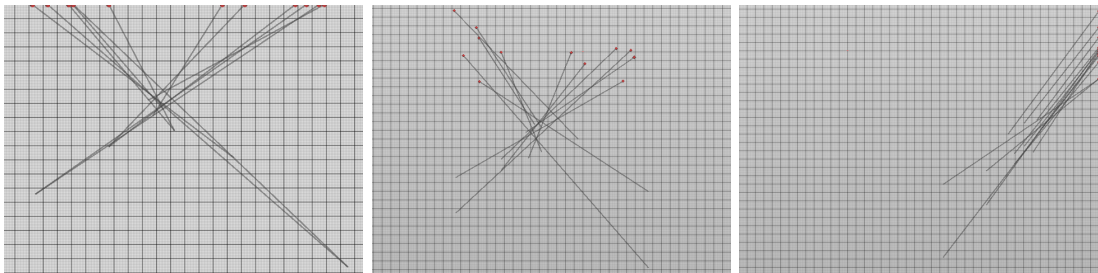


Figure 10-6 - The top (left), front (middle), and side (right) orthographic views provided within the 3D visualisation Shockwave® component of the analytical site of impact estimation application.

<b>Mouse and Function Key Combination</b>	<b>Perspective View</b>	<b>Top View</b>	<b>Front View</b>	<b>Side View</b>
Left Click	Rotate	Pan	Pan	Pan
Shift+Left Click	Pan up/down Pan left/right	Rotate	N/A	N/A
Control+Left Click	Zoom Rotate left/right	Zoom	Zoom	Zoom
Alt+Left Click	Pan left/right Pan forward/backwards	N/A	N/A	N/A

Table 10-1 - The camera navigation for the four cameras generated within the 3D virtual site of impact estimation environment.

#### **10.4.1.2 Geometry Selection and Numerical Data Presentation**

Interaction with the 3D virtual site of impact estimation environment is further achieved in the perspective view of the 3D CG environment through the inclusion of geometry selection functionality. By using the right mouse button to click on specific object geometries within the 3D environment, the application user can retrieve estimate data specific to any particular feature represent by a 3D model within the virtual investigative environment. Once selected, the geometry in question is highlight within the visualisation using a bright yellow geometry shader, as indicated in Figure 10-7.

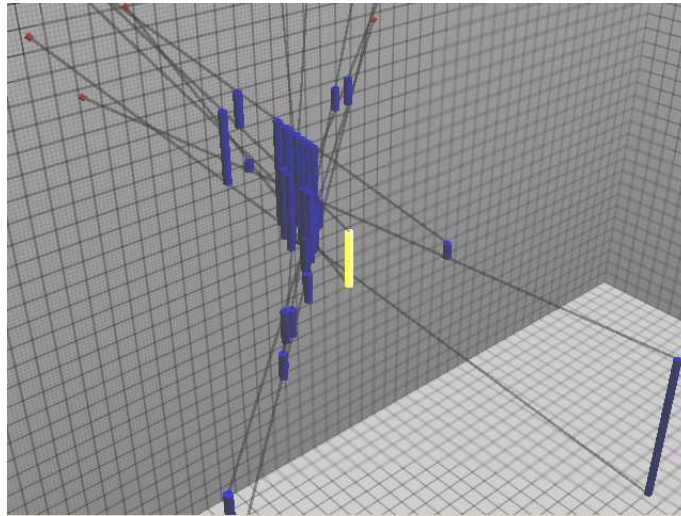


Figure 10-7 - An example of a selected intersection geometry highlighted in yellow.

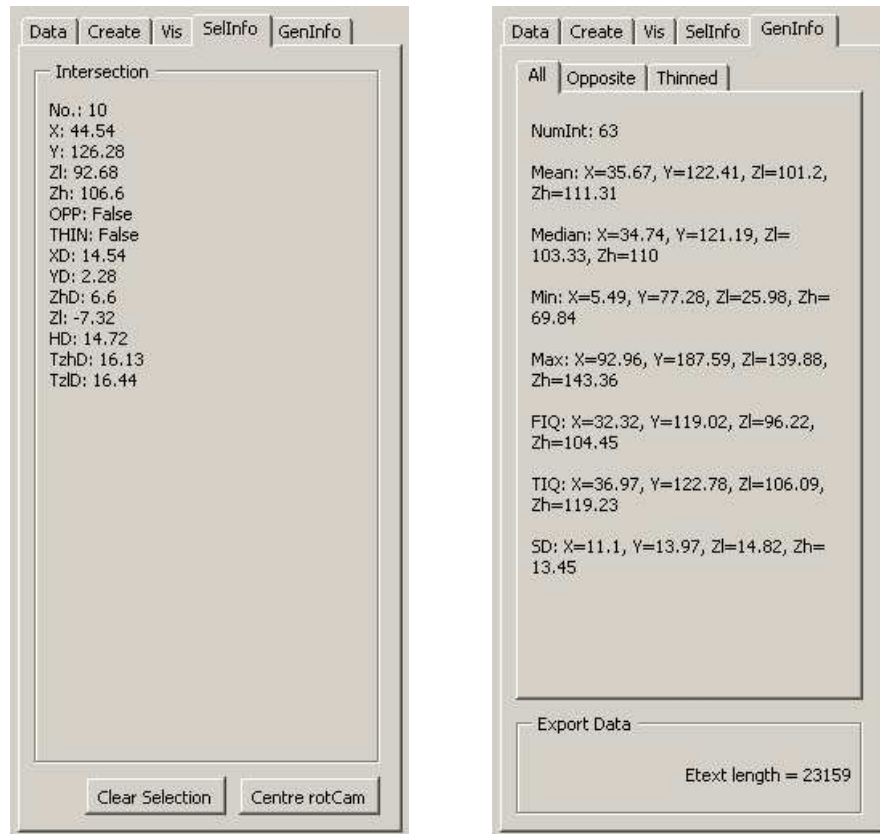


Figure 10-8 - The selection information (left) and general information (right) panels of the VB macro interface.

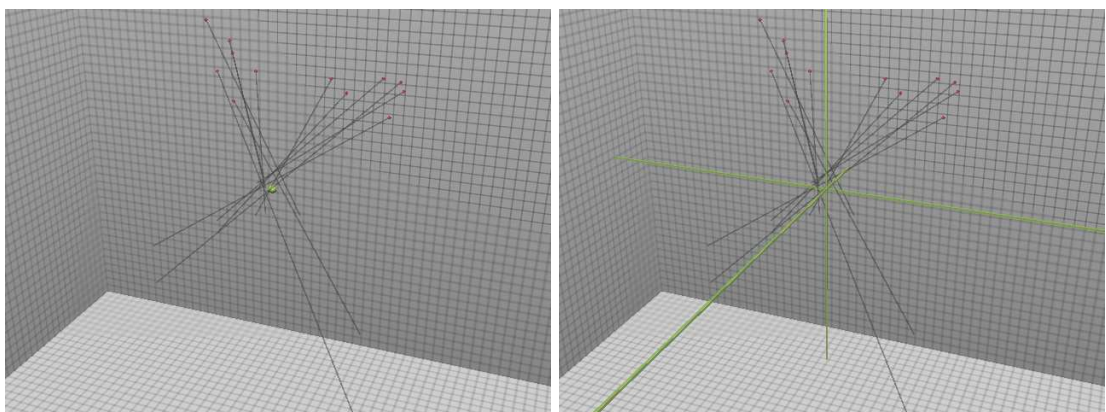
The Shockwave® movie, in a reciprocal procedure to that involved in the passing of data from the VB macro to the visualisation, passes a string-based indicator of the specific geometry selected to the VB macro. The VB macro, using the text



parsing capabilities inherent to VBA, interprets this indicator and displays the relevant estimate data within the 'SelInfo' panel of the application interface, as shown in Figure 10-8. As a result, the precise numerical basis for any particular estimate feature included within the 3D visualisation can be interactively displayed, and a degree of numerical-visualisation integration achieved. Additional interactive functionality is also available from within the 'SelInfo' panel of the VB macro interface, as the current object selection can be cleared from this panel, as well as the focus of the perspective camera given to the currently selected object, to facilitate the detailed visual analysis of this particular estimate feature. The general site of impact estimate data that corresponds to the current visualisation can also be viewed within the VB interface at any time during the investigation of the 3D CG environment through the 'GenInfo' tab. An example of the mean, median, range, and inter-quartile range of each of the three trajectory intersection data sets generated during a single sample estimate visualisation is illustrated in Figure 10-8.

#### **10.4.1.3 Known Site of Impact Visualisation**

The location of a known impact site, where this has been included for analysis, is modelled by the visualisation component of the analytical site of impact estimation application, to provide a means of visually evaluating and comparing any estimates constructed. The 3D positional data stored on this location within the VB macro is passed to the visualisation program, where it is processed to provide two alternative geometrical representations of the impact event location.



*Figure 10-9 - The visualisation of the point (left) and axes (right) representations of the location of a known impact site.*

A single sphere geometry is used to provide a point-based version of the known impact site, while three cuboidal geometries, which extend across the extent of the 3D environment, are generated to provide an axial representation of this location. This axial visualisation of the known impact site location data is included as it can provide a more effective positional indicator where considerable amounts of other visualisation geometry are being viewed simultaneously within the 3D virtual investigative environment. An example of these two alternative known impact site visualisations are illustrated in Figure 10-9.

#### **10.4.1.4 Spatter Bloodstain Visualisation**

The collections of spatter bloodstain analysed during the construction of a site of impact estimate are also visualised through the Shockwave® movie. Each spatter bloodstain is visualised as a hemisphere, which is positioned relative to its measured location within the 3D investigative environment, and rotated to correspond to the orientation and normal of the target surface plane upon which it was observed. Where a sample of spatter bloodstains are selected from a larger impact pattern population, three visualisation options are provided through the 'BSvis' interface panel. The total spatter bloodstain population, represented by the entire spatter bloodstain data set pre-processed by the VB macro can be viewed. Alternatively, the selected sub-population of interest, or sample drawn from this sub-population can be viewed. Where these latter two options are selected, the locations of the total spatter bloodstain population are still visualised, although the individual bloodstains not included in the selected groups are rendered as opaque grey hemispheres. The spatter bloodstains within each selected group are rendered as solid red hemispheres by default. An example of the visualisation of a total spatter bloodstain population and a sub-population of interest selected from it are shown in Figure 10-10.

The ability to view the independent data quality assessments made for each spatter bloodstain analysed by the VB macro are also included within the visualisation. Two alternative geometry shading schemes are employed in which the colour of each spatter bloodstain is indicative of its independent data quality, as illustrated in Figure 10-11. Both the horizontal and 3D independent data qualities associated with each spatter bloodstain are viewable within the 3D virtual environment. A very poor level of data quality, corresponding to an error of greater than 45 centimetres, is indicated with a blue geometry shader. As the

independent data quality improves the shader colour moves through blue, into green, and eventually through yellow into a red colour, which corresponds to a error level of smaller than 5 centimetre. The visualisation of this spatter bloodstain quality assessment information provides a mean of evaluating the potential accuracy of a collection of spatter bloodstains, as well as providing a visual spatial assessment of how the levels of data quality are distributed across the target surface plane within any particular spatter bloodstain collection.

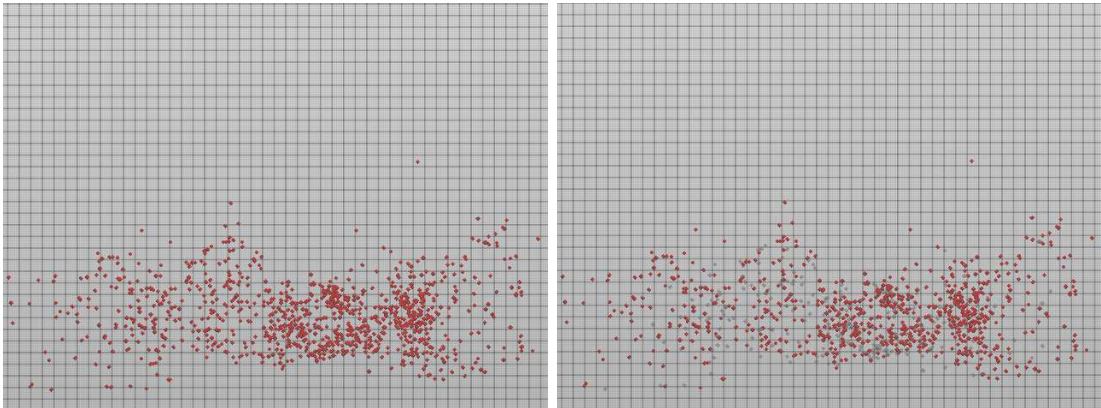


Figure 10-10 - The visualisation of a total spatter bloodstain population (left), and a selected sub-population of interest (right).

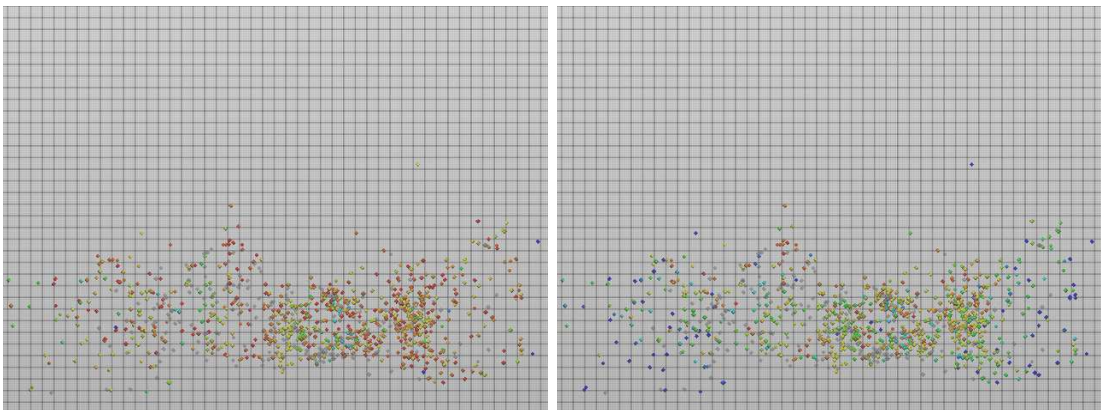


Figure 10-11 - The visualisation of the horizontal independent data quality (left) and 3D independent data quality (right) of a selected sub-population of interest.

#### **10.4.2 Single Sample Estimate Visualisation**

This section will discuss the visualisation methodology employed in the construction of a virtual 3D single sample site of impact estimate from the

estimate data generated by the analytical VB macro. The generation of the 3D geometry used to represent the fundamental estimate features of straight-line trajectory approximations, and the trajectory intersection data sets established during the construction of an estimate will be described. The methods through which the analyses conducted on the trajectory intersection data sets of an estimate are visualised will also be addressed. An example of a virtual 3D site of impact estimate situated within the VB macro interface is illustrated in Figure 10-12. The 'SingVis' panel of the VB macro interface shown in this example provides additional interactivity in the visualisation of a single sample estimate. The panel allows each feature of the single sample estimate visualisation to be shown or hidden within the 3D environment, as well as enabling a selection to be made between a number of the options provided for the visualisation of the estimate geometry, which are described below.

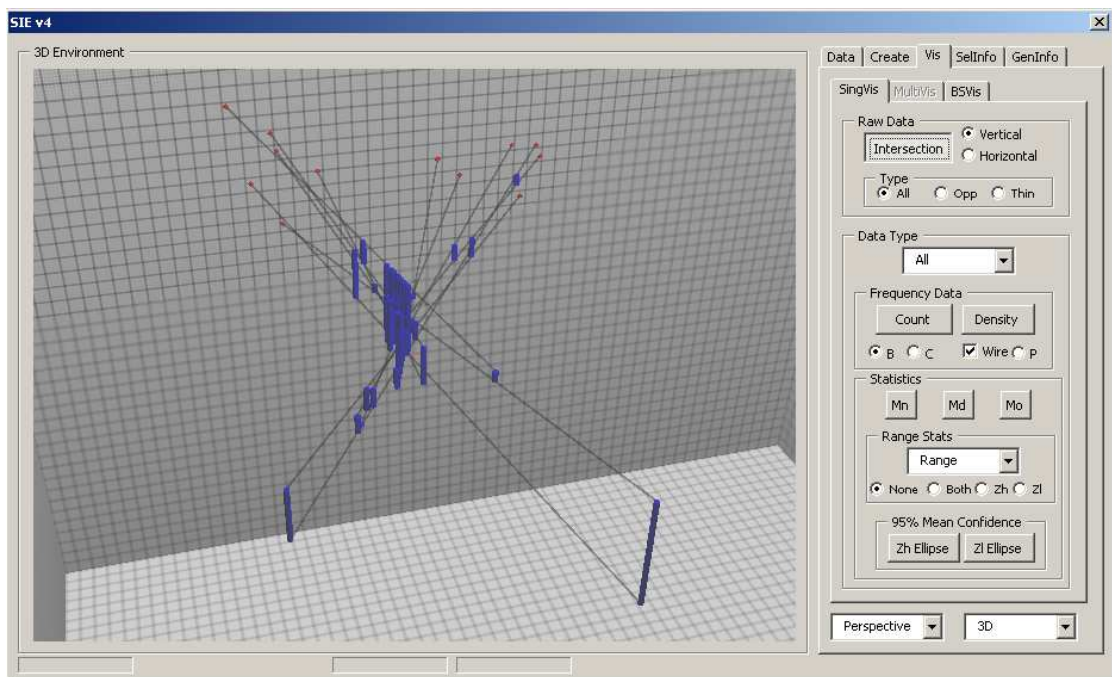
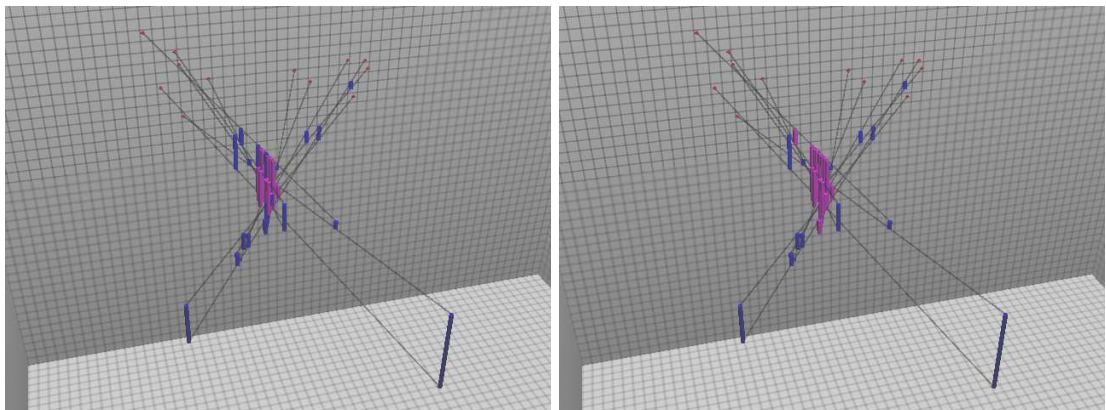


Figure 10-12 - An example of the visualisation of a collection of spatter bloodstains analysed, their associated straight-line trajectory approximations, and the intersections between this trajectories.

#### 10.4.2.1 Straight-Line Trajectory and Intersection Visualisation

The fundamental reconstructive information involved in a single site of impact estimate is transformed into viewable 3D geometry within the 3D investigation environment by the Shockwave® movie component of the analytical site of impact estimation application. The straight-line trajectory approximations generated for

each spatter bloodstain analysed are rendered within the 3D investigative environment as long thin cuboidal geometries, which are orientated within the environment relative to the horizontal and vertical angles calculated through the VB macro and positioned to correspond with the origin of each trajectory - its associated spatter bloodstain. The length of each trajectory is also set to correspond to the distance needed to reach the trajectory intersection established along its length that is furthest away from its origin. Each trajectory intersection established during the construction of single sample site of impact estimate is also included as geometry within the 3D investigation environment, where the number of intersections is less than 2000. Each trajectory intersection geometry is modelled as a cylinder, whose x- and y-axis location corresponds to the locations of a horizontal trajectory intersection, and the top and bottom of the cylinder correspond to the upper and lower heights of the two horizontally intersecting trajectories respectively. The trajectory intersection geometry visualised within the 3D environment of the Shockwave<sup>®</sup> movie are assigned a deep blue shader, although the intersections which correspond to either of the opposite or thinned approaches to the intersections of trajectory intersection data set can be highlight using a purple geometry shader, as illustrated in Figure 10-13.



*Figure 10-13 - The visualisation of trajectory intersections which correspond to the alternative bracketing (left) and thinned (right) approaches.*

The number of intersections visualised is restricted by the visualisation component of the site of impact estimation application to 2000, although the numerical data for the full distributions is still calculated and analysed. This is primarily to avoid an over complicated visualisation and examination of a site of impact estimate which can occur with such high numbers of geometrical features included within the 3D investigative environment, but also to avoid any excessive

slow down of the visualisation procedure which can occur when the application is attempting to interactively render significant numbers of geometry polygons.

#### 10.4.2.2 Visualisation of Intersection Data Set Analyses

The detailed statistical and spatial analyses conducted through the VB macro on the trajectory intersection data set of an estimate are visualised in the 3D CG investigative environment in a number of different ways. Firstly, the point-based summaries of the trajectory intersection data sets are modelled as cylinder geometries in the same manner as the trajectory intersection data outlined above (Section 10.4.2.1). The x- and y-axis locations of each cylinder indicate the horizontal location of the particular measure of central tendency, while the top and bottom of the cylinder indicate the central tendency of the upper and lower height estimate distribution respectively. The mean and median cylinder geometries of the total, opposite and thinned trajectory intersection data sets are visualised using blue, green and yellow geometry shaders respectively. An example of the visualisation of a mean site of impact estimate for a total trajectory intersection data set is illustrated in Figure 10-14.

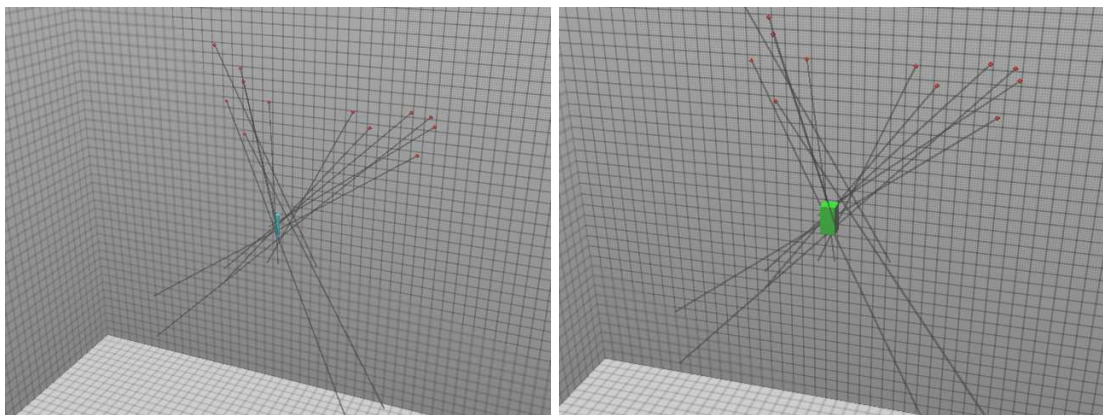


Figure 10-14 - The 3D visualisation of the mean (left) and mode (right) data generated for a trajectory intersection data.

Secondly, the 3D mode generated for both the upper and lower height estimate data for each of the three alternative trajectory intersection data sets are also visualised within the application. The data provided on each 3D mode is covered by the visualisation application into a cuboid geometry, which is scaled and positioned to cover the region within the 3D environment that corresponds with each mode established. The mode or modes of the upper intersection height data

is indicated with a green shader, while a blue geometry shader indicates the mode of the lower intersection height data. An example of the visualisation of the 3D mode of a site of impact estimate constructed by the analytical site of impact estimation application is shown in Figure 10-14.

Thirdly, the information provided on the dispersion of a trajectory intersection data set in form of the range, inter-quartile range, and standard deviation of the three separate distributions is also presented visually through the 3D CG visualisation component of the site of impact application. An example of the visualisation method employed in the presentation of this dispersion data is illustrated in Figure 10-15. The data provided on the minimum and maximum locations of these four measures of dispersion is used by the visualisation program to generate and locate cuboid geometry, which corresponds to the volumetric region created from the univariate dispersion of the trajectory intersection data sets with respect to the x- and y-axes, and the upper and lower height intersection estimates generated. Each of the four volumetric measures of dispersion can be viewed for each of the three alternative trajectory intersection data sets, which can also be viewed in terms of the dispersion of the upper or lower height estimate, or the maximum dispersion, if both heights are considered.

Fourthly, the multivariate mean confidence region and univariate mean bootstrap confidence intervals for the mean estimate of each trajectory intersection data set are visualised within the 3D investigative environment, as demonstrated in Figure 10-15. The bootstrap confidence interval for the mean of each site of impact estimate is processed and visualised using the same method employed for the generation of the 3D cuboid geometry used to represent the volumetric dispersion of each estimate intersection data set. The multivariate mean confidence data passed to the visualisation application is processed to transform a spherical primitive geometry with a single unit radius into its ellipsoidal geometry described by the eigenvectors and confidence dependent axial lengths calculated for each trajectory intersection distribution. The axis aligned sphere is scaled to correspond with the axial lengths of the confidence ellipsoid, rotated relative to the eigenvectors of the variance-covariance of the trajectory intersection distribution, and positioned relative to the mean of the distribution. This process is repeated for each of the three possible trajectory intersection distributions analysed. The mean confidence ellipsoid for each trajectory intersection data set is visualised with a transparent solid red shader, with the

external edge of the ellipsoid highlighted by a black line. Visualised in this way the external definition of the confidence region can be assessed relative to any viewpoint selected.

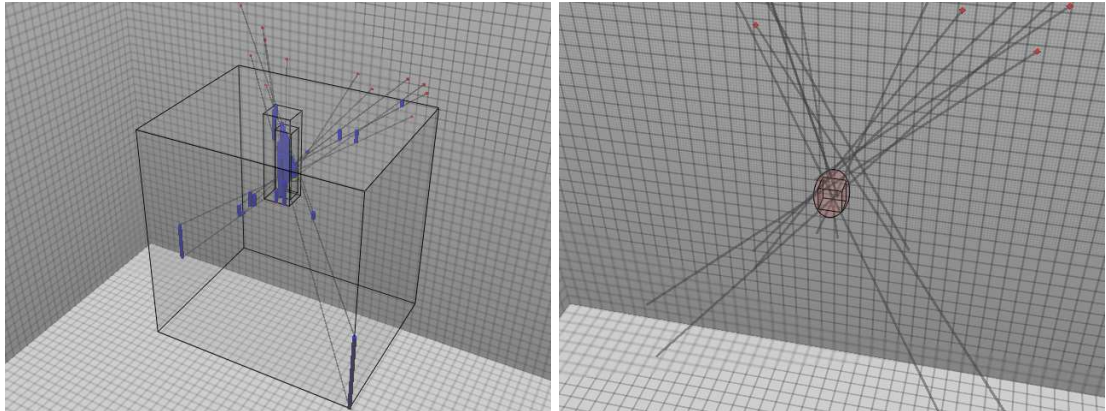


Figure 10-15 - The visualisation of the dispersal data (left) and mean confidence data (right) generated for a trajectory intersection data set.

The joint distribution count data generated during the analysis of the horizontal distribution of the trajectory intersection data set of a site of impact estimate is visualised by the Shockwave® movie component of the analytical site of impact estimation application as a 3D histogram. Each class interval within the horizontal plane of the 3D investigative environment that contains at least one trajectory intersection is covered by a single cuboid geometry. The heights of each of these cuboids are subsequently scaled relative to the number of intersections located within the particular class interval that they represent. The maximum class interval count over the three joint distribution counts generated for the three alternative trajectory intersection data sets is used as the benchmark against which all the other heights are scaled. Two alternative geometry shading schemes are employed to aid the interpretation of the joint distribution count data. The first geometry shader scheme assigns a colour to each column of the three possible 3D histograms relative to the number of the size of the count that each column represents. The seven colours used to represent this count data in ascending order are blue, cyan, green, chartreuse, yellow, orange, and red. In contrast to the height of the histogram columns, the geometry shaders are assigned relative to the largest single count established for each of the three possible joint distribution counts. As a result, while the height of the histogram columns can be used to compare the various 3D histograms produced, the colour of the columns can be used to compare count data within each histogram. The second geometry shader scheme employed within the visualisation application



assigns a colour to each column of the 3D histograms based on the probability of achieving such a count given the distribution of the non-zero counts, as calculated within the analytical VB macro. A blue shader is assigned for a probability level of less than 0.1, and cyan, green, yellow and red chasers applied to the histogram columns for probabilities levels corresponding to 0.1, 0.05, 0.01, and 0.001 respectively. An example of the 3D histogram visualisation of the horizontal intersection joint distribution count data and the two alternative geometry shader schemes are demonstrated in Figure 10-16.

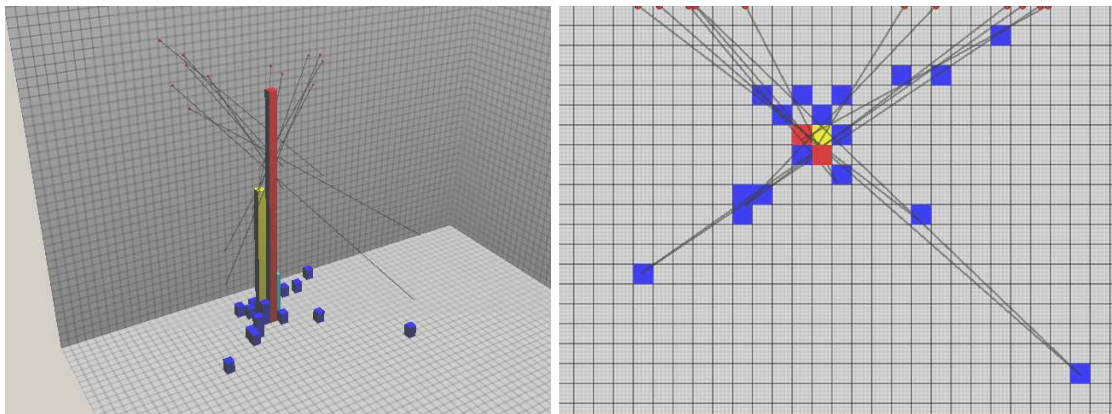
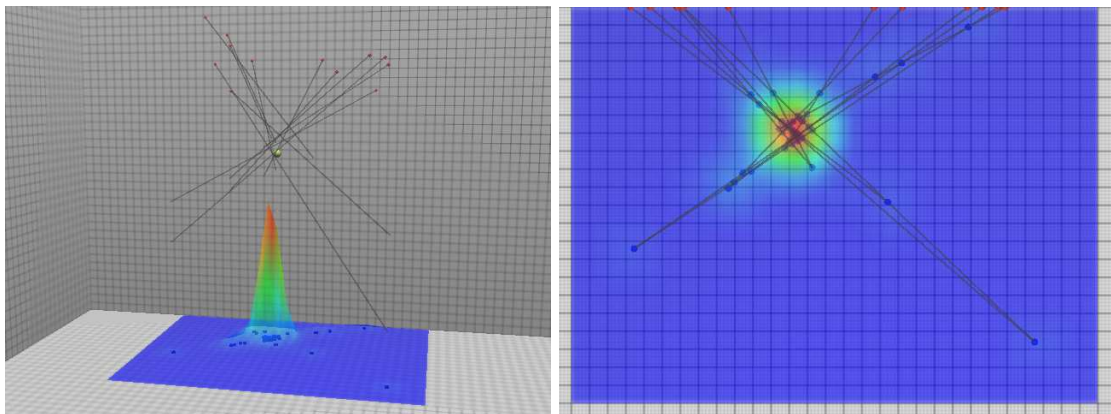


Figure 10-16 – The visualisation of a joint distribution count of the horizontal data of a trajectory intersection data set (left), and the same 3D histogram viewed in an orthographic top view with IRP comparative texturing (right).

The EPDF data generated by the VB macro is also passed to the visualisation application for inclusion within the 3D investigative environment. The EPDF data is processed by the visualisation Shockwave<sup>®</sup> movie to produce a surface geometry based on a single 3D plane. The width and length of the plane are set to correspond with the extent of the calculated EPDF surface, and the plane positioned accordingly. The number of width and length vertices of the 3D plane is set to correspond to the number of horizontal sample points used in the creation of the EPDF, and the height of each vertex is manipulated to provide a relative height which is indicative of the density of trajectory intersections at each sample location. The height of each vertex is scaled relative to the largest single point-sample reading generated during the construction of the three possible EPDF by the analytical VB macro. Three separate shading schemes are also implemented to aid the interpretation of the EPDF surface data.

The first shading scheme uses the point-sample data of each calculated EPDF to produce a relative density texture. The volume under each section of the EPDF

enclosed within four adjacent sample points is calculated by the visualisation application, and the maximum single volume region for each of the three possible EPDFs established. A dynamic texture is created within the visualisation application, which has the corresponding number of pixels to the number of volume regions under the EPDFs. Each pixel is assigned a colour according to the relative standing of the volume within that region compared to the maximum established for each separate EPDF. A colour scheme using eighty separate shades is used to indicate the relative density of trajectory intersections across each of the three EPDFs, ranging from a deep blue indicating low density, through green, and yellow to a deep red colour to indicate high relative density. An example of the 3D EPDF surface geometry and the relative density shader generated by the visualisation component of the analytical site of impact estimation application is shown in Figure 10-17.



*Figure 10-17 – The relative density texturing of an EPDF viewed from a perspective viewpoint (left) and an orthographic top view.*

The second shading scheme employed also involves the generation of dynamic texture maps. The level of density calculated for a trajectory intersection at each sample point across the EPDF is compared to the level expected from a constant density IRP. Where the average level of density across the four sample points which surround a single 5 by 5 centimetre region is above that expected given a hypothesis of a IRP, then the corresponding pixel on the dynamic texture map is coloured red. Where the average density level is equal to or below this expected level the texture map is coloured blue. This method of texturing provides a visual method of assessing the potential pattern randomness present within each of the three possible EPDFs, an example of which is illustrated in Figure 10-18. The final shading scheme employed for the visualisation of the EPDF data is the simplest of the three, and involves the shading of each of the three EPDFs with a

separate colour to provide a method for the direct visual comparison of each individual EPDF, as demonstrated in Figure 10-18. Under this comparative colour scheme, the total intersection EPDF is assigned a blue shader, the opposite intersection EPDF a green shader, and the thinned intersection EPDF an orange shader. The EPDF surface of each trajectory intersection data set, regardless of the texturing scheme applied is also viewable as a wire frame model to provide an alternative visualisation method where a more transparent version of the EPDF surface models may be beneficial.

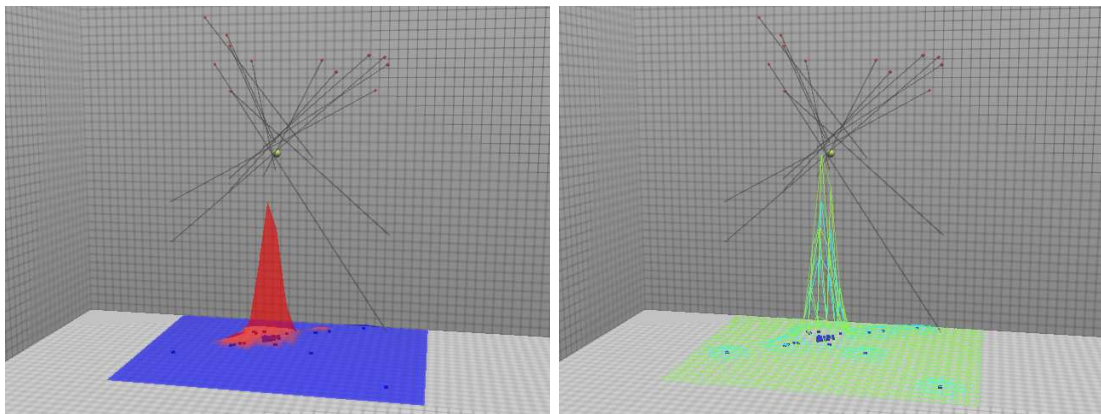


Figure 10-18 – The IRP texturing of a single EPDF (left) and the single colour comparative texturing of EPDF surfaces generated for two alternative trajectory intersection data sets (right).

### 10.4.3 Multiple Sample Visualisation

This section will discuss the visualisation methodology employed in the visualisation of virtual 3D multiple sample site of impact estimates derived from the results of analyses conducted within the analytical VB macro. The description of the construction of a multiple sample estimate is divided into two further sections that will outline the procedures used to visualise the individual multiple mean estimates for each analysis, and the generation of the geometry to represent the confidence regions calculated by the VB macro for the sampling distribution of these mean estimates. The 'MultiVis' panel of the VB macro interface, illustrated in Figure 10-19, provides the interactivity necessary to control and analyse various aspects of the visualisation of a 3D multiple sample estimate. The visualisation features of each set of estimates constructed for the four possible alternative sample sizes, and the three possible trajectory intersection data sets can be hidden and made visible from this interface panel.

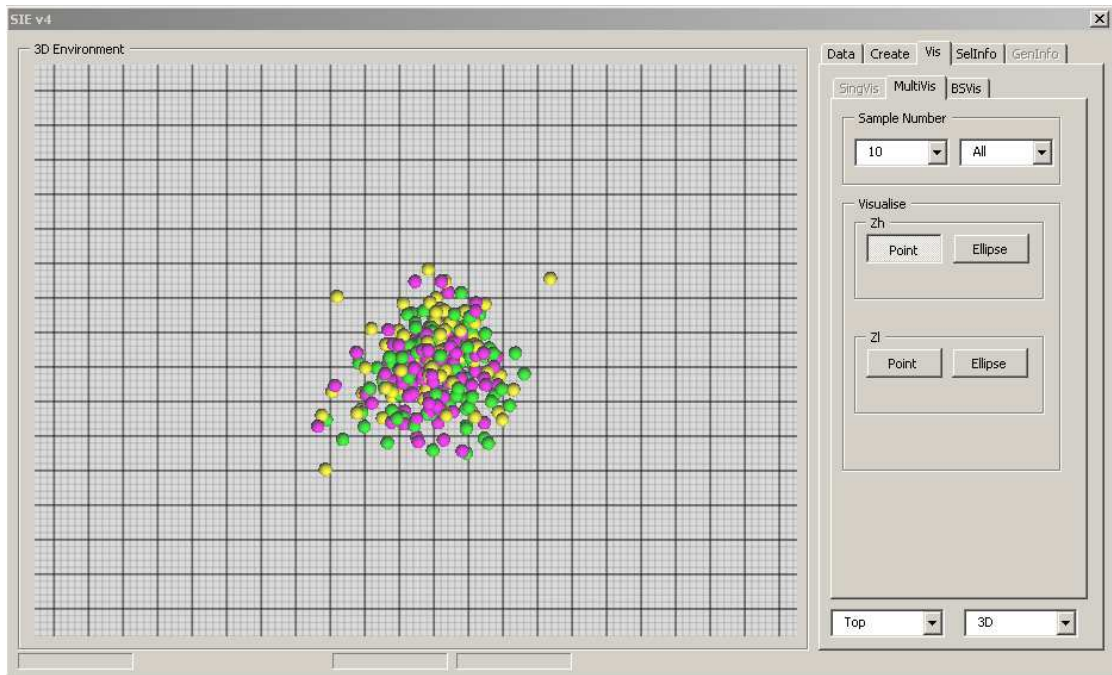


Figure 10-19 - The top orthographic visualisation of the 100 mean multiple sample data generated for the total (green), opposite (purple), and thinned (yellow) data sets.

#### 10.4.4 Mean Data Visualisation

The Shockwave<sup>®</sup> movie component of the analytical site of impact estimation application transforms the 100 single sample means generated for each of the three possible trajectory intersection data sets, at each of the four possible sample sizes, into spherical geometries to construct a point-based visualisation of the multiple sample data. Each mean point-summary is represented by a 3D sphere that is centred on the location of the mean provided through the data passed to the visualisation application via the VB macro. Two sets of mean points are generated to visualise the 3D means in terms of both their mean upper and lower intersection height estimates. The alternative means generated, according to the different approaches to the interpretation of trajectory intersection data sets, are identified using different geometry shader schemes. The total intersection approach is represented a green geometry shader, while the opposite and thinned approaches are represented by purple and yellow geometry shaders respectively, as illustrated in Figure 10-19. As a result, the distribution of the estimate means for each approach to the analysis trajectory intersection data, at both the upper and lower intersection heights, and at all the sample sizes

analysed, can be compared, contrasted and evaluated within the interactive 3D virtual investigative environment.

#### 10.4.5 Sampling Distribution Confidence Interval Visualisation

In addition to the construction of multiple mean-point geometries, the Shockwave® movie component of the analytical site of impact estimation application constructs geometry to represent the multivariate confidence regions for the sampling distribution of the mean generated during the analysis of multiple samples through the VB macro. The ellipsoidal population confidence intervals are constructed using the same method outlined for the generation of 3D mean confidence intervals in the visualisation of a single sample estimate (see Section 10.4.2.2).

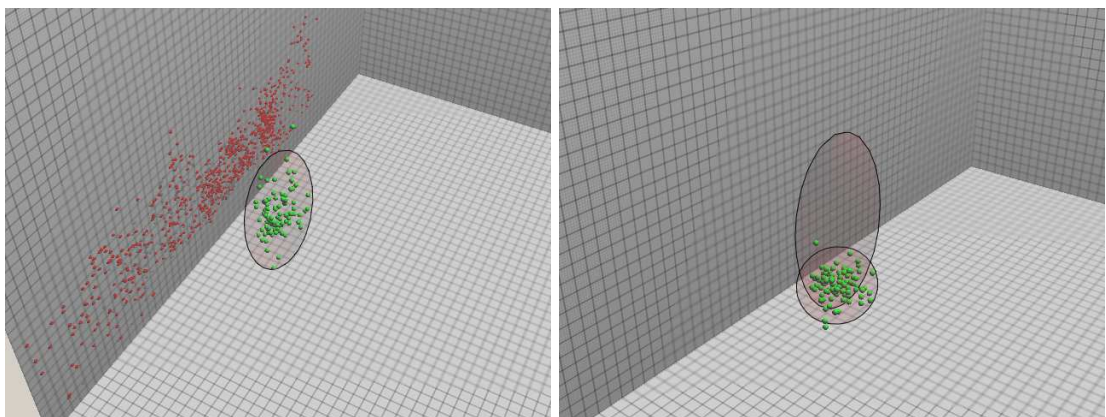


Figure 10-20 - The 95% confidence region generated for a 3D mean estimate population from a multiple sample estimate (left) and the comparison of a population confidence region for an estimates upper and lower intersection heights (right).

For the multiple sample visualisation, however, a possible total of 24 confidence region geometries are constructed to provide an assessment of the sampling distribution of the mean data sets of the total, opposite and thinned approaches, at both the upper and lower intersection heights, at sample sizes of 10, 20, 50, and 100. The visualisation of the multiple sample estimate confidence ellipsoidal geometries provides a method of visually assessing the uncertainty present in the mean estimate of any particular sampling methodology, highlighting any potential single estimates within the grouping which do not correspond to the general trend, and facilitating the comparison of mean estimate uncertainty in alternative

approaches to the interpretation of trajectory intersection data, as demonstrated in Figure 10-20.

## 10.5 Conclusions

The Shockwave® movie developed using the Macromedia® Director® IDE, and integrated within the VB macro interface through the Shockwave® ActiveX Control, provides a visual means of investigating, evaluating and presenting the results of the detailed numerical analyses conducted during the construction and analysis of a site of impact estimate by the analytical VB macro. The 3D interactive investigation virtual environment provides a user-led investigative experience within which estimate data can be interpreted in relation to the native 3D spatial context of both the original spatter bloodstain data, and the construction of the site of impact estimate. While the use of 3D modelling software within BPA is already proving effective in the construction and presentation of site of impact estimates (see Section 3.4.2), the integrated interactive potential of such 3D virtual environment technologies is not currently exploited to the level of the analytical site of impact estimation application developed as part of this research project.

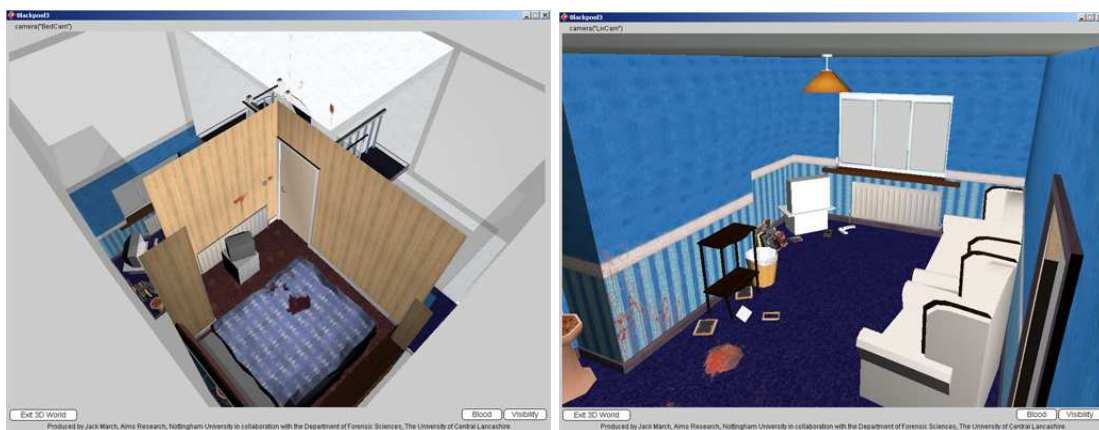


Figure 10-21 - An interactive crime scene environment developed as a prototype BPA training and visualisation application.

The visualisation methodology employed within the 3D virtual Shockwave® environment, in conjunction with its interactive functionality, enables multiple features of an estimate, and the results of its analysis, to be compared and evaluated in an immediately more accessible medium than that provided by the consideration of often-complex numerical results of an analysis in isolation. The

provision of such an integrated visual approach to the analysis of site of impact estimate has the potential to both increase the informational value of complex numerical data generated during the construction of an estimate, as well as to condense large and diverse numerical data sets into a rapidly interpretable format (Ware, 2000). By the same token, the visualisation of estimate information can also facilitate the dissemination of such technical data and promote an improved understand in others, who do not necessarily have the same in-depth understanding of the reconstructive process (Noond et al, 2002).

While the visualisation methodology employed during this research project is largely decontextualised, in the sense that the visualisation takes place in a sterile investigative environment, with additional development, and integration within other 3D crime scene capture and 3D CG reconstruction technologies, the interpretive and presentational potential of the 3D interactive visualisation of detailed site of impact estimate data could be further enhanced. The incorporation of estimate data within a 3D CG reconstruction of a crime scene, such as the example shown in Figure 10-21, for example, could provide additional or alternative spatial or situational constraints within which a constructed estimate may require explicit evaluation, as well as providing a contextualised setting for the presentation and discussion of case-specific site of impact estimates and wider CSRs. As the generation and presentation of 3D CG visualisations and reconstructions of forensic information become increasingly accepted within legal contexts, the detailed numerical analysis and 3D visualisation of site of impact estimate information, with continued development, may ultimately provide site of impact estimation with a consistent means of providing, proving, and presenting a consistent, appropriate, and sound scientific basis for its status as expert forensic CSR evidence.

## **11 Experimental Data Analysis**

### **11.1 Introduction**

This chapter will describe and examine the analysis of the three experimental impact spatter patterns generated for the purposes of this research into site of impact estimation and estimate uncertainty. This discussion of the experimental data analysis undertaken during this research project is divided into four main sections. Firstly, the screening process conducted on the spatter bloodstain data contained within each experimental impact spatter patterns will be described, and the reasoning behind the reduction of the total enumerated data sets explained. Secondly, the large number of estimates constructed using the analytical site of impact estimation application during this research project will be discussed, and the structured sampling methodology employed in the generation of this data for the purposes of investigating estimate uncertainty for each of the three experimental impact spatter patterns will be examined. The third and fourth sections of this chapter will provide a relatively brief examination of the detailed site of impact estimation data generated in the analysis of six of the spatter bloodstain sampling strategies investigated during this research project. The specific sampling strategies were chosen for this discuss in an attempt to provide some preliminary insights into the potential effects and manifestations of estimate uncertainty, and the investigative potential of the analytical procedures included within the analytical site of impact estimation application in an attempt to evaluate this information.

### **11.2 Impact Spatter Pattern Screening**

While the data on the entire observable spatter bloodstain population of each of the three experimental impact spatter patterns was collected during the exhaustive recording procedure (see Section 5.3), a restricted screened version of these impact spatter pattern data sets was deemed more appropriate for the investigation of site of impact estimate uncertainty proposed by this research project. Each of the three impact spatter patterns is screened during analysis within the VB macro component of the analytical site of impact estimation application to remove spatter bloodstains with a subjective classification of OSC, DIST, PSAT, PDS or NDLE. Any spatter bloodstain with a subjective classification of OSC, DIST, or PSAT is precluded from pre-processing within the VB macro



during the data acquisition phase (see Section 8.3.1), as the data collectable from the morphologies of potentially oscillatory, distorted, and satellite spatter bloodstains is not appropriate for the purposes of site of impact estimation. These spatter bloodstains, as a result, are automatically omitted from analysis by the analytical VB macro. The remaining spatter bloodstains within each impact spatter pattern are defined here as 'Usable' spatter bloodstains.

Spatter bloodstains with a classification of either PDS or NDLE, however, are omitted from the analyses here during the sub-population definition phase of the analytical procedure of the VB macro. These subjective spatter bloodstain types are removed from the analyses in an attempt to replicate the types of spatter bloodstain data that might be usable in the construction of site of impact estimates under casework rather than experimental conditions. To achieve this aim spatter bloodstains with a subjective classification of PDS, potentially distorted spatter bloodstains, are removed from consideration, as the quantification of the morphology of these bloodstains is likely to be less accurate than in spatter bloodstains that are not distorted to the same degree. Spatter bloodstains with a classification of NDLE, where no leading edge is identifiable, are also omitted as the directionality of these spatter bloodstain was not independently assignable during the exhaustive recording procedure. The determination of the angle of orientation for this spatter bloodstain type was only possible due to the *a priori* knowledge of the location of the impact site of each experimental impact event. While some approximation of this process may be possible under casework conditions through the interpretation of directionality based on other spatter bloodstains within close proximity, the straight-line trajectory approximations for these spatter bloodstains are dependent on their assumed association with other bloodstains, and as a result are disregarded from the remaining research within this project. The remaining spatter bloodstains within each impact spatter pattern following this screening procedure are defined here as 'Screened' spatter bloodstains.

As the impact spatter pattern bloodstain data is only screened during the sub-population definition phase of the analytical site of impact estimation procedure, the full experimental impact spatter pattern data (with OSC, DIST, and PSAT spatter bloodstains excluded) is available for future analysis, should additional or alternative investigative directions be required of these large-scale site of impact estimation data sets. The total number of spatter bloodstain recorded for each of the three experimental impact spatter patterns, and the number of usable and

screened spatter bloodstains, defined through the VB macro data acquisition and project specific sampling strategy respectively, are shown in Table 11-1.

<b>Pattern</b>	<b>Total Number of Spatter Bloodstains Recorded</b>	<b>Number of Useable Spatter Bloodstains</b>	<b>Useable / Total Ratio (2 d.p.)</b>	<b>Number of Screened Spatter Bloodstains</b>	<b>Screened / Total Ratio (2 d.p.)</b>	<b>Screened / Usable Ratio (2 d.p.)</b>
ES-A	1022	979	0.96	746	0.73	0.76
ES-B	430	408	0.95	343	0.8	0.84
ES-C	957	891	0.93	661	0.69	0.74

*Table 11-1 - The number of spatter bloodstain available for analysis before and after the removal of the spatter bloodstains with either a PDS or NDLE subjective classification.*

### **11.3 Site of Impact Estimate Sampling Strategy**

A wide-ranging sampling strategy was devised for the analysis of site of impact estimation and estimate uncertainty proposed by this research project utilising the analytical potential of the site of impact estimation computer application developed. Each of the three experimental impact spatter patterns generated during the research project were analysed using the 34 separate spatter bloodstain sampling criteria outlined in Table 11-2. This sampling strategy was designed to investigate the potential of specific collections of spatter bloodstains in providing information on the location of a spatter-producing impact site and to identify and analyse the composition of groups of spatter bloodstains within each impact spatter pattern which could be considered to provide a reasonable degree of accuracy.

<b>Upward Moving (degrees)</b>	<b>Downward Moving (degrees)</b>	<b>Impact Angle (degrees)</b>	<b>Flight Distance (cm)</b>	<b>Size (mm)</b>	<b>Horizontal Quality (cm)</b>	<b>3D Quality (cm)</b>	<b>Total</b>
All	All	0-45	0-25	0-1	0-5	0-5	All
0-45	0-45	45-90	25-50	1-3	0-10	0-10	
45-90	45-90	0-30	50-75	3+	0-15	0-15	
0-30	0-30	30-60	75-100	0-3			
30-60	30-60	60-90	100+	1+			
60-90	60-90						

*Table 11-2 - The 34 individual spatter bloodstain sampling strategies employed in the investigation of site of impact estimation uncertainty as part of this research project.*

In the former sample group, a number of spatter bloodstain variables, which are often applied in spatter bloodstain selection during site of impact estimation (see Section 4.7), are included. A range of samples based on the vertical angle

defined by the straight-line trajectory approximation ('Upward' and 'Downward' columns), the impact angles of the spatter bloodstains, the minimum straight-line flight distance of the spatter bloodstain-producing blood droplets, and the size of the spatter bloodstain were included within the strategy to provide a means of evaluating and comparing collections of spatter bloodstains which could be considered likely to be both accurate and inaccurate, in the construction of a site of impact estimate. An additional total screened impact spatter pattern strategy was also provided to act as a theoretical base against which other sampling methodologies can be compared, and an assessment of a total pattern estimate construction methodology could be made. In the latter sample group, sampling strategies were included in the investigation of the experimental impact spatter patterns that were based on a range of horizontal and 3D independent data quality assessments made for each spatter bloodstain during data pre-processing.

Each of these sampling strategies was applied in isolation during the analysis of the experimental impact spatter patterns undertaken using the analytical site of impact estimation macro during this research project. While this is not necessarily representative of sampling methodologies employed during the construction of site of impact estimates which typically employ selection using multiple variables, the application of individual sampling strategies was considered to represent an appropriate and logical starting point for the analysis of impact spatter bloodstain patterns, site of impact estimation, and estimate uncertainty using the detailed analytical methodology employed as an integral part of this research project. The analysis of more complex multiple variable sampling strategies represents one of the potential future avenues for the continuation and advancement of this type of structured research into the uncertainty present within the construction of site of impact estimates.

Even without the inclusion of combinations of multiple sample strategies, which would have greatly increased the number of estimates constructed, a total of 612 estimates were constructed during this research. Both a single and multiple sample site of impact estimate were constructed using the 34 spatter bloodstain samples for each of the three experimental impact spatter patterns. This construction of 68 estimates was conducted three times to produce 204 site of impact estimates for each impact spatter pattern. The first series of 68 estimates were constructed using two spatter bloodstain sub-populations, one representing spatter bloodstains that were situated to the left, and the other made up of spatter bloodstain situated to the right of the known location of the impact site

within the target surface upon which the impact spatter pattern was observed. This series of estimates was constructed to provide data on a methodological approach to site of impact estimate that corresponds to the straight-line trajectory bracketing hypothesis, which can be considered to provide a more accurate indication of the location of an impact site (Laber and Epstein, 2004; Carter and Podworny, 1991). The second and third series of estimates were constructed using a single spatter bloodstain sub-population that was made up of spatter bloodstains from either the left or the right of the known location of the site of impact estimation. These directionally-restricted site of impact estimates were constructed to provide a series of results which could be considered to correspond to impact spatter patterns that demonstrated distributions of spatter bloodstains, which do not provide an opportunity to generate bracketing estimates. In the following discussion of the analysis of these samples, where no specific sub-population approach is defined, the data being described will correspond to the dual directional sub-population division of the impact spatter pattern data.

The sampling strategy employed in the analysis of the experimental impact spatter patterns, consequently, provides a large amount of information for the evaluation and comparison of varying approaches to spatter bloodstain sampling and estimate construction given different impact spatter pattern distributions. The data provided by the analytical site of impact estimation application on the entire series of estimates, however, represents a considerable quantity of numerical and visual information, the description of which is physically beyond the scope of this thesis. The results of the analysis of each of the samples are provided on the DVD-ROMs that accompany this thesis, as this data represents a considerable repository of empirical site of impact estimate data, which could prove useful in further research into estimate uncertainty, or in addressing specific estimate questions arising during casework.

Of the series of estimates constructed during this research project, the general results generated from two potentially important sampling strategies, in terms of investigating site of impact uncertainty, will be examined in the remainder of this chapter. These sampling strategies represent a total reconstruction model within which all screened spatter bloodstains are considered for each impact spatter pattern, and the 3D 0-10 centimetre independent data quality samples for each impact spatter pattern, which represent what can be considered to be a relatively accurate collection of spatter bloodstains from within the overall bloodstain

population. Within these two approaches to the construction of site of impact estimates, both the dual directional and the two single directionally-restricted version of the spatter bloodstain data will be discussed.

#### **11.4 Total Spatter Bloodstain Population Analysis**

This section will outline and examine the results of the analyses conducted into site of impact estimation and estimate uncertainty using the total spatter bloodstain populations provided by each of the three screened experimental impact spatter patterns. The discussion of these results will be presented in two sections, which relate to the two approaches to the construction of site of impact estimate provided through the analytical site of impact estimation application. Firstly, the results of the construction of single sample estimates using the entire screened spatter bloodstain populations will be described and discussed. Secondly, the results of the construction of multiple sample estimates using the random selection of smaller spatter bloodstain samples from within these total screened spatter bloodstain populations will be examined.

Before discussing the results of these site of impact estimation procedures, the examination of the potential accuracy of each impact spatter pattern, in terms of the independent data quality assessment calculated for each spatter bloodstain during data pre-processing by the analytical site of impact estimation application, has implication for the construction of these estimates, and provides additional information for the interpretation of their results. The horizontal and 3D independent data quality assessments made for the total screened spatter bloodstain populations are illustrated in Figure 11-1 and Figure 11-2 respectively. This independent data quality assessment data indicates a considerably degree of variation between the three patterns. Pattern ES-C has the largest proportion of spatter bloodstains with what could be considered to be a reasonable data quality, with 64 and 88 percent of bloodstains providing a 3D quality, and 83 and 94 percent providing a horizontal data quality of less than 10 and 15 centimetres respectively. For pattern ES-A, the next most accurate pattern in terms of independent data quality, these proportions are reduced to 26 and 50 percent for 3D, and 63 and 85 for horizontal quality. Patterns ES-B provides the lowest proportions of spatter bloodstains with a reasonable level of data quality, with percentages of 11 and 20 for the 3D data quality, and 53 and 77 in terms of horizontal data quality. The construction of site of both single population

estimates, and multiple random smaller sample estimates could, as a result, produce some considerable variation between the three experimental impact spatter patterns.

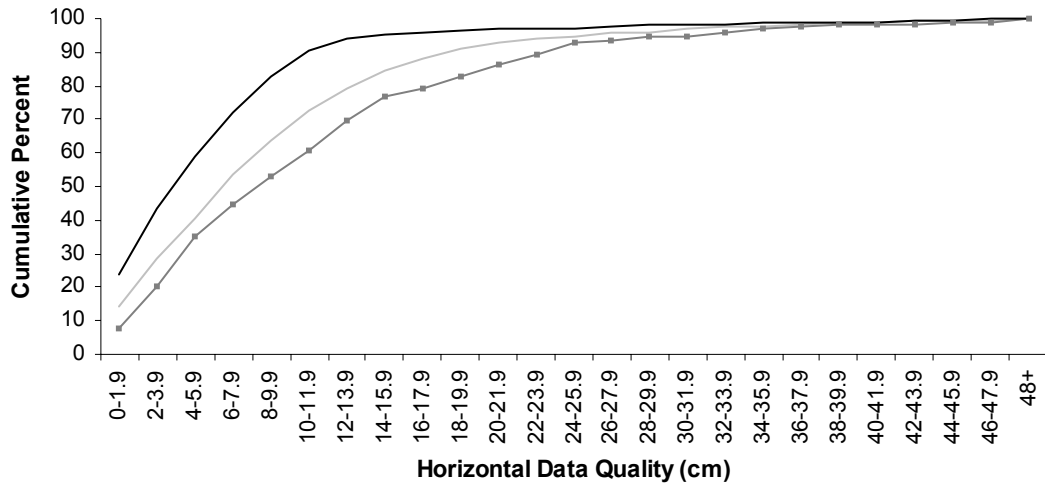


Figure 11-1 - The cumulative percentage of spatter bloodstains with a horizontal independent data quality in five centimetre wide categories for patterns ES-A (light grey line), ES-B (dark grey line with squares), and ES-C (black line).

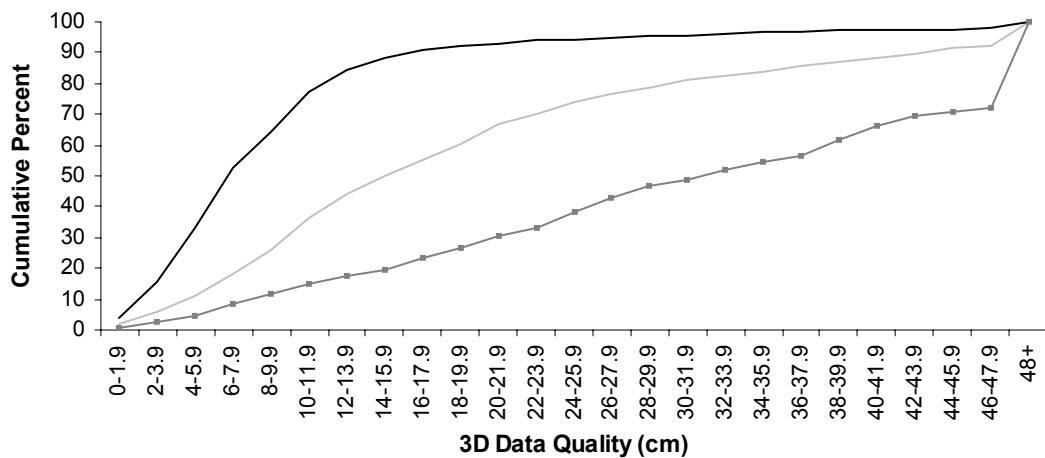


Figure 11-2 - The cumulative percentage of spatter bloodstains with a 3D independent data quality in five centimetre wide categories for patterns ES-A (light grey line), ES-B (dark grey line with squares), and ES-C (black line).

### 11.4.1 Single Sample Estimation

The construction of single samples site of impact estimates using the entire spatter bloodstain populations of the three screened experimental impact spatter

patterns provides two main investigative functions. Firstly, the construction of these estimates provides a means of evaluating the potential utility of a total population estimate methodology, and the potential variation in estimate data given this approach. Secondly, the data produced from the construction of a single population-based site of impact estimate should provide the estimate parameters around which the statistics generated through the repeated smaller sample estimation approach of the multiple sample technique are distributed.

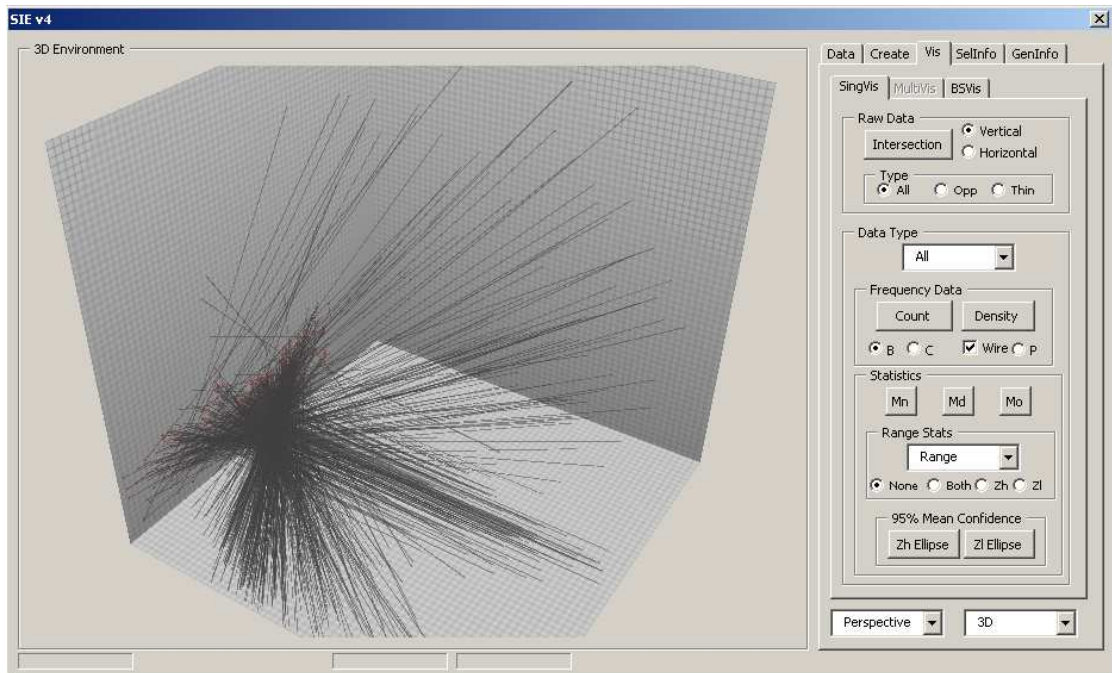


Figure 11-3 - The straight-line trajectory approximations from the 746 screened spatter bloodstains within impact spatter pattern ES-A.

As would be expected from the previous discussions on the rapid increase in the numbers of trajectory intersections given increases in spatter bloodstains the numbers considered in the construction of an estimate (see Sections 4.7), a single sample site of impact estimate consisting of several hundred spatter bloodstains generates considerable amounts of trajectory intersection data. An example of the complex estimation data in the form of the straight-line trajectory approximations established for the single sample estimate of the 746 spatter bloodstains with the screened pattern ES-A is illustrated in Figure 11-3. The total number of trajectory intersection established for the total estimate of the screened spatter bloodstain populations of pattern ES-A, ES-B, and ES-C are 227558, 47506, and 158837 respectively.

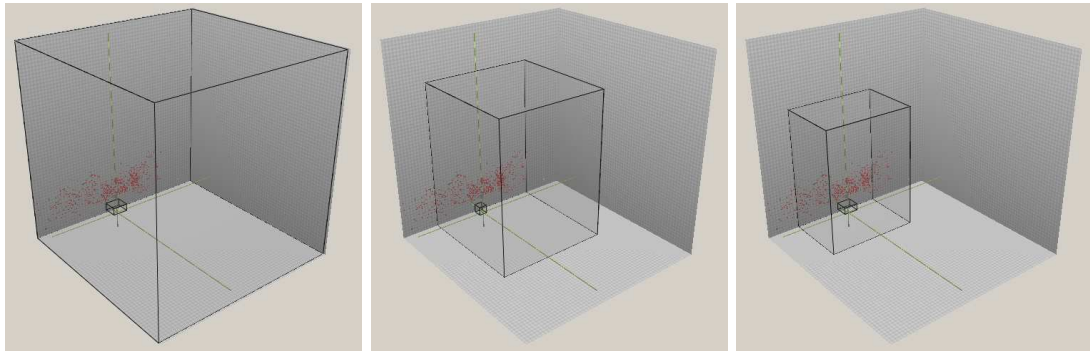


Figure 11-4 - The range and inter-quartile ZI range data for the total (left), opposite (centre) and thinned (right) trajectory intersection data sets generated during the population estimate for pattern ES-A.

<b>Pattern</b>	<b>X (cm)</b>	<b>Y (cm)</b>	<b>Zh (cm)</b>	<b>ZI (cm)</b>	<b>OX (cm)</b>	<b>OY (cm)</b>
ES-A	297.13	298.35	299.18	298.88	176.04	173.59
ES-B	296.90	297.23	296.17	279.17	171.27	153.20
ES-C	220.65	296.68	297.94	132.98	71.60	164.65

<b>Pattern</b>	<b>OZh (cm)</b>	<b>OZI (cm)</b>	<b>TX (cm)</b>	<b>TY (cm)</b>	<b>TZh (cm)</b>	<b>TZI (cm)</b>
ES-A	292.23	230.39	98.91	141.43	294.75	192.19
ES-B	285.63	258.88	130.19	168.13	291.91	258.88
ES-C	175.18	107.26	56.24	77.24	138.56	105.02

Table 11-3 - The ranges of intersection data for the population estimates generated for each of the three experimental impact spatter patterns, employing the three alternative approaches to the interpretation of trajectory intersection data sets.

Table 11-3 and Figure 11-4 indicate the size of the ranges of the distribution of trajectory intersections within the population estimates, for each of the three approaches to the interpretation of trajectory intersection data sets. These ranges tend to be relatively large volumetric regions in comparison to both the total extent of the investigative environment, and the spatial reconstructive aims of site of impact estimation. While the range statistic can provide useful information in the description of the distribution of trajectory intersections for each estimate, the inter-quartile range is adopted for the evaluation of intersection dispersion for each estimate during this analysis. As the smaller of the two cuboids in each of the three visualisations illustrated in Figure 11-4 indicates, the inter-quartile range of a population estimate provides a much more spatially-restricted region within the investigative environment, while still indicating the 3D volume within which the central 113779, 23753, and 79418 trajectory intersections are situated in the estimates constructed for pattern ES-A, ES-B, and ES-C respectively. As a result, the inter-quartile range statistic, especially in the case of these large-scale estimates is likely to provide a more



appropriate means of assessing trajectory intersection distribution for the purposes of the interpretation of the site of impact estimate data.

Figure 11-5, Figure 11-6, and Figure 11-7 show the inter-quartile ranges, means and medians generated during the analysis of the three trajectory intersection data sets constructed for the population estimates of pattern ES-A, ES-B, and ES-C respectively, presented in terms of the estimate error indicated by the distance of each statistic from the location of the known impact site. Each of the three population estimates achieves a relatively high degree of locative accuracy in the horizontal plane of analysis, with pattern ES-B, which exhibits the largest degree of error of the three patterns, providing mean and mode point estimates within 10 centimetres of the known location of the pattern-producing impact event.

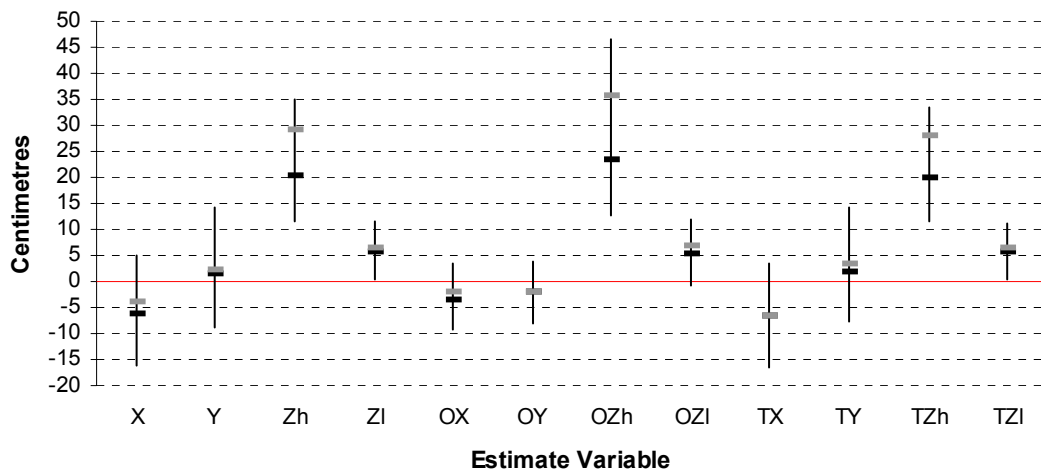


Figure 11-5 – The inter-quartile range (vertical bar), median (black horizontal bar), and mean (grey horizontal bar) of the error of the population estimate constructed for pattern ES-A.

Of the two height estimates generated through the analytical site of impact estimation application, the lower,  $p_{zl}$ , estimate provides the consistently more accurate estimate across all of the analyses. Both the mean and the mode statistics of the  $p_{zl}$  height data for the estimates constructed for pattern ES-A and ES-C provide relatively accurate approximations of the height of pattern-producing impact site, especially given the theoretical difficulties involved in establishing height estimates from straight-line trajectory approximations. Pattern ES-B, as might be expected from the distribution of independent data assessments, exhibits the greatest error in terms of height estimation, both within the  $p_{zl}$  and  $p_{zh}$  intersection variables. Of the horizontal estimate variables the  $p_x$  estimates, the location of the estimate perpendicular to the plane of the

target surface, as opposed to the  $p_y$  variable, the location of the estimate parallel to the plane of the target surface, appears to demonstrate the largest degree of estimate error in majority of cases.

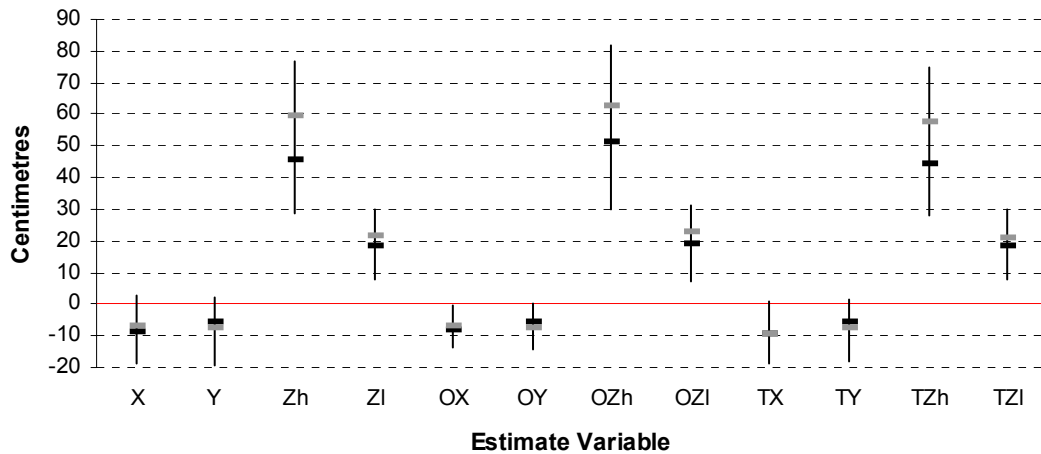


Figure 11-6 - The inter-quartile range (vertical bar), median (black horizontal bar), and mean (grey horizontal bar) of the error of the population estimate constructed for pattern ES-B.

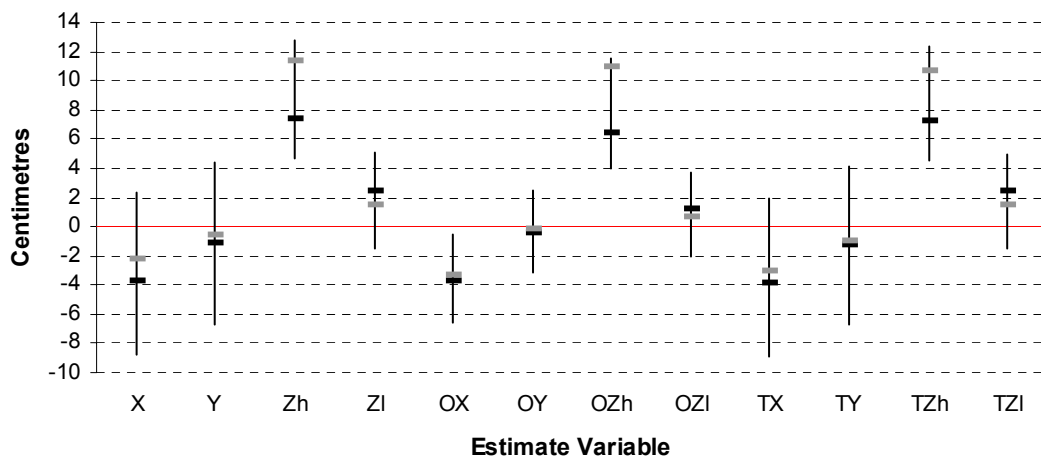


Figure 11-7 - The inter-quartile range (vertical bar), median (black horizontal bar), and mean (grey horizontal bar) of the estimate error of the population estimate constructed for pattern ES-C.

While the application of opposite and thinned approaches to the interpretation of intersection intersections does affect the statistics generated on each population estimate, these do not appear to be significant compared to the accuracy of the statistical descriptions of the total trajectory intersection data. The application of the opposite approach produces the largest change in the estimate results, although this only appears to have a consistent affect of reducing the inter-quartile range of the  $p_x$  and  $p_y$  intersection data.

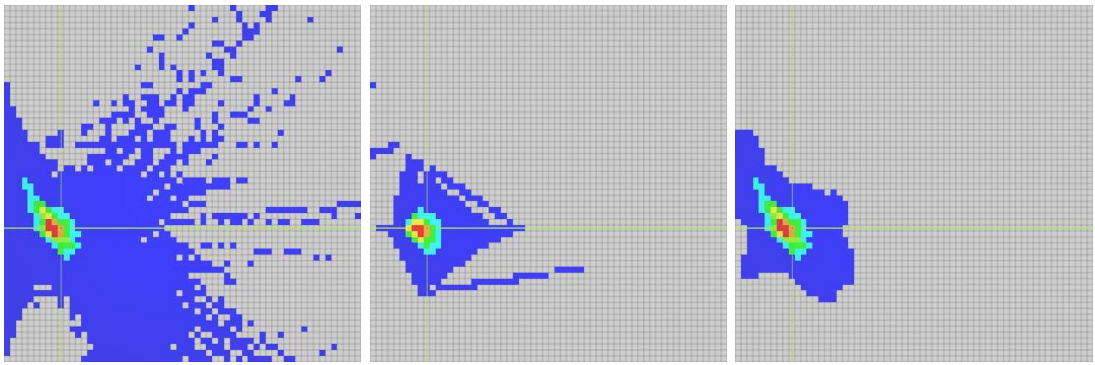


Figure 11-8 - The 3D histogram visualisations generated for the total (left), opposite (centre), and thinned (right) approach to trajectory intersection for the population estimate of pattern ES-A.

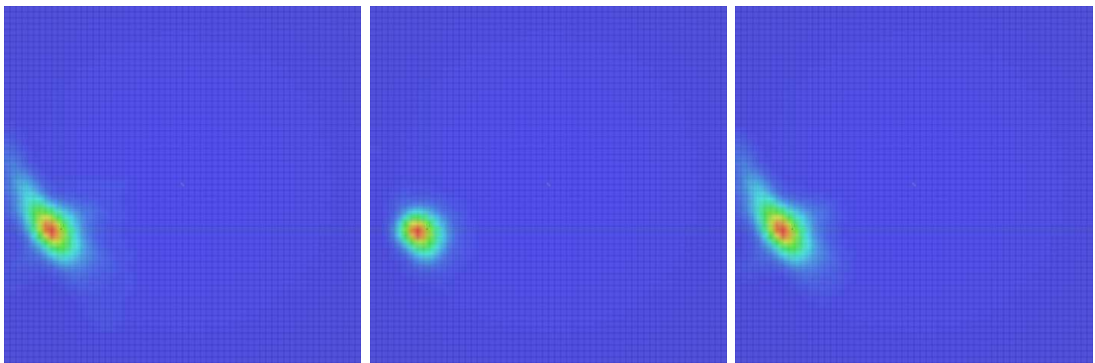


Figure 11-9 - The relative density visualisations generated for the total (left), opposite (centre), and thinned (right) approach to trajectory intersection for the population estimate of pattern ES-A.

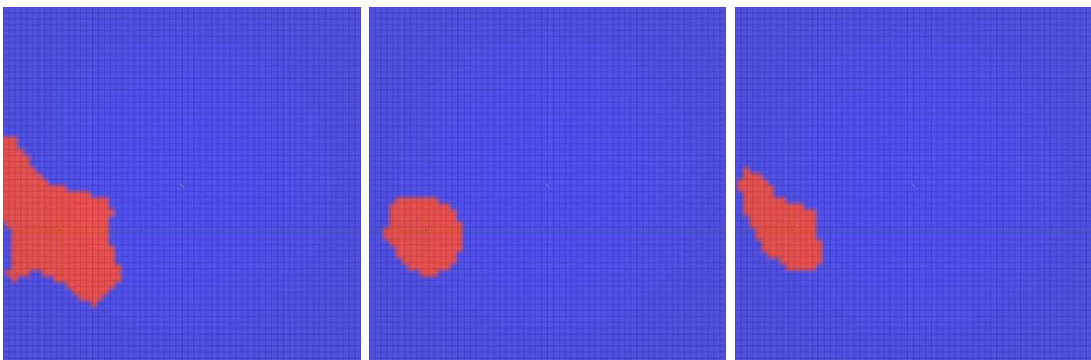


Figure 11-10 - The aggregated density visualisations generated for the total (left), opposite (centre), and thinned (right) approach to trajectory intersection for the total single reconstruction of pattern ES-A.

The differences in the distribution of trajectory intersections given the three alternative approaches to the interpretation of this data are demonstrated for pattern ES-A in Figure 11-8, Figure 11-9, Figure 11-10. The reduction in the spatial extent of the trajectory intersection distributions in the horizontal plane achieved through the opposite and thinned trajectory intersection data sets can

be clearly seen in visualisation of the 3D histograms and intersection density estimates. While the opposite approach changes the distribution of intersections throughout the distribution, indicated by the change in both size and shape of the zone of relatively high quadrat counts, the thinned approach maintains the internal structure of the distribution of the data provided by the total trajectory intersection data, while removing a large amount of the extreme observations. Each of the three approaches to the interpretation of trajectory intersection data sets exhibit a good correspondence between the regions of relative high quadrat count and intersection density and the known location of the impact site.

The effect on the population estimates of the restriction of spatter bloodstain to those bloodstains that are located either to the left or right of the location of the known impact site within the vertical plane of the recording target surface are illustrated in Figure 11-11, Figure 11-12, and Figure 11-13 for pattern ES-A, ES-B and ES-C respectively. As previously discussed, directionally-restricted spatter bloodstain samples were included within this research project to approximate the effect on estimate accuracy that may occur in the analysis of impact spatter patterns where the entire spatter bloodstain distribution is located to one side of the location of the pater-producing impact event. The directionally-restricted population estimate data generated for each of the three experimental impact patterns presents a relatively consistent pattern of the effects that the reliance of such spatter bloodstain data could have on the accuracy of estimate construction. The predominant effect on the estimate data appears to be evident in the horizontal plane of analysis. Whether a left or right directionally-restricted population is used to construct the estimate, the inter-quartile range, mean and mode of the trajectory intersection data sets in the x-axis demonstrate a shift away from the location of the impact site, back towards the target surface upon which the impact spatter patterns were observed. In the y-axis, movement in the inter-quartile range, mean and mode of the trajectory intersection data sets are also evident, although in this axis the direction of this movement is towards the direction in which the restricted spatter bloodstain distribution is located. While the change in the mean and mode of the horizontal trajectory intersection estimate data is not particular large for pattern ES-C, the differences in side-restricted estimates for pattern ES-A, and ES-B exhibit a more significant increase in error within both the x- and y-axes.

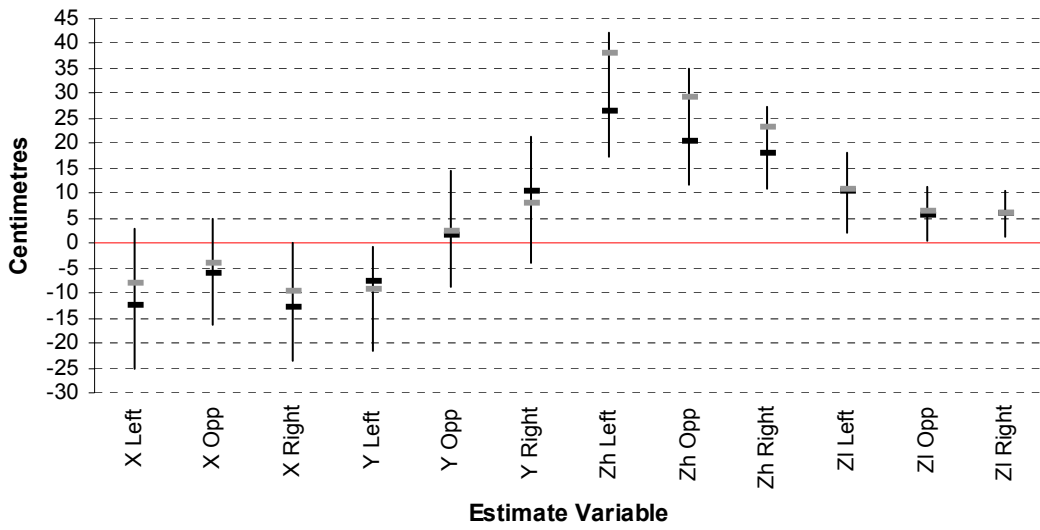


Figure 11-11 - The inter-quartile range (vertical bar), median (black horizontal bar), and mean (grey horizontal bar) of the error of the population estimates constructed for pattern ES-A using the left, right, and dual directional sub-populations.

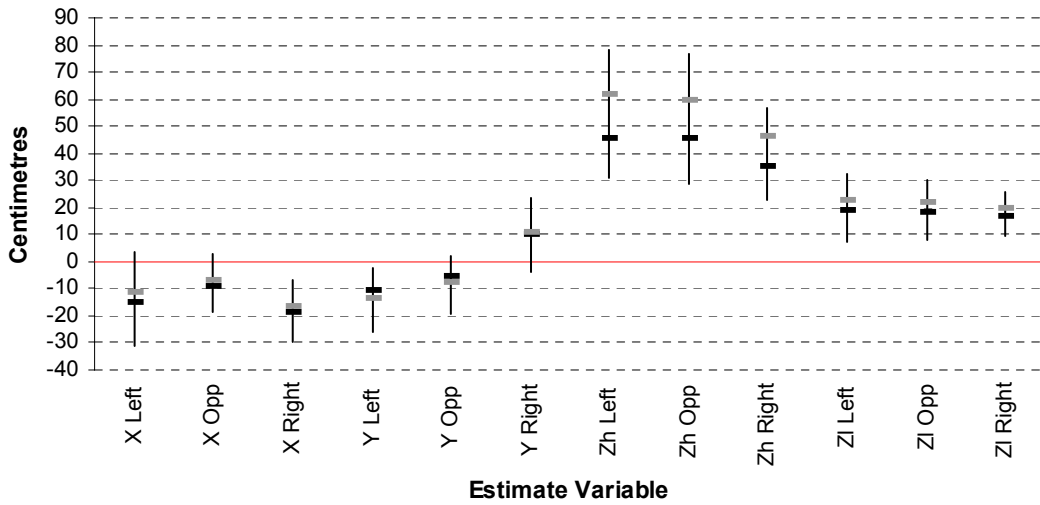


Figure 11-12 - The inter-quartile range (vertical bar), median (black horizontal bar), and mean (grey horizontal bar) of the error of the population estimates constructed for pattern ES-B using the left, right, and dual directional sub-populations.

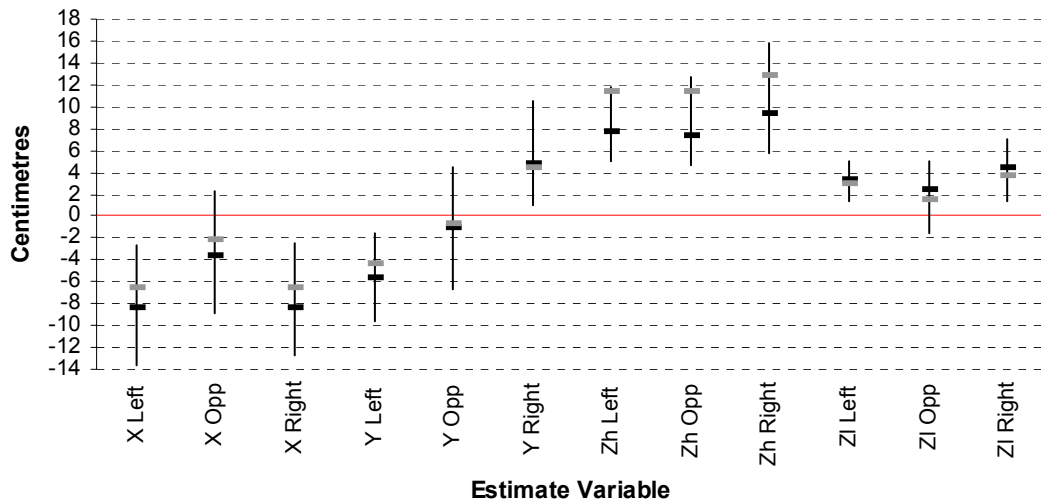


Figure 11-13 - The inter-quartile range (vertical bar), median (black horizontal bar), and mean (grey horizontal bar) of the error of the population estimates constructed for pattern ES-C using the left, right, and dual directional sub-populations.

The effects of the construction of the population estimates where the spatter bloodstain data is restricted to a single direction either side of the known impact site in the vertical target surface on the distribution of the trajectory intersection data set of the estimate is indicated in Figure 11-14. Where the spatter bloodstain distribution is situated to the left of the impact site the distribution of trajectory intersections is directionally skewed in the direction that the straight-line trajectory approximations of the majority of spatter bloodstains describe. Where the spatter bloodstains are situated to the left of the impact site, for example, the straight-line trajectories will tend to be orientated in a left to right direction, and, as a result, produce a trajectory intersection data set that is skewed in this direction. This directional variation in estimates constructed using the directionally-restricted impact pattern population data is also evident in the thinned trajectory intersection data set.

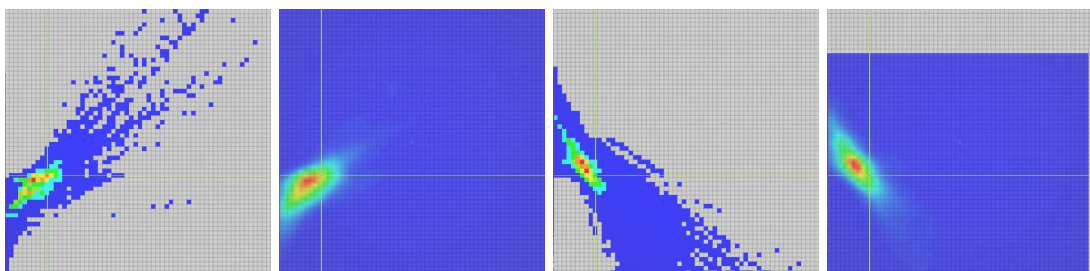


Figure 11-14 - The 3D histogram visualisations generated using the total trajectory intersection data set of spatter bloodstains from the left (far left and centre left) and the right (centre right and far right) subpopulations of pattern ES-A.

### 11.4.2 Multiple Sample Estimation

The multiple sample estimates generated during this research project for each of the three screened impact spatter pattern populations were produced to provide an assessment of the potential variation in sample-based estimates where the spatter bloodstain samples are selected randomly from an impact spatter pattern. This sampling strategy, and the estimate results generated from it are considered to represent a base level of sample-based estimate uncertainty, against which other more structured sampling strategies employed in attempts to select accurate spatter bloodstains for the construction of site of impact estimates could be compared.

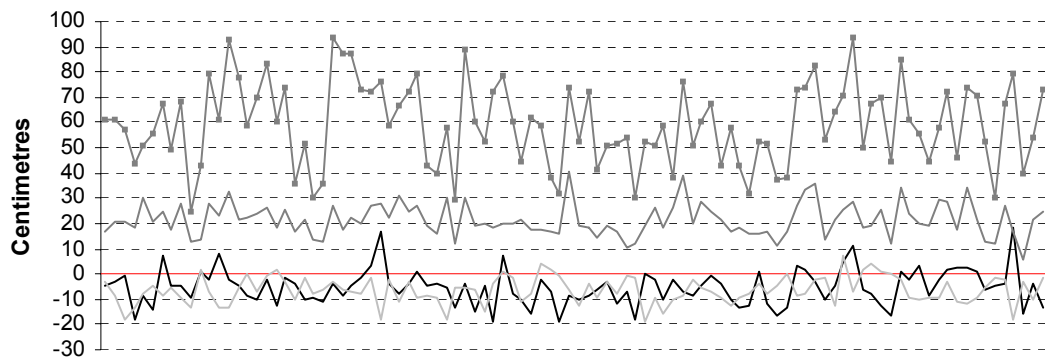


Figure 11-15 - The x (black line), y (light grey line), zI (dark grey line) and zh (dark grey line with squares) of total trajectory intersection mean site of impact estimate errors for the 100 samples of 10 spatter bloodstain selected randomly from pattern ES-B.

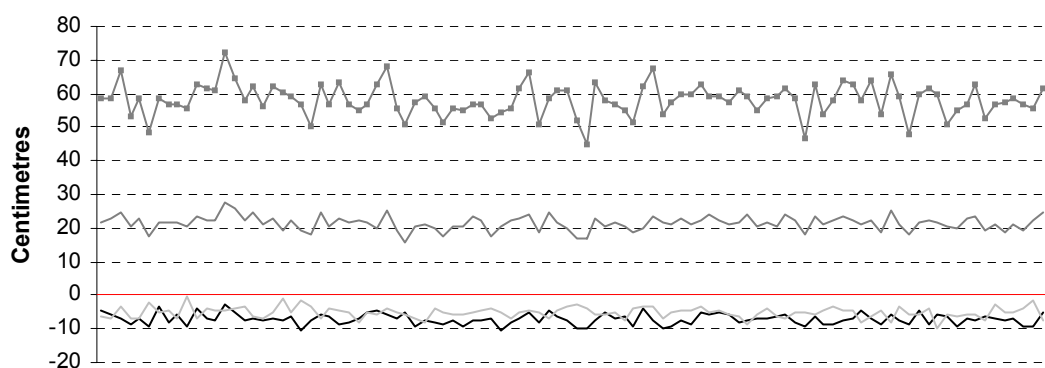


Figure 11-16 - The x (black line), y (light grey line), zI (dark grey line) and zh (dark grey line with squares) total trajectory intersection mean site of impact estimate errors for the 100 samples of 100 spatter bloodstains selected randomly from pattern ES-B.

Figure 11-15 and Figure 11-16 illustrate a series of results generated from the 100 site of impact estimates generated by the analytical site of impact estimation application using samples selected randomly from the total screened population of pattern ES-B with sample sizes of 10 and 100 spatter bloodstains respectively. As would be expected given sampling distribution theory, the multiple sample results exhibit a trend towards a decrease in estimate variation around the population estimate as the sample sizes considered increase. Within the two sample sizes, which represent the smallest and largest sample sizes investigated, the lower,  $p_{zl}$ , height estimate, as with the population estimate data, provides the more accurate height estimate for pattern ES-B. The upper,  $p_{zh}$ , not only provides the largest degree of error of any of the four estimate variables for pattern ES-B, but also appears to demonstrate the largest degree of variation between its individual estimates.

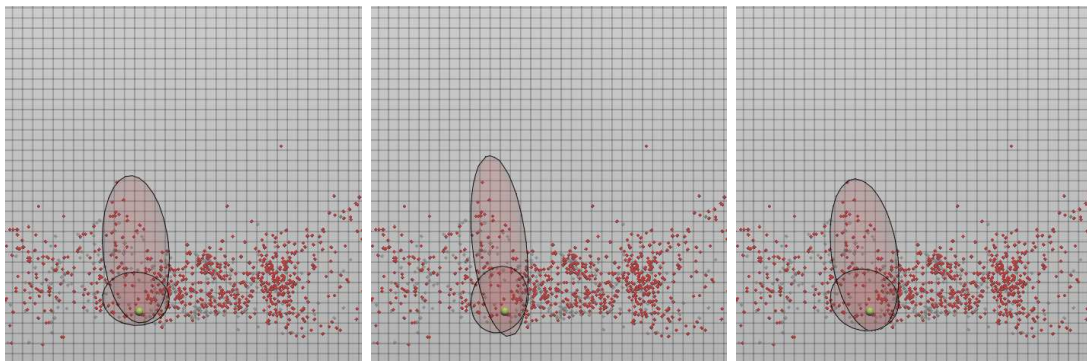


Figure 11-17 - The comparison of  $z_l$  (smallest) and  $z_h$  (largest) 95% confidence regions for the 100 mean estimate points of the total, opposite, and thinned trajectory intersection datasets for the samples of 10 bloodstains selected randomly from pattern ES-A.

The difference in the variation between the  $p_{zl}$  and  $p_{zh}$  height estimate variables for the 10-spatter sample size multiple sample estimate generated for pattern ES-A is illustrated in Figure 11-17. The 95 percent confidence ellipsoids generated for the multiple sample mean estimates for this pattern indicate that the upper estimate, which in population terms has a much lower error value than for pattern ES-B, can provide a reasonable height approximation for the impact site, with the confidence region encompassing the location of the known impact site. The extended nature and vertical orientation of this ellipsoidal region, however, demonstrates that a relatively large degree of variation exists between the individual estimates, and, as a result, any single sampled estimate generated using a random sample of 10 spatter bloodstains could also provide a  $p_{zh}$  with a positive estimate error of approximately 60 centimetres. The  $p_{zl}$  mean height



estimation data, in contrast, demonstrates a much smaller, and less vertically extended confidence ellipsoid, indicating the variation in height estimate data using this estimate variable is considerably smaller than the  $p_{zh}$  height estimates, even at this relatively small sample size.

A statistical description of the horizontal distance between the mean and median estimates generated for the 100 random sample estimates from pattern ES-B for samples sizes of 10 and 50 spatter bloodstains are shown in Figure 11-18 and Figure 11-19 respectively. The summary of the distribution of the horizontal accuracy of each of these the 100 sample estimates are illustrated for the total (MeanHD and MedHD), opposite (OMeanHD and OMedHD), and thinned (TMeanHD and TMedHD) trajectory intersection data sets constructed during the analysis of each individual estimate. This multiple sample data indicates that the use of the opposite and thinned trajectory intersection data sets in the construction of site of impact estimates, given the specific sampling strategy employed, do not provide any consistent improvement in the horizontal accuracy of the point-based statistical descriptions of the central tendency of an estimate distribution compared to the analysis of the total intersection data set. The application of alternative mean and mode methods of defining the central tendency of the distribution of the trajectory intersection data set of each individual estimate generated also appear to provide little consistent benefit in providing an accurate assessment of the location of a site of impact estimate.

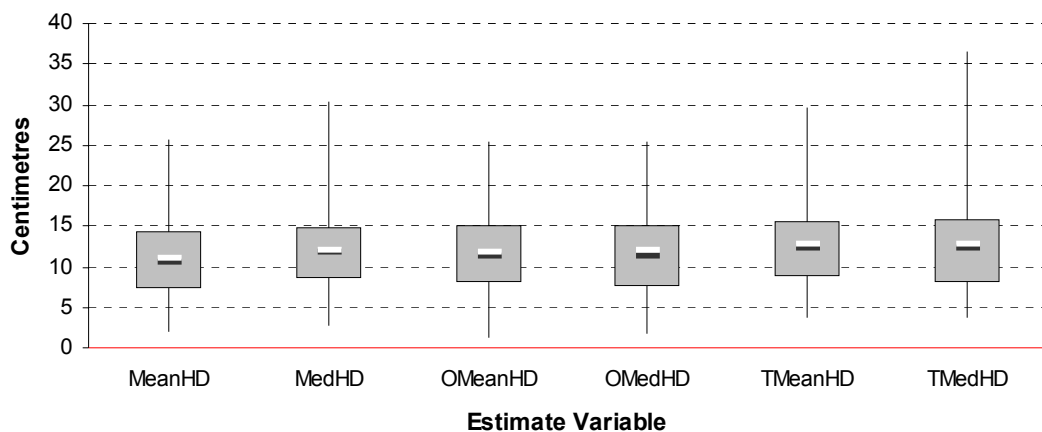


Figure 11-18 – The range, inter-quartile range, mean (white bar), and median (black bar) of the total horizontal estimate error of the mean and median site of impact estimates for the 100 samples of 10 spatter bloodstain selected randomly from pattern ES-B.

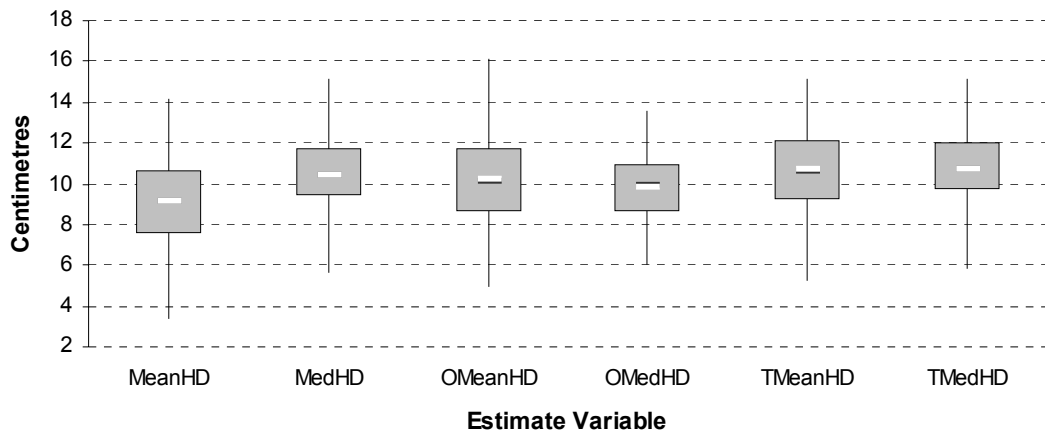


Figure 11-19 - The range, inter-quartile range, mean (white bar), and median (black bar) of the total horizontal estimate error of the mean and median site of impact estimates for the 100 samples of 50 spatter bloodstain selected randomly from pattern ES-B.

Given this apparent correspondence between the various methods employed in the construction, and the description of the central tendency of an estimate's intersection distribution for the multiple estimates generated for pattern ES-B, which exhibits the greatest degree of variation in data quality of the three experimental patterns, a more detailed assessment of the distribution of the accuracies of the mean of the total trajectory intersection data set of the 100 sample estimates generated for each of the four spatter bloodstain sample sizes for each impact spatter pattern are provided in Figure 11-20 to Figure 11-25.

The general indication from the distributions of this multiple sample estimate error data is that, even where spatter bloodstain selection with an dual directional definition of the total screened impact spatter pattern bloodstain population is completely random, the construction of sample-based site of impact estimates can provide a reasonable degree of accuracy. The application of even small sample sizes of 10 or 20 spatter bloodstains appear to demonstrate an ability to provide a high proportion of reasonably accurate horizontal and 3D estimates for both pattern ES-A, and EC-C. And although this ability is not necessarily surprising given the higher proportion of independently accurate straight-line trajectories within both of these patterns, what could be potentially significant for site of impact estimation is that the mechanics of the estimation process appear to produce larger proportions of sample estimates with a high degree of accuracy than the proportions of spatter bloodstains within these patterns that achieve high independent data assessments (see Figure 11-1 and Figure 11-2). The multiple random samples of pattern ES-B, however, do not demonstrate the same

degree of accuracy as the other two patterns. The horizontal accuracy of these estimates still provides reasonably high proportions of sample estimate accuracy, albeit with increases error levels and large sample sizes. The 3D estimate accuracy, however, as indicated by both the independent data quality assessment and the results of the total population site of impact estimate, appears to be relatively poor.

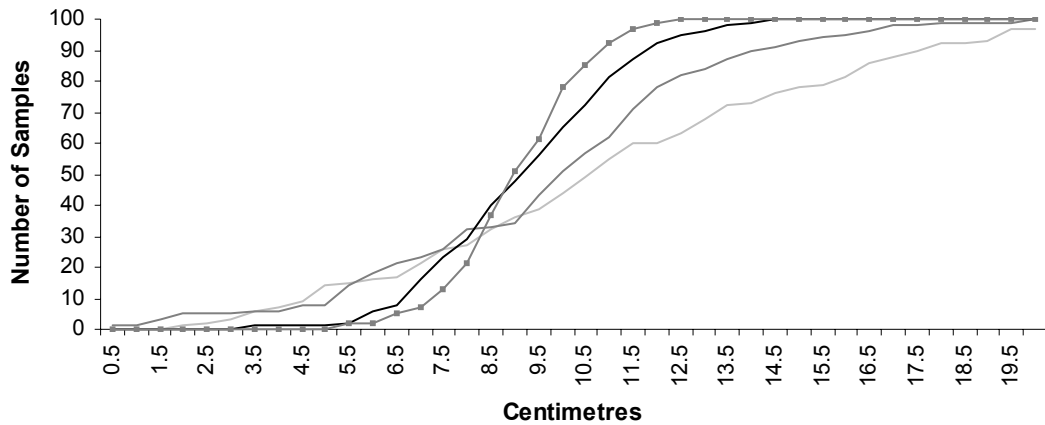


Figure 11-20 – The number of samples selected randomly from pattern ES-B that achieve a given level of mean estimate horizontal error. Sample size of 10, 20, 50, and 100 are represented by the light grey, dark grey, black, and dark grey with squares lines respectively.

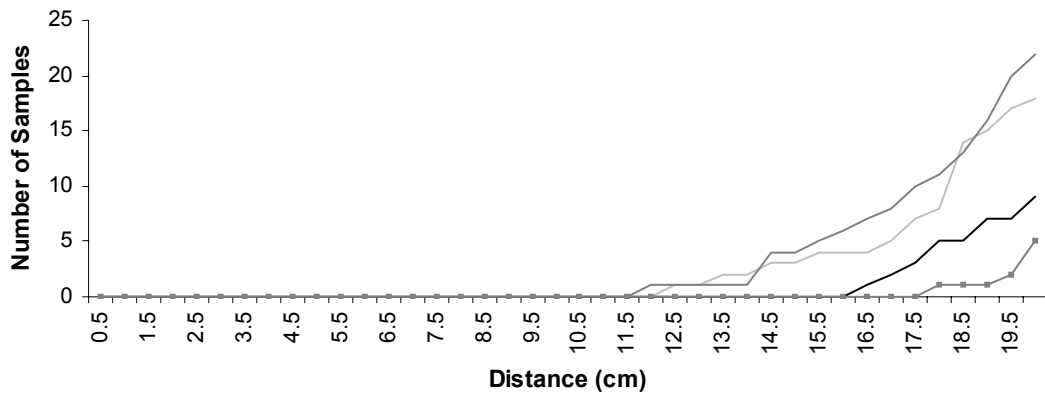


Figure 11-21 - The number of samples selected randomly from pattern ES-B that achieve a given level of mean estimate 3D error. Sample size of 10, 20, 50, and 100 are represented by the light grey, dark grey, black, and dark grey with squares lines respectively.

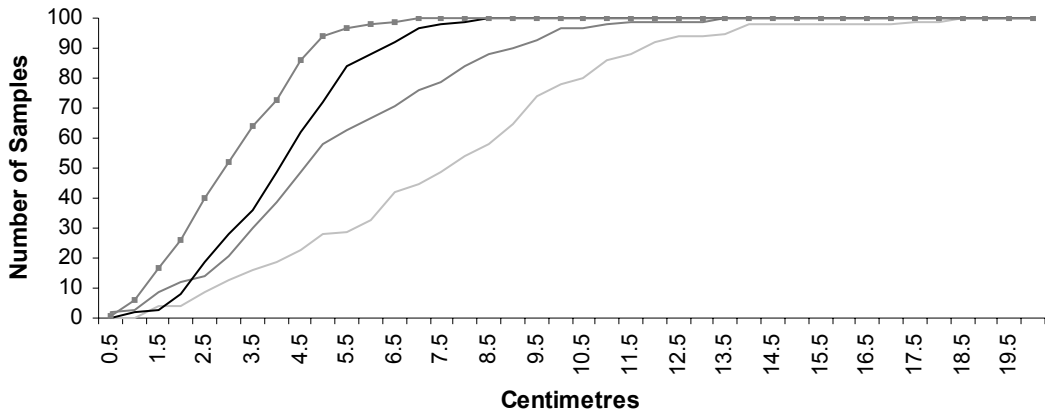


Figure 11-22 – The number of samples selected randomly from pattern ES-A that achieve a given level of mean estimate horizontal error. Sample size of 10, 20, 50, and 100 are represented by the light grey, dark grey, black, and dark grey with squares lines respectively.

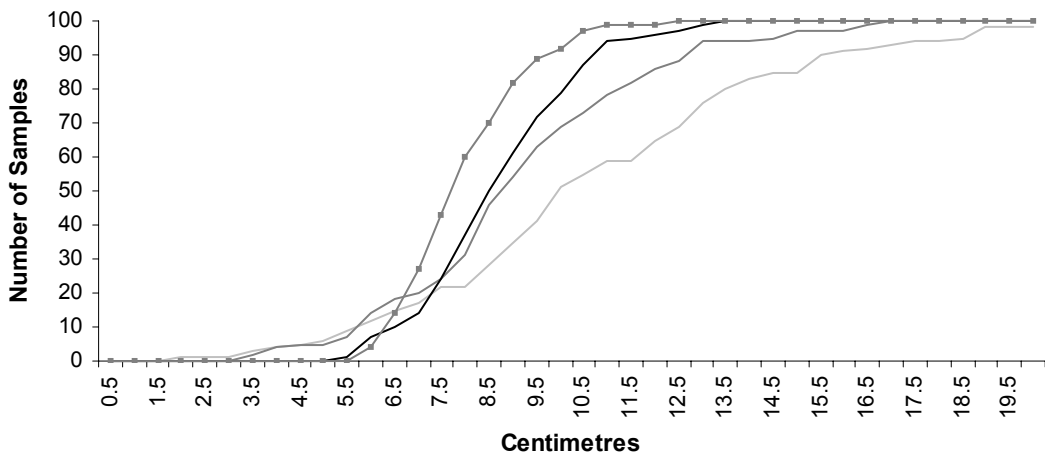


Figure 11-23 – The number of samples selected randomly from pattern ES-A that achieve a given level of mean estimate 3D error. Sample size of 10, 20, 50, and 100 are represented by the light grey, dark grey, black, and dark grey with squares lines respectively.

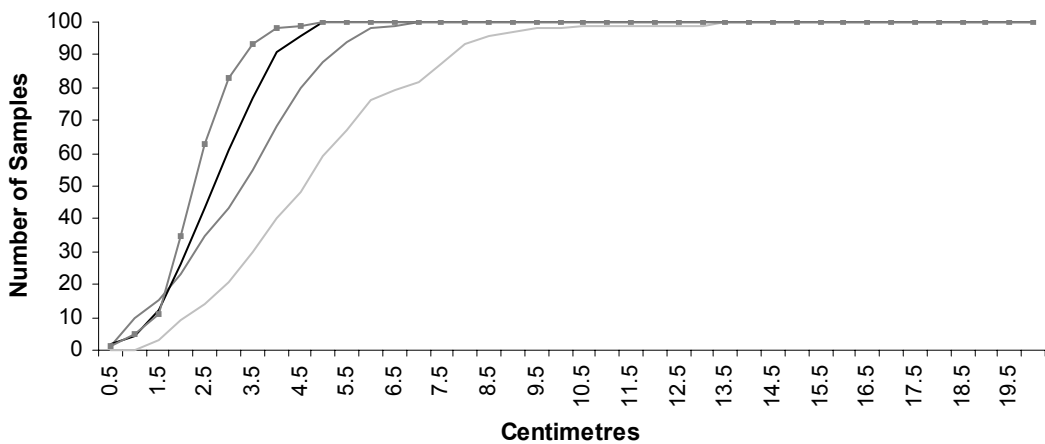


Figure 11-24 – The number of samples selected randomly from t pattern ES-C that achieve a given level of mean estimate horizontal error. Sample size of 10, 20, 50, and 100 are represented by the light grey, dark grey, black, and dark grey with squares lines respectively.

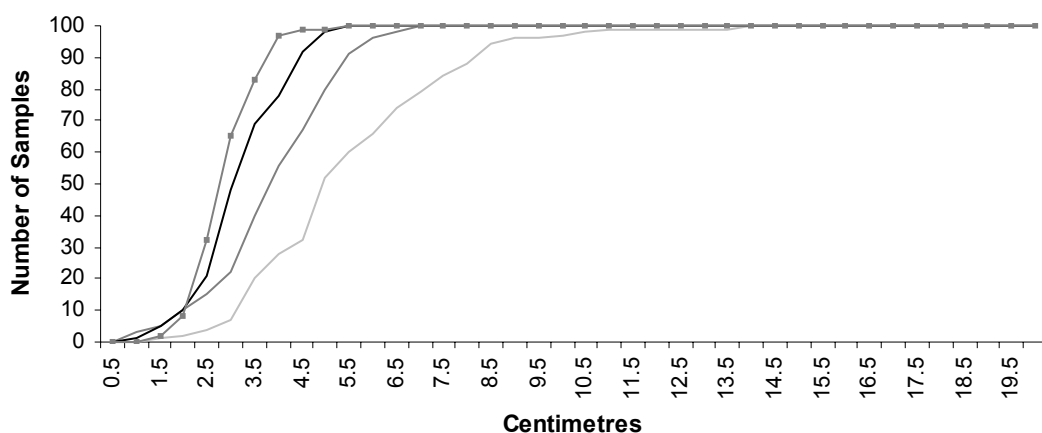


Figure 11-25 - The number of samples selected randomly from pattern ES-C that achieve a given level of mean estimate 3D error. Sample size of 10, 20, 50, and 100 are represented by the light grey, dark grey, black, and dark grey with squares lines respectively.

The effect on the construction of the multiple sample estimates where the spatter bloodstain data is restricted to a single direction either side of the known impact site is illustrated in Figure 11-26, Figure 11-27, and Figure 11-28. The information depicted consists of the multiple sample estimate data generated for pattern ES-A with a sample size of 10 spatter bloodstains for the dual directional, left, and right directionally-restricted versions of the population data respectively. The data produced from this multiple sample analysis, as expected, reflects the results obtained in the side-restricted single population estimates already described.

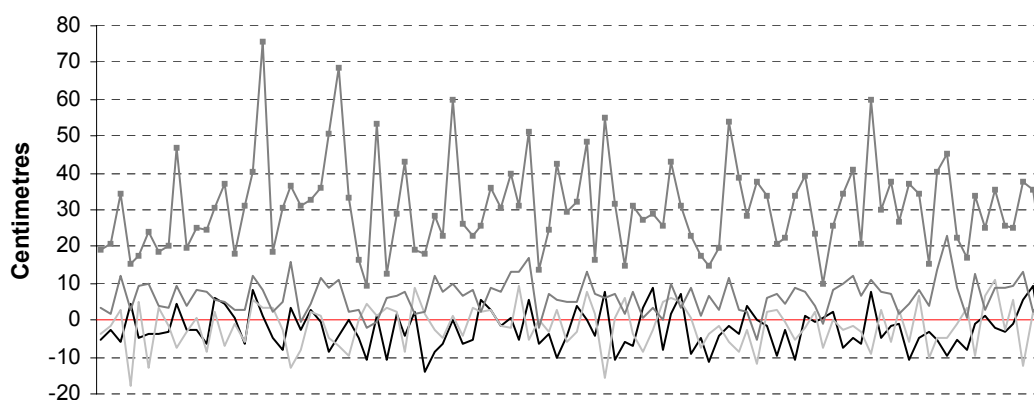


Figure 11-26 - The x (black line), y (light grey line), zl (dark grey line) and zh (dark grey line with squares) total trajectory intersection mean site of impact estimate errors for the 100 samples of pattern ES-A with a sample size of 10 taken randomly from the dual directional sub-populations.

The accuracy of the x-axis estimates in both the left- and right-restricted populations decreases, representing a movement towards the plane of the target surface. In the y-axis, the multiple sample estimates generated gravitate towards the direction in which the spatter bloodstain population is restricted, moving away from the more accurate central estimates generated in the analysis of the dual directional version of the spatter bloodstain population. The height estimates produced from this multiple estimate data also appear to be affected by the directional restriction of the spatter bloodstain population of pattern ES-A, although this factor is likely a product of the distribution of accurate spatter bloodstains within the pattern itself, as illustrated in Figure 11-29.

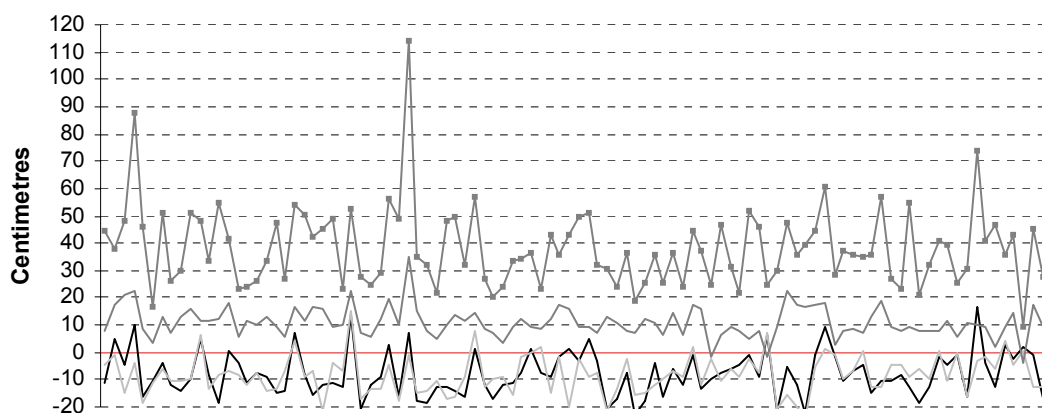


Figure 11-27 - The x (black line), y (light grey line), z1 (dark grey line) and zh (dark grey line with squares) total trajectory intersection mean site of impact estimate errors for the 100 samples of pattern ES-A with a sample size of 10 taken randomly from the left sub-population.

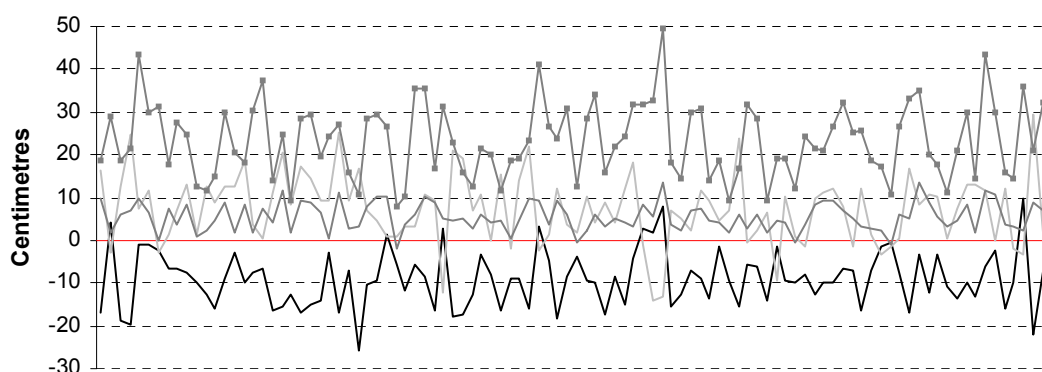


Figure 11-28 The x (black line), y (light grey line), z1 (dark grey line) and zh (dark grey line with squares) total trajectory intersection mean site of impact estimate errors for the 100 samples of pattern ES-A with a sample size of 10 taken randomly from the right sub-population.

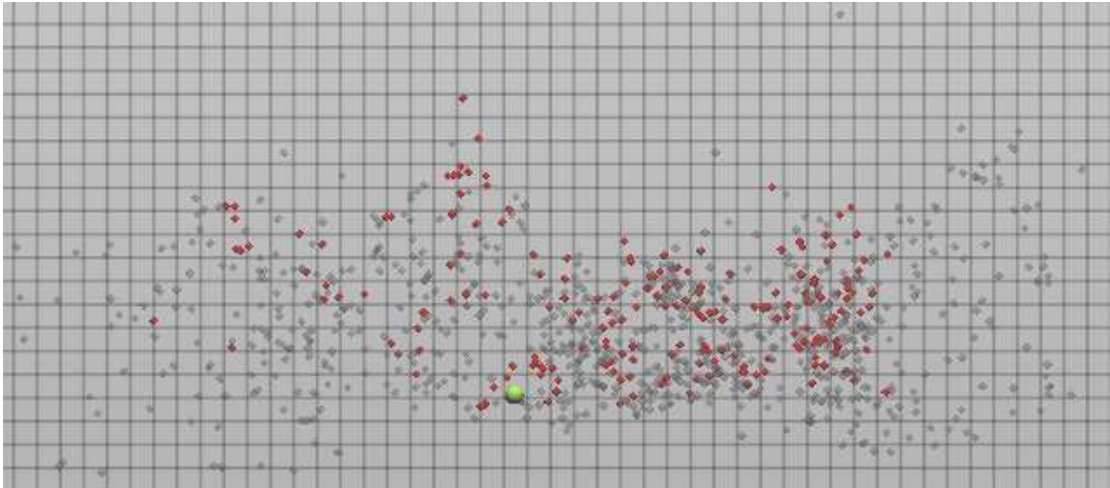


Figure 11-29 - The locations of the spatter bloodstains within the selected 10-centimetre data quality group in relation to the known impact site, and other spatter bloodstains in the target surface of pattern ES-A.

The effects of this side-restricted distribution of the spatter bloodstain data used in the construction of the multiple samples estimates can be seen in Figure 11-30, which illustrates the ellipsoidal confidence regions calculated for this multiple sample estimate data in the horizontal plane. Where the full distribution is made available for analysis the confidence regions exhibit a near circular shape, which is approximately centred on the known location of the impact site. Where the spatter bloodstain distributions are restricted to a single side of the known location of the impact site the confidence regions form accentuated elliptical shapes, which are orientated relative to the direction of the distribution of spatter bloodstains.

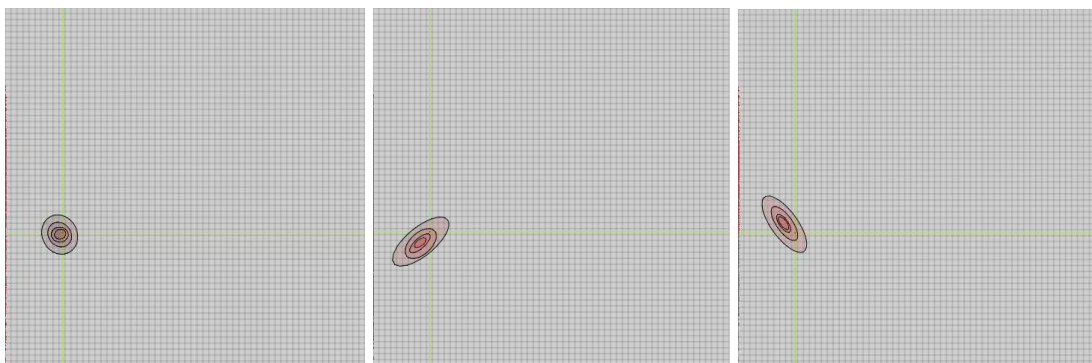


Figure 11-30 - The top viewpoint visualisations of the 95% 3D confidence regions for the mean estimate of the total trajectory intersection data set at sample sizes of 10, 20, 50, and 100 selected randomly from the dual directional (left), left (centre), and right (right) sub-populations of pattern ES-A.

A left-to-right orientation relative to the plane of the target surface is exhibited where the spatter distribution is restricted to the left of the impact site, and a right-to-left orientation is present where the spatter distribution is restricted to the right of the impact site. The movement in the mean of the sampling distribution is also indicated by the shift in the centre of these ellipses in the direction of the spatter bloodstain distributions, and towards the target surface. This same pattern is replicated in the thinned trajectory data sets generated for each estimate by the analytical site of impact estimation application. The opposite trajectory intersection data set, given the single-sided distribution of the impact spatter pattern, cannot be formed.

### **11.5 3D Data Quality Sub-Population Analysis**

This section will describe and discuss the results obtained from the analysis of the collection of spatter bloodstains within each of the three screened impact spatter pattern bloodstain populations whose 3D independent data quality assessments correspond to a level of 10 centimetres or less. Three aspects of the investigation of this specific spatter bloodstain sub-population will be addressed. Firstly, the composition of each of the samples selected from the impact spatter pattern bloodstain populations with respect to a number of spatter bloodstain variables will be examined. Secondly, the results of the single sample site of impact estimates generated using the entire spatter bloodstains sub-populations identified for each impact spatter pattern will be evaluated. Finally, the multiple sample estimates generated from this potentially accurate site of impact estimation spatter bloodstain data will be discussed.

#### **11.5.1 Sub-population Composition**

The combination of the total pattern enumeration methodology employed during this research project, and the independent data quality assessment and spatter bloodstain collection characterisation functionality included within the analytical site of impact estimation application makes available a considerable amount of information for the evaluation and comparison of any particular collection of experimentally generated spatter bloodstains. In terms of the analysis of the composition of the sub-populations within each of the three screened experimental impact spatter patterns that correspond to a 3D independent data



quality of 10 centimetres or less (referred to hereafter as 3D data quality sub-populations), the investigative opportunity is provided to compare the distributions of spatter bloodstain variables of empirically established accurate collections of spatter bloodstains to practical and theoretical spatter bloodstain selection criteria, which are often employed in site of impact estimate in an attempt to both provide, and accurately interpret, reliable estimate data from within an observed impact spatter pattern. The composition of the empirical 3D data quality sub-populations identified during the analysis of the three experimental impact spatter patterns is present in terms of three specific spatter bloodstain variables:

- The vertical angle of the straight-line trajectory approximation.
- The width-to-length ratio of the spatter bloodstains
- The minimum 3D flight distance of the spatter-causing droplet.

Each of these variables have been highlighted in the discussion of site of impact estimation theory and methodology as having a utility in the selection of spatter bloodstains in constructing accurate and/or appropriate site of impact estimates (see Chapter 4). To facilitate the investigation of the distributions of these variables, the composition data generated during the analysis of the total screened spatter bloodstain populations, and the relative relationships between these source populations and the empirically derived 3D data quality spatter bloodstain sub-populations are provided for comparison.

An initial comparison of the numbers and ratios of spatter bloodstain within each of the screened experimental spatter bloodstain populations and their respective 3D data quality sub-populations, as shown in Table 11-4, demonstrates a considerable degree of variation between the three impact spatter patterns which could well be reflected in other areas of the composition of the 3D data quality sub-populations. While a firm independent variable cannot be suggested as the cause of this variation, due to the relatively uncontrolled experimental impact spatter pattern generation procedure employed during this research project, both the total number and relative ratios of 3D data quality spatter bloodstain within each of the impact spatter patterns do seem to correspond inversely to the perpendicular impact site-target surface distances set for each of the three patterns during their creation (see Section 5.2.4).

Pattern	Number of Screened Bloodstains	Number of 3D Quality $\leq 10$ Centimetres	Ratio
ES-A	746	196	0.26
ES-B	343	39	0.11
ES-C	661	423	0.64

Table 11-4 - The number and ratio of spatter bloodstain within each experimental impact spatter pattern that correspond to a 3D data quality assessment of 10 centimetres or less.

### 11.5.1.1 Vertical Angle

The composition of the 3D data quality sub-populations identified within the screened experimental impact spatter patterns ES-A, ES-B, and ES-C, in terms of the vertical angle of the straight-line trajectory approximations constructed for each spatter bloodstain, are illustrated in Figure 11-31, Figure 11-32, and Figure 11-33 respectively.

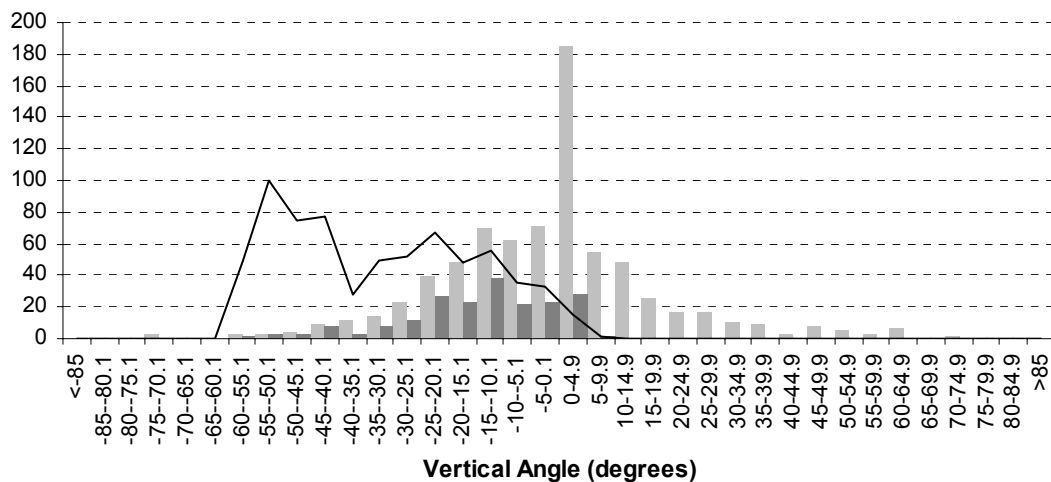


Figure 11-31 - The vertical straight-line trajectory angle of pattern ES-A. The total number (light grey bars), the number with the selected 10-centimetre 3D data quality grouping (dark grey bars), and the percentage of selected bloodstains (black line) are shown.

Each of the three 3D data quality sub-populations identified for the screened experimental impact spatter patterns demonstrate distributions of vertical trajectory angles that are almost exclusively restricted to downward elevations. These downward elevations correspond to spatter-producing droplets, which have an upward moving trajectory on contact with the target surface, and, as a result, provide a degree of empirical support for the theoretical principles of straight-line

trajectory theory in relation to site of impact height estimation (see Section 2.5.3).

The distributions of the vertical trajectory angles for both the total and sub-populations also seem to reflect the distances between the locations of the pattern-producing impact events and their respective recording target surfaces. The relative proportions of upward vertical trajectory angles within each total population appear to decrease as the distance between the impact site and target surface of the three impact patterns is reduced. Pattern ES-B, which has the greatest impact site-target surface distance of the three patterns, demonstrates the largest proportion of these upward vertical angle elevations. This is followed by patterns ES-A and ES-C respectively, which were created using increasingly smaller impact site-target surface distances. This increase in upward vertical angle proportionality with greater impact site-target surface distances is likely to be the result of the occurrence of curvature in the flight path of a spatter-producing blood droplet as the flight distance and potential flight time increases. Such an interpretation must be made cautiously, however, as the unknown variable of droplet velocity and any variation in this variable between the three impact events, where present, could also be influential in producing similar distributions.

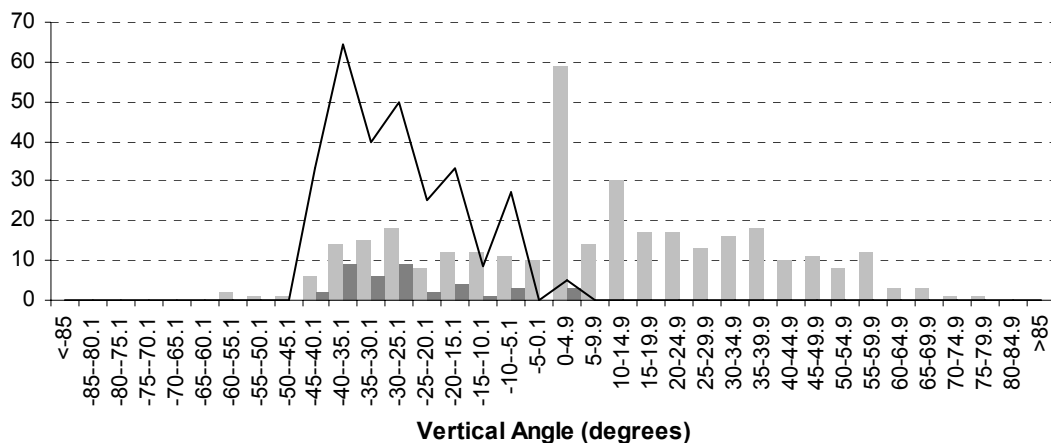


Figure 11-32 - The vertical straight-line trajectory angle of pattern ES-B. The total number (light grey bars), the number with the selected 10-centimetre 3D data quality grouping (dark grey bars), and the percentage of selected bloodstains (black line) are shown.

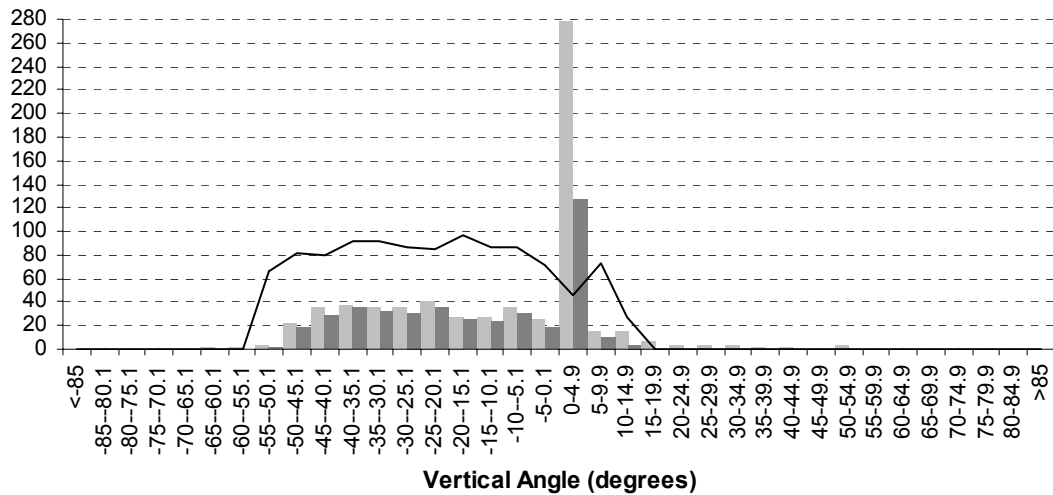


Figure 11-33 - The vertical straight-line trajectory angle of pattern ES-C. The total number (light grey bars), the number with the selected 10-centimetre 3D data quality grouping (dark grey bars), and the percentage of selected bloodstains (black line) are shown.

### 11.5.1.2 Width-to-Length Ratio

The composition of each of the three 3D data quality sub-populations in relation to the width-to-length ratios established for their constituent spatter bloodstains are demonstrated in Figure 11-34, Figure 11-35, and Figure 11-36.

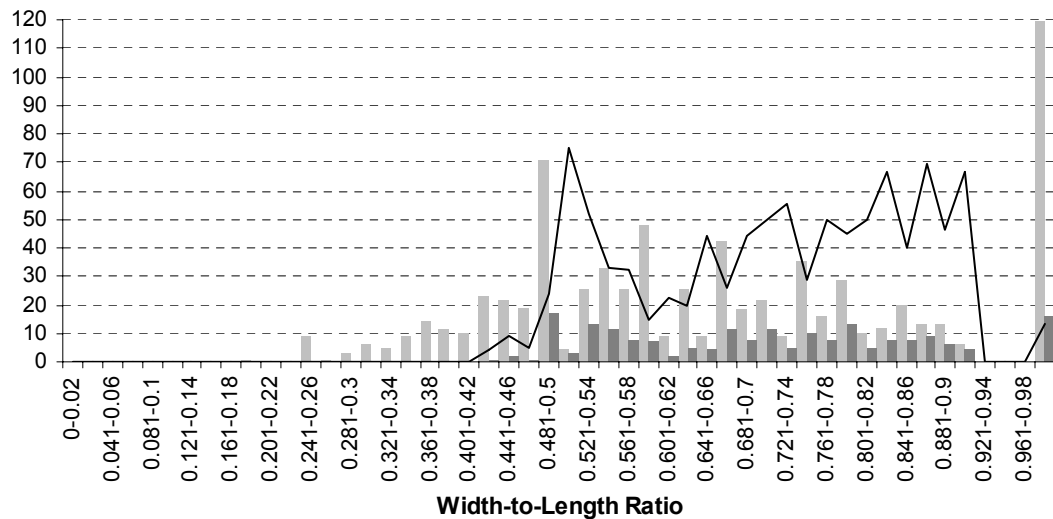


Figure 11-34 - The width-to-length ratios of pattern ES-A. The total number (light grey bars), the number with the selected 10-centimetre 3D data quality grouping (dark grey bars), and the percentage of selected bloodstains (black line) are shown.

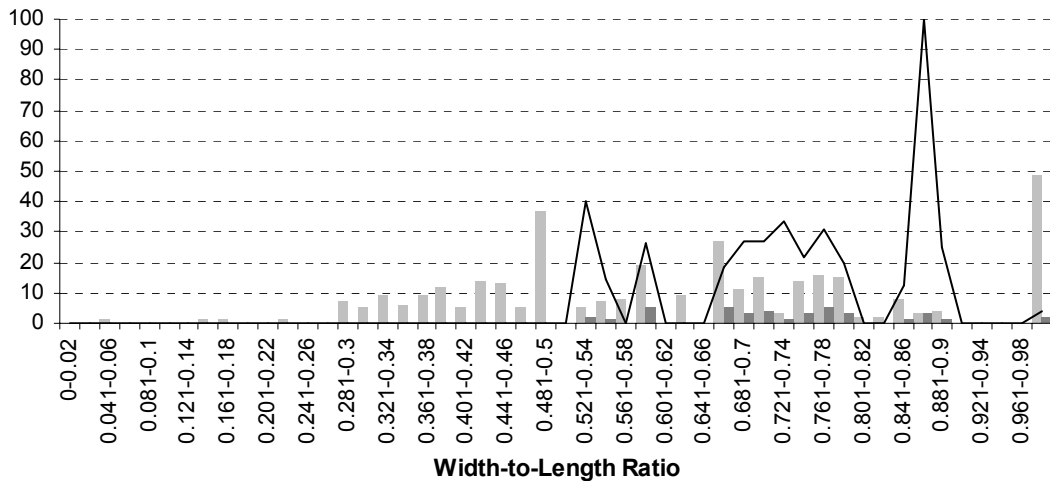


Figure 11-35 - The width-to-length ratios of pattern ES-B. The total number (light grey bars), the number with the selected 10-centimetre 3D data quality grouping (dark grey bars), and the percentage of selected bloodstains (black line) are shown.

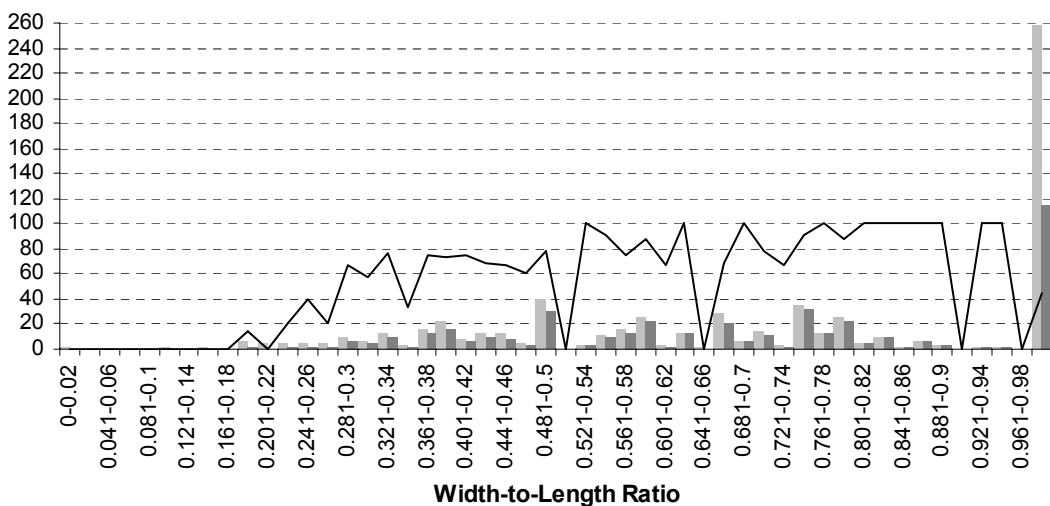


Figure 11-36 - The width-to-length ratios of pattern ES-C. The total number (light grey bars), the number with the selected 10-centimetre 3D data quality grouping (dark grey bars), and the percentage of selected bloodstains (black line) are shown.

The distribution of the width-to-length ratios of the spatter bloodstains the 3D data quality sub-populations for three experimental impact spatter patterns appear to demonstrate two distinct relationships. Both patterns ES-A, and ES-B, despite a considerable difference in the percentages of spatter bloodstains within each category, have sub-population distributions made up predominantly of spatter bloodstains with width-to-length ratios of between approximately 0.5 and 0.9. As a result, the majority of spatter bloodstains with these two sub-populations exhibit impact angles ranging from approximately 30 to 64 degrees.

The 3D data quality sub-population of pattern ES-C, in contrast, demonstrates a relatively high proportion of spatter bloodstain across a range of width-to-length ratios of between approximately 0.24 and 0.96, corresponding to impact angles of between 14 and 73 degrees. While both of these width-to-length distributional relationships display some degree of correspondence to suggested selection criteria for spatter bloodstains based on width-to-length configurations (see Chapter 4), both also include impact angles not commonly associated with providing accurate site of impact estimation data. The 3D data quality sub-populations of both pattern ES-A and ES-B contain spatter bloodstains with impact angles of above the postulated accurate range of 20 to 45 degrees, while the sub-population of pattern ES-C includes angles both above and below this range (Reynolds, 2004a; Willis et al., 2001). The comparison of the empirical width-to-length ratio distributions to such ideal ranges, however, is not necessarily straightforward. The suggestions made for the selection of spatter bloodstain for purposes of site of impact estimation based on width-to-length ratios are generally concerned with the ability to accurately interpret and quantify the morphology of spatter bloodstains, as well as avoid any potential increases in error through the sine-based calculation procedure (Willis et al., 2001; Wonder, 2001; Reynolds, 2004a). The composition of the empirical 3D data quality sub-populations does not provide any evidence to suggest that this variability in spatter measurement and impact angle calculation is not present in the spatter bloodstain with impact angles that fall outside of this range. The results of this analysis do appear to suggest, however, that some practical utility may be achievable using spatter bloodstain that exhibit less acute impact angles than generally deemed acceptable.

### **11.5.1.3 Minimum Droplet Flight Distance**

The distribution of the minimum blood droplet flight distances of the spatter bloodstain within the three 3D data quality sub-populations, which are approximated using the 3D straight-line distance between the location of the known impact site and each spatter bloodstain within the 3D investigational environment, is illustrated for pattern ES-A, ES-B and ES-C in Figure 11-37, Figure 11-38, and Figure 11-39 respectively.

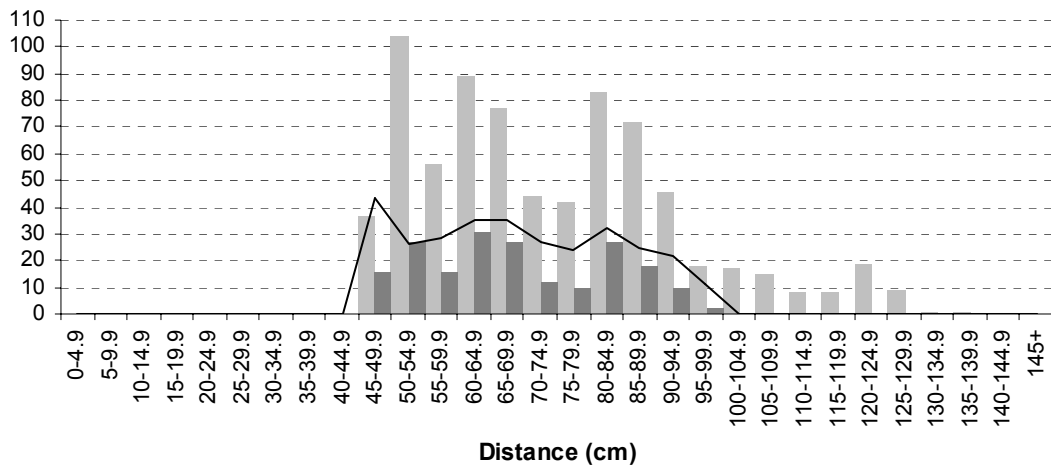


Figure 11-37 - The minimum 3D flight distances of pattern ES-A. The total number (light grey bars), the number with the selected 10-centimetre 3D data quality grouping (dark grey bars), and the percentage of selected bloodstains (black line) are shown.

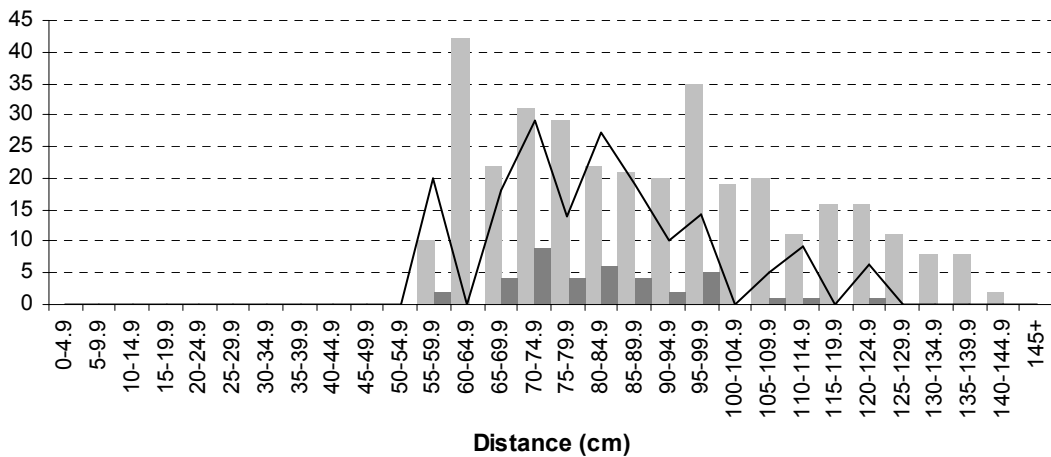


Figure 11-38 - The minimum 3D flight distances of pattern ES-B. The total number (light grey bars), the number with the selected 10-centimetre 3D data quality grouping (dark grey bars), and the percentage of selected bloodstains (black line) are shown.

The distribution of minimum calculated flight distances for each spatter bloodstain within the 3D data quality sub-populations established for patterns ES-A, ES-B, and ES-C exhibit a concentration of lower values relative to their shortest possible flight distance (the perpendicular impact site-target surface distance). The larger flight distance values for each distribution appear to be either under represented, such as in pattern ES-B, or totally absent, as in patterns ES-A and ES-C, with the predominant proportion of each distribution situated within 50 centimetres of their specific smallest possible minimum flight distance. These distributions, in conjunction with the total proportions of spatter bloodstain within the three 3D data quality sub-populations reinforce the suggestion that the general quality of

the spatter bloodstain data within the three experimental impact spatter patterns are directly related to their impact site-target surface distance. While any consistent difference in droplet velocity between the impact spatter patterns can still not be ruled out as an influencing factor within these results, the general correspondence between different variable distributions and the common hammer-strike pattern-producing impact event employed in each case would suggest that the likelihood of this scenario is diminished.

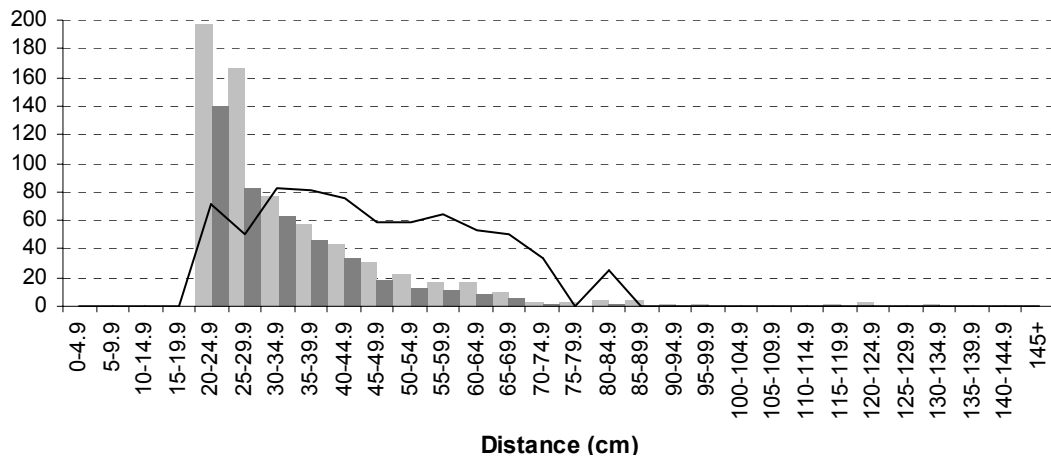


Figure 11-39 - The minimum 3D flight distances of pattern ES-C. The total number (light grey bars), the number with the selected 10-centimetre 3D data quality grouping (dark grey bars), and the percentage of selected bloodstains (black line) are shown.

### 11.5.2 Single Sample Estimation

As with the construction of the single population estimates for the screened impact spatter pattern population data, the generation of a single sample estimate for the complete 10 centimetre 3D independent data quality samples selected from each of the three experimental impact spatter patterns provide two main investigative directions for the analysis of estimate uncertainty. Firstly, the construction of a single sample estimate utilising the complete data quality samples will provide a means of assessing the utility of a total estimate methodology where an accurate spatter bloodstain sample can be selected, as well as indicate the potential variation that exists in this approach to site of impact estimation. Secondly, the data produced from the construction of these single sample high data quality estimates will provide an indication of the estimate parameters around which the descriptive statistics generated for the



repeated multiple sample estimates constructed using this sampling strategy will be distributed.

Figure 11-40, Figure 11-41, and Figure 11-42 illustrate the inter-quartile ranges, means and medians of the trajectory intersection distributions generated during the construction of the single sample estimates using the 3D independent data quality samples selected from each of the three screened experimental impact spatter patterns. The statistical descriptions of the 3D data quality sample estimates demonstrate a relatively high degree of estimate accuracy, as would be expected from the sampling strategy employed. A number of the trends observed in the total population estimate data are also reflected in the results of these single sample estimates. The  $p_{zh}$  height estimate variable, for example, consistently demonstrates the poorest of the two height estimates, although for these estimates the difference is not as pronounced as when a total population is considered. There also does not appear to be any consistent improvement in estimate accuracy through the consideration of the opposite and thinned trajectory intersection data sets, with the exception of some small decrease in the size of the opposite intersections inter-quartile ranges.

The largest degree of estimate error in the horizontal plane, as in the case of the total population estimates, appears to be in the  $p_x$  variable. This degree of error, however, is more consistent within the results of the estimates of the 3D data quality sub-populations, and is further highlighted by the fact that that  $p_{zi}$  height estimate demonstrates a much reduced level of estimate error, meaning that in the majority of cases the  $p_x$  variable could contribute the greatest proportion of error to a 3D site of impact estimate. A degree of error in the interpretation of the morphology of a number of the spatter bloodstains within the 3D data quality sub-populations of each impact spatter pattern, however, is indicated by these estimate results. The distribution of the lower,  $p_{zi}$ , height estimate data demonstrates that a proportion of the distribution of observations within this estimate variable is situated below the known height of the pattern-producing impact events. Given the principles of straight-line trajectory theory (see Section 2.5.3), the presence of trajectory approximations that pass below the known height of their origin are only possible where some error is introduced in the interpretation of spatter bloodstain morphology, and, consequently, the construction of its associated straight-line trajectory approximation.

An additional interesting feature of the results of the single sample estimates for the 3D quality data sub-populations selected from the screened experimental impact spatter patterns is that, although slight improvements are noted for the estimates in pattern ES-A and ES-C, these do not appear to be particularly significant given the level of accuracy demonstrated in the total population estimates, especially in the horizontal plane of analysis. However, for pattern ES-B, which was created with the largest impact site-target surface distance and demonstrates the lowest proportions of accurate 3D independent data quality assessments, the selection and analysis of the 3D data quality sub-population does provide a considerable increase in estimate accuracy, especially in terms of the vertical variables, and to a lesser extent in the horizontal plane of analysis.

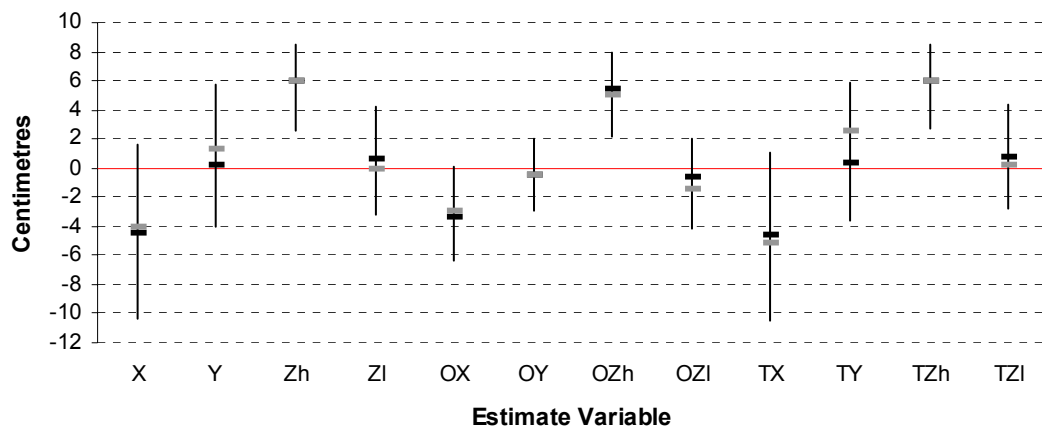


Figure 11-40 – The inter-quartile range (vertical bar), median (black horizontal bar), and mean (grey horizontal bar) of the error of the total sample estimate constructed for pattern ES-A from the 3D data quality sub-populations.

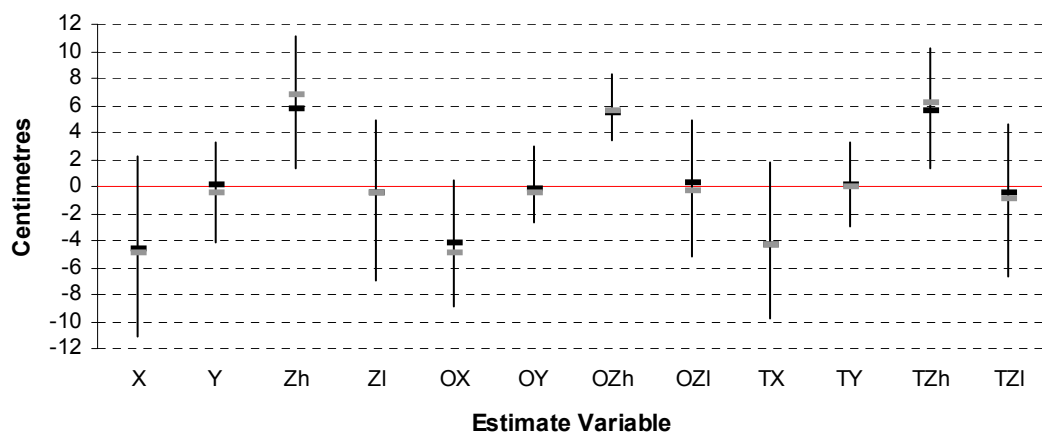


Figure 11-41 – The inter-quartile range (vertical bar), median (black horizontal bar), and mean (grey horizontal bar) of the error of the total sample estimate constructed for pattern ES-B from the 3D data quality sub-populations.

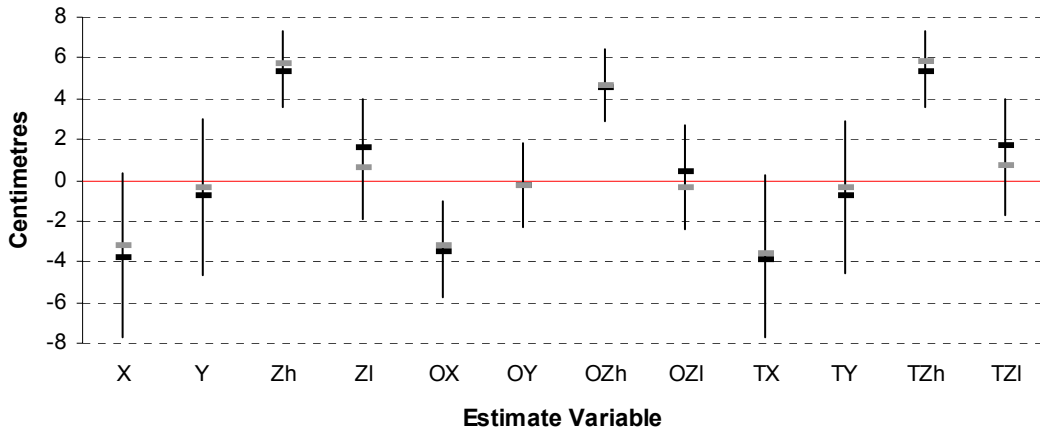


Figure 11-42 - The inter-quartile range (vertical bar), median (black horizontal bar), and mean (grey horizontal bar) of the error of the total sample estimate constructed for pattern ES-C from the 3D data quality sub-population.

The effect of the directionally-restricted spatter bloodstain populations on the total 3D data quality estimates for each of the three screened experimental impact spatter patterns are illustrated in Figure 11-43, Figure 11-44, and Figure 11-45. The same relationship that was demonstrated in the results of the total population estimates also appears to be present in the 3D data quality estimates for pattern ES-A and ES-C.

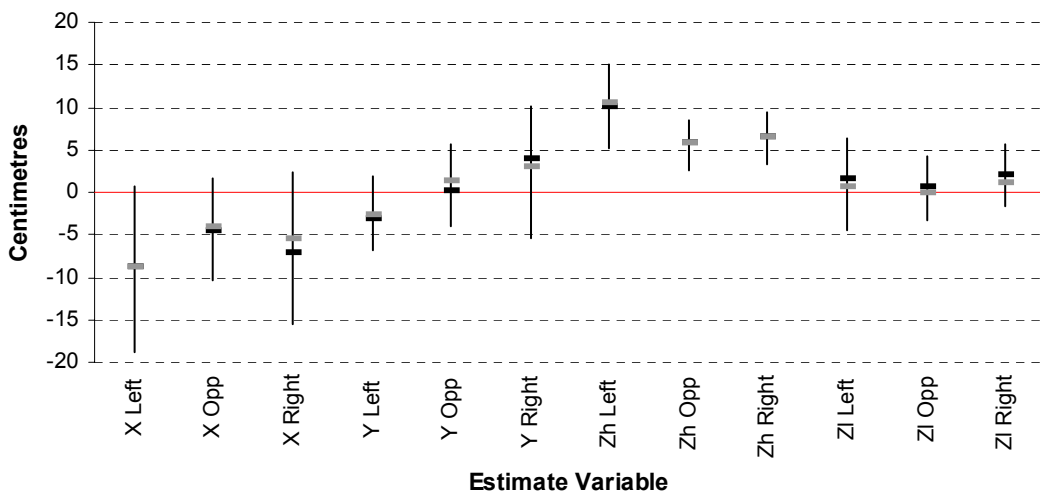


Figure 11-43 - The inter-quartile range (vertical bar), median (black horizontal bar), and mean (grey horizontal bar) of the error of the total sample estimate constructed for pattern ES-A using the left, right, and dual directional 3D data quality sub-populations.

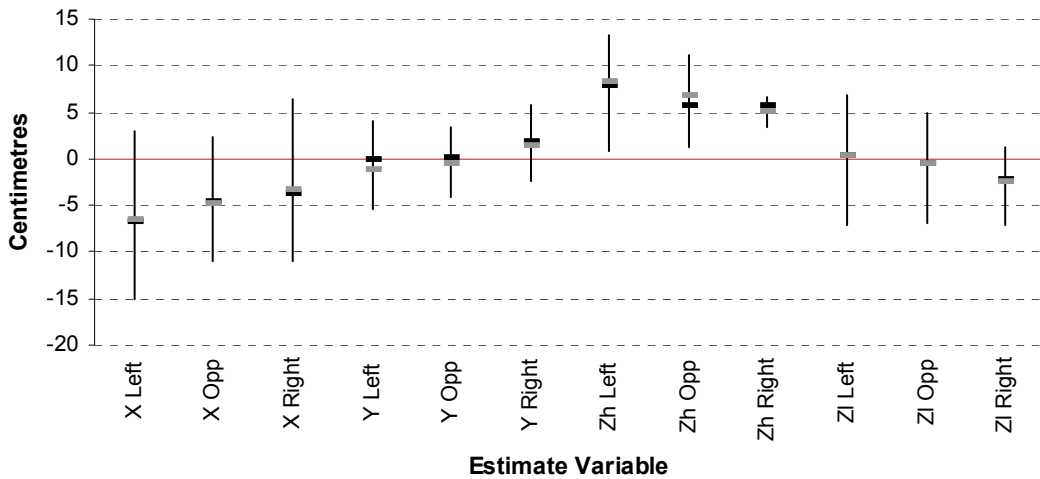


Figure 11-44 - The inter-quartile range (vertical bar), median (black horizontal bar), and mean (grey horizontal bar) of the error of the total sample estimate constructed for pattern ES-B using the left, right, and dual directional 3D data quality sub-populations.

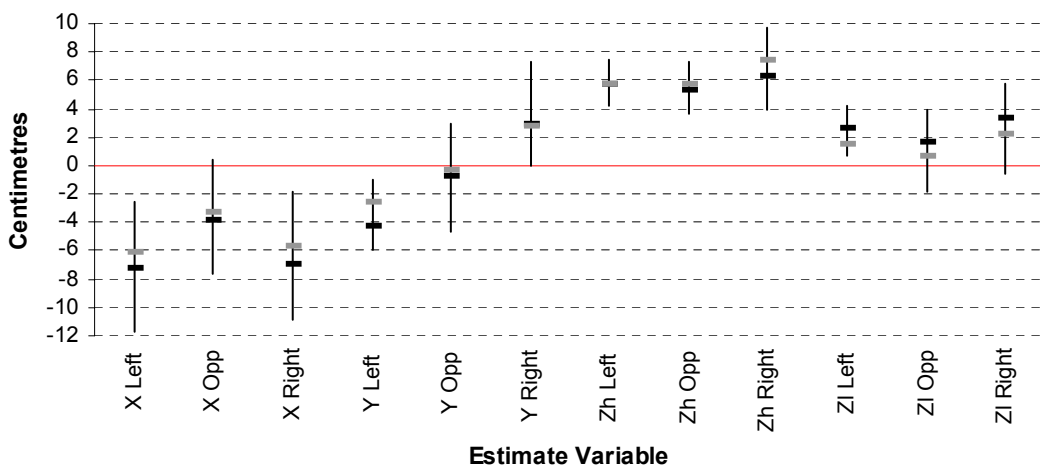
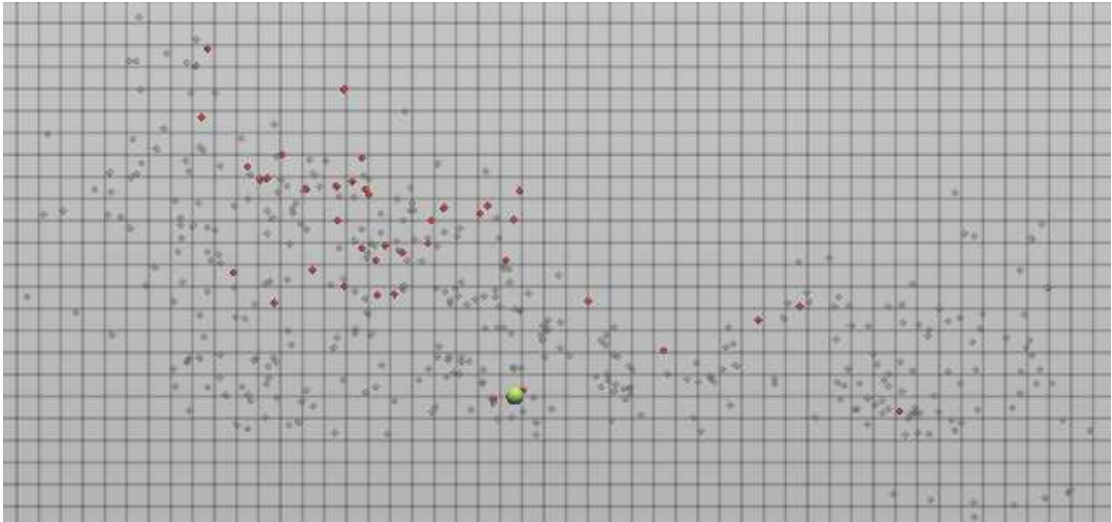
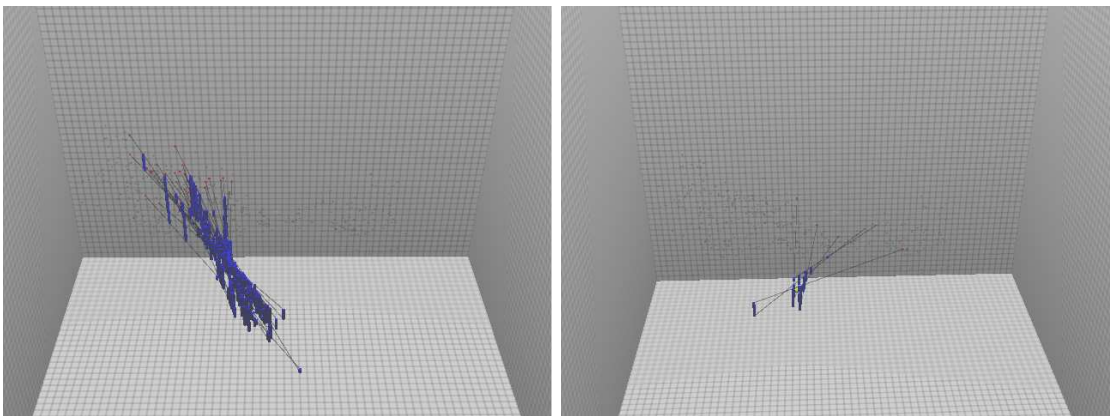


Figure 11-45 - The inter-quartile range (vertical bar), median (black horizontal bar), and mean (grey horizontal bar) of the error of the total sample estimate constructed for pattern ES-C using the left, right, and dual directional 3D data quality sub-populations.

For both of these impact spatter patterns the generation of an estimate from a directionally-restricted sub-population, whether this is to the left or the right of the impact site, produces an increase in the inter-quartile range in that x-axis estimate data, as well as increasing the error in the point-based central tendency statistics in the direction of the plane of the target surface. In the y-axis, the accuracy of the mean and mode of the distribution of the trajectory intersection data is also increased, moving the location of these statistics away from the relatively accurate dual directional sub-population estimate, towards which ever direction the spatter distribution is restricted.



*Figure 11-46 - The locations of the spatter bloodstains within the selected 10-centimetre data quality group in relation to the known impact site, and other spatter bloodstains in the target surface of pattern ES-B.*



*Figure 11-47 - The substantial difference in estimate data in the consideration of the left (left), and right (right) directionally-restricted spatter bloodstain distributions for pattern ES-B.*

This trend in the variation in the results of estimates given the different directionally-restricted sub-populations, however, is not replicated in the 3D data quality estimates for pattern ES-B. While the estimate in which the spatter distribution is restricted to the right side of the location of the pater-producing impact event within the plane of the vertical target surface does indicate a comparable change in estimate distribution and accuracy in the horizontal plane of analysis, this relationship is not evident where the spatter bloodstain distribution is restricted to the right side of the impact site. The potential reason for this is unclear, although a contributory factor may well be the small number of spatter bloodstains that correspond to this 3D data quality group which are situated to the right of the location of the impact site, as demonstrated in Figure

11-46. The effects of the directionally biased distribution of spatter bloodstain with the 3D data quality sub-population on the potential trajectory intersection estimate data for pattern ES-B is highlighted in Figure 11-47.

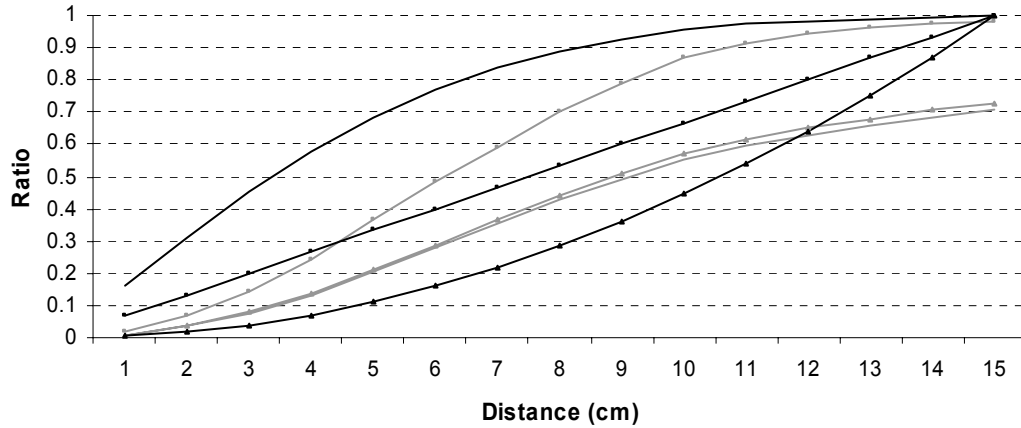


Figure 11-48 – The percentage of trajectory intersections with a given radius of the location of the impact site for the dual directional 3D data quality estimate for pattern ES-A. The constant intensity (black line with triangles), equal number (black line with squares), and normal distribution models (black line), and the total (grey line), opposite (grey line with squares), and thinned trajectory intersection data sets (grey line with triangles) are shown.

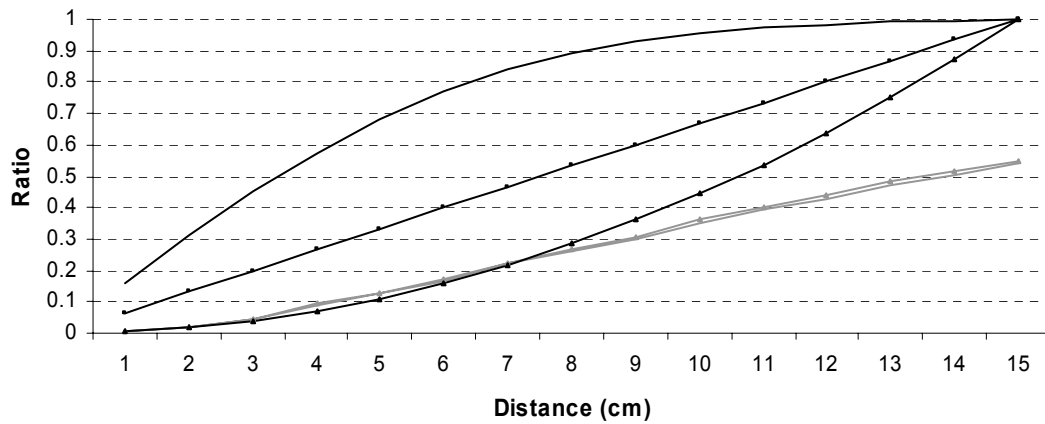


Figure 11-49 - The percentage of trajectory intersections with a given radius of the location of the impact site for the left-restricted 3D data quality estimate for pattern ES-A. The constant intensity (black line with triangles), equal number (black line with squares), and normal distribution models (black line), and the total (grey line) and thinned trajectory intersection data sets (grey line with triangles) are shown.

The effect of the change in location, and density of the distributions of the trajectory intersection estimate data constructed using a directionally-restricted sub-population of spatter bloodstains is further illustrated in Figure 11-48 and Figure 11-49. The total, opposite, and thinned approaches to the interpretation

of trajectory intersection data all demonstrate a degree of aggregation close to the location of the known impact site in excess of the constant intensity theoretical model, while the opposite approach also indicates a degree of excess aggregation compared to the equal count theoretical model over much of the 15 centimetre circular area considered. In the case of the 3D data quality estimate using the left-restricted sub-population data, however, the ratio of spatter bloodstains within each concentric circular region investigated, as well as the apparent excess theoretical aggregation, appears to have been considerably reduced for both the total and thinned data sets (the opposite approach not being application to this spatter bloodstain data).

### 11.5.3 Multiple Sample Estimation

The multiple sample estimates generated during this research project for each of the 3D data quality sub-populations of the three screened impact spatter patterns were produced to provide an assessment of the potential variation in sample-based estimates given the potential high degree of accuracy of all of the selected spatter bloodstains. An example of the visualisation of a selection of this multiple estimate data generated for pattern ES-A within the 3D virtual investigative environment of the analytical site of impact estimation application is illustrated in Figure 11-50.

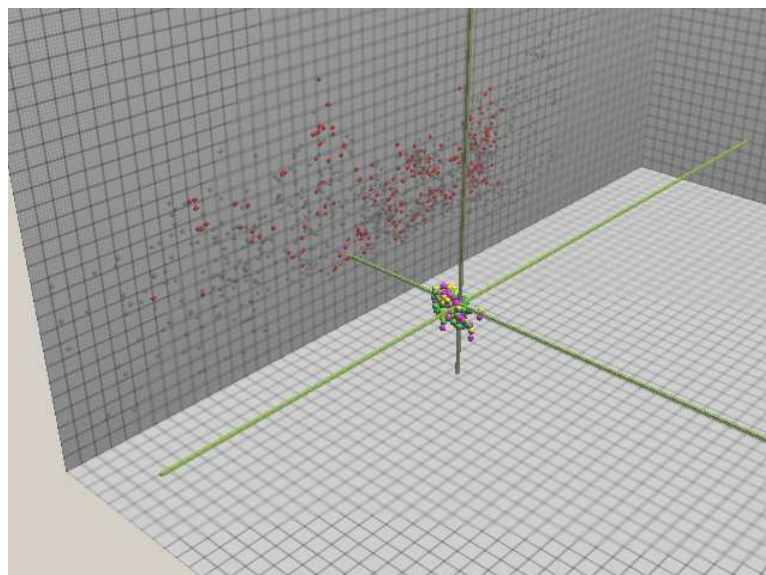


Figure 11-50 – The visualisation of the 100 mean estimate points generated using a sample size of 10 spatter bloodstains with a 3D data quality from pattern ES-A. The means of the total, opposite and thinned  $p_{21}$  trajectory intersection data sets for each individual estimate are shown.

The statistical description of the distribution of the estimates constructed through the multiple sample estimation process in terms of both the horizontal and 3D accuracy of the mean and mode descriptions of central tendency for the three alternative approaches to the interpretation of trajectory intersection data sets are illustrated for pattern ES-A, ES-B, and ES-C in Figure 11-51, Figure 11-52, and Figure 11-53 respectively. Each of the distributions analysed is the result of the 100 estimates constructed with a sample size of 10 spatter bloodstains from within the 3D data quality sub-population of each impact spatter pattern.

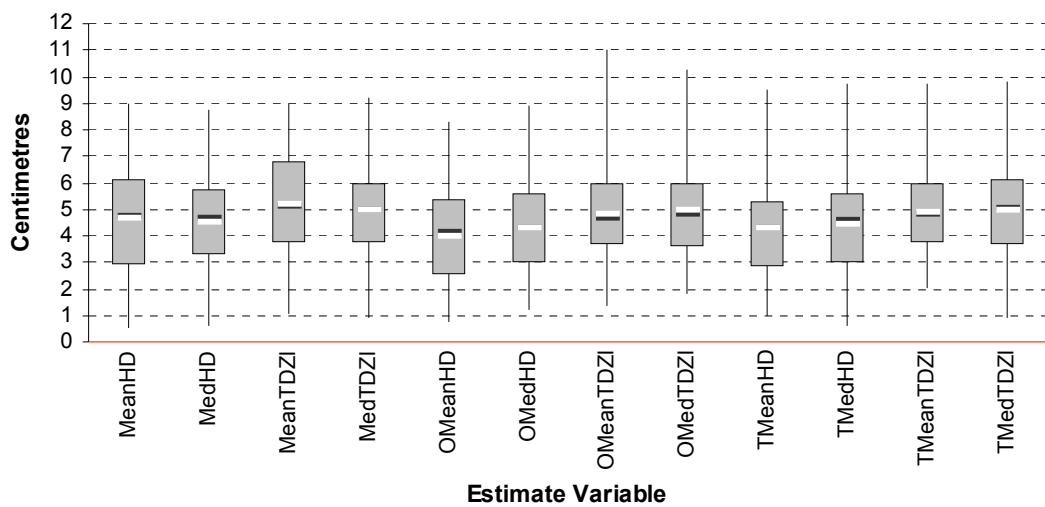


Figure 11-51 - The range, inter-quartile range, mean (white bar), and median (black bar) of the total horizontal error of the mean and median site of impact estimates for the 100 samples of 10 spatter bloodstain selected randomly from the 3D data quality sub-population of pattern ES-A.

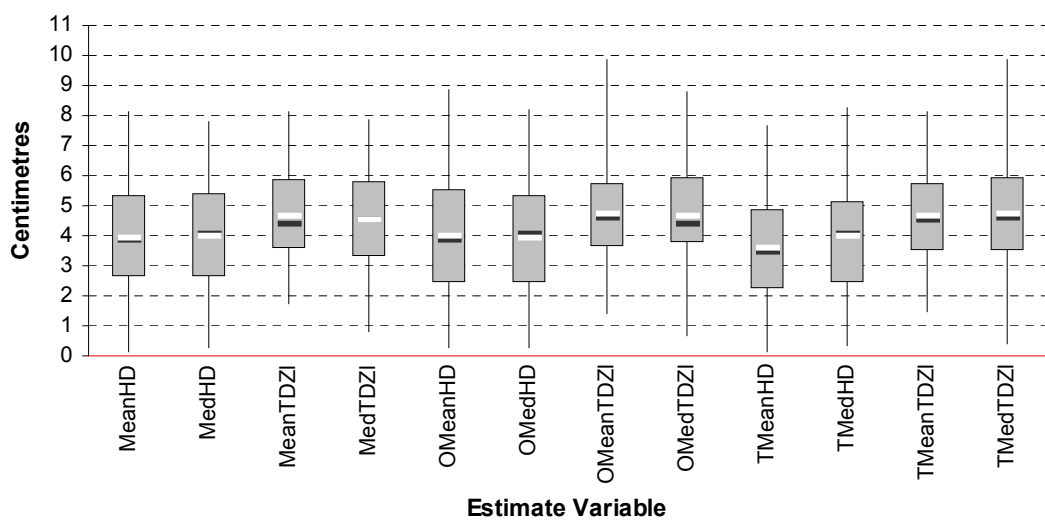


Figure 11-52 - The range, inter-quartile range, mean (white bar), and median (black bar) of the total horizontal error of the mean and median site of impact estimates for the 100 samples of 10 spatter bloodstain selected randomly from the 3D data quality sub-population of pattern ES-B.



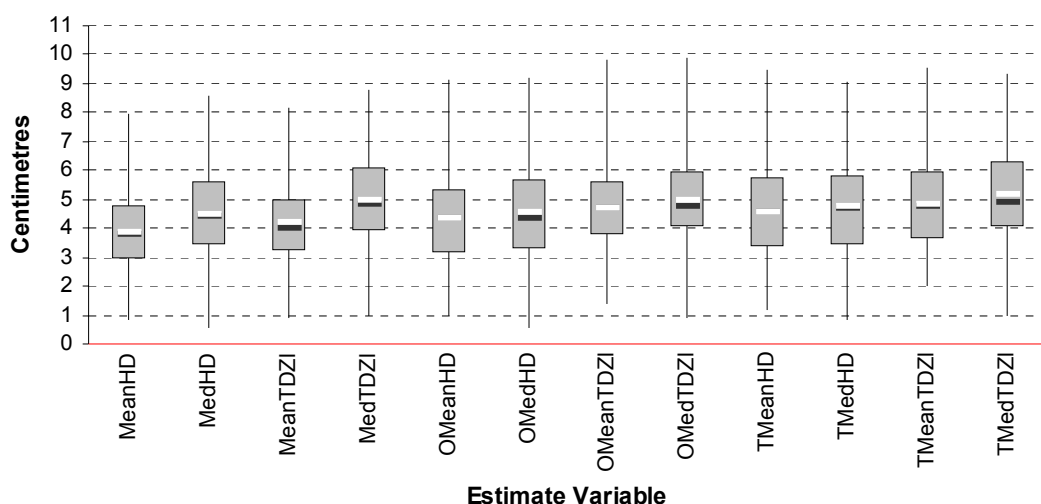


Figure 11-53 - The range, inter-quartile range, mean (white bar), and median (black bar) of the total horizontal error of the mean and median site of impact estimates for the 100 samples of 10 spatter bloodstain selected randomly from the 3D data quality sub-population of pattern ES-C.

The majority of the multiple sample estimate distributions generated using the smallest sample size of 10 spatter bloodstains produced an estimate error in terms of both the horizontal and 3D estimate of less than 10 centimetres, and 75 percent achieving a error level of less than 6 centimetres. As in the case of the analysis of the results of the multiple sample estimates generated for the total population data, the suggestion from this analysis is that the application of opposite and thinned trajectory intersection data sets in the construction of the estimates using the 3D data quality sampling strategy do not appear to provide any considerable or consistent advantage in terms of horizontal or 3D accuracy of the statistical descriptions of the individual estimate distributions over that the provided by a total trajectory intersection approach. The use of the alternative mean and mode methods of defining the central tendency of the individual estimate distributions also appears to provide no consistent benefit in terms of increased estimate accuracy.

The affect on the construction of the multiple sample estimates using directionally-restricted versions of the 3D data quality sub-populations are illustrated in Figure 11-54, Figure 11-55, and Figure 11-56 using the 3D visualisation of the results generated for pattern ES-A as an example. The same predominant relationship that was identified in the analysis of 95 percent confidence regions of the total population multiple sample estimates appear to be demonstrated by the results of the analysis of the 3D data quality sub-population.

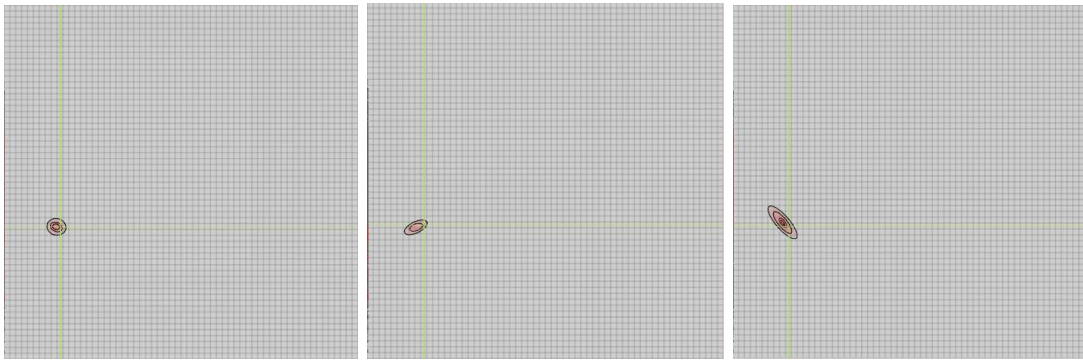


Figure 11-54 – The 95% confidence regions for the 100 mean estimates for pattern ES-A at each sample size possible using the dual directional (left), left (centre) and right (right) sub-populations viewed in the horizontal plane of analysis.

While the dual directional sub-population approach produces an approximately circular confidence region within the horizontal plane, the directionally restriction spatter bloodstain distributions result in accentuated elliptical shapes, whose long axes are orientated towards the direction in which the spatter bloodstains are located. The size of the ellipsoidal regions generated during the 3D data quality multiple sample estimation process, however, are considerably smaller than those constructed for the multiple estimate analysis of the total screened spatter bloodstain populations (see Figure 11-30), highlighting the reduced variation in this multiple sample estimate data. Although some differences in the left and right-restricted confidence regions are evident in the multiple sample estimates of the total screened spatter bloodstain population of pattern ES-A, these relative variations in size and shape are not as accentuated as in the data generated for the multiple sample estimates presented here. The ellipsoidal confidence region generated for the results of the estimates generated using the spatter bloodstain distribution situated to the right of the impact site exhibits a much more elongated elliptical shape than the confidence region constructed for the left-restricted spatter bloodstains. The cause of this variation is likely to be the result of the relatively smaller number of spatter bloodstains within the 3D data quality sub-population which are situated to the left of the impact site, as illustrated in Figure 11-55. As a comparison between Figure 11-55 and Figure 11-56 indicates, however, the extended ellipsoidal geometry evident in the horizontal axis of the 3D investigative environment does not appear to significantly affect the accuracy and variation in the vertical component of the estimate.

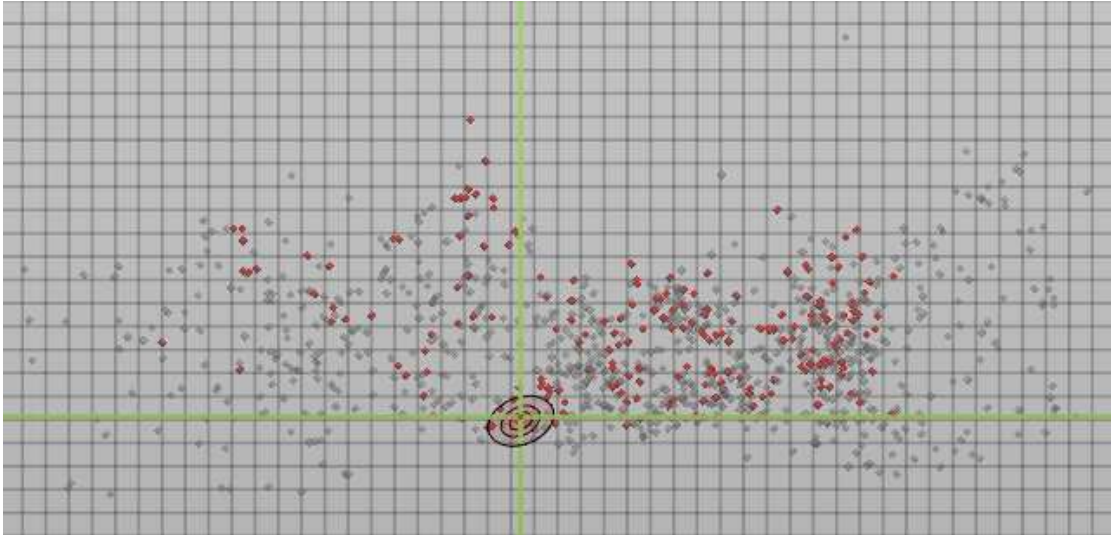


Figure 11-55 – The 95% confidence regions for the  $\mathbf{p}_{z_i}$  total trajectory intersection data set generated for the 3D data quality sub-population of pattern ES-A.

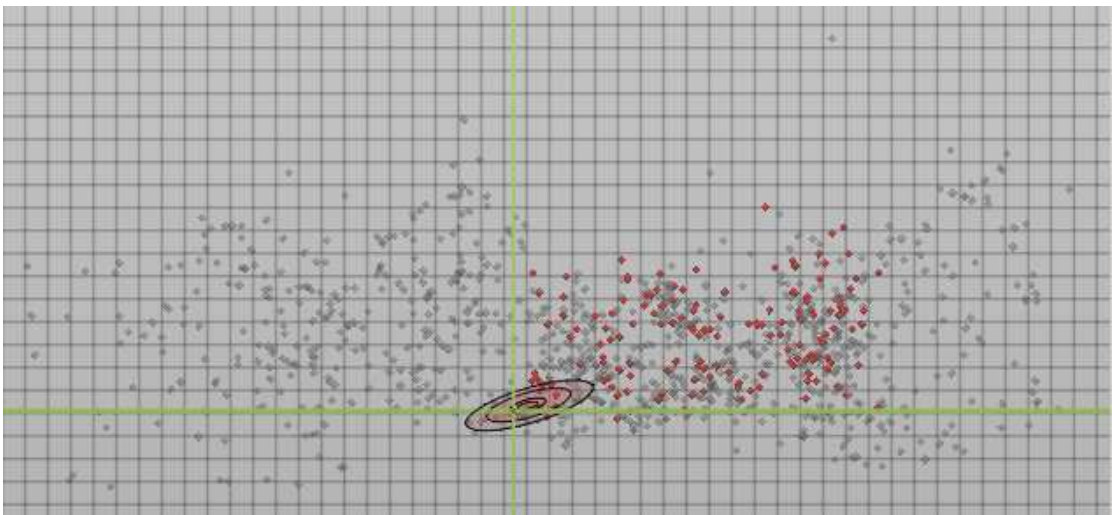


Figure 11-56 - The 95% confidence regions for the  $\mathbf{p}_{z_i}$  total trajectory intersection data set generated for right-restricted 3D data quality sub-population of pattern ES-A.

## 11.6 Conclusions

A considerable amount of site of impact estimation data has been generated during this research project, the production of which was made possible through the combined investigative potential of the various analytical techniques included in the site of impact estimation application and the total enumeration methodology employed in the recording of the experimentally produced impact spatter patterns. Each of the three impact spatter patterns produced were screened to remove data that could be considered to be unusable within non-

experimental conditions, and were subsequently analysed using an extensive sampling strategy designed to identify and investigate the site of impact estimation potential of specific sub-populations of spatter bloodstains from within the wider total pattern populations. The various samples within this investigative strategy were included to provide some analysis of the potential accuracy and uncertainty involved in the construction of site of impact estimates, where the selection of either potentially accurate or inaccurate spatter bloodstains are made, or where no explicit selection criteria are employed.

Of the wide range of spatter sub-populations analysed, the results of six specific examples for each impact spatter pattern, a relatively small proportion of the total site of impact estimation data produced, have been specifically addressed within this chapter. These six examples demonstrate the results of the site of impact estimation analysis, given the dual directional and two directionally-restricted sub-population definitions of both the total useable spatter bloodstain data within each impact spatter patterns, and the collection of spatter bloodstains within each impact spatter pattern that exhibit 3D independent data quality assessments of 10 centimetres or less. The discussion, evaluation and comparison of the analysis of these two collections of spatter bloodstains, and the three alternative directional sub-population approaches to their definition, were considered to provide a degree of insight into the potential uncertainty involved in site of impact estimation through, two essentially opposing approaches to estimate construction. The analysis of the total populations provides information on the potential accuracy and uncertainty in site of impact estimates of what could be considered to be a potentially inaccurate approach to estimation, where no specific spatter bloodstain selection is made. The analysis of the 3D data quality sub-populations, in contrast, provides evidence for the actual level of accuracy, and the potential uncertainty in the construction of site of impact estimates in what could be considered to be a 'best case' scenario, where the entire distribution of reasonably accurate spatter bloodstains within an isolated impact spatter pattern are empirically established.

While the discussion of these results are only general in nature, given the detailed analytical potential of the single and multiple sample estimates constructed through the site of impact estimation application, they do appear to demonstrate a number of implications for the construction and evaluation of site of impact estimates, as well as indicate some of the investigative benefits of the detailed impact spatter recording and analysis methodologies employed during

this research project. Firstly, the analysis and comparison of the dual directional, and left and right directionally-restricted versions of both the total and 3D data quality sub-populations appear to exhibit a consistent relationship that could have implications for the interpretation of estimates generated from impact spatter patterns whose entire spatter bloodstain demonstrates a solely directionally-restricted distribution. The comparison of the estimate results generated from both the single and multiple sample analyses indicate that where a distribution is directionally-restricted, the trajectory intersection data exhibits a locative bias both towards the direction of the target surface upon which the spatter bloodstain are observed, and in the direction from which the directionally-restricted spatter distribution originate. While these results have not been directly compared to site of impact estimates generated from completely directionally-restricted impact spatter bloodstains, the implication is that a directionally consistent error may be introduced during the construction of these estimates, and, as a result may require explicit consideration in the evaluation of the estimate results.

A second but related trend in the results of the single sample estimates for the 3D data quality sub-population estimates indicates that the x-axis estimate consistently provides the largest single directional degree of error within the estimates for each of the three impact spatter patterns. While this error is relatively small, within five centimetres for each experimental impact spatter pattern, this apparent trend could have implications for the interpretation of site of impact estimate results where the estimate accuracy of the selected spatter bloodstains and constructed straight-line trajectory approximations are not known, but inferred. The suggestion could also be made, although not investigated here, that if the error in the direction perpendicular to the target surface plane, that the consideration of spatter bloodstains on multiple target surfaces, where these are present, could potentially provide further improved estimate accuracies. This apparent general directional bias in estimate results is also reflected in the results of the horizontal estimates of the total population single sample estimate results, although to a less clearly defined degree. This factor, however, is not necessarily surprising, given the potential effect of the total combined error of all of the straight-line trajectory estimates considered.

Thirdly, the analysis and comparison of the composition of spatter bloodstain populations and smaller purposive samples selected from them have been shown to provide investigative potential. The composition of the 3D data quality sub-populations in terms of vertical trajectory angles, for example, appear to provide

a degree of empirical support for the theoretical principles of straight-line trajectory theory, with the sub-populations consisting almost exclusively of downward elevated angles. The distribution of vertical trajectory angles within the total pattern populations also suggests that the proportionality of upward and downward elevations, at least for the three experimental impact spatter patterns analysed, is indicative of both the distance of the impact site from the recording target surface, and the general estimate quality of the individual impact spatter patterns. While neither of these conclusions is particularly unexpected, they do indicate the potential of the experimental techniques applied during this research project to provide detailed empirical evidence in support of site of impact estimation concepts. The potential benefits of quantifying and characterising an entire observable impact spatter pattern in terms of providing a structured basis for the selection of spatter bloodstain sample, and enhancing the general analysis, interpretation, and evaluation of impact spatter patterns are also arguably exemplified.

An additional and potentially advantageous feature of the empirical analysis of impact spatter patterns is suggested by the analysis of the composition of the 3D data quality samples with regards to the width-to-length ratios of their constituent spatter bloodstains. Each of the three 3D data quality sub-populations investigated during this research project seem to indicate that some practical estimate utility can be achieved using the data provided by spatter bloodstains that exhibit less acute impact angles than usually considered viable. While this does not suggest that the variation and error in the measurement and calculation of impact angles is not present, nor that such spatter bloodstains should be immediately and routinely used in site of impact estimates, the potential of an empirical total-pattern investigative methodology to highlight possible spatter bloodstain selection criteria, either pre-existing or identified through the empirical analysis itself, could benefit from further investigation. Despite the investigative potential demonstrated, the method of composition analysis employed within this research project is could be considered to be limited. Arguably, each of the spatter bloodstain variables is analysed using a univariate approach, which is neither particularly representative of either the multivariate nature of spatter bloodstain information, nor spatter bloodstain sample selection technique which are typically based on the consideration of a number of variables simultaneously. Additional benefit in the investigation of pattern and sample composition may, consequently, be gained from the application of high-dimensional multivariate analytical techniques, which explicitly

analyse the combinations of multiple attributes of objects within a data set. Combined with the detailed analysis of the total pattern enumeration approach and the construction of independent data quality assessments for spatter bloodstain within experimental contexts, the application of techniques such as principle component analysis, or multiple discriminate function analysis, which can be used to determine variables which provide the highest discriminatory value within and between grouped data, could be trained and tested using alternative experimental impact spatter bloodstain data. Such methods could, with significant development, provide additional empirically-based spatter bloodstain selection criteria, which applied along side theoretical selection criteria, and given an analyst's interpretive skill and experience, could ultimately provide site of impact estimation with a comprehensive, detailed and quantifiable approach to the interpretation of impact spatter patterns, and the selection of spatter bloodstain samples for analysis.

Fifthly, of the two height estimation techniques applied through the analytical site of impact estimation macro, the results of the analysis of the  $p_{zl}$  data sets (which includes all of the lower trajectory heights at the location of horizontal intersection of two trajectories for a single estimate) demonstrate a consistently greater degree of estimate accuracy than the  $p_{zh}$  (upper trajectory height) data across each of the estimates generated. The results of the single estimate analysis of the total pattern populations also indicate that, where the potential height estimate quality of the data analysed is unknown, the  $p_{zh}$  height estimate data also demonstrates the greatest degree of variation signified by the relatively large inter-quartiles ranges, and a relatively large disparity between the mean and mode estimates of central tendency, suggesting a consistently positively skewed distribution. This greater degree of variation between the  $p_{zh}$  data estimates is also suggested in the analysis of the total population multiple samples. While these results are not necessarily surprising given the fact that, in straight-line trajectory theory all accurately interpreted trajectories should pass over the impact site either at, or more likely above, the actual height at which the particular impact event took place, the empirical investigation of this consistent approach to height estimation method, as opposed to relatively ad hoc methods of limited trajectory selection, could provide complementary alternative techniques for the investigation, interpretation, and evaluation of the potential height estimate data provided within the construction of a site of impact estimate.

A sixth implication is suggested in the comparison of the results provided by the alternative total, opposite, and thinned approaches to the interpretation of trajectory intersection data sets in each analysis conducted, which do not seem to demonstrate that any consistent benefit in terms of the point-based description of the central tendency of an estimate is achieved in the application of any single approach. A similar lack of consistent benefit in terms of the accuracy of an estimate is also demonstrated throughout the various estimates constructed and analysed in terms of the application of the mean and median approaches to the definition of the central tendency of a trajectory intersection data set. The inclusion of the various analytical methods within the site of impact estimation application, however, does provide additional and detailed information that can aid the investigation and evaluation of individual estimate distributions. The inclusion of robust descriptions of dispersion and spatial count- and density-based analytical techniques, for example, have been shown to provide potentially significant and detailed information on the spatial distribution and aggregation of trajectory intersection data sets, which is not currently associated with computer-based site of impact estimation techniques. The combined analysis of numerous statistical and spatial analytical techniques, whether they are those included with this research, or other more applicable or appropriate methods, where identified, provide alternative and interpretatively complementary results, which can increase both the value of site of impact estimation data and the weight attributed to its analysis. The inclusion and evaluation of such wide-ranging analyses within a site of impact estimation application, as has been demonstrated within this chapter, provide a level of investigational functionality which promotes a methodological approach whereby if a choice of analytical technique is deemed necessary in terms of analysing or reporting the results of an estimate, this choice can be made on the merits of individual estimate, and the data generated from its analysis.

Perhaps the most significant implication in terms of evidential support for the current sampled-based methodological approaches employed in the construction of site of impact estimates is suggested by the results of the multiple sample estimates. The results of the analysis of the dual directional definition of the three total screened pattern populations, for example, indicate that, even where spatter bloodstain selection is completely random, the construction of sample-based site of impact estimates can provide reasonable levels of estimate accuracy. In the cases of pattern ES-A, and ES-C, where the potential 3D data quality of the entire pattern is comparatively good, a relatively high 3D multiple



sample estimate accuracy is exhibited, whereas in the case of pattern ES-B, which demonstrates the poorest potential 3D data quality, a reasonably high level of estimate accuracy is only achieved in the horizontal plane of analysis. Perhaps most significantly, pattern ES-A, which represents the median pattern in terms of 3D independent data quality, seems to achieve a higher proportion of estimates within a certain level of 3D estimate accuracy than is indicated by the proportions of its constituent spatter bloodstains with similar levels of 3D independent data quality, even where the sample size analysed is small. The implication of these results for current sample-based site of impact estimation methods, which could be investigated further using other pattern sample data generated during this project but not analysed within this chapter, is that even where some improved estimate accuracy through spatter bloodstain selection can be achieved, then even relatively small size sample methodologies could potentially provide reasonable accurate site of impact estimates.

An additional feature of the results of the multiple sample estimate analysis conducted during this research project could also have implications for the practice of site of impact estimation. The results suggest that, as would be expected from the fundamental statistical principles of sampling distributions, and central limit theory, the larger the spatter bloodstain sample size involved in the construction of an estimate, the less variation is observed in statistical descriptions between estimate, and the closer these description corresponds to that of the population parameter, however this population (i.e. total or sub-population) is defined. Consequently, in the consideration of sample-based site of impact estimation, the accuracy of the population parameter, and the relative population and sample sizes can all be important factors in interpreting estimate accuracy and reliability. The construction of single sample total (sub-)population estimate, could, as result, be recommended as a more appropriate method of producing a site of impact estimate. Within such an estimate, any sample-based variation, even where potentially small in real dimensional terms, is avoided, and the total distribution of trajectory intersections of the spatter bloodstain population investigated can be explicitly and comprehensively assessed. Given current practical spatter bloodstain recording and morphological quantification methodologies, however, such an approach to estimate construction is not currently viable under typical casework conditions.

A final, but crucial point concerning the interpretation of the data presented in the chapter, however, is that despite the potentially far-reaching implications of a

number of the conclusions suggested, the data upon which these conclusions are based is relatively limited in nature. Only three impact spatter patterns, which were created under similar conditions, have been analysed during the course of this research project, and only a small amount of the potentially informative estimate data generated through the broad sampling strategy employed during this research project has been explicitly evaluated and discussed. Consequently, the firmest conclusion that might be reliably drawn from the analysis of this data is that the empirical estimate analyses made possible through the analytical site of impact estimation computer application and exhaustive total impact spatter pattern recording methodology, demonstrate considerable potential for the further scientific investigation of site of impact estimation, estimate uncertainty, and estimate construction methodologies. With continued experimentation, analysis and development, the application of the kind of analytical approaches to site of impact estimation suggested within this research project, could, ultimately, provide BPA with one method for demonstrating, proving and maintaining the acceptance and reliability of site of impact estimation as 'scientific' expert evidence, as well as helping to preserve the potentially valuable application of this evidence within CSRs, and wider criminal investigations and legal contexts.

## **12 Research Conclusions**

### **12.1 Introduction**

This chapter will provide a review of the justification for the research into site of impact estimation and estimate uncertainty described within this thesis. The main investigational research questions will be repeated, and the potential answers provided from the results of this research project postulated. The final section of this chapter will describe potential issues involved in the construction and analysis of site of impact estimates, which have been identified during this research project, and will highlight the research results that could benefit from further investigation.

### **12.2 The Limitation of Current Site of Impact Estimation**

Blood is one of the most common forms of evidence found at the scene of violent crimes. The investigation of the morphology and distribution of the bloodstain evidence found at a crime scene reveals considerable information concerning the physical, spatial, and temporal components of a crime scene dynamic through the analytical and inferential techniques of BPA. Despite being an established and functional component of CSR and wider criminal investigations, BPA is facing a series of complex challenges surrounding the future of its utility and admissibility as expert forensic evidence within legal contexts.

Site of impact estimation, a term defined within this thesis to describe the range of BPA techniques which attempt to infer the location in which an impact event took place from its resultant impact spatter bloodstain pattern, can be a significant issue in the reconstruction of a crime scene. The general technique combines aspects of physics, ballistics, biochemistry, fluid dynamics and mathematics in both its theoretical foundation and practical implementation. The established principles of spatter bloodstain directionality, impact angle calculation, and straight-line trajectory reconstruction, are utilised within these techniques to retrace the flight paths of spatter-producing droplets through a crime scene, and where these trajectories intersect can subsequently be interpreted as the pattern-producing impact site, the location within the scene where a blood source encountered an impacting force.

Of the various site of impact estimation methodologies, computer-based estimation techniques, which have been in development for nearly 20 years, are emerging as the method of choice within BPA. The practical and theoretical benefits of this type of approach to site of impact estimation include the provision of mathematically defined straight-line trajectory approximations; both a numerical and graphical representation of an estimate; the separation of the horizontal and vertical components of an estimate; a relatively quick and less cumbersome reconstruction methodology; an analytical method that can be conducted independently of the physical scene; a valuable presentational tool; computer processing power facilitating the consideration of increased number of spatter bloodstains within any particular estimate; and the potential for the re-evaluation of an estimate. As computer-based site of impact estimation are gradually replacing physical estimation techniques within BPA, 3D CG and virtual investigative environments are also beginning to complement the more traditional 'virtual stringing' approaches. Consequently, the potential additional benefits of 3D crime scene scanning technologies, and the virtual 3D CG investigation and presentation of the results of site of impact estimation are also being to be incorporated within the computer-based construction of site of impact estimates.

While the benefits of computer-based techniques have given rise to claims that the techniques of BackTrack<sup>®</sup>/Win, for example, can be considered to provide a site of impact estimation sound scientific methodology, the theoretical foundation and practical implementation of the principles of site of impact estimation are not without their limitations (Carter, 2001). The review of the fundamental theoretical and practical principles of site of impact estimation within this thesis, for example, has highlighted the intrinsic uncertainty that is involved in the construction, analysis, and evaluation of site of impact estimates. The sources of this uncertainty are both wide and varied, originating from elements of the estimation process such as the theoretical definition and practical approximation of an impact site; the theoretical justification for impact angle calculation; the practical processes of spatter bloodstain sample selection; the dimensional interpretation of spatter bloodstain morphology; the inability to fully incorporate droplet flight dynamics; and the limited numerical methods used to describe an estimate. While this largely pervasive uncertainty has not precluded the estimation process from achieving a level of accuracy that is typically considered sufficient for the purposes of practical reconstructions, it is questionable as to what extent such 'practicality' corresponds to the more rigid investigative and

conclusive criteria that are increasingly being required of the analysis and interpretation of forensic evidence within legal contexts.

During the discussion of estimate uncertainty, a number of research questions were identified, which, if addressed, could be significant in defining the future of the practical and theoretical application of computer-based site of impact estimation techniques, potentially strengthening the 'sound scientific' methodology of this valuable reconstructive technique through the explicit investigation and incorporation of estimate uncertainty within the analysis, evaluation, and presentation of the results of site of impact estimation. Four main questions, which were deemed necessary for further investigation, were formulated:

- Could the provision of alternative detailed statistical and spatial analyses of estimate data provide both an assessment of the uncertainty involved in the construction of an estimate, and a firmer basis for the formation and evaluation of reconstructive conclusions drawn from this data?
- Can the investigation of spatter bloodstain sampling procedures provide information on the level of uncertainty associated within the construction of a site of impact estimate, and what confidence can be attributed to estimates constructed using both qualitative spatter bloodstain selection criteria, and where no appropriate spatter bloodstains are observed?
- Can the construction of site of impact estimates benefit from a more explicit and considered 3D volumetric estimation process, and can this process be facilitated through the provision of a 3D CG virtual investigative environment?
- Could a less subjective approach to the quantification of spatter bloodstain morphology provide site of impact estimates with a reproducible quantitative, and quantifiable qualitative analysis of the evidence upon which the construction of an estimate depends?

These research questions were investigated using an experimental computer-based research design. This process involved the experimental creation of a series of impact spatter patterns, and the development and implementation of an exhaustive spatter bloodstain recording methodology, through which the experimental impact spatter patterns were totally enumerated. The extensive experimental spatter bloodstain data collected was subsequently analysed through an analytical site of impact estimation computer application developed

specifically for this research. This computer application provided a number of alternative numerical approaches to the construction and analysis of site of impact estimates, which included detailed and precise sample selection; the compositional analysis of collections of spatter bloodstains; the creation of single and multiple sample estimates; three alternative approaches to the definition of trajectory intersection data sets; and the provision of a range of statistical and spatial analytical methods to examine any estimate data produced. An integrated 3D CG virtual investigative site of impact estimation environment was also developed, within which the detailed estimate data produced could be visualised, investigated, and evaluated within an approximation of the data's natural spatial context. The analysis of the experimental impact spatter pattern data undertaken during this research was conducted using an extensive sampling strategy to provide estimate data on a range of specific sub-populations of spatter bloodstains, which could be analysed, compared and evaluated. Two additional pilot projects were also conducted during this research into site of impact estimation uncertainty to investigate the potential utility of a rapid large-scale sampled photographic approach to the recording of spatter bloodstains, and the possible effectiveness of an automated IA procedure in the quantification of spatter bloodstain morphologies.

### **12.3 Results of the Research**

The results of this research project into site of impact estimation uncertainty suggest a number of potential answers for the four questions outlined above, as well as indicating areas of further investigation in which the analysis of estimate uncertainty, and the incorporation of this uncertainty within practical estimate construction methodologies could be advanced. Firstly, the provision of alternative analytical techniques for the investigation of site of impact estimation data has been shown to provide a more considered basis for the evaluation of the results of an estimate, and to provide some degree of assessment concerning the potential uncertainty exhibited within this data. The provision of alternative descriptive statistical methods of summarising the size, shape, and central tendency of trajectory intersection data sets, and the inclusion of spatial count and density-based analyses have been demonstrated to provide detailed assessments of both the spatial distribution and aggregation of trajectory intersection data sets. As a result, they provide a conceptual indication of the uncertainty or agreement within the data upon which any particular estimate is

based. The provision of alternative but complementary analytical methods has also been shown to facilitate the evaluation of the nature of the distribution of an estimate, and the potential significance of such measures, given the particular structure of that distribution. The analysis of alternative approaches to the definition of trajectory intersection data sets within this research project, such as the two height estimate distributions, and the total, opposite and thinned trajectory intersection data sets, further suggest that the comparison and consideration of alternative analytical approaches to the construction and investigation of site of impact estimates can provide additional functionality for the detailed consideration and incorporation of uncertainty with the construction and evaluation of an estimate. The analysis of site of impact estimation presented within this thesis, as a result, indicates that the formation and evaluation of reconstructive conclusions from site of impact estimate data can be enhanced through the comprehensive investigation and description of the potentially detailed trajectory intersection data generated during the construction of an estimate. The results of this analysis, however, are limited, in the sense that a detailed consideration is not given to the full complement of analytical techniques provided within the analytical site of impact estimation application. The analytical methods discussed are also relatively unsophisticated, given the detailed nature of the trajectory intersection data sets constructed, and the potential of higher-dimensional multivariate and more complex spatial analytical approaches to the description, investigation, and statistical evaluation of the spatial dependence and association of variables within the observed estimate. The identification and application of appropriate analytical techniques, which give explicit consideration to the spatial nature and potential complexity of the distribution of the data upon which the evaluation of an estimate is ultimately based, even given these limitations, have been shown to increase both the value of this data and the potential weight attributed to its analysis. The inclusion and evaluation of a range of alternative and complementary analytical techniques within site of impact estimation also arguably promotes a methodological approach whereby a considered evaluation of the estimate data is possible, and the distillation of this data into reconstructive locative conclusions can be made, with explicit consideration being given to structure of the estimate data.

Secondly, the investigation of sample-based site of impact estimation methodologies within this research project has suggested some potentially significant implications concerning the uncertainty associated with such approaches to the construction of site of impact estimates. The practical results

of the analyses conducted during this research suggest that sampled approaches can provide a reasonable degree of estimate accuracy, even where the spatter bloodstain sample size is relatively small. This degree of accuracy appears to be comparatively high within the horizontal plane of analysis, as would be expected given straight-line trajectory theory, while, in the vertical plane of analysis some selection of potentially accurate straight-line trajectories in terms of height estimation, if such spatter bloodstains are not well represented within the total pattern population, may be necessary. While the data analysed during this research project suggests such a conclusion, the actual analysis of spatter bloodstain samples that correspond to such spatter bloodstain selection have not been evaluated. The estimate data from such samples, however, has been generated as part of the extensive sampling strategy employed during this research project, and as such the data necessary to full investigate this proposition is available for future research. Where spatter bloodstain distributions are directionally-restricted, a pattern configuration not typically considered to be as accurate as dual directional distributions, the results of this research have suggested comparable levels of estimate accuracy, although no direct comparison to totally directionally-restricted impact spatter patterns has been attempted. In the interpretation and evaluation of such impact spatter pattern distributions, however, certain directional biases, which are shown to be present within the construction of estimates, may require explicit consideration. Despite the indications of an achievable degree of estimate accuracy through sampled estimate construction methodologies, the investigation of the construction of sample-based site of impact estimates has also highlighted the effect that the fundamental statistical principles of sampling distribution and central limit theory can have on the potential levels of uncertainty within a sampled site of impact estimate. The results of this research emphasize the relationship between the potential accuracy and uncertainty involved in the construction of a sampled estimate, the accuracy of the statistical parameters of a site of impact estimate constructed using the total spatter bloodstain population from which a sample is drawn, and the relative size of the spatter bloodstain sample compared to that of the spatter bloodstain population, however this may be defined. The proposition could, therefore, be made that, despite being currently impractical, given spatter bloodstain recording and data processing methodologies, the potential variation in estimate construction, even where this is potentially small, could be avoided if a total or at least large-scale sampling regime is implemented in the selection of spatter bloodstains from some pre-defined bloodstain population for the purposes of the construction of site of



impact estimates. The potential utility of the analysis and comparison of the composition of spatter bloodstain populations and the smaller samples selected from them has also been highlighted the site of impact estimate analyses undertaken within this research project. Despite being limited by the univariate analytical approach employed within the site of impact estimation application, the empirical investigation of the composition of specific collections of spatter bloodstains has exhibited some investigative potential in terms of both reinforcing and challenging accepted spatter bloodstain selection criteria, and providing additional analytical techniques for the interpretation and evaluation of impact spatter patterns, and the structured selection of spatter bloodstain samples from these patterns.

Thirdly, this research has demonstrated, at least to some degree, the potential advantages that a 3D CG virtual environment developed specifically for the investigation, interpretation, and presentation of site of impact estimate data can provide. The use of 3D modelling software within BPA is already proving effective in the construction and presentation of site of impact estimates. Arguably, however, the interactive analytical potential of such 3D virtual environments, which is likely to become increasing viable with the inclusion of site of impact estimation techniques within 3D crime scene scanning and reconstruction technologies is not currently exploited to the level of that achieved within this research project. The 3D CG interactive virtual estimation environment developed for this research project provides an information-rich user-led investigative experience, which enables the analysis and interpretation of site of impact estimate data, and the evaluation of the potential significance of this data within an approximation of the native 3D spatial context of the spatter bloodstain data, and the spatter-producing impact event. The interactive visual medium offered by such approaches to the presentation and investigation of large and complex numerical data sets provides an immediately more accessible method for the representation and interpretation site of impact estimation data and the results of its analysis. The interactive visualisation methodology employed within the 3D virtual environment enables multiple features of an estimate to be visually compared and evaluated in relation to their spatial locations, sizes, configurations and associations, as well as reviewing the numerical results upon which a number of the less complex geometrical estimate features are based. While no direct critical comparison has been made with other computer-based methods of the representation and interpretation of site of impact estimation data, the interpretatively significant orthographic projections associated with widely

accepted computer-based site of impact estimation methodologies are provided within the data visualisation methodology developed for this research project. As a result, the benefits of both integrated 3D interactive perspective-based and orthographic plan- and elevation-based representations of site of impact estimate data, which are both included within the 3D CG virtual environment, are clearly demonstrated. The visualisation methodology developed, however, can be considered to be limited in both its analytical and interpretive functionality. While the virtual environment represents a sterile investigative context within which the detailed and isolated analysis of site of impact estimate data can be conducted, the results of this analysis remain largely decontextualised from the physical crime scene context from which the spatter bloodstain data was derived. In addition, although the visualisation methodology can be considered to be interactive, in the sense that the 3D virtual environment can be freely navigated, and the data visualised controlled, the methodology is not truly analytically interactive in the sense that the construction and analysis of an estimate cannot be refined or manipulated during the investigative process.

Finally, the results of the pilot project conducted into the utility of an automated IA approach to the quantification of spatter morphology indicate that an objective, reproducible, and quantifiably qualitative assessment of spatter bloodstain data for the purposes of site of impact estimation can be achieved. While limited in terms of the preliminary nature of the investigation, the idealised spatter bloodstain shapes and binary images analysed and the limited range of IA techniques applied, the analytical potential of such techniques in providing reproducible quantitative data concerning the morphology of spatter bloodstains, and specifically those characteristics required for site of impact estimation, has been demonstrated. In order to provide a time- and cost-effective method for recording large amounts of spatter bloodstain data analogous to the exhaustive manual recording methodology developed during this research project, however, the implementation and application of such automated IA techniques will require a substantial amount of further research and development. The potential advantages of such an automated IA system arguably warrant such development, with its ability to provide BPA with a structured and consistent methodology for the interpretation and quantification of spatter bloodstain morphologies, and a firmer evidential base for the analysis and investigation of impact spatter patterns and the construction and evaluation of site of impact estimates and estimate uncertainty. The spatter bloodstain data necessary for such development could initially be provided from the scaled-photographic images taken of the three

experimental impact spatter patterns during the recording phase of this research, or the images generated during the other additional pilot project, conducted during this research project, into the potential utility of a sampled scaled-photographic spatter bloodstain recording methodology. This data, and the recording methodology that created it, could represent an interim stage in the development of rapid large-scale impact spatter pattern capture and spatter bloodstain morphological analysis techniques. Given continued development, and the integration of site of impact estimation techniques within 3D crime scene geometry-capture techniques and the potential of detailed empirical analysis and detailed estimate construction methodologies demonstrated by this research project, rapid large-scale photographic recording methodologies could become increasingly practical and possibly indispensable within site of impact estimation. Where this collection of large amounts of raw spatter bloodstain data can be achieved with a reliable and high degree of accuracy, the potential for the detailed investigation and interpretation of impact spatter bloodstain patterns, their associated site of impact estimates and estimate uncertainty, is likely to be considerably enhanced when compared to current relatively small-scale spatter bloodstain analyses.

#### **12.4 Future Work**

It has been suggested that computer-aided analysis is an area within BPA that is ripe for development, allowing analysts to utilise more in-depth analytical techniques in the investigation and evaluation of bloodstain evidence and test their reconstructive hypotheses. The possible application of such computer-based analyses, however, has received little attention in terms of exploring and defining the future of such applications in this forensic reconstructive field (Bevel and Gardner, 2002). The potential demonstrated by the analytical computer-based approaches developed and implemented within this research project to facilitate the investigation, construction and evaluation of site of impact estimates could represent one such future for computer-aided analysis within BPA. The relatively preliminary and innovative nature of this research, however, means that the application of its findings, and its analytical techniques are not without a number of limitations, which would benefit from further research.

Firstly, the identification and implementation of alternative analytical techniques for the investigation of spatter bloodstain and site of impact estimation data could

provide additional and potentially more appropriate methods for the analysis of the large-scale and detailed spatter bloodstain and trajectory intersection data sets considered within this research project. The application of alternative and potentially more probative analytical techniques for the description, investigation and statistical evaluation of the spatial location, distribution, dependence and association of trajectory intersection estimate data, for example, could provide alternative investigative methods for the examination and evaluation of constructed estimates and the interpretation of estimate uncertainty. The analysis of the composition of collections of spatter bloodstains could also benefit from the identification and application of more appropriate analytical techniques. The application of multivariate analyses, for example, could be better suited to analysing the range of variables that are associated with each spatter bloodstain through the pre-processing and intersection calculation phases of the analytical site of impact estimation application. Combined with the empirical total impact spatter pattern enumeration methodology and independent data quality assessment functionality of the analytical approach employed during this research project, the application of such techniques, with future development, could prove effective in highlighting, investigating, and evaluating spatter bloodstain selection criteria. Whether these criteria are pre-existing or empirically established, the explicit and detailed analysis of experimental impact spatter pattern data could, where applied in conjunction with established theoretical and practical selection criteria, and the interpretive skill and experience of a BPA practitioner, provide site of impact estimation with a comprehensive, quantifiable, and structured approach to selection of spatter bloodstain samples for the purposes of constructing site of impact estimates, as well as the investigation and interpretation of impact spatter patterns in terms of the spatial distribution, similarity and dissimilarity of their constituent spatter bloodstain variables.

Secondly, the visualisation methodology employed during this research project is another area which would benefit from further development and investigation. The potential of interactive 3D CG virtual environments in the construction and analysis of site of impact estimates could become increasingly significant given the migration of computer-based estimation methodologies into 3D crime scene capture and reconstruction technologies. As a result, the integration of the 3D site of impact estimation visualisation methodologies within contextual crime scene models could prove to be a significant area of future research. While the development of such functionality could present a necessary contextual aspect to evaluation of site of impact estimate data, as well as provide a potential valuable

presentational tool, the advantages and limitations of such an approach, especially concerning the scientific validity of the combination of reconstruction and estimate construction, require explicit investigation. Another area in which the potential of the 3D virtual site of impact estimation environment could potentially be improved is in the provision of a truly interactive analytical investigative methodology. The ability to interact with, manipulate, and define the nature of the estimate constructed within the context of a 3D CG environment could provide additional and probative functionality which could aid the investigation and interpretation of impact spatter pattern data, the construction, analysis and evaluation of site of impact estimates, and the examination and assessment of potential estimate uncertainty.

Thirdly, a potentially fundamental limitation in the application of the findings of this research project is the restricted nature of the data upon which the analysis of site of impact estimation and estimate uncertainty is based. To provide a wider and more representative evidential base for the extension of the findings of this, and any future research that utilises the extensive and detailed impact spatter pattern data recorded during this research project, the number and nature of the impact spatter patterns analysed arguably requires some diversification. The validity of the extension of the results of the experimental impact spatter generation and recording methodologies employed during this research project to the varied nature and manifestation of non-experimental impact and pattern creation mechanics, and the contextual recording of spatter bloodstains within casework scenarios, for example, could be queried. The future creation and investigation of alternative impact spatter patterns could, consequently, be a viable avenue of further research. The production of impact spatter patterns using alternative impact methods, volumes of blood, impact site structure, target surface configurations, blood temperatures, and the development and implementation of a practical exhaustive recording methodology for the recording of spatter bloodstain upon the target surface geometry on which they were deposited, could all provide the potentially probative results of the analysis of site of impact estimate uncertainty with a more representative evidential foundation. The generation and analysis of impact spatter patterns with specific controlled variables could also provide additional investigative potential for the detailed analytical techniques developed and implemented within this research project for the analysis of impact spatter patterns and the construction of site of impact estimates. In addition to the questions concerning the extension of the results generated from the restricted

evidential base of this research project, the actual analysis of the potential site of impact estimation data generated during this research project was necessarily limited in the discussion of the research results produced. While six out of the potential of 612 estimates, constructed in line with the extensive sampling procedure employed during this research project, were selected and explicitly analysed based on their potential probative and comparative value, the results of a large number of other potentially informative site of impact estimates are still awaiting examination. A future direction for the investigation of the utility of the site of impact estimation application and the investigation estimate uncertainty would, consequently, be in the identification, examination, and evaluation of the outcomes of a significant number of these other estimates, and the investigation of the additional analytical techniques that were included within the site of impact estimation computer application, but not explicitly evaluated in respect to the estimate results discussed within this thesis.

Finally, and perhaps the most crucially for the practical further empirical investigation of site of impact estimation uncertainty using large-scale impact spatter patterns data, and the development of a viable version of the detailed analytical estimate methodology that can be applied in casework conditions, the further investigation and application of automated IA technologies in the quantification of spatter bloodstain morphologies is arguably essential. As already discussed, the potential utility of even a relatively limited automated IA procedure has been successfully demonstrated within this research. The development and implementation of totally automated techniques, however, where multiple spatter bloodstains are identified and isolated from variable background surfaces, and accurately measured in terms of the attributes required for the construction of straight-line trajectory approximations, present a number of specific analytical requirements beyond those of the pilot project, which require further research. In addition to some of the more procedural aspects of IA, the development of image capture methodologies, which can provide sufficient resolution for the accurate measurement of spatter bloodstains, but still provide a comparatively rapid and accurate method for recording large amounts of spatter bloodstain data within an environmental co-ordinate system, will require further investigation and practical experimentation.

## References

3rdTech, (2004a) '*SceneVision-3D*' to work with '*BackTrack*' for 3D Blood Spatter Analysis [online]. Available at < [http://www.3rdtech.com/SceneVision\\_BackTrack\\_news\\_release.htm](http://www.3rdtech.com/SceneVision_BackTrack_news_release.htm) >. Last accessed April 2005.

3rdTech (2004b) *Revolutionary 3D Scene Capture, Viewing and Analysis* [online]. Available at < <http://www.3rdtech.com/images/deltadsforweb.pdf> >. Last accessed April 2005.

3rdTech (2005) *Revolutionary 3D Scene Capture, Viewing and Analysis* [online]. Available at < [http://www.deltasphere.com/deltasphere\\_crimeaccident.htm](http://www.deltasphere.com/deltasphere_crimeaccident.htm) >. Last accessed April 2005.

ACSR (2005) *Association of Crime Scene Reconstruction* [online]. Available at < <http://www.acsr.org/> >. Last Accessed June 2005.

Adobe Systems Incorporated (1999) Adobe® Photoshop® 5.5. Adobe Systems Incorporated, 345 Park Avenue, San Jose, CA, USA.

Adobe Systems Incorporated (2001) Adobe® Illustrator® 10. Adobe Systems Incorporated, 345 Park Avenue, San Jose, CA, USA.

Aitken, C.G.G. (1995) *Statistics and the Evaluation of Evidence for Forensic Scientists*. John Wiley and Sons: Chichester.

Bailey, T.C. and Gatrell, A.C. (1995) *Interactive Spatial Data Analysis*. Longman: Harlow.

Barndorff-Nielsen, O.E., Kendall, W.S. and van Lieshout, M.N.M. (1999) *Stochastic Geometry: Likelihood and Computation*. Chapman and Hall/CRC: London.

Benecke, M. and Barksdale, L. (2003) Distinction of Bloodstain Patterns from Fly Artifacts. *Forensic Science International*, 137: 152-159.

- Bevel, T. and Gardner, R.M. (2002) *Bloodstain Pattern Analysis: with an Introduction to Crime Scene Reconstruction* (2<sup>nd</sup> Ed.). CRC Press: London.
- Bevington, P.R., and Robinson, D.K. (1992) *Data Reduction and Error Analysis for the Physical Sciences*. McGraw-Hill: USA.
- Bohan T.L. and Yergin, A.A. (1999) Computer-Generated Trial Exhibits: A Post-Daubert Update. *Accident Reconstruction: Technology and Animation 9*, Warrendale, USA, Society of Automotive Engineers: 199-210.
- Bowman, A.W. and Azzalini, A. (1997) *Applied Smoothing Techniques for Data Analysis: The Kernel Approach with S-Plus Illustrations*. Oxford University Press: Oxford.
- Brady, T., Tigmo, J. and Graham, G. (2002) Extreme Temperature Effects on Bloodstain Pattern Analysis. *IABPA Newsletter*, June: 3-20 [online]. Available at < <http://www.iabpa.org/June2002News.pdf> >. Last accessed August, 2005.
- Carl Zeiss Ltd (2005) KS 400 version 3.1. Carl Zeiss Ltd, PO Box 78, Hertfordshire. AL7 1LU.
- Carter, A.L. and Podworny, E.J. (1991) Bloodstain Pattern Analysis with a Scientific Calculator. *Journal of the Canadian Society of Forensic Sciences*, 24 (1): 37-42.
- Carter, A.L. (1998) Bloodstain Pattern Analysis with a Computer. In S.H. James (Ed.) *Scientific and Legal Application of Bloodstain Pattern Interpretation*, pp17-32. CRC Press: London.
- Carter, A. L. (2001) The Directional Analysis of Bloodstain Patterns, Theory and Experimental Validation. *Journal of the Canadian Society of Forensic Sciences*, 34 (4): 173-189.
- Carter, A.L. (2004a) *Bloodspatter Analysis with Computers* [online]. Available at < <http://www.physics.carleton.ca/~carter/> >. Last accessed April 2005.



- Carter, A.L. (2004b) *Alfred L. Carter Ph.D.* [online]. Available at < <http://www.physics.carleton.ca/~carter/alcarter.htm> >. Last accessed April 2005.
- Carter, A.L., Collins, R., Larocque, S. and Yamashita, B. (2004) The Directional Analysis of a Bloodstain Pattern Located on a Sloped Ceiling. *IABPA Annual Conference*, Tucson, Arizona, USA. October 6th – 8<sup>th</sup>.
- Chafe, F. (2003) Determination of Impact Angle Using Mathematical Properties of the Ellipse. *IABPA Newsletter*, March: 5-9 [online]. Available at < <http://www.iabpa.org/March2003News.pdf> >. Last accessed August 2005.
- Cheatham, C.S. and Flach, N.W. (2003) A National Survey of Police Exposure to Bloodstain Pattern Analysis. *IABPA Newsletter*, June: 4-13 [online]. Available at < <http://www.iabpa.org/Jun2003News.pdf> >. Last accessed September, 2005.
- Chernick, M.R. (1999) *Bootstrap Methods: A Practitioner's Guide*. John Wiley and Sons: Chichester.
- Chisum, W.J. (2000) *A Commentary on Bloodstain Analyses in the Sam Sheppard Case* [online]. Available at < [http://law-forensic.com/bloodstain\\_2.htm](http://law-forensic.com/bloodstain_2.htm) >. Last accessed October 2002.
- Clegg, F. (1982) *Simple Statistics*. Cambridge University Press: Cambridge.
- Cooley, C.H. (2001) *Law, Reliability and the Reconstructionist: Why the Supreme Court and Federal Rules of Evidence Require the Reconstructionist to Employ the Scientific Method* [online]. Available at < [http://www.law-forensic.com/annual\\_training\\_conference\\_vegas.htm](http://www.law-forensic.com/annual_training_conference_vegas.htm) >. Last accessed February 2003.
- Cressie, N.A.C. (1993) *Statistics for Spatial Data*. John Wiley and Sons: Chichester.
- Davis, J.C. (1986) *Statistics and Data Analysis in Geology* (2<sup>nd</sup> Ed.). John Wiley and Sons: Chichester.

- Diggle, P. (2003) *Statistical Analysis of Point Patterns* (2<sup>nd</sup> Ed.). Arnold: London.
- Dillon, W.R. and Goldstein, M. (1984) *Multivariate Analysis: Methods and Applications*. John Wiley and Sons: Chichester.
- Douglas, J.F., Gasiorek, J.A. and Swaffield, J.A. (1995) *Fluid Mechanics* (3<sup>rd</sup> Ed.). Longman Scientific and Technical: London.
- eFunda (2005) *Engineering Fundamentals* [online]. Available at < <http://www.efunda.com/math/areas/EllipseGen.cfm> >. Last accessed August 2005.
- Eikelenboom, R. (2003) Bloodstain Pattern Analysis: The Professional Approach. Proceedings of the 3<sup>rd</sup> European Academy of Forensic Science Meeting, Istanbul, Turkey, 22-27 September. *Forensic Science International*, 136 (Supplement 1): 21.
- Eliason, A. and Malarky, R. (1999) *Visual Basic 6: Environment, Programming and Application*. Que, Macmillan Computer Publishing: Indianapolis, Indiana, USA.
- Emes, A. and Price, C. (2004) Bloodstain Pattern Analysis. In P.C. White (Ed.) *Crime Scene to Court: The essentials of forensic science*, pp115-141. Royal Society of Chemistry: London.
- Everitt, B.S., Landau, S. and Leese, M. (2001) *Cluster Analysis* (4<sup>th</sup> Ed.). Arnold: London.
- Evident Crime Scene Products (2002) *Blood Spatter and Trajectory Equipment* [online]. Available at < <http://www.evidentcrimescene.com/cata/blood/blood.htm> >. Last Accessed January 2003.
- Fischer, W.C. (1998) Defining the 'Address' of Bloodstain and Other Evidence at the Crime Scene. In S.H. James (Ed.) *Scientific and Legal Application of Bloodstain Pattern Interpretation*, pp1-15. CRC Press: London.

- Fischer, W.C. (2001) Velocity Problems and Pressure Differentials in the Formation of Bloodstains (Letter to the Editor). *IABPA Newsletter*, June: 5-8 [online]. Available at < [www.iabpa.org/June2001News.pdf](http://www.iabpa.org/June2001News.pdf) >. Last accessed March 2004.
- Fotherington, A.S., Brunsdon, C. and Charlton, M. (2000) *Quantitative Geography: Perspectives on Modern Spatial Analysis*. Sage Publications: London.
- Forensic Computing of Ottawa Inc., Ottawa, Ontario, Canada (2001a) Tracks® 2.2 (Demonstration version),
- Forensic Computing of Ottawa Inc., Ottawa, Ontario, Canada (2001b) BackTrack®/Win 3.05 (Demonstration version).
- Forensic Computing of Ottawa Inc., Ottawa, Ontario, Canada (2001c) BackTrack®/Images 3.05 (Demonstration version).
- Frohn, A. and Roth, N. (2000) *Dynamics of Droplets*. Springer Verlag: London.
- Gatrell, A.C., Bailey, T.C., Diggle, P.J. and Rowlingson, B.S. (1996) Spatial point pattern analysis and its application in geographical epidemiology. *Transactions of the Institute of British Geographers*, 21: 256-274.
- Geometric Tools (2005) *Source Code Page* [online]. Available at < <http://www.geometrictools.com/SourceCode.html> >. Last Accessed August 2005.
- Goodwin, L. (2005) *Visualising Vehicle Accidents: Evidence Uncertainty, Presentation and Admissibility*. Thesis submitted to the University of Nottingham for the degree of Doctor of Philosophy, 2004.
- Grimes W. D. (1994) Classifying the Elements in a Scientific Animation. *Accident Reconstruction: Technology and Animation 4*, Warrendale, USA, Society of Automotive Engineers: 397-404.
- Guttorp, P (1995) *Stochastic Modeling of Scientific Data*. Chapman and Hall: London.

- Hart, D., and Croft, T. (1988) *Modelling with Projectiles*. Ellis Horwood: Chichester.
- Henderson, C. (1998) Legal and Ethical Aspects of Bloodstain Evidence. In S.H. James (Ed.) *Scientific and Legal Applications of Bloodstain Pattern Interpretation*, pp 91-120. CRC Press: London.
- Heuvelink, G.M.B. (1998) *Error Propagation in Environmental Modelling with GIS*. Taylor and Francis: London.
- Hulse-Smith, L., Mehdizadeh, N.Z. and Chandra, S. (2005) Deducing Drop Size and Impact Velocity from Circular Bloodstains. *Journal of Forensic Sciences*, 50 (1): 54-63.
- IABPA (2004a) *International Association of Bloodstain Pattern Analysts* [online]. Available at < <http://www.iabpa.org/> >. Last Accessed October 2004.
- IABPA (2004b) *Terminology List* [online]. Available at < <http://www.iabpa.org/Terminology.pdf> >. Last Accessed June 2005.
- IABPA (2004c) *International Association of Bloodstain Pattern Analysts Bloodstain Pattern Analysis Basic Course: Course Requirements* [online]. Available at < <http://www.iabpa.org/RevEduc.pdf> >. Last Accessed June 2005.
- IAI (2004) *International Association of Identification Bloodstain Pattern Analysis Certification* [online]. Available at < <http://www.theiai.org/certifications/bloodstain/index.html> >. Last Accessed October 2004.
- Jackson, A.R.W, and Jackson, J.M (2004) *Forensic Science*. Pearson, Prentice Hall: London.
- Jackson, J.E. (1991) *A User Guide to Principle Components*. John Wiley and Sons: Chichester.
- James, S.H., and Eckert, W.G. [Eds.] (1998) *Interpretation of Bloodstain Evidence at Crime Scenes* (2<sup>nd</sup> Ed.). CRC Press: London.

- James, S.H., and Sutton, T.P. (1998a) Low-Velocity Impact and Angular Considerations of Bloodstains. In James, S.H. and Eckert, W.G. (Eds.) *Interpretation of Bloodstain Evidence at Crime Scenes* (2<sup>nd</sup> Ed.), pp 19-58. CRC Press: London.
- James, S.H., and Sutton, T.P. (1998b) Medium- and High-Velocity Impact Spatter. In James, S.H. and Eckert, W.G. (Eds.) *Interpretation of Bloodstain Evidence at Crime Scenes* (2<sup>nd</sup> Ed.), pp 56-83. CRC Press: London.
- James, S.H. (1998a) Introduction to Bloodstain Pattern Interpretations and Properties of Blood. In James, S.H. and Eckert, W.G. (Eds.) *Interpretation of Bloodstain Evidence at Crime Scenes* (2<sup>nd</sup> Ed.), pp 1-17. CRC Press: London.
- James, S.H. (1998b) The Significance of Partially Dried, Clotted, Aged and Physically Altered Bloodstains. In James, S.H. and Eckert, W.G. (Eds.) *Interpretation of Bloodstain Evidence at Crime Scenes* (2<sup>nd</sup> Ed.), pp 85-103. CRC Press: London.
- James, S.H. (1998c) Outline of Basic Laboratory Experiments for Bloodstain Pattern Interpretation. In S.H. James (Ed.) *Scientific and Legal Applications of Bloodstain Pattern Interpretation*, CRC Press: London.
- James, S.H. (1998d) The Documentation, Collection, and Evaluation of Bloodstain Evidence. In James, S.H. and Eckert, W.G. (Eds.) *Interpretation of Bloodstain Evidence at Crime Scenes* (2<sup>nd</sup> Ed.), pp 125-151. CRC Press: London.
- Johnson, R.A and Wichern, D.W. (2002) *Applied Multivariate Statistical Analysis* (5<sup>th</sup> Ed.). Pearson Education: New Jersey, USA.
- Kish, P.E. (1998) Approach to Case Evaluation and Report Writing. In S.H. James (Ed.) *Scientific and Legal Applications of Bloodstain Pattern Interpretation*, pp 71-89. CRC Press: London,

- Kou, C., Lin, C. and Springsteel, F. (1992) HABSIS: An Expert System to Reconstruct Crime Scene based on Bloodstain Interpretations. *Proceedings of the 26<sup>th</sup> IEEE Annual International Carnahan Conference on Security Technology*, October. 14-16, pp 74-80.
- Krzanowski, W.J. (2000) *Principles of Multivariate Analysis: A User's Perspective* (Revised Edition). Oxford University Press: Oxford.
- Krzanowski, W.J. and Marriott, F.H.C. (1994) *Multivariate Analysis, Part 1: Distributions, Ordination and Inference*. Edward Arnold: London.
- Lee, H.C., Palmbach, T. and Miller, M.T. (2001) *Henry Lee's Crime Scene Handbook*. Academic Press: London.
- Lewis, J. (2003) Personal Communication.
- Laber, T., and Epstein, B. (2004) *Bloodstain Pattern Analysis Introductory Course*. Forensic Access, Culham, Oxfordshire, UK. 6<sup>th</sup> February, 2004.
- Landau, D.P. and Binder, K. (2000) *A Guide to Monte Carlo Simulations in Statistical Physics*. Cambridge University Press: Cambridge.
- Lawson, A.B. (2001) *Statistical Methods in Spatial Epidemiology*. John Wiley and Sons: Chichester.
- MacDonell, H.L. (1996) *Crime Scene Evidence: Blood Spatters and Smears and Other Physical Evidence* [online]. Available at < [http://www.law-forensic.com/bloodstain\\_1.htm](http://www.law-forensic.com/bloodstain_1.htm) >. Accessed September 2002.
- MacDonell, H.L., (2004) Another Confusing Bloodstain Pattern [online]. *IABPA Newsletter*, September 2004: 11-15. Available at < <http://www.iabpa.org/Sept2004News.pdf> >. Accessed April 2005.
- Macromedia Inc. (2001) Macromedia<sup>®</sup> Director 8.5<sup>®</sup>. Macromedia, Inc. 601 Townsend Street, San Francisco, CA 94103. USA.

- Macromedia Inc. (2005) Macromedia® Director® [online]. Available at < <http://www.macromedia.com/software/director/> >. Last accessed September, 2005.
- Marriner, B. (1991) *Forensic Clues to Murder: Forensic Science in the Art of Crime Detection*. Arrow: London.
- Mavin, T.J. (2002) A Laser Angle Gauge for Use in Stringing Blood Patterns. *IABPA News*, September 2002 [Online]. Available at < <http://www.iabpa.org/Sept2002News.pdf> >. Last Accessed November 2004.
- McKinney, B. (1997) *Hardcore Visual Basic* (2<sup>nd</sup> Ed.). Microsoft Press: Washington, USA.
- Microsoft Corporation (1999) Microsoft Office 2000. Microsoft Corporation, One Microsoft Way, Redmond, WA, USA.
- Microsoft Corporation (2005) *Visual Basic for Applications Overview* [online]. Available at < <http://msdn.microsoft.com/isv/technology/vba/overview/default.aspx> >. Last accessed August 2005.
- Moore, C.C. (2002) Three Dimensional Models for Bloodstain Pattern Analysis. *Journal of Forensic Identification*, 52 (2):182-203.
- Morrison, D.F. (2005) *Multivariate Statistical Methods* (4<sup>th</sup> Ed.). Brooks/Cole: California, USA.
- Murray, D.C. (2000a) *An Advocates Approach to Bloodstain Pattern Analysis Evidence (Part 1)* [online]. Available at < <http://www.iabpa.org/sep2000htm> >. Last accessed September 2002.
- Murray, D.C. (2000b) *An Advocates Approach to Bloodstain Pattern Analysis Evidence (Part 2)* [online]. Available at < [www.iabpa.org/june2000htm](http://www.iabpa.org/june2000htm) >. Last accessed September 2002.

- Nakayama, Y., and Boucher, R.F. (1999) *Introduction to Fluid Mechanics*. Arnold: London.
- NBS (2005) *The National Blood Service* [online]. Available at < <http://www.blood.co.uk/> >. Last Accessed June 2005.
- Nelson, E.L. (1999) Bloodspatter [online]. Was available at < [www.xmisson.com/~elnelson/blood-spatter/spatter-matters.html](http://www.xmisson.com/~elnelson/blood-spatter/spatter-matters.html) >. Last accessed June 2002. Website no longer available.
- NIST/SEMATECH (2005) *Engineering Statistics Handbook* [online]. Available at < <http://www.itl.nist.gov/div898/handbook/> >. Last accessed August 2005.
- Noond J., Schofield D., March J. and Evison M. (2002) Visualising the Scene: Computer Graphics and Evidence Presentation, *Science and Justice*, Journal of The Forensic Science Society, 42(2): 89 – 96.
- Norton, P. and Groh, M. (1998) *Guide to Visual Basic 6*. Sams, Macmillan Computer Publishing: Indianapolis, Indiana, USA.
- NZFSS (2001) Future Forensics. *New Zealand Forensic Society Newsletter* [online], December 2001: 9. Available at < <http://www.nifs.com.au/ANZFSS/States/NZNewsletterDecember2001.PDF> >. Last Accessed June 2005.
- Ott, R.L. and Longnecker, M. (2001) *An introduction to Statistical Methods and Data Analysis* (5<sup>th</sup> Ed.). Duxbury: California, USA.
- O’Sullivan, D. and Unwin, D.J. (2003) *Geographical Information Analysis*, John Wiley and Sons: Chichester.
- Peel Regional Police (2004) *Bloodstain Patterns* [online]. Available at < <http://www.peelpolice.on.ca/FIS/Blood-Pat.html> >. Last Accessed November 2004.
- Pizzola, P.A., Roth, S. and DeForest, P.R (1986a) Blood Droplet Dynamics – 1. *Journal of Forensic Sciences*, 31 (1): 36-49.



- Pizzola, P.A., Roth, S. and DeForest, P.R (1986b) Blood Droplet Dynamics – 2. *Journal of Forensic Sciences*, 31 (1): 50-64.
- Pace, A. (2004a) Personal Communication.
- Pace, A. (2004b) *Bloodstain Pattern Analysis* [online]. Available at < <http://www.bloodstain-forensics.com/> >. Last Accessed April 2005.
- Perry, G. (1998) *Teach yourself Visual Basic 6 in 21 days*. Sams, Macmillan Computer Publishing: Indianapolis, Indiana, USA.
- Rabinovich, S. (1995) *Measurement Errors: Theory and Practice*. American Institute of Physics: New York, USA.
- Raymond, M.A., Smith, E.R. and Liesegang, J. (1996a) The Physical Properties of Blood – Forensic Considerations. *Science and Justice*, 36 (3): 153-160.
- Raymond, M.A., Smith, E.R. and Liesegang, J. (1996b) Oscillating Blood Droplets – Implications for Crime Scene Reconstruction. *Science and Justice*, 36 (3): 161-171.
- Reselman, B, Pruchniak, W. Peasley, R.A., and Smith E.A. (1999) *Practical Visual Basic 6*. Que, Macmillan Computer Publishing: Indianapolis, Indiana, USA.
- Reynolds, M. (2004a) Target Surface Influence on Angle of Impact. *IABPA Newsletter* [online], March 2004: 4-5. Available at < <http://www.iabpa.org/March2004News.pdf> >. Last Accessed April 2005.
- Reynolds, M. (2004b) Personal Communication.
- Rinehart, D.J. (2000) *Computers vs. Strings: 2 cases in point* [online]. Available at < <http://crime-scene-investigator.net/computersvstrings.ntml> >. Accessed May 2002.
- Ripley, B.D. (1981) *Spatial Statistics*. John Wiley and Sons: Chichester.

- Ristenbatt, R.R. and Shaler, R.C. (1995) A Bloodstain Pattern Interpretation in a Homicide Case Involving an Apparent "Stomping". *Journal of Forensic Sciences*, 40 (1): 139-145.
- Rogerson, P.A. (2001) *Statistical Methods for Geography*. Sage Publications: London.
- Saccoccio, M.E. (1998) *Bloodstain Pattern Interpretation: A Post-Conviction Analysis*. In S.H. James (Ed.) *Scientific and Legal Applications of Bloodstain Pattern Interpretation*, pp 121-156. CRC Press: London,
- Saferstein, R. (1995) *Criminalistics: An introduction to forensic science*. Prentice Hall: New Jersey, USA.
- Schofield D., Noond J., Goodwin L., and March J. (2002) Interactive Evidence: New Ways To Present Accident Investigation Information. *Proceedings of the Workshop on the Investigation and Reporting of Incidents and Accidents*, University of Glasgow, pp 194 - 203, 17<sup>th</sup> - 20<sup>th</sup> July 2002.
- Schofield D. (2005) Personal Communication.
- Siegel, A.F. and Morgan, C.J. (1996) *Statistics and Data Analysis: An Introduction* (2<sup>nd</sup> Ed.). John Wiley and Sons: Chichester.
- Silk, J. (1981) *Statistical Concepts in Geography*. Allen and Unwin: London.
- Silverman, B.W. (1986) *Density Estimation for Statistics and Data Analysis*. Chapman and Hall: London.
- Sirignano, W.A. (1999) *Fluid Dynamics and Transportation of Droplets and Sprays*. Cambridge University Press: Cambridge.
- Slemko, J. (2002) *Bloodstain Pattern Analysis Tutorial* [online]. Available at < <http://www.bloodspatter.com/BPATutorial.htm> >. Last accessed Spetember 2005.
- Stoyan, D., Kendall, W.S. and Mecke, J. (1987) *Stochastic Geometry and its Applications*. John Wiley and Sons: Chichester.

- SWGSTAIN (2002) Bylaws of the Scientific Working Group on Bloodstain Pattern Analysis (SWGSTAIN). *Forensic Science Communications*, 2002; 4(3) [online]. Available at < <http://www.fbi.gov/hq/lab/fsc/backissu/july2002/swgstain.htm> >. Last accessed October 2004.
- Taylor, H.M. and Karlin, S. (1998) *An Introduction to Stochastic Modelling* (3<sup>rd</sup> Ed.). Academic Press: London.
- Taylor, P.J. (1977) *Quantitative Methods in Geography: An Introduction to Spatial Analysis*. Houghton Muffin: USA.
- Taylor, J.R. (1997) *An Introduction to Error Analysis: The Study of Uncertainties in Physical Measurements* (2<sup>nd</sup> Ed.) University Science Books: USA.
- The Bloody Sunday Inquiry (2005) *The Bloody Sunday Inquiry website*. Available at < <http://www.bloody-sunday-inquiry.org.uk/> >. Last accessed September 2005.
- Tulloch, S. [Ed.] (1995) *The Oxford Dictionary and Thesaurus*. Oxford University Press: Oxford.
- Upton, G. and Fingleton, B. (1985) *Spatial Data Analysis by Example. Volume 1: Point Pattern and Quantitative Data*. John Wiley and Sons: Chichester.
- University of Bradford (2004) *Bloodspatter* (The Department of Chemical and Forensic Sciences) [online]. Available at < <http://www.bradford.ac.uk/acad/chemistry/localaccess/pwrdreqd/FEESM/FEESM%20session8-2002.html> >. Last Accessed October 2004.
- Unwin, D. (1981) *Introductory Spatial Analysis*. Methuen: London.
- Van Stratton, M.J. (2003) *SWGSTAIN Report, Winter 2003* [online]. Available at < <http://www.asclid.org/newsletter/winter2003/swg.html> >. Last Accessed October 2004.

- Van Stratton, M.J. (2004) *SWGSTAIN Report*, Summer 2004 [online]. Available at < <http://www.asclid.org/newsletter/summer2004/committee.html> >. Last Accessed October 2004.
- Van Zyl, M. (2001) The value of Bloodstain Pattern Interpretation in Criminal Investigations. *Proceedings of the 2<sup>nd</sup> World Conference on Modern Criminal Investigation, Organised Crime and Human Rights*, Durban, South Africa. December 3<sup>rd</sup> –7<sup>th</sup> [online]. Available at < <http://www.crimeinstitute.ac.za/2ndconf/papers/vanzyl.pdf> >. Last accessed September, 2005.
- Veilleux, D.R. (1993) Admissibility in Criminal Prosecution, of Expert Opinion Evidence as to 'Blood Splatter' Interpretation. *American Law Reports*, 9 A.L.R. 5<sup>th</sup> 369.
- Walton J. (2003) *NAG's Iris Explorer*. In C.R. Johnson and C.D. Hansen (Eds.) *Visualization Handbook*. Academic Press: Cheshire.
- Wand, M.P. and Jones, M.C. (1995) *Kernel Smoothing*. Chapman and Hall: London.
- Ware, C. (2000) *Information Visualization: Perception for Design*. Morgan Kaufmann: USA.
- Watson, N. (2004) The Analysis of Bodily Fluids. In P.C. White (Ed.) *Crime Scene to Court: The essentials of forensic science*, pp377-413. Royal Society of Chemistry: London.
- Weiss, N.A. (1999) *Elementary Statistics* (4<sup>th</sup> Ed.). Addison-Wesley: Harlow.
- Weisstein, E. W. (1999) *Inverse Sine* [online]. From Mathworld, a Wolfram Web Resource. Available at < <http://mathworld.wolfram.com/InverseSine.html> > Last accessed July 2005.
- Willis, C., Piranian, A.K., Donaggio, J.R., Barnett, R.J. and Rowe, W.F. (2001) Errors in the Estimation of the Distance of Fall and Angles of Impact Blood Drops. *Forensic Science International*, 123: 1-4.

Wonder, A. (2001) *Blood Dynamics*. Academic Press: Cheshire.

Yen, K., Thali, M.D., Kneubuehl, B.P., Peschel, O., Zollinger, U. and Dirnhofer, R.  
(2003) Blood-Spatter Patterns: Hands Hold Clues for the Forensic  
Reconstruction of the Sequence of Events. *American Journal of Forensic  
Medicine and Pathology*, 23 (2): 132-140.

Zhang, J., and Goodchild, M. (2002) *Uncertainty in Geographical Information*.  
Taylor and Francis: London.

## Appendix A – Forensic Alliance Limited Examination of Biological Contaminated Material Information Sheet

### Examination of Biologically Contaminated Material

It is Forensic Alliance policy that all staff dealing with potentially biologically contaminated material will receive all appropriate training and inoculations. At present staff are routinely vaccinated against:

Hepatitis A and B  
Polio  
Tetanus  
TB

Staff will not be routinely vaccinated against meningitis because bacterial meningitis does not survive outside the body and therefore does not constitute a risk. \*

\*Information received from the Meningitis Research Foundation

### Blood-borne Pathogens

Hepatitis B is considered potentially the most infectious blood-borne pathogen but although Hepatitis C and HIV are considered significantly less infectious, these present more of a risk because presently no vaccine is available for either.

### Liquid Blood

The table below lists the chance of infection if a needle stick occurs with a syringe of highly contaminated blood:

Hepatitis B	30%
Hepatitis C	3%
HIV	0.3%

These levels are very approximate and apply to infected liquid blood transmitted directly into the blood stream. The risks of the same infected blood transmitting via mucous membranes are less, for example in the case of HIV, this falls to 0.1%.

All liquid blood samples will be opened and used within a fume hood and universal precautions will be taken during the examination. All sharps used during the examination will be disposed of in the sharps' bin inside the fume hood. Used syringes should be immediately disposed of without attempting to bend, break or re-sheath the needle.

### Dried Blood

There are no published risk ratings for the possibility of infection from dried blood and although the risk will be considerably reduced again, infection still remains a possibility, however slight. Following advice from NHS medical advisors and various published documents\*, Forensic Alliance has determined that universal precautions should be taken during all potential contact with biologically contaminated items. These are listed in FAL SI 11. In cases where an item is heavily bloodstained or there is an increased chance of blood flaking and dusting these precautions will include use of a fume hood or wearing safety goggles and a dust proof face mask, EN149 or above.

**Other Body fluids**

Other body fluids such as semen and vaginal material are also considered potentially infectious and although faeces, nasal secretions, saliva, sputum, sweat, tears, urine and vomit are considered to present a minimal risk, unless they contain blood, all biological examinations will be treated as a "worse case scenario" with the universal precautions outlined for blood still applying.

**Actions after exposure to potential infection**

- Immediately wash off splashes on skin with soap and running water
- Encourage bleeding if the skin has been broken and flush out the wound with running water
- Wash out splashes to the eye with eyewash from a fresh bottle
- Wash out splashes to the nose or mouth with tap water
- Report the incident without delay to the health and safety or line manager who will then arrange medical attention.
- Record the incident in the accident book

**\*see attached references**

**Attached References**

Protection against blood-borne pathogens in the work place: HIV and hepatitis  
Advisory Committee on Dangerous Pathogens

Blood-borne viruses in the workplace Guidance for employers and employees  
Health & Safety Executive

Exposure to blood What health care workers need to know  
CDC Department of Health and Human Services

HIV and its transmission  
CDC National Centre for HIV, STD and TB prevention

Updated U.S public health service guidelines for the management of occupational exposure to HBV, HCV and HIV and recommendations for post-exposure prophylaxis  
CDC MMWR

OSHA and blood-borne pathogens – 1 and 2

## Appendix B – Forensic Alliance Limited Bloodstain Experimentation Information Sheet

FORENSIC ALLIANCE LTD		FAL/LGN/	
HEALTH AND SAFETY	Bloodstain Experiments	Issue 1	March 2003

### General requirements

Where possible, transfusion blood should be used as this has been screened.

A person coughing or sneezing blood should use their own blood. This must be drawn by a qualified medical person, e.g at AEON.

Scene suit with hood up (or hair net), gloves, mask and visor must be worn by person(s) carrying out experiment and anyone else in immediate vicinity. Shoe covers must also be worn. Scene suit cuffs should be tucked into gloves and secured with tape.

A bucket of water should be present and any blood making contact with the skin should be washed off immediately.

### Set up

Where possible, the gazebo in the garage should be used. Fresh paper should be used to line the walls, floor and ceiling of the gazebo.

Surrounding items that may get splashed with blood should either be removed or covered with paper prior to commencement.

Where a pig carcass or other biohazardous material is to be attached to the dummy, the dummy should first be covered (e.g with a bin liner) in order to prevent the biohazardous material coming into direct contact with the dummy.

### Clean up

Visors should be cleaned with water and bleach solution after each stage.

Gloves, shoe covers and masks should be disposed of in biohazard bags after use;

Boiler suits/ scene suits should either be a) allowed to dry then packaged in clearly labelled brown paper bags for future examination or b) disposed of in biohazard bags.

Any weapons used should either be a) allowed to dry then packaged in clearly labelled brown paper bags for future examination or b) thoroughly cleaned in bleach solution

All lining paper in the gazebo, coverings for other items in the garage and coverings for the dummy should be disposed of in biohazard bags. Target boards or target sheets of paper should be allowed to dry and then packaged in clearly labelled brown paper bags for future examination.

The surface of the dummy and any exposed floor and framework should be washed down with bleach solution.

Any pig carcass should be correctly disposed of in adequate biohazard bags. Where the biohazardous material won't fit in biohazard bags, Grundons waste disposal company

<b>This procedure has been substantially revised</b>	
<b>The registered recipient is responsible for destroying all superceded documents</b>	
Author	
Approved by	
Approved by	



<b>FORENSIC ALLIANCE LTD</b>		<b>FAL/LGN/</b>	
<b>HEALTH AND SAFETY</b>	<b>Bloodstain Experiments</b>	<b>Issue 1</b>	<b>March 2003</b>

should be contacted to arrange delivery of an appropriately sized bin. The pig carcass should then be placed in the bin and the bin disposed of by Grundons.

All non disposable equipment used should be cleaned with bleach solution.

**Use of Sharp Weapons**

A thick butchers glove should be worn on the stabbing hand.

When stabbing a pig carcass, areas with bone should be avoided.

**Use of Rat/ Mouse Traps**

Care should be taken whilst using the trap. The trap should be placed on a flat surface before use.

Also refer to FAL-SI-11 and LGN- 13.

<b>This procedure has been substantially revised</b>	
<b>The registered recipient is responsible for destroying all superceded documents</b>	
Author	
Approved by	
Approved by	

## Appendix C – Forensic Alliance Limited Experimentation Risk Assessment

### Risk Assessment – New or Changed Procedure

Each new procedure or change in procedure is to be Risk Assessed in line with those carried out and documented in FAL/RA/14a and 14b. This form represents such an assessment for the specified procedure or change.

<b>Title of Procedure</b>	BLOOD TRAINING COURSE / EXPERIMENTS		
Reason for Risk Assessment (Please tick)	New Procedure		Change in Procedure

Step 1: List all procedural tasks and identify the associated hazard as specified in FAL/RA/14.

Task	Hazard Reference (FAL/RA/14)*
Setting up of courses/ experiments <sup>1</sup>	8, 11, 12, 19
Splashing, spraying, dripping, pouring of blood <sup>2</sup>	1, 3, 7, 8, 11, 12, 13, 19, 24
Use of mannequin/ pig	1, 3, 4, 8
Observing the above <sup>2</sup>	3, 13, 24
Cleaning up after course/ experiment	1, 2, 3, 7, 8, 24

\*This document must be updated if a new hazard is identified.

1. Experiments involving blood should be carried out in the garage with biohazard warning signs displayed on garage door 2. Blood used must have been previously screened. Universal precautions for examination of bloodstained items apply - see FAL SI 11.

Step 2: Follow up actions

a	Has a new hazard been identified? (please tick)	NO	Go to section (b)
		YES	Assess the hazard in terms of Risk Rating and Precautions in line with FAL/RA/14
b	Is the use of chemicals involved in the procedure or change in procedure? (please tick)	NO	Go to section (c)
		YES	Carry out a COSHH assessment.
c	What class of procedure is it? (please tick)	General	Update FAL/RA/14a
		Lab	Update FAL/RA/14b

Step 3: Cross Check

- Where required, all new HAZARD assessments have been carried out and FAL/RA/14 updated.
- Where required, all new COSHH assessments have been carried out.
- The relevant Risk Assessment document FAL/RA/14a(b) has been updated.

Author..... dated.....

Checker..... dated.....

New Procedure Approved by MD..... dated.....

8. Manual handling - equipment	2	3	6	Suitably trained staff <sup>e</sup> Purchase sufficient equipment where possible Use of appropriate aids
9. Manual handling - exhibits	1	3	3	Suitably trained staff <sup>e</sup> Use of appropriate aids Preferential storage at low levels Clear labelling Storage areas kept sufficiently uncluttered
10. Heat hazard	1	3	3	Suitably trained staff <sup>f</sup> PPE where appropriate
11. Electrical hazard	1	5	5	Suitably trained staff <sup>f</sup> Regular maintenance by qualified staff
12. Mechanical hazard	2	3	6	Suitably trained staff <sup>f</sup> Regular maintenance by qualified staff PPE <sup>d</sup>
13. Aerosol production	1	3	3	Suitably trained staff <sup>f</sup> Capped tubes, covered rotor PPE <sup>d</sup>
14. Non ionising radiation	1	3	3	Suitably trained staff <sup>f</sup> PPE <sup>d</sup>
15. Eye strain	1	2	2	Suitably trained staff <sup>g</sup> Regular breaks
16. Incorrect posture	1	3	3	Suitably trained staff <sup>f</sup> Correct seating

This procedure has been substantially revised  
The registered recipient is responsible for destroying all superseded documents

Author	
Approved by	
Approved by	

8. Manual handling - equipment	2	3	6	Suitably trained staff <sup>6</sup> Purchase sufficient equipment where possible Use of appropriate aids
9. Manual handling - exhibits	1	3	3	Suitably trained staff <sup>6</sup> Use of appropriate aids Preferential storage at low levels Clear labelling Storage areas kept sufficiently uncluttered
10. Heat hazard	1	3	3	Suitably trained staff <sup>1</sup> PPE where appropriate <sup>4</sup>
11. Electrical hazard	1	5	5	Suitably trained staff <sup>7</sup> Regular maintenance by qualified staff
12. Mechanical hazard	2	3	6	Suitably trained staff <sup>1</sup> Regular maintenance by qualified staff PPE <sup>4</sup>
13. Aerosol production	1	3	3	Suitably trained staff <sup>1</sup> Capped tubes, covered rotor PPE <sup>4</sup>
14. Non ionising radiation	1	3	3	Suitably trained staff <sup>1</sup> PPE <sup>6</sup>
15. Eye strain	1	2	2	Suitably trained staff <sup>1,8</sup> Regular breaks
16. Incorrect posture	1	3	3	Suitably trained staff <sup>1</sup> Correct seating

This procedure has been substantially revised  
The registered recipient is responsible for destroying all superseded documents

Author  
Approved by  
Approved by

17. Obstruction (low headroom)	3	2	6	Warning signs
18. Falling material	1	3	3	Appropriate stacking Use of appropriate aids
19. Falling from height	1	3	3	Suitably trained staff <sup>1</sup> Use of appropriate aids (e.g. ladders, kickstool etc)
20. Broken glass – non exhibit	1	3	3	Use of appropriate aids
21. Working : low lighting environment	1	2	2	Suitably trained staff <sup>1</sup> Work areas free from clutter Use of appropriate aids
22. Road traffic accident	1	7	7	Suitably trained staff <sup>9</sup> Regular maintenance of vehicle
23. Scene environment	1	5	5	Suitably trained staff <sup>9</sup> Lase with appropriate emergency services
24. Slipping on wet floor	1	3	3	Clean up any spillages immediately Ensure appropriate warning signs are used
25. Production of ozone	1	1	1	Ensure suitable ventilation
26. Noise hazard	1	3	3	Suitably trained staff PPE <sup>4</sup>

Notes : 1. General Laboratory Practice (locally given) 2. Working Procedure FAL/SI/11 3. Cleaning protocol FAL/SI/12 4. Provision of Personal Protective Equipment FAL/SI/21 & 5. Firearms Safety FAL/SI/24 6. HSE Document Getting to Grips with Manual Handling INDG143 7. HSE Document Electrical Safety and You INDG231 8. HSE document Working with VDUs INDG36 9. AEA Document Safe Driving SEGN201 10. Scene Risk Assessment FAL/GN/08

This procedure has been substantially revised	
The registered recipient is responsible for destroying all superseded documents	
Author	
Approved by	
Approved by	

## Appendix D – Forensic Alliance Limited Laboratory Working Procedure

FORENSIC ALLIANCE LTD		FAL/S1/11
HEALTH AND SAFETY Laboratory Working Procedure	Handling of Biological Samples Issue 3	June 2001

### Working Procedure

1. No eating, drinking, or applying make-up is allowed in the laboratory areas.
2. Personnel must wear laboratory coats and handle biological material wearing disposable gloves. Heavily and/or wet stained items must be examined in a fume cupboard.
3. All potentially contaminated material must be disposed of in a suitable, identified safety container.
4. All sharps (contaminated or not) must be disposed of in a suitable, identified sharps container.
5. The laboratory cleaning protocol (FAL/SI/12) must be adhered to.
6. Only sealed tubes are to be used in centrifuges. Wherever possible a cover should be used over the rotor.

<b>This procedure has been substantially revised</b>	
<b>The registered recipient is responsible for destroying all superceded documents</b>	
Author	Robert Burgess
Approved by	

## Appendix E – Spatter Bloodstain Recording Process Assessment

Process Assessment  
(Room B11 Biolaboratory Building L4 Laboratories) Page:1

UNIVERSITY OF NOTTINGHAM – SCHOOL OF CHEMICAL, ENVIRONMENTAL AND MINING ENGINEERING

Section: Building L4  
Assessor: Jack March (PG)  
Rig Name: N/A  
Rig Number: N/A  
Supervisor Signature:

Actions required: YES / NO  
Date: 9 October 2003 Issue: 1  
Rig Location: Biohazards Laboratory

School Safety officer Signature:

Hazard Likelihood: 5	Severity / Consequence: 3	Risk Score: 15
<b>1. Persons at Risk:</b> Operator and anyone in close proximity.		<b>8. Emergency Shut Off Procedure:</b> N/A
<b>2. Physical Conditions:</b> Temperature range: Ambient Pressure Range: Ambient		<b>9. Other Notes:</b> Contaminated waste materials including personal protective equipment will be collected in yellow biohazards bag for disposal.
<b>3. Chemicals involved:</b> Bleach solution (Sodium Hypochlorite < 5%) Plasti-Kote Super Spray Paint no. 1138 Dried screened human transfusion blood		<b>10. Experimental Procedure:</b> <ol style="list-style-type: none"> <li>Bloodstained brown paper unrolled and fixed using Plasti-Kote spray paint.</li> <li>Bloodstain pattern divided into 10cm<sup>2</sup> sections and photographed.</li> <li>Individual bloodspatters identified, counted and measured within each 10cm<sup>2</sup> section.</li> <li>Measurements include width, length and directional angle of the bloodstains, as well as position within overall pattern.</li> <li>Identified bloodstain individually and section photographed.</li> <li>Areas in contact with contaminated material will be cleaned with a bleach solution at the end of each recording session.</li> <li>Four patterns will be recorded in all.</li> </ol>
<b>4. Special Precautions for Chemicals:</b> Low risk as defined by Forensic Alliance Limited.		
<b>5. Biological Effects:</b> NONE		
<b>6. Rig Hazards:</b> Presence of dried human blood.		
<b>7. Special Precautions:</b> Paper fixed with Plasti-Kote to prevent bloodstain flaking. Full Forensic suit, face mask and double latex gloves worn at all times while in proximity to dried blood as defined by Forensic Alliance Limited universal blood experimentation policy. Area within biohazard laboratory restricted to researcher access during recording procedure.		
<b>Hazard Likelihood:</b> <ol style="list-style-type: none"> <li>Highly unlikely</li> <li>Remote Possibility</li> <li>Occasional Occurrence</li> <li>Fairly Frequent</li> <li>Frequent and Regular</li> <li>Almost a Certainty (Daily)</li> </ol>		
<b>Severity / Consequence:</b> <ol style="list-style-type: none"> <li>Negligible Injury</li> <li>Minor Injuries</li> <li>Major Injuries</li> <li>Single Fatality</li> <li>Multiple Fatality</li> <li>As 5 including off-site</li> </ol>		

Date of Printing: 13 October 2003

## Appendix F – Spatter Bloodstain Recording Risk Assessment

### Amendment to Bloodstain Experiment Risk Assessment – Recording Procedure to be conducted in SChEME Biohazards laboratory, University of Nottingham.

12/8/03  
Jack March

Task	Hazard Reference (FAL/RA/14)
Photography and measurement of dried bloodstains <sup>1</sup>	3, 8, 11, 12

1. Blood previously screened – see FAL/LGN and Examination of Biologically Contaminated Material.

Working Procedure will follow those set out in FAL/S1/11.

A full forensic scene suit, latex gloves and face mask (at least EN149) will be worn throughout the recording procedure. To further guard against flaking dried blood the contaminated material will initially be sprayed with a plastic coating (Plasti-Kote Super Spray Paint no. 1138, Clear Acrylic – as recommended by FAL staff)

Areas of Laboratory that have come into contact with bloodstained material will be cleaned down with a water-bleach solution after each recording session.

The contaminated material will be repackaged and stored in the biohazard laboratory in between recording sessions. The packages will be clearly marked as a biohazard and will provide contact numbers of relevant personnel.



## Appendix G – Plasti-Kote Material Safety Data Sheet

SECTION I - MATERIAL SAFETY DATA SHEET						PAGE 1 OF 2																																										
<p><b>PLASTI-KOTE CO., INC.</b></p> <p>1000 LAKE ROAD MEDINA, OHIO 44256 1-330-725-4511 1-800-255-3924 24 Hour Emergency Only</p>						DATE PREPARED: 09/29/00																																										
						<p><b>PRODUCT CLASS: AEROSOL SPRAY PAINT</b></p> <p>SHIPPING NAME: CONSUMER COMMODITY ORM-D INT'L UN NO. : 1950 NE = NONE ESTABLISHED NA = NONE AVAILABLE</p>																																										
<b>HAZARD RATING</b>		<b>HMS</b>			<b>NFPA</b>																																											
4 = SEVERE		HEALTH 1			HEALTH 2																																											
3 = SERIOUS		FLAMMABILITY 4			FLAMMABILITY 4																																											
2 = MODERATE		REACTIVITY 0			REACTIVITY 0																																											
1 = SLIGHT		PERSONAL -			OTHER --																																											
0 = MINIMAL		PROTECTION E																																														
SECTION II - HAZARDOUS INGREDIENTS.																																																
<b>PRODUCT NAME :</b>						<b>PRODUCT#</b>																																										
						<table border="1" style="width: 100%; border-collapse: collapse;"> <tr> <td style="width: 15%;">1100, 1102, 1104,</td> <td style="width: 10%;">1103</td> <td style="width: 10%;">1116</td> <td style="width: 10%;">CLEAR</td> <td style="width: 10%;">1140</td> <td style="width: 10%;">1150</td> <td style="width: 10%;">1146</td> </tr> <tr> <td>1105, 1107, 1108</td> <td></td> <td>1122</td> <td>1138</td> <td>1142</td> <td>THRU</td> <td>1147</td> </tr> <tr> <td>1109, 1112, 1113,</td> <td></td> <td></td> <td></td> <td></td> <td>1157</td> <td>1148</td> </tr> <tr> <td>1114, 1115, 1117,</td> <td></td> <td></td> <td></td> <td></td> <td></td> <td></td> </tr> <tr> <td>1120, 1123, 1126,</td> <td></td> <td></td> <td></td> <td></td> <td></td> <td></td> </tr> <tr> <td>1128, 1130, 1132, 1134</td> <td>% (wt)</td> <td></td> <td>% (wt)</td> <td>% (wt)</td> <td></td> <td></td> </tr> </table>							1100, 1102, 1104,	1103	1116	CLEAR	1140	1150	1146	1105, 1107, 1108		1122	1138	1142	THRU	1147	1109, 1112, 1113,					1157	1148	1114, 1115, 1117,							1120, 1123, 1126,							1128, 1130, 1132, 1134
1100, 1102, 1104,	1103	1116	CLEAR	1140	1150	1146																																										
1105, 1107, 1108		1122	1138	1142	THRU	1147																																										
1109, 1112, 1113,					1157	1148																																										
1114, 1115, 1117,																																																
1120, 1123, 1126,																																																
1128, 1130, 1132, 1134	% (wt)		% (wt)	% (wt)																																												
<b>ULTRA SPRAY ENAMEL</b>																																																
<b>INGREDIENT</b>	<b>CAS NUMBER</b>	<b>ACGIH TWA PPM</b>	<b>OSHA PEL PPM</b>	<b>OTHER TLV PPM</b>	<b>VAPOR PRESSURE mmHg at 20 C</b>	<b>1128, 1130, 1132, 1134</b>	<b>% (wt)</b>	<b>PROD.#</b>	<b>PROD.#</b>	<b>PROD.#</b>	<b>PROD.#</b>	<b>PROD.#</b>																																				
ACETONE	67-64-1	750	1000	---	186	33-42	33-42	33-42	30-35	15-35	32-40	10-15																																				
ALIPHATIC HYDROCARBON	64742-89-8	NE	NE	300	38							5-10																																				
AROMATIC HYDROCARBON	64742-95-6	NE	NE	100	3		0-5	0-5																																								
ETHYL ACETATE	141-78-6	400	400	---	69			0-5																																								
ISOPROPYL ALCOHOL	67-63-0	400	400	---	33	0-5						0-5																																				
ETHYL ALCOHOL	64-17-5	1000	1000	---	40	5-10	5-10	5-10				5-10																																				
ETHYL 3-ETHOXY PROPIONATE	763-69-9	NE	NE	50	.67	5-10	0-5	5-10				5-10																																				
* METHYL ETHYL KETONE	78-93-3	200	200	---	70	0-5	0-5	0-5				0-5																																				
MINERAL SPIRITS	64742-48-9	NE	NE	100	2.0					0-5																																						
* XYLENE	1330-20-7	100	100	---	5.1	5-10	5-10	5-10	35-40	25-55	5-10	30-40																																				
PROPANE-ISOBUTANE MIXTURE	68476-86-8	NE	1000	---	---	23	23	23	23	23	23	25																																				
* THIS CHEMICAL IS SUBJECT TO THE REPORTING REQUIREMENTS OF SECTION 313 OF SARA TITLE III.																																																
SECTION III - PHYSICAL DATA																																																
<b>BOILING RANGE:</b>	133° - 331° F			<b>VAPOR DENSITY:</b>	_X_ Heavier ___ Lighter than air																																											
<b>MELTING POINT:</b>	Estimated min. 1500° F			<b>WEIGHT PER GALLON:</b>	7.8 - 8.0 (PAINT)																																											
<b>VAPOR PRESSURE:</b>	Unknown for products.			<b>SPECIFIC GRAVITY :</b>	(H2O=1): < 1																																											
<b>SOLUBILITY IN WATER:</b>	Slight to moderate			<b>EVAPORATION RATE:</b>	___ Faster _X_ Slower than ether.																																											
<b>APPEARANCE AND ODOR:</b>	Typical solvent paint			<b>EVAPORATION RATE:</b>																																												
<b>PERCENT VOLATILE BY VOLUME:</b>	80-90			(Butyl Acetate = 1) Section 1 products > 1																																												
<b>See Section II for volatile, hazardous components.</b>				Propellants > 1				( Propellant faster)																																								
Continue on page 2																																																

STANDARD		PAGE 2 OF 2	
<b>SECTION IV - FIRE AND EXPLOSION HAZARD DATA</b>			
<b>FLAMMABILITY CLASSIFICATION:</b> (EXTREMELY FLAMMABLE)	<b>OSHA: IA</b>	<b>FLASH POINT:</b> 0° F (-18° C) TCC (Propellant = -100° F)	
<b>EXTINGUISHING MEDIA:</b>	<b>UNIFORM FIRE CODE:</b> LEVEL 3 AEROSOL ALCOHOL FOAM, CO2, DRY CHEMICAL	<b>LEL 1.0</b>	
<b>UNUSUAL FIRE AND EXPLOSION HAZARDS:</b> Closed containers may explode and/or autoignite when exposed to extreme heat, vapors are heavier than air and may travel along the ground or may be moved by ventilation and ignited by pilot lights, other flames, sparks, heaters, smoking, electric motors or other locations distant from material handling point.			
<b>SPECIAL FIRE FIGHTING PROCEDURES:</b> Water spray may be ineffective. Water may be used to cool closed containers to prevent pressure build and possible autoignition or explosion when exposed to extreme heat. If water is used, fog nozzles are preferable use self-contained breathing apparatus with full face piece operated in pressure demand or other positive pressure mode.			
<b>SECTION V - HEALTH HAZARD DATA</b>			
<b>ROUTE(S) OF ENTRY:</b>	<input checked="" type="checkbox"/> INHALATION	<input checked="" type="checkbox"/> SKIN	<input type="checkbox"/> INGESTION <input checked="" type="checkbox"/> EYES
<b>CARCINOGENICITY:</b>	<input type="checkbox"/> NTP	<input checked="" type="checkbox"/> IARC	<input type="checkbox"/> OSHA
Contains ethylbenzene as a component of xylene and/or mineral spirits. Ethylbenzene is classified by IARC as possibly carcinogenic to humans based on animal data; however there is inadequate evidence for cancer in exposed humans.			
<b>SYMPTOMS OF OVEREXPOSURE:</b>			
<b>ACUTE:</b>	<b>BREATHING -</b>	EXCESSIVE INHALATION OF VAPORS CAN CAUSE NASAL AND RESPIRATORY IRRITATION, DIZZINESS, WEAKNESS, FATIGUE, NAUSEA, HEADACHE, POSSIBLE UNCONSCIOUSNESS AND EVEN ASPHYXIATION.	
	<b>EYE CONTACT -</b>	CAN CAUSE SEVERE IRRITATION, REDNESS, TEARING, BLURRED VISION.	
	<b>SWALLOWING -</b>	CAN CAUSE GASTROINTESTINAL IRRITATION, NAUSEA, VOMITING, DIARRHEA.	
	<b>SKIN CONTACT -</b>	CAN CAUSE IRRITATION, PROLONGED CONTACT CAN CAUSE DRYNESS AND CRACKING OF SKIN	
<b>CHRONIC:</b>	None known for product(s) in Section 1.		
REPORTS HAVE ASSOCIATED REPEATED AND PROLONGED OCCUPATIONAL OVEREXPOSURE TO SOLVENTS WITH PERMANENT BRAIN AND NERVOUS SYSTEM DAMAGE, SEVERE OVEREXPOSURE IN LABORATORY ANIMALS HAS ALSO CAUSED LIVER ABNORMALITIES AND DAMAGE TO KIDNEYS, LUNGS, AND SPLEEN, HEART AND ADRENALS. INTENTIONAL MISUSE BY DELIBERATELY CONCENTRATING AND INHALING THE CONTENTS MAY BE HARMFUL OR FATAL.			
<b>MEDICAL CONDITIONS:</b>	Generally Aggravated By Exposure - Can cause respiratory and/or skin reaction.		
<b>FIRST AID-EMERGENCY PROCEDURES:</b>			
	1. IF BREATHED - REMOVE INDIVIDUAL TO FRESH AIR. IF BREATHING IS DIFFICULT, ADMINISTER OXYGEN. IF BREATHING IS STOPPED, GIVE ARTIFICIAL RESPIRATION AND SEEK MEDICAL HELP.		
	2. IF IN EYES - FLUSH WITH WATER FOR 15 MINUTES WHILE HOLDING EYELIDS OPEN. GET PROMPT MEDICAL ATTENTION		
	3. IF SWALLOWED - DO NOT INDUCE VOMITING (ASPIRATION OF MATERIAL INTO LUNGS CAN CAUSE PNEUMONITIS, WHICH CAN BE FATAL). KEEP PERSON WARM, QUIET AND GET MEDICAL ATTENTION / POISON CONTROL CENTER.		
	4. IF ON SKIN - WASH WITH SOAP AND WATER OR VARIOUS HAND CLEANERS, AND WASH CLOTHING .		
<b>SECTION VI - REACTIVITY DATA</b>			
<b>STABILITY:</b>	<input type="checkbox"/> UNSTABLE <input checked="" type="checkbox"/> STABLE	<b>HAZARDOUS POLYMERIZATION:</b>	<input type="checkbox"/> MAY OCCUR <input checked="" type="checkbox"/> WILL NOT OCCUR
<b>CONDITIONS TO AVOID:</b>	Heat, Sparks and open flame.		
<b>INCOMPATIBILITY (Materials to avoid):</b>	Avoid contact with strong oxidizing agents and heat.		
<b>HAZARDOUS DECOMPOSITION:</b>	May form toxic materials, carbon dioxide / carbon monoxide, various hydrocarbons, nitrogen compounds, etc., when burned.		
<b>CONDITIONS TO AVOID:</b>	Not applicable.		
<b>SECTION VII - SPILL OR LEAK PROCEDURES</b>			
<b>STEPS TO BE TAKEN IN CASE MATERIAL IS RELEASED OR SPILLED:</b> ELIMINATE ALL IGNITION SOURCES, VENTILATE AREA, ABSORB LIQUID ON PAPER, VERMICULITE, FLOOR ABSORBENT, OR OTHER ABSORBENT MATERIAL AND TRANSFER TO A CLOSED CONTAINER.			
<b>WASTE DISPOSAL METHOD:</b>	MATERIAL COLLECTED ON ABSORBENT MATERIAL MAY BE DEPOSITED IN A POSTED TOXIC SUBSTANCE LANDFILL IN ACCORDANCE WITH LOCAL, STATE, AND FEDERAL REGULATIONS.		
<b>PRECAUTIONS TO BE TAKEN IN HANDLING AND STORING:</b>	DO NOT PUNCTURE OR INCINERATE.		DO NOT STORE IN AREAS ABOVE 120° F. (49°C)
	OR IN DIRECT SUNLIGHT, OR NEAR HEAT OR OPEN FLAMES.		
<b>STORAGE CATEGORY:</b>	STORE LARGE QUANTITIES IN BUILDING PROTECTED FOR STORAGE OF FLAMMABLE LIQUIDS.		
<b>SECTION VIII - SPECIAL PROTECTION INFORMATION</b>			
<b>RESPIRATORY PROTECTION:</b>	FOR CASUAL / OCCASIONAL USE - TO AVOID BREATHING VAPORS OR SPRAY MIST, OPEN WINDOWS AND DOORS OR USE OTHER MEANS TO ENSURE FRESH AIR ENTRY DURING APPLICATION AND DRYING. IF YOU EXPERIENCE EYE WATERING, HEADACHE, OR DIZZINESS, INCREASE FRESH AIR, WEAR RESPIRATORY PROTECTION (NIOSH/MSHA APPROVED), OR LEAVE THE AREA.		
<b>VENTILATION:</b>	FOR REGULAR / CONTINUOUS USE - PROVIDE SUFFICIENT MECHANICAL (GENERAL) AND/OR LOCAL EXHAUST VENTILATION TO MAINTAIN EXPOSURE BELOW TLV'S IN SECTION II.		
<b>PROTECTIVE GLOVES:</b>	WEAR CHEMICAL RESISTANT GLOVES, SUCH AS NEOPRENE. IF SKIN CONTACT IS TO BE AVOIDED.		
<b>EYE PROTECTION:</b>	CHEMICAL SPLASH GOGGLES, IN COMPLIANCE WITH OSHA REGULATIONS, ARE ADVISED.		
<b>OTHER EQUIPMENT:</b>	WHERE SPECIAL OR UNUSUAL CONDITIONS EXIST, SEEK THE EXPERT ASSISTANCE OF AN INDUSTRIAL HYGIENIST.		
<b>WORK/HYGIENIC PRACTICES:</b>	WASH HANDS BEFORE EATING OR USING WASHROOM. AS WITH ALL CHEMICALS, MINIMIZE PERSONAL CONTACT.		
THE INFORMATION CONTAINED ABOVE IS BELIEVED TO BE ACCURATE. BUT IS NOT WARRANTED. RECIPIENTS ARE ADVISED TO CONFIRM IN ADVANCE OF NEED THAT THE INFORMATION IS CURRENT, APPLICABLE, AND SUITABLE TO CIRCUMSTANCES.			
<b>MSDS SHEET PREPARED BY:</b> Plasti-Kote Technical Department		<b>DATE:</b> 9/29/00	

# Appendix H – Sodium Hypochlorite Material Safety Data Sheet

<p>UNIVERSITY OF NOTTINGHAM SCHOOL OF CHEMICAL ENVIRONMENTAL &amp; MINING ENGINEERING [L3 LABS] UNIVERSITY PARK NG7 2RD United Kingdom</p>	<p>SIGMA-ALDRICH CO. LTD. Fancy Road Poole BH12 4QH United Kingdom</p> <p>In Emergency Contact: DUTY CONTACT Sigma-Aldrich Company Ltd. Fancy Road Poole Dorset BH17 7NH Telephone: 01202 731114 Our Delivery Note: 0044853169</p>
<p>M A T E R I A L   S A F E T Y   D A T A   S H E E T</p>	
<p>DATE PRODUCED: 24-JAN-2003</p>	
SECTION 1. . . . .	CHEMICAL IDENTIFICATION. . . . .
PRODUCT #: 239305	NAME: SODIUM HYPOCHLORITE SOLUTION, AVAILABLE CHLORINE 4% (MINIMUM)
SECTION 2. . . . .	COMPOSITION/INFORMATION ON INGREDIENTS . . . . .
CAS #: 7681-52-9	MF: CLMO
EC NO: 231-668-3	SYNONYMS
<p>ANTI-FORMIN * B-K LIQUID * CABREL-DAKIN SOLUTION * CHLOROS * CHLOROX * CLOKROX * DAKINS SOLUTION * DEOSAN * HYPOCHLORITE SOLUTION CONTAINING &gt;7% AVAILABLE CHLORINE BY WT. (UN1791) * JAVEX * KLOBROX * MILTON * NEO-CLEANER * NEOSEPTAL CL * PAROZONE * PIRIN B * SODIUM CHLORIDE OXIDE * SODIUM HYPOCHLORITE * SODIUM OXYCHLORIDE * SURCHLOR *</p>	
SECTION 3. . . . .	HAZARDS IDENTIFICATION . . . . .
<p>LABEL PRECAUTIONARY STATEMENTS</p> <p>IRRITANT</p> <p>CONTACT WITH ACIDS LIBERATES TOXIC GAS.</p> <p>IRRITATING TO EYES AND SKIN.</p> <p>IN CASE OF CONTACT WITH EYES, RINSE IMMEDIATELY WITH PLENTY OF WATER AND SEEK MEDICAL ADVICE.</p> <p>WEAR SUITABLE PROTECTIVE CLOTHING.</p>	
SECTION 4. . . . .	FIRST-AID MEASURES. . . . .
<p>IF SWALLOWED, WASH OUT MOUTH WITH WATER PROVIDED PERSON IS CONSCIOUS. CALL A PHYSICIAN.</p> <p>DO NOT INDUCE VOMITING.</p>	
SECTION 5. . . . .	FIRE FIGHTING MEASURES . . . . .
<p>IF INVOLVED, REMOVE TO FRESH AIR. IF NOT BREATHING GIVE ARTIFICIAL RESPIRATION. IF BREATHING IS DIFFICULT, GIVE OXYGEN.</p> <p>IN CASE OF SKIN CONTACT, FLUSH WITH COPIOUS AMOUNTS OF WATER FOR AT LEAST 15 MINUTES. REMOVE CONTAMINATED CLOTHING AND SHOES. CALL PHYSICIAN.</p> <p>IN CASE OF CONTACT WITH EYES, FLUSH WITH COPIOUS AMOUNTS OF WATER FOR AT LEAST 15 MINUTES. ASSURE ADEQUATE FLUSHING BY SEPARATING THE EYELIDS WITH FINGERS. CALL A PHYSICIAN.</p>	
SECTION 6. . . . .	ACCIDENTAL RELEASE MEASURES. . . . .
<p>EXTINGUISHING MEDIA</p> <p>CARBON DIOXIDE, DRY CHEMICAL POWDER OR APPROPRIATE FOAM.</p> <p>SPECIAL FIRE-FIGHTING PROCEDURES</p> <p>WEAR SELF-CONTAINED BREATHING APPARATUS AND PROTECTIVE CLOTHING TO PREVENT CONTACT WITH SKIN AND EYES.</p> <p>UNUSUAL FIRE AND EXPLOSION HAZARDS</p> <p>EMITS TOXIC FUMES UNDER FIRE CONDITIONS.</p>	
SECTION 7. . . . .	HANDLING AND STORAGE. . . . .
<p>REFER TO SECTION 6.</p>	
SECTION 8. . . . .	EXPOSURE CONTROLS/PERSONAL PROTECTION. . . . .
<p>WEAR SELF-CONTAINED BREATHING APPARATUS, RUBBER BOOTS AND HEAVY RUBBER GLOVES.</p> <p>EVACUATE AREA.</p> <p>ABSORB ON SAND OR VERMICULITE AND PLACE IN CLOSED CONTAINERS FOR DISPOSAL.</p> <p>VENTILATE AREA AND WASH SPILL SITE AFTER MATERIAL PICKUP IS COMPLETE.</p>	
SECTION 9. . . . .	PHYSICAL AND CHEMICAL PROPERTIES . . . . .
<p>APPEARANCE AND ODOR</p> <p>LIQUID.</p> <p>PHYSICAL PROPERTIES</p> <p>SPECIFIC GRAVITY: 1.097</p> <p>VAPOR PRESSURE: 17.5 MMHG @ 20 C</p>	
SECTION 10. . . . .	STABILITY AND REACTIVITY . . . . .

STABILITY  
 STABLE  
 INCOMPATIBILITIES  
 STRONG ACIDS  
 ORGANIC MATERIALS  
 FINELY POWDERED METALS  
 FORMS EXPLOSIVE MIXTURES WITH:  
 AMINES  
 AZIDES  
 HYDROPEROXIDES  
 METANOL  
 HAZARDOUS COMBUSTION OR DECOMPOSITION PRODUCTS  
 CHLORINE  
 HAZARDOUS POLYMERIZATION  
 WILL NOT OCCUR.

SECTION 11. TOXICOLOGICAL INFORMATION

ACUTE EFFECTS  
 CAUSES BURNS.  
 MAY BE HARMFUL IF ABSORBED THROUGH THE SKIN.  
 MATERIAL IS EXTREMELY DESTRUCTIVE TO THE TISSUE OF THE MUCOUS MEMBRANES  
 AND UPPER RESPIRATORY TRACT.  
 MAY BE HARMFUL IF INHALED.  
 MATERIAL IS EXTREMELY DESTRUCTIVE TO TISSUE OF THE MUCOUS MEMBRANES  
 AND UPPER RESPIRATORY TRACT, EYES AND SKIN.  
 INHALATION MAY RESULT IN SPASM, INFLAMMATION AND EDEMA OF THE  
 LARYNX AND BRONCHI, CHEMICAL PNEUMONITIS AND PULMONARY EDEMA.  
 SYMPTOMS OF EXPOSURE MAY INCLUDE BURNING SENSATION, COUGHING,  
 HEEZING, LARYNGITIS, SHORTNESS OF BREATH, HEADACHE, NAUSEA AND  
 VOMITING.  
 CHRONIC EFFECTS  
 THIS PRODUCT IS OR CONTAINS A COMPONENT THAT IS NOT CLASSIFIABLE AS  
 TO ITS CARCINOGENICITY BASED ON ITS IARC, ACGIH, NTP OR EPA  
 CLASSIFICATION.  
 RTECS #: NH486300  
 HYPOCHLOROUS ACID, SODIUM SALT  
 IRRITATION DATA  
 TOXICITY TO MG/KG TPAP9 55,501,1980  
 ORL-MUS IDE0-5800 MG/KG SHEZAP 27,553,1986  
 TARGET ORGAN DATA  
 BEHAVIORAL (SOMNOLENCE)  
 VASCULAR (BP LOWERING NOT CHARACTERIZED IN AUTONOMIC SECTION)  
 LINGS, THIRAX OR RESPIRATION (OTHER CHANGES)  
 GASTROINTESTINAL (NAUSEA OR VOMITING)  
 SKIN AND APPENDAGES (CORROSIVE)  
 ONLY SELECTED REGISTRY OF TOXIC EFFECTS OF CHEMICAL SUBSTANCES  
 (RTECS) DATA IS PRESENTED HERE. SEE ACTUAL ENTRY IN RTECS FOR  
 COMPLETE INFORMATION.

SECTION 12. ECOLOGICAL INFORMATION

DATA NOT YET AVAILABLE.

SECTION 13. DISPOSAL CONSIDERATIONS

CONTACT A LICENSED PROFESSIONAL WASTE DISPOSAL SERVICE TO DISPOSE OF  
 THIS MATERIAL.  
 DO NOT MIX THE MATERIAL WITH A COMBUSTIBLE SOLVENT AND BURN IN A  
 CHEMICAL INCINERATOR EQUIPPED WITH AN AFTERBURNER AND SCRUBBER.  
 OBSERVE ALL FEDERAL, STATE AND LOCAL ENVIRONMENTAL REGULATIONS.

SECTION 14. TRANSPORT INFORMATION

CDG UK  
 PROPER SHIPPING NAME:  
 HYPOCHLORITE SOLUTION  
 UN NO: 1791 PACKING GROUP: III  
 MAJOR HAZARD CLASS: 8.0  
 SUBSID HAZARD CLASS(ES):  
 ICAO/IATA  
 MAJOR HAZARD CLASS: 8.0  
 SUBSID HAZARD CLASS(ES):  
 PROPER SHIPPING NAME:  
 HYPOCHLORITE SOLUTION  
 UN NO: 1791 PACKING GROUP: III  
 MAJOR HAZARD CLASS: 8.0  
 SUBSID HAZARD CLASS(ES):

SECTION 15. REGULATORY INFORMATION

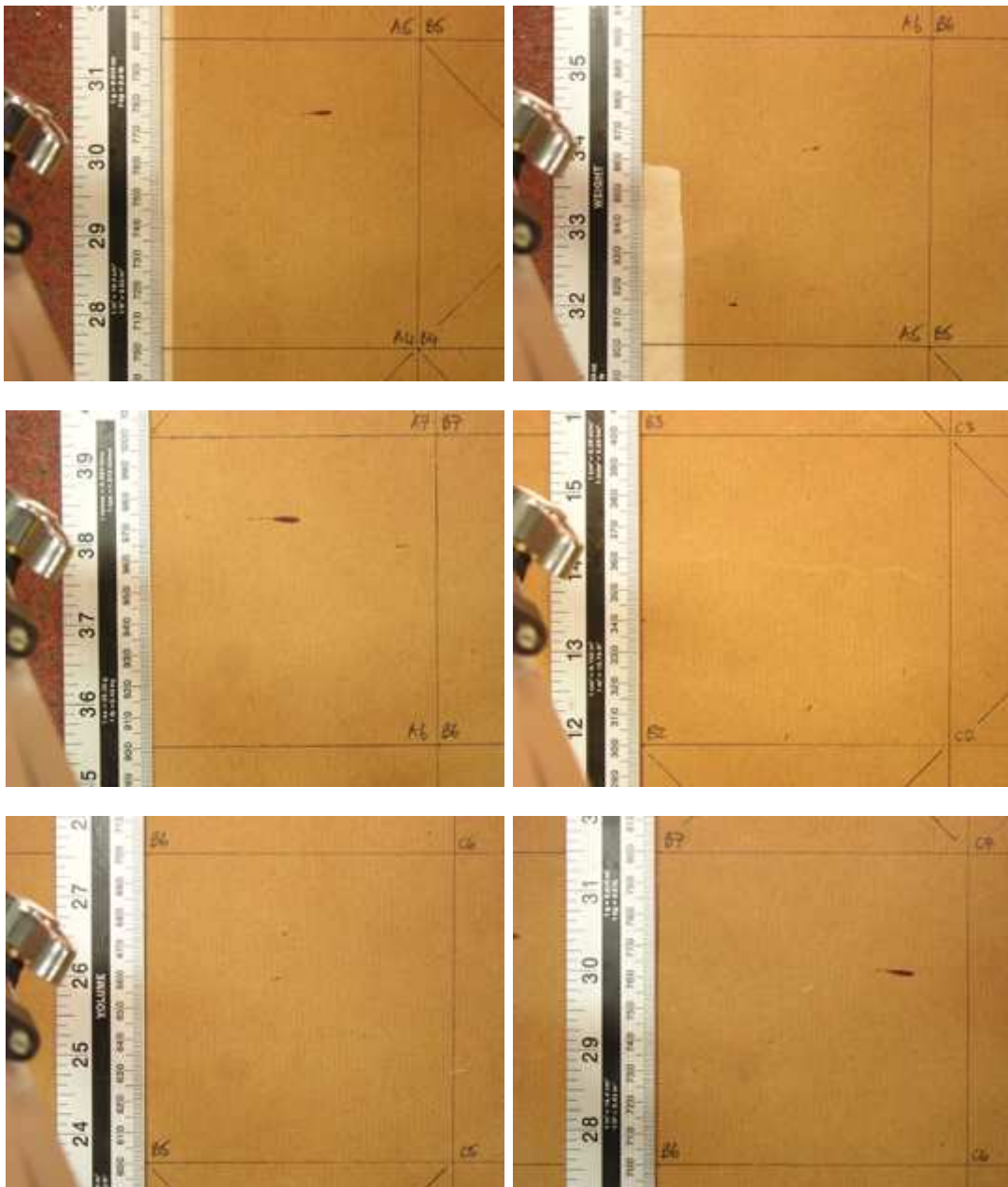
EUROPEAN INFORMATION  
 EC INDEX NO: 017-011-01-9  
 IRRITANT  
 R 31  
 CONTACT WITH ACIDS LIBERATES TOXIC GAS.  
 R 36/38  
 IRRITATING TO EYES AND SKIN.  
 S 26  
 IN CASE OF CONTACT WITH EYES, RINSE IMMEDIATELY WITH PLENTY OF  
 WATER AND SEEK MEDICAL ADVICE.  
 S 36  
 WEAR SUITABLE PROTECTIVE CLOTHING.  
 REVIEW, STANDARDS, AND REGULATIONS  
 BELMAG  
 IARC CANCER REVIEW: ANIMAL INADEQUATE EVIDENCE IHBPT 53,159,1991  
 IARC CANCER REVIEW: HUMAN 30 AVAILABLE DATA IHBPT 53,159,1991  
 IARC CANCER REVIEW: GROUP 3 IHBPT 53,159,1991  
 EPA FIFRA 1988 PESTICIDE SUBJECT TO REGISTRATION OR RE-REGISTRATION  
 FERRAC 54,7740,1989  
 NOS 1974: HD 69090; NIS 202; TNP 70228; NOS 111; TNE 556664  
 NOS 1983: HD 69090; NIS 168; TNP 23747; NOS 132; TNE 562423; TNE  
 265913  
 EPA GENETOX PROGRAM 1988, POSITIVE; E COLI FOLA WITHOUT S9  
 EPA GENETOX PROGRAM 1988, POSITIVE/DOSE RESPONSE; IN VITRO  
 CYTOGENETICS-NONHUMAN  
 EPA GENETOX PROGRAM 1988, POSITIVE/DOSE RESPONSE; IN VITRO  
 CYTOGENETICS-HUMAN LYMPHOCYTE

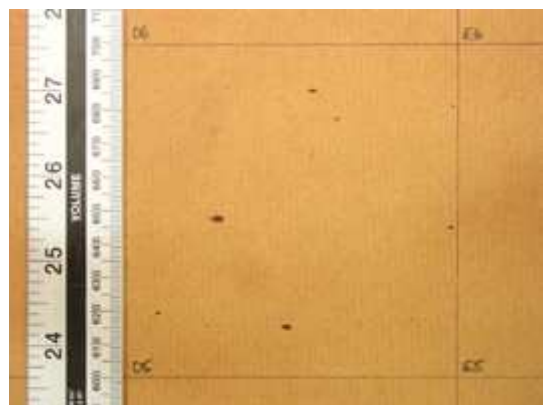
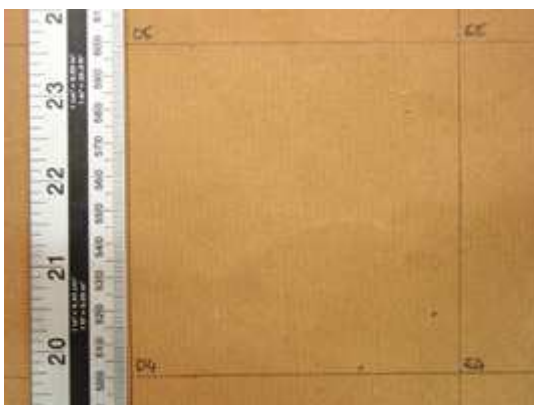
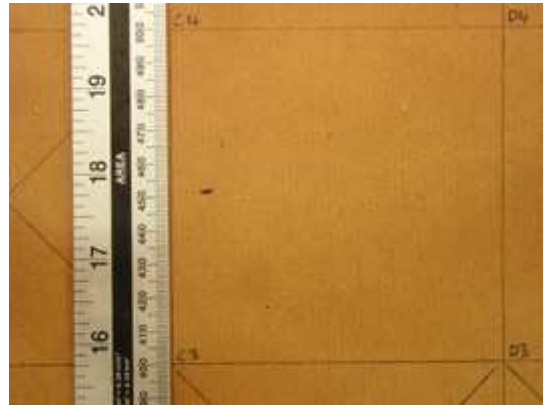
EPA GENETOX PROGRAM 1988, INCONCLUSIVE, HISTIDINE REVERSION-AMES TEST  
EPA TSCA SECTION 8(B) CHEMICAL INVENTORY  
EPA TSCA SECTION 8(D) UNPUBLISHED HEALTH/SAFETY STUDIES  
EPA TSCA TEST SUBMISSION (TSCATS) DATA BASE, JANUARY 2001  
SECTION 16. . . . . OTHER INFORMATION. . . . .

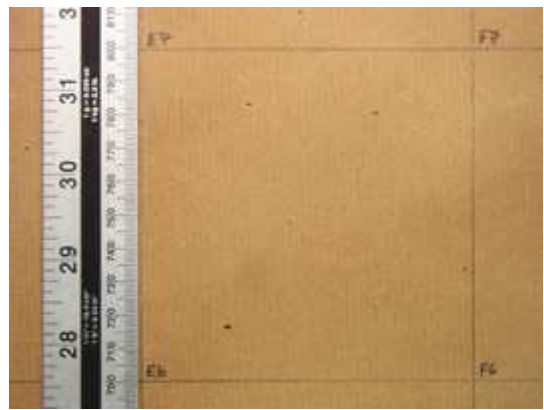
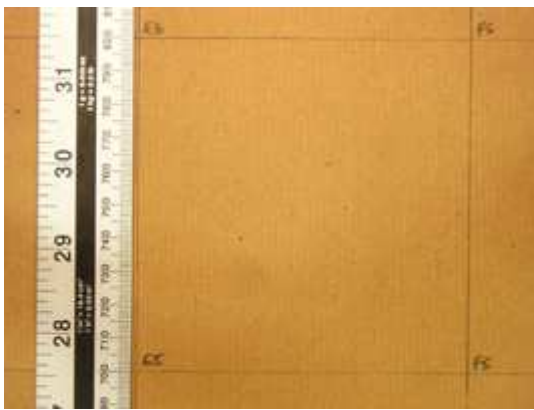
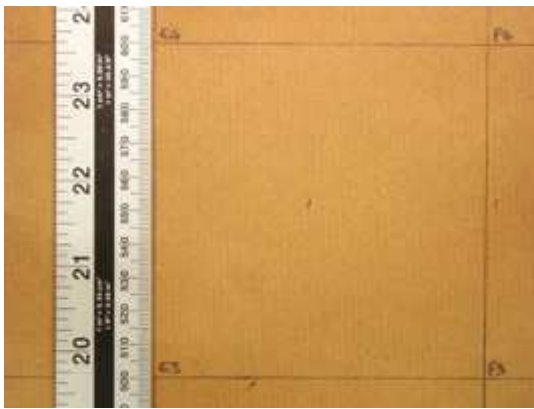
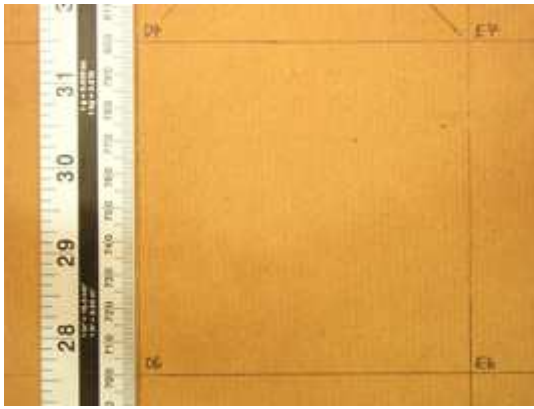
## Appendix I – Experimental Impact Spatter Pattern Photographic Recording

A sample of the scaled and spatter numbered photographs taken during the recording process for experimental impact spatter pattern ES-A are shown below. The full series of photographs for each of the three experimental impact spatter patterns at their full resolution are included on the DVD-ROMs that accompany this thesis.

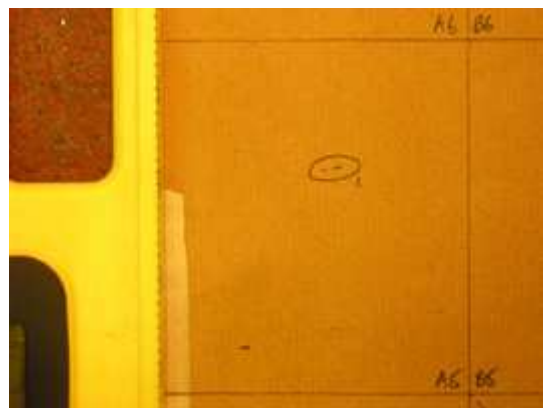
### Scaled Grid



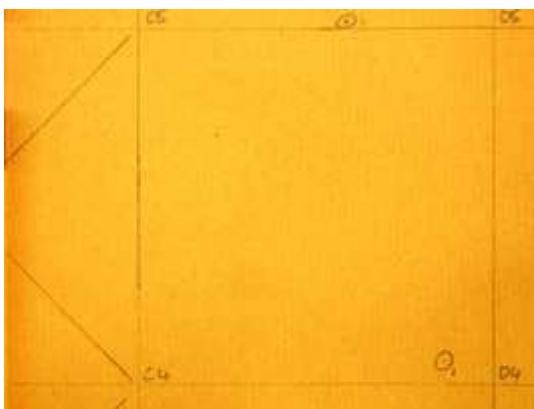
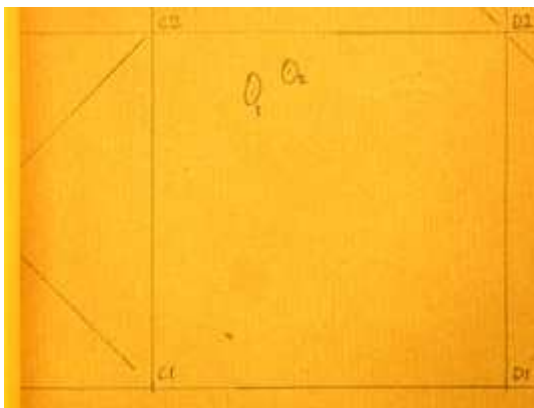
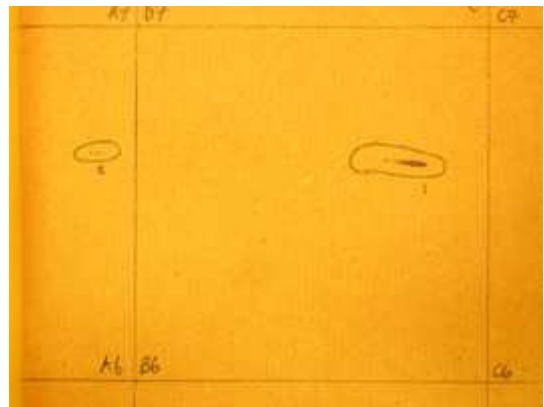
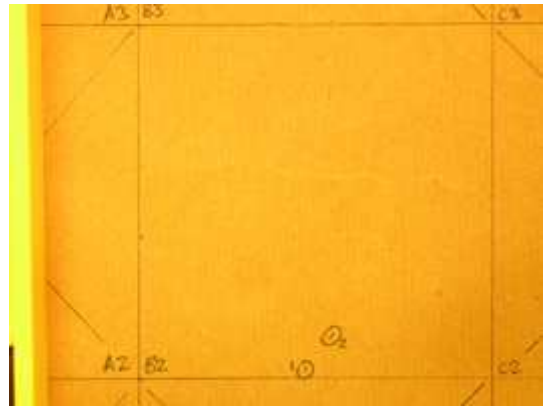
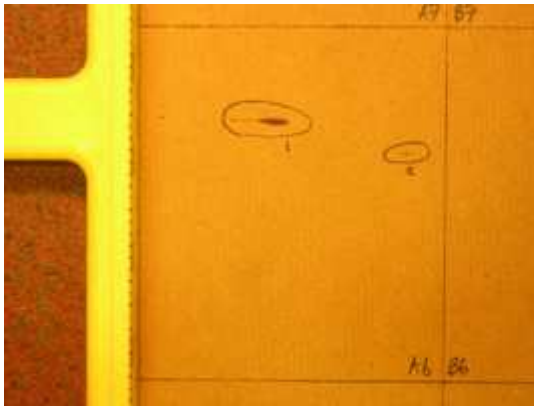


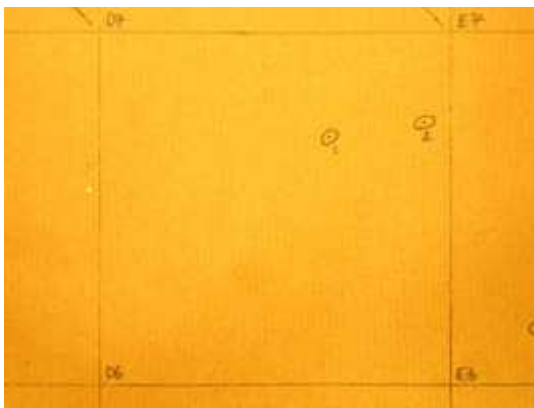
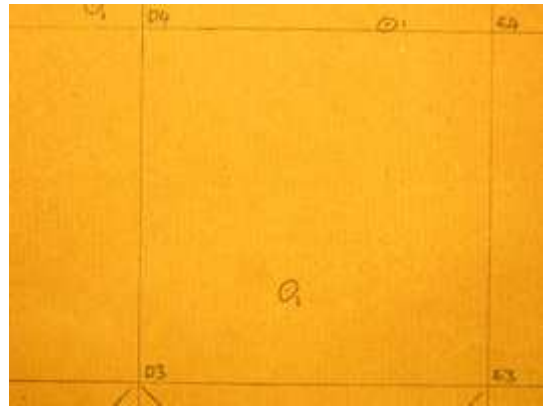


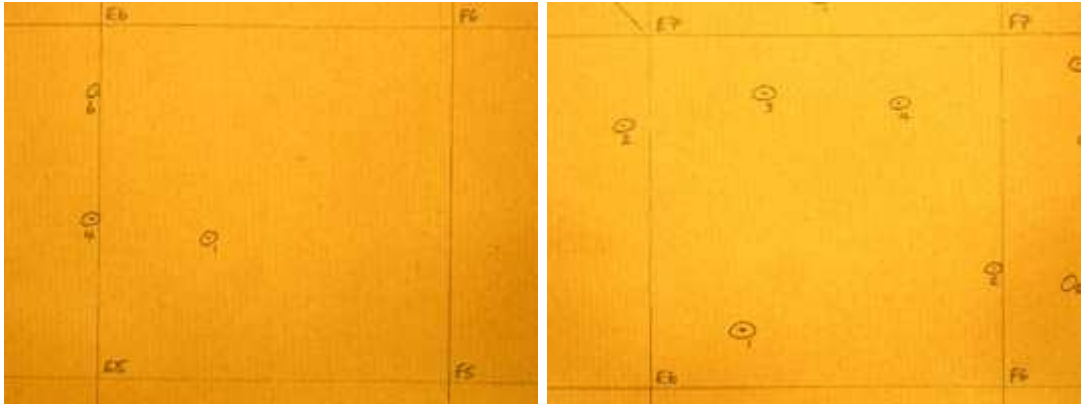
**Numbered**







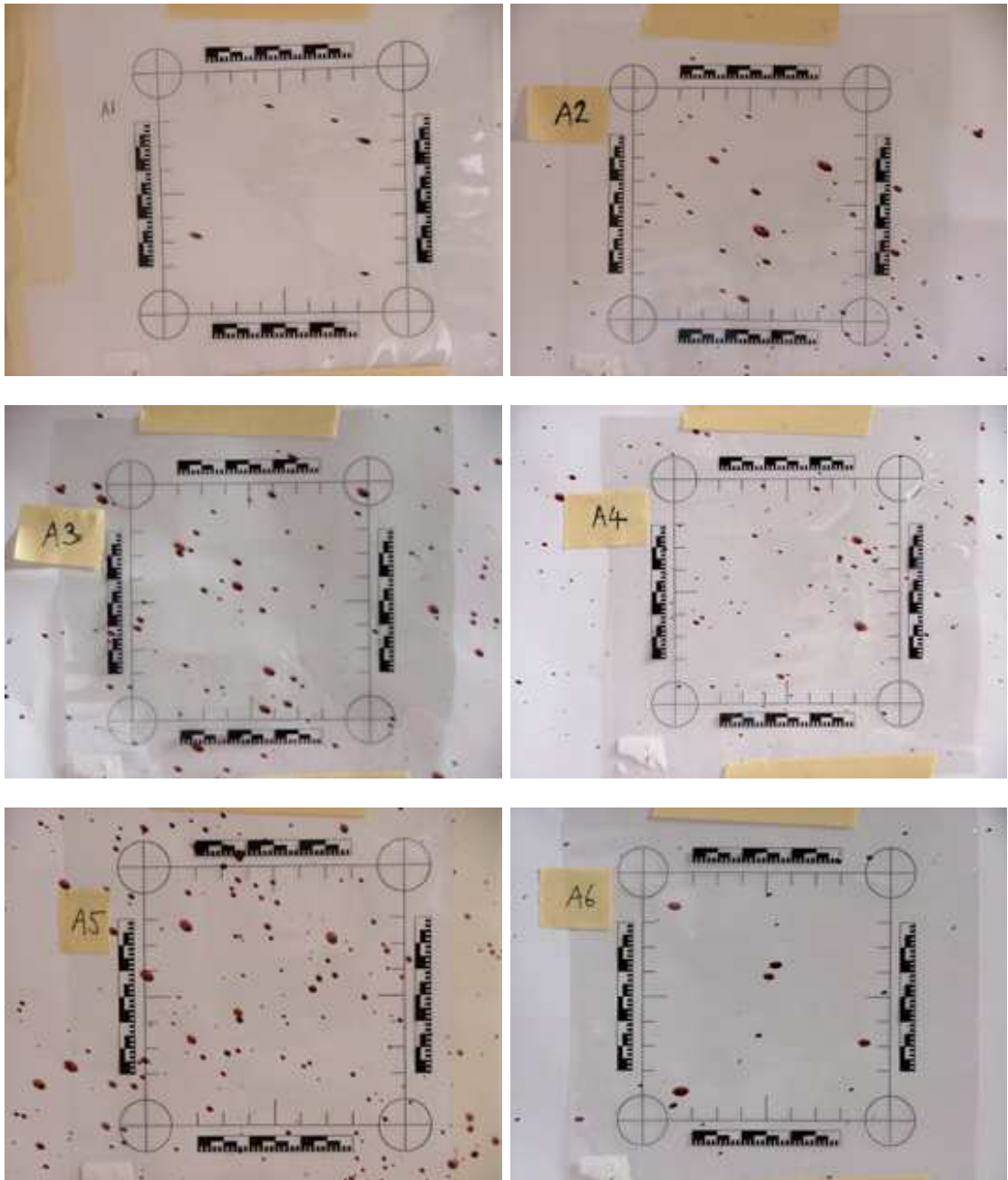


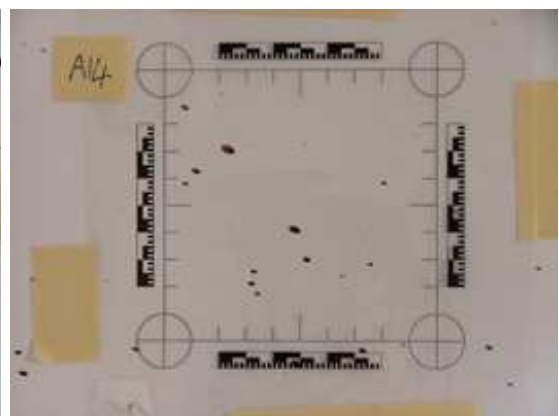
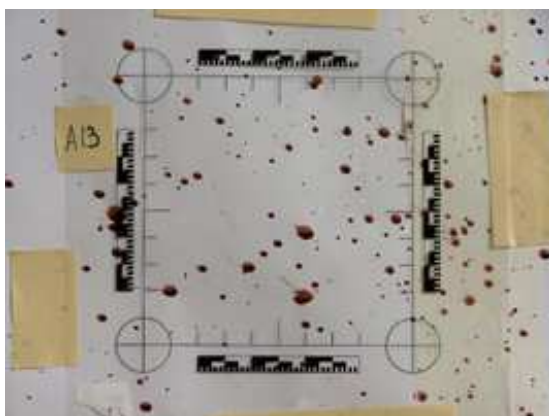
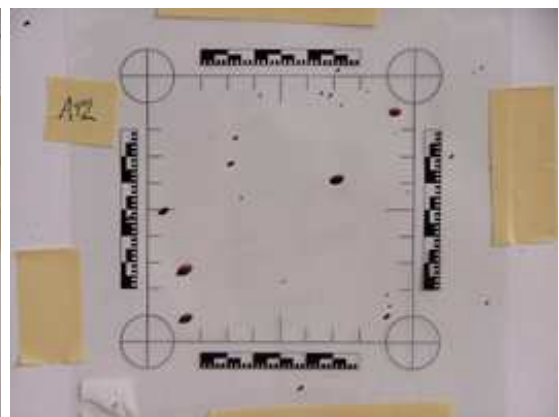
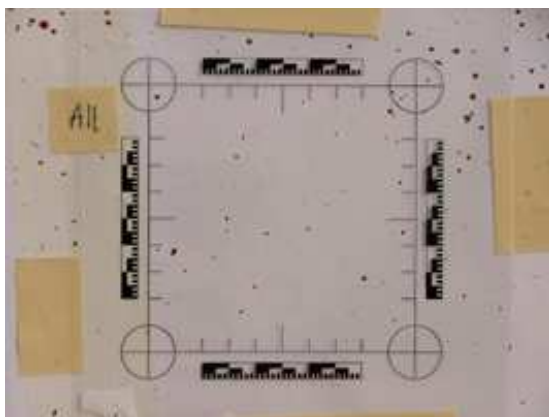
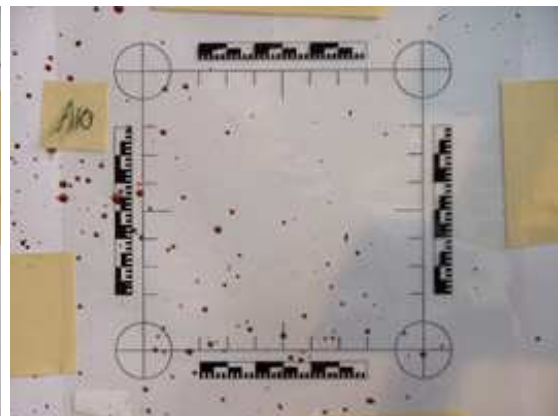
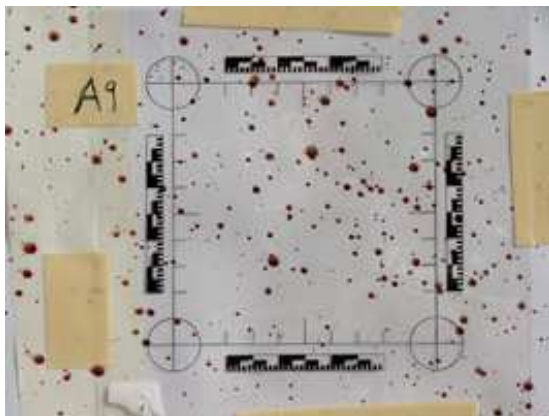
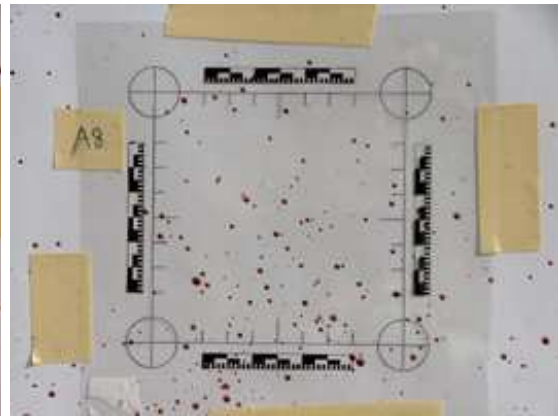
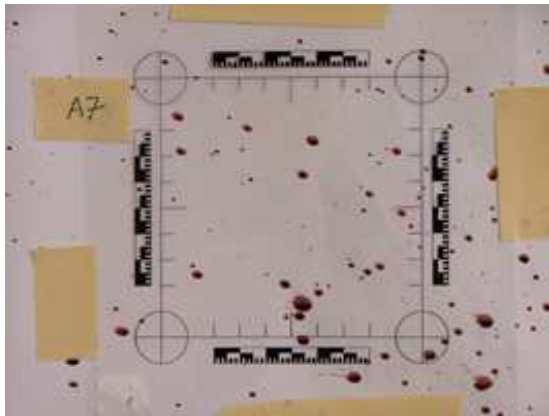


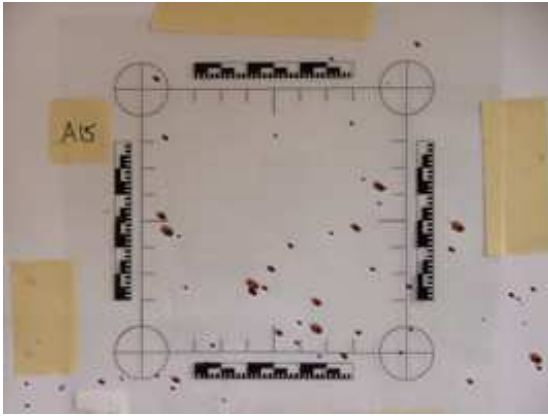
## Appendix J – Sampled Photographic Recording

The photographic spatter bloodstain samples taken during this research project are displayed below. The full series of images at their full resolution are also included on the DVD-ROMs that accompany this thesis.

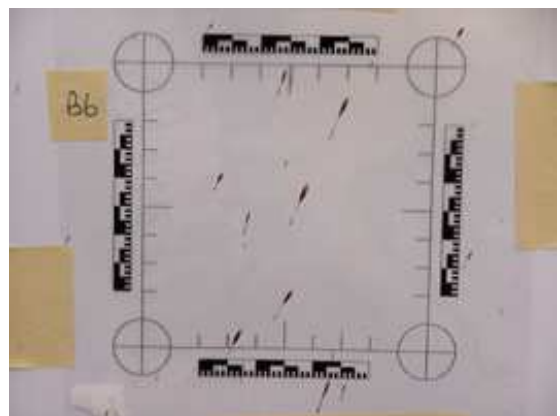
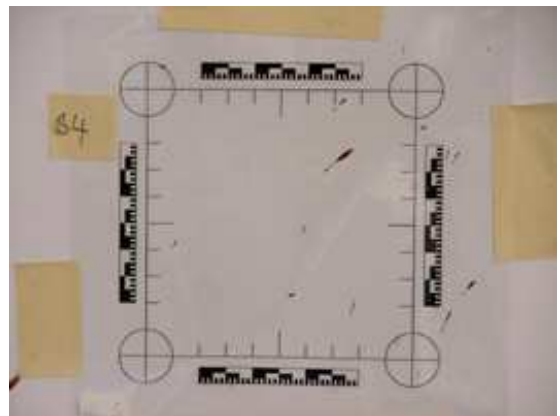
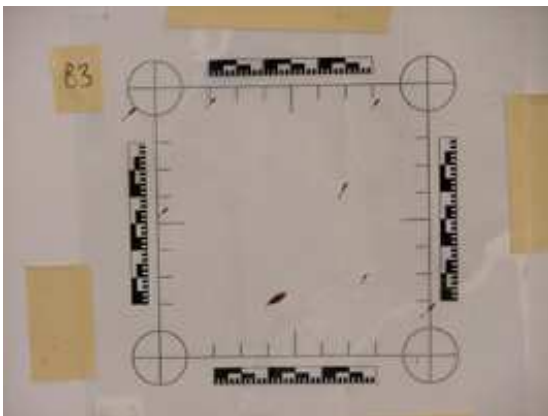
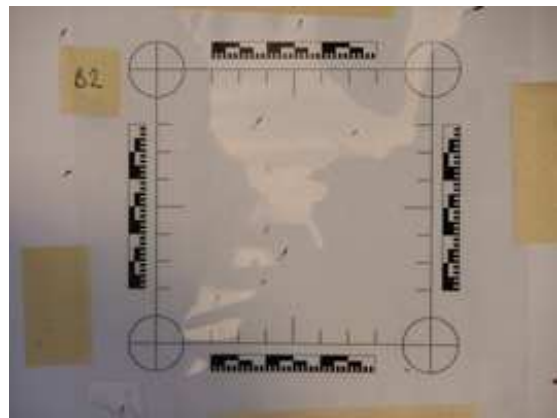
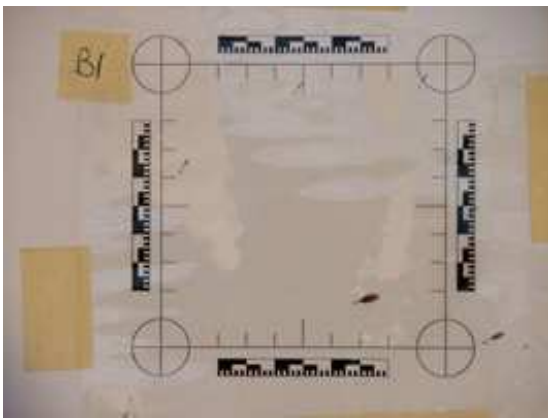
### Pattern MS-A

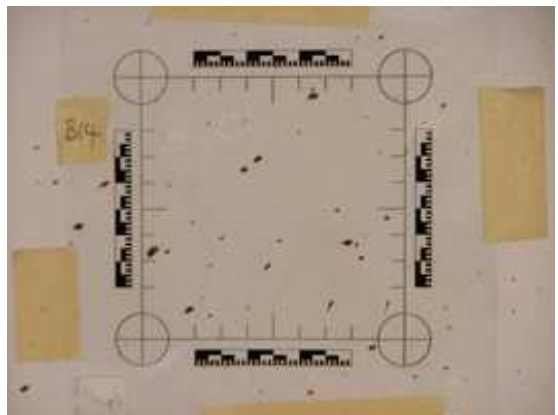
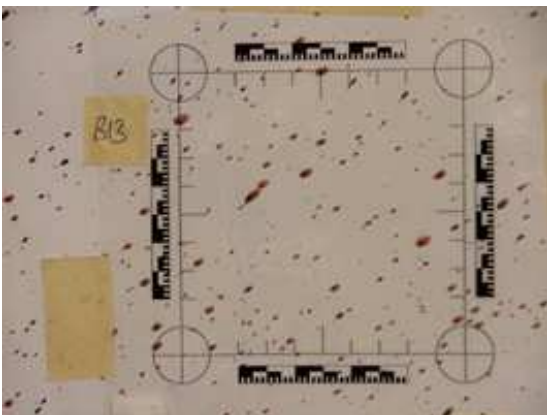
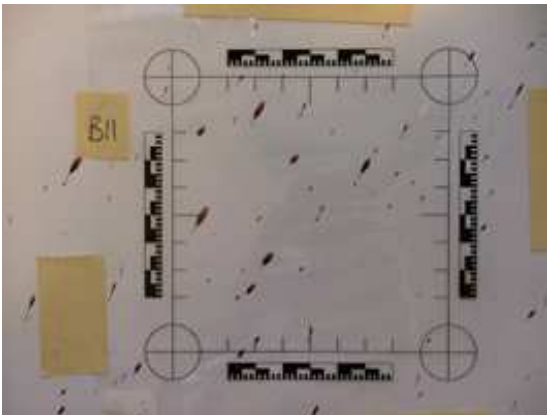
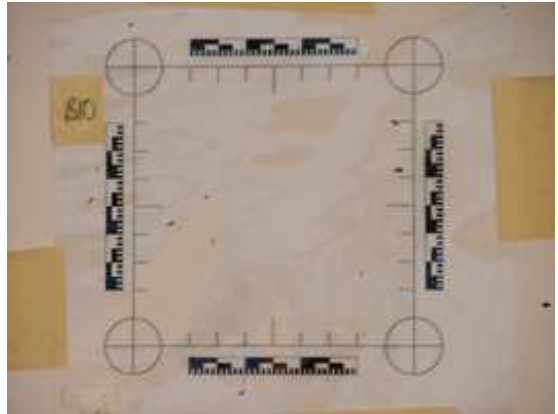
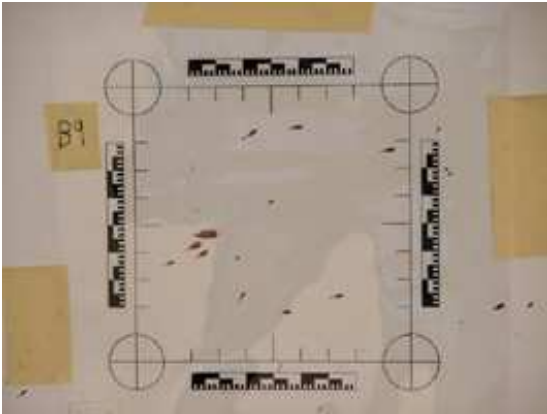
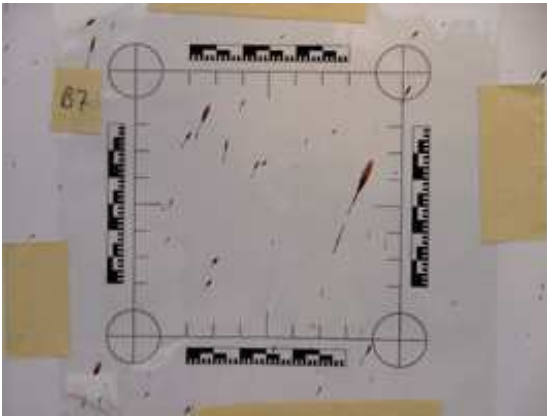


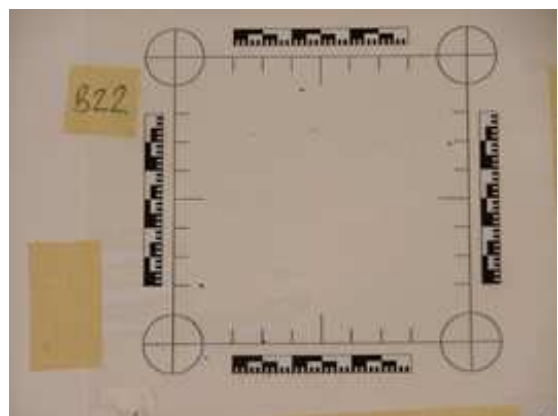
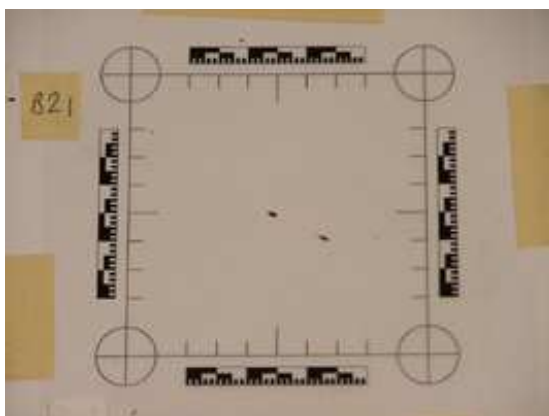
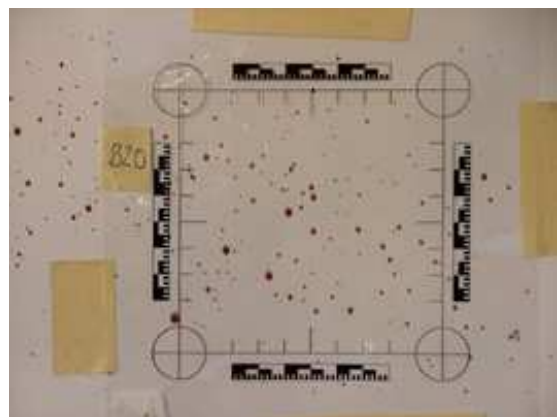
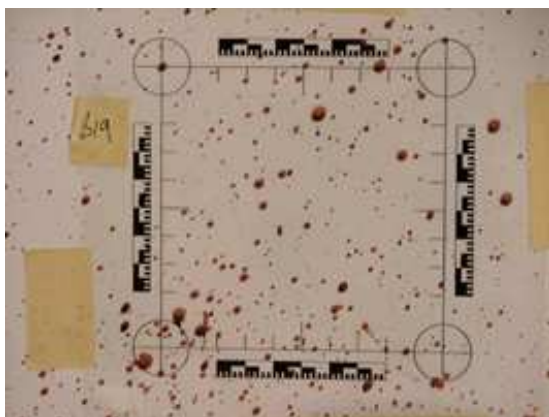
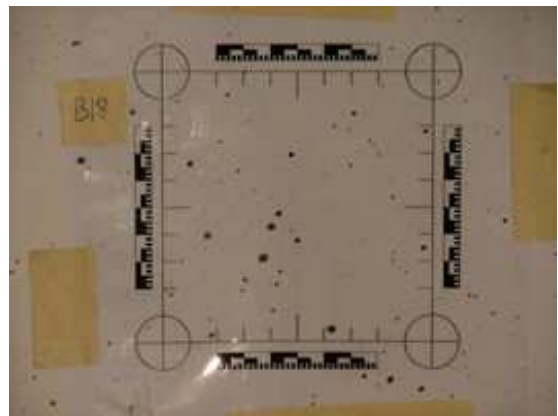
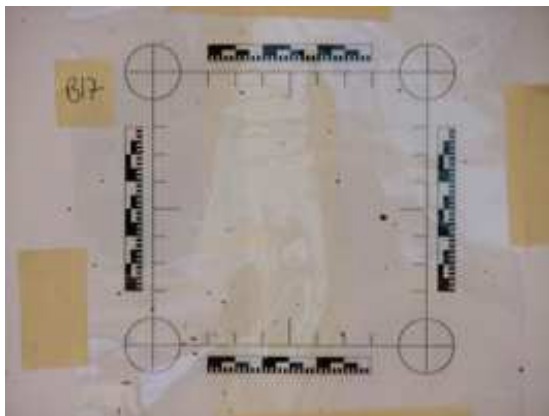
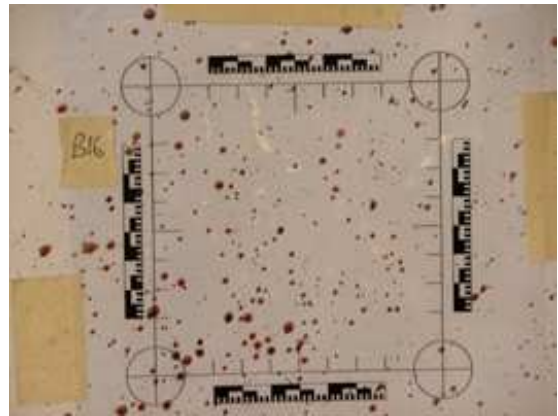
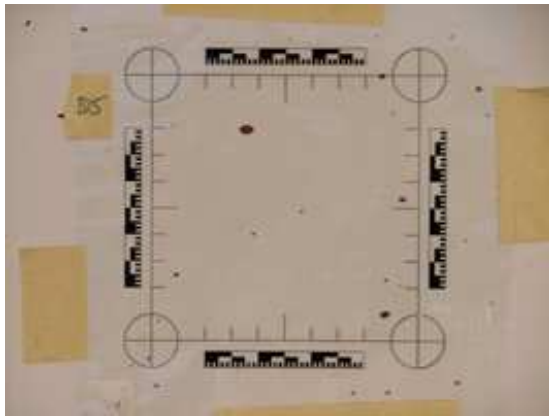




Pattern MS-B









## Appendix K – The Automated Image Analysis Macro

The following code is the macro developed to analyse the six idealised spatter bloodstain shapes using the Zeiss KS400 (Carl Zeiss Ltd, 2005) IA software application:

```
DBreset
fcnload "d002xls.fcn"

StainCounter = 0
threshold1=110
threshold2=110
thresholdupper = 220

MSsetprop "CONNECT",8

imgdelete "*"
! imgload "c:\TaoWu\Blood\Images\ShapeA.bmp",1
FilePath = "C:\\TaoWU\\Blood\\Results\\"
SampleName0= "ShapeA"
read SampleName0, "Name the sameple"
Results = FilePath + SampleName0 + ".xls"

MSFilePath = "C:\\TaoWU\\MS\\"
MSFileName="default.ms"
LoadMSFile = MSFilePath + MSFileName
MSload LoadMSFile
MSsetprop
"REGIONFEAT", "FERETRATIO, ANGLEFMAX, ANGLEFMIN, CGRAVX, CGRAVY, PERIM, P
ERIMF, AREA, AREA, FERETMAX, FERETMIN"

DBnew SampleName0,11
DBsetcolumn SampleName0,1,"NO","Int" #Eroding counter
DBsetcolumn SampleName0,2,"AREA","Float","micron"
DBsetcolumn SampleName0,3,"PERIM","Float","micron"
DBsetcolumn SampleName0,4,"PERIMF","Float","micron"
DBsetcolumn SampleName0,5,"FERETRATIO","Float"
DBsetcolumn SampleName0,6,"FERETMAX","Float","micron"
DBsetcolumn SampleName0,7,"FERETMIN","Float","micron"
DBsetcolumn SampleName0,8,"CGRAVX","Float","micron"
DBsetcolumn SampleName0,9,"CGRAVY","Float","micron"
DBsetcolumn SampleName0,10,"ANGLEFMAX","Float","deg"
DBsetcolumn SampleName0,11,"ANGLEFMIN","Float","deg"

DistanceTransform = SampleName0+"DT"
DBnew DistanceTransform,256
for i =1, i <= 256, i= i + 1
    ColumnName = "greyscale"+string(i)
    DBsetcolumn DistanceTransform,i,ColumnName,"Float","%"
endfor

dislev 1,2,255,88,1
MSmeasmask 2,1,"DATABASE",0,1,10
distance 2,3,1
histo[256] := 0.0
imgstathisto 3,0,"histo"
```

```

# Distance transform
DBaddline DistanceTransform
for i = 1, i <= 256, i= i + 1
    ColumnName = "greyscale"+string(i)
    value = histo[i]
    DBsetvalue DistanceTransform, ColumnName,value
endfor

dislev 3,4,2,255,1

RGnew 4,4
RGnextregion
RegionExist = _STATUS
i=1
while RegionExist
    dislev 3,4,i+1,255,1

    MSmeasmask 4,4,"DATABASE",0,1,10
    i=i+1

    DBfirstline "DATABASE"
    if _STATUS
        DBgetvalue "DATABASE", "AREA", Area
        DBgetvalue "DATABASE", "CGRAVX", CGravX
        DBgetvalue "DATABASE", "CGRAVY", CGravY
        DBgetvalue "DATABASE", "PERIMF", PerimF
        DBgetvalue "DATABASE", "PERIM", Perim
        DBgetvalue "DATABASE", "FERETMAX", FeretMax
        DBgetvalue "DATABASE", "FERETMIN", FeretMin
        DBgetvalue "DATABASE", "FERETRATIO", FeretRatio
        DBgetvalue "DATABASE", "ANGLEFMAX", AngleFMax
        DBgetvalue "DATABASE", "ANGLEFMIN", AngleFMin
        DBaddline SampleName0
        DBsetvalue SampleName0,"NO", StainCounter
        DBsetvalue SampleName0,"AREA", Area
        DBsetvalue SampleName0,"PERIM",Perim
        DBsetvalue SampleName0,"PERIMF",PerimF
        DBsetvalue SampleName0,"FERETRATIO",FeretRatio
        DBsetvalue SampleName0,"FERETMAX",FeretMax
        DBsetvalue SampleName0,"FERETMIN",FeretMin
        DBsetvalue SampleName0,"CGRAVX",CGravX
        DBsetvalue SampleName0,"CGRAVY",CGravY
        DBsetvalue SampleName0, "ANGLEFMAX", AngleFMax
        DBsetvalue SampleName0, "ANGLEFMIN", AngleFMin
    endif

    RGnew 4,4
    RGnextregion
    RegionExist = _STATUS
endwhile

DBgetpath DBpath
WrkFile1= DBpath + "\\\" + SampleName0
D002XLS WrkFile1, Results, "StainDetected", 3
wait 2000
WrkFile2= DBpath + "\\\" + DistanceTransform
D002XLS WrkFile2, Results, "DistanceTransform", 3

write Results
stop

```

## Appendix L – Automated Image Analysis Results

All results are reported to 1 decimal place where necessary. The full tabulated results of the automated IA procedures conducted on the six idealised spatter bloodstain shapes are also included on the DVD-ROMs that accompany this thesis.

### Shape IS-A

Iteration	Area (pixels)	Perimeter (pixels)	Feret Maximum Length (pixels)	Feret Minimum Length (pixels)	Centre Gravity X (pixels)	Centre Gravity Y (pixels)	Feret Maximum Angle (degrees)	Feret Minimum Angle (degrees)
1	12038	450.8	177.7	88.2	87.6	102.4	118.1	28.1
2	11658	445.1	175.9	86.5	87.6	102.4	118.1	28.1
3	11282	438.9	174.2	84.7	87.6	102.4	118.1	28.1
4	10911	433.2	172.4	82.9	87.6	102.4	118.1	28.1
5	10544	427.5	170.7	81.2	87.6	102.4	118.1	28.1
6	10181	421.9	168.9	79.4	87.6	102.4	123.8	28.1
7	9822	415.1	167.0	77.6	87.6	102.4	118.1	22.5
8	9469	409.4	165.2	75.8	87.6	102.4	118.1	22.5
9	9120	403.7	163.5	73.9	87.6	102.4	118.1	22.5
10	8775	398.1	161.7	72.1	87.6	102.4	118.1	22.5
11	8434	390.7	159.8	70.3	87.6	102.4	118.1	22.5
12	8100	385.0	158.1	68.4	87.6	102.4	118.1	22.5
13	7770	378.8	156.2	66.6	87.6	102.4	118.1	22.5
14	7445	372.5	154.0	64.7	87.6	102.4	118.1	22.5
15	7125	366.3	152.2	62.9	87.6	102.4	118.1	22.5
16	6810	360.0	149.9	61.0	87.6	102.4	118.1	22.5
17	6500	354.4	148.2	59.2	87.6	102.4	118.1	22.5
18	6194	347.6	145.5	57.3	87.6	102.4	118.1	22.5
19	5894	340.7	143.2	55.5	87.6	102.4	118.1	22.5
20	5600	334.5	141.0	53.6	87.6	102.4	118.1	22.5
21	5311	327.1	138.3	51.8	87.6	102.4	118.1	22.5
22	5029	320.2	136.0	49.9	87.6	102.4	118.1	22.5
23	4753	314.6	134.2	48.1	87.6	102.4	118.1	22.5
24	4481	307.8	131.5	46.2	87.6	102.4	118.1	22.5
25	4215	301.5	129.3	44.4	87.6	102.4	118.1	22.5
26	3954	294.1	126.6	42.5	87.6	102.4	118.1	22.5
27	3700	285.9	123.4	40.7	87.6	102.5	118.1	22.5
28	3453	279.6	121.6	38.8	87.6	102.5	118.1	22.5
29	3211	271.4	118.1	37.0	87.6	102.5	118.1	22.5
30	2976	265.1	115.8	35.1	87.6	102.4	118.1	22.5
31	2746	258.3	113.1	33.3	87.6	102.4	118.1	22.5
32	2522	250.9	110.4	31.5	87.6	102.4	118.1	22.5

33	2305	243.5	107.7	29.6	87.6	102.4	118.1	22.5
34	2095	236.7	105.0	27.8	87.6	102.4	118.1	22.5
35	1891	227.0	100.5	25.9	87.6	102.4	112.5	22.5
36	1695	220.2	97.9	24.1	87.6	102.4	112.5	22.5
37	1505	212.8	95.3	22.2	87.6	102.4	112.5	22.5
38	1322	203.9	91.8	20.4	87.6	102.4	112.5	22.5
39	1147	195.7	88.2	18.5	87.6	102.5	112.5	22.5
40	979	188.9	85.6	16.7	87.6	102.5	112.5	22.5
41	817	178.6	81.2	14.8	87.6	102.4	112.5	22.5
42	664	171.2	78.5	13.0	87.6	102.5	112.5	22.5
43	518	161.5	74.1	11.1	87.6	102.5	112.5	22.5
44	380	149.9	69.2	9.3	87.6	102.5	112.5	22.5
45	255	131.4	60.7	7.4	87.5	102.3	112.5	22.5
46	145	106.1	49.0	5.6	87.5	102.2	112.5	22.5
47	56	69.1	31.9	3.7	87.4	102.2	112.5	22.5

### Shape IS-B

Iteration	Area (pixels)	Perimeter (pixels)	Feret Maximum Length (pixels)	Feret Minimum Length (pixels)	Centre Gravity X (pixels)	Centre Gravity Y (pixels)	Feret Maximum Angle (degrees)	Feret Minimum Angle (degrees)
1	13283	534.2	189.6	95.3	107.2	114.0	118.1	28.1
2	12840	513.9	187.9	93.5	107.3	114.2	118.1	28.1
3	12413	495.1	185.6	91.7	107.3	114.4	118.1	28.1
4	12004	481.4	182.5	89.0	107.4	114.5	118.1	28.1
5	11607	470.6	179.4	87.2	107.4	114.5	118.1	28.1
6	11220	462.4	176.8	85.5	107.3	114.6	118.1	28.1
7	10840	454.1	175.0	83.7	107.3	114.6	118.1	28.1
8	10467	447.9	173.2	81.9	107.3	114.6	118.1	28.1
9	10099	440.8	171.5	80.2	107.3	114.6	118.1	28.1
10	9736	434.6	169.7	78.4	107.3	114.6	118.1	28.1
11	9378	426.9	167.5	76.7	107.2	114.6	118.1	28.1
12	9026	420.7	165.7	74.8	107.2	114.6	118.1	22.5
13	8679	414.4	163.9	73.0	107.2	114.6	118.1	22.5
14	8337	408.2	161.7	71.1	107.2	114.6	118.1	22.5
15	8000	398.5	158.1	69.3	107.1	114.5	118.1	22.5
16	7671	390.3	155.6	67.5	107.1	114.5	118.1	22.5
17	7349	384.0	153.9	65.6	107.1	114.4	118.1	22.5
18	7032	377.8	151.6	63.8	107.0	114.4	118.1	22.5
19	6720	371.5	149.8	61.9	107.0	114.3	118.1	22.5
20	6413	365.9	148.1	60.1	106.9	114.3	118.1	22.5
21	6110	360.2	146.3	58.2	106.9	114.2	118.1	22.5
22	5811	354.0	144.1	56.4	106.8	114.1	118.1	22.5
23	5517	347.7	141.8	54.5	106.8	114.1	118.1	22.5
24	5228	340.3	139.6	52.7	106.7	114.0	118.1	22.5
25	4946	334.7	137.8	50.8	106.7	114.0	118.1	22.5

26	4668	325.8	134.2	49.0	106.6	114.0	118.1	22.5
27	4398	319.0	131.5	47.1	106.6	113.9	118.1	22.5
28	4134	311.4	128.4	45.3	106.5	113.8	118.1	22.5
29	3876	305.1	126.2	43.4	106.5	113.7	118.1	22.5
30	3623	297.5	123.5	41.6	106.4	113.6	118.1	22.5
31	3376	290.6	120.8	39.7	106.3	113.6	118.1	22.5
32	3135	283.8	118.1	37.9	106.3	113.5	118.1	22.5
33	2901	274.1	114.1	36.0	106.2	113.4	112.5	22.5
34	2674	265.9	111.8	34.2	106.1	113.3	112.5	22.5
35	2454	259.1	109.6	32.3	106.0	113.1	112.5	22.5
36	2240	250.8	106.5	30.5	105.9	112.9	112.5	22.5
37	2033	244.6	104.2	28.7	105.8	112.8	112.5	22.5
38	1831	238.4	102.0	26.8	105.7	112.6	112.5	22.5
39	1634	230.7	98.8	25.0	105.6	112.4	112.5	22.5
40	1443	221.9	95.3	23.1	105.4	112.3	112.5	22.5
41	1261	210.8	90.5	21.3	105.3	112.1	112.5	22.5
42	1087	201.7	87.3	19.4	105.1	111.8	112.5	22.5
43	920	194.3	85.1	17.6	104.9	111.4	112.5	22.5
44	761	183.2	80.6	15.7	104.6	111.0	112.5	22.5
45	610	173.0	76.5	13.9	104.4	110.5	112.5	22.5
46	468	155.9	68.9	12.0	104.1	110.0	112.5	22.5
47	341	137.2	61.1	10.2	103.8	109.5	112.5	22.5
48	228	118.7	52.9	8.3	103.4	108.9	112.5	22.5
49	132	96.0	42.9	6.5	103.2	108.8	112.5	22.5
50	51	46.3	20.6	4.6	103.6	110.4	112.5	22.5
51	15	22.7	10.3	2.8	102.4	108.1	118.1	22.5

### Shape IS-C

Iteration	Area (pixels)	Perimeter (pixels)	Feret Maximum Length (pixels)	Feret Minimum Length (pixels)	Centre Gravity X (pixels)	Centre Gravity Y (pixels)	Feret Maximum Angle (degrees)	Feret Minimum Angle (degrees)
1	13535	638.9	273.8	89.1	127.2	161.6	118.1	28.1
2	13004	571.5	244.2	87.3	127.8	162.7	118.1	28.1
3	12536	553.4	236.6	85.5	128.1	163.3	118.1	28.1
4	12079	538.1	229.9	83.8	128.4	163.7	118.1	28.1
5	11632	520.7	222.4	82.0	128.6	164.2	118.1	28.1
6	11199	513.1	219.2	80.3	128.8	164.6	118.1	28.1
7	10773	502.6	214.8	78.5	129.0	165.0	118.1	28.1
8	10356	490.1	209.4	76.7	129.2	165.4	118.1	28.1
9	9947	479.0	204.9	75.0	129.4	165.7	118.1	28.1
10	9547	470.8	201.8	73.2	129.6	166.0	118.1	22.5
11	9155	458.3	196.4	71.3	129.8	166.3	118.1	22.5
12	8773	447.2	191.9	69.5	129.9	166.6	118.1	22.5
13	8399	439.6	188.8	67.6	130.1	166.9	118.1	22.5
14	8032	431.1	185.6	65.8	130.2	167.2	118.1	22.5

15	7671	417.8	180.2	63.9	130.3	167.4	118.1	22.5
16	7319	408.7	176.6	62.1	130.5	167.6	118.1	22.5
17	6974	401.1	173.5	60.2	130.6	167.9	118.1	22.5
18	6636	391.4	169.9	58.4	130.7	168.1	118.1	22.5
19	6305	380.3	165.0	56.6	130.8	168.3	118.1	22.5
20	5983	370.4	161.0	54.7	130.9	168.5	118.1	22.5
21	5668	363.6	158.3	52.9	131.0	168.7	118.1	22.5
22	5360	351.9	153.3	51.0	131.1	168.9	118.1	22.5
23	5061	343.7	150.2	49.2	131.2	169.0	118.1	22.5
24	4769	333.8	146.2	47.3	131.2	169.2	118.1	22.5
25	4484	324.7	142.6	45.5	131.3	169.3	118.1	22.5
26	4206	315.9	139.4	43.6	131.4	169.4	118.1	22.5
27	3936	308.2	136.3	41.8	131.4	169.6	118.1	22.5
28	3672	298.6	131.8	39.9	131.5	169.7	118.1	22.5
29	3416	290.4	128.2	38.1	131.5	169.8	118.1	22.5
30	3167	282.1	125.1	36.2	131.6	169.9	118.1	22.5
31	2925	273.9	121.5	34.4	131.6	170.0	112.5	22.5
32	2690	265.0	118.0	32.5	131.7	170.1	112.5	22.5
33	2463	258.2	115.4	30.7	131.7	170.2	112.5	22.5
34	2242	250.0	111.8	28.8	131.8	170.3	112.5	22.5
35	2028	241.1	108.3	27.0	131.8	170.4	112.5	22.5
36	1822	231.5	103.8	25.1	131.8	170.5	112.5	22.5
37	1624	222.7	100.3	23.3	131.9	170.5	112.5	22.5
38	1434	214.4	96.8	21.4	131.9	170.6	112.5	22.5
39	1251	204.8	92.3	19.6	131.9	170.7	112.5	22.5
40	1076	197.9	89.7	17.8	131.9	170.7	112.5	22.5
41	907	187.7	85.2	15.9	132.0	170.8	112.5	22.5
42	747	178.9	81.7	14.1	132.0	171.0	112.5	22.5
43	595	170.6	78.2	12.2	132.1	171.1	112.5	22.5
44	449	155.5	71.5	10.4	132.2	171.3	112.5	22.5
45	317	139.1	63.9	8.5	132.1	171.3	112.5	22.5
46	200	119.7	55.3	6.7	132.1	171.3	112.5	22.5
47	100	87.6	40.5	4.8	132.1	171.1	112.5	22.5
48	26	43.8	20.2	2.9	132.4	172.0	112.5	16.9

### Shape IS-D

Iteration	Area (pixels)	Perimeter (pixels)	Feret Maximum Length (pixels)	Feret Minimum Length (pixels)	Centre Gravity X (pixels)	Centre Gravity Y (pixels)	Feret Maximum Angle (degrees)	Feret Minimum Angle (degrees)
1	14722	915.1	284.5	98.0	124.8	176.4	118.1	28.1
2	13958	906.5	282.2	96.2	125.9	178.5	118.1	28.1
3	13206	846.8	280.5	93.4	127.0	180.8	118.1	22.5
4	130	92.6	42.5	7.1	53.0	37.1	118.1	28.1
5	59	49.1	22.8	5.3	50.9	33.3	118.1	33.8
6	23	34.6	16.1	3.5	50.6	32.9	118.1	28.1

7	10928	516.9	198.6	77.7	129.8	186.4	118.1	28.1
8	10504	499.0	194.6	76.0	130.0	186.7	118.1	28.1
9	10095	484.5	190.1	74.2	130.1	186.9	118.1	28.1
10	9700	468.4	186.9	72.4	130.2	187.1	118.1	28.1
11	9314	456.5	182.5	70.7	130.2	187.3	118.1	28.1
12	8938	445.4	178.0	68.9	130.3	187.5	118.1	28.1
13	8570	435.7	173.9	67.1	130.3	187.6	118.1	28.1
14	8210	426.1	170.8	65.4	130.3	187.7	118.1	28.1
15	7858	415.8	167.2	63.6	130.3	187.8	118.1	28.1
16	7515	408.2	164.1	61.8	130.3	187.9	118.1	28.1
17	7178	398.5	160.5	60.1	130.3	187.9	118.1	28.1
18	6849	390.3	157.3	58.3	130.3	188.0	118.1	28.1
19	6527	382.0	153.8	56.6	130.3	188.0	118.1	28.1
20	6212	372.4	150.6	54.8	130.3	188.0	112.5	28.1
21	5905	365.5	148.8	53.0	130.2	187.9	112.5	22.5
22	5604	359.3	146.9	51.1	130.2	187.9	112.5	22.5
23	5308	351.6	145.1	49.3	130.2	187.8	112.5	22.5
24	5018	343.4	142.5	47.4	130.1	187.8	112.5	22.5
25	4735	337.7	140.6	45.6	130.1	187.8	112.5	22.5
26	4456	330.1	138.4	43.7	130.1	187.7	112.5	22.5
27	4183	323.8	136.5	41.9	130.0	187.7	112.5	22.5
28	3915	316.2	133.4	40.0	130.0	187.6	112.5	22.5
29	3653	309.9	131.1	38.2	130.0	187.5	112.5	22.5
30	3396	300.3	128.9	36.3	130.0	187.5	112.5	22.5
31	3147	292.9	126.7	34.5	129.9	187.4	112.5	22.5
32	2905	286.6	124.5	32.6	129.9	187.4	112.5	22.5
33	2668	280.4	122.2	30.8	129.9	187.3	112.5	22.5
34	2436	274.7	120.4	28.9	129.9	187.2	112.5	22.5
35	2208	265.9	116.8	27.1	129.9	187.2	112.5	22.5
36	1989	254.8	112.0	25.3	129.9	187.1	112.5	22.5
37	1778	247.2	108.8	23.4	129.8	187.0	112.5	22.5
38	1573	239.5	105.7	21.6	129.8	186.9	112.5	22.5
39	1374	232.7	103.5	19.7	129.7	186.8	112.5	22.5
40	1181	225.9	101.2	17.9	129.7	186.6	112.5	22.5
41	994	216.8	97.7	16.0	129.7	186.5	112.5	22.5
42	814	209.1	94.9	14.2	129.7	186.5	112.5	22.5
43	640	200.9	91.8	12.3	129.8	186.5	112.5	22.5
44	473	193.2	88.6	10.5	130.0	186.8	112.5	22.5
45	312	178.8	82.3	8.6	130.5	187.6	112.5	22.5
46	169	121.4	56.1	5.6	131.7	190.2	112.5	22.5
47	67	83.6	38.6	3.8	132.2	191.2	112.5	22.5

## Shape IS-E

Iteration	Area (pixels)	Perimeter (pixels)	Feret Maximum Length (pixels)	Feret Minimum Length (pixels)	Centre Gravity X (pixels)	Centre Gravity Y (pixels)	Feret Maximum Angle (degrees)	Feret Minimum Angle (degrees)
1	15559	594.8	237.4	98.0	126.6	182.8	118.1	22.5
2	15066	585.1	235.6	96.1	126.8	183.1	118.1	22.5
3	14584	577.4	233.9	94.3	126.9	183.4	118.1	22.5
4	14108	564.6	229.0	92.5	127.1	183.7	118.1	22.5
5	13644	556.3	225.9	90.6	127.2	183.9	118.1	22.5
6	13187	546.7	222.8	88.8	127.3	184.1	118.1	22.5
7	12738	537.9	219.6	86.9	127.4	184.4	118.1	22.5
8	12297	529.0	216.9	85.1	127.5	184.6	118.1	22.5
9	11864	523.4	215.2	83.2	127.6	184.8	118.1	22.5
10	11435	517.7	213.4	81.4	127.8	185.0	118.1	22.5
11	11010	512.1	211.6	79.5	127.9	185.3	118.1	22.5
12	10589	505.2	209.8	77.7	128.0	185.5	118.1	22.5
13	10174	499.0	208.1	75.8	128.1	185.8	118.1	22.5
14	9764	492.2	206.3	74.0	128.3	186.1	118.1	22.5
15	9360	485.3	204.1	72.1	128.4	186.4	118.1	22.5
16	8962	478.5	202.2	70.3	128.6	186.7	118.1	22.5
17	8570	471.7	200.5	68.4	128.8	187.1	118.1	22.5
18	8184	464.8	198.2	66.6	129.0	187.5	118.1	22.5
19	7804	451.8	193.3	64.7	129.2	187.8	118.1	22.5
20	7435	442.9	189.7	62.9	129.4	188.2	118.1	22.5
21	7075	429.6	183.9	61.0	129.6	188.5	118.1	22.5
22	6725	418.6	178.9	59.2	129.8	188.8	118.1	22.5
23	6383	407.5	174.0	57.3	130.0	189.1	118.1	22.5
24	6051	393.0	167.7	55.5	130.1	189.4	118.1	22.5
25	5731	379.7	161.9	53.7	130.2	189.6	118.1	22.5
26	5420	370.0	158.3	51.8	130.3	189.8	118.1	22.5
27	5117	360.6	154.7	50.0	130.4	189.9	118.1	22.5
28	4823	354.4	152.5	48.1	130.5	190.1	118.1	22.5
29	4534	347.5	149.8	46.3	130.6	190.2	118.1	22.5
30	4251	339.3	146.6	44.4	130.7	190.4	118.1	22.5
31	3975	333.1	144.3	42.6	130.8	190.6	118.1	22.5
32	3704	326.8	142.1	40.7	130.9	190.8	118.1	22.5
33	3438	320.6	139.9	38.9	131.1	191.1	118.1	22.5
34	3177	312.3	136.8	37.0	131.2	191.4	118.1	22.5
35	2923	306.1	134.5	35.2	131.4	191.8	118.1	22.5
36	2674	299.8	132.3	33.3	131.6	192.3	118.1	22.5
37	2430	288.8	127.3	31.5	131.9	192.8	118.1	22.5
38	2201	253.1	111.1	29.6	132.1	193.3	112.5	22.5
39	1996	237.2	104.0	27.8	132.1	193.4	112.5	22.5
40	1801	228.9	100.5	25.9	132.1	193.4	112.5	22.5
41	1613	219.3	96.0	24.1	132.1	193.4	112.5	22.5



42	1433	211.0	92.5	22.2	132.1	193.4	112.5	22.5
43	1260	202.0	88.4	20.4	132.1	193.4	112.5	22.5
44	1094	195.7	86.2	18.5	132.1	193.4	112.5	22.5
45	933	189.5	83.9	16.7	132.1	193.4	112.5	22.5
46	777	180.4	79.8	14.8	132.1	193.4	112.5	22.5
47	628	174.2	77.6	13.0	132.1	193.5	112.5	22.5
48	484	165.9	74.1	11.2	132.2	193.6	112.5	22.5
49	347	157.7	70.5	9.3	132.3	193.9	112.5	22.5
50	68	46.0	20.6	5.7	122.8	170.7	112.5	16.9
51	32	37.0	17.1	3.7	122.7	170.4	112.5	16.9
52	28	37.0	17.1	3.4	137.0	205.6	112.5	16.9

### Shape IS-F

Iteration	Area (pixels)	Perimeter (pixels)	Feret Maximum Length (pixels)	Feret Minimum Length (pixels)	Centre Gravity X (pixels)	Centre Gravity Y (pixels)	Feret Maximum Angle (degrees)	Feret Minimum Angle (degrees)
1	36	26.1	10.8	5.7	62.6	20.0	123.8	16.9
2	16	19.3	8.6	3.6	62.4	19.8	123.8	28.1
3	12531	541.5	231.7	85.8	144.2	177.1	118.1	28.1
4	12081	533.8	228.6	84.0	144.5	177.5	118.1	28.1
5	11637	521.3	223.2	82.2	144.7	177.9	118.1	28.1
6	11202	508.8	217.9	80.4	144.9	178.3	118.1	22.5
7	10778	501.2	214.8	78.6	145.1	178.7	118.1	22.5
8	10361	486.5	208.5	76.7	145.3	179.0	118.1	22.5
9	9954	474.6	204.0	74.9	145.5	179.3	118.1	22.5
10	9556	468.3	201.8	73.1	145.7	179.6	118.1	22.5
11	9164	457.8	197.3	71.2	145.8	179.9	118.1	22.5
12	8779	446.8	192.8	69.4	146.0	180.2	118.1	22.5
13	8403	438.5	189.6	67.5	146.1	180.5	118.1	22.5
14	8035	428.0	185.2	65.7	146.3	180.8	118.1	22.5
15	7674	417.0	180.2	63.8	146.4	181.0	118.1	22.5
16	7322	411.3	178.5	62.0	146.5	181.3	118.1	22.5
17	6975	399.6	173.9	60.1	146.7	181.5	118.1	22.5
18	6637	389.7	169.9	58.3	146.8	181.8	118.1	22.5
19	6306	380.1	165.9	56.4	146.9	182.0	118.1	22.5
20	5983	372.4	162.8	54.6	147.0	182.2	118.1	22.5
21	5667	363.4	159.2	52.7	147.1	182.4	118.1	22.5
22	5358	352.3	154.2	50.9	147.2	182.5	118.1	22.5
23	5057	343.5	150.6	49.0	147.3	182.7	118.1	22.5
24	4764	332.4	146.2	47.2	147.3	182.9	118.1	22.5
25	4480	326.1	143.9	45.3	147.4	183.0	118.1	22.5
26	4202	315.1	139.0	43.5	147.5	183.2	118.1	22.5
27	3932	306.8	135.4	41.6	147.5	183.3	118.1	22.5
28	3669	298.6	131.8	39.8	147.6	183.4	118.1	22.5
29	3413	290.9	128.7	37.9	147.7	183.5	118.1	22.5

30	3163	282.1	125.1	36.1	147.7	183.6	118.1	22.5
31	2921	274.7	122.5	34.2	147.8	183.7	112.5	22.5
32	2686	266.5	118.9	32.4	147.8	183.8	112.5	22.5
33	2458	258.2	115.4	30.6	147.8	183.9	112.5	22.5
34	2237	248.6	110.9	28.7	147.9	184.0	112.5	22.5
35	2024	239.7	107.4	26.9	147.9	184.1	112.5	22.5
36	1819	231.5	103.8	25.0	148.0	184.2	112.5	22.5
37	1621	222.7	100.3	23.2	148.0	184.3	112.5	22.5
38	1431	213.0	95.8	21.3	148.0	184.3	112.5	22.5
39	1249	205.6	93.2	19.5	148.0	184.4	112.5	22.5
40	1074	197.3	89.7	17.6	148.1	184.5	112.5	22.5
41	906	187.7	85.2	15.8	148.1	184.6	112.5	22.5
42	746	178.9	81.7	13.9	148.2	184.7	112.5	22.5
43	594	170.6	78.2	12.1	148.2	184.9	112.5	22.5
44	450	156.7	72.4	10.2	148.3	185.1	112.5	22.5
45	316	135.4	62.6	8.4	148.3	185.2	106.9	22.5
46	202	119.7	55.3	6.5	148.3	185.0	112.5	22.5
47	102	94.4	43.6	4.7	148.3	185.0	112.5	22.5
48	23	41.8	19.3	2.8	147.7	183.5	112.5	22.5

## Appendix M – Experimental Impact Spatter Pattern ES-A

An example of the spatter bloodstain data collected for experimental impact spatter pattern ES-A is provided in the table below. The raw spatter bloodstain data collected on each of the three experimental impact spatter patterns analysed during this research project are available in Excel® format on the DVD-ROMs that accompany this thesis.

Plane	Normal	X (cm)	Y (cm)	Z (cm)	Width (mm)	Length (mm)	Orientation Angle (degrees)	Subjective Comment
YZ	+	0	7.2	37.65	1.4	5.6	86.5	TAI
YZ	+	0	6.45	46.4	0.7	2	80	TSAT
YZ	+	0	5.5	57.3	2	8.2	93	TSAT
YZ	+	0	8.9	56.4				PSAT(B6-1)
YZ	+	0	14.75	10.3	0.4	1.6	26	
YZ	+	0	15.5	11.35	0.6	1.2	47	
YZ	+	0	14.4	45.95	0.4	2	80	TSAT
YZ	+	0	18.25	56.1	1.8	7.4	97	ESAT(A6-2)/ HSAT
YZ	+	0	22.85	8.35				PSAT(?)
YZ	+	0	23.9	8.95	0.3	1.6	21	PDS/ NDLE
YZ	+	0	22.9	21.7	0.5	1.2	51.5	
YZ	+	0	21.25	25.2	1.3	3.6	82	TSAT
YZ	+	0	25.1	24.55				PSAT(?)
YZ	+	0	28.65	30.7	0.4	1	19	
YZ	+	0	25.9	40.25	0.7	1.2	58	
YZ	+	0	27.6	42.7	0.8	1.3	71	
YZ	+	0	25.8	46.25	1.3	2.8	92	TAI
YZ	+	0	24.8	55.6	1.2	2.6	94.5	TSAT
YZ	+	0	25.6	57.85	0.5	1.4	41	TAI
YZ	+	0	34.2	22.7	0.4	1.1	30	
YZ	+	0	37	30.2	0.7	1.2	56	TSAT
YZ	+	0	39.2	31.8	0.8	1.3	64	
YZ	+	0	35.15	38.2	0.3	0.5	76.4	PDLE
YZ	+	0	34.95	41.5	1.6	2.8	96	
YZ	+	0	31	41.95	0.7	1.2	76	
YZ	+	0	32.9	44.75	2	3.1	91	TAI(?)
YZ	+	0	39.85	44.5	0.7	1.3	82	
YZ	+	0	36.4	47.8	0.7	1	74	
YZ	+	0	39.9	48.15	0.5	0.8	67	PDLE
YZ	+	0	35.7	48.6	1.1	2	94	
YZ	+	0	36.6	57	0.6	0.8	59	
YZ	+	0	39.3	57.4	0.6	1	81	
YZ	+	0	47.85	10.4	0.2	0.6	11.5	PDS/ NDLE
YZ	+	0	49.6	10.15	0.4	1.2	20	
YZ	+	0	48.8	18.8	0.4	0.8	34	
YZ	+	0	43.05	19.85	0.7	1.9	46	TSAT

YZ	+	0	44.65	25.35	0.5	1.6	20	
YZ	+	0	49.15	29.05	0.3	1	11	NDLE
YZ	+	0	46.8	31.35	0.8	1.3	74	
YZ	+	0	47.05	32	1.5	2.5	81	
YZ	+	0	44.4	36.8	0.4	0.6	38	NDLE
YZ	+	0	43.15	44.05	0.5	0.9	74	
YZ	+	0	42.7	51.6	1.1	1.7	100	TAI
YZ	+	0	49.8	53.35	0.6	0.8	105.5	PDLE
YZ	+	0	43.3	58.3	0.7	1.1	101	
YZ	+	0	47.1	58.05	0.7	0.9	91	
YZ	+	0	44.85	61.1	0.6	0.9	77	
YZ	+	0	44.4	64.25	0.8	1.4	113	
YZ	+	0	45.7	65.35	0.7	1.4	99	
YZ	+	0	48.9	65.95	1.2	1.9	82	TAI
YZ	+	0	43.9	67.8	0.8	1.4	113	
YZ	+	0	58	10.5	0.3	1.1	11	NDLE
YZ	+	0	50.35	25.4	0.4	1.6	13.5	
YZ	+	0						Not Blood
YZ	+	0	56.35	26.1	0.3	0.6	31	NDLE
YZ	+	0	57.3	26.6	0.8	1.6	74	TAI
YZ	+	0	56	29.95	0.5	0.9	52	
YZ	+	0	58.75	32.5	0.4	0.9	20	
YZ	+	0	58.5	34.95	0.2	0.4	57.5	NDLE
YZ	+	0	51.75	35.7	1.8	2.8	91	
YZ	+	0	51.75	37.1	1.6	2.4	7.75	TAI
YZ	+	0	56	36.25	0.4	0.7	56	
YZ	+	0	59.35	38.15	0.4	0.5	93	PDLE
YZ	+	0	59.7	38.95	0.3	0.5	45	NDLE
YZ	+	0	58.3	39.65	0.5	0.8	83	
YZ	+	0	56.45	39.9	0.3	0.4	75.5	NDLE
YZ	+	0	52.8	42.9	0.4	0.7	23	
YZ	+	0	57.95	44.8	0.3	0.5	90	
YZ	+	0	57.8	50.6	0.3	0.6	103.5	
YZ	+	0	58.65	50.35	0.4	0.8	89	
YZ	+	0	57.7	52.1	0.5	0.9	106	
YZ	+	0	58.65	52.05	0.5	0.8	102	
YZ	+	0	51.9	52.95	0.2	0.4	47	NDLE
YZ	+	0	57.75	55.05	0.8	1.7	109	
YZ	+	0	53.6	56.6	1	1.8	118	
YZ	+	0	53.05	56.5	0.4	0.7	109	
YZ	+	0	52.5	56.9	0.9	1.6	117.5	
YZ	+	0	55.35	57.4	0.5	0.9	113	
YZ	+	0	53.7	58.35				DIST
YZ	+	0	52.1	59.1				DIST
YZ	+	0	54.75	60.8	0.5	0.9	84	
YZ	+	0	52.4	63.4	1.2	2.2	124	TAI
YZ	+	0	50.35	66.05	1.9	3.5	116	
YZ	+	0	52.35	66	0.8	1.6	123.5	TAI
YZ	+	0	57.9	67.35	0.8	1.6	108	
YZ	+	0	64.95	9.45	0.3	0.7	10	PDLE
YZ	+	0	69.55	15.4	0.3	0.8	13.5	NDLE

YZ	+	0	60.1	17.4				PSAT(?)
YZ	+	0	66.6	20.1	0.5	1	29	
YZ	+	0	67.85	20.2	0.5	0.8	24.5	
YZ	+	0	69	20.5	0.3	0.9	14	NDLE
YZ	+	0	62.7	22.4	0.4	0.9	49	
YZ	+	0	65.9	26.15	0.8	1.3	78	TAI
YZ	+	0	69.1	26.15	0.8	1.1	67.5	
YZ	+	0	69.9	25.7	0.3	0.4	20.5	NDLE
YZ	+	0	61.55	28.05				PSAT(?)
YZ	+	0	61.2	29.65	1.2	2.2	76.5	
YZ	+	0	60.1	33.3				DIST – by grid line.
YZ	+	0	63.2	33.35	0.5	0.7	36	
YZ	+	0	68.35	33.8	0.3	0.5	34	PDLE
YZ	+	0	61.65	36.95	0.5	0.8	54	
YZ	+	0	62.8	36.15	0.9	1.6	82.5	TAI
YZ	+	0	64.05	35.55	0.6	0.8	82	
YZ	+	0	64.45	35.5	0.4	0.9	47.5	PDLE
YZ	+	0	68.05	35.65	0.9	1.4	80	
YZ	+	0	68.5	37.15	0.7	1	76	
YZ	+	0	68.25	37.4	1.3	1.9	92	
YZ	+	0	67.8	38.5	0.4	0.6	52	NDLE
YZ	+	0	68.85	39.45	0.6	0.8	78	NDLE
YZ	+	0	64.65	39.5	0.2	0.5	85	NDLE
YZ	+	0	66.7	41.35	1.4	2.4	82	
YZ	+	0	61.95	42.45	0.5	0.9	84	
YZ	+	0	61.7	44.15	1	2.2	97	TAI
YZ	+	0	69.25	42.8				DIST
YZ	+	0	68.15	45.15	0.3	0.5	46	NDLE
YZ	+	0	69.7	47.05	0.7	0.8	100	NDLE
YZ	+	0	65.15	49.2	0.7	1.2	96	TAI
YZ	+	0	61.25	47.35	0.3	0.4	57	NDLE
YZ	+	0	62.75	51.8	1.5	3	109	TSAT
YZ	+	0	65.05	52.6	2.5	4.8	119	
YZ	+	0	66.6	52.65	0.4	0.6	72	NDLE
YZ	+	0	67.05	52.5	0.9	1.6	122	
YZ	+	0	67.75	51.9	0.8	1.2	124	
YZ	+	0	69.9	51.4	0.2	0.2		CIRC
YZ	+	0	61.1	55.75	0.5	0.7	83	
YZ	+	0	68.9	58	0.2	0.3	121.5	NDLE
YZ	+	0	66.3	60.1	0.5	0.8	128	
YZ	+	0	61.55	63.3	1.4	2.6	119	
YZ	+	0	62.85	77.45	0.8	1	78	
YZ	+	0	74.25	13.3	0.6	1.2	12	
YZ	+	0	74.95	13.25	0.2	0.5	9	
YZ	+	0	70.7	22.5	0.4	0.5	52	NDLE
YZ	+	0	72.35	27.75	1.1	1.8	54	PDS
YZ	+	0	74.35	28.05				DIST
YZ	+	0	76.65	27.3	0.5	0.5		CIRC/PDS
YZ	+	0	73	31.1	1.1	1.4	54	
YZ	+	0	71.85	31.85	0.4	0.6	48	NDLE

YZ	+	0	71.5	32.7	0.9	1.3	85	PDLE
YZ	+	0	73.25	34.9	0.5	0.7	39	NDLE
YZ	+	0	73.8	39.35	1.2	1.5	62	PDLE
YZ	+	0	77.35	38.75	0.8	0.8		CIRC/PDS
YZ	+	0	79.15	39.4	0.6	0.6		CIRC/PDS
YZ	+	0	75.1	41.05	0.2	0.4	26	NDLE
YZ	+	0	74.2	42.65	0.3	0.4	33	NDLE
YZ	+	0	75.8	43.95	0.2	0.3	37	NDLE
YZ	+	0	75.85	44.2	0.3	0.4	66	NDLE
YZ	+	0	79.1	43.8	0.3	0.3		CIRC
YZ	+	0	77.25	44.8	0.5	0.5		CIRC
YZ	+	0	70.75	45.9	0.5	0.7	54	
YZ	+	0	71.45	46.1	1.3	1.8	118	
YZ	+	0	74.6	46.5	0.8	1	125	
YZ	+	0	72.3	47.5	0.4	0.5	94	NDLE
YZ	+	0						Not Blood
YZ	+	0	71.9	49.05	1	1.4	132	
YZ	+	0	73.5	49.9	0.4	0.5	91	NDLE
YZ	+	0	72.8	50.95	1.5	2	134.5	PDS
YZ	+	0	75.45	52.3	1.2	1.4	128	
YZ	+	0	77.3	52.45	1.4	2.2	133	
YZ	+	0						Not Blood
YZ	+	0	71	57.9	0.4	0.6	131.5	
YZ	+	0	71.15	62.65	0.4	0.8	21	NDLE
YZ	+	0	75.2	72.5	0.8	1.1	132	PDLE
YZ	+	0	86.7	26.2	0.8	1	53.5	NDLE
YZ	+	0	85	27.75	0.6	0.8	53	
YZ	+	0	80.3	30.3	0.4	0.4		CIRC
YZ	+	0	87.3	31	0.4	0.6	30	NDLE
YZ	+	0	84.95	34.05	0.6	0.7	74.5	
YZ	+	0	87.35	34.4	2.9	3.4	97	
YZ	+	0	80.3	35.5	1	1.2	69	
YZ	+	0	85.8	36.6	0.7	0.8	115	
YZ	+	0	84.3	38.15	0.7	0.9	61	NDLE
YZ	+	0	88.95	39.4	0.7	0.7		CIRC
YZ	+	0	87.85	44.3	0.3	0.3		CIRC
YZ	+	0	80.15	47.25	1.4	1.8	124	
YZ	+	0	89.85	49.45	0.5	0.6	45	NDLE
YZ	+	0	83.35	52.15	0.4	0.5	80	NDLE
YZ	+	0						Not Blood
YZ	+	0	88.05	52.15	0.2	0.2		CIRC
YZ	+	0	86.8	53.5	0.8	0.8		CIRC/PDS
YZ	+	0	82.1	55.25	2.4	2.8	136	CREN
YZ	+	0	84.1	55.1	0.6	0.8	113	NDLE
YZ	+	0	82.55	56.25	3.2	3.8	144	CREN
YZ	+	0	83	56.8	0.3	0.3		CIRC
YZ	+	0	83.15	57.4	0.4	0.6	126	NDLE
YZ	+	0	83.45	61.95	0.4	0.6	146	NDLE
YZ	+	0	83.2	62.7	1.2	2	142.5	
YZ	+	0	82.05	63.8	0.7	1.2	136	NDLE
YZ	+	0	84.65	63.7	0.9	1.4	142	PDLE

YZ	+	0	85.95	63.7	0.9	1.2	141	
YZ	+	0	88.6	64.3	0.2	0.2		CIRC
YZ	+	0	89.95	68.6	0.4	0.6	149	NDLE
YZ	+	0	90.85	22.95	0.6	0.8	19	NDLE
YZ	+	0	93.3	26.15	1.4	1.6	70	
YZ	+	0	98.85	25.45	1.4	1.6	29	
YZ	+	0	99.55	25.1	1.4	1.6	62.5	
YZ	+	0	91.2	27.35	0.6	0.6		CIRC
YZ	+	0	93.4	28.1	0.3	0.5	14	
YZ	+	0	95.95	27.7	1	1.2	71	NDLE
YZ	+	0	96.7	28.45				DIST
YZ	+	0	97.3	28.6	0.4	0.4		CIRC
YZ	+	0						Not Blood
YZ	+	0	94.5	29.15	0.4	0.5	46	
YZ	+	0	91.35	30.05	1.2	1.4	87	PDLE
YZ	+	0	99.35	30.1	0.7	0.7		CIRC
YZ	+	0	93.1	31.2	1.1	1.1		CIRC
YZ	+	0	90.8	32.5	3.3	4.5	84	CREN
YZ	+	0	90	34.05	0.3	0.6	9	NDLE
YZ	+	0	91.05	34.75	0.9	1.1	71	NDLE
YZ	+	0	91.9	35.2	2.2	2.4	94.5	
YZ	+	0	95.1	34.75	1	1.2	48	NDLE
YZ	+	0	96.2	34.45	1.3	1.5	44	NDLE
YZ	+	0	91.55	39.8	2.3	2.8	136	
YZ	+	0	96.45	39.8	0.4	0.4		CIRC
YZ	+	0	97.9	38.9	0.4	0.4		CIRC
YZ	+	0	92.9	41.95	1	1		CIRC
YZ	+	0	95.5	41.25	1.2	1.2		CIRC
YZ	+	0	93.8	42.65	0.9	1.2	136	PDLE
YZ	+	0	92.8	43.25	1.6	2	124	PDLE
YZ	+	0	99.4	41.7	0.2	0.2		CIRC
YZ	+	0	90.25	46.8	0.2	0.2		CIRC
YZ	+	0	93.4	46.65	1	1		CIRC
YZ	+	0	95.25	47.85	1.7	2	127	NDLE
YZ	+	0	98.65	45.8	2.3	2.6	125	
YZ	+	0	99.3	45.1	1.6	2.2	138	PDLE
YZ	+	0	92.95	50.15	0.3	0.6	170	NDLE
YZ	+	0	93.25	50.2	0.5	0.6	40	NDLE
YZ	+	0	93.7	51.1	0.2	0.2		CIRC
YZ	+	0	94.05	51.6	0.3	0.5	27	NDLE
YZ	+	0	92.25	53.7	0.9	1	139	NDLE
YZ	+	0	98.5	53.4	2.5	2.8	166	
YZ	+	0	99.87	53.7	1	1.2	132	NDLE
YZ	+	0	99.25	54.15	0.8	1	152	NDLE
YZ	+	0	99.95	55.55	0.8	0.9	165	NDLE
YZ	+	0	90.6	55.3	0.3	0.3		CIRC
YZ	+	0	92.45	56.2	0.2	0.2		CIRC
YZ	+	0	90.3	58.95	1.2	1.6	131	NDLE
YZ	+	0	90.1	63	0.3	0.4	145	NDLE
YZ	+	0	96.25	63.2	0.6	0.7	167	PDLE
YZ	+	0	98.9	64.35	1.6	2.2	167	

YZ	+	0	90.1	67.55	0.7	0.7		CIRC
YZ	+	0	91.4	69.35	0.4	0.6	151	NDLE
YZ	+	0	92.9	70.6	0.3	0.4	156	NDLE
YZ	+	0	98.05	72.5	0.5	0.7	158.5	
YZ	+	0	99.2	72.55	1.3	2	163	
YZ	+	0	98.9	79.45	0.5	1.2	162	
YZ	+	0	103.6	20.6	0.3	0.4	13	NDLE
YZ	+	0	102.3	22.95	0.4	0.7	13.5	NDLE
YZ	+	0	105.1	23.2	0.9	0.9		CIRC
YZ	+	0	105.95	23.7	0.5	0.5		CIRC
YZ	+	0	108.25	24.05	1.3	1.6	3.5	
YZ	+	0	107.8	27.25	1.3	1.3		CIRC
YZ	+	0	107.25	29.1	0.8	1.1	18	NDLE
YZ	+	0	101.8	29.3	1.2	1.2		CIRC
YZ	+	0	102.55	32.7	1	1.2	166.5	NDLE
YZ	+	0	101.9	34.35	0.9	1	54	
YZ	+	0	109.75	38.3	0.4	0.6	168	NDLE
YZ	+	0	108.85	38.5	0.2	0.2		CIRC
YZ	+	0	105.4	38.65	0.3	0.3		CIRC
YZ	+	0	104.7	42.6	0.2	0.8	2	NDLE
YZ	+	0	105.7	43.7	0.4	0.4		CIRC
YZ	+	0	109.5	44.5	0.4	0.6	176.5	
YZ	+	0	102.25	44.65	0.6	0.8	143	NDLE
YZ	+	0	102	44.7	1.2	1.6	147	NDLE
YZ	+	0	105.55	46.2				DIST
YZ	+	0	108.3	46.85	0.9	1.2	163	PDLE/PDS
YZ	+	0	106	47	2.3	2.8	162	CREN
YZ	+	0	104.65	46.8	0.4	0.4		CIRC
YZ	+	0	101.9	47.15	1.8	2.2	163.5	
YZ	+	0	102.55	47.9	1.2	1.6	157	
YZ	+	0	103.65	49.1	0.6	0.7	160	NDLE
YZ	+	0	103.75	49.7	1.7	2.2	164	
YZ	+	0	101.05	52.4	0.3	0.3		CIRC
YZ	+	0	104.6	54.2	0.5	0.7	165	NDLE
YZ	+	0	108.65	54.05	0.5	0.7	176	NDLE
YZ	+	0	102.4	55.3	0.7	0.9	176	NDLE
YZ	+	0	105	55.55	0.3	0.6	165	NDLE
YZ	+	0	100.45	56	0.2	0.4	6	NDLE
YZ	+	0	100.85	55.95	2.8	3.5	159	
YZ	+	0	106.2	57.5	0.9	1.1	7	PDLE
YZ	+	0	108.5	57.15	0.3	0.6	176	NDLE
YZ	+	0	100.8	58.25	1.6	2	144	
YZ	+	0	105.15	59.2	0.6	0.8	177	NDLE
YZ	+	0	100.4	59.65	0.2	0.2		CIRC
YZ	+	0	104.1	62.15	1.1	1.6	169	
YZ	+	0	109.6	62.5	0.6	0.8	172	PDLE
YZ	+	0	100.25	65.55	0.3	0.5	171	NDLE
YZ	+	0	100.75	68.7	0.5	0.7	164	PDLE
YZ	+	0	102.4	69.2	0.3	0.4	172	NDLE
YZ	+	0	106.35	70.4	1.1	1.4	176	
YZ	+	0	100.3	72.8	1	1.6	166	



YZ	+	0	102.4	73.4	1	1.4	168	
YZ	+	0	106.25	72.5	0.6	0.8	175	PDLE
YZ	+	0	100.75	74.5	0.8	1.3	168	
YZ	+	0	104.55	80.5	0.4	0.7	177	
YZ	+	0	101.25	89.2	1.1	2	166.5	
YZ	+	0	114.95	20.75	0.2	0.5	350	NDLE
YZ	+	0	119.4	21.65				DIST
YZ	+	0	115.3	22.95	0.2	0.3	352	NDLE
YZ	+	0	117.55	23.3	0.2	0.6	354	NDLE
YZ	+	0	111.3	24.85	1	1		CIRC
YZ	+	0	113.5	24.2	1.2	1.4	351	
YZ	+	0	114.45	24.1	0.6	1	351	
YZ	+	0	119.45	24.1	1	1		CIRC
YZ	+	0	118	26.4	0.7	0.9	336	NDLE
YZ	+	0	117.9	29.8	1	1		CIRC
YZ	+	0	110.65	29.3	0.3	0.3		CIRC
YZ	+	0	111.85	31.8	0.8	0.8		CIRC
YZ	+	0	118.45	31.2	0.8	0.8		CIRC
YZ	+	0	116.3	32.05	2	2		CIRC
YZ	+	0	117.95	31.8	0.3	0.3		CIRC
YZ	+	0	119.85	32	0.4	0.4		CIRC
YZ	+	0	116.8	32.75	0.3	0.3		CIRC
YZ	+	0	119.95	32.9	1	1		CIRC/PDS
YZ	+	0	116.6	33.7	0.3	0.3		CIRC
YZ	+	0	115.6	35.6	0.9	1	202	
YZ	+	0	117.15	35.3				DIST
YZ	+	0	118.4	35.75	0.3	0.3		CIRC
YZ	+	0	118.95	35.15	1.6	1.6		CIRC/PDS
YZ	+	0	118.75	38.4	0.3	0.3		CIRC
YZ	+	0	112.2	41.2	0.3	0.4	150	NDLE
YZ	+	0	118.2	41.05	1.5	1.8	214	NDLE
YZ	+	0	119.7	40.75				DIST
YZ	+	0	119.25	41.55	0.4	0.4		CIRC
YZ	+	0	119.75	44.35	0.7	0.8	207	
YZ	+	0	115.5	45.2	0.3	0.3		CIRC
YZ	+	0	111.55	46.15	0.9	0.9		CIRC/PDS
YZ	+	0	115.5	46.9	0.9	1.1	198	PDLE
YZ	+	0	117.3	46.25	0.5	0.5		CIRC
YZ	+	0	118.75	46.75	0.6	0.8	203	NDLE
YZ	+	0	116.5	47.8	1.6	2	136/316	OCS
YZ	+	0	118.75	47.95	0.6	0.7	194	NDLE
YZ	+	0	119.75	48.15	0.6	0.8	201	NDLE
YZ	+	0	113.4	49.6	0.2	0.4	179	NDLE
YZ	+	0	116.4	51.8	1.2	1.6	185	
YZ	+	0	117.7	51.3	2.2	2.5	200	CREN
YZ	+	0	117.95	51.75	0.5	0.7	201	
YZ	+	0	118.9	54.3				DIST
YZ	+	0	116.3	55.6	0.8	1	192.5	
YZ	+	0	114.25	61.15	0.4	0.5	186	NDLE
YZ	+	0	113.6	62.6	0.8	0.9	192	PDS
YZ	+	0	111.65	64.3	0.2	0.4	176	NDLE

YZ	+	0	111.05	65.3	1	1.4	183	
YZ	+	0	114.55	66.15	1.1	1.4	200	
YZ	+	0						Not Blood
YZ	+	0	112.5	68.1	0.4	0.4		CIRC
YZ	+	0	120.25	19.75	0.2	0.3	348	NDLE
YZ	+	0	123.45	17.95	0.2	0.2		CIRC
YZ	+	0	124.05	19.15	0.4	0.6	331	NDLE
YZ	+	0						Not Blood
YZ	+	0	122.55	20.55	0.2	0.2		CIRC
YZ	+	0	125.7	21.25	0.5	0.5		CIRC
YZ	+	0	127.65	21.5	0.4	0.4		CIRC
YZ	+	0	122.75	22.75	0.3	0.3		CIRC
YZ	+	0	122.2	24.35	0.3	0.3		CIRC
YZ	+	0	123.75	24.2	1	1.1	304	
YZ	+	0	121.25	26.35	0.8	0.8		CIRC
YZ	+	0	123.1	26.15	1.2	1.2		CIRC/CREN
YZ	+	0	121.55	28.75	0.7	0.7		CIRC
YZ	+	0	125.55	27.45	0.6	0.6		CIRC
YZ	+	0	125.9	28	0.8	0.8		CIRC
YZ	+	0	127	27.75	0.7	0.7		CIRC
YZ	+	0	129.75	27.95	0.8	0.8		CIRC
YZ	+	0	126.45	29.25	0.4	0.4		CIRC
YZ	+	0	128.65	28.8	0.2	0.4	346	NDLE
YZ	+	0	120.45	31.2	0.3	0.3		CIRC
YZ	+	0						Not Blood
YZ	+	0	124	31.85	0.3	0.6	345	NDLE
YZ	+	0	126.2	30.45	0.4	0.4		CIRC
YZ	+	0	129.9	31.8	0.5	0.5		CIRC
YZ	+	0	125.85	32.15	0.7	0.9	242	NDLE
YZ	+	0	126.15	33	0.6	0.6		CIRC
YZ	+	0	126.2	33.2	0.6	0.7	263	
YZ	+	0	120.75	35.1	1	1.1	325	
YZ	+	0	122.05	34.85	0.8	0.9	248	NDLE
YZ	+	0	123.95	34.35	0.3	0.6	344	
YZ	+	0	126.9	34.25	0.6	0.6		CIRC
YZ	+	0	127.6	34.2	0.4	0.4		CIRC
YZ	+	0	120.1	36.85	0.3	0.6	324	NDLE
YZ	+	0	122.65	36.35	0.9	0.9		CIRC
YZ	+	0	122.9	35.55	0.6	0.6		CIRC
YZ	+	0	124.4	36.2	0.3	0.4	236	NDLE
YZ	+	0	124.4	36.75	0.3	0.3		CIRC
YZ	+	0	125	36.6	0.4	0.6	326	
YZ	+	0	126.6	35.85	0.4	0.4		CIRC
YZ	+	0	126.7	35.75	1.1	1.2	240	
YZ	+	0	127.25	36.1	0.3	0.3		CIRC
YZ	+	0	127.7	35.65	0.9	1	296	NDLE
YZ	+	0	126.7	36.75	0.4	0.4		CIRC
YZ	+	0	121.75	38.95	0.5	0.5		CIRC
YZ	+	0	126.55	39.4	0.8	0.8		CIRC
YZ	+	0	127.5	37.9	0.5	0.5		CIRC
YZ	+	0	128.95	37.1	1.4	1.6	255	NDLE/CREN

YZ	+	0	129.05	36.95	0.2	0.6	348	NDLE
YZ	+	0	128.95	38.85	0.7	0.7		CIRC/PDS
YZ	+	0	124.75	39.95	0.4	0.6	328	NDLE
YZ	+	0	123.95	40.45	0.9	1.1	221	PDLE
YZ	+	0	128.1	40.75	0.8	1	239	
YZ	+	0	124.7	41.5	0.7	0.8	220	PDLE
YZ	+	0	120.8	42.5	1.2	1.6	211	
YZ	+	0	122.9	43	1.1	1.1		CIRC
YZ	+	0	124.25	42.25	1.2	1.4	191	NDLE
YZ	+	0	126	43.25	1.8	2.2	211	
YZ	+	0	127.9	42.75	0.2	0.6	339	NDLE
YZ	+	0	129.7	42.7				DIST
YZ	+	0	129.6	43.55	0.5	0.7	226	
YZ	+	0	121.85	44.15	0.7	0.9	201.5	
YZ	+	0	129.3	44.15	0.6	0.7	257.5	NDLE
YZ	+	0	122.95	46.3	1.2	1.4	205	
YZ	+	0	127.45	46.1	0.8	0.8		CIRC
YZ	+	0	129.2	45.95	0.3	0.3		CIRC
YZ	+	0	123.1	47.6	1	1		CIRC
YZ	+	0	125.3	47.4	0.3	0.3		CIRC
YZ	+	0	127.1	47.3				DIST
YZ	+	0	127.9	46.75	0.5	0.5		CIRC
YZ	+	0	125.7	49.1	0.9	1.1	203	PDS
YZ	+	0	127	48.45	0.3	0.3		CIRC
YZ	+	0	123.05	50.5	2.2	2.4	191	CREN
YZ	+	0	125.2	50.95	0.4	0.8	333	NDLE
YZ	+	0	127.8	52.1	0.7	0.8	251	NDLE
YZ	+	0	125.75	53.85	0.6	0.7	202	NDLE
YZ	+	0	123.6	54.85	2.3	2.8	197.5	
YZ	+	0	126.1	55.45	1.6	1.9	231	
YZ	+	0	138.5	21.3	0.2	0.2		CIRC
YZ	+	0	138.55	21.2	1.2	1.4	310	
YZ	+	0	138.3	22.05	0.3	0.6	282	NDLE
YZ	+	0	139.8	22.8	0.3	0.4	324	NDLE
YZ	+	0	131.35	23.35	0.6	0.8	318	
YZ	+	0	134.9	23.75	0.7	0.8	277	
YZ	+	0	135.1	23.85	0.6	0.8	307	NDLE
YZ	+	0	136.55	23.95	0.9	1.3	291	
YZ	+	0	137.7	23.3	0.7	0.8	296	NDLE
YZ	+	0	136.15	24.45	0.2	0.3	329	NDLE
YZ	+	0	139.7	24.3	0.8	1.1	269	NDLE
YZ	+	0	133.8	26	0.4	0.6	300	NDLE
YZ	+	0	137.7	25.3	1	1.2	274	HSAT
YZ	+	0	139.35	25.85	0.6	0.7	289	NDLE
YZ	+	0	130.15	28.15	0.3	0.6	334	NDLE
YZ	+	0	130.6	27.95	0.5	0.5		CIRC
YZ	+	0	131.4	27.3	0.1	0.1		CIRC
YZ	+	0	131.45	27.35	0.2	0.2		CIRC
YZ	+	0	131.5	27.4	0.2	0.3	334	NDLE
YZ	+	0	134.1	27.25	0.2	0.3	342	NDLE
YZ	+	0	134.9	28.85	0.8	0.9	262	

YZ	+	0	139.5	28.15	0.3	0.4	299	NDLE
YZ	+	0	137	29.6	0.7	0.8	274	
YZ	+	0	137.2	29.5	0.4	0.5	272	
YZ	+	0	132.9	30.1	0.6	0.8	318	
YZ	+	0	133.6	30.65	1.2	1.4	253	
YZ	+	0	131.8	32	0.9	1	256	
YZ	+	0	134.95	31.75				DIST
YZ	+	0	137.35	32.1				DIST
YZ	+	0	130.95	32.75	0.2	0.2		CIRC
YZ	+	0	131.05	32.6	0.7	0.8	284	NDLE
YZ	+	0	133	32.6	1	1.2	246	
YZ	+	0	133.85	33.1	0.5	0.6	244	NDLE
YZ	+	0	137.7	33.05	1	1.1	251	
YZ	+	0	131.2	33.45	0.3	0.3		CIRC
YZ	+	0	132.2	33.2	0.5	0.5		CIRC
YZ	+	0	133.52	33.5	0.3	0.3		CIRC
YZ	+	0	130.05	35.3	1	1.1	285	NDLE
YZ	+	0	132.05	34.35	0.3	0.3		CIRC
YZ	+	0	135.35	34.45	0.7	0.8	259	PDLE
YZ	+	0	130.2	35.75	0.4	0.5	229	NDLE
YZ	+	0	131.85	36	0.7	0.8	253	PDLE
YZ	+	0	132.65	35.5	0.5	0.5		CIRC
YZ	+	0	137.65	35.95	0.4	0.5	252	
YZ	+	0	138.7	36.2	0.6	0.8	255.5	
YZ	+	0	139.25	35.9	0.3	0.4	252	NDLE
YZ	+	0	131.8	37.15	1.7	2	251.5	
YZ	+	0	134.55	37	0.7	0.9	258	
YZ	+	0	137.45	37.1	0.4	0.6	273	
YZ	+	0	130.25	39.05	0.5	0.5		CIRC
YZ	+	0	138.5	39.3	0.3	0.5	333	
YZ	+	0	131.2	40.05	1.6	1.9	244	CREN
YZ	+	0	133.2	41.05	0.9	1	234	
YZ	+	0	134.2	41.75	0.3	0.3		CIRC
YZ	+	0	135.3	41.7	1.1	1.3	247	
YZ	+	0	132.35	43.55	0.7	0.8	229	
YZ	+	0	133.8	43.25	1.1	1.3	254	
YZ	+	0	138.35	44.4	0.7	0.9	232	
YZ	+	0	130.05	46.2	1.3	1.6	229	
YZ	+	0	131.65	46.5	0.4	0.4		CIRC
YZ	+	0	133.65	46.7	0.9	1.1	238.5	
YZ	+	0	134.2	47.05	0.4	0.6	257	NDLE
YZ	+	0	135.1	47.7	1	1.3	271	
YZ	+	0	138.35	47.25	1.6	1.8	274	
YZ	+	0	136.2	49.6	0.4	0.5	241	
YZ	+	0	135.75	50.3	0.3	0.3		CIRC
YZ	+	0	135.9	54.15	0.4	0.6	219	
YZ	+	0	137.2	54.2	0.7	1	230	
YZ	+	0	137.1	54.95	0.5	0.6	228	
YZ	+	0	139.8	54.1	2.6	3.4	254	PDS
YZ	+	0	135.85	58.5	0.8	1.2	222	
YZ	+	0	138.7	61.35				DIST

YZ	+	0	141.3	22.25	0.3	0.6	292	NDLE
YZ	+	0	143.95	23	0.2	0.2		CIRC
YZ	+	0	145.7	23.75	0.3	0.4	295	NDLE
YZ	+	0	145.65	23.7	0.4	7	289	NDLE
YZ	+	0	141.45	24.3	0.6	0.8	289	
YZ	+	0	149.9	24.25	0.4	0.6	296	NDLE
YZ	+	0	141.25	26.25	0.4	0.5	303	NDLE
YZ	+	0	142.45	26.1	0.6	0.8	270	NDLE
YZ	+	0	144.4	25.4	0.4	0.5	272.5	NDLE
YZ	+	0	145.4	25.9	0.3	0.4	270.5	NDLE
YZ	+	0	147.4	25.25	0.3	0.4	301	NDLE
YZ	+	0	149.7	25.9	0.6	0.8	268.5	
YZ	+	0	141.35	26.55	0.5	0.7	275	NDLE
YZ	+	0	142.95	26.55				DIST
YZ	+	0	140.8	27.4	0.5	0.6	271	NDLE
YZ	+	0	142.5	27.9	0.2	0.3	317	NDLE
YZ	+	0	143.85	27.95	0.8	0.9	267	
YZ	+	0	145.3	28.15	0.3	0.3		CIRC
YZ	+	0	147.75	28.5	0.4	0.6	291	
YZ	+	0	149.35	27.95	0.4	0.6	277	
YZ	+	0	142.2	29				DIST
YZ	+	0	143	29	2.2	3.2	259	CREN
YZ	+	0	144.2	29.7	0.6	0.8	264	NDLE
YZ	+	0	144.85	29.15	0.4	0.5	276	
YZ	+	0	146.6	29.65	0.2	0.3	277	NDLE
YZ	+	0	146.9	29.25	0.3	0.5	273	
YZ	+	0	141.05	30.7	0.7	1	266	CREN
YZ	+	0	147.55	30.05	0.7	1	276.5	
YZ	+	0	142.55	31.8	0.7	1.3	244	
YZ	+	0	143.4	31.3	0.2	0.2		CIRC
YZ	+	0	147.1	31.45	0.4	0.7	278	
YZ	+	0	149.35	31	0.5	0.5		CIRC
YZ	+	0	149	32.2	0.4	0.6	271	NDLE
YZ	+	0	146.7	33.2	0.2	0.2		CIRC
YZ	+	0	147.55	33	0.4	0.6	265	PDLE
YZ	+	0	148.6	32.85	0.8	1	251	PDS/CREN
YZ	+	0	140.4	35.1	0.3	0.3		CIRC
YZ	+	0	145.9	34.2	0.8	1	261	
YZ	+	0	147	34.85	0.4	0.7	264	
YZ	+	0	142.6	36.05	0.4	0.8	337	
YZ	+	0	147.85	36.3	0.7	0.9	248	
YZ	+	0	140	39.5	1	1.3	234	PDS
YZ	+	0	141.5	39.95	0.5	0.7	237	
YZ	+	0	142.5	39.95	0.8	1	316.5	
YZ	+	0	146.1	39.65	0.3	0.3		CIRC
YZ	+	0	148.4	40.15	0.4	0.6	255	NDLE
YZ	+	0	145.9	41.85	0.2	0.3	272	NDLE
YZ	+	0	148.2	42.65	0.2	0.4	317	NDLE
YZ	+	0	149.1	41.95	0.3	0.4	279	PDLE
YZ	+	0						Not Blood
YZ	+	0	149.15	43.95	0.4	0.6	308	NDLE

YZ	+	0	148.05	44	0.2	0.2		CIRC
YZ	+	0	142.9	44.95	0.8	0.9	238	
YZ	+	0	144.4	44.6	0.4	0.5	249	
YZ	+	0	145.35	45.1	0.3	0.5	298	PDLE
YZ	+	0	147.1	44.7	0.6	0.7	236	PDLE
YZ	+	0	148.4	44.75	0.3	0.3		CIRC
YZ	+	0	148.9	45.75	0.5	0.6	242	PDLE
YZ	+	0	149.3	46.1	0.4	0.6	268	NDLE
YZ	+	0	142.85	46.8	1	1.3	237	TAI
YZ	+	0	143.85	46.55	1	1.7	238	HSAT
YZ	+	0	144.3	46.4	0.3	0.4	269	NDLE
YZ	+	0	146.2	46.4	0.8	0.9	238	
YZ	+	0	147.45	46.9	0.6	0.6		CIRC/PDS
YZ	+	0	145	47.15				DIST
YZ	+	0	145.7	47.5	0.4	0.4		CIRC
YZ	+	0	140.8	48.45	0.7	0.9	243	PDLE
YZ	+	0	144.5	48	1.5	1.8	274	
YZ	+	0	141.85	49.55	0.9	1.5	238	
YZ	+	0	144.7	48.6	2	2.5	240	
YZ	+	0	145.5	49.4	0.6	0.6		CIRC/PDS
YZ	+	0	145.7	49.5				DIST
YZ	+	0	145.8	49.25	0.4	0.4		CIRC
YZ	+	0	146.85	49.75	0.7	1	236	
YZ	+	0	147.3	49.65	0.8	0.9	233	NDLE
YZ	+	0	147.35	48.7	1.6	1.9	242	
YZ	+	0	147.4	48.6	0.8	0.9	238	NDLE
YZ	+	0	148.2	49.45	1.6	1.8	234	HSAT/CREN
YZ	+	0	141.1	50.9	0.5	0.7	235	
YZ	+	0	142	51.25	0.3	0.5	232	NDLE
YZ	+	0	142.25	50.9	1.6	2.2	234	HSAT
YZ	+	0	142.95	51.45				DIST
YZ	+	0	144	50.7	0.8	1.2	231	NDLE
YZ	+	0	145.4	50.3	0.6	0.6		CIRC/PDS
YZ	+	0	146.75	50.95	0.6	0.8	232	NDLE
YZ	+	0	141.25	51.75	0.6	0.9	217	
YZ	+	0	142.55	52.7				DIST
YZ	+	0	143.4	52	2.4	3	237	
YZ	+	0	145.95	51.7	1.4	1.8	246	
YZ	+	0	149.35	52	0.9	1.2	247	
YZ	+	0	146	52.5	1.9	2.2	218	
YZ	+	0	146.7	52.7	1.2	1.6	248	PDLE
YZ	+	0	147.25	52.8	1.1	1.4	234	
YZ	+	0	145.65	53.3	0.9	1.1	239	
YZ	+	0	146.35	53.25	2.2	2.6	224	
YZ	+	0	140.9	53.35	0.4	0.5	234	NDLE
YZ	+	0	143.8	53.6	0.4	0.7	224	PDLE
YZ	+	0	144.2	55.5	0.7	1	223.5	
YZ	+	0	144.4	57.9				DIST
YZ	+	0	146.75	57.05	0.8	1	206	
YZ	+	0	154	23.95	0.2	0.3	307	NDLE
YZ	+	0	150.4	24.75	0.5	0.7	289	

YZ	+	0	151.45	25.6	0.2	0.3	317	NDLE
YZ	+	0	154.05	25.9	0.3	0.5	308	
YZ	+	0	159.4	25.2	0.5	0.7	289	
YZ	+	0	151.3	28.95	0.6	0.8	267	PDLE
YZ	+	0	151.75	29.15	0.4	0.4		CIRC
YZ	+	0	152.4	28.7	0.2	0.2		CIRC
YZ	+	0	152.95	28.2	0.3	0.5	287	
YZ	+	0	153.65	28.45	0.2	0.2		CIRC
YZ	+	0	155.1	28.25	0.9	1.5	272	
YZ	+	0	155.6	27.65	0.6	0.9	281	
YZ	+	0	159.3	27.05	0.6	0.8	289	PDLE
YZ	+	0	159.7	28.3	0.2	0.3	296	NDLE
YZ	+	0	154	29.65	0.4	0.6	262	
YZ	+	0	157.2	29.5	0.9	1.4	273	TAI
YZ	+	0	159.5	29.6	0.4	0.7	271	
YZ	+	0	155.75	30.25	0.3	0.4	289	PDLE
YZ	+	0	156.15	30.35	0.6	0.9	272	PDS
YZ	+	0	156.15	30.85	0.7	1.1	268	NDLE
YZ	+	0	155.25	31.2	1.4	3.3	270	FRAG
YZ	+	0	155.6	31.6	0.5	0.8	266	
YZ	+	0	151.85	32.5	1	1.5	269	PDS
YZ	+	0	151.8	32.35	0.5	0.6	268	
YZ	+	0	153.8	32.45	0.9	1.2	281	PDS
YZ	+	0	155.25	32.85	0.7	1	263.5	
YZ	+	0	155.55	31.8	0.2	0.5	280	
YZ	+	0	159.2	32.35	1	1.4	276	HSAT
YZ	+	0	159.8	32.8	0.6	0.9	275	PDLE
YZ	+	0	150.9	34.25				DIST/FRAG
YZ	+	0	151.85	34.65	0.6	0.6		CIRC
YZ	+	0	153.15	34	0.3	0.3		CIRC
YZ	+	0	152.6	35.2	0.8	1.1	261	
YZ	+	0	153.9	34.85	0.6	0.9	261	
YZ	+	0	157.4	33.75	0.6	1	260.5	
YZ	+	0	159.25	33.9	0.6	0.9	265	
YZ	+	0	153	36.15	0.5	0.7	266.5	PDLE
YZ	+	0	155.8	35.45	0.4	0.5	271	PDLE
YZ	+	0	156.6	35.25	1.5	2	263	HSAT/CREN
YZ	+	0	157.8	35.75	1.1	1.4	265.5	PDS
YZ	+	0	158.15	36.25	0.6	1	261	
YZ	+	0	159.2	36.5	0.6	0.9	262	NDLE
YZ	+	0	152.25	36.9	0.2	0.4	310	NDLE
YZ	+	0	152.8	32.8	0.3	0.4	314	PDLE
YZ	+	0	152.1	37.7	0.3	0.4	277	
YZ	+	0	156.95	39.55	0.5	0.9	255	PDS
YZ	+	0	158.6	38.35	1.5	1.9	263	TSAT
YZ	+	0	159.25	38.75	0.2	0.4	292	NDLE
YZ	+	0	159.1	39.2	0.4	0.5	264	
YZ	+	0	152.7	42.05	1	1.3	253	
YZ	+	0	154.05	41.65	0.4	0.6	260	PDLE
YZ	+	0	156.8	41.75	0.7	1	251	PDLE
YZ	+	0	151.65	43.1	0.8	1.1	254	FRAG/HSAT

YZ	+	0	154.05	43.15	0.6	0.8	256	
YZ	+	0	155.25	43.45	1	1.6	249	
YZ	+	0	156.95	43.65	0.2	0.4	266	NDLE
YZ	+	0	150.5	44.4	0.5	0.6	233	
YZ	+	0	151	43.95	0.4	0.5	248	
YZ	+	0	159.65	44.2	1.2	2.2	253.5	
YZ	+	0	150.95	45.65				DIST
YZ	+	0	152	45.15	0.4	0.6	254	
YZ	+	0	152.3	45.55	0.3	0.3		CIRC
YZ	+	0	155.65	45.45				DIST
YZ	+	0	157.65	46.05	1	1.5	246	HSAT
YZ	+	0	157.2	46.5	1.4	2.4	245	PDS/HSAT
YZ	+	0	150.5	47.8	1.5	2	275	
YZ	+	0	151.7	47.4	1.9	2.4	234	HSAT
YZ	+	0	151.8	47.9	0.8	1	234	PDS
YZ	+	0	154.45	47.65	1	1.7	243.5	HSAT
YZ	+	0	150.55	49.25	0.9	1.5	233	
YZ	+	0	152.15	48.7	2.9	3.6	237	CREN/HSAT
YZ	+	0	154.55	49.5	0.5	0.8	250	
YZ	+	0	156.15	48.6	0.7	1.2	248	FRAG
YZ	+	0	158.25	50.05	1	1.6	245	PDS
YZ	+	0	158.35	51.55	0.5	0.8	243	
YZ	+	0	158.7	51.5	0.9	1.8	244	TSAT/PDS
YZ	+	0	154.25	52.95	1.5	2.4	275	
YZ	+	0	152.2	56.45	1	1.4	234	
YZ	+	0	153.1	60.4	1.1	2	232	
YZ	+	0	158.1	62.65	1.1	2.3	237.5	
YZ	+	0	155.35	77.55	0.7	1	234	
YZ	+	0	160.9	16.85	0.2	0.5	325	NDLE
YZ	+	0	161.55	20.1				PSAT(?)
YZ	+	0	160.75	23.2	0.3	0.5	323	NDLE
YZ	+	0	166.6	23	1.5	3.3	299	TAI/HSAT
YZ	+	0	162.75	25.15	0.9	1.3	293	
YZ	+	0	169.1	24.75	0.6	0.9	287	
YZ	+	0	161.05	27	0.6	1	276.5	PDLE
YZ	+	0	163.7	25.95	0.3	0.5	306	NDLE
YZ	+	0	164.1	25.9	0.2	0.4	309	NDLE
YZ	+	0	161.05	28.4	0.5	0.8	277	
YZ	+	0	161.6	28.2	0.6	0.8	282	PDS
YZ	+	0	162.2	27.85	1.6	2.3	274.5	FRAG
YZ	+	0	166.6	28				PSAT(?)
YZ	+	0	165.2	28.65	0.9	1.7	277	
YZ	+	0	164.05	29.9	0.6	0.9	270	
YZ	+	0	165.05	27	0.2	0.3	289	NDLE
YZ	+	0	169.15	27	0.3	0.4	303	NDLE
YZ	+	0	161.6	30	1	1.2	263	HSAT/CREN
YZ	+	0	161.25	30.6	0.7	1	265	
YZ	+	0	165.95	30.65	0.5	0.7	272	TAI
YZ	+	0	161.4	31.55	0.6	0.8	268	
YZ	+	0	165	31.9	0.5	0.7	297.5	
YZ	+	0	163.05	32.95	0.6	0.9	285	



YZ	+	0	166.5	33.5	0.6	0.8	261	
YZ	+	0	167.1	33.5	0.4	0.7	281	
YZ	+	0	167.5	33.15	2.5	4.4	275	TAI/FRAG
YZ	+	0	160.8	34.25	0.8	1.2	273	
YZ	+	0	160.5	35.85	1.8	2.7	264	PDS
YZ	+	0	160.2	36.5	0.7	1.2	267	PDLE
YZ	+	0	167.45	35.85	0.8	0.9	266	PDLE
YZ	+	0	167.95	35.8	0.6	1.1	276	
YZ	+	0	164.75	38.2	0.4	0.6	302	
YZ	+	0	165.65	37.7	0.2	0.3	273.5	NDLE
YZ	+	0	164.35	38.8	0.5	0.8	289	PDLE
YZ	+	0	162.1	39.75	0.2	0.4	268.5	PDLE
YZ	+	0	167.15	39.25	0.6	1.2	271	PDS
YZ	+	0	163.2	40.15	0.9	1.6	260.5	
YZ	+	0	163.9	40.4	1.6	2.4	263	PDS
YZ	+	0	168.3	40.8	0.8	1.3	266	
YZ	+	0	168.55	41.95	0.5	0.7	258	
YZ	+	0	167.6	42.15	0.3	0.6	265.5	
YZ	+	0	163.65	44.45	0.6	0.9	258	
YZ	+	0	165.4	44.6	0.9	1.6	254	TAI
YZ	+	0	165.65	44.05	0.6	1	257	
YZ	+	0	166.5	44.4	0.6	0.9	250	
YZ	+	0	168.05	44.3	0.2	0.3	318	NDLE
YZ	+	0	169.9	44.05	0.3	0.5	286	NDLE
YZ	+	0	168.3	47.4	0.6	1	257	
YZ	+	0	166.4	49.7	0.6	1.4	244	
YZ	+	0	162.3	52.7	1.6	2.9	247.5	FRAG
YZ	+	0	169.5	56.7	1.4	2.4	243	HSAT
YZ	+	0	164.15	59.85	0.4	0.6	246	PDLE
YZ	+	0	167.35	70.05	1	1.8	235.5	TAI
YZ	+	0	172.9	0.85				PSAT(?)
YZ	+	0	170.65	18.2	0.2	0.4	336	NDLE
YZ	+	0	175.7	19.95	0.5	0.9	306	PDS
YZ	+	0	175.9	19.7	0.2	0.6	310	PDLE
YZ	+	0	175.05	20.15	0.5	0.8	287	
YZ	+	0	175.7	21.25	0.4	0.8	292	
YZ	+	0	179.35	20.45	0.6	1.1	288	
YZ	+	0	176.25	24.35	0.3	0.6	311	
YZ	+	0	176.6	25.3	0.4	0.6	304	
YZ	+	0	178.1	24.05	0.3	0.6	302	
YZ	+	0	178.1	24.25	0.2	0.4	303.5	NDLE
YZ	+	0	179.9	23.7	1	2.2	283	HSAT
YZ	+	0	179.45	25.2	1	1.9	281	TAI
YZ	+	0	173.4	26.3	0.7	1.1	288.5	
YZ	+	0	179.25	26.6	0.2	0.4	312	PDLE
YZ	+	0	176.05	28.15	1.1	1.9	275	
YZ	+	0	177.8	29.6	0.4	0.8	276	
YZ	+	0	179.2	29.35	1	2	279	
YZ	+	0	177.1	30.45	0.3	0.6	289	
YZ	+	0	174.75	31.3	0.7	1.2	277	
YZ	+	0	173.6	32.7	0.4	0.6	281	

YZ	+	0	176.65	32	1.3	2.3	272	CREN
YZ	+	0	178.6	31.95	1.4	2.7	266	TAI/CREN
YZ	+	0	175.65	33.3	0.4	0.9	272.5	
YZ	+	0	176.8	33.55	0.7	1.2	268	FRAG/HSAT
YZ	+	0	173.35	35.5	0.4	0.6	268	
YZ	+	0	175.1	35.6	0.3	0.6	289	
YZ	+	0	176.45	34.8	0.6	1.2	268	
YZ	+	0	172.6	36.25	0.4	0.7	267	
YZ	+	0	174.3	36.9	1.4	2.6	258	CREN/HSAT
YZ	+	0	175.3	36.1	0.2	0.4	328	NDLE
YZ	+	0	176.3	36.6	1.5	2.8	262	HSAT
YZ	+	0	177.3	36.45	0.8	1.8	260	
YZ	+	0	177.8	36.75	2.2	4.4	261	FRAG/ HSAT/ TSAT
YZ	+	0	179.45	37.1	0.4	0.6	281	
YZ	+	0	179.25	36.1	0.2	0.4	319	NDLE
YZ	+	0	178.8	37.5	0.6	1.2	263	
YZ	+	0	177.25	37.7	1.1	2.1	266	CREN
YZ	+	0	178.7	38.45	0.8	1.2	268	TAI/HSAT
YZ	+	0	179.7	38.9	0.2	0.4	321	NDLE
YZ	+	0	170.05	37.65	0.2	0.4	308	NDLE
YZ	+	0	172.7	37.9	0.2	0.4	336	NDLE
YZ	+	0	174	38.1	0.6	1	268	
YZ	+	0	172.3	38.9	1.2	1.7	256	
YZ	+	0	173.6	39.8	0.4	0.8	262	
YZ	+	0	174.95	39.9	1.2	2.2	252	
YZ	+	0	175.9	39.25	0.5	0.8	275	
YZ	+	0	176.5	38.85				DIST
YZ	+	0	172.1	40.85	0.5	0.8	268	
YZ	+	0	178.55	40.5	0.5	0.7	261	
YZ	+	0	179.9	40.4	0.3	0.6	263	
YZ	+	0	170.6	42.3	3.8	5.9	256	FRAG/ HSAT/ TSAT
YZ	+	0	178.2	42.6	1.4	3	258	HSAT/TSAT
YZ	+	0	178.05	41.65	0.3	0.6	276	PDLE
YZ	+	0	179.5	41.15	1.5	2.9	262	
YZ	+	0	170.4	43.6	1.3	2.4	262	
YZ	+	0	171	44.9	2.2	3.6	256	TAI
YZ	+	0	172.75	44.55	0.2	0.4	256	NDLE
YZ	+	0	173	44.35	1.7	2.8	268	CREN/ HSAT/ TSAT
YZ	+	0	172.3	41.85	0.3	0.6	273	
YZ	+	0	172.6	42.6	0.3	0.4	276	PDLE
YZ	+	0	176.45	44.2	1	1.8	262	HSAT
YZ	+	0	177.95	43.25	0.3	0.4	274	PDLE
YZ	+	0	178.75	44.2	0.6	1.2	263	
YZ	+	0	177.85	44.65	2.8	5.7	259	TAI/ TSAT/ CREN
YZ	+	0	179.7	44.95	0.7	0.9	262	
YZ	+	0	179.8	45.5	1.2	3	259	TAI/PDS
YZ	+	0	174.9	45.5	0.5	1	255	

YZ	+	0	175.5	45.6	0.9	1.8	260	
YZ	+	0	174.55	46.15	1	2.1	257	
YZ	+	0	176.2	46.1	0.8	1.8	262	
YZ	+	0	177.9	46.35	1.6	3.2	257	TSAT/ TAI/ CREN
YZ	+	0	172.75	48.25	0.6	1	261	TAI
YZ	+	0	174.6	47.45	0.7	1.3	255.5	
YZ	+	0	175.2	47.25	0.3	0.5	275	
YZ	+	0	176.65	47.2	0.8	1.6	257	TAI
YZ	+	0	177.3	47.3	3.3	5.6	254	FRAG/ TSAT
YZ	+	0	177.3	47.85	1.3	3.5	255	TAI
YZ	+	0	177.5	48.6	1.2	2.6	253	
YZ	+	0	174.95	48.9	1	2.4	257	
YZ	+	0	176.4	49.45	0.7	1.2	251.5	
YZ	+	0	174.8	46.6	0.3	0.5	14	
YZ	+	0	175.9	45.45	0.2	0.4	308	NDLE
YZ	+	0	173.05	50.3	0.5	1	253	
YZ	+	0	176.55	50.3	1.4	2.9	252	TAI/HSAT
YZ	+	0	171.7	51	0.5	0.8	265	
YZ	+	0	173.5	51.45	0.4	0.7	252	
YZ	+	0	173.85	51.4	1.6	2.5	251	
YZ	+	0	170.8	53.7	0.3	0.5	268.5	NDLE
YZ	+	0	172.25	53.35	0.8	1.3	256	
YZ	+	0	174.75	53.3	0.3	0.5	273.5	
YZ	+	0	175.65	53.3				DIST
YZ	+	0	177.85	52.2	0.4	0.6	271	
YZ	+	0	179.5	53.05	1	2.1	254.5	
YZ	+	0	179.2	54.25	0.8	1.5	253	
YZ	+	0	171.05	55.25	1.6	3.3	252	
YZ	+	0	173.9	57.2	1.4	2.6	244	FRAG/TSAT
YZ	+	0	173.4	58.3	1.3	2.4	246.5	
YZ	+	0	178.85	57.6	0.3	0.6	268.5	NDLE
YZ	+	0	178.95	59.85	0.9	1.7	243	FRAG
YZ	+	0	172.65	60.95	0.6	0.8	245.5	
YZ	+	0	174.6	63.8	0.6	0.9	252	
YZ	+	0	177.75	63.2	0.6	1	254	TAI
YZ	+	0	179.2	62	0.6	1.4	248	TSAT
YZ	+	0	170.4	68.5	0.6	1.3	239	PDS
YZ	+	0	182.55	14.9	0.2	0.4	340	NDLE
YZ	+	0	186.55	15.2	0.5	1.1	296	HSAT
YZ	+	0	187.2	15.45	0.2	0.6	321	NDLE
YZ	+	0	189.4	13.7	0.6	1.1	302	
YZ	+	0	184.4	17.85	0.3	0.3		CIRC
YZ	+	0	185.35	19.35	0.8	1.5	287	TAI
YZ	+	0	186	21.75	0.6	1.1	289	
YZ	+	0	182.05	23.15	0.4	0.7	301	
YZ	+	0	181.55	24.45	0.6	1.1	286	
YZ	+	0	184.5	24.7	1	1.9	287	
YZ	+	0	186.05	25.2	1.7	3.9	279	TAI
YZ	+	0	187.75	24.7	0.9	2	283	
YZ	+	0	189.7	23.25	0.5	1	292	

YZ	+	0	181.1	25.35	0.3	0.6	293	
YZ	+	0	181.6	26.7	0.3	0.5	301	NDLE
YZ	+	0	185.1	28.8	0.7	1.3	275	
YZ	+	0	185.8	28.85	0.6	1.4	277	
YZ	+	0	187.3	27.35	1.6	3.4	277	HSAT
YZ	+	0	188.15	27.05	0.5	1	279	TSAT
YZ	+	0	182.65	29.6	0.2	0.5	329	NDLE
YZ	+	0						Not Blood
YZ	+	0	180.65	30.65	0.5	1.2	275	TAI
YZ	+	0	183.15	30.65	0.8	1.6	272	HSAT
YZ	+	0	183.7	30.3	0.2	0.4	301	HSAT
YZ	+	0	183.95	30.85	0.6	1.3	276	TAI
YZ	+	0	186.65	31	0.5	0.8	285	
YZ	+	0	185	30.7	0.6	0.8	282	
YZ	+	0	180.75	33.8	0.6	1.2	272.5	TSAT/TAI
YZ	+	0	180.9	34.6	0.8	1.6	265	
YZ	+	0	182.35	34.05	0.6	1	281	HSAT/ TAI
YZ	+	0	182.75	33.9	0.4	0.6	286	
YZ	+	0	185.9	33.15	1	2.4	267	TAI
YZ	+	0	183.3	34.8	0.4	0.9	274	
YZ	+	0	181.6	36.05	1.2	2.2	265	TAI
YZ	+	0	185.5	35.05	0.8	1.5	273	
YZ	+	0	187.7	35.35	0.6	1.2	268	TSAT
YZ	+	0	181.05	37.25	1.6	3	264	TSAT
YZ	+	0	182.05	107	2.9	4.4	262	FRAG/ TAI/ TSAT
YZ	+	0	183.15	36.95	0.5	1.1	269	TSAT
YZ	+	0	182.45	38.15	0.4	0.8	269	TSAT
YZ	+	0	183.8	37.9	3.4	7.6	266	FRAG/TSAT
YZ	+	0	185.05	37.3	0.3	0.5	280	
YZ	+	0	187.45	37.8	0.3	0.5	301	
YZ	+	0	187.5	38.3	0.4	0.7	267.5	
YZ	+	0	180.7	39.55	0.2	0.4	279	
YZ	+	0	184.65	39.5	1.9	5.1	260	FRAG/TSAT
YZ	+	0	185.9	39.5	1	2.3	267	
YZ	+	0	188.85	39.25	0.4	0.8	279	
YZ	+	0	180.4	41.1	0.4	0.5	277	
YZ	+	0	181.05	41.15				DIST
YZ	+	0	182.2	41	0.4	0.5	275	
YZ	+	0	183.2	41.35	0.6	1.4	268	HSAT
YZ	+	0	186.05	41.1	1	2.4	262.5	HSAT
YZ	+	0	186.5	40.8	0.3	0.6	285	NDLE
YZ	+	0	186.85	40.1	1.6	3.8	265	TAI/HSAT
YZ	+	0	187.8	40.25	0.5	0.8	270	
YZ	+	0	180.15	42.4	1.3	2.4	264	TSAT
YZ	+	0	180.75	42.15	3	5.6	258	TSAT/HSAT
YZ	+	0	183.2	41.9	0.6	1.3	272.5	
YZ	+	0	183.45	42.65	0.6	1.3	262	TAI/TSAT
YZ	+	0	183.2	43.05	1.5	3.2	263	TSAT
YZ	+	0	182.35	43.5	0.4	0.8	258	
YZ	+	0	186.45	43.3	0.5	0.9	261	

YZ	+	0	189.85	42.3	0.4	0.6	281	
YZ	+	0	184.3	44.8	0.2	0.6	297	NDLE
YZ	+	0	188.4	44.4	1.4	2.9	256	TAI/HSAT
YZ	+	0	181.25	46.6	0.3	0.7	266	
YZ	+	0	183.5	46.4	2.2	4	255	FRAG/ CREN/ HSAT
YZ	+	0	184.1	46.45	1.1	2.3	263	
YZ	+	0	180.55	47.45	1.4	2.9	256	FRAG/ TSAT/ PDS
YZ	+	0	181.55	47.4	2.2	4.4	253.5	FRAG/TSAT
YZ	+	0	183.65	48.35	0.6	1.2	252.5	
YZ	+	0	184.2	48.05	0.8	1.7	260	
YZ	+	0	184.75	47.45	2.8	5.2	256	FRAG/TSAT
YZ	+	0	188.9	47.25	1.4	2.7	257	TAI/TSAT
YZ	+	0	188.75	48.2	0.2	0.4	285	NDLE
YZ	+	0	182.7	49.95	0.3	0.4	290	PDLE
YZ	+	0	182.9	49.85	0.3	0.6	270	TAI
YZ	+	0	183.7	49.4	0.8	1.6	254	
YZ	+	0	183.8	49	0.4	0.5	282	
YZ	+	0	183.65	50.1	0.4	0.8	259	
YZ	+	0	184.5	50.15	0.9	1.9	258.5	
YZ	+	0	186.95	50	0.4	0.8	266	
YZ	+	0	183.5	50.4	2.2	4.1	249	CREN/ TSAT
YZ	+	0	185.7	50.9	0.2	0.6	279	NDLE
YZ	+	0	186.05	50.6	0.4	0.6	269	
YZ	+	0	182.7	51.9	3.6	6.8	258	CREN/ FRAG/ TSAT
YZ	+	0	186.1	52.15	2.8	6.5	251	FRAG/ TAI/ TSAT
YZ	+	0	185.15	54.7	0.3	0.5	281	
YZ	+	0	185.55	54.6				DIST
YZ	+	0	187.1	54.5	0.7	1.3	253.5	TSAT
YZ	+	0	188.5	54.1	0.6	1.1	264	
YZ	+	0	189.15	55.15	0.6	1.2	256	
YZ	+	0	180.4	57.7	1.3	2.6	244	CREN/ TSAT
YZ	+	0	183.6	58.35	0.4	0.8	254	
YZ	+	0	188.6	58.95	1.4	3.2	252	TAI/TSAT
YZ	+	0	185.65	59.9	0.8	1.8	244	TAI/HSAT
YZ	+	0	181.95	64.2	0.6	1	243	
YZ	+	0	184.4	65.7	0.7	1.4	247.5	TSAT
YZ	+	0	192.9	13.4	0.2	0.6	321	TAI
YZ	+	0	192	17.45	0.7	1.3	291	TSAT
YZ	+	0	196.85	16.55	0.5	1.2	294	HSAT
YZ	+	0	193.4	20.95	1.2	3.2	284	TSAT
YZ	+	0	192.6	22.3	1.4	3.2	280	TAI
YZ	+	0	190.25	23.95	0.7	1.5	283	
YZ	+	0	194.75	23.05	0.8	1.9	282	
YZ	+	0	198.3	21.9	0.2	0.5	307	
YZ	+	0	191.9	26.15	1	2.1	276	
YZ	+	0	193	26.6	0.4	0.9	284	
YZ	+	0	198.35	24.35	0.2	0.8	322	NDLE

YZ	+	0	192.9	27.4	0.3	0.5	317	
YZ	+	0	197.8	26.3	1.2	3	282	TAI/HSAT
YZ	+	0	198.5	26.05				DIST
YZ	+	0	195.1	30.45	0.5	0.9	289	
YZ	+	0	194	32.35	1	2.2	282	TAI/HSAT
YZ	+	0	192.5	37.5	0.4	0.6	288	
YZ	+	0	193.1	38.65				DIST
YZ	+	0	195.3	40.35	1	2.3	266	HSAT
YZ	+	0	190.85	41.5	0.5	1	267	
YZ	+	0	195.35	44.45				DIST
YZ	+	0	195.5	44.15	0.3	0.4	311	
YZ	+	0	197.95	46.8	2	5.4	257.5	TAI/HSAT
YZ	+	0	198.6	47.65	0.6	1.2	276	
YZ	+	0	190.15	49.7	0.4	0.6	275	
YZ	+	0	197.45	48.6	0.3	0.7	282	
YZ	+	0	191.9	44.5	0.2	0.5	266	NDLE
YZ	+	0	198.55	51.5	0.3	0.6	283	
YZ	+	0	198.05	53.35	0.4	0.9	267	
YZ	+	0	192.2	55.75	2.5	5.5	253	TAI/HSAT
YZ	+	0	193.65	57.5	0.6	1.2	256	
YZ	+	0	197.7	58.6	0.5	1.2	265	HSAT
YZ	+	0	192.75	59.5	0.4	0.8	263	
YZ	+	0	194.8	62.8	0.6	1.4	256	
YZ	+	0	197.15	63.15	0.5	0.9	274.5	
YZ	+	0	194.45	65.95	0.8	2	252	HSAT
YZ	+	0	202.35	14.85	0.5	1.2	296	HSAT
YZ	+	0	201.4	18.6	2.1	4.9	283	TAI/TSAT
YZ	+	0	205.45	18.3	1.4	3.6	289	TAI
YZ	+	0	209.2	17.6	0.4	1	310	
YZ	+	0	200.25	30	0.4	0.9	297	PDS
YZ	+	0	206.9	20.6	0.2	0.8	317	TAI
YZ	+	0	208.05	22.4	0.2	0.7	323	NDLE
YZ	+	0	205.15	33.15	0.4	0.9	284	HSAT
YZ	+	0	208.25	33.6	0.8	1.8	298	TAI/TSAT
YZ	+	0	204	42.95	0.6	1.6	271	HSAT
YZ	+	0	206.5	45.25	0.7	1.7	272.5	HSAT
YZ	+	0	206.25	50.35	0.7	1.3	270	
YZ	+	0	202.2	56.2	0.6	1	268	TAI/TSAT
YZ	+	0	208.45	54.95	0.8	2.7	264	
YZ	+	0	201.35	59.65	0.4	0.8	272	
YZ	+	0	206.6	57.35	0.3	0.8	307	
YZ	+	0	200.8	62.45	0.4	0.6	303	
YZ	+	0	202.85	65.2	0.8	1.4	255	HSAT
YZ	+	0	202.35	66.1	0.5	0.9	264	TAI
YZ	+	0	205.65	74.1	0.4	0.8	302	
YZ	+	0	208.3	73.15	0.5	1	252	HSAT
YZ	+	0	207.95	82.6	1.1	2.6	247	TAI/TSAT
YZ	+	0	210.9	16.6	0.6	1.3	305	TSAT
YZ	+	0	219	21.85	0.7	2	305	HSAT
YZ	+	0	212.5	27.5	0.4	0.8	316	NDLE
YZ	+	0	219.2	27.05	0.8	2	279	TSAT

YZ	+	0	210.85	37.8	0.5	1	292	
YZ	+	0	214.8	40.3	1.6	4.2	270	TAI/HSAT
YZ	+	0	214.1	41.5	0.4	1.1	294	
YZ	+	0	211.25	43.65	0.3	0.7	292	
YZ	+	0	212.4	45.8	0.2	0.7	312	NDLE
YZ	+	0	216	51.1	0.2	0.8	325	NDLE
YZ	+	0	213.3	57.9	1.3	3.7	273	
YZ	+	0	219.3	65.2	0.6	1.7	262	HSAT
YZ	+	0	212.65	71.55	0.8	2.2	256	TAI/TSAT
YZ	+	0	216.25	70.8	0.4	1	264	TSAT
YZ	+	0	216.1	72.15	0.6	1.6	255	HSAT
YZ	+	0	210.9	72.4	1.7	5.3	253	PDS
YZ	+	0	211.25	72.3	1.8	4.9	250	TAI/TSAT/ PDS
YZ	+	0	212.6	74.9	0.6	1.4	259	TSAT
YZ	+	0	215.5	76	1.5	6	249	FRAG/TAI
YZ	+	0	219.4	78.2	0.5	1.5	256	HSAT
YZ	+	0	218.65	78.75	2.8	5.5	247	FRAG/TAI/ TSAT
YZ	+	0	225	22.3	0.8	3.2	284	TAI
YZ	+	0	226.8	25.7	0.8	2.8	281	
YZ	+	0	226.75	27.35	1.4	4.2	276	FRAG/ TAI/ TSAT
YZ	+	0	227.2	27.55	0.9	2.9	278.5	TAI/TSAT
YZ	+	0	226	29.65	1.6	3.8	275	TAI
YZ	+	0	226.5	32.1	0.6	1.4	286	HSAT
YZ	+	0	221.95	35.8	0.4	1.6	286	HSAT
YZ	+	0	224.4	49.5	0.4	0.9	291	
YZ	+	0	226.75	49.6	0.5	1.4	289	HSAT
YZ	+	0	224.3	50.15	1.1	3	284	
YZ	+	0	226.65	51.1	0.4	1.4	282	TSAT
YZ	+	0	222.45	53	0.5	1.6	268	HSAT
YZ	+	0	222	53.8				PSAT(?)
YZ	+	0	225.6	53	0.9	2.5	267	TAI
YZ	+	0	225.9	55.25	0.4	1.3	292	
YZ	+	0	221.6	61.4	0.7	2	265	TSAT
YZ	+	0	221.95	65.6	0.5	1.4	270	HSAT
YZ	+	0	224.5	66.35	0.4	1	291	
YZ	+	0	220.3	81.9	0.8	2.6	252	TSAT
YZ	+	0	231.65	25.7	0.5	1.6	179	TSAT
YZ	+	0	233.85	73.9	0.4	1.5	189	HSAT

## Appendix N – Converted BackTrack®/Win Experimental Data

The four spatter bloodstain data examples provided with the demonstration version of BackTrack®/Win (Forensic Computing of Ottawa, 2001b) which are included within the analytical site of impact estimation macro for analysis are shown in the tables below. The data has been converted from the original format to adhere to the measurement standards required by the VB macro, and the pre-defined investigative environment size used throughout this research project.

### Front Wall

Plane	Normal	X (cm)	Y (cm)	Z (cm)	Width (mm)	Length (mm)	Orientation Angle (degrees)
XZ	-	76.2	300	173.7	1.67	3.57	136.1
XZ	-	89	300	164	2.1	3.85	147
XZ	-	90.5	300	158	2.19	4.12	147.3
XZ	-	81.6	300	147.9	1.97	3.95	139
XZ	-	103.2	300	149.8	1.5	2.56	158
XZ	-	90.7	300	133	2.13	3.4	123.1
XZ	-	143.3	300	149.6	2.2	4.27	202
XZ	-	151.2	300	143.2	1.63	3	218.1
XZ	-	169.1	300	152	2.48	5.15	226
XZ	-	177.5	300	151	2.19	4.98	227
XZ	-	179.4	300	146.9	1.83	4.49	235.2
XZ	-	173	300	133.2	2.33	4.49	240

### Back Wall

Plane	Normal	X (cm)	Y (cm)	Z (cm)	Width (mm)	Length (mm)	Orientation Angle (degrees)
XZ	+	123.8	0	173.7	1.67	3.57	136.1
XZ	+	111	0	164	2.1	3.85	147
XZ	+	109.5	0	158	2.19	4.12	147.3
XZ	+	118.4	0	147.9	1.97	3.95	139
XZ	+	96.8	0	149.8	1.5	2.56	158
XZ	+	109.3	0	133	2.13	3.4	123.1
XZ	+	56.7	0	149.6	2.2	4.27	202
XZ	+	48.8	0	143.2	1.63	3	218.1
XZ	+	30.9	0	152	2.48	5.15	226
XZ	+	22.5	0	151	2.19	4.98	227
XZ	+	20.6	0	146.9	1.83	4.49	235.2
XZ	+	27	0	133.2	2.33	4.49	240



### Right Wall

Plane	Normal	X (cm)	Y (cm)	Z (cm)	Width (mm)	Length (mm)	Orientation Angle (degrees)
YZ	-	300	123.8	173.7	1.67	3.57	136.1
YZ	-	300	111	164	2.1	3.85	147
YZ	-	300	109.5	158	2.19	4.12	147.3
YZ	-	300	118.4	147.9	1.97	3.95	139
YZ	-	300	96.8	149.8	1.5	2.56	158
YZ	-	300	109.3	133	2.13	3.4	123.1
YZ	-	300	56.7	149.6	2.2	4.27	202
YZ	-	300	48.8	143.2	1.63	3	218.1
YZ	-	300	30.9	152	2.48	5.15	226
YZ	-	300	22.5	151	2.19	4.98	227
YZ	-	300	20.6	146.9	1.83	4.49	235.2
YZ	-	300	27	133.2	2.33	4.49	240

### Left Wall

Plane	Normal	X (cm)	Y (cm)	Z (cm)	Width (mm)	Length (mm)	Orientation Angle (degrees)
YZ	+	0	76.2	173.7	1.67	3.57	136.1
YZ	+	0	89	164	2.1	3.85	147
YZ	+	0	90.5	158	2.19	4.12	147.3
YZ	+	0	81.6	147.9	1.97	3.95	139
YZ	+	0	103.2	149.8	1.5	2.56	158
YZ	+	0	90.7	133	2.13	3.4	123.1
YZ	+	0	143.3	149.6	2.2	4.27	202
YZ	+	0	151.2	143.2	1.63	3	218.1
YZ	+	0	169.1	152	2.48	5.15	226
YZ	+	0	177.5	151	2.19	4.98	227
YZ	+	0	179.4	146.9	1.83	4.49	235.2
YZ	+	0	173	133.2	2.33	4.49	240